

**Ongoing Face Recognition
Vendor Test (FRVT)**
Part 1: Verification

Patrick Grother
Mei Ngan
Kayee Hanaoka
*Information Access Division
Information Technology Laboratory*

This publication is available free of charge from:
<https://www.nist.gov/programs-projects/face-recognition-vendor-test-frvt-ongoing>

2021/08/02

ACKNOWLEDGMENTS

The authors are grateful to staff in the NIST Biometrics Research Laboratory for infrastructure supporting rapid evaluation of algorithms.

DISCLAIMER

Specific hardware and software products identified in this report were used in order to perform the evaluations described in this document. In no case does identification of any commercial product, trade name, or vendor, imply recommendation or endorsement by the National Institute of Standards and Technology, nor does it imply that the products and equipment identified are necessarily the best available for the purpose.

INSTITUTIONAL REVIEW BOARD

The National Institute of Standards and Technology's Research Protections Office reviewed the protocol for this project and determined it is not human subjects research as defined in Department of Commerce Regulations, 15 CFR 27, also known as the Common Rule for the Protection of Human Subjects (45 CFR 46, Subpart A).

FRVT STATUS

This report is a draft NIST Interagency Report, and is open for comment. It is the twenty first edition of the report since the first was published in June 2017. Prior editions of this report are maintained on the FRVT [website](#), and may contain useful information about older algorithms and datasets no longer used in FRVT.

FRVT remains open: All [four tracks](#) of the FRVT are open to new algorithm submissions.

2021-08-02 changes since 2021-06-25:

- ▷ We have added results for first algorithms from eight new developers: Bee the Data, Closeli Inc, Coretech Knowledge Inc, Deepsense (France), ioNetworks Inc, Kakao Pay Corp, Seventh Sense Artificial Intelligence, and SK Telecom.
- ▷ We have added results for new algorithms from fifteen returning developers: Alchera Inc, Adera Global PTE, Aware, Bresee Technology, Cyberlink Corp, Expasoft LLC, Fujitsu Research and Development Center, Gorilla Technology, Idemia, Neurotechnology, NEO Systems, NHN Corp, Paravision, Panasonic R+D Center Singapore, and Shenzhen University-Macau University of Science and Technology.
- ▷ We have retired results for twelve algorithms per our policy to only list results for two algorithms per developer. Results for retired algorithms appear in prior versions of this report in the [archive](#).

2021-06-25 changes since 2021-05-21:

- ▷ We have added results for first algorithms from six new developers: Alice Biometrics, BOE Technology Group, Fincore, Neosecu, Sodec App, and Yuntu Data and Technology.
- ▷ We have added results for new algorithms from seven returning developers: Incode Technologies, HyperVerge, Mobbeel Solutions, Guangzhou Pixel Solutions, Remark Holdings, Sensetime, and Vietnam Posts and Telecommunications Group.
- ▷ We have retired results for four algorithms per our policy to only list results for two algorithms per developer. Results for retired algorithms appear in prior versions of this report in the [archive](#).

2021-05-21 changes since 2021-04-26:

- ▷ We have added results for first algorithms from five new developers: Ekin Smart City Technologies, Suprema ID, Tripleize, Taiwan-Certificate Authority, and Vision Intelligence Center of Meituan.
- ▷ We have added results for new algorithms from eight returning developers: ID3 Technology, Imagus Technology, Momentum Digital, N-Tech Lab, NSENSE, Shanghai Jiao Tong University, Vision-Box, and Yuan High-Tech Development
- ▷ We have retired results for seven algorithms per our policy to only list results for two algorithms per developer. Results for retired algorithms appear in prior versions of this report in the [archive](#).

2021-04-26 changes since 2021-04-16:

- ▷ We have added results for first algorithms from three new developers: Quantasoft, Rendip, and NEO Systems.
- ▷ We have added results for new algorithms from four returning developers: 3Divi, Realnetworks, Veridas Digital Authentication Solutions, and Universidade de Coimbra.

- ▷ We have retired results for three algorithms per our policy to only list results for two algorithms per developer. Results for retired algorithms appear in prior versions of this report in the [archive](#).

2021-04-16 changes since 2021-03-19:

- ▷ We have added results for first algorithms from six new developers: 20Face, Beijing DeepSense Technologies, BitCenter UK, Enface, FaceTag, InsightFace AI, Line Corporation, Lema Labs, Nanjing Kiwi Network Technology, Omnidarde, Regula Forensics, and Suprema.
- ▷ We have added results for new algorithms from ten returning developers: CloudSmart Consulting, Dermalog, GeoVision, Neurotechnology, Panasonic R+D Center Singapore, Samsung S1, Securif AI, Trueface.ai, Vigilant Solutions, and Visidon.
- ▷ We have retired results for ten algorithms per our policy to only list results for two algorithms per developer. Results for retired algorithms appear in prior versions of this report in the [archive](#).

2021-03-19 changes since 2021-03-05:

- ▷ We have added results for first algorithms from six new developers: Ajou University, AuthenMetric, Code Everest, Corsight, Papilon Savunma, and NHN Corp
- ▷ We have added results for new algorithms from seven returning developers: Alchera, Deepglint, Fiber-home Telecommunication Technologies, Kakao Enterprise, Kookmin University, Megvii/Face++, and NotionTag Technologies.
- ▷ We have updated many of the hyperlinked HTML report-cards to include seven figures on demographic dependence. Figures of this kind first appeared, and are documented in, the December 2019 document, [NIST Interagency Report 8280](#) on demographic differentials in face recognition. The figures quantify false negative dependence on demographics using “visa-border” comparisons, and false positive dependence using comparisons of “application” photos that uniformly of quality and similar to visa photos.

2021-03-05 changes since 2021-01-19:

- ▷ We have added results for first algorithms from three new developers: IVA Cognitive, Mobbeel, and MoreDian Technology.
- ▷ We have added results for new algorithms from returning developers: Ability Enterprise - Andro Video, ACI Software, Adera Global, AnyVision, BioID Technologies, China Electronics Import-Export, Cognitec Systems, Fujitsu Research and Development Center, Glory, Guangzhou Pixel Solutions, Hengrui AI Technology, Incode Technologies, Intel Research, iQIYI, Mobai, Oz Forensics, Paravision, VisionLabs, and Xforward AI Technology.
- ▷ We have added a new “resources” tab to the main [webpage](#). It includes sortable columns for data related to speed, model size, storage, and memory consumption.
- ▷ We have retired results for 13 algorithms per our policy to only list results for two algorithms per developer. Results for retired algorithms appear in prior versions of this report in the [archive](#).

2021-01-19 changes since 2020-12-18:

- ▷ This report adds results for first algorithms from four developers: Herta Security, Irex AI, Shenzhen University-Macau University of Science and Technology, and Vietnam Posts and Telecommunications Group. See Table 5 for more information.
- ▷ The report also includes results for thirteen developers who have previously submitted algorithms: Bresee Technology, Canon (previously Canon Information Technology (Beijing)), Cyberlink, CSA IntelliCloud Technology, Dahua Technology, ID3 Technology, Imagus Technology (Vixvizon), Moontime Smart Technology, N-Tech Lab, Thales Cogent, Veridas Digital Authentication Solutions, Vocord, and Yuan High-Tech Development.
- ▷ We have retired results for ten algorithms per our policy to only list results for two algorithms per developer. Results for retired algorithms appear in prior versions of this report in the [archive](#).

2020-12-18 changes since 2020-10-09:

- ▷ This report adds results for first algorithms from ten developers: BitCenter UK, CloudSmart Consulting, Cubox, Institute of Computing Technology, Naver Corp, Minivision, NSENSE Corp, Viettel Group, Visage Technologies, and Xiamen University. See Table 5 for more information.
- ▷ The report also includes results for eighteen developers who have previously submitted algorithms: ADVANCE.AI, Awidit Systems, Chosun University, Dermalog, GeoVision, ICM Airport Technics, Idemia, Institute of Information Technologies, Kakao Enterprise, Neurotechnology, Panasonic R+D Center Singapore, Rank One Computing, Sensetime Group, Shanghai Jiao Tong University, TigerIT Americas LLC, Vigilant Solutions, Winsense, and YooniK
- ▷ We have retired results for twelve algorithms per our policy to only list results for two algorithms per developer. Results for retired algorithms appear in prior versions of this report in the [archive](#).

Changes since September 18, 2020:

- ▷ This report adds results for first algorithms from five developers: Aigen, Cortica, Kookmin University, Securif AI and Vinai.
- ▷ The report also includes results for three developers who have previously submitted algorithms: Fujitsu Laboratories, Hengrui AI, and X-Forward AI.
- ▷ In the per-algorithm report-cards linked from tables and the main webpage, we have added a chart to showing reduction in error rates over the course of FRVT i.e. from 2017 onwards for all algorithms supplied by that developer. Similarly we have added a chart showing error rate reductions for our test of protective face mask verification.
- ▷ We plan to continue evaluating algorithms on various mask datasets. We hold that algorithms should be capable of detecting masks and verifying identity of all combinations of masked and unmasked faces. We have accordingly increased the amount of time allowed to extract those features from 1.0 to 1.5 seconds.

Changes since August 25, 2020:

- ▷ This report adds results for first algorithms from eight new developers: Akurat Satu Indonesia, Cybercore, Decatur Industries, Innef Labs, Satellite Innovation/Eocortex, Expasoft, and Mobai.
- ▷ The report includes results for seven developers who have previously submitted algorithms: 3Divi, BioID Technologies, Incode Technologies, Innovatrics, iSAP Solution, Synology, and Tevian.

- ▷ We have retired results for five algorithms per our policy to only list results for two algorithms per developer. Results for retired algorithms appear in prior versions of this report in the [archive](#).

Changes since July 27, 2020:

- ▷ We have introduced per-algorithm report sheets. These are HTML documents linked from the accuracy tables in this report (i.e. Table 21) and on the FRVT 1:1 [homepage](#). The sheets contain interactive graphics allowing, for example, mouseover exploration of FNMR(T) and FMR(T). Some of their content had previously appeared in this document.
- ▷ This report adds results for algorithms from six new developers. ACI Software, Bresee Technology, Fiberhome Telecommunication Technologies, Imageware Systems, Oz Forensics, and Pensees.
- ▷ The report includes results for thirteen developers who have previously submitted algorithms: Canon Information Technology (Beijing), Cyberlink, Dahua Technology, Gorilla Technology, ID3 Technology, Intel Research Group, iQIYI Inc, Momentum Digital, Netbridge Technology, Tech5 SA, Shenzhen AiMall Tech, Vigilant Solutions, and VisionLabs.
- ▷ We have retired results for nine algorithms per our policy to only list results for two algorithms per developer. Results for retired algorithms appear in prior versions of this report in the [archive](#).

Changes since May 18, 2020:

- ▷ The report is the first FRVT update since the pandemic closed it from March to June 2020.
- ▷ This report includes results for algorithms from nine new developers: GeoVision Inc, Su Zhou NaZhi-TianDi Intelligent Technology, YooniK, AYF Technology, PXL Vision AG, Yuan High-Tech Development, Beihang University-ERCACAT, ICM Airport Technics, and Staqu Technologies
- ▷ This report includes results for algorithms from 15 returning developers Acer Incorporated, Antheus Technologia, Chosun University, Chunghwa Telecom, Idemia, Moontime Smart Technology, Neurotechnology, Guangzhou Pixel Solutions, Panasonic R+D Center Singapore, Rank One Computing, Scanovate, Shanghai Universiy - Shanghai Film Academy, Synesis, Trueface.ai, and Veridas Digital Authentication Solutions
- ▷ We have retired results for ten algorithms per our policy to only list results for two algorithms per developer. Results for retired algorithms appear in prior versions of this report in the [archive](#).
- ▷ We separated timing and other resource consumption from the main participation table. The new Table 13 includes template generation durations for four kinds of images, not just mugshots.
- ▷ We have published a separate report, [NIST Interagency Report 8311](#) on accuracy of pre-pandemic algorithms on subjects wearing face masks. We plan to track improvements in accuracy on masked images going forward. In particular, we invite submission of algorithms that can detect whether a person is wearing a mask, extract features from the full face or the exposed periocular region, and do appropriate comparison. We do not intend to evaluate algorithms that assume 100% of images will be of masked individuals.

Changes since March 25, 2020:

- ▷ The report is a maintenance release - it does not add any new algorithms, and FRVT has been closed to new algorithms since mid March 2020.
- ▷ We modified the primary accuracy summary, Table 21, as follows:

- ▷▷ For visa images, the column for FNMR at FMR = 0.0001 has been removed. The visa images are so highly controlled that the error rates for the most accurate algorithms are dominated by false rejection of very young children and by the presence of a few noisy greyscale images. For now, two visa columns remain: FNMR at $FMR = 10^{-6}$ and, for matched covariates, FNMR at $FMR = 10^{-4}$.
- ▷▷ We have inserted a new column labelled “BORDER” giving accuracy for comparison of moderately poor webcam border-crossing photos that exhibit pose variations, poor compression, and low contrast due to strong background illumination. The accuracies are the worst from all cooperative image datasets used in FRVT.
- ▷ Accordingly, we updated the failure-to-template rates in Table 27.
- ▷ We withdrew a figure showing how false matches are concentrated in certain visa images used in cross-comparison, because it didn’t attempt to include demographic information.

Changes since February 27, 2020:

- ▷ The report adds results algorithms from two new developers: Beijing Alleyes Technology, and the Chinese University of Hong Kong. Results for newly submitted algorithms from two other developers will appear in the next report.
- ▷ The report adds results for algorithms from thirteen returning developers: ASUSTek Computer, Aware, Cyberlink Corp, Gorilla Technology, Innovative Technology, Kakao Enterprise, Lomonosov Moscow State University, Panasonic R+D Center Singapore, Shenzhen AiMall Technology, Shenzhen Intellifusion Technologies, Synology, Tech5 SA, and Via Technologies.
- ▷ Per policy to only list results for two algorithms per developer, we have dropped results for algorithms from Aware, Cyberlink, Gorilla Technology, Kakao Enterprise, Lomonosov Moscow State University, Panasonic R+D Center Singapore, and Tech5 SA.

Changes since January 20, 2020:

- ▷ The report adds results for five new developers: Ability Enterprise (Andro Video), Chosun University, Fujitsu Research and Development Center, University of Coimbra, and Xforward AI Technology.
- ▷ The report adds results for algorithms from six returning developers: AlphaSSTG, Incode Technologies, Kneron, Shanghai Jiao Tong University, Vocord, and X-Laboratory.
- ▷ We have corrected template comparison timing numbers for algorithms submitted September 2019 to January 2020. The values reported previously were slower due to a software bug.
- ▷ We have dropped results for algorithms from Vocord and Incode per policy to only list results for two algorithms per developer.
- ▷ The [FRVT 1:1 homepage](#) has been updated with latest accuracy results.
- ▷ The [FRVT 1:N homepage](#) now includes an update to the September 2019 NIST Interagency Report 8271. The new report adds results for one-to-many search algorithms submitted to NIST from June 2019 to January 2020.

Changes since January 6, 2020:

- ▷ Section 2 has been updated to better describe the Visa and Border images. The caption for Table 21 has been updated to better relate the accuracy values to particular image comparisons.

- ▷ The report adds results for five new developers: Acer, Advance.AI, Expasoft, Netbridge Technology, and Videmo Intelligent Videoanalyse.
- ▷ The report adds results for algorithms from 7 returning developers: China Electronics Import-Export Corp, Intel Research Group, ITMO University, Neurotechnology, N-Tech Lab, Rokid, and VisionLabs.
- ▷ We have dropped results from this edition of the report per policy to only list results for two algorithms per developer: N-Tech Lab, Neurotechnology, ITMO, Visionlabs, and CEIEC.
- ▷ The [FRVT homepage](#) has been updated with latest accuracy results.

Changes since November 11, 2019:

- ▷ Table 13 has been updated to include runtime memory usage. This is the first time such a quantity has been reported. The value is the peak size of the resident set size logged during enrollment of single images.
- ▷ We have migrated summary results table to a new platform that supports sortable tables:
<https://pages.nist.gov/frvt/html/frvt11.html>
- ▷ The report adds results for four new developers: Antheus Technologia, BioID Technologies SA, Canon Information Tech. (Beijing), Samsung S1 (listed in the tables as S1), and Taiwan AI Labs.
- ▷ The report adds results for algorithms from 13 returning developers: Anke Investments, Chunghwa Telecom, Deepglint, Institute of Information Technologies, iQIYI, Kneron, Ping An Technology, Paravision, KanKan Ai, Rokid Corporation, Shanghai Universiy - Shanghai Film Academy, Veridas Digital Authentication Solutions, and Videonetics Technology.
- ▷ We have dropped results from this edition of the report per policy to only list results for two algorithms per developer: remarkai-000, veridas-001, sensetime-001, iit-000, anke-003, and everai-002. Results for these are available in prior editions of this report linked from the FRVT page.
- ▷ We issued [NIST Interagency Report 8280: FRVT Part 3: Demographics](#) on 2019-12-19. It includes results for many of the algorithms covered by this report.

Changes since October 16, 2019:

- ▷ The report adds results for ten new developers: Ai-Union Technology, ASUSTek Computer, DiDi ChuXing Technology, Innovative Technology, Luxand, MVision, Pyramid Cyber Security + Forensic, Scanovate, Shenzhen AiMall Tech, and TUPU Technology.
- ▷ The report adds results for 12 returning developers: CTBC Bank Glory Gorilla Technology Guangzhou Pixel Solutions Imagus Technology Incode Technologies Lomonosov Moscow State University Rank One Computing Samtech InfoNet Shanghai Ulucu Electronics Technology Synesis, and Winsense.
- ▷ We have dropped results from this edition of the report per policy to only list results for two algorithms per developer: glory-000, gorilla-002, incode-003, rankone-006, and synesis-004.
- ▷ Results for five recently submitted algorithms will appear in the next report.

Changes since September 11, 2019:

- ▷ The report adds results for five new participants: Awidit Systems (Awiros), Momentum Digital (Sertis), Trueface AI, Shanghai Jiao Tong University, and X-Laboratory.

- ▷ The report adds results for five new algorithms from returning developers: Cyberlink, Hengrui AI Technology, Idemia, Panasonic R+D Singapore, and Tevian. This causes three algorithm, to be de-listed from the report per policy to list results for two algorithms per developer.

Changes since July 31 2019:

- ▷ The HTML table on the [FRVT 1:1 homepage](#) has been updated to include a column for cross-domain Visa-Border verification. Results for this new dataset appeared in the July 29 report under the name "CrossEV" - these are now renamed "Visa-Border".
- ▷ The [FRVT 1:1 homepage](#) lists algorithms according to lowest mean rank accuracy:

$$\begin{aligned} \text{Rank(FNMR}_{\text{VISA}} \text{ at FMR} = 0.000001) + \\ \text{Rank(FNMR}_{\text{VISA-BORDER}} \text{ at FMR} = 0.000001) + \\ \text{Rank(FNMR}_{\text{MUGSHOT}} \text{ at FMR} = 0.00001 \text{ after 14 years}) + \\ \text{Rank(FNMR}_{\text{WILD}} \text{ at FMR} = 0.00001) \end{aligned}$$

This ordering rewards high accuracy across all datasets.
- ▷ The main results in Table 21 is now in landscape format to accomodate extra columns for the Visa-Border set, and mugshot comparisons after at least 12 years.
- ▷ The report adds results for nine new participants: Alpha SSTG, Intel Research, ULSee, Chungwa Telecon, iSAP Solution, Rokid, Shenzhen EI Networks, CSA Intellicloud, Shenzhen Intellifusion Technologies.
- ▷ The reports adds results for six new algorithms from returning developers: Innovatrics, Dahua Technology, Tech5 SA, Intellivision, Nodeflux and Imperial College, London. One algorithm, from Imperial has been retired, per policy to list results for two algorithms per developer.
- ▷ The cross-country false match rate heatmaps have been replotted to reveal more structure by listing countries by region instead of alphabetically.
- ▷ The next version of this report will be posted around October 18, 2019.

Changes since July 3 2019:

- ▷ The HTML table on the [FRVT 1:1 homepage](#) has been updated to list the 20 most accurate developers rather than algorithms, choosing the most accurate algorithm from each developer based on visa and mugshot results. Also, the algorithms are ordered in terms of lowest mean rank across mugshot, visa and wild datasets, rewarding broad accuracy over a good result on one particular dataset.
- ▷ This report includes results for a new dataset - see the column labelled "visa-border" in Table 5. It compares a new set of high quality visa-like portraits with a set webcam border-crossing photos that exhibit moderately poor pose variations and background illumination. The two new sets are described in sections 2.3 and 2.4. The comparisons are "cross-domain" in that the algorithm must compare "visa" and "wild" images. Results for other algorithms will be added in future reports as they become available.
- ▷ This report adds results for algorithms from 9 developers submitted in early July 2019. These are from 3DiVi, Camvi, EverAI-Paravision, Facesoft, Farbar (F8), Institute of Information Technologies, Shanghai U. Film Academy, Via Technologies, and Ulucu Electronics Tech. Six of these are new participants.
- ▷ Several other algorithms have been submitted and are being evaluated. Results will be released in the next report, scheduled for September 5. That report will include results for new datasets.
- ▷ Older algorithms from Everai, Camvi and 3DiVi, have been retired, per the policy to list only two algorithms per developer.

Changes since June 20 2019:

- ▷ This report adds results for algorithms from 18 developers submitted in early June 2019. These are from CTBC Bank, Deep Glint, Thales Cogent, Ever AI Paravision, Gorilla Technology, Imagus, Incode, Kneron, N-Tech Lab, Neurotechnology, Notiontag Technologies, Star Hybrid, Videonetics, Vigilant Solutions, Winsense, Anke Investments, CEIEC, and DSK. Nine of these are new participants.

- ▷ Several other algorithms have been submitted and are being evaluated. Results will be released in the next report, scheduled for August 1.
- ▷ Older algorithms from Everai, Thales Cogent, Gorilla Technology, Incode, Neurotechnology, N-Tech Lab and Vigilant Solutions have been retired, per the policy to list only two algorithms per developer.

Changes since April 2019:

- ▷ This report adds results for nine algorithms from nine developers submitted in early June 2019. These are from Tencent Deepsea, Hengrui, Kedacom, Moontime, Guangzhou Pixel, Rank One Computing, Synesis, Sensetime and Vocord.
- ▷ Another 23 algorithms have been submitted and are being evaluated. Results will be released in the next report, scheduled for July 3.
- ▷ Older algorithms for Rank One, Synesis, and Vocord have been retired, per the policy to list only two algorithms per developer.

Changes since February 2019:

- ▷ This report adds results for 49 algorithms from 42 developers submitted in early March 2019.
- ▷ This report omits results for algorithms that we retired. We retired for three reasons: 1. The developer submitted a new algorithm, and we only list two. 2. The algorithm needs a GPU, and we no longer allow GPU-based algorithms. 3. Inoperable algorithms.
- ▷ Previous results for retired algorithms are available in older editions of this report linked [here](#).
- ▷ The mugshot database used from February 2017 to January 2019 has been replaced with an extract of the mugshot database documented in NIST Interagency Report 8238, November 2018. The new mugshot set is described in section [2.5](#) and is adopted because:
 - ▷▷ It has much better identity label integrity, so that false non-match rates are substantially lower than those reported in FRVT 1:1 reports to date - see Figure [68](#).
 - ▷▷ It includes images collected over a 17 year period such that ageing can be much better characterized - - see Figure [251](#).
- ▷ Using the new mugshot database, Figure [251](#) shows accuracy for four demographic groups identified in the biographic metadata that accompanies the data: black females, black males, white females and white males.
- ▷ The report adds Figure [17](#) with results for the twenty human-difficult pairs used in the May 2018 paper *Face recognition accuracy of forensic examiners, superrecognizers, and face recognition algorithms* by Phillips et al. [[1](#)].
- ▷ The report uses an update to the wild image database that corrects some ground truth labels.
- ▷ Some results for the child exploitation database are not complete. They are typically updated less frequently than for other image sets.

Contents

ACKNOWLEDGMENTS	1
DISCLAIMER	1
INSTITUTIONAL REVIEW BOARD	1
1 METRICS	40
1.1 CORE ACCURACY	40
2 DATASETS	41
2.1 CHILD EXPLOITATION IMAGES	41
2.2 VISA IMAGES	41
2.3 APPLICATION IMAGES	41
2.4 BORDER CROSSING IMAGES	42
2.5 MUGSHOT IMAGES	42
2.6 WILD IMAGES	42
3 RESULTS	43
3.1 TEST GOALS	43
3.2 TEST DESIGN	43
3.3 FAILURE TO ENROLL	46
3.4 RECOGNITION ACCURACY	52
3.5 GENUINE DISTRIBUTION STABILITY	253
3.5.1 EFFECT OF BIRTH PLACE ON THE GENUINE DISTRIBUTION	253
3.5.2 EFFECT OF AGEING	282
3.5.3 EFFECT OF AGE ON GENUINE SUBJECTS	303
3.6 IMPOSTOR DISTRIBUTION STABILITY	333
3.6.1 EFFECT OF BIRTH PLACE ON THE IMPOSTOR DISTRIBUTION	333
3.6.2 EFFECT OF AGE ON IMPOSTORS	337

List of Tables

1 PARTICIPANT INFORMATION	17
2 PARTICIPANT INFORMATION	18
3 PARTICIPANT INFORMATION	19
4 PARTICIPANT INFORMATION	20
5 PARTICIPANT INFORMATION	21
6 ALGORITHM SUMMARY	22
7 ALGORITHM SUMMARY	23
8 ALGORITHM SUMMARY	24
9 ALGORITHM SUMMARY	25
10 ALGORITHM SUMMARY	26
11 ALGORITHM SUMMARY	27
12 ALGORITHM SUMMARY	28
13 ALGORITHM SUMMARY	29
14 FALSE NON-MATCH RATE	30
15 FALSE NON-MATCH RATE	31
16 FALSE NON-MATCH RATE	32
17 FALSE NON-MATCH RATE	33
18 FALSE NON-MATCH RATE	34
19 FALSE NON-MATCH RATE	35
20 FALSE NON-MATCH RATE	36

21	FALSE NON-MATCH RATE	37
22	FAILURE TO ENROL RATES	46
23	FAILURE TO ENROL RATES	47
24	FAILURE TO ENROL RATES	48
25	FAILURE TO ENROL RATES	49
26	FAILURE TO ENROL RATES	50
27	FAILURE TO ENROL RATES	51

List of Figures

1	PERFORMANCE SUMMARY: FNMR VS. TEMPLATE SIZE TRADEOFF	38
2	PERFORMANCE SUMMARY: FNMR VS. TEMPLATE TIME TRADEOFF	39
3	EXAMPLE IMAGES	43
(A)	VISA	43
(B)	MUGSHOT	43
(C)	WILD	43
(D)	BORDER	43
4	PERFORMANCE ON 20 HUMAN-DIFFICULT PAIRS	53
5	PERFORMANCE ON 20 HUMAN-DIFFICULT PAIRS	54
6	PERFORMANCE ON 20 HUMAN-DIFFICULT PAIRS	55
7	PERFORMANCE ON 20 HUMAN-DIFFICULT PAIRS	56
8	PERFORMANCE ON 20 HUMAN-DIFFICULT PAIRS	57
9	PERFORMANCE ON 20 HUMAN-DIFFICULT PAIRS	58
10	PERFORMANCE ON 20 HUMAN-DIFFICULT PAIRS	59
11	PERFORMANCE ON 20 HUMAN-DIFFICULT PAIRS	60
12	PERFORMANCE ON 20 HUMAN-DIFFICULT PAIRS	61
13	PERFORMANCE ON 20 HUMAN-DIFFICULT PAIRS	62
14	PERFORMANCE ON 20 HUMAN-DIFFICULT PAIRS	63
15	PERFORMANCE ON 20 HUMAN-DIFFICULT PAIRS	64
16	PERFORMANCE ON 20 HUMAN-DIFFICULT PAIRS	65
17	PERFORMANCE ON 20 HUMAN-DIFFICULT PAIRS	66
18	ERROR TRADEOFF CHARACTERISTIC: VISA IMAGES	67
19	ERROR TRADEOFF CHARACTERISTIC: VISA IMAGES	68
20	ERROR TRADEOFF CHARACTERISTIC: VISA IMAGES	69
21	ERROR TRADEOFF CHARACTERISTIC: VISA IMAGES	70
22	ERROR TRADEOFF CHARACTERISTIC: VISA IMAGES	71
23	ERROR TRADEOFF CHARACTERISTIC: VISA IMAGES	72
24	ERROR TRADEOFF CHARACTERISTIC: VISA IMAGES	73
25	ERROR TRADEOFF CHARACTERISTIC: VISA IMAGES	74
26	ERROR TRADEOFF CHARACTERISTIC: VISA IMAGES	75
27	ERROR TRADEOFF CHARACTERISTIC: VISA IMAGES	76
28	ERROR TRADEOFF CHARACTERISTIC: VISA IMAGES	77
29	ERROR TRADEOFF CHARACTERISTIC: VISA IMAGES	78
30	ERROR TRADEOFF CHARACTERISTIC: VISA IMAGES	79
31	ERROR TRADEOFF CHARACTERISTIC: VISA IMAGES	80
32	ERROR TRADEOFF CHARACTERISTIC: VISA IMAGES	81
33	ERROR TRADEOFF CHARACTERISTIC: VISA IMAGES	82
34	ERROR TRADEOFF CHARACTERISTIC: VISA IMAGES	83
35	ERROR TRADEOFF CHARACTERISTIC: VISA IMAGES	84
36	ERROR TRADEOFF CHARACTERISTIC: VISA IMAGES	85
37	ERROR TRADEOFF CHARACTERISTIC: VISA IMAGES	86
38	ERROR TRADEOFF CHARACTERISTIC: VISA IMAGES	87
39	ERROR TRADEOFF CHARACTERISTIC: VISA IMAGES	88
40	ERROR TRADEOFF CHARACTERISTIC: VISA IMAGES	89
41	ERROR TRADEOFF CHARACTERISTIC: VISA IMAGES	90

42	ERROR TRADEOFF CHARACTERISTIC: VISA IMAGES	91
43	ERROR TRADEOFF CHARACTERISTIC: VISA IMAGES	92
44	ERROR TRADEOFF CHARACTERISTIC: VISA IMAGES	93
45	ERROR TRADEOFF CHARACTERISTIC: VISA IMAGES	94
46	ERROR TRADEOFF CHARACTERISTIC: VISA IMAGES	95
47	ERROR TRADEOFF CHARACTERISTIC: VISA IMAGES	96
48	ERROR TRADEOFF CHARACTERISTIC: VISA IMAGES	97
49	ERROR TRADEOFF CHARACTERISTIC: VISA IMAGES	98
50	ERROR TRADEOFF CHARACTERISTIC: VISA IMAGES	99
51	ERROR TRADEOFF CHARACTERISTIC: VISA IMAGES	100
52	ERROR TRADEOFF CHARACTERISTIC: MUGSHOT IMAGES	101
53	ERROR TRADEOFF CHARACTERISTIC: MUGSHOT IMAGES	102
54	ERROR TRADEOFF CHARACTERISTIC: MUGSHOT IMAGES	103
55	ERROR TRADEOFF CHARACTERISTIC: MUGSHOT IMAGES	104
56	ERROR TRADEOFF CHARACTERISTIC: MUGSHOT IMAGES	105
57	ERROR TRADEOFF CHARACTERISTIC: MUGSHOT IMAGES	106
58	ERROR TRADEOFF CHARACTERISTIC: MUGSHOT IMAGES	107
59	ERROR TRADEOFF CHARACTERISTIC: MUGSHOT IMAGES	108
60	ERROR TRADEOFF CHARACTERISTIC: MUGSHOT IMAGES	109
61	ERROR TRADEOFF CHARACTERISTIC: MUGSHOT IMAGES	110
62	ERROR TRADEOFF CHARACTERISTIC: MUGSHOT IMAGES	111
63	ERROR TRADEOFF CHARACTERISTIC: MUGSHOT IMAGES	112
64	ERROR TRADEOFF CHARACTERISTIC: MUGSHOT IMAGES	113
65	ERROR TRADEOFF CHARACTERISTIC: MUGSHOT IMAGES	114
66	ERROR TRADEOFF CHARACTERISTIC: MUGSHOT IMAGES	115
67	ERROR TRADEOFF CHARACTERISTIC: MUGSHOT IMAGES	116
68	ERROR TRADEOFF CHARACTERISTIC: MUGSHOT IMAGES	117
69	ERROR TRADEOFF CHARACTERISTIC: WILD IMAGES	118
70	ERROR TRADEOFF CHARACTERISTIC: WILD IMAGES	119
71	ERROR TRADEOFF CHARACTERISTIC: WILD IMAGES	120
72	ERROR TRADEOFF CHARACTERISTIC: WILD IMAGES	121
73	ERROR TRADEOFF CHARACTERISTIC: WILD IMAGES	122
74	ERROR TRADEOFF CHARACTERISTIC: WILD IMAGES	123
75	ERROR TRADEOFF CHARACTERISTIC: WILD IMAGES	124
76	ERROR TRADEOFF CHARACTERISTIC: WILD IMAGES	125
77	ERROR TRADEOFF CHARACTERISTIC: WILD IMAGES	126
78	ERROR TRADEOFF CHARACTERISTIC: WILD IMAGES	127
79	ERROR TRADEOFF CHARACTERISTIC: WILD IMAGES	128
80	ERROR TRADEOFF CHARACTERISTIC: WILD IMAGES	129
81	ERROR TRADEOFF CHARACTERISTIC: WILD IMAGES	130
82	ERROR TRADEOFF CHARACTERISTIC: WILD IMAGES	131
83	ERROR TRADEOFF CHARACTERISTICS: CHILD EXPLOITATION IMAGES	132
84	ERROR TRADEOFF CHARACTERISTICS: CHILD EXPLOITATION IMAGES	133
85	ERROR TRADEOFF CHARACTERISTICS: CHILD EXPLOITATION IMAGES	134
86	CMC CHARACTERISTICS: CHILD EXPLOITATION IMAGES	135
87	CMC CHARACTERISTICS: CHILD EXPLOITATION IMAGES	136
88	CMC CHARACTERISTICS: CHILD EXPLOITATION IMAGES	137
89	CMC CHARACTERISTICS: CHILD EXPLOITATION IMAGES	138
90	CMC CHARACTERISTICS: CHILD EXPLOITATION IMAGES	139
91	FALSE MATCH RATES WITHIN AND ACROSS DEMOGRAPHIC GROUPS	140
92	FALSE MATCH RATES WITHIN AND ACROSS DEMOGRAPHIC GROUPS	141
93	FALSE MATCH RATES WITHIN AND ACROSS DEMOGRAPHIC GROUPS	142
94	FALSE MATCH RATES WITHIN AND ACROSS DEMOGRAPHIC GROUPS	143
95	FALSE MATCH RATES WITHIN AND ACROSS DEMOGRAPHIC GROUPS	144
96	FALSE MATCH RATES WITHIN AND ACROSS DEMOGRAPHIC GROUPS	145
97	FALSE MATCH RATES WITHIN AND ACROSS DEMOGRAPHIC GROUPS	146
98	FALSE MATCH RATES WITHIN AND ACROSS DEMOGRAPHIC GROUPS	147

99	FALSE MATCH RATES WITHIN AND ACROSS DEMOGRAPHIC GROUPS	148
100	FALSE MATCH RATES WITHIN AND ACROSS DEMOGRAPHIC GROUPS	149
101	FALSE MATCH RATES WITHIN AND ACROSS DEMOGRAPHIC GROUPS	150
102	FALSE MATCH RATES WITHIN AND ACROSS DEMOGRAPHIC GROUPS	151
103	FALSE MATCH RATES WITHIN AND ACROSS DEMOGRAPHIC GROUPS	152
104	FALSE MATCH RATES WITHIN AND ACROSS DEMOGRAPHIC GROUPS	153
105	FALSE MATCH RATES WITHIN AND ACROSS DEMOGRAPHIC GROUPS	154
106	FALSE MATCH RATES WITHIN AND ACROSS DEMOGRAPHIC GROUPS	155
107	FALSE MATCH RATES WITHIN AND ACROSS DEMOGRAPHIC GROUPS	156
108	SEX AND RACE EFFECTS: MUGSHOT IMAGES	157
109	SEX AND RACE EFFECTS: MUGSHOT IMAGES	158
110	SEX AND RACE EFFECTS: MUGSHOT IMAGES	159
111	SEX AND RACE EFFECTS: MUGSHOT IMAGES	160
112	SEX AND RACE EFFECTS: MUGSHOT IMAGES	161
113	SEX AND RACE EFFECTS: MUGSHOT IMAGES	162
114	SEX AND RACE EFFECTS: MUGSHOT IMAGES	163
115	SEX AND RACE EFFECTS: MUGSHOT IMAGES	164
116	SEX AND RACE EFFECTS: MUGSHOT IMAGES	165
117	SEX AND RACE EFFECTS: MUGSHOT IMAGES	166
118	SEX AND RACE EFFECTS: MUGSHOT IMAGES	167
119	SEX AND RACE EFFECTS: MUGSHOT IMAGES	168
120	SEX AND RACE EFFECTS: MUGSHOT IMAGES	169
121	SEX AND RACE EFFECTS: MUGSHOT IMAGES	170
122	SEX AND RACE EFFECTS: MUGSHOT IMAGES	171
123	SEX AND RACE EFFECTS: MUGSHOT IMAGES	172
124	SEX AND RACE EFFECTS: MUGSHOT IMAGES	173
125	SEX EFFECTS: VISA IMAGES	174
126	SEX EFFECTS: VISA IMAGES	175
127	SEX EFFECTS: VISA IMAGES	176
128	SEX EFFECTS: VISA IMAGES	177
129	SEX EFFECTS: VISA IMAGES	178
130	SEX EFFECTS: VISA IMAGES	179
131	SEX EFFECTS: VISA IMAGES	180
132	SEX EFFECTS: VISA IMAGES	181
133	SEX EFFECTS: VISA IMAGES	182
134	SEX EFFECTS: VISA IMAGES	183
135	SEX EFFECTS: VISA IMAGES	184
136	SEX EFFECTS: VISA IMAGES	185
137	SEX EFFECTS: VISA IMAGES	186
138	SEX EFFECTS: VISA IMAGES	187
139	SEX EFFECTS: VISA IMAGES	188
140	SEX EFFECTS: VISA IMAGES	189
141	SEX EFFECTS: VISA IMAGES	190
142	SEX EFFECTS: VISA IMAGES	191
143	SEX EFFECTS: VISA IMAGES	192
144	SEX EFFECTS: VISA IMAGES	193
145	SEX EFFECTS: VISA IMAGES	194
146	SEX EFFECTS: VISA IMAGES	195
147	SEX EFFECTS: VISA IMAGES	196
148	SEX EFFECTS: VISA IMAGES	197
149	SEX EFFECTS: VISA IMAGES	198
150	SEX EFFECTS: VISA IMAGES	199
151	SEX EFFECTS: VISA IMAGES	200
152	SEX EFFECTS: VISA IMAGES	201
153	FALSE MATCH RATE CALIBRATION: MUGSHOT IMAGES	202
154	FALSE MATCH RATE CALIBRATION: MUGSHOT IMAGES	203

155	FALSE MATCH RATE CALIBRATION: MUGSHOT IMAGES	204
156	FALSE MATCH RATE CALIBRATION: MUGSHOT IMAGES	205
157	FALSE MATCH RATE CALIBRATION: MUGSHOT IMAGES	206
158	FALSE MATCH RATE CALIBRATION: MUGSHOT IMAGES	207
159	FALSE MATCH RATE CALIBRATION: MUGSHOT IMAGES	208
160	FALSE MATCH RATE CALIBRATION: MUGSHOT IMAGES	209
161	FALSE MATCH RATE CALIBRATION: MUGSHOT IMAGES	210
162	FALSE MATCH RATE CALIBRATION: MUGSHOT IMAGES	211
163	FALSE MATCH RATE CALIBRATION: MUGSHOT IMAGES	212
164	FALSE MATCH RATE CALIBRATION: MUGSHOT IMAGES	213
165	FALSE MATCH RATE CALIBRATION: MUGSHOT IMAGES	214
166	FALSE MATCH RATE CALIBRATION: MUGSHOT IMAGES	215
167	FALSE MATCH RATE CALIBRATION: MUGSHOT IMAGES	216
168	FALSE MATCH RATE CALIBRATION: MUGSHOT IMAGES	217
169	FALSE MATCH RATE CALIBRATION: MUGSHOT IMAGES	218
170	FALSE MATCH RATE CALIBRATION: VISA IMAGES	219
171	FALSE MATCH RATE CALIBRATION: VISA IMAGES	220
172	FALSE MATCH RATE CALIBRATION: VISA IMAGES	221
173	FALSE MATCH RATE CALIBRATION: VISA IMAGES	222
174	FALSE MATCH RATE CALIBRATION: VISA IMAGES	223
175	FALSE MATCH RATE CALIBRATION: VISA IMAGES	224
176	FALSE MATCH RATE CALIBRATION: VISA IMAGES	225
177	FALSE MATCH RATE CALIBRATION: VISA IMAGES	226
178	FALSE MATCH RATE CALIBRATION: VISA IMAGES	227
179	FALSE MATCH RATE CALIBRATION: VISA IMAGES	228
180	FALSE MATCH RATE CALIBRATION: VISA IMAGES	229
181	FALSE MATCH RATE CALIBRATION: VISA IMAGES	230
182	FALSE MATCH RATE CALIBRATION: VISA IMAGES	231
183	FALSE MATCH RATE CALIBRATION: VISA IMAGES	232
184	FALSE MATCH RATE CALIBRATION: VISA IMAGES	233
185	FALSE MATCH RATE CALIBRATION: VISA IMAGES	234
186	FALSE MATCH RATE CALIBRATION: VISA IMAGES	235
187	FALSE MATCH RATE CALIBRATION: VISA IMAGES	236
188	FALSE MATCH RATE CALIBRATION: VISA IMAGES	237
189	FALSE MATCH RATE CALIBRATION: VISA IMAGES	238
190	FALSE MATCH RATE CALIBRATION: VISA IMAGES	239
191	FALSE MATCH RATE CALIBRATION: VISA IMAGES	240
192	FALSE MATCH RATE CALIBRATION: VISA IMAGES	241
193	FALSE MATCH RATE CALIBRATION: VISA IMAGES	242
194	FALSE MATCH RATE CALIBRATION: VISA IMAGES	243
195	FALSE MATCH RATE CALIBRATION: VISA IMAGES	244
196	FALSE MATCH RATE CALIBRATION: VISA IMAGES	245
197	FALSE MATCH RATE CALIBRATION: VISA IMAGES	246
198	FALSE MATCH RATE CALIBRATION: VISA IMAGES	247
199	FALSE MATCH RATE CALIBRATION: VISA IMAGES	248
200	FALSE MATCH RATE CALIBRATION: VISA IMAGES	249
201	FALSE MATCH RATE CALIBRATION: VISA IMAGES	250
202	FALSE MATCH RATE CALIBRATION: VISA IMAGES	251
203	FALSE MATCH RATE CALIBRATION: VISA IMAGES	252
204	EFFECT OF COUNTRY OF BIRTH ON FNMR	254
205	EFFECT OF COUNTRY OF BIRTH ON FNMR	255
206	EFFECT OF COUNTRY OF BIRTH ON FNMR	256
207	EFFECT OF COUNTRY OF BIRTH ON FNMR	257
208	EFFECT OF COUNTRY OF BIRTH ON FNMR	258
209	EFFECT OF COUNTRY OF BIRTH ON FNMR	259
210	EFFECT OF COUNTRY OF BIRTH ON FNMR	260
211	EFFECT OF COUNTRY OF BIRTH ON FNMR	261

212	EFFECT OF COUNTRY OF BIRTH ON FNMR	262
213	EFFECT OF COUNTRY OF BIRTH ON FNMR	263
214	EFFECT OF COUNTRY OF BIRTH ON FNMR	264
215	EFFECT OF COUNTRY OF BIRTH ON FNMR	265
216	EFFECT OF COUNTRY OF BIRTH ON FNMR	266
217	EFFECT OF COUNTRY OF BIRTH ON FNMR	267
218	EFFECT OF COUNTRY OF BIRTH ON FNMR	268
219	EFFECT OF COUNTRY OF BIRTH ON FNMR	269
220	EFFECT OF COUNTRY OF BIRTH ON FNMR	270
221	EFFECT OF COUNTRY OF BIRTH ON FNMR	271
222	EFFECT OF COUNTRY OF BIRTH ON FNMR	272
223	EFFECT OF COUNTRY OF BIRTH ON FNMR	273
224	EFFECT OF COUNTRY OF BIRTH ON FNMR	274
225	EFFECT OF COUNTRY OF BIRTH ON FNMR	275
226	EFFECT OF COUNTRY OF BIRTH ON FNMR	276
227	EFFECT OF COUNTRY OF BIRTH ON FNMR	277
228	EFFECT OF COUNTRY OF BIRTH ON FNMR	278
229	EFFECT OF COUNTRY OF BIRTH ON FNMR	279
230	EFFECT OF COUNTRY OF BIRTH ON FNMR	280
231	EFFECT OF COUNTRY OF BIRTH ON FNMR	281
232	ERROR TRADEOFF CHARACTERISTIC: MUGSHOT IMAGES	283
233	ERROR TRADEOFF CHARACTERISTIC: MUGSHOT IMAGES	284
234	ERROR TRADEOFF CHARACTERISTIC: MUGSHOT IMAGES	285
235	ERROR TRADEOFF CHARACTERISTIC: MUGSHOT IMAGES	286
236	ERROR TRADEOFF CHARACTERISTIC: MUGSHOT IMAGES	287
237	ERROR TRADEOFF CHARACTERISTIC: MUGSHOT IMAGES	288
238	ERROR TRADEOFF CHARACTERISTIC: MUGSHOT IMAGES	289
239	ERROR TRADEOFF CHARACTERISTIC: MUGSHOT IMAGES	290
240	ERROR TRADEOFF CHARACTERISTIC: MUGSHOT IMAGES	291
241	ERROR TRADEOFF CHARACTERISTIC: MUGSHOT IMAGES	292
242	ERROR TRADEOFF CHARACTERISTIC: MUGSHOT IMAGES	293
243	ERROR TRADEOFF CHARACTERISTIC: MUGSHOT IMAGES	294
244	ERROR TRADEOFF CHARACTERISTIC: MUGSHOT IMAGES	295
245	ERROR TRADEOFF CHARACTERISTIC: MUGSHOT IMAGES	296
246	ERROR TRADEOFF CHARACTERISTIC: MUGSHOT IMAGES	297
247	ERROR TRADEOFF CHARACTERISTIC: MUGSHOT IMAGES	298
248	ERROR TRADEOFF CHARACTERISTIC: MUGSHOT IMAGES	299
249	ERROR TRADEOFF CHARACTERISTIC: MUGSHOT IMAGES	300
250	ERROR TRADEOFF CHARACTERISTIC: MUGSHOT IMAGES	301
251	ERROR TRADEOFF CHARACTERISTIC: MUGSHOT IMAGES	302
252	EFFECT OF SUBJECT AGE ON FNMR	304
253	EFFECT OF SUBJECT AGE ON FNMR	305
254	EFFECT OF SUBJECT AGE ON FNMR	306
255	EFFECT OF SUBJECT AGE ON FNMR	307
256	EFFECT OF SUBJECT AGE ON FNMR	308
257	EFFECT OF SUBJECT AGE ON FNMR	309
258	EFFECT OF SUBJECT AGE ON FNMR	310
259	EFFECT OF SUBJECT AGE ON FNMR	311
260	EFFECT OF SUBJECT AGE ON FNMR	312
261	EFFECT OF SUBJECT AGE ON FNMR	313
262	EFFECT OF SUBJECT AGE ON FNMR	314
263	EFFECT OF SUBJECT AGE ON FNMR	315
264	EFFECT OF SUBJECT AGE ON FNMR	316
265	EFFECT OF SUBJECT AGE ON FNMR	317
266	EFFECT OF SUBJECT AGE ON FNMR	318

267	EFFECT OF SUBJECT AGE ON FNMR	319
268	EFFECT OF SUBJECT AGE ON FNMR	320
269	EFFECT OF SUBJECT AGE ON FNMR	321
270	EFFECT OF SUBJECT AGE ON FNMR	322
271	EFFECT OF SUBJECT AGE ON FNMR	323
272	EFFECT OF SUBJECT AGE ON FNMR	324
273	EFFECT OF SUBJECT AGE ON FNMR	325
274	EFFECT OF SUBJECT AGE ON FNMR	326
275	EFFECT OF SUBJECT AGE ON FNMR	327
276	EFFECT OF SUBJECT AGE ON FNMR	328
277	EFFECT OF SUBJECT AGE ON FNMR	329
278	EFFECT OF SUBJECT AGE ON FNMR	330
279	EFFECT OF SUBJECT AGE ON FNMR	331
280	WORST CASE REGIONAL EFFECT FNMR	334
281	IMPOSTOR DISTRIBUTION SHIFTS FOR SELECT COUNTRY PAIRS	336

	Location	Developer Name	Short Name	Seq. Num.	Validation Date
1	NL	20Face	20face-000	000	2021-04-12
2	US	3Divi	3divi-005	005	2020-08-28
3	US	3Divi	3divi-006	006	2021-04-14
4	TH	ACI Software	acisw-003	003	2020-08-03
5	TH	ACI Software	acisw-006	006	2021-02-25
6	SG	ADVANCE.AI	advance-002	002	2019-12-19
7	TW	ASUSTek Computer Inc	asusaics-000	000	2019-10-24
8	TW	ASUSTek Computer Inc	asusaics-001	001	2020-02-25
9	CN	AYF Technology	ayftech-001	001	2020-07-06
10	TW	Ability Enterprise - Andro Video	androvideo-000	000	2021-01-25
11	TW	Acer Incorporated	acer-000	000	2020-01-08
12	TW	Acer Incorporated	acer-001	001	2020-06-30
13	SG	Adera Global PTE	adera-002	002	2021-02-16
14	SG	Adera Global PTE	adera-003	003	2021-07-12
15	TH	Ai First	aifirst-001	001	2019-11-21
16	TW	AiUnion Technology	aiunionface-000	000	2019-10-22
17	TH	Aigen	aigen-001	001	2020-10-06
18	TH	Aigen	aigen-002	002	2021-03-15
19	KR	Ajou University	ajou-001	001	2021-03-08
20	ID	Akurat Satu Indonesia	ptakuratsatu-000	000	2020-09-11
21	KR	Alchera Inc	alchera-002	002	2021-03-05
22	KR	Alchera Inc	alchera-003	003	2021-07-13
23	ES	Alice Biometrics	alice-000	000	2021-06-15
24	RU	Alivia / Innovation Sys	isystems-001	001	2018-06-12
25	RU	Alivia / Innovation Sys	isystems-002	002	2018-10-18
26	IN	AllGoVision	allgovision-000	000	2019-03-01
27	CN	AlphaSSTG	alphaface-001	001	2019-09-03
28	CN	AlphaSSTG	alphaface-002	002	2020-02-20
29	GB	Amplified Group	amplifiedgroup-001	001	2019-03-01
30	CN	Anke Investments	anke-004	004	2019-06-27
31	CN	Anke Investments	anke-005	005	2019-11-21
32	BR	Antheus Technologia	antheus-000	000	2019-12-05
33	BR	Antheus Technologia	antheus-001	001	2020-06-25
34	GB	AnyVision	anyvision-004	004	2018-06-15
35	GB	AnyVision	anyvision-005	005	2021-02-03
36	CN	AuthenMetric	authenmetric-002	002	2021-03-10
37	US	Aware	aware-005	005	2020-02-27
38	US	Aware	aware-006	006	2021-07-03
39	IN	Awidit Systems	awiros-001	001	2019-09-23
40	IN	Awidit Systems	awiros-002	002	2020-10-28
41	JP	Ayonix	ayonix-000	000	2017-06-22
42	CN	BOE Technology Group	boetech-001	001	2021-06-22
43	ES	Bee the Data	beethedata-000	000	2021-07-26
44	CN	Beihang University-ERCACAT	ercacat-001	001	2020-07-06
45	CN	Beijing Alleyes Technology	alleyes-000	000	2020-03-09
46	CN	Beijing DeepSense Technologies	deepsense-000	000	2021-03-19
47	CN	Beijing Vion Technology Inc	vion-000	000	2018-10-19
48	CH	BioID Technologies SA	bioidtechswiss-001	001	2020-08-28
49	CH	BioID Technologies SA	bioidtechswiss-002	002	2021-02-17
50	UK	BitCenter UK	farfaces-001	001	2021-04-09
51	CN	Bitmain	bm-001	001	2018-10-17
52	CN	Bresee Technology	bresee-001	001	2020-12-30
53	CN	Bresee Technology	bresee-002	002	2021-06-30
54	CN	CSA IntelliCloud Technology	intellicloudai-001	001	2019-08-13
55	CN	CSA IntelliCloud Technology	intellicloudai-002	002	2020-12-17
56	TW	CTBC Bank	ctbcbank-000	000	2019-06-28
57	TW	CTBC Bank	ctbcbank-001	001	2019-10-28
58	US	Camvi Technologies	camvi-002	002	2018-10-19
59	US	Camvi Technologies	camvi-004	004	2019-07-12
60	CN	Canon Inc	canon-002	002	2020-12-29
61	CN	Canon Inc	cib-001	001	2020-08-05
62	CN	China Electronics Import-Export Corp	ceiec-003	003	2020-01-06
63	CN	China Electronics Import-Export Corp	ceiec-004	004	2021-01-18
64	CN	China University of Petroleum	upc-001	001	2019-06-05
65	CN	Chinese University of Hong Kong	cuhkee-001	001	2020-03-18
66	KR	Chosun University	chosun-001	001	2020-07-01
67	KR	Chosun University	chosun-002	002	2020-11-25
68	TW	Chunghwa Telecom	chtface-002	002	2019-12-07
69	TW	Chunghwa Telecom	chtface-003	003	2020-06-24
70	CN	Closeli Inc	closeli-001	001	2021-07-15

Table 1: Summary of participant information included in this report.

	Location	Developer Name	Short Name	Seq. Num.	Validation Date
71	US	CloudSmart Consulting LLC	csc-001	001	2020-11-20
72	US	CloudSmart Consulting LLC	csc-002	002	2021-03-24
73	CN	Cloudwalk - Hengrui AI Technology	cloudwalk-hr-003	003	2020-09-25
74	CN	Cloudwalk - Hengrui AI Technology	cloudwalk-hr-004	004	2021-02-10
75	CN	Cloudwalk - Moontime Smart Technology	cloudwalk-mt-002	002	2020-07-02
76	CN	Cloudwalk - Moontime Smart Technology	cloudwalk-mt-003	003	2020-12-22
77	IN	Code Everest Pvt	facex-001	001	2021-03-08
78	DE	Cognitec Systems GmbH	cognitec-000	000	2018-10-19
79	DE	Cognitec Systems GmbH	cognitec-002	002	2021-02-24
80	TW	Coretech Knowledge Inc	coretech-000	000	2021-07-12
81	IL	Corsight	corsight-001	001	2021-03-11
82	IL	Cortica	cor-001	001	2020-09-24
83	KR	Cubox	cubox-001	001	2020-12-07
84	JP	Cybercore	cybercore-000	000	2020-08-26
85	US	Cyberextruder	cyberextruder-001	001	2017-08-02
86	US	Cyberextruder	cyberextruder-002	002	2018-01-30
87	TW	Cyberlink Corp	cyberlink-006	006	2021-01-08
88	TW	Cyberlink Corp	cyberlink-007	007	2021-07-16
89	CN	DSK	dsk-000	000	2019-06-28
90	CN	Dahua Technology	dahua-005	005	2020-08-13
91	CN	Dahua Technology	dahua-006	006	2020-12-30
92	US	Decatur Industries Inc	decatur-000	000	2020-08-18
93	CN	Deepglint	deepglint-002	002	2019-11-15
94	CN	Deepglint	deepglint-003	003	2021-03-03
95	FR	Deepsense	dps-000	000	2021-07-16
96	DE	Dermalog	dermalog-006	006	2018-10-18
97	DE	Dermalog	dermalog-008	008	2021-03-25
98	CN	DiDi ChuXing Technology	didiglobalface-001	001	2019-10-23
99	GB	Digital Barriers	digitalbarriers-002	002	2019-03-01
100	TR	Ekin Smart City Technologies	ekin-002	002	2021-05-04
101	RU	Enface	enface-000	000	2021-04-09
102	RU	Expasoft LLC	expasoft-001	001	2020-09-03
103	RU	Expasoft LLC	expasoft-002	002	2021-07-26
104	GB	FaceSoft	facesoft-000	000	2019-07-10
105	KR	FaceTag Co	facetag-000	000	2021-03-22
106	TW	FarBar Inc	f8-001	001	2019-07-11
107	UK	Fincore Ltd	fincore-000	000	2021-06-07
108	CN	Fujitsu Research and Development Center	fujitsulab-002	002	2021-02-24
109	CN	Fujitsu Research and Development Center	fujitsulab-003	003	2021-07-12
110	US	Gemalto Cogent	cogent-004	004	2019-06-14
111	US	Gemalto Cogent	cogent-005	005	2020-12-29
112	TW	GeoVision Inc	geo-001	001	2020-10-30
113	TW	GeoVision Inc	geo-002	002	2021-04-01
114	JP	Glory	glory-002	002	2019-11-12
115	JP	Glory	glory-003	003	2021-01-15
116	TW	Gorilla Technology	gorilla-006	006	2020-07-31
117	TW	Gorilla Technology	gorilla-007	007	2021-06-28
118	CN	Guangzhou Pixel Solutions	pixelall-005	005	2021-02-05
119	CN	Guangzhou Pixel Solutions	pixelall-006	006	2021-06-17
120	ES	Herta Security	hertasecurity-000	000	2021-01-05
121	CN	Hikvision Research Institute	hik-001	001	2019-03-01
122	IN	HyperVerge Inc	hyperverge-001	001	2020-12-13
123	IN	HyperVerge Inc	hyperverge-002	002	2021-05-27
124	AU	ICM Airport Technics	icm-002	002	2020-11-13
125	FR	ID3 Technology	id3-006	006	2020-12-17
126	FR	ID3 Technology	id3-007	007	2021-05-17
127	RU	ITMO University	itmo-006	006	2019-03-01
128	RU	ITMO University	itmo-007	007	2020-01-06
129	RU	IVA Cognitive	ivacognitive-001	001	2021-01-29
130	FR	Idemia	idemia-007	007	2020-12-04
131	FR	Idemia	idemia-008	008	2021-07-07
132	US	Imageware Systems	iws-000	000	2020-08-12
133	AU	Imagus Technology Pty	imagus-002	002	2020-12-31
134	AU	Imagus Technology Pty	imagus-003	003	2021-05-18
135	GB	Imperial College London	imperial-000	000	2019-03-01
136	GB	Imperial College London	imperial-002	002	2019-08-28
137	US	Incode Technologies Inc	incode-008	008	2021-01-19
138	US	Incode Technologies Inc	incode-009	009	2021-06-22
139	IN	Innef Labs	inneflabs-000	000	2020-09-04
140	GB	Innovative Technology	innovativetechnologyltd-001	001	2019-10-22

Table 2: Summary of participant information included in this report.

	Location	Developer Name	Short Name	Seq. Num.	Validation Date
141	GB	Innovative Technology	innovativetechnologyltd-002	002	2020-02-26
142	SK	Innovatrics	innovatrics-006	006	2019-08-13
143	SK	Innovatrics	innovatrics-007	007	2020-08-19
144	CN	InsightFace AI	insightface-000	000	2021-03-17
145	CN	Institute of Computing Technology	icthtc-000	000	2020-11-29
146	RU	Institute of Information Technologies	iit-002	002	2019-12-04
147	RU	Institute of Information Technologies	iit-003	003	2020-12-01
148	IS	Intel Research Group	intelresearch-002	002	2020-07-24
149	IS	Intel Research Group	intelresearch-003	003	2021-01-18
150	US	Intellivision	intellivision-001	001	2017-10-10
151	US	Intellivision	intellivision-002	002	2019-08-23
152	US	IrexAI	irex-000	000	2020-12-17
153	IL	Is It You	isityou-000	000	2017-06-26
154	KR	Kakao Enterprise	kakao-004	004	2020-10-28
155	KR	Kakao Enterprise	kakao-005	005	2021-03-09
156	KR	Kakao Pay Corp	kakaopay-001	001	2021-07-06
157	SG	Kedacom International Pte	kedacom-000	000	2019-06-03
158	US	Kneron Inc	kneron-003	003	2019-07-01
159	US	Kneron Inc	kneron-005	005	2020-02-21
160	KR	Kookmin University	kookmin-001	001	2020-09-28
161	KR	Kookmin University	kookmin-002	002	2021-03-05
162	IN	Lema Labs	lemalabs-001	001	2021-04-13
163	JP	Line Corporation	line-000	000	2021-03-31
164	RU	Lomonosov Moscow State University	intsysmsu-001	001	2019-10-22
165	RU	Lomonosov Moscow State University	intsysmsu-002	002	2020-03-12
166	IN	Lookman Electroplast Industries	lookman-002	002	2018-06-13
167	IN	Lookman Electroplast Industries	lookman-004	004	2019-06-03
168	US	Luxand Inc	luxand-000	000	2019-11-07
169	RU	MVision	mvision-001	001	2019-11-12
170	CN	Megvii/Face++	megvii-002	002	2018-10-19
171	CN	Megvii/Face++	megvii-003	003	2021-03-08
172	GB	MicroFocus	microfocus-001	001	2018-06-13
173	GB	MicroFocus	microfocus-002	002	2018-10-17
174	CN	Minivision	minivision-000	000	2020-10-28
175	NO	Mobai	mobai-000	000	2020-08-26
176	NO	Mobai	mobai-001	001	2021-02-17
177	ES	Mobbeel Solutions	mobbl-000	000	2021-01-28
178	ES	Mobbeel Solutions	mobbl-001	001	2021-06-16
179	TH	Momentum Digital	sertis-000	000	2019-10-07
180	TH	Momentum Digital	sertis-002	002	2021-05-13
181	CN	MoreDian Technology	moreedian-000	000	2021-02-24
182	RU	N-Tech Lab	ntechlab-009	009	2020-12-30
183	RU	N-Tech Lab	ntechlab-010	010	2021-04-30
184	CA	NEO Systems	neosystems-001	001	2021-03-02
185	CA	NEO Systems	neosystems-002	002	2021-07-03
186	KR	NHN Corp	nhn-001	001	2021-03-15
187	KR	NHN Corp	nhn-002	002	2021-07-15
188	KR	NSENSE Corp	nsensecorp-001	001	2020-10-20
189	KR	NSENSE Corp	nsensecorp-002	002	2021-05-06
190	CN	Nanjing Kiwi Network Technology	kiwitech-000	000	2021-03-19
191	KR	Naver Corp	clova-000	000	2020-10-21
192	KR	Neosecu Co	openface-001	001	2021-06-15
193	TW	Netbridge Technology Incoporation	netbridgetech-001	001	2020-01-08
194	TW	Netbridge Technology Incoporation	netbridgetech-002	002	2020-08-11
195	LT	Neurotechnology	neurotechnology-011	011	2021-03-26
196	LT	Neurotechnology	neurotechnology-012	012	2021-07-26
197	ID	Nodeflux	nodeflux-002	002	2019-08-13
198	IN	NotionTag Technologies Private Limited	notionntag-000	000	2019-06-12
199	IN	NotionTag Technologies Private Limited	notionntag-001	001	2021-03-04
200	US	Omnigarde Ltd	omnigarde-000	000	2021-04-05
201	RU	Oz Forensics LLC	oz-001	001	2020-07-29
202	RU	Oz Forensics LLC	oz-002	002	2021-01-18
203	CH	PXL Vision AG	pxl-001	001	2020-06-30
204	SG	Panasonic R+D Center Singapore	psl-007	007	2021-03-19
205	SG	Panasonic R+D Center Singapore	psl-008	008	2021-07-21
206	TR	Papilon Savunma	papsav1923-001	001	2021-03-10
207	US	Paravision (EverAI)	paravision-004	004	2019-12-11
208	US	Paravision (EverAI)	paravision-008	008	2021-06-30
209	SG	Pensees Pte	pensees-001	001	2020-08-17
210	IN	Pyramid Cyber Security + Forensic (P)	pyramid-000	000	2019-11-04

Table 3: Summary of participant information included in this report.

	Location	Developer Name	Short Name	Seq. Num.	Validation Date
211	CZ	Quantasoft	quantasoft-003	003	2021-04-19
212	US	Rank One Computing	rankone-009	009	2020-06-26
213	US	Rank One Computing	rankone-010	010	2020-11-05
214	US	Realnetworks Inc	realnetworks-002	002	2019-02-28
215	US	Realnetworks Inc	realnetworks-004	004	2021-04-15
216	US	Regula Forensics	regula-000	000	2021-04-13
217	CN	Remark Holdings	remarkai-001	001	2019-03-01
218	CN	Remark Holdings	remarkai-003	003	2021-06-22
219	SG	Rendip	rendip-000	000	2021-04-19
220	CN	Rokid Corporation	rokid-000	000	2019-08-01
221	CN	Rokid Corporation	rokid-001	001	2019-12-13
222	KR	SK Telecom	sktelecom-000	000	2021-07-09
223	DE	Saffe	saffe-001	001	2018-10-19
224	DE	Saffe	saffe-002	002	2019-03-01
225	KR	Samsung S1 Corp	s1-001	001	2019-12-06
226	KR	Samsung S1 Corp	s1-002	002	2021-03-24
227	IN	Samtech InfoNet Limited	samtech-001	001	2019-10-15
228	RU	Satellite Innovation/Eocortex	eocortex-000	000	2020-08-26
229	IL	Scanovate	scanovate-001	001	2019-11-12
230	IL	Scanovate	scanovate-002	002	2020-06-26
231	RO	Securif AI	securifai-001	001	2020-10-06
232	RO	Securif AI	securifai-002	002	2021-03-19
233	CN	Sensetime Group	sensetime-004	004	2020-11-20
234	CN	Sensetime Group	sensetime-005	005	2021-05-24
235	SG	Seventh Sense Artificial Intelligence	seventhsense-000	000	2021-06-29
236	US	Shaman Software	shaman-000	000	2017-12-05
237	US	Shaman Software	shaman-001	001	2018-01-13
238	CN	Shanghai Jiao Tong University	sjtu-003	003	2020-11-02
239	CN	Shanghai Jiao Tong University	sjtu-004	004	2021-05-13
240	CN	Shanghai Ulucus Electronics Technology	uluface-002	002	2019-07-10
241	CN	Shanghai Ulucus Electronics Technology	uluface-003	003	2019-11-12
242	CN	Shanghai University - Shanghai Film Academy	shu-002	002	2019-12-10
243	CN	Shanghai University - Shanghai Film Academy	shu-003	003	2020-06-24
244	CN	Shanghai Yitu Technology	yitu-003	003	2019-03-01
245	CN	Shenzhen AiMall Tech	aimall-002	002	2020-03-12
246	CN	Shenzhen AiMall Tech	aimall-003	003	2020-08-12
247	CN	Shenzhen EI Networks	einetworks-000	000	2019-08-13
248	CN	Shenzhen Inst Adv Integrated Tech CAS	siat-002	002	2018-06-13
249	CN	Shenzhen Inst Adv Integrated Tech CAS	siat-004	004	2019-03-01
250	CN	Shenzhen Intellifusion Technologies	intellifusion-001	001	2019-08-22
251	CN	Shenzhen Intellifusion Technologies	intellifusion-002	002	2020-03-18
252	CN	Shenzhen University-Macau University of Science and Technology	sztu-000	000	2020-12-17
253	CN	Shenzhen University-Macau University of Science and Technology	sztu-001	001	2021-07-13
254	DE	Smilart	smilart-002	002	2018-02-06
255	DE	Smilart	smilart-003	003	2018-06-18
256	TR	Sodec App Inc	sodec-000	000	2021-06-02
257	IN	Staqu Technologies	st aqu-000	000	2020-07-15
258	CN	Star Hybrid Limited	starhybrid-001	001	2019-06-19
259	CN	Su Zhou NaZhiTianDi intelligent technology	nazhai-000	000	2020-06-25
260	KR	Suprema	suprema-000	000	2021-03-31
261	KR	Suprema ID Inc	supremaid-001	001	2021-05-04
262	RU	Synesis	synesis-006	006	2019-10-10
263	RU	Synesis	synesis-007	007	2020-06-24
264	TW	Synology Inc	synology-000	000	2019-10-23
265	TW	Synology Inc	synology-002	002	2020-08-20
266	CN	TUPU Technology	tuputech-000	000	2019-10-11
267	TW	Taiwan AI Labs	ailabs-001	001	2019-12-18
268	TW	Taiwan-Certificate Authority Incorporatio)	twface-000	000	2021-05-14
269	CH	Tech5 SA	tech5-004	004	2020-03-09
270	CH	Tech5 SA	tech5-005	005	2020-07-24
271	CN	Tencent Deepsea Lab	deepsea-001	001	2019-06-03
272	RU	Tevian	tevian-005	005	2019-09-21
273	RU	Tevian	tevian-006	006	2020-09-11
274	US	TigerIT Americas LLC	tiger-003	003	2018-10-16
275	US	TigerIT Americas LLC	tiger-004	004	2020-12-01
276	RU	Tinkoff Bank	tinkoff-001	001	2021-05-13
277	CN	TongYi Transportation Technology	tongyi-005	005	2019-06-12
278	JP	Toshiba	toshiba-002	002	2018-10-19
279	JP	Toshiba	toshiba-003	003	2019-03-01
280	JP	Tripleize	aize-001	001	2021-04-23

Table 4: Summary of participant information included in this report.

	Location	Developer Name	Short Name	Seq. Num.	Validation Date
281	US	Trueface.ai	trueface-001	001	2020-07-20
282	US	Trueface.ai	trueface-002	002	2021-03-29
283	CN	ULSee Inc	ulsee-001	001	2019-07-31
284	PT	Universidade de Coimbra	visteam-000	000	2020-01-14
285	PT	Universidade de Coimbra	visteam-001	001	2021-03-16
286	US	VCognition	vcog-002	002	2017-06-12
287	ES	Veridas Digital Authentication Solutions S.L.	veridas-004	004	2020-07-21
288	ES	Veridas Digital Authentication Solutions S.L.	veridas-006	006	2021-04-15
289	TW	Via Technologies Inc	via-000	000	2019-07-08
290	TW	Via Technologies Inc	via-001	001	2020-01-08
291	DE	Videmo Intelligente Videoanalyse	videmo-000	000	2019-12-19
292	IN	Videonetics Technology Pvt	videonetics-001	001	2019-06-19
293	IN	Videonetics Technology Pvt	videonetics-002	002	2019-11-21
294	VN	Vietnam Posts and Telecommunications Group	vnpt-001	001	2021-01-08
295	VN	Vietnam Posts and Telecommunications Group	vnpt-002	002	2021-06-08
296	VN	Viettel Group	vts-000	000	2020-11-04
297	US	Vigilant Solutions	vigilantsolutions-009	009	2020-12-07
298	US	Vigilant Solutions	vigilantsolutions-010	010	2021-04-07
299	VN	VinAI Research VietNam	vinai-000	000	2020-09-24
300	SE	Visage Technologies	visage-000	000	2020-12-09
301	FI	Visidon	vd-001	001	2019-02-26
302	FI	Visidon	vd-002	002	2021-04-12
303	CN	Vision Intelligence Center of Meituan	meituan-000	000	2021-05-14
304	PT	Vision-Box	visionbox-001	001	2019-03-01
305	PT	Vision-Box	visionbox-002	002	2021-04-29
306	RU	VisionLabs	visionlabs-009	009	2020-07-27
307	RU	VisionLabs	visionlabs-010	010	2021-01-25
308	RU	Vocord	vocord-008	008	2020-01-31
309	RU	Vocord	vocord-009	009	2020-12-28
310	CN	Winsense	winsense-001	001	2019-10-16
311	CN	Winsense	winsense-002	002	2020-11-20
312	CN	Xforward AI Technology	xforwardai-001	001	2020-09-25
313	CN	Xforward AI Technology	xforwardai-002	002	2021-02-10
314	CN	Xiamen Meiya Pico Information	meiya-001	001	2019-03-01
315	CN	Xiamen University	xm-000	000	2020-10-19
316	PT	Yoonik	yoonik-000	000	2020-06-24
317	PT	Yoonik	yoonik-001	001	2020-10-26
318	TW	Yuan High-Tech Development	yuan-001	001	2021-01-08
319	TW	Yuan High-Tech Development	yuan-002	002	2021-05-17
320	CN	Yuntu Data and Technology	ytu-000	000	2021-06-16
321	CN	Zhuhai Yisheng Electronics Technology	yisheng-004	004	2018-06-12
322	CN	iQIYI Inc	iqface-000	000	2019-06-04
323	CN	iQIYI Inc	iqface-003	003	2021-02-23
324	TW	iSAP Solution Corporation	isap-001	001	2019-08-07
325	TW	iSAP Solution Corporation	isap-002	002	2020-09-01
326	TW	ioNetworks Inc	ionetworks-000	000	2021-07-20

Table 5: Summary of participant information included in this report.

ALGORITHM			CONFIG	LIBRARY	TEMPLATE								COMPARISON ⁴		
NAME			DATA	DATA	MEMORY	SIZE	GENERATION TIME (ms) ⁴				TIME (ns) ⁵				
			(KB) ¹	(KB) ²	(MB) ³	(B)	MUGSHOT	480x720	960x1440	1600x2400	3000x4500	GENUINE	IMPOSTOR		
1	20face-000	119967175	324083	170905	1792048 ± 0	35232 ± 1	19223 ± 1	14226 ± 4	12222 ± 1	11224 ± 1	30644880 ± 134	30544462 ± 163			
2	3divi-005	270436716	53870	60431	1552048 ± 0	268993 ± 83	2371136 ± 88	2491309 ± 137	2281348 ± 131	2081671 ± 166	81790 ± 20	79791 ± 23			
3	3divi-006	280439478	52656	70472	1772048 ± 0	164654 ± 1	118651 ± 0	102660 ± 1	86678 ± 2	84759 ± 13	78775 ± 19	78770 ± 22			
4	acer-000	112369572	88323	73478	2092048 ± 0	33222 ± 0	21233 ± 4	17238 ± 4	16262 ± 18	19356 ± 46	1011065 ± 40	1121109 ± 35			
5	acer-001	37530576	66086	57417	25512 ± 0	29199 ± 0	22237 ± 28	15229 ± 26	15242 ± 37	13259 ± 21	1862453 ± 44	1882461 ± 62			
6	acisw-003	288798384	35664	39282	32818467 ± 8	36232 ± 1	26267 ± 22	57488 ± 28	163990 ± 24	2422977 ± 129	328847908 ± 16757	329851850 ± 17018			
7	acisw-006	288798384	36107	43303	32718465 ± 8	32219 ± 0	20227 ± 0	35410 ± 1	127838 ± 1	2342532 ± 10	326548137 ± 16513	326549586 ± 9238			
8	ader-a-002	0	749797	177921	3195120 ± 0	3211394 ± 11	2671381 ± 1	251393 ± 1	2341403 ± 1	1971464 ± 2	1752163 ± 32	1762158 ± 28			
9	ader-a-003	0	749778	173917	3185120 ± 0	3191381 ± 12	2681385 ± 1	2581394 ± 1	2321401 ± 1	1981469 ± 1	1742148 ± 34	1732130 ± 32			
10	advance-002	263345868	20434	41295	852048 ± 0	212811 ± 2	162803 ± 2	114696 ± 2	90699 ± 4	73718 ± 1	95987 ± 10	95988 ± 45			
11	aifirst-001	229537224	808777	75485	1962048 ± 0	133587 ± 2	93568 ± 2	80584 ± 3	66601 ± 6	83755 ± 5	1091099 ± 14	1111087 ± 45			
12	aigen-001	263125848	595227	2111136	1692048 ± 0	3281448 ± 9	2751451 ± 8	2721759 ± 6	2682594 ± 4	2585691 ± 44	2253772 ± 57	2233736 ± 56			
13	aigen-002	210228007	1316138	164874	972048 ± 0	131586 ± 24	96582 ± 4	168920 ± 4	2511758 ± 5	2565427 ± 17	2223678 ± 44	2213646 ± 48			
14	ailabs-001	1079975494	338989	2221252	1732048 ± 0	169664 ± 4	154774 ± 50	2231145 ± 12	2591972 ± 74	2545205 ± 272	317104034 ± 661	7922103415 ± 722			
15	aimall-002	379040058	25210	2571576	1782048 ± 0	203776 ± 4	195927 ± 27	173940 ± 21	155955 ± 34	1321003 ± 75	31672811 ± 7399	31571216 ± 6286			
16	aimall-003	516428479	171935	2731913	531024 ± 0	168662 ± 1	144740 ± 51	130752 ± 62	104741 ± 46	94807 ± 47	30134565 ± 93	30234598 ± 118			
17	aiunionface-000	247442204	840295	52402	1092048 ± 0	157637 ± 13	149754 ± 41	1941025 ± 28	2011179 ± 29	2061639 ± 47	1031072 ± 19	1081080 ± 47			
18	aize-001	274899563	168970	2461436	2132048 ± 0	80437 ± 10	55440 ± 8	72542 ± 17	110756 ± 27	2031583 ± 53	1631937 ± 22	1611919 ± 23			
19	ajou-001	317975940	31734	63442	1522048 ± 0	110530 ± 0	85536 ± 0	70535 ± 0	57549 ± 0	46577 ± 0	38597 ± 19	43596 ± 13			
20	alchera-002	415139706	22275	2201233	1952048 ± 0	262968 ± 1	206976 ± 2	184979 ± 1	162988 ± 1	1341025 ± 2	2193488 ± 63	2193430 ± 63			
21	alchera-003	499423744	24613	2361376	1532048 ± 0	229854 ± 3	178862 ± 2	153870 ± 1	141882 ± 2	117918 ± 1	2163426 ± 57	2163383 ± 53			
22	alice-000	1783085023	19355	2651732	2894096 ± 0	255950 ± 2	197933 ± 1	177949 ± 1	1681011 ± 3	1741264 ± 8	28114975 ± 201	28014890 ± 229			
23	alleyes-000	519819601	997090	162857	2192048 ± 0	205784 ± 1	204970 ± 61	182974 ± 62	152943 ± 69	1411057 ± 23	1251298 ± 34	1271303 ± 51			
24	allgovision-000	176649434	155862	103561	1742048 ± 0	68384 ± 8	48395 ± 17	37413 ± 14	37471 ± 14	71710 ± 21	29929903 ± 406	30029735 ± 194			
25	alphaface-001	266086261	81636	93527	1122048 ± 0	146612 ± 1	104613 ± 3	88612 ± 1	70619 ± 1	58640 ± 2	981008 ± 10	981002 ± 19			
26	alphaface-002	787451788	70692	2451434	2032048 ± 0	153628 ± 2	146746 ± 19	129751 ± 18	115779 ± 22	100828 ± 40	88945 ± 25	90935 ± 17			
27	amplifiedgroup-001	0	47053	981	50866 ± 2	893 ± 0	-	-	-	-	31357803 ± 4210	31056365 ± 196			
28	androvideo-000	179043623	585063	53403	1262048 ± 0	45277 ± 0	33285 ± 0	22314 ± 0	22372 ± 1	53620 ± 0	2002860 ± 28	2002847 ± 22			
29	anke-004	357773976	410776	130706	2452056 ± 0	151625 ± 1	108627 ± 2	98635 ± 3	80653 ± 2	128982 ± 8	53633 ± 22	58632 ± 34			
30	anke-005	336438306	429160	2101134	2492056 ± 0	134590 ± 2	100594 ± 5	84601 ± 3	76638 ± 4	99821 ± 24	61685 ± 19	67687 ± 26			
31	antheus-000	122319905	41994	17116	40520 ± 0	13109 ± 1	16187 ± 1	12189 ± 1	9195 ± 1	12236 ± 2	2576901 ± 268	2566936 ± 103			
32	antheus-001	122319905	41962	181118	39520 ± 0	16120 ± 1	25265 ± 13	50468 ± 22	2091223 ± 27	2352660 ± 87	2546218 ± 47	2526216 ± 45			
33	anyvision-004	410625029	630797	2071102	601024 ± 0	63355 ± 1	-	-	-	-	1611891 ± 51	1561829 ± 85			
34	anyvision-005	195563434	116595	184963	581024 ± 0	265985 ± 1	208997 ± 1	1921004 ± 1	164995 ± 1	130995 ± 1	71733 ± 14	74733 ± 16			
35	asusaics-000	263596044	245320	114605	1892048 ± 0	95484 ± 13	77506 ± 21	148850 ± 26	2531789 ± 61	2606305 ± 188	2405455 ± 78	2405422 ± 12			
36	asusaics-001	263596114	245330	110595	2964096 ± 0	226842 ± 17	2091008 ± 20	2562423 ± 28	2672423 ± 277	2637284 ± 277	2678618 ± 42	2678638 ± 36			
37	authenmetric-002	460742912	91489	2091112	1632048 ± 0	252942 ± 1	201950 ± 1	180960 ± 1	157960 ± 1	129991 ± 2	1451712 ± 20	1461719 ± 19			
38	aware-005	307217546	26320	2241265	791572 ± 0	243886 ± 23	2201038 ± 21	2181121 ± 22	2261337 ± 58	2212195 ± 144	1341475 ± 63	1321427 ± 115			
39	aware-006	305708324	14124	181943	14352 ± 0	2941148 ± 3	2421146 ± 2	2301190 ± 2	2231306 ± 20	2121754 ± 84	1932598 ± 42	1942559 ± 60			
40	awiros-001	15871971	87480	1388	26512 ± 0	1097 ± 6	598 ± 4	8138 ± 6	13225 ± 7	42556 ± 8	1051079 ± 44	1031050 ± 45			
41	awiros-002	295953108	203723	104562	1472048 ± 0	92479 ± 0	75500 ± 0	69534 ± 0	69618 ± 0	123946 ± 1	1651966 ± 31	1661957 ± 25			
42	ayftech-001	200113346	43580	135731	22512 ± 0	75408 ± 23	63476 ± 52	137814 ± 108	2541827 ± 384	2555412 ± 1029	47615 ± 16	88885 ± 44			
43	ayonix-000	59909936	5252	569	651036 ± 0	218 ± 2	-	-	-	-	48621 ± 23	53620 ± 26			
44	beethedata-000	233318297	1087592	101555	1192048 ± 0	88465 ± 0	61467 ± 0	49468 ± 0	36467 ± 0	24467 ± 0	1722121 ± 34	1722110 ± 38			

Notes

- 1 The configuration size does not capture static data included in libraries.
- 2 The library size is the combined total of all files provided in the submission lib folder. These libraries e.g. OpenCV may or may not be installed on any end user's platform natively and would not need to be installed with the algorithm. Some developers put neural network models in their libraries.
- 3 The memory usage is the peak resident set size reported by the ps system call during template generation.
- 4 The median template creation times are measured on Intel®Xeon®@CPU E5-2630 v4 @ 2.20GHz processors.
- 5 The comparison durations, in nanoseconds, are estimated using std::chrono::high_resolution_clock which on the machine in (2) counts 1ns clock ticks. Precision is somewhat worse than that however. The ± value is the median absolute deviation times 1.48 for Normal consistency.

Table 6: Summary of algorithms and properties included in this report. The red superscripts give ranking for the quantity in that column.

ALGORITHM				CONFIG	LIBRARY	TEMPLATE						COMPARISON ⁴									
NAME		DATA	DATA	MEMORY	SIZE	GENERATION TIME (ms) ⁴					TIME (ns) ⁵										
		(KB) ¹	(KB) ²	(MB) ³	(B)	MUGSHOT	480x720	960x1440	1600x2400	3000x4500	GENUINE	IMPOSTOR									
45	bioidtechswiss-001	1207059515	120811	249	1455	24	512 ± 0	261	966 ± 4	261	1270 ± 270	246	1294 ± 96	235	1409 ± 157	215	1793 ± 79	194	2610 ± 25	196	2624 ± 32
46	bioidtechswiss-002	762660868	114842	192	993	21	512 ± 0	247	917 ± 2	196	930 ± 2	179	952 ± 2	154	947 ± 3	142	1058 ± 11	176	2177 ± 29	177	2170 ± 31
47	bm-001	294640228	38076	21	148	1	64 ± 0	82	444 ± 88	-	-	-	-	-	-	-	-	160	1887 ± 31	160	1877 ± 26
48	boetech-001	267649084	88710	238	1384	108	2048 ± 0	43	271 ± 1	28	268 ± 1	18	273 ± 0	17	286 ± 1	15	318 ± 1	314	68519 ± 1921	314	67648 ± 822
49	bresee-001	294790077	23227	217	1214	193	2048 ± 0	307	1223 ± 3	252	1216 ± 1	253	1331 ± 1	211	1227 ± 1	187	1360 ± 1	302	37240 ± 655	303	37167 ± 884
50	bresee-002	321154814	30902	277	1956	146	2048 ± 0	194	743 ± 4	240	1143 ± 2	224	1146 ± 2	196	1148 ± 2	163	1176 ± 2	150	1778 ± 22	150	1775 ± 23
51	camvi-002	241949538	225285	136	737	51	1024 ± 0	175	677 ± 7	139	726 ± 36	152	869 ± 28	190	1129 ± 43	239	2785 ± 113	44	612 ± 26	47	603 ± 20
52	camvi-004	287471548	615819	174	919	102	2048 ± 0	197	59 ± 10	177	861 ± 17	187	986 ± 34	220	1279 ± 51	241	2891 ± 158	89	948 ± 40	91	963 ± 31
53	canon-002	457207046	130232	168	891	300	4096 ± 0	317	1308 ± 2	266	1315 ± 1	252	1326 ± 2	227	1345 ± 1	196	1452 ± 1	253	6211 ± 25	251	6194 ± 25
54	ceiec-003	266620201	88707	59	430	164	2048 ± 0	215	817 ± 4	186	883 ± 57	161	897 ± 60	146	899 ± 72	122	944 ± 72	180	2256 ± 38	181	2241 ± 54
55	ceiec-004	269799940	67011	54	408	123	2048 ± 0	274	1024 ± 1	213	1027 ± 1	196	1027 ± 1	172	1030 ± 1	140	1055 ± 1	157	1844 ± 26	157	1836 ± 20
56	chosun-001	783990750	707	79	491	160	2048 ± 0	204	783 ± 2	165	826 ± 4	271	1662 ± 13	273	3679 ± 67	270	11694 ± 243	96	998 ± 25	102	1035 ± 11
57	chosun-002	239617968	31875	65	450	131	2048 ± 0	37	248 ± 3	30	273 ± 3	267	1495 ± 14	276	7920 ± 90	273	80302 ± 1349	50	623 ± 17	60	634 ± 13
58	chtface-002	371869498	369529	206	1100	107	2048 ± 0	129	584 ± 14	134	712 ± 41	202	1038 ± 42	255	1861 ± 75	253	4661 ± 232	181	2264 ± 26	180	2234 ± 13
59	chtface-003	371869498	369529	213	1178	191	2048 ± 0	138	594 ± 16	138	720 ± 33	205	1050 ± 41	258	1884 ± 90	257	5606 ± 334	171	2110 ± 37	179	2219 ± 65
60	cib-001	446723681	133766	154	836	93	2048 ± 0	160	651 ± 2	132	707 ± 13	122	716 ± 15	100	728 ± 3	98	820 ± 5	226	3783 ± 38	225	3765 ± 32
61	closeli-001	430430427	9851	139	773	287	4096 ± 0	225	839 ± 1	171	843 ± 1	145	841 ± 1	130	845 ± 1	108	865 ± 1	239	5404 ± 17	239	5400 ± 25
62	cloudwalk-hr-003	392949139	144263	190	984	256	2057 ± 0	142	606 ± 0	97	588 ± 0	81	594 ± 0	68	612 ± 1	-	-	259	6982 ± 80	257	6972 ± 32
63	cloudwalk-hr-004	514986414	520169	240	1394	229	2049 ± 0	237	873 ± 1	184	877 ± 1	157	876 ± 1	140	879 ± 1	114	902 ± 3	272	11652 ± 127	271	11608 ± 13
64	cloudwalk-mt-002	297731560	145340	157	844	228	2049 ± 0	125	573 ± 1	136	717 ± 78	117	700 ± 66	107	749 ± 96	89	770 ± 80	264	7205 ± 204	262	7211 ± 24
65	cloudwalk-mt-003	502133796	494959	232	1342	227	2049 ± 0	248	923 ± 1	194	918 ± 1	171	926 ± 1	149	925 ± 1	121	936 ± 1	271	11620 ± 179	272	11661 ± 128
66	clova-000	203182777	6824	68	464	120	2048 ± 0	81	437 ± 0	51	431 ± 0	41	435 ± 0	33	452 ± 2	27	508 ± 7	152	1794 ± 16	155	1795 ± 19
67	cogent-004	740269228	389164	199	1059	83	1983 ± 0	267	987 ± 50	-	-	-	-	-	-	-	-	283	15536 ± 75	283	15964 ± 103
68	cogent-005	1921839276	75276	298	2806	267	2523 ± 0	306	1221 ± 2	255	1236 ± 1	243	1289 ± 2	238	1420 ± 4	204	1602 ± 5	295	24854 ± 69	294	24858 ± 74
69	cognitec-000	486154134	27371	80	495	235	2052 ± 0	34	224 ± 1	-	-	-	-	-	-	-	-	227	3835 ± 108	227	3782 ± 82
70	cognitec-002	403546749	62354	117	624	242	2052 ± 0	27	192 ± 6	18	219 ± 6	16	233 ± 8	14	241 ± 6	14	314 ± 10	213	3250 ± 41	214	3241 ± 46
71	cor-001	1223627342	11240	221	1249	258	2060 ± 0	185	699 ± 3	179	863 ± 76	151	865 ± 80	136	872 ± 89	125	952 ± 39	324	282686 ± 117	324	282686 ± 117
72	coretech-000	190897979	43964	51	393	23	512 ± 0	140	602 ± 15	116	659 ± 12	221	1139 ± 24	197	1149 ± 25	160	1165 ± 23	15	333 ± 14	321	1171 ± 13
73	corsight-001	1472269967	31525	281	2040	260	2064 ± 0	315	1291 ± 3	262	1285 ± 1	245	1293 ± 1	222	1303 ± 2	188	1379 ± 3	323	249340 ± 1713	323	248929 ± 193
74	csc-001	0	240698	102	557	43	544 ± 0	52	302 ± 1	35	303 ± 0	20	304 ± 0	18	309 ± 1	17	341 ± 4	18	354 ± 8	20	344 ± 11
75	csc-002	0	519768	237	1376	44	544 ± 0	90	473 ± 0	72	494 ± 0	53	481 ± 1	42	490 ± 1	31	514 ± 5	19	367 ± 11	21	371 ± 16
76	ctbcbank-000	263381717	599238	106	570	223	2048 ± 0	123	568 ± 43	102	606 ± 38	111	690 ± 53	95	711 ± 50	101	831 ± 51	221	3551 ± 87	234	4805 ± 109
77	ctbcbank-001	282123885	599238	112	603	154	2048 ± 0	162	652 ± 35	156	781 ± 30	156	875 ± 43	145	898 ± 51	135	1030 ± 47	228	3926 ± 45	228	3924 ± 56
78	cubox-001	378498689	75427	120	649	104	2048 ± 0	245	907 ± 1	193	902 ± 1	163	903 ± 0	148	917 ± 0	119	931 ± 0	126	1379 ± 37	131	1417 ± 38
79	cuhkree-001	806762318	74917	292	2515	239	2052 ± 0	263	977 ± 31	-	-	-	-	-	-	-	-	196	2719 ± 60	198	2783 ± 56
80	cybercore-000	88073082	55441	31	200	33	512 ± 0	166	655 ± 3	125	689 ± 71	101	649 ± 6	77	648 ± 8	66	680 ± 6	280	14800 ± 75	282	15757 ± 72
81	cyberextruder-001	124120800	13629	26	178	3	256 ± 0	244	893 ± 25	-	-	-	-	-	-	-	-	106	1083 ± 16	107	1079 ± 19
82	cyberextruder-002	172963574	13924	30	194	222	2048 ± 0	112	532 ± 6	-	-	-	-	-	-	-	-	154	1803 ± 14	153	1779 ± 22
83	cyberlink-006	349866738	102456	241	1400	324	6212 ± 0	181	690 ± 1	129	702 ± 0	119	703 ± 0	96	712 ± 0	80	741 ± 0	10	270 ± 13	12	271 ± 13
84	cyberlink-007	389168020	102446	266	1743	323	6212 ± 0	190	725 ± 1	142	732 ± 1	125	734 ± 1	102	736 ± 1	88	767 ± 1	13	304 ± 19	13	304 ± 16
85	dahua-005	1624985571	169478	323	7360	293	4096 ± 0	325	1418 ± 34	-	-	-	-	-	-	-	-	90	957 ± 23	93	969 ± 19
86	dahua-006	851600617	119261	319	5068	158	2048 ± 0	322	1398 ± 2	270	1397 ± 1	259	1404 ± 1	233	1402 ± 1	190	1402 ± 1	7	249 ± 13	9	250 ± 11
87	decatur-000	358907752	171271	171	907	306	4100 ± 0	272	1024 ± 2	-	-	-	-	-	-	-	-	270	11439 ± 80	270	11418 ± 12
88	deepglint-002	470673814	272878	261	1614	297	4096 ± 0	174	677 ± 2	166	826 ± 74	146	848 ± 42	131	849 ± 55	110	886 ± 27	279	13633 ± 87	277	12905 ± 40

Notes

- 1 The configuration size does not capture static data included in libraries.
- 2 The library size is the combined total of all files provided in the submission lib folder. These libraries e.g. OpenCV may or may not be installed on any end user's platform natively and would not need to be installed with the algorithm. Some developers put neural network models in their libraries.
- 3 The memory usage is the peak resident set size reported by the ps system call during template generation.
- 4 The median template creation times are measured on Intel®Xeon®CPU E5-2630 v4 @ 2.20GHz processors.
- 5 The comparison durations, in nanoseconds, are estimated using std::chrono::high_resolution_clock which on the machine in (2) counts 1ns clock ticks. Precision is somewhat worse than that however. The ± value is the median absolute deviation times 1.48 for Normal consistency.

Table 7: Summary of algorithms and properties included in this report. The red superscripts give ranking for the quantity in that column.

	ALGORITHM	CONFIG	LIBRARY	TEMPLATE								COMPARISON ⁴									
				NAME	DATA	DATA	MEMORY	SIZE	GENERATION TIME (ms) ⁴				TIME (ns) ⁵								
									(KB) ¹	(KB) ²	(MB) ³	(B)	MUGSHOT	480x720	960x1440	1600x2400	3000x4500	GENUINE	IMPOSTOR		
89	deepglint-003	858178673	262081	287	2374	321	6144 ± 0	295	1159 ± 1	241	1145 ± 1	225	1148 ± 1	195	1148 ± 1	159	1163 ± 1	285	17227 ± 41	285	17210 ± 61
90	deepsea-001	151037339	336250	47	358	55	1024 ± 0	154	630 ± 7	148	752 ± 37	128	746 ± 30	99	727 ± 32	97	820 ± 32	129	1401 ± 37	133	1467 ± 50
91	deepsense-000	365684327	936618	324	7618	92	2048 ± 0	170	664 ± 3	114	645 ± 1	103	660 ± 2	88	687 ± 2	95	808 ± 3	25	480 ± 22	27	459 ± 34
92	dermalog-006	0	452387	187	970	2	128 ± 0	113	532 ± 12	-	-	-	-	-	-	-	-	29	506 ± 23	28	459 ± 23
93	dermalog-008	0	937895	318	4989	30	512 ± 0	72	404 ± 2	49	410 ± 3	39	424 ± 5	29	430 ± 5	25	477 ± 5	24	468 ± 31	17	328 ± 13
94	didiglobalface-001	266086235	70680	92	527	98	2048 ± 0	145	612 ± 1	112	633 ± 3	97	634 ± 3	79	650 ± 15	64	666 ± 4	93	973 ± 20	94	988 ± 20
95	digitalbarriers-002	84994577	598577	275	1930	250	2056 ± 0	30	209 ± 11	24	250 ± 19	36	411 ± 37	120	808 ± 72	223	2236 ± 123	277	13409 ± 228	278	13267 ± 206
96	dps-000	607	2211812	197	1058	277	4096 ± 0	233	868 ± 2	190	893 ± 6	264	1445 ± 9	270	2910 ± 38	266	9345 ± 17	133	1473 ± 37	134	1479 ± 37
97	dsk-000	12254510	782905	34	252	27	512 ± 0	53	304 ± 47	36	317 ± 33	191	1001 ± 96	269	2660 ± 170	269	10451 ± 832	263	7152 ± 115	260	7134 ± 11
98	einetworks-000	381551539	219883	166	880	255	2056 ± 0	159	645 ± 3	-	-	-	-	-	-	-	-	236	4876 ± 66	235	5156 ± 77
99	ekin-002	52668576	278	19139	270	3072 ± 0	301	1186 ± 13	246	1180 ± 12	228	1181 ± 11	205	1191 ± 11	168	1207 ± 8	232	4294 ± 80	243	5569 ± 112	
100	enface-000	378468370	153781	123	662	59	1024 ± 0	122	555 ± 4	91	558 ± 4	105	669 ± 6	161	987 ± 15	227	2349 ± 54	261	7059 ± 62	258	6980 ± 65
101	eocortex-000	262080175	59432	33	224	221	2048 ± 0	64	305 ± 22	41	341 ± 25	45	440 ± 47	34	464 ± 45	29	513 ± 44	87	923 ± 11	89	918 ± 11
102	ercacat-001	831102356	58012	299	2816	240	2052 ± 0	280	1052 ± 3	-	-	-	-	-	-	-	-	190	2551 ± 62	189	2501 ± 81
103	expasoft-001	39994987	983064	20	142	137	2048 ± 0	670	0 ± 0	374	0 ± 0	377	0 ± 0	373	0 ± 0	374	0 ± 0	141	1660 ± 35	142	1676 ± 48
104	expasoft-002	39691196	59825	23	168	218	2048 ± 0	434	0 ± 0	234	0 ± 0	234	0 ± 0	134	0 ± 0	134	0 ± 0	268	8870 ± 78	268	8838 ± 78
105	f8-001	279529297	19668	225	1276	157	2048 ± 0	221	822 ± 39	-	-	-	-	-	-	-	-	282	15262 ± 139	281	15277 ± 212
106	facesoft-000	379002927	10612	143	796	106	2048 ± 0	173	675 ± 18	119	669 ± 3	109	686 ± 3	84	675 ± 5	67	687 ± 2	179	2239 ± 28	182	2277 ± 96
107	facetag-000	1261907727	4022	186	965	49	684 ± 0	62	355 ± 17	45	369 ± 8	189	989 ± 33	266	2408 ± 91	264	7930 ± 316	315	72003 ± 625	316	71912 ± 62
108	facex-001	312396751	930372	302	2931	103	2048 ± 0	76	422 ± 4	53	434 ± 4	67	520 ± 7	103	737 ± 13	207	1670 ± 27	158	1871 ± 23	158	1846 ± 23
109	farfaces-001	354810878	44581	35	261	29	512 ± 0	298	1179 ± 1	248	1180 ± 1	227	1180 ± 0	202	1185 ± 1	169	1209 ± 2	85	855 ± 25	85	860 ± 31
110	fiberhome-nanjing-002	212375748	596827	151	826	61	1024 ± 0	305	1217 ± 2	264	1294 ± 30	250	1312 ± 12	243	1477 ± 14	183	1326 ± 11	138	1582 ± 57	137	1560 ± 51
111	fiberhome-nanjing-003	361365058	1482309	159	845	213	2048 ± 0	290	1136 ± 7	236	1134 ± 4	220	1132 ± 3	194	1139 ± 3	155	1154 ± 5	108	1097 ± 38	110	1083 ± 12
112	fincore-000	262774045	19409	95	535	133	2048 ± 0	104	508 ± 3	76	505 ± 0	63	508 ± 1	49	513 ± 2	36	535 ± 1	148	1765 ± 31	148	1763 ± 22
113	fujitsulab-002	0	1088887	260	1613	310	4104 ± 0	311	1237 ± 2	253	1222 ± 2	236	1236 ± 1	214	1251 ± 2	185	1327 ± 2	198	2836 ± 25	199	2809 ± 14
114	fujitsulab-003	678158225	318209	322	6907	308	4104 ± 0	257	951 ± 20	200	941 ± 19	178	952 ± 19	159	971 ± 20	138	1045 ± 21	199	2855 ± 16	201	2849 ± 17
115	geo-001	264721293	70163	45	344	217	2048 ± 0	283	1079 ± 0	224	1076 ± 0	208	1076 ± 0	182	1078 ± 0	149	1102 ± 0	211	3163 ± 47	211	3158 ± 38
116	geo-002	378781240	98667	193	1018	129	2048 ± 0	207	791 ± 1	158	793 ± 0	133	794 ± 0	117	795 ± 1	92	803 ± 1	215	3407 ± 45	218	3422 ± 51
117	glory-002	0	385177	188	982	265	2106 ± 0	139	594 ± 3	143	740 ± 3	176	948 ± 3	261	2168 ± 6	919	191 ± 15	256	6787 ± 85	254	6551 ± 24
118	glory-003	0	536910	242	1400	312	4234 ± 0	97	489 ± 0	92	565 ± 0	124	732 ± 0	257	1876 ± 2	265	8941 ± 20	249	6020 ± 90	250	6003 ± 72
119	gorilla-006	176888996	1318812	165	874	313	4240 ± 0	84	454 ± 3	67	484 ± 3	61	497 ± 5	56	543 ± 25	118	928 ± 60	224	3755 ± 38	224	3737 ± 14
120	gorilla-007	451643974	708166	262	1691	325	6288 ± 0	136	592 ± 1	98	592 ± 1	86	603 ± 1	72	625 ± 2	74	722 ± 9	223	3686 ± 37	222	3709 ± 36
121	hertasecurity-000	5	780014	89	516	5	256 ± 0	11	99 ± 0	698	0 ± 0	5	100 ± 0	5	107 ± 0	6	139 ± 0	66	710 ± 31	63	667 ± 28
122	hik-001	683894884	9290	321	6597	72	1408 ± 0	161	651 ± 0	118	667 ± 8	107	677 ± 16	87	686 ± 13	78	737 ± 12	26	488 ± 19	29	477 ± 22
123	hyperverge-001	267079500	88624	84	507	187	2048 ± 0	177	682 ± 20	126	695 ± 17	233	1196 ± 37	265	2400 ± 68	262	7178 ± 204	251	6026 ± 40	249	5984 ± 80
124	hyperverge-002	3022745705	198832	278	1975	54	1024 ± 0	250	938 ± 1	199	939 ± 1	174	941 ± 1	153	945 ± 1	127	975 ± 1	250	6023 ± 37	248	5966 ± 40
125	icm-002	636504686	903	74	484	95	2048 ± 0	276	1031 ± 7	-	-	-	-	-	-	-	-	294	24052 ± 118	293	24049 ± 124
126	icthtc-000	176598609	1471004	269	1805	198	2048 ± 0	61	338 ± 11	40	338 ± 9	42	437 ± 16	93	705 ± 24	211	1719 ± 44	238	5284 ± 63	238	5290 ± 54
127	id3-006	215159624	7706	189	982	38	520 ± 0	178	683 ± 0	225	1088 ± 1	231	1192 ± 1	208	1209 ± 1	175	1270 ± 1	243	5547 ± 34	242	5563 ± 34
128	id3-007	189471032	7728	191	988	10	264 ± 0	271	1016 ± 1	239	1139 ± 1	278	3911 ± 2	278	1052 ± 12	274	135182 ± 1912	241	5500 ± 29	241	5486 ± 35
129	idemlia-007	361720312	67485	196	1051	15	468 ± 0	70	384 ± 0	47	389 ± 0	32	393 ± 1	25	405 ± 2	22	441 ± 8	212	3243 ± 63	213	3202 ± 63
130	idemlia-008	382993834	69922	214	1194	13	348 ± 0	85	457 ± 1	60	461 ± 0	47	466 ± 1	38	476 ± 2	30	513 ± 10	208	3080 ± 41	206	3046 ± 56
131	iit-002	265809599	52070	134	731	87	2048 ± 0	105	514 ± 1	79	531 ± 2	76	547 ± 1	60	583 ± 1	76	733 ± 2	99	1023 ± 7	99	1011 ± 66
132	iit-003	267559145	53791	149	817	149	2048 ± 0	94	482 ± 0	70	493 ± 0	64	509 ± 0	54	541 ± 0	62	661 ± 0	14	324 ± 17	16	326 ± 8

Notes

- 1 The configuration size does not capture static data included in libraries.
- 2 The library size is the combined total of all files provided in the submission lib folder. These libraries e.g. OpenCV may or may not be installed on any end user's platform natively and would not need to be installed with the algorithm. Some developers put neural network models in their libraries.
- 3 The memory usage is the peak resident set size reported by the ps system call during template generation.
- 4 The median template creation times are measured on Intel®Xeon®CPU E5-2630 v4 @ 2.20GHz processors.
- 5 The comparison durations, in nanoseconds, are estimated using std::chrono::high_resolution_clock which on the machine in (2) counts 1ns clock ticks. Precision is somewhat worse than that however. The ± value is the median absolute deviation times 1.48 for Normal consistency.

Table 8: Summary of algorithms and properties included in this report. The red superscripts give ranking for the quantity in that column.

	ALGORITHM	CONFIG	LIBRARY	TEMPLATE								COMPARISON ⁴			
				NAME		DATA		MEMORY		SIZE		GENERATION TIME (ms) ⁴			
				(KB) ¹	(KB) ²	(MB) ³	(B)	MUGSHOT	480x720	960x1440	1600x2400	3000x4500	GENUINE	IMPOSTOR	
133	imagus-002	233233236	318409	⁵⁶ 411	¹⁷⁰ 2048 ± 0	²⁰⁶ 786 ± 1	¹⁵¹ 766 ± 2	¹⁵⁹ 885 ± 3	²³⁹ 1430 ± 3	²⁵⁰ 4080 ± 10	⁵⁷ 676 ± 16	⁵⁰ 630 ± 20			
134	imagus-003	260977219	378019	⁸² 498	¹⁸² 2048 ± 0	²³² 865 ± 2	¹⁹⁸ 938 ± 1	²⁷⁰ 1577 ± 1	²⁷¹ 3002 ± 3	²⁶⁷ 9521 ± 16	⁷³ 738 ± 26	⁶³ 683 ± 25			
135	imperial-000	379002927	10623	¹⁴⁴ 796	¹⁶⁵ 2048 ± 0	¹⁷¹ 669 ± 1	¹²² 675 ± 3	¹⁰⁸ 683 ± 17	⁸⁵ 676 ± 2	⁶⁸ 689 ± 2	¹⁷³ 2130 ± 32	¹⁷⁰ 2052 ± 100			
136	imperial-002	483663560	16134	²⁷⁰ 1826	²²⁰ 2048 ± 0	¹²⁴ 569 ± 1	⁹⁵ 581 ± 15	⁷⁹ 575 ± 5	⁵⁹ 576 ± 2	⁴⁸ 588 ± 3	¹⁸² 2278 ± 90	¹⁷⁴ 4131 ± 44			
137	incode-008	272489716	21014	²⁵¹ 1469	¹⁵¹ 2048 ± 0	¹⁰⁰ 500 ± 0	⁶⁹ 493 ± 0	⁶⁰ 496 ± 0	⁴⁸ 506 ± 1	³⁸ 537 ± 0	¹⁰² 1070 ± 28	¹⁰⁹ 081 ± 34			
138	incode-009	272489716	21014	¹⁷⁹ 939	¹⁸⁶ 2048 ± 0	¹⁰¹ 503 ± 0	⁶⁸ 490 ± 1	⁶² 498 ± 0	⁴⁷ 505 ± 0	³⁷ 537 ± 0	¹¹⁰ 1102 ± 28	¹¹³ 113 ± 29			
139	innefuleabs-000	379482783	162172	⁶¹ 439	²²⁴ 2048 ± 0	²⁶⁹ 1006 ± 3	²¹² 1025 ± 3	¹⁹⁸ 1030 ± 4	¹⁷⁶ 1041 ± 2	¹⁵² 1135 ± 3	²⁴⁵ 5782 ± 41	²⁴⁷ 3741 ± 45			
140	innovativetechnologyltd-001	181485901	335757	⁴⁴ 341	¹⁷⁵ 2048 ± 0	⁷⁸ 433 ± 7	⁵⁷ 446 ± 8	⁴³ 439 ± 4	³² 452 ± 4	²⁶ 485 ± 7	¹⁵⁹ 1877 ± 42	¹⁶² 924 ± 97			
141	innovativetechnologyltd-002	178114027	372324	¹⁷² 912	¹⁸³ 2048 ± 0	¹⁶⁷ 661 ± 2	¹⁴⁰ 726 ± 4	¹⁸⁵ 981 ± 27	¹⁶⁵ 997 ± 40	⁸⁷ 766 ± 3	¹⁵⁶ 1841 ± 50	¹⁵⁹ 857 ± 59			
142	innovatrics-006	74	466269	²⁰⁸ 1107	⁴¹ 538 ± 0	²¹⁸ 820 ± 5	¹⁶⁰ 799 ± 4	¹³⁵ 805 ± 3	¹¹⁸ 796 ± 9	¹¹¹ 890 ± 15	²⁴⁶ 5855 ± 204	²³⁶ 5266 ± 118			
143	innovatrics-007	74	493269	²⁷⁶ 1937	⁶⁸ 1064 ± 0	³³⁰ 1485 ± 7	²⁷⁷ 1785 ± 184	²⁷⁴ 2078 ± 24	²⁶⁰ 2123 ± 15	²²² 2210 ± 42	²⁴⁸ 5978 ± 88	²⁴⁶ 5690 ± 102			
144	insightface-000	826320727	16606	³¹² 3912	²⁸⁶ 4096 ± 0	²⁷⁰ 1009 ± 1	²¹¹ 1019 ± 2	¹⁹³ 1017 ± 2	¹⁶⁹ 1020 ± 2	¹³⁶ 1032 ± 2	¹⁴⁹ 1778 ± 31	¹⁴⁹ 773 ± 35			
145	intellicloudai-001	226131619	868246	¹²¹ 655	¹¹⁶ 2048 ± 0	⁸⁹ 468 ± 2	⁵⁸ 456 ± 1	⁴⁸ 466 ± 3	⁴⁴ 492 ± 1	⁵⁴ 632 ± 2	¹⁰⁰ 1056 ± 4	¹⁰⁴ 151 ± 72			
146	intellicloudai-002	265264200	58559	³⁰⁶ 3584	³⁰⁴ 4100 ± 0	²²⁷ 847 ± 1	¹⁷² 847 ± 2	¹⁴⁷ 849 ± 1	¹³³ 853 ± 1	¹⁰⁹ 878 ± 4	⁸³ 822 ± 28	⁸² 818 ± 23			
147	intellifusion-001	278397082	289387	¹³⁷ 762	¹⁴⁰ 2048 ± 0	¹⁹⁸ 764 ± 38	¹⁵³ 774 ± 39	¹³⁴ 797 ± 42	¹¹⁹ 803 ± 34	⁹³ 805 ± 33	¹¹¹ 1112 ± 28	¹¹⁵ 128 ± 41			
148	intellifusion-002	781037413	385841	¹⁸⁰ 941	²⁹⁸ 4096 ± 0	²⁵⁶ 950 ± 2	²²⁹ 1096 ± 42	²¹¹ 1088 ± 33	¹⁹⁹ 1168 ± 31	¹⁶¹ 1171 ± 10	¹⁴⁶ 1713 ± 57	¹⁴¹ 1655 ± 87			
149	intellivision-001	44741184	11649	⁷ 74	²⁵² 2056 ± 0	⁵ 62 ± 2	-	-	-	-	¹⁹¹ 2573 ± 91	¹⁹² 4544 ± 38			
150	intellivision-002	44741184	14505	¹⁰ 81	²⁴³ 2056 ± 0	⁵⁶ 322 ± 1	⁴² 355 ± 2	²⁹ 372 ± 1	²⁸ 422 ± 2	⁴⁹ 600 ± 1	²⁷⁸ 13525 ± 134	²⁷⁶ 12782 ± 278			
151	intelresearch-002	463719162	86454	²⁴³ 1420	¹⁴³ 2048 ± 0	¹⁸⁸ 707 ± 2	¹⁵⁷ 790 ± 33	¹³² 788 ± 26	¹²⁵ 831 ± 29	¹⁰⁶ 862 ± 22	²³⁰ 4204 ± 91	²²⁹ 1553 ± 93			
152	intelresearch-003	410975551	85085	²¹² 1177	¹²⁸ 2048 ± 0	³⁰⁹ 1232 ± 3	²⁵⁶ 1237 ± 2	²³⁸ 1242 ± 2	²¹⁸ 1263 ± 2	¹⁸² 1324 ± 3	²³⁴ 4443 ± 75	²³² 1374 ± 77			
153	intsysmsu-001	393635676	172480	¹⁴² 789	⁸⁸ 2048 ± 0	¹⁴⁷ 614 ± 2	¹⁰⁶ 615 ± 2	¹⁰⁰ 642 ± 2	¹⁰⁸ 750 ± 3	¹⁵⁸ 1159 ± 4	⁴⁹ 621 ± 8	⁵⁰ 621 ± 31			
154	intsysmsu-002	784303912	172298	¹⁴¹ 786	⁵⁶ 1024 ± 0	¹³⁷ 593 ± 1	¹⁵⁹ 793 ± 2	¹⁴⁰ 827 ± 1	¹³⁸ 875 ± 104	¹⁷⁸ 1293 ± 3	³¹ 549 ± 25	³⁴ 548 ± 29			
155	ionetworks-000	294511946	51236	⁴⁶ 351	¹⁵⁶ 2048 ± 0	⁷⁷ 430 ± 0	⁵⁴ 435 ± 0	⁴⁰ 433 ± 0	³⁰ 432 ± 0	²³ 444 ± 0	²⁵⁸ 6913 ± 102	²⁶¹ 7150 ± 160			
156	iqface-000	275271315	596337	¹²⁹ 704	³¹⁵ 4750 ± 32	¹¹⁵ 538 ± 26	⁷¹ 494 ± 2	⁷⁴ 543 ± 3	¹⁰¹ 734 ± 4	¹⁸⁹ 1393 ± 4	³²⁸ 636433 ± 38446	³²⁸ 632654 ± 85615			
157	iqface-003	379702979	963398	¹⁴⁸ 817	³¹⁶ 4763 ± 37	¹⁰⁸ 529 ± 1	⁸⁰ 532 ± 2	⁸³ 599 ± 8	¹³² 850 ± 2	²⁰⁹ 1694 ± 2	³²⁷ 575924 ± 2601	³²⁷ 576633 ± 2051			
158	irex-000	759705187	47419	²⁸² 2086	²⁷² 3080 ± 0	²²⁸ 852 ± 2	¹⁷⁴ 850 ± 1	¹⁵⁵ 874 ± 2	¹⁵⁰ 939 ± 1	¹⁷³ 1249 ± 5	⁴ 201 ± 11	⁵ 208 ± 8			
159	isap-001	101427082	204201	¹ 18	²⁸⁰ 4096 ± 0	¹ 0 ± 0	-	-	-	-	²³ 459 ± 17	²⁶ 456 ± 11			
160	isap-002	262928187	49931	⁴⁰ 288	¹⁴² 2048 ± 0	²⁰¹ 769 ± 3	²¹⁴ 1027 ± 2	¹⁵⁸ 877 ± 2	¹¹³ 761 ± 1	¹¹⁶ 912 ± 2	²⁰⁶ 3045 ± 94	²⁰² 1973 ± 66			
161	isityou-000	49163234	36621	¹⁵ 110	³²⁹ 19200 ± 0	¹⁴ 113 ± 5	-	-	-	-	³²² 237517 ± 1318	³²² 237349 ± 1279			
162	isystems-001	281212446	639268	²⁰⁵ 1091	¹¹⁵ 2048 ± 0	⁴⁹ 291 ± 9	-	-	-	-	³² 557 ± 16	³⁴ 564 ± 22			
163	isystems-002	367599646	803389	²⁵⁹ 1595	⁸⁹ 2048 ± 0	²²⁰ 822 ± 8	-	-	-	-	⁷⁴ 749 ± 31	⁵⁴ 652 ± 28			
164	itmo-006	613567913	96762	²⁵³ 1489	²⁶⁶ 2121 ± 0	²¹⁴ 814 ± 1	¹⁶⁸ 831 ± 26	¹⁴¹ 830 ± 17	¹²⁴ 830 ± 3	¹²⁴ 952 ± 38	²⁹⁷ 26154 ± 148	²⁹⁶ 26128 ± 260			
165	itmo-007	425962652	245376	²⁸⁶ 2199	¹⁹² 2048 ± 0	¹⁹³ 741 ± 2	-	-	-	-	¹⁸⁹ 2551 ± 50	¹⁹¹ 1529 ± 80			
166	ivacognitive-001	263125888	62791	¹⁸² 947	¹¹¹ 2048 ± 0	³¹⁶ 1292 ± 3	²⁶³ 1289 ± 4	²⁴⁴ 1292 ± 4	²²¹ 1292 ± 3	¹⁸¹ 1321 ± 4	²³¹ 4228 ± 41	²³⁰ 1226 ± 41			
167	iws-000	31616555	3063	⁸ 77	¹⁹ 512 ± 0	⁴⁴ 277 ± 5	³² 283 ± 1	⁵⁹ 494 ± 3	¹⁶⁰ 984 ± 3	²⁴³ 2987 ± 39	⁹⁷ 999 ± 40	⁹⁸ 982 ± 22			
168	kakao-004	424357647	135270	²⁶⁸ 1783	⁸⁶ 2048 ± 0	²³⁰ 856 ± 1	¹⁷⁶ 855 ± 0	¹⁴⁹ 857 ± 0	¹³⁴ 858 ± 0	¹⁰⁵ 860 ± 1	¹⁶⁴ 1957 ± 28	¹⁶⁵ 1953 ± 37			
169	kakao-005	424259623	152216	²⁵⁸ 1581	²³⁴ 2052 ± 0	²⁸² 1068 ± 1	²²³ 1073 ± 1	²⁰⁹ 1079 ± 0	¹⁸¹ 1077 ± 1	¹⁴⁷ 1089 ± 1	¹⁷⁰ 2067 ± 26	¹⁶⁹ 2043 ± 34			
170	kakaopay-001	407413757	179869	¹²⁶ 684	²⁸² 4096 ± 0	⁸³ 448 ± 0	⁸⁰ 542 ± 0	⁷³ 542 ± 0	⁵⁵ 542 ± 0	⁴¹ 553 ± 0	⁵² 633 ± 22	⁵³ 630 ± 22			
171	kedacom-000	251179996	37401	³²⁸ 23574	¹¹ 292 ± 0	¹⁰² 506 ± 3	⁸⁹ 547 ± 10	⁹⁰ 614 ± 9	⁶² 588 ± 10	⁶³ 665 ± 24	⁶⁰ 684 ± 14	⁶⁴ 682 ± 16			
172	kiwitech-000	378584700	21375	¹⁴⁶ 808	¹²⁵ 2048 ± 0	¹³⁵ 591 ± 0	⁹⁹ 594 ± 0	⁸² 595 ± 1	⁶⁵ 596 ± 0	⁵⁰ 609 ± 0	¹⁴⁷ 1755 ± 20	¹⁴⁷ 734 ± 16			
173	kneron-003	59767577	1747	²⁷ 188	²⁰⁸ 2048 ± 0	⁴⁶ 281 ± 3	³¹ 280 ± 1	²³ 315 ± 13	²¹ 365 ± 7	¹⁷¹ 1224 ± 30	²³⁷ 5237 ± 63	²³⁷ 3274 ± 99			
174	kneron-005	384383985	13633	⁶⁷ 457	¹⁰⁰ 2048 ± 0	¹⁰⁷ 518 ± 2	⁷⁸ 522 ± 4	⁷⁸ 556 ± 5	¹¹¹ 757 ± 19	²¹³ 1760 ± 25	¹⁶² 1922 ± 11	¹⁶³ 1926 ± 20			
175	kookmin-001	239617968	31875	⁶² 439	¹³⁵ 2048 ± 0	¹⁵ 114 ± 1	⁹ 110 ± 1	⁶ 116 ± 1	⁷ 128 ± 1	⁸ 172 ± 1	⁵¹ 629 ± 35	⁵² 616 ± 11			
176	kookmin-002	380693533	30734	¹⁵² 827	¹³⁸ 2048 ± 0	²⁷⁸ 1038 ± 2	²²¹ 1047 ± 1	²⁰³ 1045 ± 1	¹⁸⁰ 1061 ± 1	¹⁵⁰ 1116 ± 1	⁵⁶ 638 ± 19	⁶¹ 636 ± 20			

Notes

- 1 The configuration size does not capture static data included in libraries.
- 2 The library size is the combined total of all files provided in the submission lib folder. These libraries e.g. OpenCV may or may not be installed on any end user's platform natively and would not need to be installed with the algorithm. Some developers put neural network models in their libraries.
- 3 The memory usage is the peak resident set size reported by the ps system call during template generation.
- 4 The median template creation times are measured on Intel®Xeon®CPU E5-2630 v4 @ 2.20GHz processors.
- 5 The comparison durations, in nanoseconds, are estimated using std::chrono::high_resolution_clock which on the machine in (2) counts 1ns clock ticks. Precision is somewhat worse than that however. The ± value is the median absolute deviation times 1.48 for Normal consistency.

Table 9: Summary of algorithms and properties included in this report. The red superscripts give ranking for the quantity in that column.

	ALGORITHM	CONFIG	LIBRARY	TEMPLATE								COMPARISON ⁴								
				NAME	DATA	DATA	MEMORY	SIZE	GENERATION TIME (ms) ⁴				TIME (ns) ⁵							
									(KB) ¹	(KB) ²	(MB) ³	(B)	MUGSHOT	480x720	960x1440	1600x2400	3000x4500	GENUINE	IMPOSTOR	
177	lemalabs-001	766361714	198794	297	2738	184	2048 ± 0	211	810 ± 0	-	-	-	-	-	-	274	11930 ± 35	274	11913 ± 37	
178	line-000	270789845	407003	108	590	96	2048 ± 0	132	586 ± 0	103	612 ± 0	87	609 ± 1	67	611 ± 0	52	618 ± 1	197	2753 ± 19	
179	lookman-002	141516916	25410	320	16518	45	548 ± 0	22	173 ± 1	-	-	-	-	-	-	43	610 ± 19	51	612 ± 22	
180	lookman-004	250650528	37401	327	23548	46	548 ± 0	103	507 ± 5	87	545 ± 12	89	613 ± 12	64	590 ± 11	59	656 ± 16	86	871 ± 29	
181	luxand-000	0	57908	234	1366	66	1040 ± 0	74	407 ± 23	52	433 ± 11	46	444 ± 14	39	464 ± 14	44	562 ± 25	84	828 ± 28	
182	megvii-002	1852993999	16491	272	1879	302	4100 ± 0	158	644 ± 0	-	-	-	-	-	-	309	50630 ± 183	309	47591 ± 16	
183	megvii-003	4536617822	42790	317	4878	292	4096 ± 0	303	1210 ± 1	254	1223 ± 0	254	1356 ± 4	246	1582 ± 7	236	2727 ± 23	320	225342 ± 3574	
184	meituwan-000	265743335	333178	98	554	101	2048 ± 0	79	436 ± 4	56	441 ± 1	91	626 ± 5	183	1098 ± 15	247	3126 ± 53	55	638 ± 17	
185	meiya-001	286777340	264913	85	507	226	2049 ± 0	150	622 ± 12	-	-	-	-	-	-	266	8356 ± 615	266	8134 ± 97	
186	microfocus-001	107032902	27242	28	190	7	256 ± 0	42	264 ± 18	-	-	-	-	-	-	6	215 ± 8	6	217 ± 10	
187	microfocus-002	98599914	27362	25	176	6	256 ± 0	39	259 ± 18	-	-	-	-	-	-	16	337 ± 34	7	230 ± 25	
188	minivision-000	856777875	16597	313	4013	284	4096 ± 0	277	1035 ± 1	218	1033 ± 2	201	1035 ± 1	175	1037 ± 1	143	1059 ± 2	187	2466 ± 26	
189	mobai-000	374222377	80573	140	786	322	6144 ± 0	199	766 ± 8	181	869 ± 6	235	1205 ± 31	256	1867 ± 45	248	3549 ± 190	284	16458 ± 333	
190	mobai-001	271664763	60164	94	534	185	2048 ± 0	144	612 ± 3	105	614 ± 3	110	687 ± 9	142	886 ± 31	210	1707 ± 103	127	1386 ± 25	
191	mobbl-000	186421478	58727	36	262	197	2048 ± 0	41	261 ± 16	27	267 ± 22	30	375 ± 92	81	655 ± 273	218	2059 ± 1129	276	12061 ± 142	
192	mobbl-001	236708614	58706	32	223	176	2048 ± 0	26	183 ± 32	15	184 ± 25	26	354 ± 76	123	823 ± 396	238	2781 ± 1166	273	11832 ± 109	
193	moreedian-000	537865562	21374	177	932	94	2048 ± 0	183	690 ± 0	127	698 ± 0	116	699 ± 0	91	700 ± 0	72	713 ± 1	155	1803 ± 11	
194	mvision-001	2329692922	149531	132	723	32	512 ± 0	182	691 ± 21	130	702 ± 19	115	697 ± 24	94	708 ± 29	70	710 ± 27	113	1123 ± 40	
195	nazhiai-000	560624381	16141	294	2716	144	2048 ± 0	179	683 ± 3	124	687 ± 2	143	835 ± 27	129	840 ± 31	103	834 ± 34	178	2230 ± 34	
196	neosystems-001	589102173	349959	216	1214	117	2048 ± 0	291	1137 ± 4	230	1098 ± 1	273	1767 ± 4	252	1769 ± 3	214	1765 ± 4	287	18557 ± 189	
197	neosystems-002	613827997	349942	219	1222	205	2048 ± 0	289	1135 ± 2	278	1855 ± 3	275	2258 ± 5	263	2238 ± 3	224	2247 ± 3	288	18752 ± 167	
198	netbridgetech-001	136302786	205875	86	508	301	4096 ± 0	785 ± 1	483 ± 0	484 ± 0	484 ± 0	492 ± 0	4	113 ± 4	269	9280 ± 74	269	9446 ± 312		
199	netbridgetech-002	263871604	49931	42	299	201	2048 ± 0	224	838 ± 6	170	838 ± 2	144	839 ± 1	128	839 ± 3	104	859 ± 3	201	2893 ± 65	
200	neurotechnology-011	372877031	51141	250	1462	36	514 ± 0	209	798 ± 1	16	802 ± 1	139	827 ± 3	137	873 ± 2	144	1059 ± 15	114	114 ± 8	
201	neurotechnology-012	151378192	51395	147	814	4	256 ± 0	69	384 ± 0	46	387 ± 0	34	404 ± 1	31	435 ± 1	47	583 ± 7	2	119 ± 7	
202	nnh-001	344464916	817674	122	662	290	4096 ± 0	275	1027 ± 3	216	1029 ± 1	197	1029 ± 1	177	1044 ± 1	148	1090 ± 1	311	56650 ± 260	
203	nnh-002	372194536	817674	124	667	278	4096 ± 0	292	1141 ± 3	238	1138 ± 2	222	1141 ± 2	198	1151 ± 6	167	1203 ± 2	310	56608 ± 579	
204	nodeflux-002	793260136	690213	69	466	225	2048 ± 0	189	708 ± 4	133	709 ± 4	121	716 ± 5	98	716 ± 7	77	736 ± 3	217	3475 ± 62	
205	notiontag-000	94979467	406791	91	525	47	584 ± 0	119	548 ± 64	90	548 ± 35	265	1450 ± 99	274	3771 ± 251	271	13146 ± 792	305	44672 ± 269	
206	notiontag-001	94979467	427967	105	566	48	584 ± 0	249	929 ± 35	226	1092 ± 39	277	3709 ± 81	277	10233 ± 180	-	304	43636 ± 286	304	43724 ± 30
207	nsensecorp-001	191919164	258593	99	554	139	2048 ± 0	60	336 ± 0	39	335 ± 0	24	336 ± 0	19	335 ± 0	16	337 ± 0	308	46605 ± 93	
208	nsensecorp-002	191919991	122407	100	554	130	2048 ± 0	59	333 ± 0	38	333 ± 0	25	337 ± 0	20	338 ± 0	18	351 ± 0	307	45965 ± 213	
209	ntechlab-009	1789996893	43730	315	4135	82	1940 ± 0	288	1115 ± 2	232	1114 ± 1	215	1119 ± 1	191	1130 ± 2	164	1202 ± 4	45	614 ± 20	
210	ntechlab-010	715357382	217167	303	2991	69	1280 ± 0	297	1177 ± 2	247	1180 ± 2	234	1197 ± 2	210	1224 ± 1	184	1326 ± 3	21	405 ± 13	
211	omnigarde-000	270395030	32882	90	523	57	1024 ± 0	254	944 ± 0	188	887 ± 0	160	888 ± 1	144	892 ± 0	115	902 ± 0	195	2671 ± 35	
212	openface-001	0	40111	14	100	127	2048 ± 0	20	148 ± 1	13	154 ± 0	28	365 ± 3	27	409 ± 9	51	616 ± 31	42	608 ± 14	
213	oz-001	311012472	238311	194	1021	311	4125 ± 0	293	1147 ± 3	250	1182 ± 3	242	1273 ± 4	247	1617 ± 7	240	2890 ± 19	321	228011 ± 5455	
214	oz-002	733207161	170261	305	3561	261	2065 ± 0	281	1064 ± 3	243	1171 ± 3	276	2953 ± 6	275	7352 ± 13	272	26658 ± 29	319	131108 ± 1408	
215	papsav1923-001	285911345	52652	72	473	204	2048 ± 0	152	626 ± 1	109	628 ± 1	92	630 ± 1	78	648 ± 2	81	744 ± 3	70	725 ± 25	
216	paravision-004	570030501	145440	256	1572	294	4096 ± 0	222	829 ± 2	169	834 ± 6	142	832 ± 2	126	833 ± 4	102	833 ± 2	72	737 ± 31	
217	paravision-008	555203492	204400	248	1448	279	4096 ± 0	186	699 ± 0	128	700 ± 0	118	701 ± 0	92	702 ± 1	69	702 ± 0	17	337 ± 17	
218	pensees-001	1658297650	408932	274	1922	326	8200 ± 0	285	1108 ± 3	274	1448 ± 17	263	1439 ± 10	242	1464 ± 5	202	1546 ± 9	210	3151 ± 34	
219	pixelall-005	0	1001355	227	1292	317	5120 ± 0	287	1112 ± 3	233	1115 ± 1	216	1120 ± 1	188	1124 ± 2	154	1143 ± 2	122	1259 ± 29	
220	pixelall-006	0	746305	178	934	268	2560 ± 0	273	1024 ± 3	215	1028 ± 2	199	1033 ± 1	173	1032 ± 1	139	1054 ± 2	75	754 ± 14	

Notes

1 The configuration size does not capture static data included in libraries.

2 The library size is the combined total of all files provided in the submission lib folder. These libraries e.g. OpenCV may or may not be installed on any end user's platform natively and would not need to be installed with the algorithm. Some developers put neural network models in their libraries.

3 The memory usage is the peak resident set size reported by the ps system call during template generation.

4 The median template creation times are measured on Intel®Xeon®CPU E5-2630 v4 @ 2.20GHz processors.

5 The comparison durations, in nanoseconds, are estimated using std::chrono::high_resolution_clock which on the machine in (2) counts 1ns clock ticks. Precision is somewhat worse than that however. The ± value is the median absolute deviation times 1.48 for Normal consistency.

Table 10: Summary of algorithms and properties included in this report. The red superscripts give ranking for the quantity in that column.

	ALGORITHM	CONFIG	LIBRARY	TEMPLATE								COMPARISON ⁴									
				NAME	DATA	DATA	MEMORY	SIZE	GENERATION TIME (ms) ⁴				TIME (ns) ⁵								
									(KB) ¹	(KB) ²	(MB) ³	(B)	MUGSHOT	480x720	960x1440	1600x2400	3000x4500	GENUINE	IMPOSTOR		
221	psl-007	977255992	524521	314	4042	275	3144 ± 0	323	1408 ± 5	272	1417 ± 3	262	1418 ± 3	237	1419 ± 2	194	1422 ± 3	9	265 ± 22	11	258 ± 17
222	psl-008	977255943	524525	309	3807	274	3144 ± 0	324	1412 ± 4	271	1415 ± 3	261	1416 ± 2	236	1418 ± 2	193	1418 ± 2	8	259 ± 22	10	252 ± 22
223	ptakuratsatu-000	29	585434	233	1347	42	538 ± 0	239	875 ± 3	180	863 ± 48	172	928 ± 9	156	958 ± 17	146	1066 ± 26	247	5900 ± 103	245	5687 ± 167
224	pxl-001	112759507	78231	22	168	31	512 ± 0	12	101 ± 5	8	104 ± 5	11	189 ± 12	26	408 ± 27	199	1470 ± 144	244	5598 ± 45	244	5590 ± 68
225	pyramid-000	381551539	219883	145	804	244	2056 ± 0	128	583 ± 2	-	-	-	-	-	-	-	262	7147 ± 59	264	7586 ± 425	
226	quantasoft-003	379410922	211354	198	1058	114	2048 ± 0	155	632 ± 2	113	634 ± 0	96	632 ± 0	73	631 ± 1	56	634 ± 0	5	201 ± 7	4	203 ± 8
227	rankone-009	441	107688	341	8	260 ± 0	24	179 ± 4	-	-	-	-	-	-	-	-	67	710 ± 32	35	552 ± 25	
228	rankone-010	441	138435	11	83	9	261 ± 0	28	193 ± 1	-	-	-	-	-	-	-	11	282 ± 13	8	234 ± 16	
229	realnetworks-002	97616019	107088	48	370	80	1848 ± 0	38	250 ± 2	23	242 ± 4	19	282 ± 5	23	381 ± 10	90	774 ± 15	124	1285 ± 17	124	1247 ± 42
230	realnetworks-004	176471448	913988	290	2467	248	2056 ± 0	57	330 ± 4	37	333 ± 3	33	402 ± 7	61	585 ± 15	191	1402 ± 51	116	1210 ± 29	122	1202 ± 17
231	regula-000	268743079	29384	115	610	134	2048 ± 0	302	1187 ± 1	235	1126 ± 1	219	1129 ± 0	192	1132 ± 1	157	1159 ± 1	28	491 ± 16	31	500 ± 22
232	remarkai-001	247662347	868314	133	730	230	2052 ± 0	223	831 ± 6	173	849 ± 18	206	1055 ± 25	206	1198 ± 34	201	1519 ± 38	119	1229 ± 20	82	805 ± 56
233	remarkai-003	287249016	58559	311	3896	305	4100 ± 0	266	986 ± 1	207	993 ± 1	190	992 ± 1	166	999 ± 3	133	1019 ± 2	80	787 ± 20	80	793 ± 22
234	rendip-000	0	437653	128	682	105	2048 ± 0	87	464 ± 2	59	458 ± 0	51	473 ± 0	40	483 ± 1	43	556 ± 4	34	576 ± 13	38	573 ± 11
235	rokid-000	264818990	396624	218	1218	246	2056 ± 0	118	546 ± 3	85	542 ± 2	75	545 ± 1	50	522 ± 3	45	563 ± 4	217	3457 ± 62	220	3463 ± 77
236	rokid-001	656613085	413733	201	1071	259	2060 ± 0	246	911 ± 2	192	901 ± 5	162	899 ± 2	147	900 ± 3	113	901 ± 3	214	3345 ± 50	215	3346 ± 149
237	s1-001	445943780	844340	138	772	264	2092 ± 0	141	605 ± 24	107	623 ± 20	166	920 ± 39	245	1567 ± 92	-	-	131	1428 ± 34	130	1415 ± 85
238	s1-002	532647605	95479	235	1374	320	6144 ± 0	313	1257 ± 1	259	1260 ± 1	240	1261 ± 1	217	1262 ± 1	177	1273 ± 1	235	4513 ± 25	233	4479 ± 25
239	saffe-001	88036907	62488	24	168	71	1280 ± 0	47	281 ± 1	-	-	-	-	-	-	-	123	1274 ± 19	126	1277 ± 26	
240	saffe-002	266877685	28285	161	855	202	2048 ± 0	216	817 ± 11	163	805 ± 15	136	809 ± 19	121	815 ± 29	96	813 ± 23	68	717 ± 7	70	714 ± 29
241	samtech-001	294996593	219883	113	605	247	2056 ± 0	51	294 ± 3	-	-	-	-	-	-	-	265	7694 ± 59	265	7678 ± 91	
242	scanovate-001	263253470	328532	111	601	214	2048 ± 0	126	577 ± 24	94	577 ± 21	94	632 ± 27	114	770 ± 28	192	1404 ± 32	275	12054 ± 699	279	13795 ± 705
243	scanovate-002	263153867	457227	160	850	132	2048 ± 0	184	696 ± 32	133	713 ± 33	126	738 ± 28	116	779 ± 32	162	1172 ± 53	205	3021 ± 38	209	3120 ± 163
244	securifai-001	123178989	12456	247	1445	307	4104 ± 0	31	211 ± 1	17	211 ± 1	13	211 ± 1	11	211 ± 1	10	211 ± 1	142	1681 ± 29	143	1701 ± 25
245	securifai-002	203595986	13496	163	863	64	1032 ± 0	18	123 ± 0	11	123 ± 0	7	123 ± 0	6	123 ± 0	5	123 ± 0	46	615 ± 22	44	597 ± 19
246	sensetime-004	977575461	30733	325	7843	63	1028 ± 0	327	1437 ± 15	-	-	-	-	-	-	-	120	1239 ± 31	120	1171 ± 22	
247	sensetime-005	783721534	37673	320	6133	62	1028 ± 0	318	1361 ± 27	265	1304 ± 1	251	1319 ± 1	229	1360 ± 1	200	1514 ± 1	118	1223 ± 28	121	1184 ± 29
248	sertis-000	271945833	68770	58	427	162	2048 ± 0	196	754 ± 0	150	759 ± 0	131	764 ± 0	112	760 ± 0	86	763 ± 0	135	1497 ± 29	139	1582 ± 38
249	sertis-002	471849050	68929	239	1391	168	2048 ± 0	300	1181 ± 1	244	1178 ± 0	229	1183 ± 0	204	1187 ± 0	170	1221 ± 0	107	1086 ± 32	105	1076 ± 31
250	seventhSense-000	378726405	1561668	150	824	233	2052 ± 0	312	1250 ± 3	258	1257 ± 1	239	1261 ± 1	216	1259 ± 1	176	1272 ± 2	153	1800 ± 35	154	1787 ± 32
251	shaman-000	0	120033	83	507	281	4096 ± 0	163	653 ± 16	-	-	-	-	-	-	-	20	380 ± 25	22	379 ± 31	
252	shaman-001	0	174446	88	511	285	4096 ± 0	50	294 ± 2	-	-	-	-	-	-	-	54	635 ± 19	24	441 ± 25	
253	shu-002	748800469	148309	167	890	283	4096 ± 0	195	751 ± 2	152	769 ± 4	169	922 ± 4	240	1431 ± 9	247	3489 ± 47	330	2930763 ± 47355	330	2929759 ± 39149
254	shu-003	439065557	146940	87	511	90	2048 ± 0	217	820 ± 6	167	828 ± 3	175	941 ± 9	224	1308 ± 15	244	3045 ± 44	188	2506 ± 26	190	2512 ± 38
255	siat-002	498527179	7738	288	2434	232	2052 ± 0	127	579 ± 0	-	-	-	-	-	-	-	77	769 ± 13	76	750 ± 13	
256	siat-004	962624717	6984	310	3860	303	4100 ± 0	172	670 ± 0	120	671 ± 7	112	693 ± 10	106	742 ± 10	120	935 ± 17	229	4013 ± 45	226	3782 ± 173
257	sjtu-003	492334366	148243	96	538	190	2048 ± 0	219	821 ± 2	164	820 ± 2	170	923 ± 3	207	1201 ± 3	229	2373 ± 9	137	1560 ± 20	138	1560 ± 14
258	sjtu-004	2000146156	241108	295	2727	314	4608 ± 0	310	1236 ± 2	251	1209 ± 2	247	1294 ± 4	244	1554 ± 5	237	2738 ± 8	207	3057 ± 14	208	3070 ± 20
259	sktelecom-000	539783520	298496	230	1311	73	1536 ± 0	286	1110 ± 1	231	1113 ± 1	213	1114 ± 1	187	1120 ± 1	156	1155 ± 1	298	26583 ± 128	297	26508 ± 126
260	smilart-002	114509977	87805	37	263	52	1024 ± 0	23	176 ± 16	-	-	-	-	-	-	-	289	18784 ± 136	290	18795 ± 151	
261	smilart-003	68956056	91670	29	192	28	512 ± 0	25	180 ± 12	14	181 ± 10	21	313 ± 22	82	665 ± 49	225	2299 ± 196	128	1395 ± 74	101	1027 ± 66
262	sodec-000	856670801	13142	304	3186	299	4096 ± 0	279	1041 ± 2	217	1032 ± 1	200	1035 ± 1	174	1037 ± 2	145	1061 ± 2	151	1794 ± 37	151	1775 ± 23
263	stacu-000	900773557	624676	200	1064	288	4096 ± 0	213	813 ± 25	-	-	-	-	-	-	-	202	2979 ± 31	205	3007 ± 75	
264	starhybrid-001	102921306	289356	158	845	124	2048 ± 0	65	358 ± 82	43	355 ± 49	31	379 ± 58	24	401 ± 79	20	393 ± 67	104	1075 ± 51	106	1078 ± 53

Notes

- 1 The configuration size does not capture static data included in libraries.
- 2 The library size is the combined total of all files provided in the submission lib folder. These libraries e.g. OpenCV may or may not be installed on any end user's platform natively and would not need to be installed with the algorithm. Some developers put neural network models in their libraries.
- 3 The memory usage is the peak resident set size reported by the ps system call during template generation.
- 4 The median template creation times are measured on Intel®Xeon®CPU E5-2630 v4 @ 2.20GHz processors.
- 5 The comparison durations, in nanoseconds, are estimated using std::chrono::high_resolution_clock which on the machine in (2) counts 1ns clock ticks. Precision is somewhat worse than that however. The \pm value is the median absolute deviation times 1.48 for Normal consistency.

Table 11: Summary of algorithms and properties included in this report. The red superscripts give ranking for the quantity in that column.

	ALGORITHM	CONFIG	LIBRARY	TEMPLATE								COMPARISON ⁴		
	NAME	DATA	DATA	MEMORY	SIZE	GENERATION TIME (ms) ⁴				TIME (ns) ⁵				
		(KB) ¹	(KB) ²	(MB) ³	(B)	MUGSHOT	480x720	960x1440	1600x2400	3000x4500	GENUINE	IMPOSTOR		
265	suprema-000	252683488	38507	¹¹⁸ 625	¹¹³ 2048 ± 0	²⁰² 771 ± 2	¹⁵⁵ 778 ± 1	¹⁵⁰ 864 ± 2	¹⁸⁵ 1109 ± 2	²²⁰ 2150 ± 4	¹⁴⁴ 1690 ± 17	¹⁴⁴ 1688 ± 13		
266	supremaid-001	264389887	23479	⁹⁷ 541	⁹¹ 2048 ± 0	⁹¹ 479 ± 1	⁶⁴ 481 ± 0	⁵⁴ 481 ± 0	⁴³ 490 ± 0	³⁵ 522 ± 0	⁶⁴ 704 ± 19	⁶² 652 ± 19		
267	synesis-006	749508090	21817	²⁵² 1472	³⁰⁹ 4104 ± 0	¹²⁰ 549 ± 1	⁸⁸ 546 ± 1	⁷⁷ 552 ± 1	⁵⁸ 558 ± 2	⁵⁷ 639 ± 28	⁶³ 697 ± 32	⁶⁸ 688 ± 31		
268	synesis-007	1477592536	24145	²⁸⁹ 2443	²⁷³ 3080 ± 0	³⁰⁴ 1215 ± 5	²⁶⁰ 1268 ± 30	²⁴⁸ 1306 ± 67	²²³ 1311 ± 58	¹⁹⁵ 1423 ± 52	⁵⁹ 684 ± 32	⁶⁶ 686 ± 25		
269	synology-000	226326270	25809	⁶⁶ 453	¹⁷¹ 2048 ± 0	⁷³ 407 ± 14	⁶⁰ 415 ± 14	¹¹³ 694 ± 31	²³¹ 1396 ± 58	²⁵² 4568 ± 211	²⁹² 19720 ± 203	²⁹¹ 19767 ± 379		
270	synology-002	262874215	25943	⁷⁷ 488	¹²² 2048 ± 0	²⁴² 886 ± 4	¹⁸⁹ 892 ± 3	¹⁶⁷ 920 ± 2	¹⁶⁷ 1000 ± 5	¹⁷⁹ 1317 ± 12	¹³² 1466 ± 32	¹³⁵ 1496 ± 45		
271	sztu-000	346765308	15871	²²⁸ 1298	¹⁴⁵ 2048 ± 0	¹¹¹ 531 ± 0	⁸¹ 532 ± 0	⁶⁸ 533 ± 0	⁵¹ 537 ± 0	³⁹ 548 ± 0	³⁵ 585 ± 11	⁴¹ 592 ± 13		
272	sztu-001	346778532	15871	²²⁹ 1298	²⁰⁷ 2048 ± 0	¹¹⁴ 535 ± 0	⁸⁴ 537 ± 0	⁷¹ 538 ± 0	⁵³ 540 ± 0	⁴⁰ 553 ± 0	⁴⁰ 599 ± 10	⁴⁶ 598 ± 10		
273	tech5-004	2468118640	118858	²⁹⁶ 2733	¹² 321 ± 0	²³⁶ 872 ± 2	²³⁴ 1117 ± 164	²¹⁴ 1114 ± 182	¹⁹³ 1134 ± 179	¹³¹ 999 ± 44	³⁹ 597 ± 13	⁴⁰ 592 ± 16		
274	tech5-005	1207059515	120517	²⁴⁴ 1426	¹⁷ 512 ± 0	³¹⁴ 1272 ± 109	²¹⁹ 1038 ± 63	²⁰⁴ 1046 ± 39	¹⁸⁹ 1124 ± 38	¹⁸⁶ 1351 ± 44	¹⁹² 2573 ± 37	¹⁹³ 2545 ± 32		
275	tevian-005	943148300	16556	²⁰³ 1083	¹⁹⁹ 2048 ± 0	¹⁵⁶ 633 ± 21	¹²¹ 672 ± 25	¹³⁸ 818 ± 37	¹⁸⁶ 1117 ± 64	²²⁸ 2364 ± 121	³³ 568 ± 22	⁴⁹ 607 ± 35		
276	tevian-006	709112566	19339	¹⁸³ 954	¹⁶¹ 2048 ± 0	¹⁴³ 611 ± 1	¹¹⁷ 666 ± 41	¹⁰⁴ 661 ± 32	⁸³ 672 ± 37	⁷⁵ 723 ± 31	³⁶ 591 ± 19	³⁹ 573 ± 28		
277	tiger-003	436392290	560292	¹³¹ 708	²⁵³ 2056 ± 0	⁸⁶ 458 ± 21	-	-	-	-	¹⁶⁷ 2031 ± 35	¹⁶⁸ 2019 ± 38		
278	tiger-004	351095179	253683	²³¹ 1336	²³¹ 2052 ± 0	²⁰⁸ 798 ± 2	-	-	-	-	³⁷ 595 ± 5	⁴⁵ 598 ± 7		
279	tinkoff-001	281251860	389272	¹⁰⁹ 592	²¹⁶ 2048 ± 0	²⁹⁶ 1176 ± 3	²⁴⁵ 1179 ± 3	²²⁶ 1178 ± 3	²⁰⁰ 1169 ± 2	¹⁶⁵ 1203 ± 3	²³³ 4361 ± 74	²³¹ 4344 ± 75		
280	tongyi-005	1168078115	138919	²⁸³ 2121	²⁶³ 2089 ± 0	²¹ 165 ± 1	-	-	-	-	²⁹⁰ 18924 ± 65	²⁹² 20158 ± 103		
281	toshiba-002	833132802	114260	-	⁷⁸ 1560 ± 0	¹¹⁷ 541 ± 0	-	-	-	-	²²⁰ 3521 ± 369	¹⁸⁶ 2449 ± 124		
282	toshiba-003	1007744192	114264	²¹⁵ 1197	⁷⁷ 1560 ± 0	¹¹⁶ 540 ± 0	-	-	-	-	¹⁸⁵ 2390 ± 41	¹⁸⁵ 2407 ± 81		
283	trueface-001	261246666	186754	¹¹⁹ 638	¹⁶ 500 ± 0	⁷¹ 390 ± 1	-	-	-	-	⁵⁸ 676 ± 26	³⁶ 538 ± 50		
284	trueface-002	260042323	123116	⁷⁶ 486	⁸⁴ 2000 ± 0	⁶⁶ 360 ± 0	⁴⁴ 361 ± 0	³⁸ 423 ± 0	⁶³ 590 ± 1	-	³ 192 ± 14	³ 186 ± 19		
285	putupitech-000	11752256	17185	²³ 33	¹⁸⁰ 2048 ± 0	¹⁷ 122 ± 4	¹⁰ 120 ± 1	⁹ 142 ± 2	¹⁰ 196 ± 5	²¹ 411 ± 14	²⁹³ 23893 ± 406	²⁹⁵ 25279 ± 406		
286	twface-000	677617540	11782	²⁹³ 2610	¹⁷² 2048 ± 0	²³⁵ 871 ± 1	¹⁸³ 873 ± 1	¹⁵⁴ 873 ± 2	¹³⁹ 876 ± 2	¹¹² 898 ± 1	¹³⁶ 1504 ± 29	¹³⁶ 1510 ± 34		
287	ulsee-001	379412284	57261	-	¹¹⁸ 2048 ± 0	¹⁶⁵ 654 ± 2	-	-	-	-	²⁵² 6065 ± 94	²⁵³ 6228 ± 77		
288	uluface-002	72	480761	²⁰⁴ 1088	¹¹⁰ 2048 ± 0	²³⁸ 873 ± 42	¹⁷⁵ 855 ± 9	¹⁸³ 978 ± 24	²¹⁹ 1271 ± 40	²²⁶ 2333 ± 68	²⁹¹ 19207 ± 1114	²⁸⁷ 18501 ± 274		
289	uluface-003	99694042	529422	²²³ 1264	²⁷¹ 3072 ± 0	²⁶⁰ 965 ± 11	²⁰³ 968 ± 10	²¹⁰ 1087 ± 20	²³⁰ 1387 ± 36	²³³ 2469 ± 86	²⁹⁶ 26057 ± 195	²⁹⁹ 26863 ± 566		
290	upc-001	0	89914	²⁰² 1077	⁶⁷ 1052 ± 0	¹²¹ 551 ± 15	¹³¹ 703 ± 56	¹²³ 724 ± 51	¹⁰⁹ 751 ± 49	¹⁰⁷ 863 ± 33	²⁰³ 3114 ± 44	²¹² 3165 ± 97		
291	vcog-002	3306941103	118946	³⁰⁷ 3666	³³⁰ 61504 ± 5	⁶⁴ 357 ± 25	-	-	-	-	³²⁵ 296154 ± 3077	³²⁵ 296436 ± 4183		
292	vd-001	174349133	44058	³⁸ 281	²⁴¹ 2052 ± 0	⁵⁵ 316 ± 6	-	-	-	-	¹²¹ 1258 ± 38	¹¹⁷ 1148 ± 109		
293	vd-002	260606257	34389	¹²⁸ 688	³⁷ 516 ± 0	¹⁸⁰ 684 ± 5	¹²³ 679 ± 4	¹⁰⁶ 676 ± 5	⁸⁹ 693 ± 5	⁸² 754 ± 5	¹² 300 ± 14	¹⁴ 319 ± 32		
294	veridas-004	201303428	160684	⁷¹ 472	¹⁸⁸ 2048 ± 0	¹⁷⁶ 678 ± 22	¹⁴⁷ 749 ± 27	²⁶⁶ 1470 ± 52	²⁷² 3228 ± 95	²⁶⁸ 10349 ± 273	²⁴² 5516 ± 42	²⁶³ 7425 ± 130		
295	veridas-006	364205776	896424	²⁸⁰ 1990	¹²¹ 2048 ± 0	²⁴¹ 880 ± 8	¹⁸⁷ 885 ± 8	²⁴¹ 1271 ± 18	²⁶⁴ 2242 ± 38	²⁶¹ 6414 ± 156	³¹² 56940 ± 149	³¹³ 66077 ± 194		
296	via-000	127408592	11151	¹⁸⁵ 964	¹⁶⁷ 2048 ± 0	¹⁸⁷ 707 ± 8	¹⁴⁵ 740 ± 5	¹⁶⁴ 906 ± 41	¹⁵¹ 941 ± 40	¹³⁷ 1040 ± 5	⁹² 966 ± 28	¹⁰⁰ 1021 ± 44		
297	via-001	379141776	11151	²⁶³ 1697	²⁰⁶ 2048 ± 0	²⁵⁹ 964 ± 3	²¹⁰ 1011 ± 3	¹⁹⁵ 1026 ± 4	¹⁷⁸ 1045 ± 3	¹⁵³ 1137 ± 28	⁹⁴ 983 ± 31	⁹⁶ 989 ± 40		
298	videmo-000	142994889	39470	⁵⁰ 390	¹⁴⁸ 2048 ± 0	¹⁹ 142 ± 5	¹² 150 ± 4	¹⁰ 150 ± 6	⁸ 151 ± 4	⁷ 155 ± 8	³⁰ 513 ± 16	³² 523 ± 38		
299	videonetics-001	31616555	5963	⁴ 61	¹⁸ 512 ± 0	⁴¹ 262 ± 3	²⁹ 273 ± 1	⁴⁴ 439 ± 3	¹²⁷ 820 ± 3	²³⁰ 2393 ± 43	¹¹⁴ 1153 ± 38	¹¹⁶ 1142 ± 65		
300	videonetics-002	124908941	6289	¹⁶ 115	²³⁸ 2052 ± 0	⁴⁸ 282 ± 5	³⁴ 295 ± 1	⁶⁵ 513 ± 4	¹⁷¹ 1029 ± 3	²⁴⁶ 3151 ± 46	¹¹⁷ 1219 ± 57	¹²⁵ 1262 ± 56		
301	vigilantsolutions-009	357169885	49973	¹⁵⁵ 840	⁷⁶ 1548 ± 0	¹⁴⁸ 615 ± 0	¹¹¹ 631 ± 0	⁹³ 632 ± 1	⁷⁴ 636 ± 0	⁶⁰ 659 ± 0	²² 452 ± 11	²⁵ 431 ± 11		
302	vigilantsolutions-010	357169886	49973	¹⁵⁶ 840	⁷⁵ 1548 ± 0	¹⁴⁹ 615 ± 0	¹¹⁰ 631 ± 0	⁹⁵ 632 ± 0	⁷⁵ 636 ± 0	⁶¹ 659 ± 0	²⁷ 490 ± 13	³⁰ 488 ± 11		
303	vinai-000	412049069	866522	¹⁹⁵ 1032	²¹¹ 2048 ± 0	²⁸⁴ 1099 ± 1	²²⁸ 1095 ± 1	²¹² 1093 ± 1	¹⁸⁴ 1099 ± 1	¹⁵¹ 1126 ± 1	²⁰³ 2996 ± 20	²⁰⁴ 2993 ± 26		
304	vion-000	233696726	7533	⁸ 498	²³⁷ 2052 ± 0	⁵⁸ 333 ± 1	-	-	-	-	³⁰³ 39839 ± 3561	²⁹⁸ 26830 ± 2241		
305	visage-000	50400173	70150	⁶ 73	²⁰ 512 ± 0	³ 27 ± 0	¹ 27 ± 0	¹ 31 ± 0	² 38 ± 0	² 63 ± 0	¹⁷⁷ 2220 ± 14	¹⁷⁸ 2218 ± 14		
306	visionbox-001	263034670	190645	¹⁰⁷ 579	¹⁴¹ 2048 ± 0	²⁶⁴ 983 ± 7	²²⁷ 1093 ± 46	²⁵⁵ 1360 ± 68	²⁶² 2181 ± 105	²⁵⁹ 5955 ± 281	¹¹⁵ 1161 ± 22	¹¹⁸ 1154 ± 20		
307	visionbox-002	265280900	135281	¹¹⁶ 612	²⁵⁷ 2059 ± 0	⁹³ 482 ± 1	⁶⁶ 482 ± 0	⁵⁵ 484 ± 1	⁴⁵ 492 ± 1	³³ 517 ± 3	¹⁶⁶ 1969 ± 44	¹⁶⁴ 1931 ± 42		
308	visionlabs-009	723046025	19862	⁶⁴ 444	³⁴ 513 ± 0	¹⁰⁶ 515 ± 41	⁶² 472 ± 1	⁵² 474 ± 1	³⁹ 476 ± 1	³⁴ 521 ± 1	⁹¹ 957 ± 28	⁹² 965 ± 32		

Notes

1 The configuration size does not capture static data included in libraries.

2 The library size is the combined total of all files provided in the submission lib folder. These libraries e.g. OpenCV may or may not be installed on any end user's platform natively and would not need to be installed with the algorithm. Some developers put neural network models in their libraries.

3 The memory usage is the peak resident set size reported by the ps system call during template generation.

4 The median template creation times are measured on Intel®Xeon®CPU E5-2630 v4 @ 2.20GHz processors.

5 The comparison durations, in nanoseconds, are estimated using std::chrono::high_resolution_clock which on the machine in (2) counts 1ns clock ticks. Precision is somewhat worse than that however. The ± value is the median absolute deviation times 1.48 for Normal consistency.

	ALGORITHM	CONFIG	LIBRARY	TEMPLATE								COMPARISON ⁴									
				NAME	DATA	DATA	MEMORY	SIZE	GENERATION TIME (ms) ⁴				TIME (ns) ⁵								
									(KB) ¹	(KB) ²	(MB) ³	(B)	MUGSHOT	480x720	960x1440	1600x2400	3000x4500	GENUINE	IMPOSTOR		
309	visionlabs-010	1092895531	19357	169	902	35	513 ± 0	191	730 ± 0	137	717 ± 1	120	709 ± 0	97	713 ± 1	79	739 ± 0	41	600 ± 41	54	626 ± 35
310	visteam-000	33514713	17740	12	83	74	1536 ± 0	96	± 7	7	102 ± 8	27	358 ± 19	170	1022 ± 50	249	3987 ± 211	255	6361 ± 87	255	6668 ± 277
311	visteam-001	190915457	30878	55	410	291	4096 ± 0	234	869 ± 7	182	872 ± 6	217	1121 ± 15	250	1719 ± 38	251	4375 ± 157	260	7054 ± 108	259	7025 ± 109
312	vnpt-001	272895047	535529	49	384	166	2048 ± 0	99	499 ± 2	74	499 ± 2	58	494 ± 3	46	502 ± 3	28	512 ± 2	168	2049 ± 29	19	337 ± 121
313	vnpt-002	278169517	3203296	78	489	194	2048 ± 0	192	739 ± 2	141	731 ± 2	127	740 ± 1	105	742 ± 2	89	763 ± 2	76	766 ± 13	77	762 ± 13
314	vocord-008	618359916	345047	255	1559	269	2688 ± 0	258	962 ± 2	205	976 ± 2	207	1061 ± 3	212	1236 ± 23	216	1851 ± 9	204	3015 ± 50	203	2988 ± 62
315	vocord-009	1413255249	201560	316	4162	81	1920 ± 0	329	1472 ± 2	276	1472 ± 1	269	1549 ± 1	248	1667 ± 2	219	2064 ± 2	169	2052 ± 50	171	2056 ± 39
316	vts-000	262747358	169760	264	1704	136	2048 ± 0	96	486 ± 1	65	481 ± 0	41	485 ± 1	32	517 ± 0	318	124209 ± 352	318	123652 ± 358		
317	winsense-001	270774312	32035	176	922	70	1280 ± 0	200	766 ± 7	222	1058 ± 47	186	983 ± 97	179	1053 ± 119	180	1320 ± 84	139	1631 ± 28	167	1964 ± 171
318	winsense-002	288132712	25780	267	1781	150	2048 ± 0	98	494 ± 2	73	498 ± 1	66	519 ± 1	52	537 ± 1	55	634 ± 1	143	1683 ± 8	143	1685 ± 7
319	x-laboratory-000	532501437	197310	254	1524	251	2056 ± 0	210	808 ± 7	191	897 ± 113	165	907 ± 103	143	886 ± 103	65	673 ± 39	69	725 ± 19	75	749 ± 34
320	x-laboratory-001	640144084	398792	271	1844	254	2056 ± 0	130	586 ± 2	101	596 ± 5	85	603 ± 6	71	620 ± 7	91	793 ± 14	82	813 ± 28	86	872 ± 32
321	xforwardai-001	348262545	51163	284	2173	99	2048 ± 0	299	1180 ± 2	249	1182 ± 1	232	1194 ± 1	203	1186 ± 2	166	1203 ± 1	79	779 ± 17	81	797 ± 13
322	xforwardai-002	724700382	51163	279	1989	295	4096 ± 0	253	944 ± 1	-	-	-	-	-	-	-	130	1406 ± 8	129	1405 ± 13	
323	xm-000	591914905	148920	127	688	236	2052 ± 0	240	878 ± 2	185	882 ± 1	188	988 ± 2	215	1258 ± 3	232	2434 ± 7	140	1634 ± 17	140	1632 ± 20
324	yisheng-004	498023846	38653	226	1279	276	3704 ± 0	67	378 ± 12	-	-	-	-	-	-	62	693 ± 137	33	526 ± 34		
325	ytu-003	1562336990	138919	308	3737	262	2082 ± 0	231	860 ± 0	-	-	-	-	-	-	286	18305 ± 71	286	18286 ± 62		
326	yoonik-000	297384719	206059	153	836	181	2048 ± 0	251	941 ± 3	202	965 ± 13	181	964 ± 10	158	964 ± 9	126	974 ± 23	112	1116 ± 34	114	1113 ± 54
327	yoonik-001	354948637	265353	282	2192	200	2048 ± 0	308	1223 ± 3	257	1238 ± 1	237	1238 ± 1	213	1240 ± 1	65	706 ± 29	69	690 ± 26		
328	ytu-000	1512817409	44032	291	2484	210	2048 ± 0	109	530 ± 0	82	533 ± 0	99	640 ± 0	135	861 ± 2	217	1949 ± 8	300	31797 ± 131	301	31794 ± 133
329	yuan-001	379364823	189558	300	2829	212	2048 ± 0	320	1383 ± 3	269	1394 ± 3	260	1408 ± 3	241	1461 ± 4	205	1615 ± 4	184	2344 ± 25	184	2325 ± 42
330	yuan-002	379363758	165662	301	2838	159	2048 ± 0	326	1420 ± 3	273	1429 ± 4	268	1511 ± 4	249	1695 ± 4	231	2408 ± 5	183	2297 ± 23	183	2310 ± 31

Notes

- 1 The configuration size does not capture static data included in libraries.
- 2 The library size is the combined total of all files provided in the submission lib folder. These libraries e.g. OpenCV may or may not be installed on any end user's platform natively and would not need to be installed with the algorithm. Some developers put neural network models in their libraries.
- 3 The memory usage is the peak resident set size reported by the ps system call during template generation.
- 4 The median template creation times are measured on Intel®Xeon®CPU E5-2630 v4 @ 2.20GHz processors.
- 5 The comparison durations, in nanoseconds, are estimated using std::chrono::high_resolution_clock which on the machine in (2) counts 1ns clock ticks. Precision is somewhat worse than that however. The ± value is the median absolute deviation times 1.48 for Normal consistency.

Table 13: Summary of algorithms and properties included in this report. The red superscripts give ranking for the quantity in that column.

Algorithm	FALSE NON-MATCH RATE (FNMR)																		
	CONSTRAINED, COOPERATIVE										LESS CONSTRAINED, NON-COOP.								
	Name	ViSAMC	VISA	MUGSHOT	MUGSHOT12+YRS	VISABORDER	BORDER	BORDER	WILD	CHILDEXP									
	FMR	0.0001	1E-06	1E-05	1E-05	1E-06	1E-06	1E-05	0.0001	0.01									
1	20face-000	0.1268	275	0.1828	274	0.1748	280	0.2768	280	0.1765	268	0.1864	226	0.0927	250	0.0405	187	-	
2	3divi-005	0.0094	148	0.0151	155	0.0078	135	0.0121	134	0.0135	134	0.0231	120	0.0156	137	0.0351	171	-	
3	3divi-006	0.0064	98	0.0094	94	0.0047	76	0.0066	75	0.0091	86	0.0191	98	0.0113	91	0.0289	91	-	
4	acer-000	0.1393	278	0.9075	320	0.9981	320	-		1.0000	317	1.0000	309	0.9998	313	0.9841	317	-	
5	acer-001	0.0294	243	0.0504	248	0.0240	239	0.0463	242	0.0436	236	0.0622	191	0.0360	213	0.0307	126	-	
6	acisw-003	0.9682	327	0.9971	327	0.7892	315	0.8738	313	0.8752	307	0.8275	283	0.6698	299	0.4470	298	-	
7	acisw-006	0.2945	292	0.9788	325	0.6044	303	-		0.9900	311	1.0000	310	0.9999	315	1.0000	329	-	
8	adera-002	0.0052	67	0.0071	62	0.0047	74	0.0064	70	0.0087	79	0.0159	77	0.0136	113	0.0990	244	-	
9	adera-003	0.0043	50	0.0059	48	0.0036	43	0.0043	31	0.0076	66	0.0151	71	0.0128	106	0.0989	243	-	
10	advance-002	0.0089	138	0.0137	140	0.0073	126	0.0115	130	0.0400	229	0.0722	199	0.0593	235	0.0498	210	-	
11	aifirst-001	0.0119	178	0.0170	170	0.0084	149	0.0127	144	0.0131	131	0.0212	108	0.0138	116	0.0432	195	0.4301	11
12	aigen-001	0.0124	183	0.0219	193	0.0143	209	0.0217	205	0.0236	202	0.8960	286	0.3255	275	0.0681	229	-	
13	aigen-002	0.0192	225	0.0343	226	0.0256	241	0.0402	237	0.0389	228	0.9196	289	0.3876	281	0.1096	252	-	
14	ailabs-001	0.0158	210	0.0276	220	0.0192	229	0.0317	228	0.0352	223	0.0608	187	0.0434	221	0.0338	160	-	
15	aimall-002	0.0119	179	0.0167	168	0.0224	235	0.0411	239	0.0233	197	0.0373	167	0.0235	188	0.0327	151	-	
16	aimall-003	0.0033	35	0.0041	26	0.0033	35	0.0035	21	0.0056	41	0.0109	44	0.0087	58	0.0312	135	-	
17	aiunionface-000	0.0104	160	0.0154	159	0.0082	147	0.0122	135	0.0141	142	0.0243	124	0.0169	145	0.0306	123	-	
18	aize-001	0.0223	232	0.0344	227	0.0199	230	0.0313	226	0.0367	224	0.0522	180	0.0359	212	0.0446	200	-	
19	ajou-001	0.0093	146	0.0147	151	0.0071	124	0.0126	139	0.0173	174	0.0274	136	0.0186	157	0.0348	166	-	
20	alchera-002	0.0107	165	0.0157	161	0.0104	177	0.0229	207	0.0144	147	0.0246	125	0.0198	170	0.0328	153	-	
21	alchera-003	0.0044	52	0.0055	46	0.0031	25	0.0039	27	0.0042	14	0.0077	12	0.0065	14	0.0339	162	-	
22	alice-000	0.0119	180	0.0192	180	0.0106	180	0.0170	182	0.0167	168	0.0265	133	0.0150	131	0.0288	84	-	
23	alleyes-000	0.0058	80	0.0090	91	0.0055	88	0.0087	106	0.0068	60	0.0105	41	0.0076	35	0.0282	58	-	
24	allgovision-000	0.0346	250	0.0527	250	0.0232	237	0.0339	229	0.0372	227	0.0620	190	0.0443	223	0.0607	224	-	
25	alphaface-001	0.0065	102	0.0097	100	0.0039	51	0.0063	69	0.0083	74	-	-	-	0.0280	44	-		
26	alphaface-002	0.0052	68	0.0075	69	0.0030	18	0.0044	32	1.0000	320	0.0115	50	0.0084	53	0.0279	37	-	
27	amplifiedgroup-001	0.5034	312	0.5848	307	0.6973	310	0.8316	308	0.7807	299	0.7724	276	0.6354	295	0.4250	296	-	
28	androvideo-000	0.0243	236	0.0438	241	0.0239	238	0.0365	236	0.0483	240	0.1870	227	0.0635	238	0.1163	255	-	
29	anke-004	0.0080	128	0.0154	158	0.0073	125	0.0112	128	0.0102	105	0.0178	91	0.0118	97	0.0288	85	0.3577	6
30	anke-005	0.0070	110	0.0109	118	0.0059	99	0.0094	109	0.0105	108	0.0142	61	0.0102	77	0.0289	89	0.3337	4
31	antheus-000	0.2564	288	0.3776	290	0.7240	311	0.8699	311	0.8899	308	0.9872	293	0.9483	305	0.7668	310	0.9233	55
32	antheus-001	0.1311	276	0.2306	279	0.5113	296	0.6797	296	0.8748	306	0.9908	294	0.9649	309	0.7586	309	-	
33	anyvision-004	0.0267	241	0.0385	236	0.0258	242	0.0487	244	0.0234	200	0.0301	145	0.0191	162	0.0470	204	0.4633	12
34	anyvision-005	0.0023	17	0.0037	18	0.0027	16	0.0035	20	0.0049	27	0.0084	18	0.0069	21	0.0285	70	-	
35	asusaics-000	0.0125	188	0.0209	187	0.0085	150	0.0134	151	0.0143	145	0.7189	270	0.0285	203	0.0295	105	-	
36	asusaics-001	0.0125	187	0.0210	188	0.0085	152	0.0134	152	0.0143	146	0.7437	273	0.0289	204	0.0295	104	-	
37	authenmetric-002	0.0092	144	0.0134	139	0.0095	168	0.0177	185	0.0192	184	0.0463	176	0.0236	189	0.0306	125	-	
38	aware-005	0.0457	257	0.0643	254	0.0603	264	0.1094	264	0.0613	247	0.1075	217	0.0491	225	0.0314	138	-	
39	aware-006	0.0487	259	0.0819	263	0.0529	260	0.1090	263	0.1011	262	0.1058	213	0.0502	227	0.0317	140	-	
40	awiros-001	0.4044	301	0.4622	297	0.5530	298	0.6518	295	0.2008	271	0.1994	230	0.1386	259	0.5584	307	-	
41	awiros-002	0.1990	283	0.2561	281	0.3319	287	0.4411	287	0.3821	285	0.9938	296	0.2634	269	0.0997	245	-	
42	ayftech-001	0.0946	272	0.1941	275	0.2438	283	0.3625	282	0.1558	266	0.1589	222	0.0936	251	0.0785	237	-	
43	ayonix-000	0.4351	305	0.4872	298	0.6150	305	0.7510	303	0.6557	293	0.6361	262	0.4981	288	0.3635	293	0.8434	49
44	beethedata-000	0.0127	189	0.0195	181	0.0092	162	0.0157	173	0.0171	171	0.0306	146	0.0204	173	0.0285	71	-	

Table 14: FNMR is the proportion of mated comparisons below a threshold set to achieve the FMR given in the header on the fourth row. FMR is the proportion of impostor comparisons at or above that threshold. The light grey values give rank over all algorithms in that column. The pink columns use only same-sex impostors; others are selected regardless of demographics. The exception, in the green column, uses “matched-covariates” i.e. impostors of the same sex, age group, and country of birth. The second pink column includes effects of extended ageing. Missing entries for border, visa, mugshot and wild images generally mean the algorithm did not run to completion. For child exploitation, missing entries arise because NIST executes those runs only infrequently. The VISA columns compare images described in section 2.2. The MUGSHOT columns compare images described in section 2.5. The VISA-BORDER column compare images described in section 2.3 with those of section 2.4. The BORDER column compares images described in section 2.4. The WILD columns compare images described in section 2.6. The CHILD-EXPLOITATION columns compare images described in section 2.1.

		FALSE NON-MATCH RATE (FNMR)																	
	Algorithm	CONSTRAINED, COOPERATIVE								LESS CONSTRAINED, NON-COOP.									
	Name	VISAMC	VISA	MUGSHOT	MUGSHOT12+YRS	VISABORDER	BORDER	BORDER	WILD	CHILDEXP									
	FMR	0.0001	1E-06	1E-05	1E-05	1E-06	1E-06	1E-06	0.0001	0.01									
45	bioditechswiss-001	0.0054	70	0.0072	63	0.0069	119	0.0124	138	0.0060	47	0.0094	26	0.0065	16	0.0313	136	-	
46	bioditechswiss-002	0.0049	58	0.0067	59	0.0064	109	0.0116	131	0.0067	59	0.0117	51	0.0086	56	0.0279	30	-	
47	bm-001	0.7431	319	0.9494	323	0.9586	316	0.9843	314	0.9049	309	0.9021	288	0.8395	302	0.9935	319	0.8845	52
48	boetech-001	0.0662	266	0.0802	262	0.0493	256	0.0791	254	0.0682	251	0.1074	216	0.0758	246	0.1719	267	-	
49	bresee-001	0.0085	134	0.0143	145	0.0086	156	0.0153	170	0.0108	112	0.0168	84	0.0115	95	0.0355	175	-	
50	bresee-002	0.0079	127	0.0101	110	0.0065	113	0.0079	90	0.0129	128	0.0263	131	0.0224	182	0.0327	152	-	
51	camvi-002	0.0125	186	0.0221	196	0.0089	160	0.0145	164	0.0142	143	0.2650	239	0.0166	144	0.0288	82	0.5760	23
52	camvi-004	0.0171	215	0.0316	222	0.0042	59	0.0049	42	0.0097	101	0.6636	265	0.0141	120	0.0284	65	0.5788	24
53	canon-002	0.0034	37	0.0050	38	0.0026	11	0.0033	18	0.0043	17	0.0182	92	0.0065	15	0.0279	34	-	
54	ceiec-003	0.0071	112	0.0107	116	0.0061	105	0.0079	91	0.0160	160	0.0316	148	0.0260	198	0.0308	131	-	
55	ceiec-004	0.0038	42	0.0051	39	0.0045	72	0.0053	49	0.0062	52	0.3939	247	0.0104	82	0.0325	148	-	
56	chosun-001	0.0525	261	0.0936	265	0.0742	268	0.1263	268	0.0978	261	1.0000	315	0.9354	304	0.4446	297	-	
57	chosun-002	0.0390	253	0.0646	255	0.0339	249	0.0576	249	0.0455	238	0.6904	267	0.1746	263	0.0696	232	-	
58	chtface-002	0.0150	205	0.0268	216	0.0096	171	0.0140	157	0.0186	180	0.0320	150	0.0194	166	0.0306	124	-	
59	chtface-003	0.0091	140	0.0146	150	0.0083	148	0.0128	146	0.0132	132	0.0220	115	0.0149	129	0.0301	115	-	
60	canon-001	0.0041	48	0.0061	52	0.0030	23	0.0041	29	0.0048	26	0.0578	183	0.0069	22	0.0279	31	-	
61	closeli-001	0.0136	194	0.0163	163	0.0039	52	0.0054	51	0.0072	65	1.0000	311	0.0094	69	0.0318	141	-	
62	cloudwalk-hr-003	0.0026	22	0.0041	27	0.0040	55	0.0058	58	0.0060	50	0.9992	303	0.0094	66	0.7206	308	-	
63	cloudwalk-hr-004	0.0009	1	0.0018	2	0.0034	36	0.0028	9	0.0052	32	0.9992	304	0.0093	65	0.1625	266	-	
64	cloudwalk-mt-002	0.0064	100	0.0085	84	0.0054	87	0.0098	116	0.0070	63	0.0108	43	0.0076	34	0.0283	63	-	
65	cloudwalk-mt-003	0.0013	2	0.0022	3	0.0026	8	0.0027	5	0.0039	8	0.0076	8	0.0067	18	0.0347	164	-	
66	clova-000	0.0099	154	0.0150	152	0.0094	166	0.0147	166	0.0136	136	0.0213	110	0.0152	134	0.0307	127	-	
67	cogent-004	0.0064	101	0.0116	127	0.0096	170	0.0134	153	0.0157	157	0.0325	152	0.0204	172	0.0379	181	0.7177	38
68	cogent-005	0.0060	90	0.0112	122	0.0064	111	0.0070	77	0.0095	97	0.0184	94	0.0135	109	0.0423	193	-	
69	cognitec-000	0.0116	173	0.0177	174	0.0118	199	0.0167	181	0.0285	215	0.9924	295	0.0435	222	0.0953	242	0.8365	48
70	cognitec-002	0.0066	103	0.0101	109	0.0079	138	0.0108	125	0.0181	176	0.0317	149	0.0237	190	0.0372	179	-	
71	cor-001	0.0075	120	0.0113	126	0.0055	90	0.0084	97	0.0091	88	0.0148	66	0.0092	64	0.0277	26	-	
72	coretech-000	0.7699	322	1.0000	330	1.0000	331	-	1.0000	330	1.0000	325	1.0000	328	1.0000	332	-		
73	corsight-001	0.0040	47	0.0057	47	0.0033	34	0.0047	36	0.0045	18	0.0095	29	0.0063	12	0.0276	17	-	
74	csc-001	0.9158	323	0.9346	321	0.9899	317	-	0.9999	315	0.9959	298	0.9906	311	0.8678	313	-		
75	csc-002	0.0099	156	0.0132	137	0.0077	132	0.0142	161	0.0126	126	0.0195	100	0.0146	125	0.1779	269	-	
76	ctbcbank-000	0.0168	212	0.0250	210	0.0146	212	0.0224	206	0.0211	191	0.8964	287	0.3779	280	1.0000	324	0.8803	51
77	ctbcbank-001	0.0155	208	0.0235	203	0.0148	217	0.0243	212	0.0207	188	0.9279	290	0.3469	277	1.0000	328	-	
78	cubox-001	0.0064	97	0.0080	78	0.0037	45	0.0055	54	0.0060	48	0.0111	45	0.0077	37	0.0300	112	-	
79	cuhkee-001	0.0036	38	0.0045	33	0.0031	28	0.0046	34	0.0051	31	0.0095	30	0.0079	41	0.1492	263	-	
80	cybercore-000	0.0728	268	0.1110	268	0.1521	278	0.2375	276	0.1874	270	0.1907	228	0.1178	256	0.1191	258	-	
81	cyberextruder-001	0.1972	281	0.2547	280	0.4686	295	0.6387	294	0.3807	284	0.3806	246	0.2582	266	0.1747	268	0.7804	47
82	cyberextruder-002	0.0811	270	0.1336	270	0.1465	277	0.2266	275	0.2086	274	1.0000	321	1.0000	330	0.1000	246	0.6105	26
83	cyberlink-006	0.0042	49	0.0054	44	0.0043	62	0.0049	40	0.0052	35	0.0097	32	0.0077	38	0.0278	27	-	
84	cyberlink-007	0.0032	33	0.0053	41	0.0041	57	0.0043	30	0.0052	34	0.0243	123	0.0084	54	0.0280	42	-	
85	dahua-005	0.0031	31	0.0046	34	0.0035	40	0.0049	43	0.0046	20	0.0076	9	0.0062	11	0.0277	23	-	
86	dahua-006	0.0027	24	0.0039	22	0.0031	27	0.0039	28	0.0039	9	0.0067	6	0.0058	7	0.0280	39	-	
87	decatur-000	0.0714	267	0.1115	269	0.0608	265	0.1106	265	0.0866	256	1.0000	313	0.0714	243	0.0658	227	-	
88	deepglint-002	0.0016	8	0.0027	12	0.0032	29	0.0033	19	0.0043	16	0.0084	19	0.0077	36	0.0280	43	0.3422	5

Table 15: FNMR is the proportion of mated comparisons below a threshold set to achieve the FMR given in the header on the fourth row. FMR is the proportion of impostor comparisons at or above that threshold. The light grey values give rank over all algorithms in that column. The pink columns use only same-sex impostors; others are selected regardless of demographics. The exception, in the green column, uses “matched-covariates” i.e. impostors of the same sex, age group, and country of birth. The second pink column includes effects of extended ageing. Missing entries for border, visa, mugshot and wild images generally mean the algorithm did not run to completion. For child exploitation, missing entries arise because NIST executes those runs only infrequently. The VISA columns compare images described in section 2.2. The MUGSHOT columns compare images described in section 2.5. The VISA-BORDER column compare images described in section 2.3 with those of section 2.4. The BORDER column compares images described in section 2.4. The WILD columns compare images described in section 2.6. The CHILD-EXPLOITATION columns compare images described in section 2.1.

Algorithm	FALSE NON-MATCH RATE (FNMR)											
	CONSTRAINED, COOPERATIVE											
	Name	ViSAMC	VISA	MUGSHOT	MUGSHOT12+YRS	VISABORDER	BORDER	BORDER	WILD	CHILDEXP		
FMR	0.0001	1E-06	1E-05	1E-05	1E-06	1E-06	1E-06	1E-05	0.0001	0.01		
89 deepglint-003	0.0027	25	0.0038	19	0.0030	21	0.0032	17	0.0043	15	0.0082	17
90 deepsea-001	0.0136	195	0.0215	190	0.0142	208	0.0214	204	0.0163	164	0.0250	126
91 depsense-000	0.0145	201	0.0265	215	0.0113	193	0.0196	197	0.0151	150	0.0215	112
92 dermalog-006	0.0253	239	0.0369	233	0.0171	224	0.0283	222	0.0217	192	0.0358	162
93 dermalog-008	0.0096	152	0.0166	167	0.0086	154	0.0133	150	0.0165	166	0.0586	186
94 didiglobalface-001	0.0055	74	0.0092	92	0.0030	19	0.0045	33	0.0088	81	0.0119	54
95 digitalbarriers-002	0.3360	297	0.3690	288	0.0877	271	0.1557	269	0.0971	260	0.0951	209
96 dps-000	0.0115	171	0.0176	173	0.0149	219	0.0185	192	0.0173	173	0.0275	138
97 dsk-000	0.1526	279	0.2169	277	0.3787	290	0.5426	291	0.3115	277	0.3089	241
98 einetworks-000	0.0099	155	0.0180	176	0.0088	159	0.0140	159	0.0130	130	0.0225	118
99 ekin-002	0.1168	274	0.2042	276	0.1530	279	0.2524	278	0.1777	269	0.2773	240
100 enface-000	0.0028	27	0.0049	37	0.0043	66	0.0072	78	0.0058	46	0.0150	69
101 eocortex-000	0.3485	298	0.6943	313	0.1122	274	0.1574	270	0.2155	275	0.2257	235
102 ercacat-001	0.0036	39	0.0044	31	0.0033	32	0.0047	37	0.0106	109	0.0202	104
103 expasoft-001	0.0328	249	0.0488	246	0.0211	233	0.0342	231	0.0629	249	0.6483	263
104 expasoft-002	0.0170	213	0.0274	218	0.0787	269	0.0768	253	0.1629	267	0.9996	305
105 f8-001	0.0249	238	0.0336	224	0.0178	226	0.0232	208	0.0303	219	0.0615	189
106 facesoft-000	0.0085	135	0.0112	124	0.0064	110	0.0107	124	0.0091	87	0.0171	87
107 facetag-000	0.2836	289	0.4081	294	0.2933	285	0.4303	285	0.3448	280	0.6312	261
108 facex-001	1.0000	331	1.0000	332	1.0000	324	-	1.0000	327	1.0000	317	1.0000
109 farfaces-001	0.4890	311	0.5860	308	0.5650	299	0.7268	300	0.8015	301	0.7511	274
110 fiberhome-nanjing-002	0.0217	231	0.0381	235	0.0874	270	0.1770	272	0.0271	210	0.0351	161
111 fiberhome-nanjing-003	0.0090	139	0.0139	143	0.0082	146	0.0144	162	0.0110	116	0.0174	88
112 fincore-000	0.0309	246	0.0502	247	0.0281	245	0.0510	246	0.0521	242	0.0815	202
113 fujitsulab-002	0.0091	143	0.0124	131	0.0105	178	0.0156	172	0.0169	170	0.0345	159
114 fujitsulab-003	0.0045	55	0.0065	57	0.0057	96	0.0083	95	0.0080	70	0.0154	74
115 geo-001	0.0180	220	0.0198	182	0.0037	46	0.0055	53	0.0070	61	0.0129	58
116 geo-002	0.0171	216	0.0187	179	0.0035	39	0.0051	48	0.0064	54	0.0117	52
117 glory-002	0.0241	234	0.0311	221	0.0116	197	0.0151	169	0.0157	158	0.0264	132
118 glory-003	0.0076	123	0.0125	134	0.0077	134	0.0103	121	0.0130	129	0.0205	105
119 gorilla-006	0.0105	164	0.0152	156	0.0106	179	0.0203	200	0.0155	153	0.0218	114
120 gorilla-007	0.0074	118	0.0111	120	0.0065	114	0.0126	140	0.0100	104	0.0151	70
121 hertasecurity-000	0.0630	264	0.0780	261	0.0503	258	0.0898	257	0.0738	252	0.0693	198
122 hik-001	0.0096	151	0.0125	132	0.0093	165	0.0164	179	0.0108	113	0.0937	207
123 hyperverge-001	1.0000	329	1.0000	329	1.0000	327	-	1.0000	322	1.0000	326	1.0000
124 hyperverge-002	0.0050	60	0.0066	58	0.0035	38	0.0051	45	0.0062	51	0.0107	42
125 icm-002	0.0143	198	0.0249	209	0.0144	210	0.0256	214	0.0236	204	0.0386	170
126 icthtc-000	0.0260	240	0.0396	237	0.0207	232	0.0339	230	0.0291	216	0.0474	177
127 id3-006	0.0072	116	0.0103	112	0.0049	79	0.0074	84	0.0095	96	0.0165	82
128 id3-007	0.0056	76	0.0078	73	0.0060	103	0.0072	80	0.0275	212	0.1374	221
129 idemia-007	0.0024	19	0.0039	23	0.0032	31	0.0038	25	0.0046	22	0.0092	25
130 idemia-008	0.0023	18	0.0032	15	0.0023	3	0.0028	6	0.0034	4	0.0067	5
131 iit-002	0.0111	169	0.0177	175	0.0085	151	0.0140	158	0.0193	185	0.0332	156
132 iit-003	0.0082	133	0.0151	154	0.0053	83	0.0084	98	0.0122	124	0.0199	102

Table 16: FNMR is the proportion of mated comparisons below a threshold set to achieve the FMR given in the header on the fourth row. FMR is the proportion of impostor comparisons at or above that threshold. The light grey values give rank over all algorithms in that column. The pink columns use only same-sex impostors; others are selected regardless of demographics. The exception, in the green column, uses "matched-covariates" i.e. impostors of the same sex, age group, and country of birth. The second pink column includes effects of extended ageing. Missing entries for border, visa, mugshot and wild images generally mean the algorithm did not run to completion. For child exploitation, missing entries arise because NIST executes those runs only infrequently. The VISA columns compare images described in section 2.2. The MUGSHOT columns compare images described in section 2.5. The VISA-BORDER column compare images described in section 2.3 with those of section 2.4. The BORDER column compares images described in section 2.4. The WILD columns compare images described in section 2.6. The CHILD-EXPLOITATION columns compare images described in section 2.1.

Algorithm	Name	FALSE NON-MATCH RATE (FNMR)												LESS CONSTRAINED, NON-COOP.					
		CONSTRAINED, COOPERATIVE								WILD CHILDEXP									
		VISAMC	VISA	MUGSHOT	MUGSHOT12+YRS	VISABORDER	BORDER	BORDER	WILD	CHILDEXP									
FMR		0.0001	1E-06	1E-05	1E-05	1E-06	1E-06	1E-05	0.0001	0.01									
133	imagus-002	0.0062	93	0.0086	85	0.0053	85	0.0075	85	0.0121	123	0.0207	106	0.0161	140	0.0735	233	-	
134	imagus-003	0.0059	88	0.0084	82	0.0059	98	0.0081	93	0.0119	120	0.0209	107	0.0162	141	0.1068	250	-	
135	imperial-000	0.0067	105	0.0108	117	0.0080	142	0.0134	154	0.0087	80	0.0581	184	0.0102	78	0.0281	48	-	
136	imperial-002	0.0058	84	0.0081	79	0.0055	89	0.0085	100	0.0083	75	0.0157	76	0.0103	79	0.0273	8	0.5151	15
137	incode-008	0.0063	95	0.0101	111	0.0046	73	0.0086	105	0.0057	42	0.0104	37	0.0074	28	0.0297	109	-	
138	incode-009	0.0044	53	0.0067	60	0.0034	37	0.0051	44	0.0049	28	0.0091	24	0.0067	19	0.0296	108	-	
139	innefulabs-000	0.0122	181	0.0199	183	0.0112	191	0.0197	198	0.0222	195	0.0372	166	0.0271	200	0.0348	167	-	
140	innovativetechnologyltd-001	0.0578	263	0.0938	266	0.0501	257	0.0981	259	0.0592	246	0.0779	201	0.0422	219	0.0449	202	-	
141	innovativetechnologyltd-002	0.0451	256	0.0716	258	0.0541	261	0.1009	261	0.0506	241	0.0682	195	0.0371	214	0.0804	239	-	
142	innovatrics-006	0.0058	83	0.0089	89	0.0061	106	0.0096	112	0.0096	99	0.0165	83	0.0103	80	0.0281	46	0.3056	3
143	innovatrics-007	0.0040	45	0.0054	45	0.0057	94	0.0078	88	0.0079	69	0.0123	55	0.0088	59	0.0282	59	-	
144	insightface-000	0.0018	13	0.0027	11	0.0029	17	0.0030	16	0.0038	7	0.0077	11	0.0068	20	0.0276	19	-	
145	intellicloudai-001	0.0142	197	0.0234	201	0.0092	164	0.0145	163	0.0162	162	0.0371	165	0.0171	148	0.0409	189	-	
146	intellicloudai-002	0.0059	87	0.0085	83	0.0060	102	0.0069	76	0.0108	111	0.2477	238	0.0171	147	0.0303	119	-	
147	intellifusion-001	0.0072	115	0.0094	96	0.0056	93	0.0085	101	0.0111	118	0.0212	109	0.0143	121	0.0289	88	0.5454	18
148	intellifusion-002	0.0059	86	0.0077	72	0.0040	54	0.0074	83	0.0085	78	0.5352	255	0.0104	83	0.0305	122	-	
149	intellivision-001	0.1335	277	0.2205	278	0.1090	272	0.1670	271	0.1385	264	0.1676	224	0.1170	255	0.2445	280	0.7766	46
150	intellivision-002	0.1000	273	0.1775	273	0.0610	266	0.1009	260	0.0805	255	0.1074	215	0.0682	239	0.0768	235	-	
151	intelresearch-002	0.0058	81	0.0082	81	0.0050	81	0.0086	103	0.0136	135	0.0434	174	0.0216	179	0.0285	75	-	
152	intelresearch-003	0.0046	56	0.0062	54	0.0038	49	0.0060	62	0.0088	83	0.0168	85	0.0136	111	0.0304	121	-	
153	intsysmsu-001	0.9543	326	0.9888	326	0.9923	318	-	-	0.9977	312	0.9955	297	0.9892	310	0.7871	311	-	
154	intsysmsu-002	0.0130	190	0.0254	212	0.0137	206	0.0267	220	0.0160	159	0.0267	135	0.0145	124	0.0289	90	-	
155	ionetworks-000	0.0060	92	0.0087	88	0.0044	67	0.0058	59	0.0080	72	0.0144	64	0.0112	89	0.0319	142	-	
156	iqface-000	0.0091	141	0.0143	144	0.0075	130	0.0110	126	0.0171	172	0.2234	233	0.0359	211	0.0381	182	0.6490	29
157	iqface-003	0.0058	82	0.0079	76	0.0051	82	0.0058	60	0.0104	107	0.0200	103	0.0193	164	0.0402	186	-	
158	irex-000	0.0052	66	0.0099	104	0.0056	92	0.0083	96	0.0137	139	0.0163	81	0.0078	40	0.0285	72	-	
159	isap-001	0.5092	313	0.6588	311	0.6899	309	0.7978	306	0.7200	296	0.7253	271	0.5373	290	0.1931	272	-	
160	isap-002	0.0114	170	0.0186	178	0.0087	157	0.0151	168	0.0156	156	0.5134	254	0.0333	207	0.0354	174	-	
161	isityou-000	0.5682	315	0.7033	314	1.0000	326	-	-	1.0000	321	1.0000	328	1.0000	320	1.0000	325	1.0000	114
162	isystems-001	0.0149	204	0.0245	207	0.0138	207	0.0210	202	0.0209	190	0.0332	155	0.0223	181	0.0524	214	0.5152	16
163	isystems-002	0.0118	175	0.0182	177	0.0111	188	0.0162	177	0.0166	167	0.0284	141	0.0195	167	0.0516	212	0.4876	13
164	itmo-006	0.0125	184	0.0220	195	0.0149	218	0.0266	219	0.0233	198	0.0383	168	0.0285	202	0.0329	154	-	
165	itmo-007	0.0080	129	0.0125	133	0.0107	181	0.0185	190	0.0167	169	0.0222	117	0.0144	123	0.0300	113	-	
166	ivacognitive-001	0.0189	223	0.0351	228	0.0123	201	0.0235	209	0.0198	186	0.0274	137	0.0155	135	0.0296	107	-	
167	iws-000	0.4824	310	0.5801	306	0.6859	308	0.8155	307	0.8251	302	0.7756	277	0.6400	297	0.3251	292	-	
168	kakao-004	0.0078	124	0.0103	113	0.0059	100	0.0102	119	0.0155	154	0.1182	218	0.0230	185	0.0277	24	-	
169	kakao-005	0.0040	44	0.0059	49	0.0036	44	0.0057	56	0.0085	77	0.0239	121	0.0125	103	0.0280	41	-	
170	kakaopay-001	0.0152	207	0.0252	211	0.0145	211	0.0270	221	0.0232	196	0.0344	158	0.0194	165	0.0416	191	-	
171	kedacom-000	0.0055	73	0.0081	80	0.0111	190	0.0120	133	0.0415	231	0.0966	211	0.0686	240	0.2511	283	0.7650	44
172	kiwitech-000	0.0076	122	0.0105	114	0.0081	144	0.0128	147	0.0096	98	0.0163	80	0.0101	75	0.0279	36	-	
173	kneron-003	0.0542	262	0.0902	264	0.0346	250	0.0562	248	0.0919	258	0.1251	220	0.0973	252	0.3053	291	0.6962	34
174	kneron-005	0.0157	209	0.0259	214	0.0126	204	0.0212	203	0.0406	230	0.0693	197	0.0542	232	0.0471	205	-	
175	kookmin-001	0.0462	258	0.0750	259	0.0489	255	0.0842	255	0.0659	250	0.8380	285	0.3212	274	0.0491	209	-	
176	kookmin-002	0.0054	72	0.0077	71	0.0043	63	0.0065	71	0.0123	125	0.7591	275	0.0198	169	0.0285	73	-	

Table 17: FNMR is the proportion of mated comparisons below a threshold set to achieve the FMR given in the header on the fourth row. FMR is the proportion of impostor comparisons at or above that threshold. The light grey values give rank over all algorithms in that column. The pink columns use only same-sex impostors; others are selected regardless of demographics. The exception, in the green column, uses “matched-covariates” i.e. impostors of the same sex, age group, and country of birth. The second pink column includes effects of extended ageing. Missing entries for border, visa, mugshot and wild images generally mean the algorithm did not run to completion. For child exploitation, missing entries arise because NIST executes those runs only infrequently. The VISA columns compare images described in section 2.2. The MUGSHOT columns compare images described in section 2.5. The VISA-BORDER column compare images described in section 2.3 with those of section 2.4. The BORDER column compares images described in section 2.4. The WILD columns compare images described in section 2.6. The CHILD-EXPLOITATION columns compare images described in section 2.1.

	Algorithm	FALSE NON-MATCH RATE (FNMR)												LESS CONSTRAINED, NON-COOP.				
		CONSTRAINED, COOPERATIVE								WILD								
		Name	VisAMC	VISA	MUGSHOT	MUGSHOT12+YRS	VisABORDER	BORDER	BORDER	WILD	CHILDEXP							
FMR		0.0001	1E-06	1E-05	1E-05	1E-06	1E-06	1E-05	1E-05	0.0001	0.01							
177	lemlabs-001	0.0111	168	0.0175	172	0.0088	158	0.0142	160	0.0143	144	0.0228	119	0.0140	118	0.0281	45	-
178	line-000	0.0172	217	0.0236	204	0.0109	185	0.0194	195	0.0183	177	0.0291	143	0.0204	174	0.0298	110	-
179	lookman-002	0.0297	244	0.0547	251	0.0339	248	0.0562	247	0.0614	248	0.0960	210	0.0790	247	0.2640	287	-
180	lookman-004	0.0074	119	0.0099	102	0.0124	203	0.0149	167	0.0430	235	0.0866	205	0.0694	241	0.2516	284	0.7664 45
181	luxand-000	0.2056	284	0.2814	282	0.4053	292	0.5365	290	0.3497	281	0.3743	244	0.2605	267	0.2222	279	-
182	megvii-002	0.0104	161	0.0145	148	0.0225	236	0.0345	232	0.0099	103	0.0286	142	0.0240	193	0.0692	231	0.3013 2
183	megvii-003	0.0064	96	0.0094	95	0.0136	205	0.0260	216	0.0050	29	0.0080	14	0.0059	9	0.0288	80	-
184	meituan-000	0.0197	226	0.0424	240	0.0078	136	0.0074	82	0.0103	106	0.0193	99	0.0164	142	0.1063	248	-
185	meiya-001	0.0171	214	0.0275	219	0.0159	222	0.0261	218	0.0311	221	0.2250	234	0.0245	195	0.0363	178	-
186	microfocus-001	0.4482	307	0.5524	305	0.7256	312	0.8416	309	0.7301	297	0.6926	268	0.5180	289	0.2567	286	0.6890 33
187	microfocus-002	0.3605	299	0.5057	300	0.5783	301	0.7223	299	0.5909	289	0.5963	260	0.4160	285	0.1582	265	0.6517 30
188	minivision-000	0.0033	34	0.0048	36	0.0038	50	0.0049	39	0.0055	40	0.0094	28	0.0079	43	0.0273	6	-
189	mobai-000	0.0360	252	0.0439	243	0.0372	252	0.0700	252	0.0367	225	0.0939	208	0.0795	248	0.2640	288	-
190	mobai-001	0.0199	228	0.0219	192	0.0047	75	0.0061	65	0.0093	94	0.0174	89	0.0138	117	0.1045	247	-
191	mobbl-000	0.2938	291	0.3861	291	0.5391	297	0.6888	297	0.6545	292	0.8027	278	0.6207	294	0.5471	305	-
192	mobbl-001	0.3208	294	0.4375	295	0.5680	300	0.7193	298	0.6282	290	0.5783	258	0.3984	282	0.1866	271	-
193	moreedian-000	0.3874	300	0.4912	299	0.9988	322	-		0.9990	313	0.9999	307	0.9998	314	0.4788	300	-
194	mvision-001	0.0191	224	0.0233	199	0.0204	231	0.0356	233	0.0198	187	0.0337	157	0.0242	194	0.0431	194	-
195	nazhiai-000	0.0040	46	0.0059	50	0.0036	41	0.0048	38	0.0057	43	0.0125	56	0.0083	50	0.0275	14	-
196	neosystems-001	1.0000	332	1.0000	331	0.2987	286	0.4382	286	0.5173	288	0.6570	264	0.4043	284	0.5091	303	-
197	neosystems-002	0.2905	290	0.4077	293	0.2028	281	0.3252	281	0.4088	286	0.5519	256	0.3331	276	0.4500	299	-
198	netbridgeTech-001	0.4749	309	0.6599	312	0.4438	293	0.5676	292	0.4491	287	1.0000	308	0.9541	306	0.1098	253	-
199	netbridgeTech-002	0.0101	158	0.0166	166	0.0077	133	0.0127	143	0.0133	133	0.8215	281	0.0523	230	0.0351	172	-
200	neurotechnology-011	0.0050	62	0.0087	86	0.0061	107	0.0097	114	0.0077	68	0.0404	173	0.0092	63	0.0293	102	-
201	neurotechnology-012	0.0051	65	0.0070	61	0.0038	47	0.0056	55	0.0066	58	0.0112	47	0.0075	31	0.0279	35	-
202	nhn-001	0.0066	104	0.0098	101	0.0053	84	0.0079	92	0.0093	91	0.0156	75	0.0109	87	0.0308	133	-
203	nhn-002	0.0068	108	0.0096	97	0.0057	97	0.0087	107	0.0136	138	0.0253	128	0.0186	158	0.0302	117	-
204	nodeflux-002	0.0186	222	0.0340	225	0.0261	243	0.0451	241	0.0548	243	1.0000	314	1.0000	317	0.0299	111	-
205	notiontag-000	0.6669	316	0.7885	315	0.3715	289	0.4978	288	0.8571	303	0.8102	280	0.6460	298	0.1807	270	0.6479 28
206	notiontag-001	0.6846	317	0.8006	316	0.3955	291	0.5247	289	0.8669	305	0.8313	284	0.6362	296	0.2221	278	-
207	nsensecorp-001	0.9909	328	0.9994	328	0.9987	321	-		1.0000	319	1.0000	316	1.0000	318	0.9858	318	-
208	nsensecorp-002	0.4277	303	0.5375	303	0.6734	307	0.7924	305	0.7194	295	0.6937	269	0.5617	291	0.5530	306	-
209	ntechlab-009	0.0039	43	0.0054	42	0.0042	61	0.0063	68	0.0275	213	0.0674	194	0.0532	231	0.0537	216	-
210	ntechlab-010	0.0013	3	0.0017	1	0.0024	6	0.0029	12	0.0031	2	0.0058	2	0.0050	2	0.0292	97	-
211	omnigarde-000	0.0633	265	0.1002	267	0.1109	273	0.2042	274	0.1288	263	0.5113	253	0.1227	257	0.0357	176	-
212	openface-001	0.1804	280	0.2921	283	0.2878	284	0.3906	284	0.2054	273	0.2338	237	0.1549	261	0.2445	281	-
213	oz-001	0.0133	191	0.0215	191	0.0109	186	0.0160	175	0.0235	201	1.0000	318	1.0000	327	0.0417	192	-
214	oz-002	0.0071	114	0.0099	107	0.0099	173	0.0100	117	0.0139	140	0.0502	178	0.0202	171	0.5084	302	-
215	papsav1923-001	0.0078	125	0.0130	136	0.0068	117	0.0105	123	0.0119	121	0.0221	116	0.0136	112	0.0293	99	-
216	paravision-004	0.0030	29	0.0046	35	0.0030	20	0.0036	22	0.0091	90	0.0188	97	0.0173	149	0.0288	83	0.2467 1
217	paravision-008	0.0018	11	0.0025	7	0.0024	4	0.0025	4	0.0036	6	0.0070	7	0.0063	13	0.0279	33	-
218	pensees-001	0.0087	137	0.0133	138	0.0071	122	0.0122	137	0.0145	148	0.0252	127	0.0195	168	0.0283	62	-
219	pixelall-005	0.0038	40	0.0052	40	0.0043	64	0.0051	46	0.0077	67	0.0839	204	0.0136	114	0.0279	29	-
220	pixelall-006	0.0032	32	0.0042	29	0.0032	30	0.0039	26	0.0063	53	0.9960	299	0.0723	244	0.0283	60	-

Table 18: FNMR is the proportion of mated comparisons below a threshold set to achieve the FMR given in the header on the fourth row. FMR is the proportion of impostor comparisons at or above that threshold. The light grey values give rank over all algorithms in that column. The pink columns use only same-sex impostors; others are selected regardless of demographics. The exception, in the green column, uses “matched-covariates” i.e. impostors of the same sex, age group, and country of birth. The second pink column includes effects of extended ageing. Missing entries for border, visa, mugshot and wild images generally mean the algorithm did not run to completion. For child exploitation, missing entries arise because NIST executes those runs only infrequently. The VISA columns compare images described in section 2.2. The MUGSHOT columns compare images described in section 2.5. The VISA-BORDER column compare images described in section 2.3 with those of section 2.4. The BORDER column compares images described in section 2.4. The WILD columns compare images described in section 2.6. The CHILD-EXPLOITATION columns compare images described in section 2.1.

Algorithm	FALSE NON-MATCH RATE (FNMR)																		
	CONSTRAINED, COOPERATIVE								LESS CONSTRAINED, NON-COOP.										
	Name	VISAMC	VISA	MUGSHOT	MUGSHOT12+YRS	VISABORDER	BORDER	BORDER	WILD	CHILDEXP									
FMR	0.0001	1E-06	1E-05	1E-05	1E-05	1E-06	1E-06	1E-05	0.0001	0.01									
221	psl-007	0.0026	23	0.0040	24	0.0027	14	0.0030	14	0.0054	36	0.0101	36	0.0081	46	0.0282	54	-	
222	psl-008	0.0026	20	0.0040	25	0.0024	5	0.0028	10	0.0041	11	0.0077	10	0.0055	5	0.0280	40	-	
223	ptakuratsatu-000	0.0060	91	0.0089	90	0.0070	120	0.0104	122	0.0096	100	0.0152	72	0.0100	72	0.0284	66	-	
224	pxl-001	0.0488	260	0.0752	260	0.0586	263	0.1087	262	0.0946	259	0.1065	214	0.0625	237	0.1088	251	-	
225	pyramid-000	0.0136	193	0.0233	200	0.0117	198	0.0192	194	0.0185	179	0.0322	151	0.0206	176	0.0304	120	-	
226	quantasoft-003	0.0081	132	0.0113	125	0.0056	91	0.0076	87	0.0091	89	0.0161	79	0.0107	86	0.0414	190	-	
227	rankone-009	0.0087	136	0.0119	128	0.0065	112	0.0086	104	0.0088	84	0.0161	78	0.0121	101	0.0323	147	-	
228	rankone-010	0.0079	126	0.0112	123	0.0061	104	0.0081	94	0.0088	82	0.0149	67	0.0117	96	0.0320	145	-	
229	realnetworks-002	0.0248	237	0.0358	230	0.0513	259	0.1127	266	0.0371	226	0.0614	188	0.0316	206	0.0334	157	-	
230	realnetworks-004	0.0075	121	0.0101	108	0.0066	115	0.0097	115	0.0108	115	0.0187	96	0.0131	108	0.0285	76	-	
231	regula-000	0.0184	221	0.0376	234	0.0103	175	0.0185	189	0.0120	122	0.0983	302	0.0231	186	0.0273	9	-	
232	remarkai-001	0.0144	199	0.0256	213	0.0102	174	0.0159	174	0.0162	163	0.0582	185	0.0185	156	0.0308	130	-	
233	remarkai-003	0.0047	57	0.0063	56	0.0033	33	0.0049	41	0.0054	37	0.0100	35	0.0072	25	0.0275	16	-	
234	rendip-000	0.0055	75	0.0077	70	0.0048	78	0.0060	63	0.0080	71	0.0142	63	0.0110	88	0.0433	196	-	
235	rokid-000	0.0093	147	0.0145	147	0.0073	127	0.0102	120	0.0164	165	0.0280	140	0.0214	178	0.0857	240	-	
236	rokid-001	0.0105	163	0.0162	162	0.0094	167	0.0163	178	0.0181	175	0.0276	139	0.0165	143	0.0325	149	-	
237	s1-001	0.0314	248	0.0651	256	0.0252	240	0.0357	234	0.0444	237	0.0653	193	0.0429	220	0.8493	312	-	
238	s1-002	0.0095	150	0.0144	146	0.0112	192	0.0196	196	0.0234	199	0.0371	164	0.0282	201	0.1167	256	-	
239	saffe-001	0.4339	304	0.5261	301	0.7539	314	0.8736	312	0.7977	300	0.9810	292	0.7435	301	0.3887	294	0.8973	53
240	saffe-002	0.0119	177	0.0206	184	0.0107	184	0.0177	184	0.0244	206	0.9998	306	0.2785	270	0.0308	129	-	
241	samtech-001	0.0197	227	0.0365	231	0.0146	215	0.0241	211	0.0238	205	0.0394	171	0.0251	196	0.0337	158	-	
242	scanovate-001	0.0175	218	0.0331	223	0.0163	223	0.0248	213	0.2476	276	0.3801	245	0.3740	279	0.4060	295	-	
243	scanovate-002	0.0175	219	0.0355	229	0.0146	213	0.0286	223	0.0269	209	0.0301	144	0.0178	151	0.0301	116	-	
244	securifai-001	0.4538	308	0.6142	309	0.5844	302	0.7428	301	0.7051	294	0.9961	300	0.9558	307	0.1963	273	-	
245	securifai-002	0.7557	321	0.8574	317	0.4550	294	0.5953	293	0.9860	310	0.9796	291	0.9158	303	0.2848	289	-	
246	sensetime-004	0.0026	21	0.0038	20	0.0022	2	0.0023	2	0.0042	13	0.0082	16	0.0078	39	0.0293	98	-	
247	sensetime-005	0.0019	14	0.0029	13	0.0022	1	0.0021	1	0.0023	1	0.0044	1	0.0039	1	0.0273	7	-	
248	sertis-000	0.0118	176	0.0208	185	0.0080	140	0.0127	142	0.0110	117	0.0176	90	0.0114	93	0.0285	74	-	
249	sertis-002	0.0049	59	0.0061	51	0.0039	53	0.0061	67	0.0055	39	0.0099	34	0.0070	23	0.0281	47	-	
250	seventhsense-000	0.0067	107	0.0099	106	0.0045	69	0.0065	72	0.0093	92	0.0169	86	0.0124	102	0.0275	15	-	
251	shaman-000	0.9297	325	0.9774	324	0.9990	323	-		0.9999	316	1.0000	312	0.9999	316	0.9575	316	0.9618	57
252	shaman-001	0.3346	296	0.4616	296	0.2368	282	0.3723	283	0.3574	282	0.3527	243	0.2304	265	0.1498	264	0.8990	54
253	shu-002	-		0.0079	77	0.0146	214	0.0308	225	1.0000	318	0.0183	93	0.0115	94	0.0284	67	-	
254	shu-003	0.0028	26	0.0041	28	0.0050	80	0.0088	108	0.0081	73	0.0133	59	0.0094	68	0.0283	64	-	
255	siat-002	0.0091	142	0.0126	135	0.0109	187	0.0190	193	0.0276	214	0.0516	179	0.0464	224	0.0520	213	0.4277	10
256	siat-004	0.0067	106	0.0099	103	0.0152	220	-		0.0275	211	0.4823	251	0.4823	286	1.0000	321	-	
257	sjtu-003	0.0017	9	0.0033	16	0.0030	22	0.0037	23	0.0058	44	0.0104	38	0.0081	47	0.0284	69	-	
258	sjtu-004	0.0014	4	0.0025	6	0.0027	13	0.0028	11	0.0046	21	0.0086	20	0.0073	26	0.0272	4	-	
259	sktelecom-000	0.0038	41	0.0054	43	0.0031	24	0.0051	47	0.0042	12	0.3418	242	0.0061	10	0.0293	101	-	
260	smilart-002	0.2440	286	0.3532	287	-		-		0.3785	283	0.4145	249	0.2611	268	-		0.6999	35
261	smilart-003	0.6944	318	0.8836	318	0.0695	267	0.1193	267	0.0894	257	0.1221	219	0.0737	245	0.1190	257	-	
262	sodec-000	0.0033	36	0.0044	32	0.0040	56	0.0053	50	0.0054	38	0.0096	31	0.0080	44	0.0274	10	-	
263	stauq-000	0.0139	196	0.0208	186	0.0104	176	0.0145	165	0.0156	155	0.8063	279	0.1408	260	0.0332	156	-	
264	starhybrid-001	0.0108	166	0.0138	141	0.0081	143	0.0113	129	0.0152	151	0.0265	134	0.0189	161	0.0350	170	0.5584	19

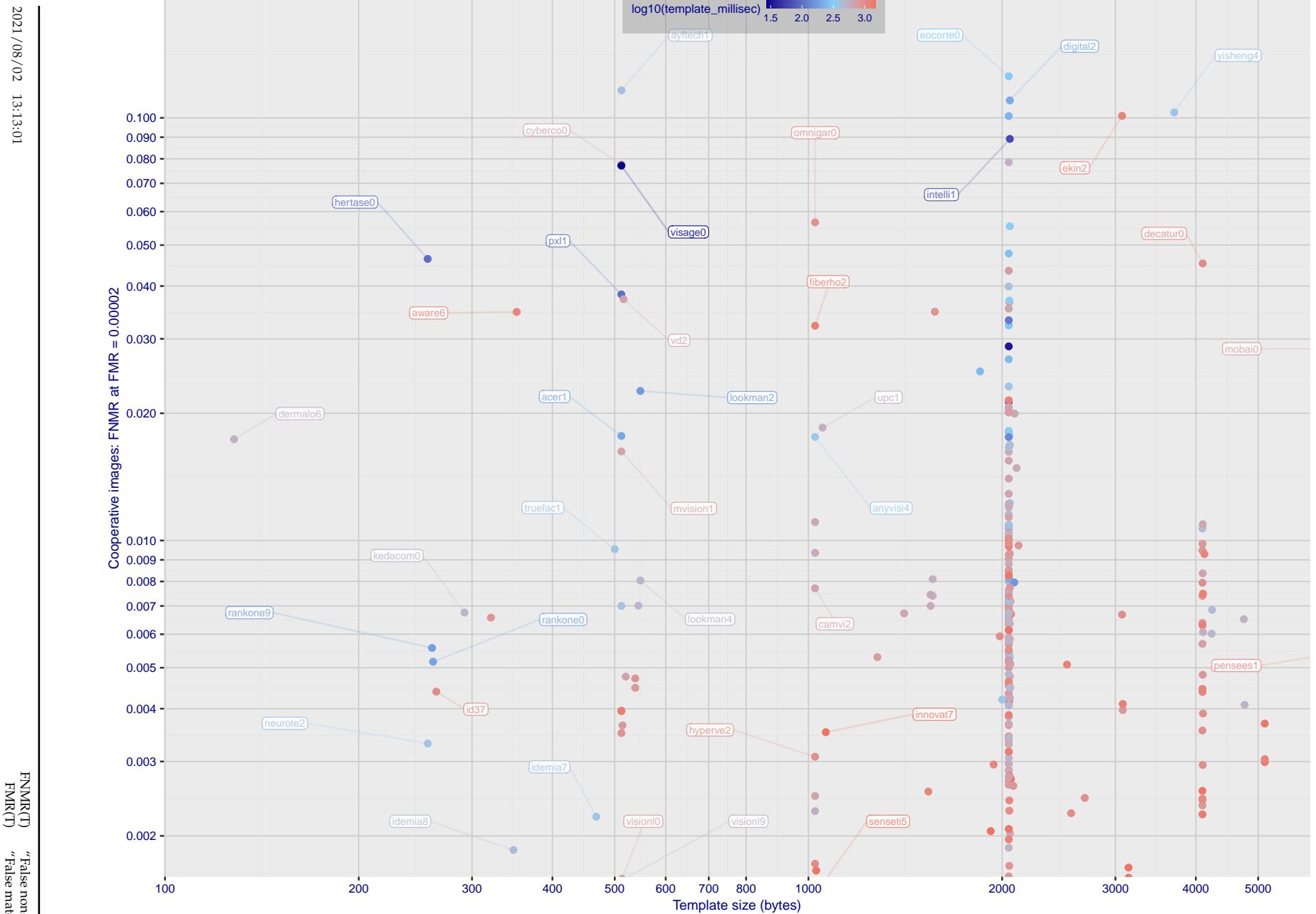
Table 19: FNMR is the proportion of mated comparisons below a threshold set to achieve the FMR given in the header on the fourth row. FMR is the proportion of impostor comparisons at or above that threshold. The light grey values give rank over all algorithms in that column. The pink columns use only same-sex impostors; others are selected regardless of demographics. The exception, in the green column, uses “matched-covariates” i.e. impostors of the same sex, age group, and country of birth. The second pink column includes effects of extended ageing. Missing entries for border, visa, mugshot and wild images generally mean the algorithm did not run to completion. For child exploitation, missing entries arise because NIST executes those runs only infrequently. The VISA columns compare images described in section 2.2. The MUGSHOT columns compare images described in section 2.5. The VISA-BORDER column compare images described in section 2.3 with those of section 2.4. The BORDER column compares images described in section 2.4. The WILD columns compare images described in section 2.6. The CHILD-EXPLOITATION columns compare images described in section 2.1.

	Algorithm	FALSE NON-MATCH RATE (FNMR)																	
		CONSTRAINED, COOPERATIVE							LESS CONSTRAINED, NON-COOP.										
		Name	ViSAMC	VISA	MUGSHOT	MUGSHOT12+YRS	VisABORDER	BORDER	BORDER	WILD	CHILDEXP								
FMR		0.0001	1E-06	1E-05	1E-05	1E-06	1E-06	1E-06	1E-05	0.0001	0.01								
265	suprema-000	0.0064	99	0.0092	93	0.0081	145	0.0096	113	0.0139	141	0.0254	130	0.0220	180	0.1131	254	-	
266	supremaid-001	0.0053	69	0.0073	66	0.0045	70	0.0066	74	0.0099	102	0.0186	95	0.0148	128	0.0352	173	-	
267	synesis-006	0.0070	111	0.0096	99	0.0107	182	0.0166	180	-	-	0.0128	57	0.0089	60	0.0292	96	-	
268	synesis-007	0.0050	61	0.0073	67	0.0062	108	0.0076	86	-	-	0.0105	39	0.0080	45	0.0288	81	-	
269	synology-000	0.0149	202	0.0238	205	0.0148	216	0.0261	217	0.0221	194	0.0331	154	0.0209	177	0.0330	155	-	
270	synology-002	0.0104	162	0.0153	157	0.0107	183	0.0184	187	0.0189	182	0.2032	232	0.0180	152	0.0312	134	-	
271	sztu-000	0.0092	145	0.0139	142	0.0091	161	0.0201	199	0.0136	137	0.0685	196	0.0118	98	0.0270	2	-	
272	sztu-001	0.0031	30	0.0043	30	0.0025	7	0.0028	8	0.0051	30	0.0113	48	0.0089	61	0.0275	12	-	
273	tech5-004	0.0123	182	0.0234	202	0.0086	155	0.0162	176	0.0065	57	0.0112	46	0.0082	48	0.0281	50	-	
274	tech5-005	0.0054	71	0.0072	64	0.0069	118	0.0122	136	0.0060	49	0.0094	27	0.0066	17	0.0349	169	-	
275	tevian-005	0.0043	51	0.0062	55	0.0057	95	0.0085	102	0.0070	62	0.0135	60	0.0119	99	0.0300	114	0.5625	22
276	tevian-006	0.0045	54	0.0061	53	0.0045	71	0.0066	73	0.0046	24	0.0091	23	0.0075	32	0.0308	132	-	
277	tiger-003	0.0313	247	0.0602	253	0.0188	228	0.0359	235	0.0344	222	-	-	-	-	0.0482	207	0.5610	21
278	tiger-004	0.0779	269	0.1393	271	0.0488	254	0.0905	258	0.0800	253	0.1640	223	0.0617	236	0.0669	228	-	
279	tinkoff-001	0.0145	200	0.0244	206	0.0318	247	0.0636	250	0.0236	203	1.0000	327	0.0339	208	0.0563	220	-	
280	tongyi-005	0.0073	117	0.0146	149	0.0187	227	0.0421	240	0.0161	161	0.0215	111	0.0149	130	0.0399	184	0.6195	27
281	toshiba-002	0.0134	192	0.0222	197	0.0097	172	0.0154	171	-	-	0.0327	153	0.0158	138	0.0434	197	0.7103	36
282	toshiba-003	0.0125	185	0.0214	189	0.0085	153	0.0131	149	-	-	0.0241	122	0.0151	133	0.0282	51	-	
283	trueface-001	0.0204	229	0.0438	242	0.0095	169	0.0138	156	0.0154	152	0.0253	129	0.0169	146	0.0772	236	-	
284	trueface-002	0.0060	89	0.0096	98	0.0048	77	0.0061	66	0.0112	119	0.0198	101	0.0155	136	0.0793	238	-	
285	tuputech-000	0.3218	295	0.3696	289	-	-	-	-	0.3237	278	0.4304	250	0.2973	273	0.9415	315	-	
286	twface-000	0.0051	64	0.0072	65	0.0041	58	0.0058	57	0.0071	64	0.0153	73	0.0100	71	0.0276	18	-	
287	ulsee-001	0.0151	206	0.0246	208	0.0113	194	0.0185	191	0.0187	181	0.6766	266	0.0181	154	0.0316	139	-	
288	ultinous-000	0.2343	285	0.3484	285	-	-	-	-	-	-	-	-	-	-	0.9447	56	-	
289	ultinous-001	0.2485	287	0.4003	292	-	-	-	-	-	-	-	-	-	-	0.6847	32	-	
290	uluface-002	0.0081	131	0.0123	129	0.0071	121	0.0095	111	0.0107	110	1.0000	324	0.0140	119	0.0444	199	0.6729	31
291	uluface-003	0.0100	157	0.0150	153	0.0079	137	0.0128	145	-	-	-	-	-	-	0.0635	226	-	
292	upc-001	0.0234	233	0.0519	249	0.0291	246	0.0490	245	0.0294	217	0.2316	236	0.0389	216	0.0314	137	0.4224	8
293	vcog-002	0.7522	320	0.9033	319	-	-	-	-	-	-	-	-	-	-	0.7523	42	-	
294	vd-001	0.0243	235	0.0452	244	0.0271	244	0.0402	238	0.0424	234	-	-	-	-	0.1389	261	-	
295	vd-002	0.0429	255	0.0704	257	0.0569	262	0.0844	256	0.0801	254	0.0937	206	0.0577	234	0.0556	219	-	
296	veridas-004	0.0281	242	0.0467	245	0.0353	251	0.0643	251	0.0424	233	0.0644	192	0.0342	209	0.0291	95	-	
297	veridas-006	0.0098	153	0.0167	169	0.0079	139	0.0127	141	0.0127	127	0.0217	113	0.0151	132	0.0286	79	-	
298	via-000	0.0216	230	0.0365	232	0.0177	225	0.0287	224	0.0296	218	0.0572	181	0.0290	205	0.0349	168	0.7638	43
299	via-001	0.0149	203	0.0229	198	0.0114	196	0.0177	186	0.0183	178	0.4056	248	0.0176	150	0.0373	180	-	
300	videmo-000	0.0298	245	0.0423	238	0.0155	221	0.0260	215	0.0246	207	0.0397	172	0.0239	192	0.0541	217	-	
301	videonetcs-001	0.5483	314	0.6446	310	0.7517	313	0.8607	310	0.8664	304	0.8255	282	0.6956	300	0.2986	290	0.7297	39
302	videonetcs-002	0.4274	302	0.5329	302	0.6081	304	0.7438	302	0.7775	298	0.7297	272	0.5756	292	0.1976	275	0.7435	41
303	vigilantsolutions-009	0.0117	174	0.0165	165	0.0075	131	0.0101	118	0.0219	193	0.0385	169	0.0238	191	0.0277	25	-	
304	vigilantsolutions-010	0.0109	167	0.0164	164	0.0074	129	0.0095	110	0.0209	189	0.0365	163	0.0233	187	0.0277	21	-	
305	vinai-000	0.0081	130	0.0124	130	0.0045	68	0.0072	79	0.0089	85	0.1814	225	0.0112	90	0.0274	11	-	
306	vion-000	0.0419	254	0.0590	252	0.0422	253	0.0478	243	0.0581	245	0.0968	212	0.0847	249	0.2479	282	0.8765	50
307	visage-000	0.0933	271	0.1441	272	0.1316	276	0.2416	277	0.1395	265	0.1920	229	0.1001	253	0.0500	211	-	
308	visionbox-001	0.0159	211	0.0270	217	0.0111	189	0.0173	183	0.0190	183	0.0315	147	0.0205	175	0.0389	183	-	

Table 20: FNMR is the proportion of mated comparisons below a threshold set to achieve the FMR given in the header on the fourth row. FMR is the proportion of impostor comparisons at or above that threshold. The light grey values give rank over all algorithms in that column. The pink columns use only same-sex impostors; others are selected regardless of demographics. The exception, in the green column, uses “matched-covariates” i.e. impostors of the same sex, age group, and country of birth. The second pink column includes effects of extended ageing. Missing entries for border, visa, mugshot and wild images generally mean the algorithm did not run to completion. For child exploitation, missing entries arise because NIST executes those runs only infrequently. The VISA columns compare images described in section 2.2. The MUGSHOT columns compare images described in section 2.5. The VISA-BORDER column compare images described in section 2.3 with those of section 2.4. The BORDER column compares images described in section 2.4. The WILD columns compare images described in section 2.6. The CHILD-EXPLOITATION columns compare images described in section 2.1.

	Algorithm	FALSE NON-MATCH RATE (FNMR)										LESS CONSTRAINED, NON-COOP.							
		CONSTRAINED, COOPERATIVE																	
		Name	VISAMC	VISA	MUGSHOT	MUGSHOT12+YRS	VISABORDER	BORDER	BORDER	WILD	CHILDEXP								
	FMR	0.0001	1E-06	1E-05	1E-05	1E-06	1E-06	1E-06	1E-05	0.0001	0.01								
309	visionbox-002	0.0058	79	0.0079	74	0.0060	101	0.0074	81	0.0084	76	0.0149	68	0.0113	92	0.0447	201	-	
310	visionlabs-009	0.0018	12	0.0025	8	0.0026	9	0.0029	13	0.0035	5	0.0064	4	0.0054	4	0.0283	61	-	
311	visionlabs-010	0.0017	10	0.0024	5	0.0026	10	0.0030	15	0.0033	3	0.0061	3	0.0052	3	0.0282	56	-	
312	visteam-000	0.9200	324	0.9489	322	0.9959	319	-	0.9994	314	0.9978	301	0.9914	312	0.8783	314	-		
313	visteam-001	0.4417	306	0.5385	304	0.6410	306	0.7788	304	0.6386	291	0.5904	259	0.4023	283	0.1413	262	-	
314	vnpt-001	0.3117	293	0.3523	286	0.3474	288	0.2747	279	0.3405	279	0.5015	252	0.4827	287	0.5337	304	-	
315	vnpt-002	0.0351	251	0.0424	239	0.0220	234	0.0316	227	0.0471	239	0.0817	203	0.0698	242	0.0400	185	-	
316	vocord-008	0.0029	28	0.0038	21	0.0042	60	0.0055	52	0.0045	19	0.0086	21	0.0073	27	0.0286	77	-	
317	vocord-009	0.0022	16	0.0029	14	0.0036	42	0.0046	35	0.0052	33	0.0098	33	0.0086	57	0.0284	68	-	
318	vts-000	0.0103	159	0.0174	171	0.0080	141	0.0129	148	0.0250	208	0.0450	175	0.0372	215	0.0596	223	-	
319	winsense-001	0.0062	94	0.0099	105	0.0092	163	0.0210	201	0.0093	93	0.0144	65	0.0098	70	0.0320	144	0.4155	7
320	winsense-002	0.0050	63	0.0073	68	0.0038	48	0.0059	61	0.0064	55	0.0118	53	0.0084	52	0.0307	128	-	
321	x-laboratory-000	0.0071	113	0.0106	115	0.0123	202	0.0138	155	0.0419	232	0.5629	257	0.2852	272	0.0295	106	0.9686	58
322	x-laboratory-001	0.0059	85	0.0110	119	0.0054	86	0.0078	89	0.0094	95	0.0142	62	0.0100	73	0.0294	103	-	
323	xforwardai-001	0.0021	15	0.0034	17	0.0027	15	0.0028	7	0.0046	23	0.0088	22	0.0079	42	0.0281	49	-	
324	xforwardai-002	0.0016	7	0.0023	4	0.0026	12	0.0025	3	0.0040	10	0.0081	15	0.0074	29	0.0282	52	-	
325	xm-000	0.0015	5	0.0026	10	0.0031	26	0.0038	24	0.0058	45	0.0105	40	0.0082	49	0.0282	55	-	
326	yisheng-004	0.1988	282	0.3329	284	0.1147	275	0.1849	273	0.2044	272	-	-	-	-	0.0908	241	0.7152	37
327	yitu-003	0.0015	6	0.0026	9	0.0066	116	0.0085	99	0.0064	56	0.0114	49	0.0103	81	0.0325	150	-	
328	yoonik-000	0.0070	109	0.0112	121	0.0074	128	0.0118	132	0.0564	244	0.2013	231	0.1160	254	0.0590	222	-	
329	yoonik-001	0.0057	77	0.0079	75	0.0043	65	0.0061	64	0.0307	220	0.0762	200	0.0556	233	0.0526	215	-	
330	ytu-000	0.0057	78	0.0087	87	0.0121	200	0.0238	210	0.0047	25	0.0078	13	0.0059	8	0.0286	78	-	
331	yuan-001	0.0116	172	0.0220	194	0.0114	195	0.0184	188	0.0149	149	0.0574	182	0.0160	139	0.0321	146	-	
332	yuan-002	0.0094	149	0.0154	160	0.0071	123	0.0110	127	0.0108	114	0.0348	160	0.0127	105	0.0319	143	-	

Table 21: FNMR is the proportion of mated comparisons below a threshold set to achieve the FMR given in the header on the fourth row. FMR is the proportion of impostor comparisons at or above that threshold. The light grey values give rank over all algorithms in that column. The pink columns use only same-sex impostors; others are selected regardless of demographics. The exception, in the green column, uses “matched-covariates” i.e. impostors of the same sex, age group, and country of birth. The second pink column includes effects of extended ageing. Missing entries for border, visa, mugshot and wild images generally mean the algorithm did not run to completion. For child exploitation, missing entries arise because NIST executes those runs only infrequently. The VISA columns compare images described in section 2.2. The MUGSHOT columns compare images described in section 2.5. The VISA-BORDER column compare images described in section 2.3 with those of section 2.4. The BORDER column compares images described in section 2.4. The WILD columns compare images described in section 2.6. The CHILD-EXPLOITATION columns compare images described in section 2.1.



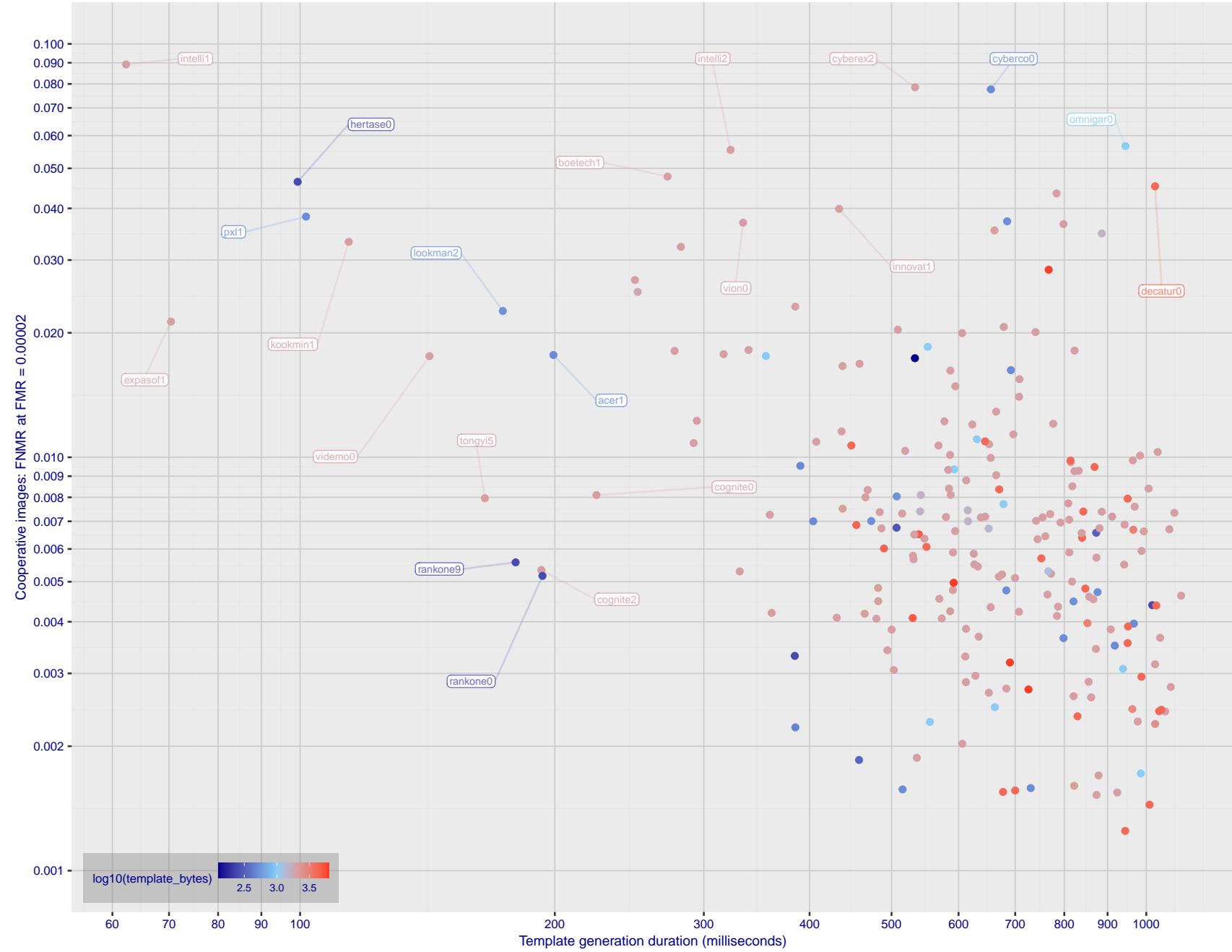


Figure 2: The points show false non-match rates (FNMR) versus the duration of the template generation operation. FNMR is the geometric mean of FNMR values for visa and mugshot images (from Figs. 51 and 68) at a false match rate (FMR) of 0.0001. Template generation time is a median estimated over 640 x 480 pixel portraits. It is measured on a single core of a c. 2016 Intel Xeon CPU E5-2630 v4 running at 2.20GHz. The color of the points encodes template size - which span two orders of magnitude. Algorithms with poor FNMR are omitted.

1 Metrics

1.1 Core accuracy

Given a vector of N genuine scores, u , the false non-match rate (FNMR) is computed as the proportion below some threshold, T:

$$\text{FNMR}(T) = 1 - \frac{1}{N} \sum_{i=1}^N H(u_i - T) \quad (1)$$

where $H(x)$ is the unit step function, and $H(0)$ taken to be 1.

Similarly, given a vector of N impostor scores, v , the false match rate (FMR) is computed as the proportion above T:

$$\text{FMR}(T) = \frac{1}{N} \sum_{i=1}^N H(v_i - T) \quad (2)$$

The threshold, T, can take on any value. We typically generate a set of thresholds from quantiles of the observed impostor scores, v , as follows. Given some interesting false match rate range, $[\text{FMR}_L, \text{FMR}_U]$, we form a vector of K thresholds corresponding to FMR measurements evenly spaced on a logarithmic scale

$$T_k = Q_v(1 - \text{FMR}_k) \quad (3)$$

where Q is the quantile function, and FMR_k comes from

$$\log_{10} \text{FMR}_k = \log_{10} \text{FMR}_L + \frac{k}{K} [\log_{10} \text{FMR}_U - \log_{10} \text{FMR}_L] \quad (4)$$

Error tradeoff characteristics are plots of FNMR(T) vs. FMR(T). These are plotted with $\text{FMR}_U \rightarrow 1$ and FMR_L as low as is sustained by the number of impostor comparisons, N. This is somewhat higher than the “rule of three” limit $3/N$ because samples are not independent, due to re-use of images.

2 Datasets

2.1 Child exploitation images

- ▷ The number of images is on the order of 10^4 .
- ▷ The number of subjects is on the order of 10^3 .
- ▷ The number of subjects with two images on the order of 10^3 .
- ▷ The images are operational. They are taken from ongoing investigations of child exploitation crimes. The images are arbitrarily unconstrained. Pose varies considerably around all three axes, including subject lying down. Resolution varies very widely. Faces can be occluded by other objects, including hair and hands. Lighting varies, although the images are intended for human viewing. Mis-focus is rare. Images are given to the algorithm without any cropping; faces may occupy widely varying areas.
- ▷ The images are usually large from contemporary cameras. The mean interocular distance (IOD) is 70 pixels.
- ▷ The images are of subjects from several countries, due to the global production of this imagery.
- ▷ The images are of children, from infancy to late adolescence.
- ▷ All of the images are live capture, none are scanned. Many have been cropped.
- ▷ When these images are input to the algorithm, they are labelled as being of type "EXPLOITATION" - see Table 4 of the FRVT API.

2.2 Visa images

- ▷ The number of images is on the order of 10^5 .
- ▷ The number of subjects is on the order of 10^5 .
- ▷ The number of subjects with two images is on the order of 10^4 .
- ▷ The images have geometry in reasonable conformance with the ISO/IEC 19794-5 Full Frontal image type. Pose is generally excellent.
- ▷ The images are of size 252x300 pixels. The mean interocular distance (IOD) is 69 pixels.
- ▷ The images are of subjects from greater than 100 countries, with significant imbalance due to visa issuance patterns.
- ▷ The images are of subjects of all ages, including children, again with imbalance due to visa issuance demand.
- ▷ Many of the images are live capture. A substantial number of the images are photographs of paper photographs.
- ▷ When these images are input to the algorithm, they are labelled as being of type "ISO" - see Table 4 of the FRVT API.

2.3 Application images

- ▷ The number of images is on the order of 10^6 .
- ▷ The number of subjects is on the order of 10^6 .
- ▷ The number of subjects with two images is on the order of 10^6 .
- ▷ The images have geometry in good conformance with the ISO/IEC 19794-5 Full Frontal image type. Pose is generally excellent.
- ▷ The images are of size 300x300 pixels. The mean interocular distance (IOD) is 61 pixels.
- ▷ The images are of subjects from greater than 100 countries, with significant imbalance due to population and immigration patterns.

- ▷ The images are of subjects of adults with imbalance due to population and immigration patterns and demand.
- ▷ All of the images are live capture.
- ▷ When these images are input to the algorithm, they are labelled as being of type "ISO" - see Table 4 of the FRVT API.

2.4 Border crossing images

- ▷ The number of images is on the order of 10^6 .
- ▷ The number of subjects is on the order of 10^6 .
- ▷ The number of subjects with two images is on the order of 10^6 .
- ▷ The images are taken with a camera oriented by an attendant toward a cooperating subject. This is done under time constraints so there are roll, pitch and yaw angle variations. Also background illumination is sometimes strong, so the face is under-exposed. There is some perspective distortion due to close range images. Some faces are partially cropped.
- ▷ The images are of subjects from greater than 100 countries, with significant imbalance due to population and immigration patterns.
- ▷ The images are of subjects of adults with imbalance due to population and immigration patterns and demand.
- ▷ The images have mean IOD of 38 pixels.
- ▷ The images are all live capture.
- ▷ When these images are input to the algorithm, they are labelled as being of type "WILD" - see Table 4 of the FRVT API.

2.5 Mugshot images

- ▷ The number of images is on the order of 10^6 .
- ▷ The number of subjects is on the order of 10^6 .
- ▷ The number of subjects with two images is on the order of 10^6 .
- ▷ The images have geometry in reasonable conformance with the ISO/IEC 19794-5 Full Frontal image type.
- ▷ The images are of variable sizes. The median IOD is 105 pixels. The mean IOD is 113 pixels. The 1-st, 5-th, 10-th, 25-th, 75-th, 90-th and 99-th percentiles are 34, 58, 70, 87, 121, 161 and 297 pixels.
- ▷ The images are of subjects from the United States.
- ▷ The images are of adults.
- ▷ The images are all live capture.
- ▷ When these images are input to the algorithm, they are labelled as being of type "mugshot" - see Table 4 of the FRVT API.

2.6 Wild images

- ▷ The number of images is on the order of 10^5 .
- ▷ The number of subjects is on the order of 10^3 .
- ▷ The number of subjects with two images on the order of 10^3 .
- ▷ The images include many photojournalism-style images. Images are given to the algorithm using a variable but generally tight crop of the head. Resolution varies very widely. The images are very unconstrained, with wide yaw and pitch pose variation. Faces can be occluded, including hair and hands.

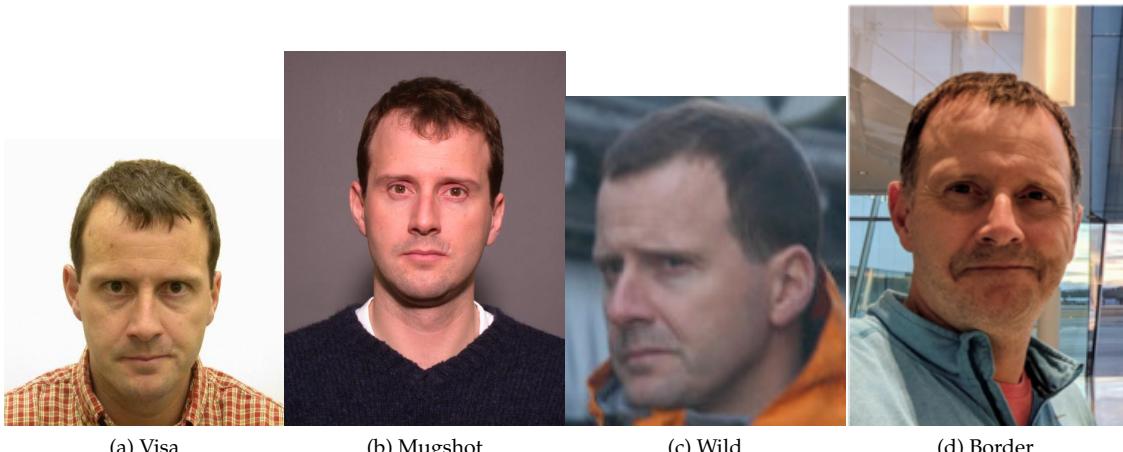


Figure 3: The figure gives simulated samples of image types used in this report.

- ▷ The images are of adults.
 - ▷ All of the images are live capture, none are scanned.
 - ▷ When these images are input to the algorithm, they are labelled as being of type "WILD" - see Table 4 of the FRVT API.

3 Results

3.1 Test goals

- ▷ To state absolute accuracy for different kinds of images, including those with and without subject cooperation.
 - ▷ To state comparative accuracy, across algorithms.

3.2 Test design

Method: For visa images:

- ▷ The comparisons are of visa photos against visa photos.
 - ▷ The number of genuine comparisons is on the order of 10^4 .
 - ▷ The number of impostor comparisons is on the order of 10^{10} .
 - ▷ The comparisons are fully zero-effort, meaning impostors are paired without attention to sex, age or other covariates. However, later analysis is conducted on subsets.
 - ▷ The number of persons is on the order of 10^5 .
 - ▷ The number of images used to make 1 template is 1.
 - ▷ The number of templates used to make each comparison score is two corresponding to simple one-to-one verification.

Method: For mugshot images:

- ▷ The comparisons are of mugshot photos against mugshot photos.

- ▷ The number of genuine comparisons is on the order of 10^6 .
- ▷ The number of impostor comparisons is on the order of 10^8 .
- ▷ The impostors are paired by sex, but not by age or other covariates.
- ▷ The number of persons is on the order of 10^6 .
- ▷ The number of images used to make 1 template is 1.
- ▷ The number of templates used to make each comparison score is two corresponding to simple one-to-one verification.

Method: For visa-border comparisons:

- ▷ The comparisons are of visa-like frontals against border crossing webcam photos.
- ▷ The number of genuine comparisons is on the order of 10^6 .
- ▷ The number of impostor comparisons is on the order of 10^8 .
- ▷ The impostors are paired by sex, but not by age or other covariates.
- ▷ The number of persons is on the order of 10^6 .
- ▷ The number of images used to make 1 template is 1.
- ▷ The number of templates used to make each comparison score is two corresponding to simple one-to-one verification.

Method: For border-border comparisons:

- ▷ The comparisons are of border crossing webcam photos.
- ▷ The number of genuine comparisons is on the order of 10^6 .
- ▷ The number of impostor comparisons is on the order of 10^8 .
- ▷ The impostors are paired by sex, but not by age or other covariates.
- ▷ The number of persons is on the order of 10^6 .
- ▷ The number of images used to make 1 template is 1.
- ▷ The number of templates used to make each comparison score is two corresponding to simple one-to-one verification.

Method: For wild images:

- ▷ The comparisons are of wild photos against wild photos.
- ▷ The number of genuine comparisons is on the order of 10^6 .
- ▷ The number of impostor comparisons is on the order of 10^7 .
- ▷ The comparisons are fully zero-effort, meaning impostors are paired without attention to sex, age or other covariates.
- ▷ The number of persons is on the order of 10^4 .
- ▷ The number of images used to make 1 template is 1.
- ▷ The number of templates used to make each comparison score is two corresponding to simple one-to-one verification.

Method: For child exploitation images:

- ▷ The comparisons are of unconstrained child exploitation photos against others of the same type.

- ▷ The number of genuine comparisons is on the order of 10^4 .
- ▷ The number of impostor comparisons is on the order of 10^7 .
- ▷ The comparisons are fully zero-effort, meaning impostors are paired without attention to sex, age or other covariates.
- ▷ The number of persons is on the order of 10^3 .
- ▷ The number of images used to make 1 template is 1.
- ▷ The number of templates used to make each comparison score is two corresponding to simple one-to-one verification.
- ▷ We produce two performance statements. First, is a DET as used for visa and mugshot images. The second is a cumulative match characteristic (CMC) summarizing a simulated one-to-many search process. This is done as follows.
 - We regard M enrollment templates as items in a gallery.
 - These M templates come from $M > N$ individuals, because multiple images of a subject are present in the gallery under separate identifiers.
 - We regard the verification templates as search templates.
 - For each search we compute the rank of the highest scoring mate.
 - This process should properly be conducted with a 1:N algorithm, such as those tested in NIST IR 8009. We use the 1:1 algorithms in a simulated 1:N mode here to a) better reflect what a child exploitation analyst does, and b) to show algorithm efficacy is better than that revealed in the verification DETs.

3.3 Failure to enroll

	Algorithm Name	Failure to Enrol Rate ¹											
		APPLICATION	BORDER	CHILD-EXPLOIT	MUGSHOT	VISA	WILD						
	Name	SEC. 2.3	SEC. 2.4	SEC. 2.1	SEC. 2.5	SEC. 2.2	SEC. 2.6						
1	20face-000	0.0000	188	0.0008	159	-	313	0.0000	98	0.0004	179	0.0004	130
2	3divi-005	0.0000	220	0.0008	152	-	115	0.0000	116	0.0002	97	0.0003	109
3	3divi-006	0.0000	170	0.0007	142	-	104	0.0001	169	0.0002	101	0.0005	167
4	acer-000	0.0000	250	0.0024	247	-	293	0.0002	211	0.0004	221	0.0008	198
5	acer-001	0.0000	169	0.0011	194	-	94	0.0001	153	0.0004	195	0.0004	141
6	acisw-003	0.0000	112	0.0000	75	-	203	0.0000	47	0.0000	70	0.0001	91
7	acisw-006	0.0000	20	0.0000	7	-	176	0.0000	44	0.0000	21	0.0001	88
8	adera-002	0.0000	252	0.0034	264	-	236	0.0003	232	0.0005	266	0.0505	301
9	adera-003	0.0000	251	0.0034	263	-	303	0.0003	233	0.0005	264	0.0505	300
10	advance-002	0.0000	145	0.0013	215	-	181	0.0000	137	0.0004	194	0.0009	204
11	aifirst-001	0.0000	24	0.0000	5	0.0000	13	0.0000	38	0.0000	15	0.0000	76
12	aigen-001	0.0000	5	0.0000	16	-	159	0.0000	28	0.0000	5	0.0000	49
13	aigen-002	0.0000	95	0.0000	45	-	304	0.0000	79	0.0000	55	0.0000	6
14	ailabs-001	0.0000	205	0.0090	302	-	264	0.0007	279	0.0005	243	0.0016	225
15	aimall-002	0.0000	253	0.0043	277	-	187	0.0012	292	0.0005	261	0.0005	174
16	aimall-003	0.0000	232	0.0012	208	-	127	0.0004	246	0.0005	235	0.0004	150
17	aiunionface-000	0.0000	107	0.0000	82	-	226	0.0000	49	0.0000	72	0.0000	77
18	aize-001	0.0001	289	0.0040	272	-	329	0.0026	309	0.0022	308	0.0058	251
19	ajou-001	0.0000	207	0.0020	238	-	234	0.0001	173	0.0004	231	0.0045	243
20	alchera-002	0.0000	140	0.0008	163	-	142	0.0001	194	0.0004	150	0.0003	124
21	alchera-003	0.0001	300	0.0013	213	-	178	0.0002	217	0.0004	198	0.0036	240
22	alice-000	0.0000	13	0.0006	122	-	132	0.0000	106	0.0004	151	0.0004	149
23	alleyes-000	0.0000	138	0.0010	179	-	154	0.0002	200	0.0004	205	0.0004	156
24	allgovision-000	0.0007	312	0.0062	293	-	305	0.0026	308	0.0052	320	0.0131	270
25	alphaface-001	0.0000	148	0.0012	200	-	192	0.0000	141	0.0004	206	0.0004	134
26	alphaface-002	0.0000	144	0.0012	201	-	179	0.0000	142	0.0004	207	0.0004	135
27	amplifiedgroup-001	0.0114	323	0.1023	325	-	169	0.0189	326	0.0279	329	0.1390	323
28	androvideo-000	0.0000	93	0.0000	43	-	302	0.0000	81	0.0000	57	0.0002	94
29	anke-004	0.0000	157	0.0011	191	0.0944	36	0.0001	177	0.0004	210	0.0006	185
30	anke-005	0.0000	184	0.0012	203	0.1228	38	0.0001	192	0.0004	222	0.0007	190
31	antheus-000	0.0000	67	0.0000	63	0.0000	21	0.0000	72	0.0000	49	0.0242	282
32	antheus-001	0.0000	128	0.0000	67	-	230	0.0000	58	0.0000	83	0.0242	283
33	anyvision-004	0.0000	240	0.0017	228	0.1660	41	0.0001	190	0.0004	186	0.0080	257
34	anyvision-005	0.0000	179	0.0013	210	-	289	0.0000	119	0.0004	153	0.0004	151
35	asusaics-000	0.0000	124	0.0000	71	-	266	0.0000	60	0.0000	85	0.0000	22
36	asusaics-001	0.0000	69	0.0000	60	-	274	0.0000	68	0.0000	45	0.0000	17
37	authenmetric-002	0.0000	35	0.0000	41	-	74	0.0000	8	0.0000	29	0.0000	69
38	aware-005	0.0000	218	0.0020	236	-	124	0.0001	199	0.0004	212	0.0011	208
39	aware-006	0.0000	175	0.0009	170	-	96	0.0000	122	0.0004	184	0.0006	181
40	awirots-001	0.0039	316	0.0369	318	-	67	0.0386	327	0.0872	330	0.3415	327
41	awirots-002	0.0000	266	0.0038	269	-	324	0.0007	277	0.0012	299	0.0208	278
42	ayftech-001	0.0002	302	0.0046	283	-	97	0.0043	316	0.0011	291	0.0091	262
43	ayonix-000	0.0053	319	0.0341	316	0.0000	3	0.0113	323	0.0137	326	0.1194	318
44	beethedata-000	0.0005	310	0.0042	276	-	288	0.0002	206	0.0010	285	0.0006	177
45	bioditechswiss-001	0.0000	190	0.0007	137	-	301	0.0000	110	0.0004	202	0.0025	236
46	bioditechswiss-002	0.0000	168	0.0007	140	-	92	0.0000	111	0.0004	200	0.0005	175
47	bm-001	0.0000	110	0.0000	76	0.0000	14	0.0000	91	0.0000	69	0.0000	36
48	boetech-001	0.0087	321	0.0272	310	-	141	0.0032	314	0.0160	327	0.0946	314
49	bressee-001	0.0000	167	0.0010	183	-	91	0.0002	205	0.0003	126	0.0003	102
50	bressee-002	0.0000	245	0.0020	239	-	85	0.0008	280	0.0004	171	0.0031	239
51	camvi-002	0.0000	94	0.0000	44	0.0000	23	0.0000	80	0.0000	56	0.0000	7
52	camvi-004	0.0000	6	0.0000	92	0.0000	8	0.0000	27	0.0000	4	0.0000	48
53	canon-002	0.0000	62	0.0000	20	-	95	0.0000	10	0.0000	31	0.0000	63
54	ceiec-003	0.0000	52	0.0013	216	-	116	0.0001	157	0.0004	201	0.0004	132
55	ceiec-004	0.0000	116	0.0008	158	-	253	0.0000	118	0.0004	158	0.0004	155
56	chosun-001	0.0000	71	0.0000	61	-	276	0.0000	69	0.0000	46	0.0000	18
57	chosun-002	0.0000	11	0.0000	14	-	130	0.0000	25	0.0000	2	0.0000	53
58	chtface-002	0.0000	264	0.0021	241	-	213	0.0002	225	0.0007	277	0.0014	222

Table 22: FTE is the proportion of failed template generation attempts. Failures can occur because the software throws an exception, or because the software electively refuses to process the input image. This would typically occur if a face is not detected. FTE is measured as the number of function calls that give EITHER a non-zero error code OR that give a “small” template. This is defined as one whose size is less than 0.3 times the median template size for that algorithm. This second rule is needed because some algorithms incorrectly fail to return a non-zero error code when template generation fails.

¹The effects of FTE are included in the accuracy results of this report by regarding any template comparison involving a failed template to produce a low similarity score. Thus higher FTE results in higher FNMR and lower FMR.

	Algorithm	Failure to Enrol Rate ¹						
		APPLICATION	BORDER	CHILD-EXPLOIT	MUGSHOT	VISA	WILD	
Name	SEC. 2.3	SEC. 2.4	SEC. 2.1	SEC. 2.5	SEC. 2.2	SEC. 2.6		
59 chtface-003	0.0000	247	0.0018	231	-	322	0.0001	161
60 cib-001	0.0000	46	0.0000	32	-	111	0.0000	22
61 closeli-001	0.0000	60	0.0000	21	-	102	0.0000	9
62 cloudwalk-hr-003	0.0000	199	0.0008	160	-	201	0.0001	160
63 cloudwalk-hr-004	0.0000	150	0.0011	199	-	191	0.0004	248
64 cloudwalk-mt-002	0.0000	200	0.0003	105	-	252	0.0001	148
65 cloudwalk-mt-003	0.0000	165	0.0007	133	-	113	0.0002	212
66 clova-000	0.0000	260	0.0022	244	-	263	0.0006	273
67 cogent-004	0.0000	26	0.0000	4	0.0000	9	0.0000	37
68 cogent-005	0.0000	15	0.0000	9	-	182	0.0000	41
69 cognitec-000	0.0005	308	0.0112	305	0.6342	58	0.0007	276
70 cognitec-002	0.0001	287	0.0069	294	-	81	0.0003	241
71 cor-001	0.0000	176	0.0006	125	-	98	0.0002	223
72 coretech-000	0.0000	55	0.0000	28	-	121	0.0000	16
73 corsight-001	0.0000	139	0.0006	127	-	136	0.0001	195
74 csc-001	0.0000	273	0.0030	254	-	291	0.0002	203
75 csc-002	0.0015	314	0.0033	260	-	77	0.0006	275
76 ctbcbank-000	0.0001	288	0.0051	287	0.3285	49	0.0011	290
77 ctbcbank-001	0.0000	268	0.0036	268	-	255	0.0005	263
78 cubox-001	0.0000	85	0.0000	50	-	296	0.0000	84
79 cuhkee-001	0.0000	185	0.0011	197	-	317	0.0000	99
80 cybercore-000	0.0000	181	0.0073	297	-	287	0.0001	168
81 cyberextruder-001	0.0029	315	0.0293	311	0.5338	56	0.0024	304
82 cyberextruder-002	0.0013	313	0.0840	324	0.2672	48	0.0027	310
83 cyberlink-006	0.0000	114	0.0005	116	-	250	0.0000	94
84 cyberlink-007	0.0000	75	0.0003	101	-	272	0.0000	96
85 dahua-005	0.0000	92	0.0000	88	-	300	0.0000	120
86 dahua-006	0.0000	118	0.0000	91	-	241	0.0000	134
87 decatur-000	0.0000	215	0.0020	235	-	61	0.0004	255
88 deepglint-002	0.0000	208	0.0004	112	0.0669	33	0.0002	218
89 deepglint-003	0.0000	189	0.0004	111	-	299	0.0002	219
90 deepsea-001	0.0000	19	0.0000	6	0.0000	11	0.0000	42
91 deepsense-000	0.0000	9	0.0006	128	-	134	0.0000	103
92 dermalog-006	0.0005	309	0.0031	257	0.1797	42	0.0013	295
93 dermalog-008	0.0000	261	0.0031	256	-	135	0.0006	269
94 didiglobalface-001	0.0000	173	0.0012	202	0.2175	44	0.0000	139
95 digitalbarriers-002	0.0001	292	0.0045	280	-	254	0.0028	312
96 dps-000	0.0000	8	0.0000	15	-	158	0.0000	29
97 dsk-000	0.0000	111	0.0000	77	0.0000	15	0.0000	45
98 einetworks-000	0.0000	267	0.0017	227	-	308	0.0002	215
99 ekin-002	0.0000	121	0.0000	93	-	245	0.0000	95
100 enface-000	0.0000	44	0.0012	207	-	112	0.0000	126
101 eocortex-000	0.0095	322	0.0602	321	-	87	0.0094	322
102 ercacat-001	0.0000	37	0.0005	117	-	80	0.0000	125
103 expasoft-001	0.0000	31	0.0000	3	-	170	0.0000	34
104 expasoft-002	0.0000	77	0.0000	57	-	319	0.0000	88
105 f8-001	0.0003	305	0.0059	292	0.2026	43	0.0035	315
106 facesoft-000	0.0000	120	0.0000	72	0.0000	19	0.0000	64
107 facetag-000	0.0000	36	0.0000	40	-	86	0.0000	4
108 facex-001	0.0001	299	0.0360	317	-	103	0.0047	318
109 farfaces-001	0.0000	265	0.0007	139	-	246	0.0003	236
110 fiberhome-nanjing-002	0.0000	226	0.0006	129	-	206	0.0001	165
111 fiberhome-nanjing-003	0.0000	64	0.0004	110	-	286	0.0000	73
112 fincore-000	0.0000	187	0.0008	161	-	294	0.0001	149
113 fujitsulab-002	0.0000	61	0.0009	168	-	105	0.0001	187
114 fujitsulab-003	0.0000	102	0.0008	154	-	220	0.0001	176
115 geo-001	0.0000	201	0.0011	190	-	243	0.0000	138
116 geo-002	0.0000	193	0.0015	219	-	218	0.0001	145

Table 23: FTE is the proportion of failed template generation attempts. Failures can occur because the software throws an exception, or because the software electively refuses to process the input image. This would typically occur if a face is not detected. FTE is measured as the number of function calls that give EITHER a non-zero error code OR that give a “small” template. This is defined as one whose size is less than 0.3 times the median template size for that algorithm. This second rule is needed because some algorithms incorrectly fail to return a non-zero error code when template generation fails.

¹ The effects of FTE are included in the accuracy results of this report by regarding any template comparison involving a failed template to produce a low similarity score. Thus higher FTE results in higher FNMR and lower FMR.

	Algorithm	Failure to Enrol Rate ¹						
		APPLICATION	BORDER	CHILD-EXPLOIT	MUGSHOT	VISA	WILD	
Name	SEC. 2.3	SEC. 2.4	SEC. 2.1	SEC. 2.5	SEC. 2.2	SEC. 2.6		
117	glory-002	0.0003	303	0.0045	279	-	108	0.0015
118	glory-003	0.0000	228	0.0027	250	-	161	0.0004
119	gorilla-006	0.0000	66	0.0006	131	-	282	0.0000
120	gorilla-007	0.0000	149	0.0009	177	-	193	0.0001
121	hertasecurity-000	0.0133	325	0.0077	300	-	167	0.0025
122	hik-001	0.0000	28	0.0000	95	-	173	0.0000
123	hyperverge-001	0.0000	282	0.0072	295	-	295	0.0015
124	hyperverge-002	0.0000	32	0.0008	153	-	75	0.0002
125	icm-002	0.0000	113	0.0001	96	-	202	0.0000
126	icthtc-000	0.0001	298	0.0047	285	-	309	0.0028
127	id3-006	0.0000	230	0.0009	176	-	123	0.0004
128	id3-007	0.0000	166	0.0041	274	-	120	0.0001
129	idemia-007	0.0000	126	0.0004	114	-	261	0.0000
130	idemia-008	0.0000	33	0.0004	113	-	78	0.0000
131	iit-002	0.0000	271	0.0021	240	-	323	0.0009
132	iit-003	0.0000	198	0.0008	162	-	204	0.0000
133	imagus-002	0.0000	236	0.0018	229	-	256	0.0000
134	imagus-003	0.0000	58	0.0000	23	-	93	0.0000
135	imperial-000	0.0000	54	0.0000	27	-	118	0.0000
136	imperial-002	0.0000	29	0.0000	1	0.0000	10	0.0000
137	incode-008	0.0000	214	0.0009	172	-	172	0.0002
138	incode-009	0.0000	225	0.0009	173	-	195	0.0002
139	innefulabs-000	0.0000	153	0.0024	246	-	166	0.0003
140	innovativetechnologyltd-001	0.0001	296	0.0050	286	-	145	0.0024
141	innovativetechnologyltd-002	0.0000	231	0.0046	282	-	126	0.0057
142	innovatrics-006	0.0000	156	0.0009	175	0.0350	28	0.0000
143	innovatrics-007	0.0000	158	0.0007	146	-	83	0.0001
144	insightface-000	0.0000	100	0.0000	85	-	212	0.0000
145	intellicloudai-001	0.0000	14	0.0000	12	-	144	0.0000
146	intellicloudai-002	0.0000	42	0.0008	155	-	71	0.0000
147	intellifusion-001	0.0000	209	0.0005	119	0.0949	37	0.0001
148	intellifusion-002	0.0000	105	0.0000	94	-	223	0.0000
149	intellivision-001	0.0042	317	0.0296	312	0.5495	57	0.0048
150	intellivision-002	0.0000	283	0.0046	281	-	155	0.0012
151	intelresearch-002	0.0000	204	0.0022	242	-	262	0.0000
152	intelresearch-003	0.0000	136	0.0006	123	-	151	0.0000
153	intsyssmsu-001	0.0000	134	0.0010	182	-	239	0.0001
154	intsyssmsu-002	0.0000	79	0.0010	181	-	332	0.0001
155	ionetworks-000	0.0000	12	0.0016	224	-	131	0.0004
156	iqface-000	0.0000	34	0.0000	42	0.0000	2	0.0000
157	iqface-003	0.0000	269	0.0076	299	-	146	0.0006
158	irex-000	0.0000	242	0.0009	174	-	258	0.0000
159	isap-001	0.0000	4	0.0000	19	-	150	0.0000
160	isap-002	0.0000	43	0.0000	35	-	68	0.0000
161	isityou-000	0.0068	320	0.0316	315	0.4714	53	0.0023
162	isystems-001	0.0000	274	0.0035	265	0.1421	40	0.0010
163	isystems-002	0.0000	275	0.0035	266	0.1421	39	0.0010
164	itmo-006	0.0000	16	0.0015	220	-	183	0.0004
165	itmo-007	0.0000	83	0.0009	166	-	330	0.0003
166	ivacognitive-001	0.0000	227	0.0011	193	-	207	0.0001
167	iws-000	0.0005	311	0.0650	322	-	190	0.0024
168	kakao-004	0.0000	108	0.0000	79	-	217	0.0000
169	kakao-005	0.0000	73	0.0000	90	-	279	0.0000
170	kakaopay-001	0.0000	210	0.0013	214	-	129	0.0001
171	kedacom-000	0.0000	51	0.0000	25	0.0000	7	0.0000
172	kiwitech-000	0.0000	155	0.0009	164	-	175	0.0004
173	kneron-003	0.0239	327	0.0306	313	0.4883	55	0.0044
174	kneron-005	0.0000	277	0.0226	308	-	208	0.0006

Table 24: FTE is the proportion of failed template generation attempts. Failures can occur because the software throws an exception, or because the software electively refuses to process the input image. This would typically occur if a face is not detected. FTE is measured as the number of function calls that give EITHER a non-zero error code OR that give a “small” template. This is defined as one whose size is less than 0.3 times the median template size for that algorithm. This second rule is needed because some algorithms incorrectly fail to return a non-zero error code when template generation fails.

¹The effects of FTE are included in the accuracy results of this report by regarding any template comparison involving a failed template to produce a low similarity score. Thus higher FTE results in higher FNMR and lower FMR.

	Algorithm	Failure to Enrol Rate ¹											
		APPLICATION	BORDER	CHILD-EXPLOIT	MUGSHOT	VISA	WILD	SEC. 2.3	SEC. 2.4	SEC. 2.1	SEC. 2.5	SEC. 2.2	SEC. 2.6
175	kookmin-001	0.0000	3	0.0000	18	-	149	0.0000	32	0.0000	9	0.0000	51
176	kookmin-002	0.0000	135	0.0000	65	-	235	0.0000	56	0.0000	81	0.0000	28
177	lemalabs-001	0.0000	25	0.0005	120	-	163	0.0002	214	0.0004	143	0.0004	137
178	line-000	0.0000	21	0.0000	8	-	177	0.0000	43	0.0000	20	0.0000	79
179	lookman-002	0.0000	41	0.0000	36	-	69	0.0000	1	0.0000	22	0.0000	72
180	lookman-004	0.0000	80	0.0000	55	0.0000	24	0.0000	86	0.0000	62	0.0000	3
181	luxand-000	0.0000	130	0.0000	66	-	228	0.0000	59	0.0000	84	0.0000	29
182	megvii-002	0.0000	23	0.0006	124	0.0274	27	0.0054	320	0.0004	152	0.0126	266
183	megvii-003	0.0000	137	0.0010	187	-	152	0.0002	221	0.0004	209	0.0011	212
184	meituan-000	0.0000	131	0.0001	98	-	227	0.0000	101	0.0002	99	0.0001	89
185	meiya-001	0.0000	272	0.0028	253	-	72	0.0004	257	0.0010	288	0.0025	235
186	microfocus-001	0.0001	295	0.0053	290	0.0791	34	0.0008	282	0.0016	304	0.0220	280
187	microfocus-002	0.0001	294	0.0053	289	0.0791	35	0.0008	283	0.0016	303	0.0220	279
188	minivision-000	0.0000	10	0.0000	13	-	128	0.0000	26	0.0000	3	0.0000	52
189	mobai-000	0.0000	248	0.0114	306	-	200	0.0003	238	0.0012	297	0.1242	319
190	mobai-001	0.0000	222	0.0040	271	-	320	0.0001	179	0.0012	296	0.0523	302
191	mobbl-000	0.0116	324	0.0720	323	-	316	0.0119	324	0.0063	322	0.1136	317
192	mobbl-001	0.0000	270	0.0052	288	-	153	0.0002	202	0.0005	259	0.0181	277
193	moreedian-000	0.0000	142	0.0009	165	-	139	0.0004	252	0.0005	239	0.0004	161
194	mvision-001	0.0000	127	0.0000	69	-	260	0.0000	62	0.0000	87	0.0000	21
195	nazhiai-000	0.0000	89	0.0000	47	-	307	0.0000	77	0.0000	53	0.0000	8
196	neosystems-001	0.0000	91	0.0000	89	-	312	0.0013	296	0.9994	332	0.0002	101
197	neosystems-002	0.0000	72	0.0000	62	-	277	0.0000	67	0.0000	44	0.0000	20
198	netbridge-tech-001	0.0000	47	0.0000	31	-	110	0.0000	23	0.0000	42	0.0000	61
199	netbridge-tech-002	0.0000	63	0.0000	64	-	284	0.0000	74	0.0000	50	0.0000	15
200	neurotechnology-011	0.0000	213	0.0013	209	-	189	0.0002	204	0.0003	134	0.0020	232
201	neurotechnology-012	0.0000	263	0.0010	189	-	278	0.0001	189	0.0004	187	0.0005	170
202	nhn-001	0.0000	182	0.0019	232	-	273	0.0001	163	0.0004	230	0.0020	233
203	nhn-002	0.0000	22	0.0004	115	-	194	0.0000	113	0.0003	111	0.0003	105
204	nodeflux-002	0.0000	162	0.0261	309	-	60	0.0008	281	0.0005	256	0.0008	203
205	notiontag-000	0.0000	98	0.0000	84	0.0000	16	0.0000	54	0.0000	78	0.0000	31
206	notiontag-001	0.0000	97	0.0000	83	-	209	0.0027	311	0.0000	80	0.0132	271
207	nsensecorp-001	0.0000	281	0.0024	245	-	325	0.0014	298	0.0101	325	0.0375	295
208	nsensecorp-002	0.0000	197	0.0009	167	-	205	0.0003	227	0.0011	289	0.0178	276
209	ntechlab-009	0.0000	241	0.0009	171	-	216	0.0001	191	0.0004	139	0.0005	164
210	ntechlab-010	0.0000	202	0.0005	118	-	242	0.0001	175	0.0004	149	0.0006	176
211	null-000	-	330	-	331	-	156	-	333	-	333	-	331
212	null-082	-	333	-	333	-	62	-	330	-	334	-	334
213	omnigarde-000	0.0000	203	0.0008	150	-	249	0.0000	109	0.0004	191	0.0003	127
214	openface-001	0.0000	254	0.0104	304	-	73	0.0004	249	0.0006	273	0.0856	311
215	oz-001	0.0000	243	0.0011	198	-	229	0.0006	274	0.0004	168	0.0014	220
216	oz-002	0.0000	104	0.0003	103	-	222	0.0000	104	0.0003	124	0.0002	99
217	papsav1923-001	0.0000	177	0.0007	141	-	101	0.0001	170	0.0002	102	0.0005	166
218	paravision-004	0.0000	237	0.0007	148	0.0570	30	0.0002	213	0.0004	172	0.0008	199
219	paravision-008	0.0000	133	0.0010	180	-	238	0.0001	164	0.0004	142	0.0003	128
220	pensees-001	0.0000	160	0.0000	39	-	82	0.0000	5	0.0000	26	0.0000	67
221	pixelall-005	0.0000	38	0.0000	38	-	79	0.0000	6	0.0000	27	0.0000	66
222	pixelall-006	0.0000	53	0.0000	26	-	117	0.0000	14	0.0000	34	0.0000	56
223	psl-007	0.0000	146	0.0007	132	-	184	0.0000	133	0.0003	125	0.0003	117
224	psl-008	0.0000	161	0.0003	104	-	65	0.0000	97	0.0003	122	0.0002	100
225	ptakuratsatu-000	0.0000	183	0.0007	147	-	321	0.0001	146	0.0003	118	0.0003	113
226	pxl-001	0.0000	286	0.0044	278	-	318	0.0005	261	0.0022	309	0.0323	291
227	pyramid-000	0.0001	291	0.0041	275	-	164	0.0005	260	0.0007	280	0.0015	223
228	quantasoft-003	0.0000	249	0.0015	222	-	248	0.0005	259	0.0006	271	0.0088	261
229	rankone-009	0.0000	76	0.0000	59	-	271	0.0000	70	0.0000	47	0.0000	74
230	rankone-010	0.0000	74	0.0000	58	-	270	0.0000	71	0.0000	48	0.0000	16
231	realnetworks-002	0.0000	234	0.0003	107	-	292	0.0004	245	0.0003	113	0.0004	153
232	realnetworks-004	0.0000	141	0.0003	102	-	138	0.0000	89	0.0002	103	0.0003	111

Table 25: FTE is the proportion of failed template generation attempts. Failures can occur because the software throws an exception, or because the software electively refuses to process the input image. This would typically occur if a face is not detected. FTE is measured as the number of function calls that give EITHER a non-zero error code OR that give a “small” template. This is defined as one whose size is less than 0.3 times the median template size for that algorithm. This second rule is needed because some algorithms incorrectly fail to return a non-zero error code when template generation fails.

¹ The effects of FTE are included in the accuracy results of this report by regarding any template comparison involving a failed template to produce a low similarity score. Thus higher FTE results in higher FNMR and lower FMR.

	Algorithm	Failure to Enrol Rate ¹							
		Name	APPLICATION	BORDER	CHILD-EXPLOIT	MUGSHOT	VISA	WILD	
	Name	SEC. 2.3	SEC. 2.4	SEC. 2.1	SEC. 2.5	SEC. 2.2	SEC. 2.6		
233	regula-000	0.0000	57	0.0000	22	-	90	0.0000	12
234	remarkai-001	0.0000	106	0.0000	81	-	225	0.0000	50
235	remarkai-003	0.0000	196	0.0007	138	-	198	0.0000	128
236	rendip-000	0.0000	235	0.0016	223	-	251	0.0002	210
237	rokid-000	0.0000	125	0.0072	296	-	267	0.0001	167
238	rokid-001	0.0000	65	0.0013	212	-	281	0.0000	75
239	s1-001	0.0000	285	0.0073	298	-	327	0.0013	293
240	s1-002	0.0000	223	0.0089	301	-	314	0.0001	185
241	saffe-001	0.0000	48	0.0000	33	0.0000	4	0.0000	21
242	saffe-002	0.0000	30	0.0000	2	-	168	0.0000	35
243	samtech-001	0.0001	290	0.0032	259	-	232	0.0004	254
244	scanovate-001	0.0208	326	0.2388	326	-	224	0.0024	303
245	scanovate-002	0.0000	211	0.0018	230	-	133	0.0000	140
246	securifai-001	0.0000	78	0.0000	56	-	315	0.0000	93
247	securifai-002	0.0000	2	0.0000	17	-	148	0.0000	30
248	sensetime-004	0.0000	147	0.0011	196	-	185	0.0000	90
249	sensetime-005	0.0000	132	0.0004	109	-	237	0.0000	114
250	sertis-000	0.0000	39	0.0007	143	-	64	0.0000	143
251	sertis-002	0.0000	27	0.0007	136	-	171	0.0000	136
252	seventhsense-000	0.0000	159	0.0006	130	-	84	0.0001	150
253	shaman-000	0.0000	115	0.0000	74	0.0000	20	0.0000	63
254	shaman-001	0.0000	101	0.0000	80	0.0000	18	0.0000	51
255	shu-002	0.0000	219	0.0010	184	-	114	0.0005	258
256	shu-003	0.0000	103	0.0007	135	-	221	0.0001	152
257	siat-002	0.0000	163	0.0012	206	0.0616	31	0.0000	124
258	siat-004	0.0000	154	0.0011	195	-	174	0.0000	112
259	sjtu-003	0.0000	68	0.0005	121	-	269	0.0000	135
260	sjtu-004	0.0000	49	0.0000	30	-	125	0.0000	13
261	sktelecom-000	0.0000	151	0.0008	157	-	162	0.0000	132
262	smilart-002	0.0000	278	0.0036	267	0.2422	47	0.0003	242
263	smilart-003	0.0003	304	0.0100	303	-	160	0.0014	297
264	sodec-000	0.0000	119	0.0000	73	-	244	0.0000	65
265	staqu-000	0.0000	109	0.0000	78	-	199	0.0000	48
266	starhybrid-001	0.0001	293	0.0033	262	0.2340	46	0.0009	286
267	suprema-000	0.0000	217	0.0017	226	-	70	0.0002	216
268	supremaid-001	0.0000	164	0.0020	237	-	66	0.0001	171
269	synesis-006	0.0000	1	0.0003	108	-	147	0.0000	131
270	synesis-007	0.0000	171	0.0013	211	-	106	0.0002	220
271	synology-000	0.0000	90	0.0000	48	-	310	0.0000	76
272	synology-002	0.0000	18	0.0000	11	-	188	0.0000	40
273	sztu-000	0.0000	86	0.0000	52	-	298	0.0000	83
274	sztu-001	0.0000	82	0.0000	54	-	328	0.0000	87
275	tech5-004	0.0000	186	0.0008	151	-	331	0.0003	229
276	tech5-005	0.0000	192	0.0007	149	-	210	0.0000	108
277	tevian-005	0.0001	297	0.0041	273	0.3606	50	0.0006	271
278	tevian-006	0.0000	99	0.0012	204	-	211	0.0003	234
279	tiger-003	0.0000	206	-	334	0.0619	32	0.0001	181
280	tiger-004	0.0000	284	0.0022	243	-	99	0.0001	180
281	tinkoff-001	0.0000	221	0.0008	156	-	100	0.0001	188
282	tongyi-005	0.0000	40	0.0000	37	0.0000	1	0.0000	3
283	toshiba-002	0.0000	17	0.0000	10	0.0000	12	0.0000	39
284	toshiba-003	0.0000	122	0.0001	97	-	247	0.0001	183
285	trueface-001	0.0000	216	0.0038	270	-	63	0.0007	278
286	trueface-002	0.0000	212	0.0046	284	-	186	0.0003	226
287	tuputech-000	0.0003	306	0.0116	307	-	285	0.0632	328
288	twface-000	0.0000	123	0.0000	70	-	265	0.0000	61
289	ulsee-001	0.0000	129	0.0000	68	-	233	0.0000	57
290	ultinous-000	-	331	-	329	0.0007	26	-	334
								0.0003	121
									- 330

Table 26: FTE is the proportion of failed template generation attempts. Failures can occur because the software throws an exception, or because the software electively refuses to process the input image. This would typically occur if a face is not detected. FTE is measured as the number of function calls that give EITHER a non-zero error code OR that give a “small” template. This is defined as one whose size is less than 0.3 times the median template size for that algorithm. This second rule is needed because some algorithms incorrectly fail to return a non-zero error code when template generation fails.

¹ The effects of FTE are included in the accuracy results of this report by regarding any template comparison involving a failed template to produce a low similarity score. Thus higher FTE results in higher FNMR and lower FMR.

	Algorithm	Failure to Enrol Rate ¹						
		APPLICATION	BORDER	CHILD-EXPLOIT	MUGSHOT	VISA	WILD	
Name	SEC. 2.3	SEC. 2.4	SEC. 2.1	SEC. 2.5	SEC. 2.2	SEC. 2.6		
291	ultinous-001	- 334	- 332	0.0007 25	- 332	0.0003 123	- 332	
292	uluface-002	0.0000 84	0.0000 49	0.0000 22	0.0000 85	0.0000 61	0.0000 12	
293	uluface-003	0.0000 7	0.0001 99	- 157	0.0002 201	0.0002 98	0.0244 285	
294	upc-001	0.0000 259	0.0003 106	0.0450 29	0.0003 228	0.0003 132	0.0011 207	
295	vcog-002	- 332	0.3719 328	0.2209 45	- 331	0.0019 307	- 333	
296	vd-001	0.0000 276	0.0030 255	- 259	0.0004 251	0.0009 283	0.0024 234	
297	vd-002	0.0000 96	0.0000 86	- 215	0.0000 53	0.0000 77	0.0000 33	
298	veridas-004	0.0000 258	0.0026 249	- 231	0.0001 182	0.0005 247	0.0006 182	
299	veridas-006	0.0000 255	0.0026 248	- 280	0.0001 184	0.0005 246	0.0006 180	
300	via-000	0.0000 45	0.0000 34	0.0000 5	0.0000 20	0.0000 40	0.0001 85	
301	via-001	0.0000 56	0.0000 29	- 119	0.0000 15	0.0000 36	0.0001 84	
302	videmo-000	0.0000 224	0.0019 233	- 333	0.0003 237	0.0012 298	0.0158 273	
303	videonetics-001	0.0004 307	0.0309 314	0.4799 54	0.0015 300	0.0010 286	0.0112 264	
304	videonetics-002	0.0000 229	0.0459 320	0.4598 52	0.0006 272	0.0005 263	0.0013 216	
305	vigilantsolutions-009	0.0000 244	0.0028 252	- 76	0.0001 155	0.0004 144	0.0005 169	
306	vigilantsolutions-010	0.0000 246	0.0028 251	- 88	0.0001 156	0.0004 146	0.0005 168	
307	vinaï-000	0.0000 88	0.0000 46	- 306	0.0000 78	0.0000 54	0.0000 9	
308	vion-000	0.0050 318	0.0392 319	0.6388 59	0.0130 325	0.0078 323	0.1389 322	
309	visage-000	0.0000 262	0.0054 291	- 268	0.0009 284	0.0006 270	0.0064 252	
310	visionbox-001	0.0000 280	0.0033 261	- 197	0.0005 267	0.0011 293	0.0028 238	
311	visionbox-002	0.0000 70	0.0017 225	- 275	0.0000 123	0.0004 232	0.0046 245	
312	visionlabs-009	0.0000 191	0.0010 178	- 214	0.0001 147	0.0004 189	0.0006 187	
313	visionlabs-010	0.0000 239	0.0009 169	- 143	0.0001 193	0.0004 180	0.0006 184	
314	visteam-000	0.0000 279	0.0031 258	- 180	0.0005 262	0.0011 290	0.0026 237	
315	visteam-001	0.0000 238	0.0014 217	- 137	0.0002 207	0.0004 192	0.0011 210	
316	vnpt-001	0.0652 329	0.2829 327	- 240	0.2116 329	0.1598 331	0.3544 328	
317	vnpt-002	0.0000 178	0.0002 100	- 283	0.0003 239	0.0003 107	0.0001 90	
318	vocord-008	0.0000 195	0.0015 221	- 196	0.0003 240	0.0001 94	0.0007 192	
319	vocord-009	0.0000 172	0.0006 126	- 107	0.0001 197	0.0003 106	0.0003 106	
320	vts-000	0.0000 233	0.0011 192	- 122	0.0001 198	0.0004 229	0.0013 215	
321	winsense-001	0.0000 50	0.0000 24	0.0000 6	0.0000 18	0.0000 38	0.0000 54	
322	winsense-002	0.0000 87	0.0000 51	- 297	0.0000 82	0.0000 58	0.0000 13	
323	x-laboratory-000	0.0247 328	0.0000 87	0.0000 17	0.0005 266	0.0002 100	0.0000 34	
324	x-laboratory-001	0.0000 152	0.0012 205	- 165	0.0001 186	0.0004 218	0.0007 188	
325	xforwardai-001	0.0000 174	0.0007 144	- 109	0.0003 230	0.0004 211	0.0004 133	
326	xforwardai-002	0.0000 180	0.0007 145	- 290	0.0003 231	0.0004 214	0.0004 131	
327	xm-000	0.0000 59	0.0007 134	- 89	0.0001 151	0.0003 114	0.0004 162	
328	yisheng-004	0.0002 301	- 330	0.4279 51	0.0013 294	0.0006 272	0.0321 290	
329	yitu-003	0.0000 81	0.0000 53	- 326	0.0009 285	0.0000 65	0.0000 1	
330	yoonik-000	0.0000 143	0.0019 234	- 140	0.0001 166	0.0004 217	0.0009 205	
331	yoonik-001	0.0000 117	0.0014 218	- 257	0.0001 196	0.0004 216	0.0017 228	
332	yitu-000	0.0000 194	0.0010 188	- 219	0.0002 222	0.0004 215	0.0011 211	
333	yuan-001	0.0000 257	0.0010 185	- 311	0.0005 264	0.0005 250	0.0005 173	
334	yuan-002	0.0000 256	0.0010 186	- 334	0.0005 265	0.0005 251	0.0005 172	

Table 27: FTE is the proportion of failed template generation attempts. Failures can occur because the software throws an exception, or because the software electively refuses to process the input image. This would typically occur if a face is not detected. FTE is measured as the number of function calls that give EITHER a non-zero error code OR that give a “small” template. This is defined as one whose size is less than 0.3 times the median template size for that algorithm. This second rule is needed because some algorithms incorrectly fail to return a non-zero error code when template generation fails.

¹ The effects of FTE are included in the accuracy results of this report by regarding any template comparison involving a failed template to produce a low similarity score. Thus higher FTE results in higher FNMR and lower FMR.

3.4 Recognition accuracy

Core algorithm accuracy is stated via:

▷ **Cooperative subjects**

- The summary table of Figure 21;
- The visa image DETs of Figure 51;
- The mugshot DETs of Figure 68;
- The mugshot ageing profiles of Figure 251;
- The human-difficult pairs of Figure 17

▷ **Non-cooperative subjects**

- The photojournalism DET of Figure 82
- The child-exploitation DET of Figure 85;
- The child-exploitation CMC of Figure 89.

Figure 203 shows dependence of false match rate on algorithm score threshold. This allows a deployer to set a threshold to target a particular false match rate appropriate to the security objectives of the application.

Figure 169 likewise shows FMR(T) but for mugshots, and specially four subsets of the population.

Note that in both the mugshot and visa sets false match rates vary with the ethnicity, age, and sex, of the enrollee and impostor. For example figure 107 summarizes FMR for impostors paired from four groups black females, black males, white females, white males.

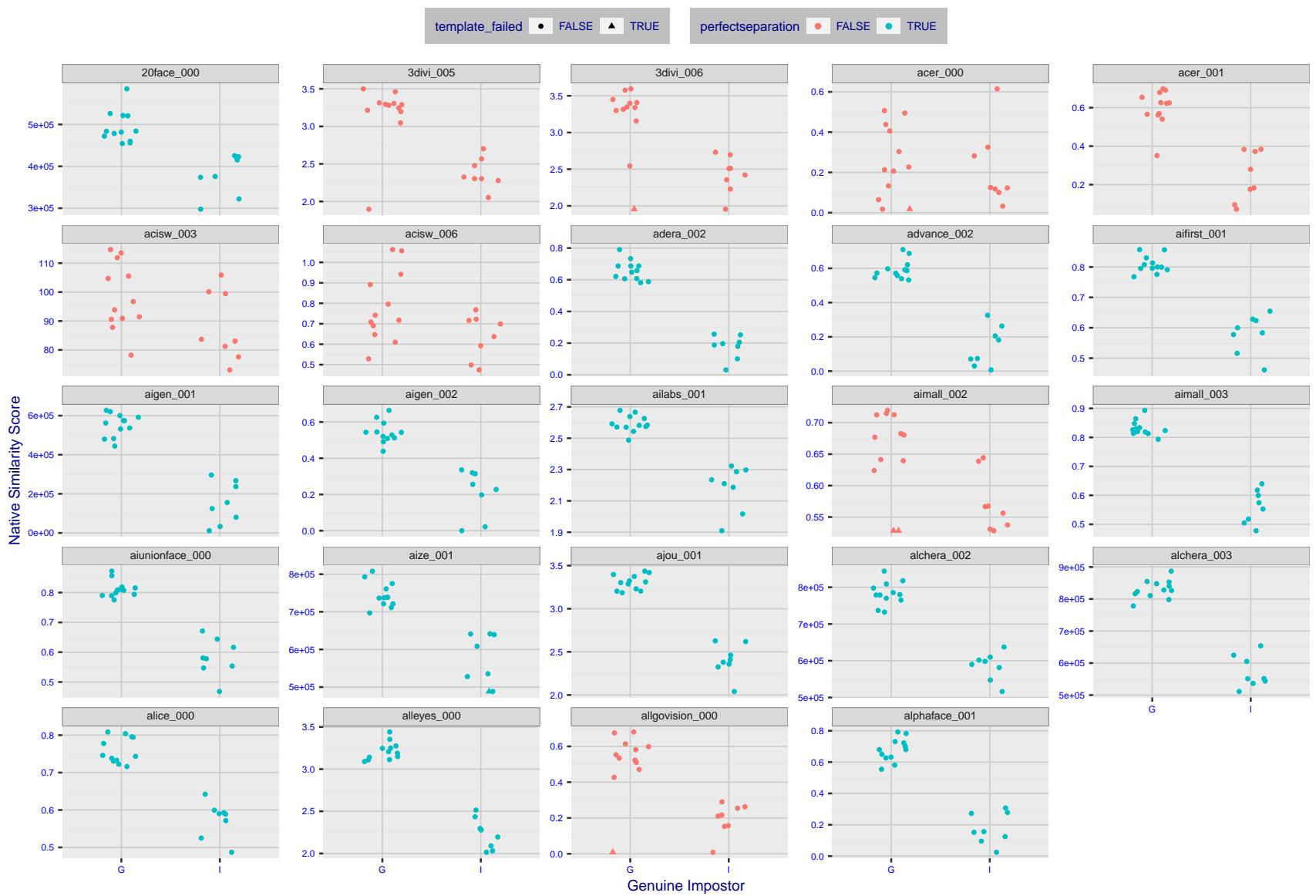


Figure 4: The Figure shows, in blue, algorithms that correctly separate the 12 genuine and 8 impostor pairs used in the May 2018 paper [Face recognition accuracy of forensic examiners, superrecognizers, and face recognition algorithms](#) (Phillips et al. [1]). In red are algorithms that are imperfect. Some algorithms fail only because they failed to make a template e.g. due to face detection failure (shown as a triangle). Others fail because the pairs were selected for that study because they had been difficult for three leading algorithms used in FRVT 2006. Caution: Given the small sample size ($n=20$) the figure may change substantially if larger or different sets were used. The images can be downloaded from the [Supplemental Information](#) page provided with that publication.



Figure 5: The Figure shows, in blue, algorithms that correctly separate the 12 genuine and 8 impostor pairs used in the May 2018 paper [Face recognition accuracy of forensic examiners, superrecognizers, and face recognition algorithms](#) (Phillips et al. [1]). In red are algorithms that imperfect. Some algorithms fail only because they failed to make a template e.g. due to face detection failure (shown as a triangle). Others fail because the pairs were selected for that study because they had been difficult for three leading algorithms used in FRVT 2006. Caution: Given the small sample size ($n=20$) the figure may change substantially if larger or different sets were used. The images can be downloaded from the [Supplemental Information](#) page provided with that publication.

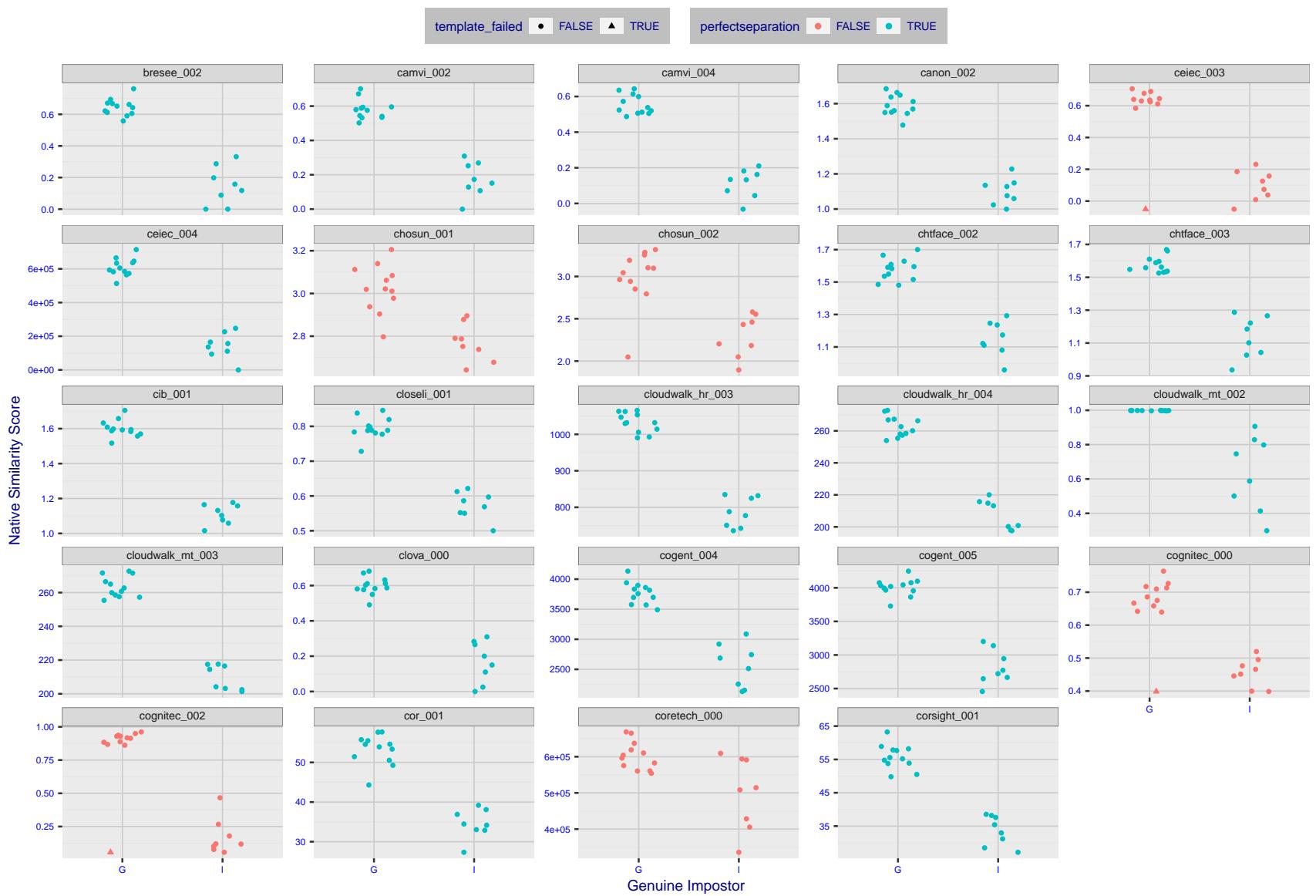


Figure 6: The Figure shows, in blue, algorithms that correctly separate the 12 genuine and 8 impostor pairs used in the May 2018 paper Face recognition accuracy of forensic examiners, superrecognizers, and face recognition algorithms (Phillips et al. [1]). In red are algorithms that are imperfect. Some algorithms fail only because they failed to make a template e.g. due to face detection failure (shown as a triangle). Others fail because the pairs were selected for that study because they had been difficult for three leading algorithms used in FRVT 2006. Caution: Given the small sample size ($n=20$) the figure may change substantially if larger or different sets were used. The images can be downloaded from the [Supplemental Information](#) page provided with that publication.



Figure 7: The Figure shows, in blue, algorithms that correctly separate the 12 genuine and 8 impostor pairs used in the May 2018 paper [Face recognition accuracy of forensic examiners, superrecognizers, and face recognition algorithms](#) (Phillips et al. [1]). In red are algorithms that are imperfect. Some algorithms fail only because they failed to make a template e.g. due to face detection failure (shown as a triangle). Others fail because the pairs were selected for that study because they had been difficult for three leading algorithms used in FRVT 2006. Caution: Given the small sample size ($n=20$) the figure may change substantially if larger or different sets were used. The images can be downloaded from the [Supplemental Information](#) page provided with that publication.



Figure 8: The Figure shows, in blue, algorithms that correctly separate the 12 genuine and 8 impostor pairs used in the May 2018 paper [Face recognition accuracy of forensic examiners, superrecognizers, and face recognition algorithms](#) (Phillips et al. [1]). In red are algorithms that are imperfect. Some algorithms fail only because they failed to make a template e.g. due to face detection failure (shown as a triangle). Others fail because the pairs were selected for that study because they had been difficult for three leading algorithms used in FRVT 2006. Caution: Given the small sample size ($n=20$) the figure may change substantially if larger or different sets were used. The images can be downloaded from the [Supplemental Information](#) page provided with that publication.

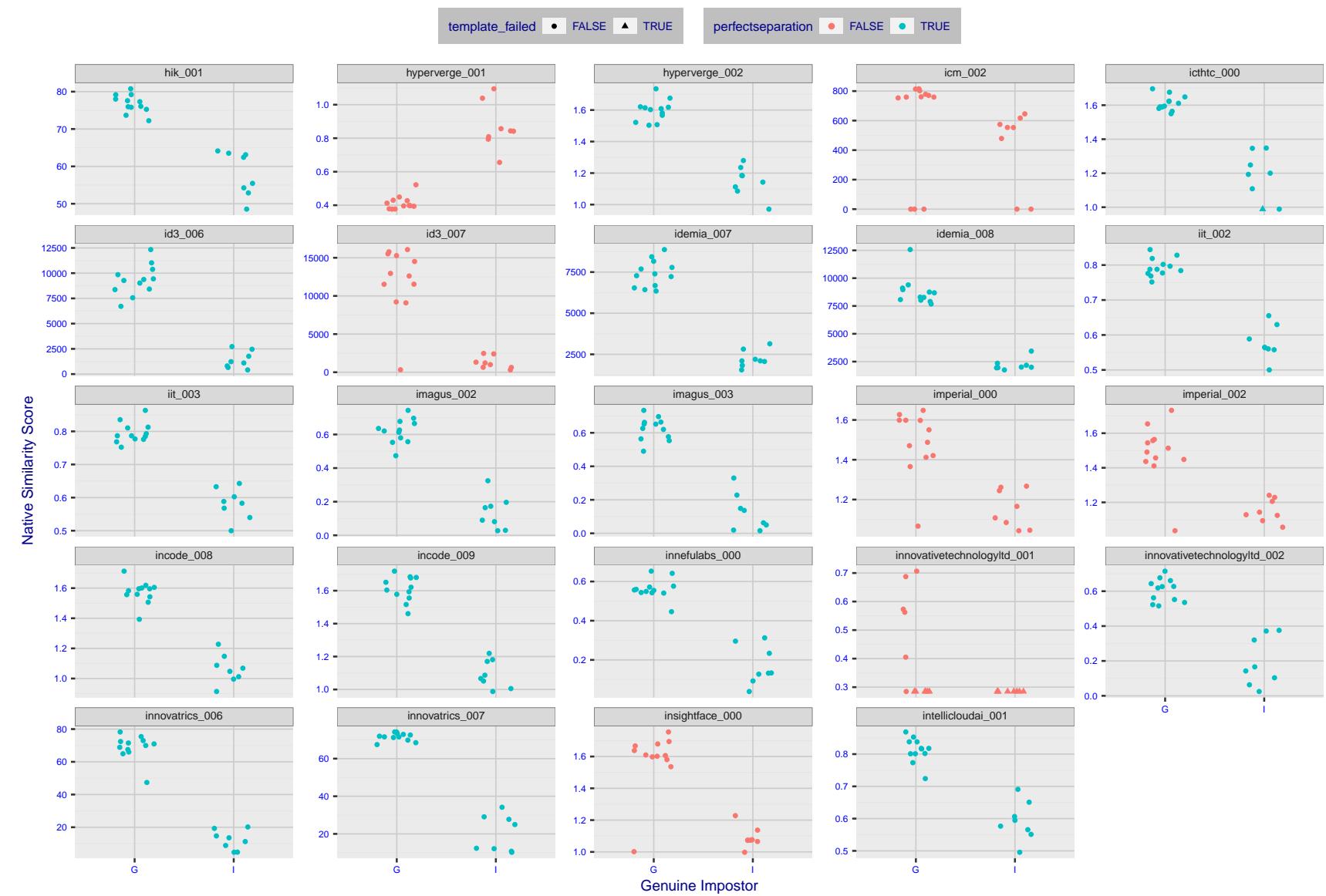


Figure 9: The Figure shows, in blue, algorithms that correctly separate the 12 genuine and 8 impostor pairs used in the May 2018 paper [Face recognition accuracy of forensic examiners, superrecognizers, and face recognition algorithms](#) (Phillips et al. [1]). In red are algorithms that are imperfect. Some algorithms fail only because they failed to make a template e.g. due to face detection failure (shown as a triangle). Others fail because the pairs were selected for that study because they had been difficult for three leading algorithms used in FRVT 2006. Caution: Given the small sample size ($n=20$) the figure may change substantially if larger or different sets were used. The images can be downloaded from the [Supplemental Information](#) page provided with that publication.

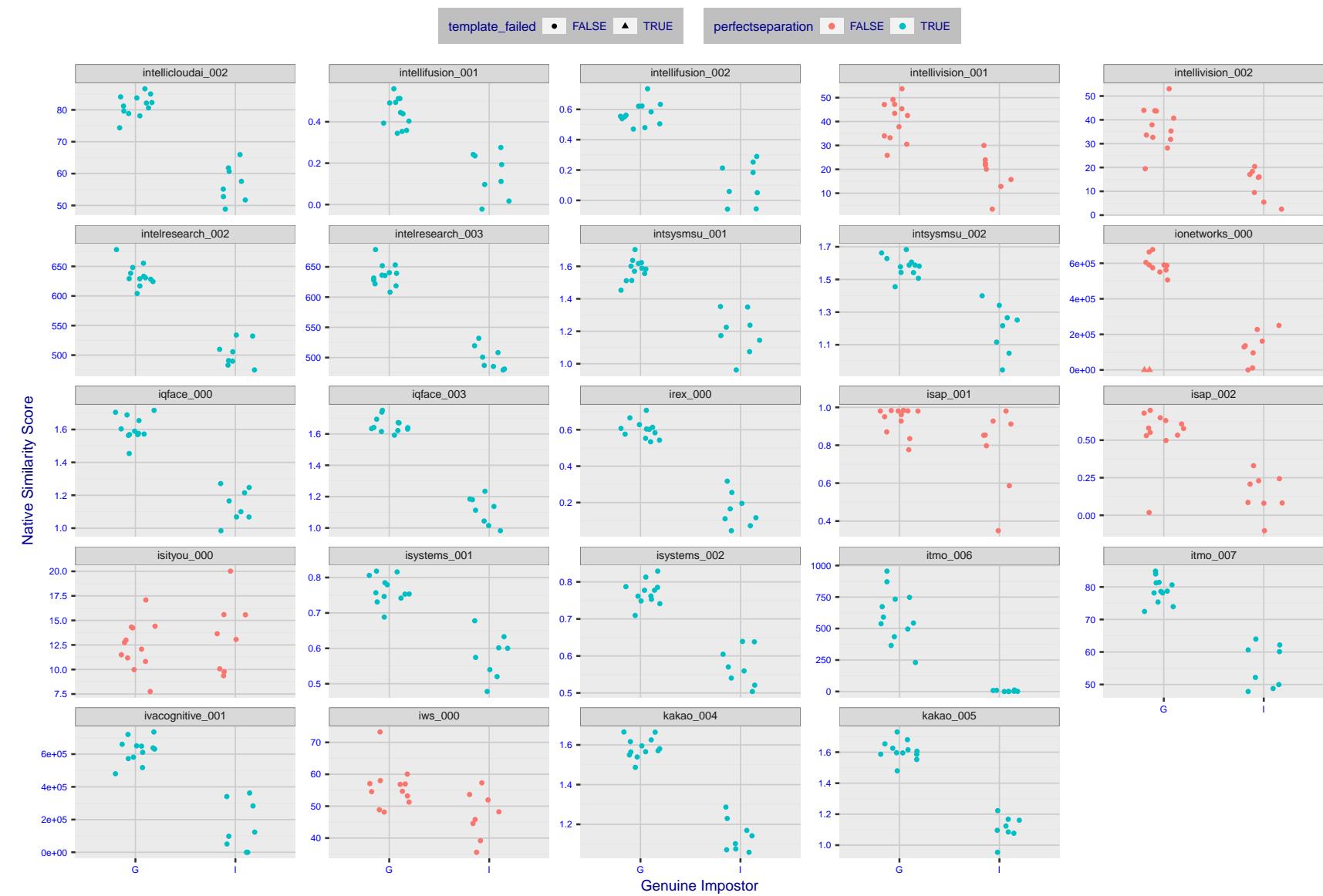


Figure 10: The Figure shows, in blue, algorithms that correctly separate the 12 genuine and 8 impostor pairs used in the May 2018 paper [Face recognition accuracy of forensic examiners, superrecognizers, and face recognition algorithms](#) (Phillips et al. [1]). In red are algorithms that are imperfect. Some algorithms fail only because they failed to make a template e.g. due to face detection failure (shown as a triangle). Others fail because the pairs were selected for that study because they had been difficult for three leading algorithms used in FRVT 2006. Caution: Given the small sample size ($n=20$) the figure may change substantially if larger or different sets were used. The images can be downloaded from the [Supplemental Information](#) page provided with that publication.

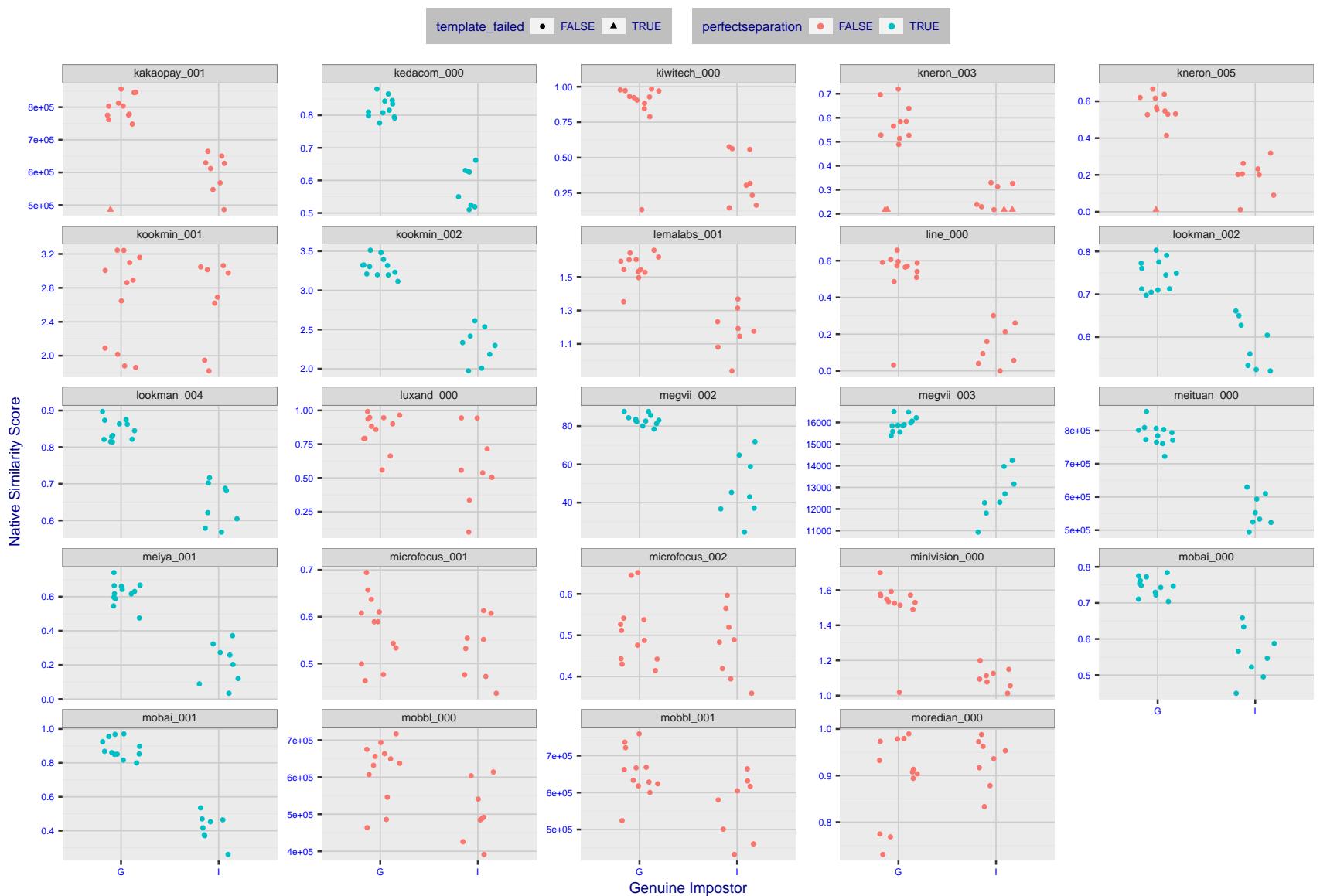


Figure 11: The Figure shows, in blue, algorithms that correctly separate the 12 genuine and 8 impostor pairs used in the May 2018 paper [Face recognition accuracy of forensic examiners, superrecognizers, and face recognition algorithms](#) (Phillips et al. [1]). In red are algorithms that are imperfect. Some algorithms fail only because they failed to make a template e.g. due to face detection failure (shown as a triangle). Others fail because the pairs were selected for that study because they had been difficult for three leading algorithms used in FRVT 2006. Caution: Given the small sample size ($n=20$) the figure may change substantially if larger or different sets were used. The images can be downloaded from the [Supplemental Information](#) page provided with that publication.

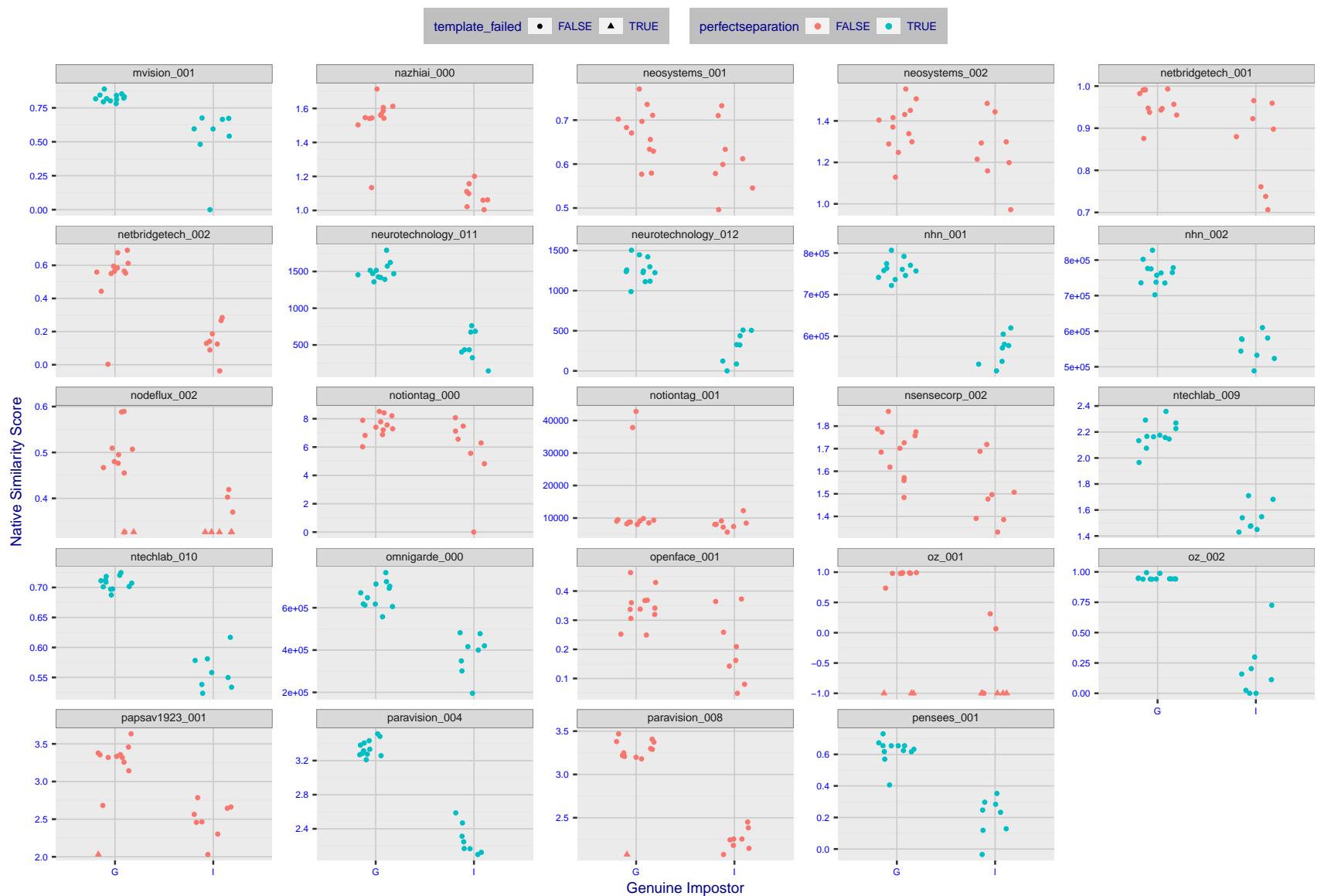


Figure 12: The Figure shows, in blue, algorithms that correctly separate the 12 genuine and 8 impostor pairs used in the May 2018 paper [Face recognition accuracy of forensic examiners, superrecognizers, and face recognition algorithms](#) (Phillips et al. [1]). In red are algorithms that are imperfect. Some algorithms fail only because they failed to make a template e.g. due to face detection failure (shown as a triangle). Others fail because the pairs were selected for that study because they had been difficult for three leading algorithms used in FRVT 2006. Caution: Given the small sample size ($n=20$) the figure may change substantially if larger or different sets were used. The images can be downloaded from the [Supplemental Information](#) page provided with that publication.



Figure 13: The Figure shows, in blue, algorithms that correctly separate the 12 genuine and 8 impostor pairs used in the May 2018 paper [Face recognition accuracy of forensic examiners, superrecognizers, and face recognition algorithms](#) (Phillips et al. [1]). In red are algorithms that are imperfect. Some algorithms fail only because they failed to make a template e.g. due to face detection failure (shown as a triangle). Others fail because the pairs were selected for that study because they had been difficult for three leading algorithms used in FRVT 2006. Caution: Given the small sample size ($n=20$) the figure may change substantially if larger or different sets were used. The images can be downloaded from the [Supplemental Information](#) page provided with that publication.



Figure 14: The Figure shows, in blue, algorithms that correctly separate the 12 genuine and 8 impostor pairs used in the May 2018 paper [Face recognition accuracy of forensic examiners, superrecognizers, and face recognition algorithms](#) (Phillips et al. [1]). In red are algorithms that are imperfect. Some algorithms fail only because they failed to make a template e.g. due to face detection failure (shown as a triangle). Others fail because the pairs were selected for that study because they had been difficult for three leading algorithms used in FRVT 2006. Caution: Given the small sample size ($n=20$) the figure may change substantially if larger or different sets were used. The images can be downloaded from the [Supplemental Information](#) page provided with that publication.

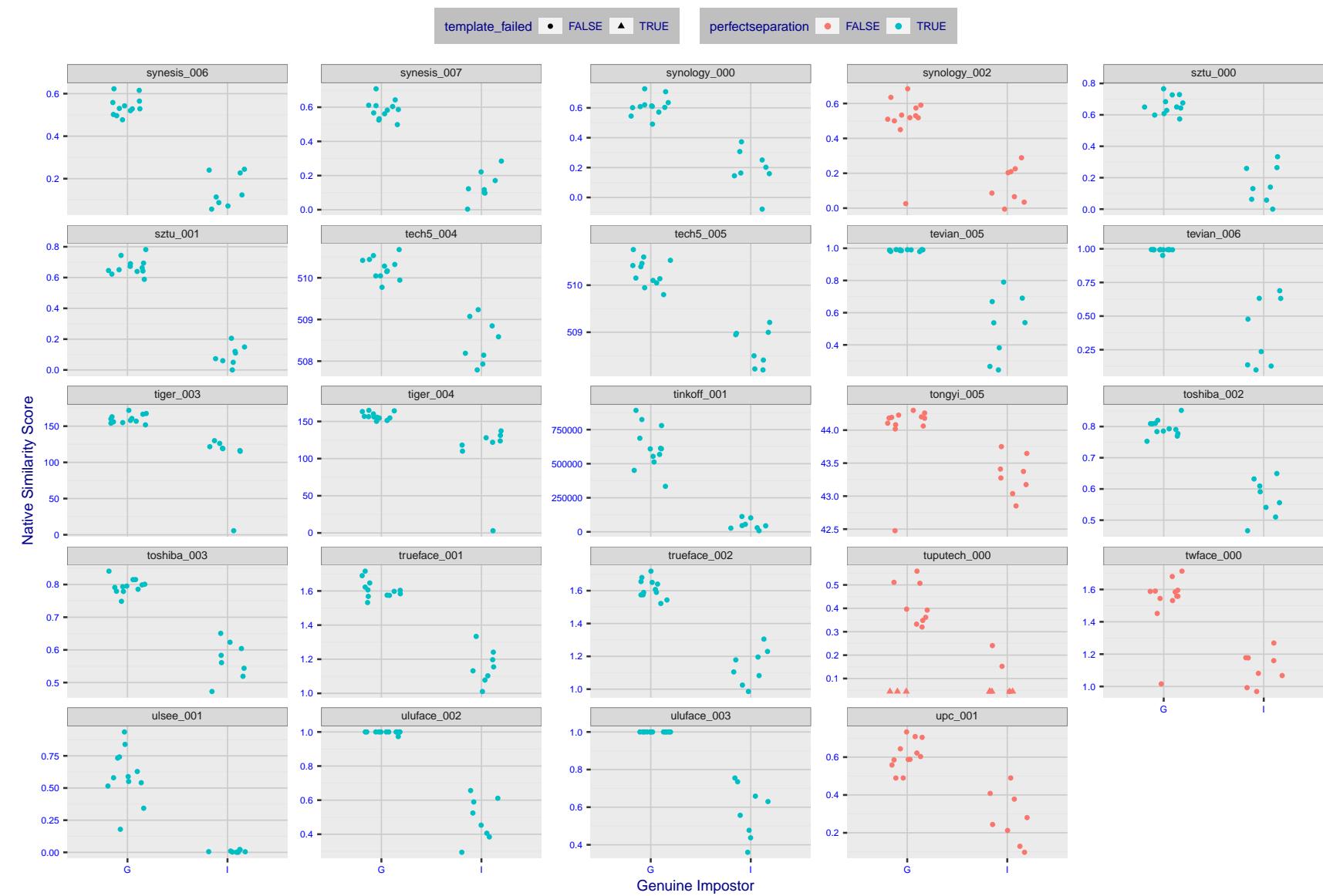


Figure 15: The Figure shows, in blue, algorithms that correctly separate the 12 genuine and 8 impostor pairs used in the May 2018 paper [Face recognition accuracy of forensic examiners, superrecognizers, and face recognition algorithms](#) (Phillips et al. [1]). In red are algorithms that are imperfect. Some algorithms fail only because they failed to make a template e.g. due to face detection failure (shown as a triangle). Others fail because the pairs were selected for that study because they had been difficult for three leading algorithms used in FRVT 2006. Caution: Given the small sample size ($n=20$) the figure may change substantially if larger or different sets were used. The images can be downloaded from the [Supplemental Information](#) page provided with that publication.

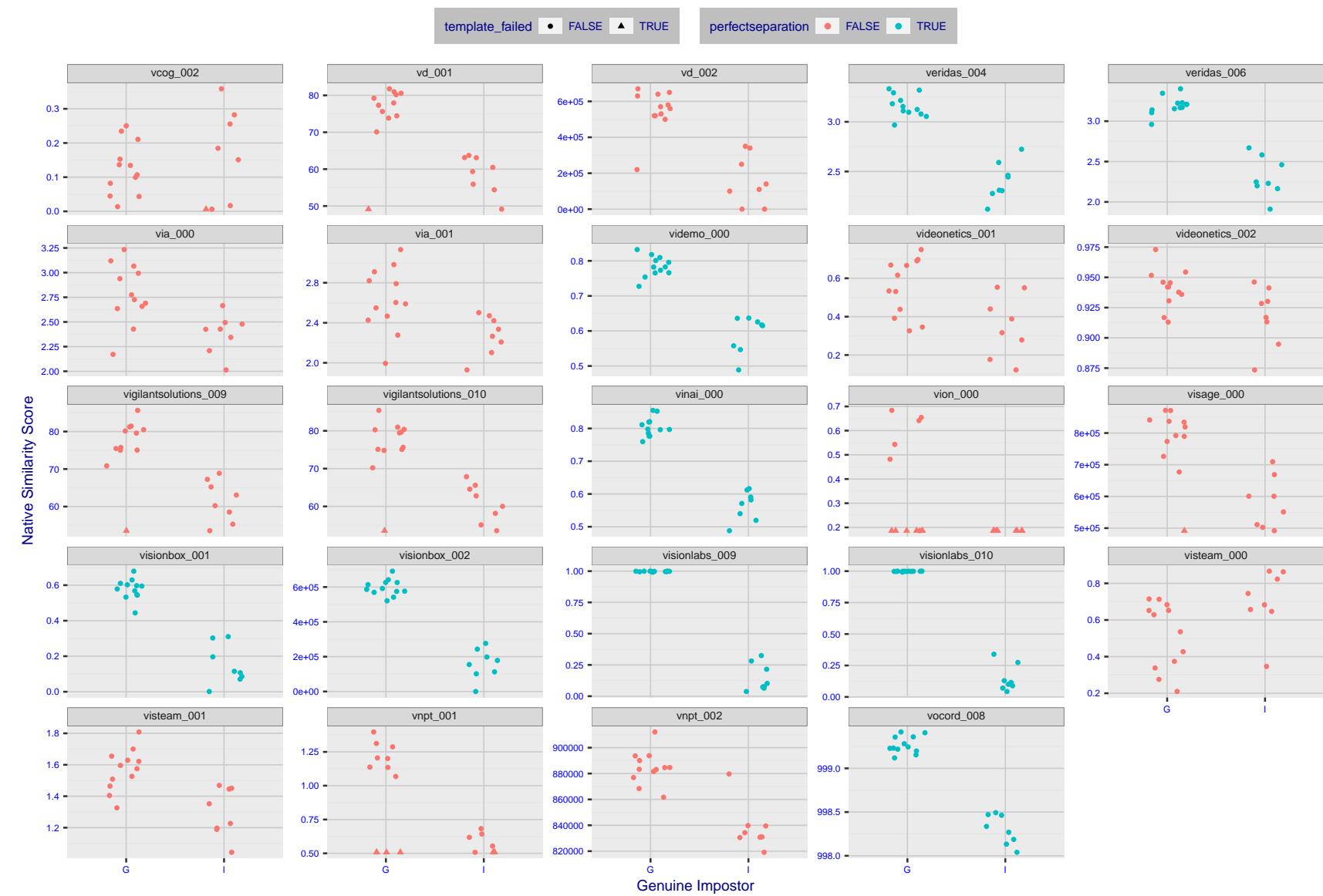


Figure 16: The Figure shows, in blue, algorithms that correctly separate the 12 genuine and 8 impostor pairs used in the May 2018 paper Face recognition accuracy of forensic examiners, superrecognizers, and face recognition algorithms (Phillips et al. [1]). In red are algorithms that are imperfect. Some algorithms fail only because they failed to make a template e.g. due to face detection failure (shown as a triangle). Others fail because the pairs were selected for that study because they had been difficult for three leading algorithms used in FRVT 2006. Caution: Given the small sample size ($n=20$) the figure may change substantially if larger or different sets were used. The images can be downloaded from the [Supplemental Information](#) page provided with that publication.

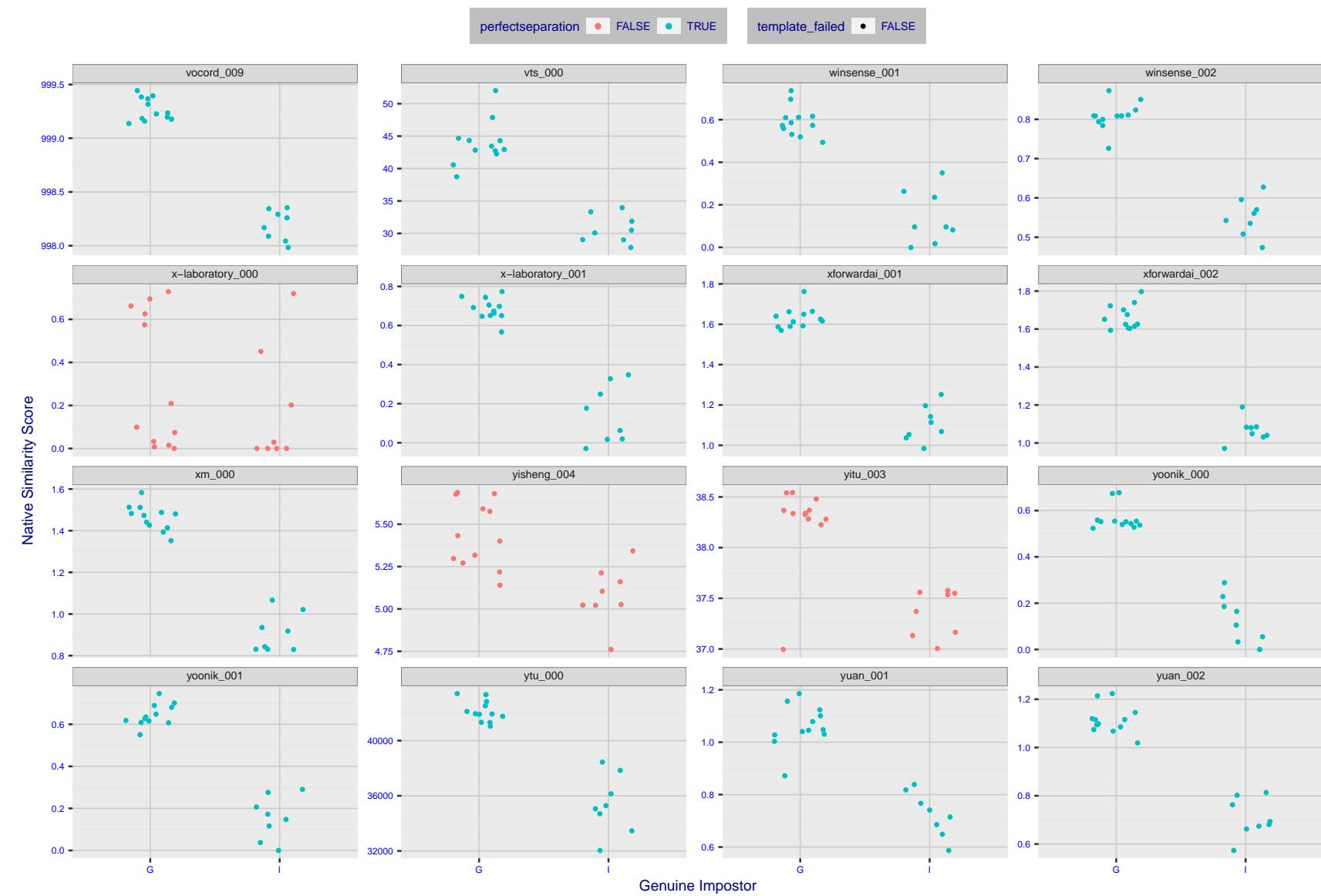


Figure 17: The Figure shows, in blue, algorithms that correctly separate the 12 genuine and 8 impostor pairs used in the May 2018 paper [Face recognition accuracy of forensic examiners, superrecognizers, and face recognition algorithms](#) (Phillips et al. [1]). In red are algorithms that are imperfect. Some algorithms fail only because they failed to make a template e.g. due to face detection failure (shown as a triangle). Others fail because the pairs were selected for that study because they had been difficult for three leading algorithms used in FRVT 2006. Caution: Given the small sample size ($n=20$) the figure may change substantially if larger or different sets were used. The images can be downloaded from the [Supplemental Information](#) page provided with that publication.

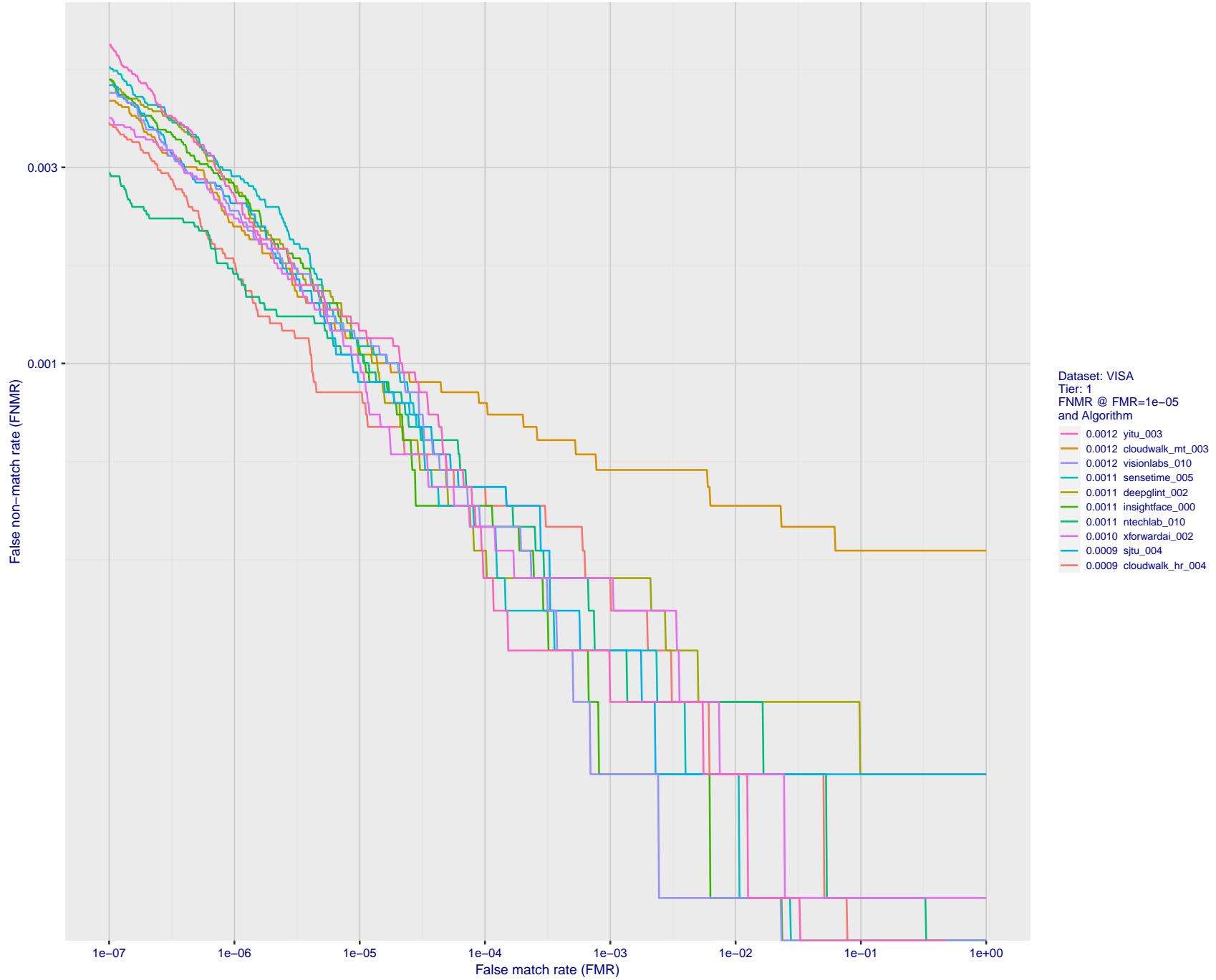


Figure 18: For the visa images, detection error tradeoff (DET) characteristics showing false non-match rate vs. false match rate plotted parametrically on threshold, T . The scales are logarithmic in order to show many decades of FMR.

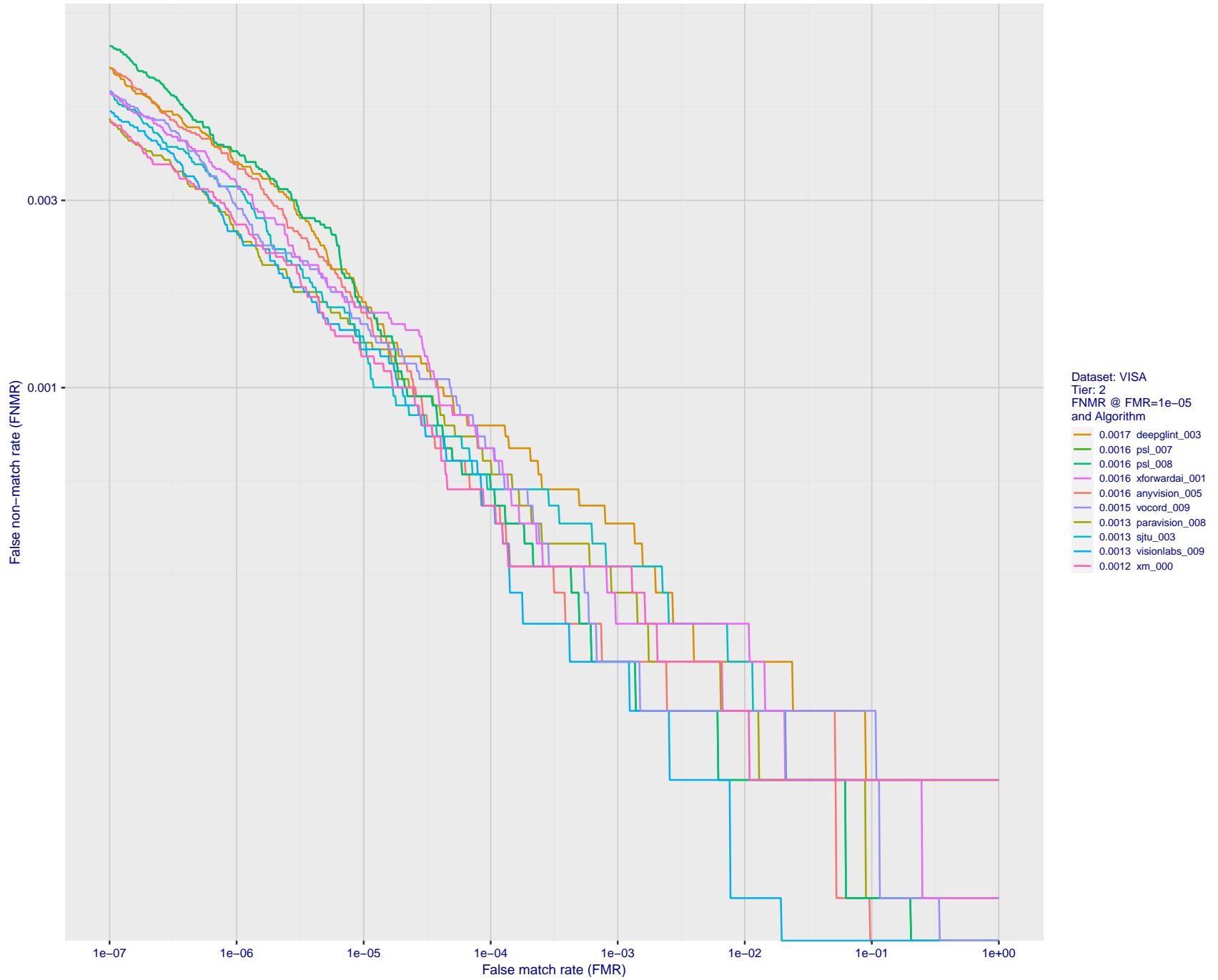


Figure 19: For the visa images, detection error tradeoff (DET) characteristics showing false non-match rate vs. false match rate plotted parametrically on threshold, T . The scales are logarithmic in order to show many decades of FMR.

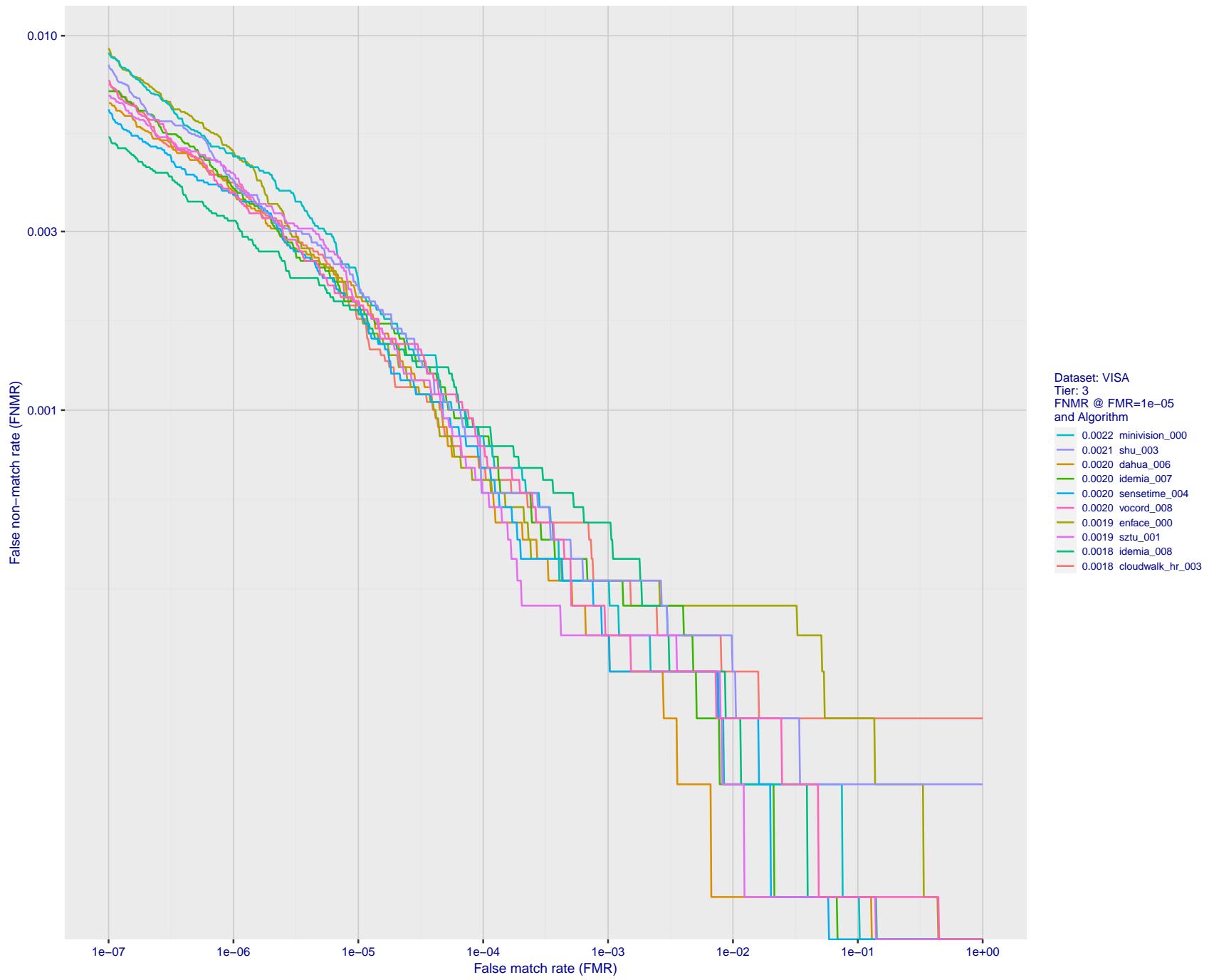


Figure 20: For the visa images, detection error tradeoff (DET) characteristics showing false non-match rate vs. false match rate plotted parametrically on threshold, T . The scales are logarithmic in order to show many decades of FMR.

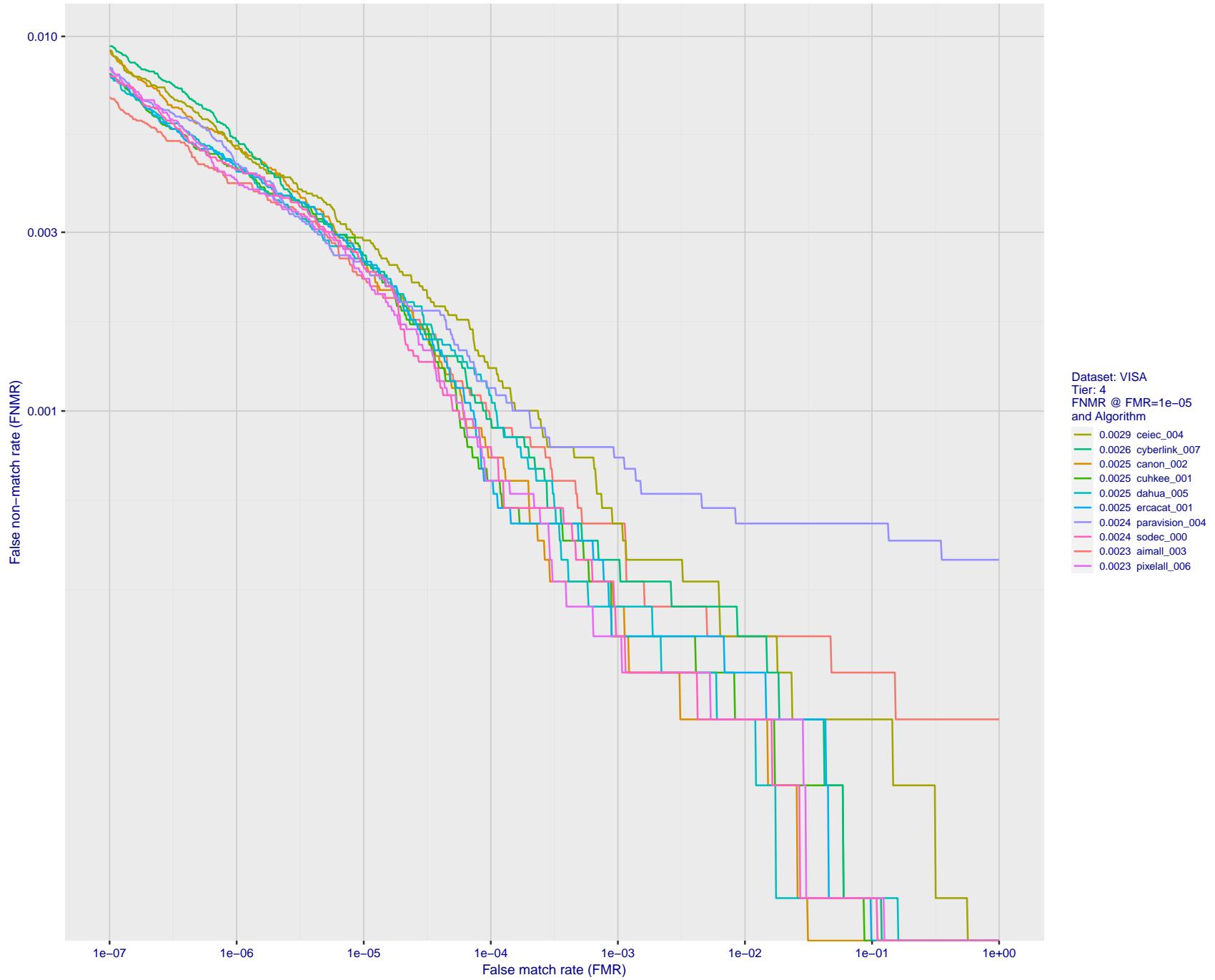


Figure 21: For the visa images, detection error tradeoff (DET) characteristics showing false non-match rate vs. false match rate plotted parametrically on threshold, T . The scales are logarithmic in order to show many decades of FMR.

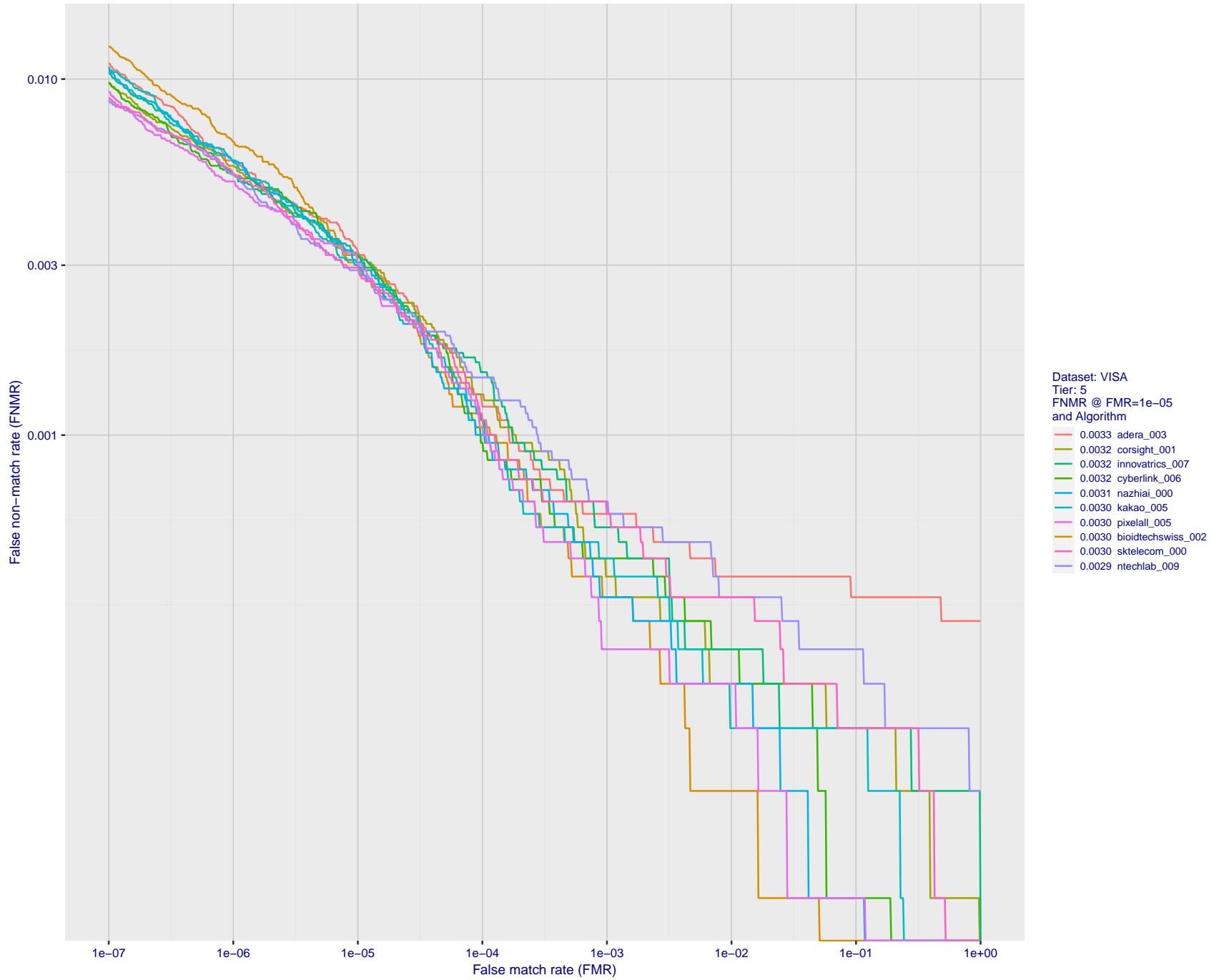


Figure 22: For the visa images, detection error tradeoff (DET) characteristics showing false non-match rate vs. false match rate plotted parametrically on threshold, T . The scales are logarithmic in order to show many decades of FMR.

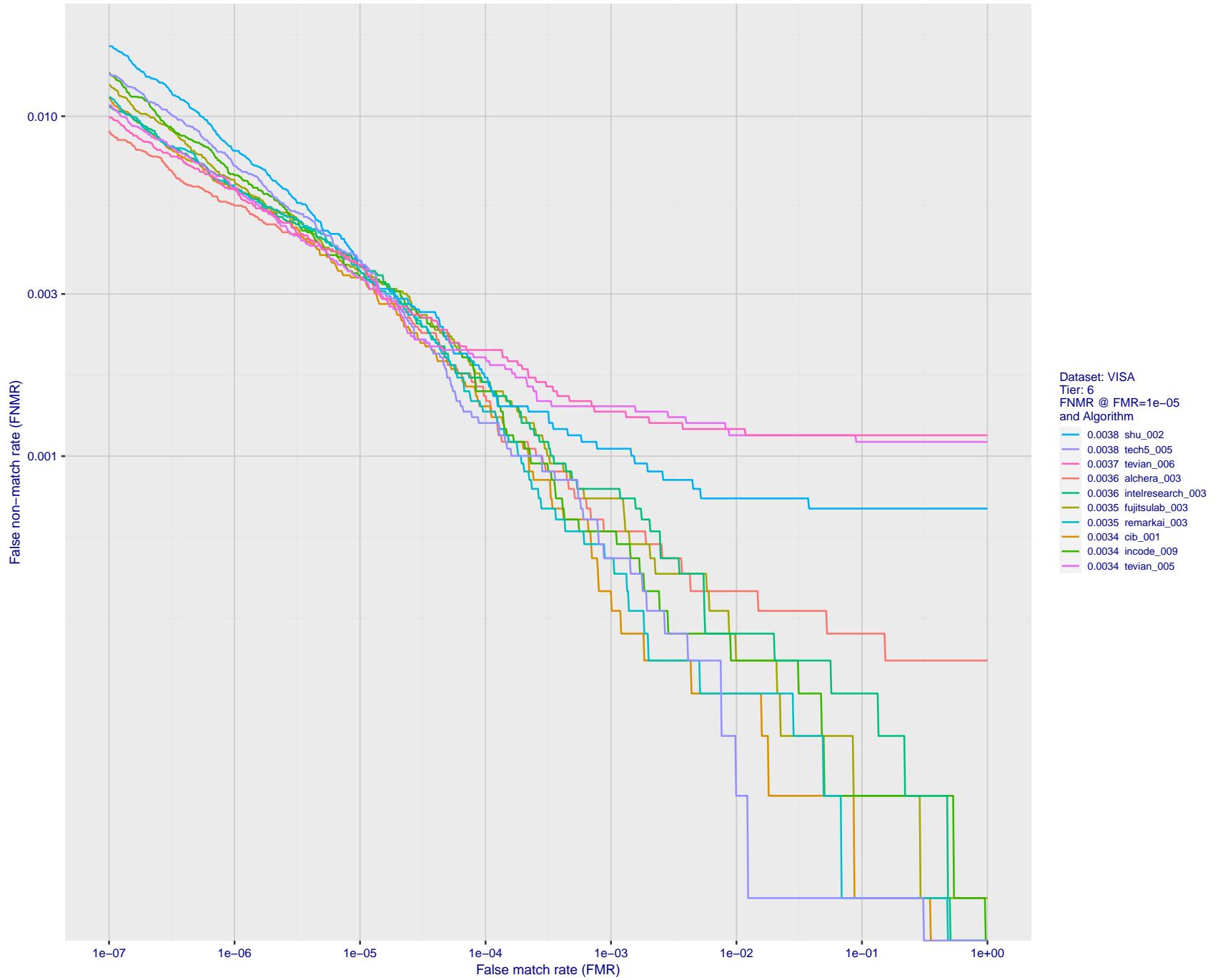


Figure 23: For the visa images, detection error tradeoff (DET) characteristics showing false non-match rate vs. false match rate plotted parametrically on threshold, T . The scales are logarithmic in order to show many decades of FMR.

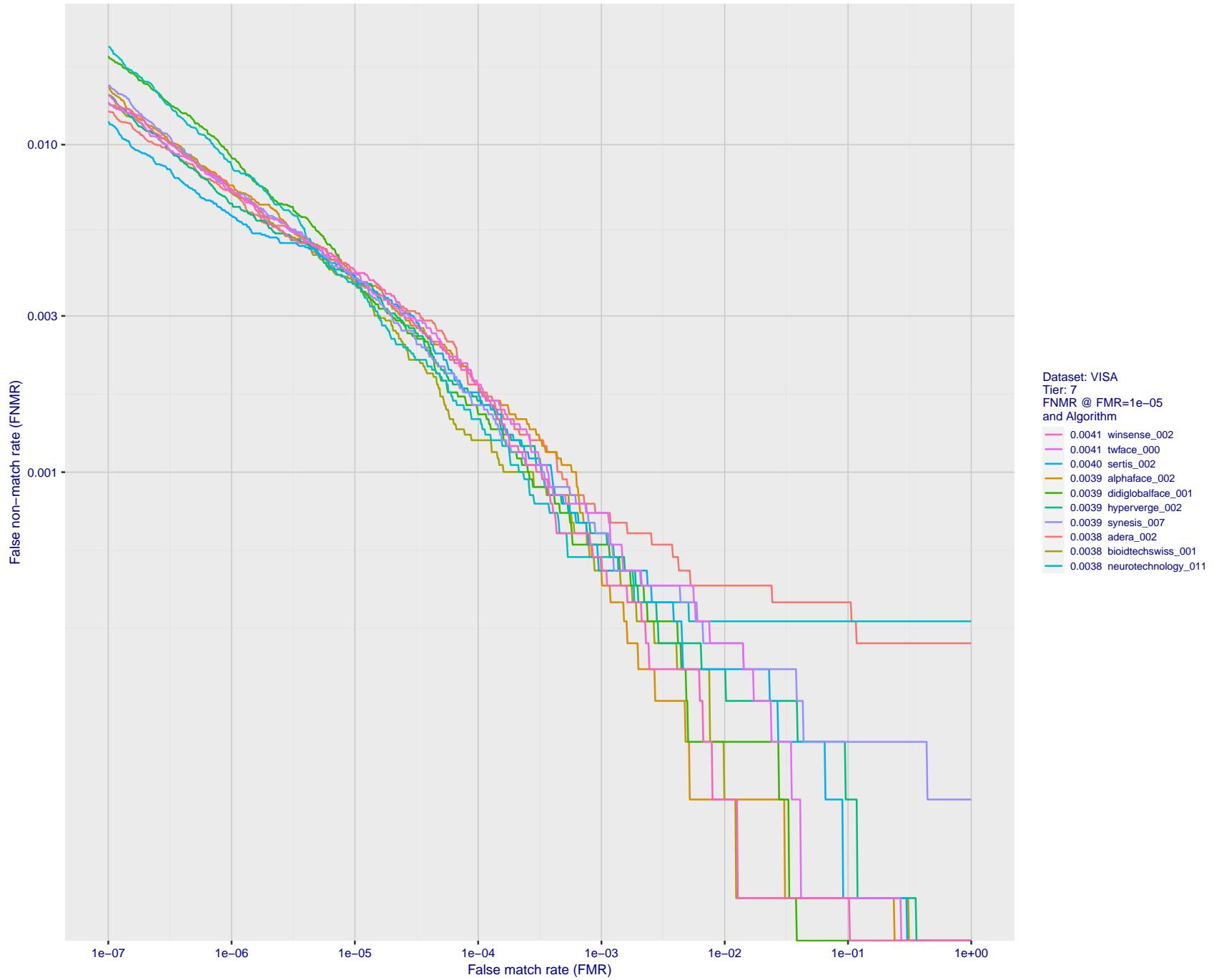


Figure 24: For the visa images, detection error tradeoff (DET) characteristics showing false non-match rate vs. false match rate plotted parametrically on threshold, T . The scales are logarithmic in order to show many decades of FMR.

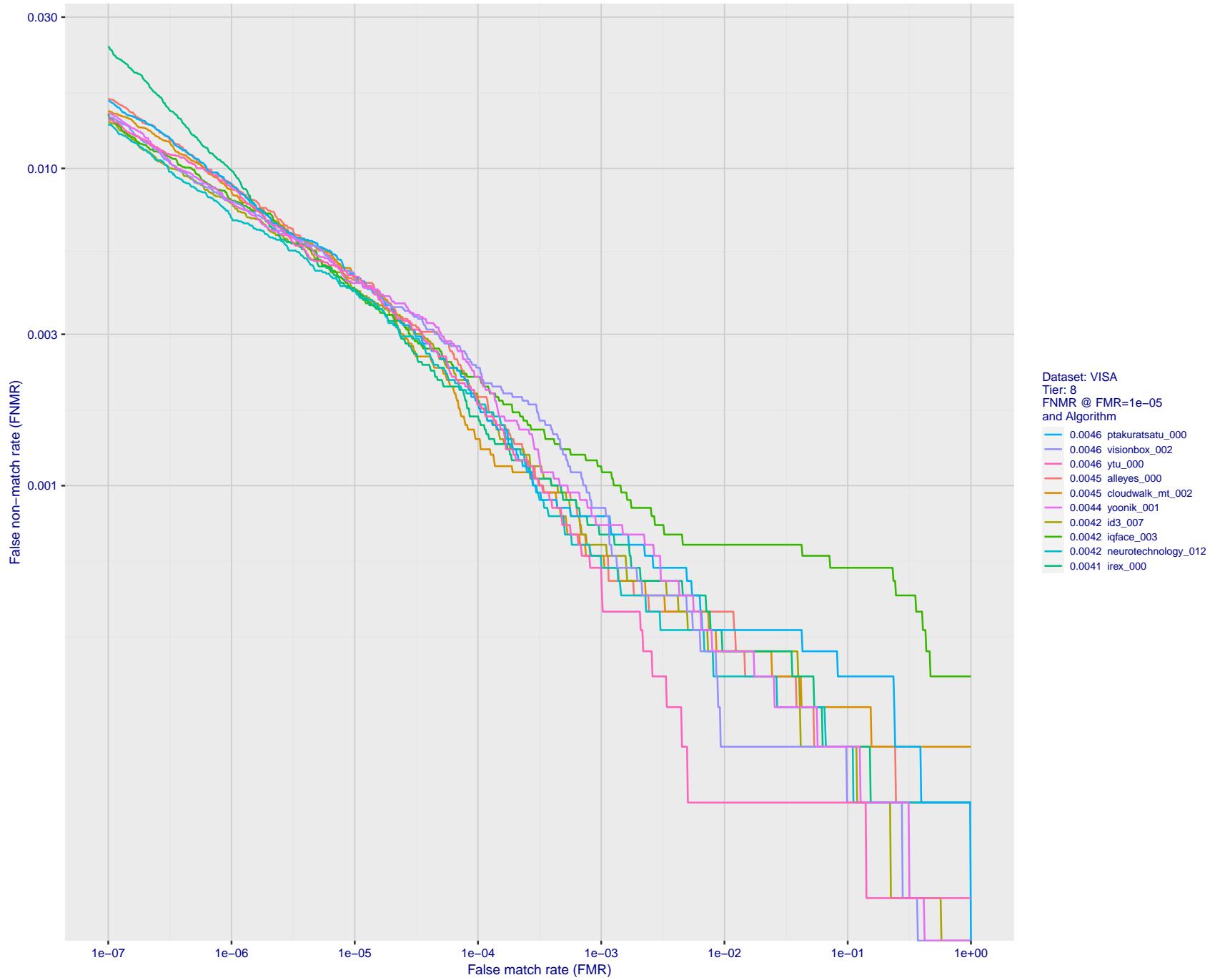


Figure 25: For the visa images, detection error tradeoff (DET) characteristics showing false non-match rate vs. false match rate plotted parametrically on threshold, T . The scales are logarithmic in order to show many decades of FMR.

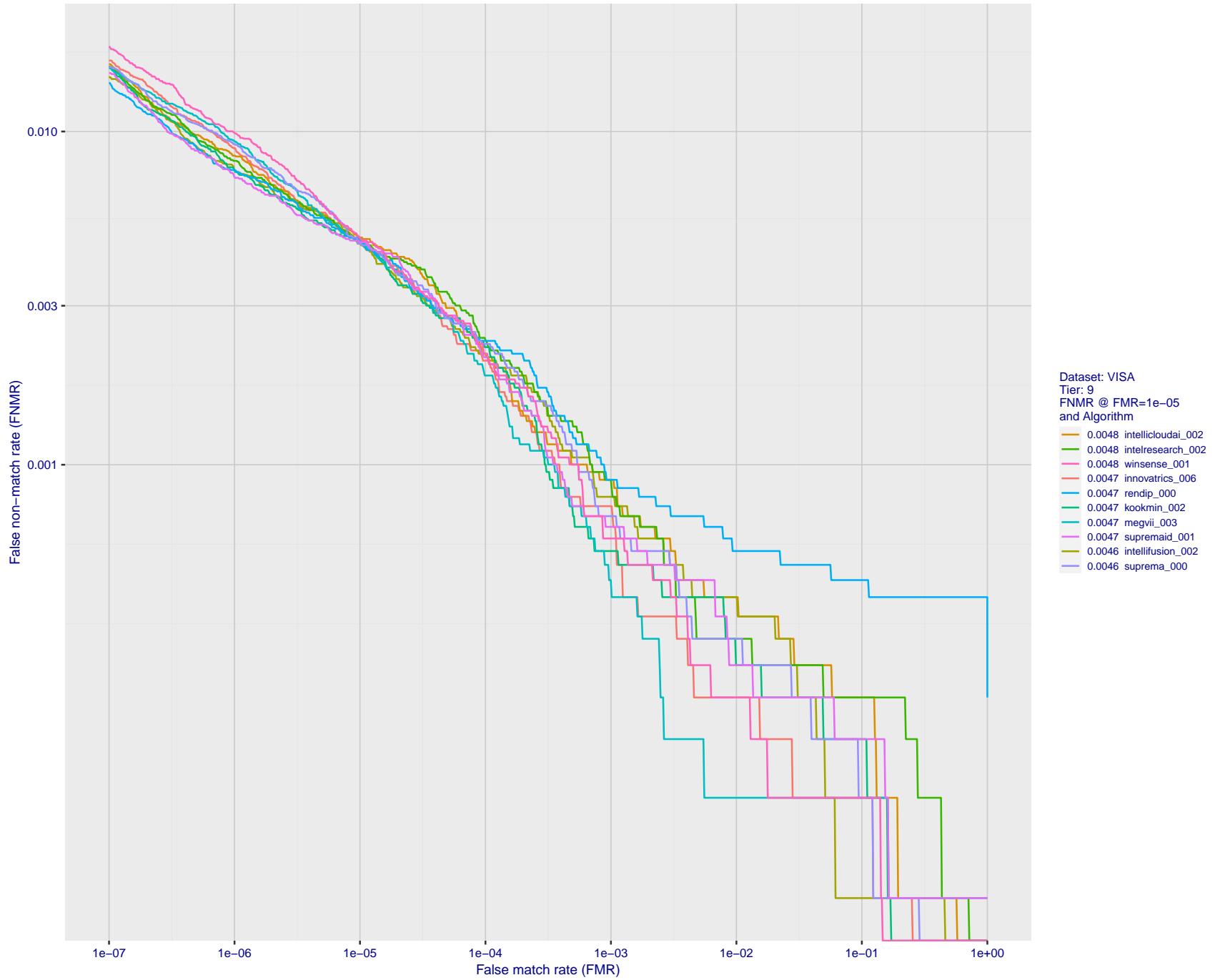


Figure 26: For the visa images, detection error tradeoff (DET) characteristics showing false non-match rate vs. false match rate plotted parametrically on threshold, T . The scales are logarithmic in order to show many decades of FMR.

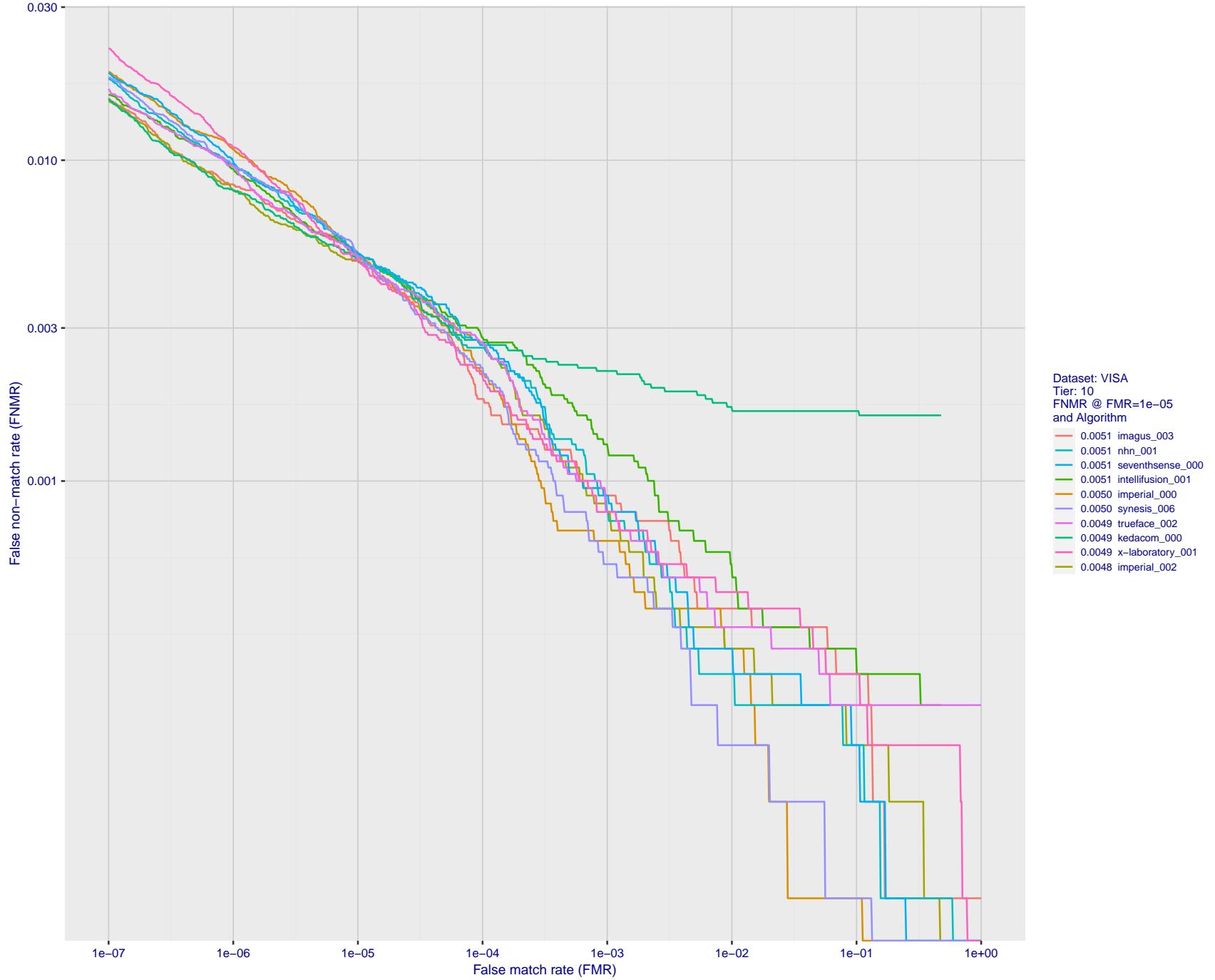


Figure 27: For the visa images, detection error tradeoff (DET) characteristics showing false non-match rate vs. false match rate plotted parametrically on threshold, T . The scales are logarithmic in order to show many decades of FMR.

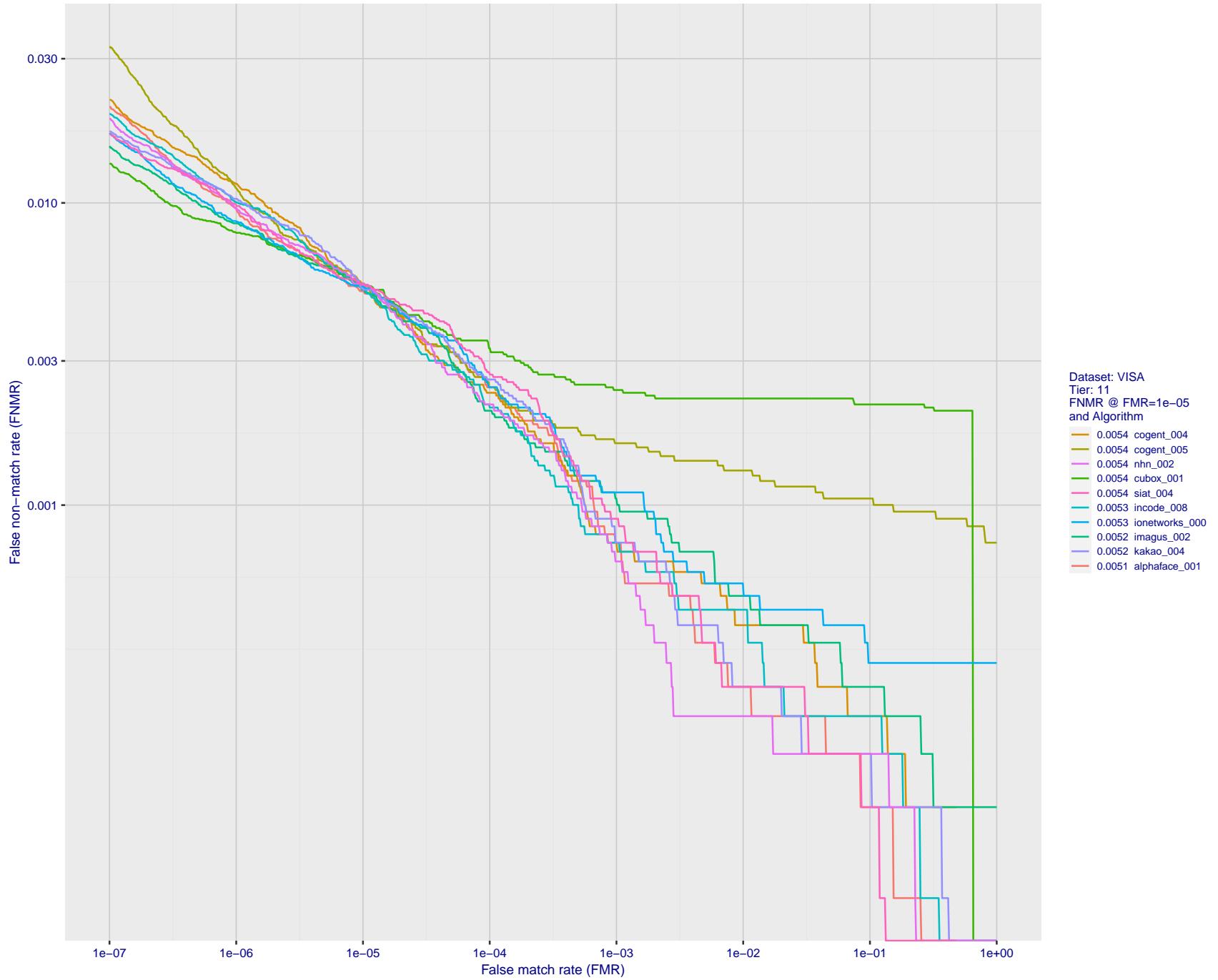


Figure 28: For the visa images, detection error tradeoff (DET) characteristics showing false non-match rate vs. false match rate plotted parametrically on threshold, T . The scales are logarithmic in order to show many decades of FMR.

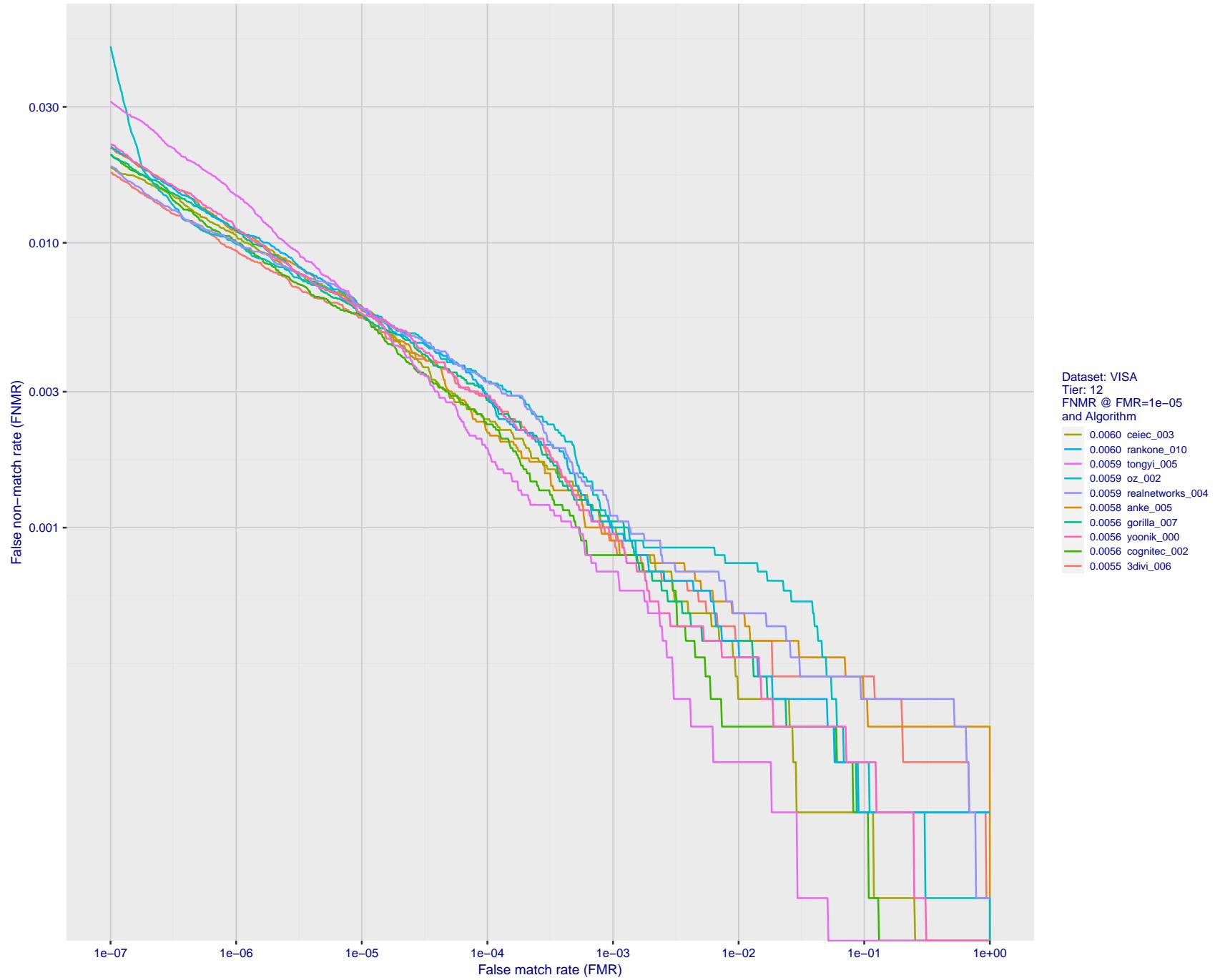


Figure 29: For the visa images, detection error tradeoff (DET) characteristics showing false non-match rate vs. false match rate plotted parametrically on threshold, T . The scales are logarithmic in order to show many decades of FMR.

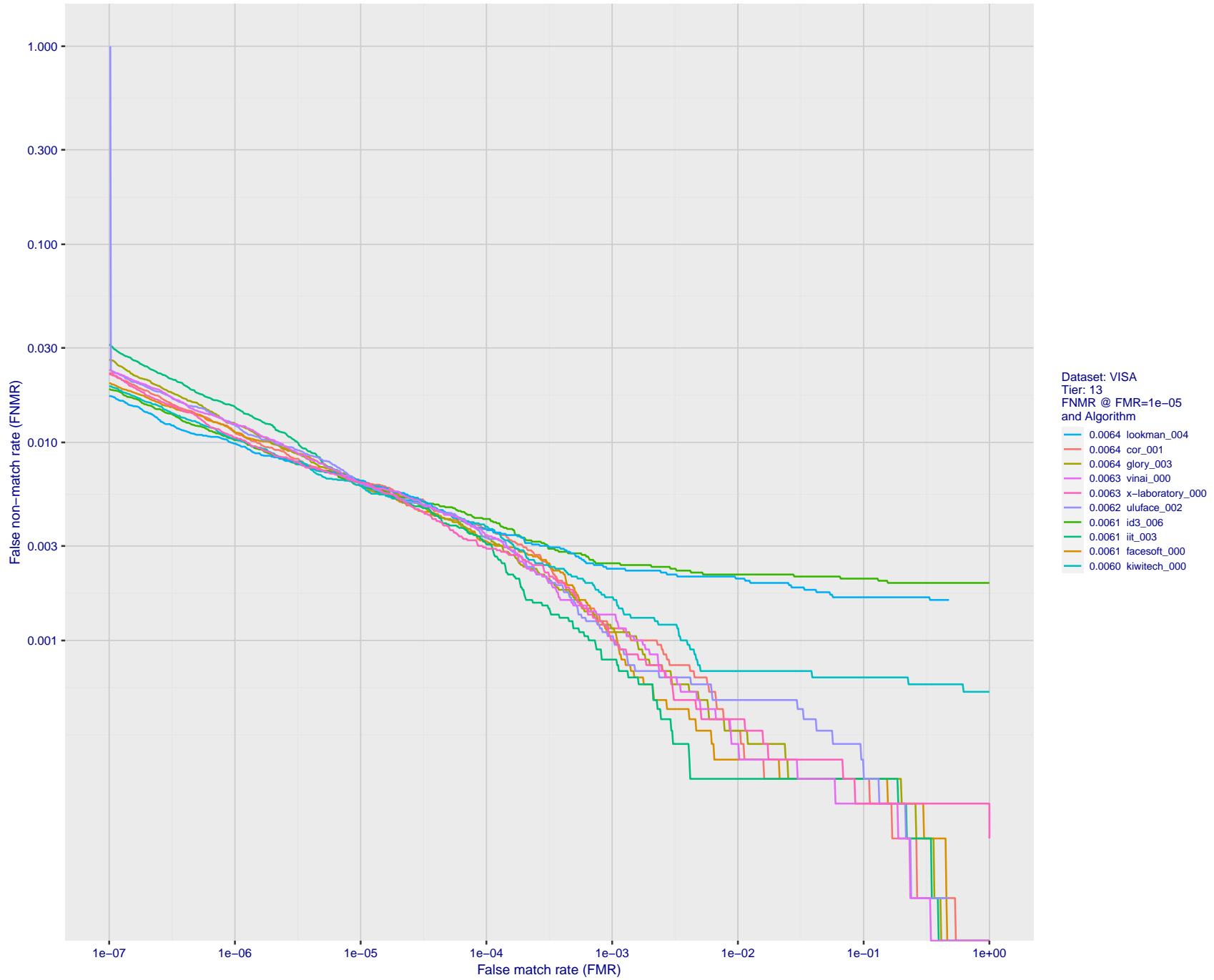


Figure 30: For the visa images, detection error tradeoff (DET) characteristics showing false non-match rate vs. false match rate plotted parametrically on threshold, T . The scales are logarithmic in order to show many decades of FMR.

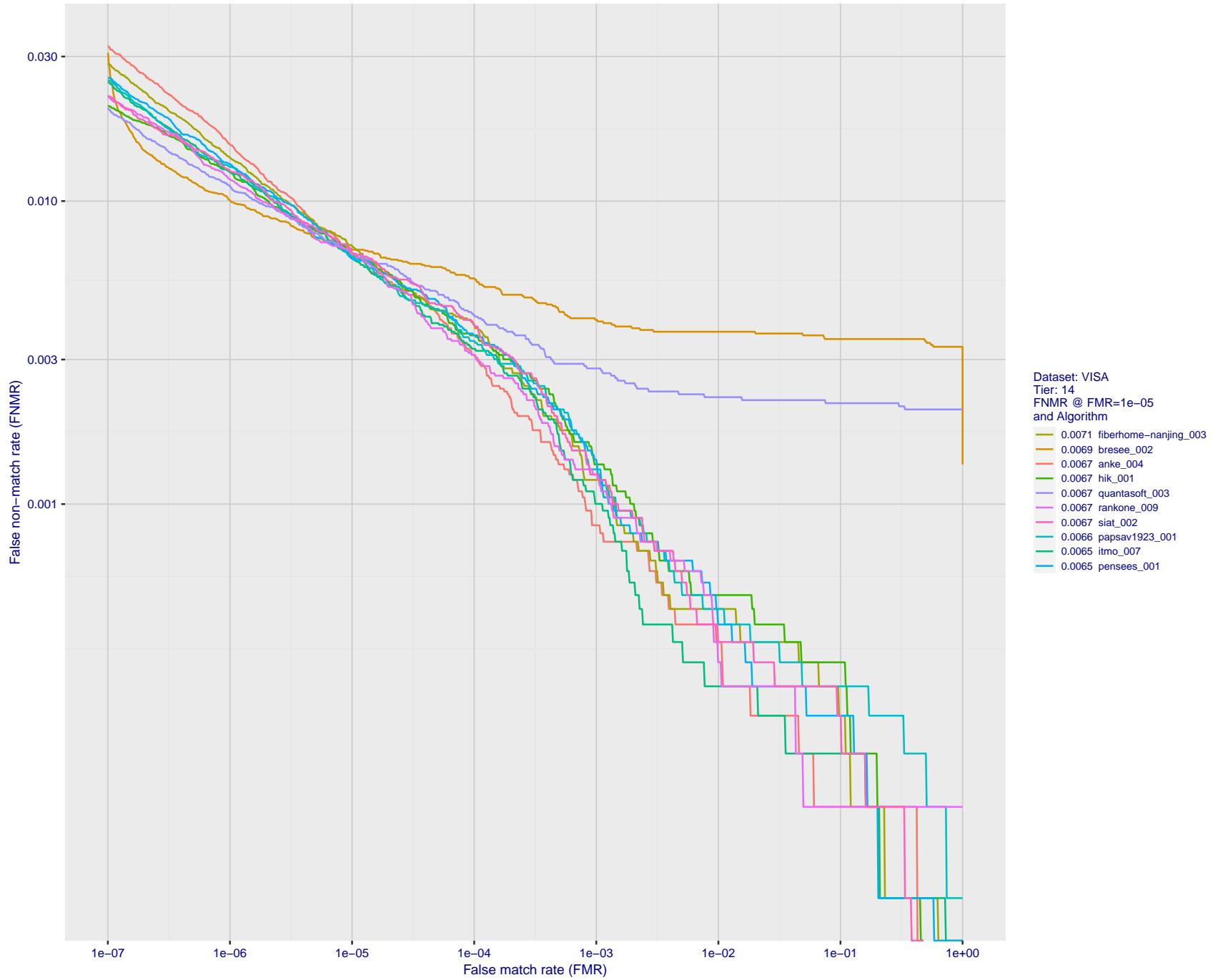


Figure 31: For the visa images, detection error tradeoff (DET) characteristics showing false non-match rate vs. false match rate plotted parametrically on threshold, T . The scales are logarithmic in order to show many decades of FMR.

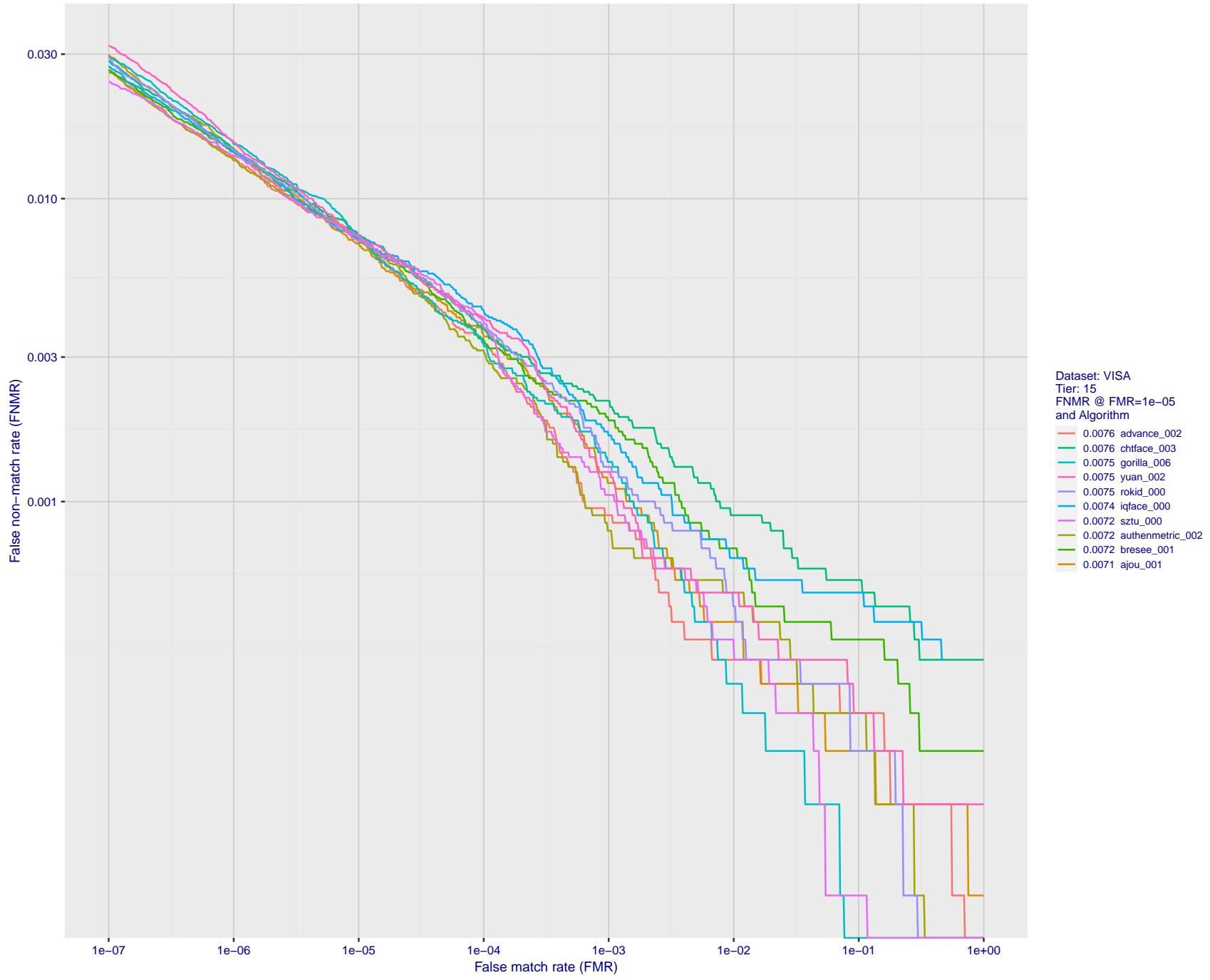


Figure 32: For the visa images, detection error tradeoff (DET) characteristics showing false non-match rate vs. false match rate plotted parametrically on threshold, T . The scales are logarithmic in order to show many decades of FMR.

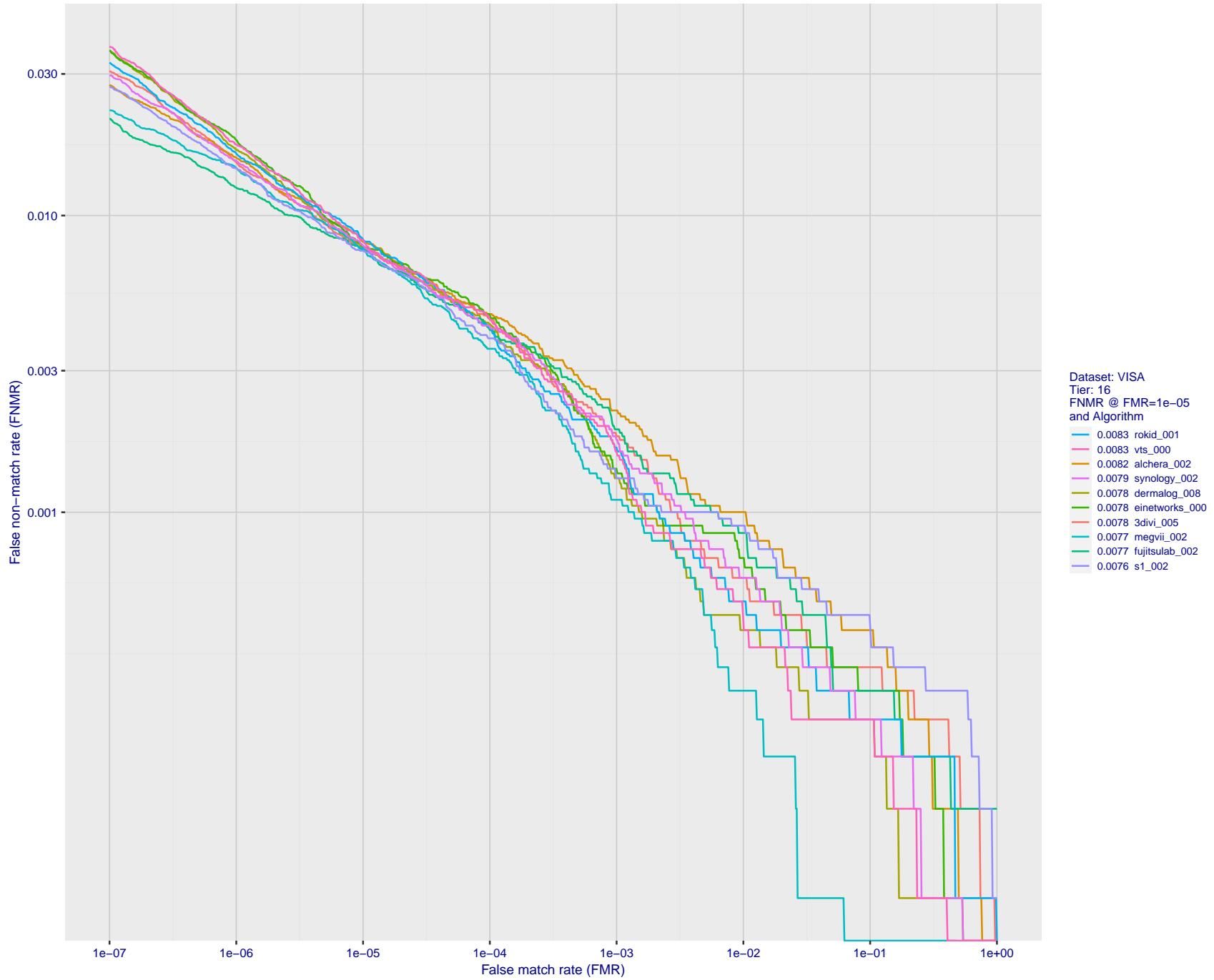


Figure 33: For the visa images, detection error tradeoff (DET) characteristics showing false non-match rate vs. false match rate plotted parametrically on threshold, T . The scales are logarithmic in order to show many decades of FMR.

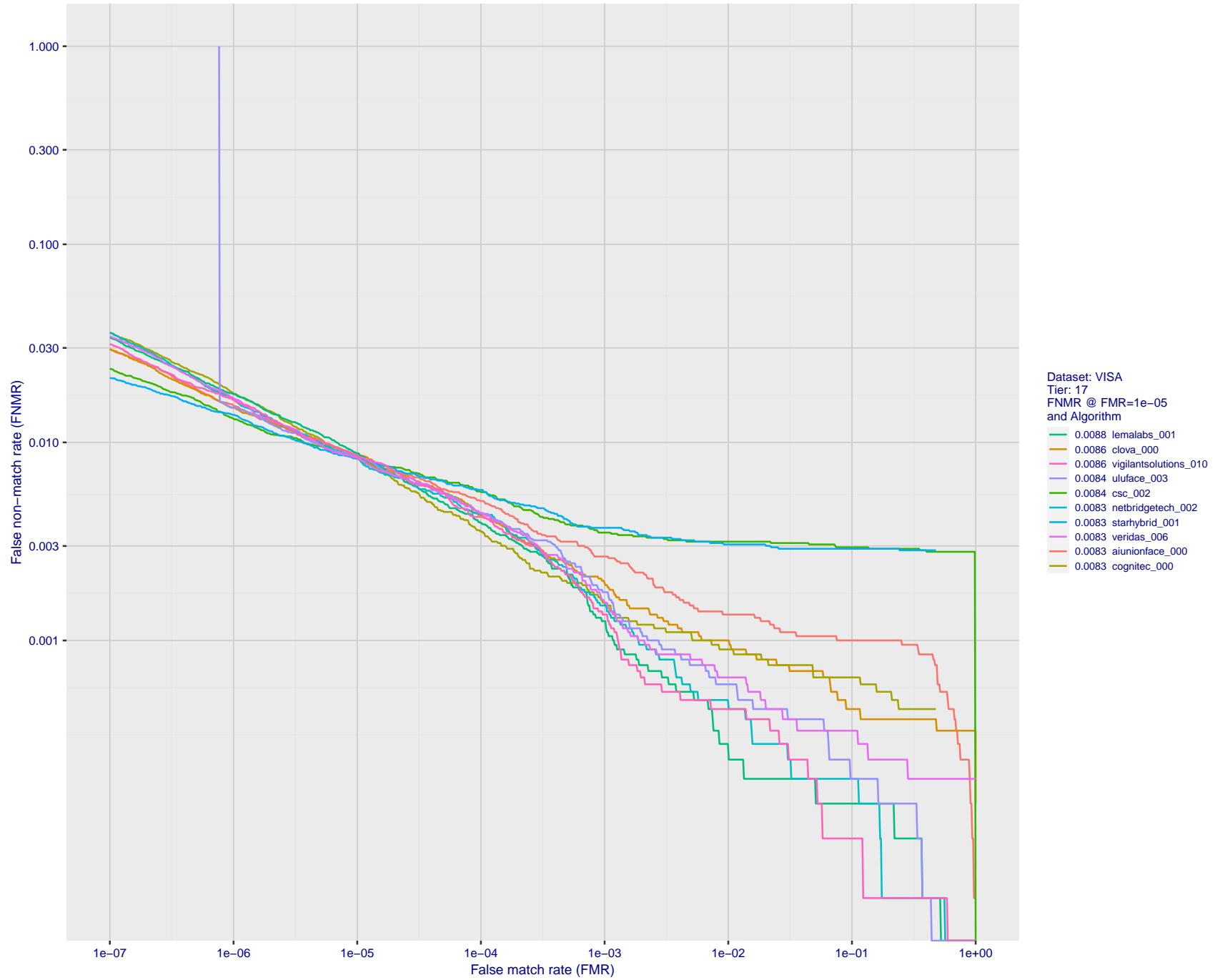


Figure 34: For the visa images, detection error tradeoff (DET) characteristics showing false non-match rate vs. false match rate plotted parametrically on threshold, T . The scales are logarithmic in order to show many decades of FMR.

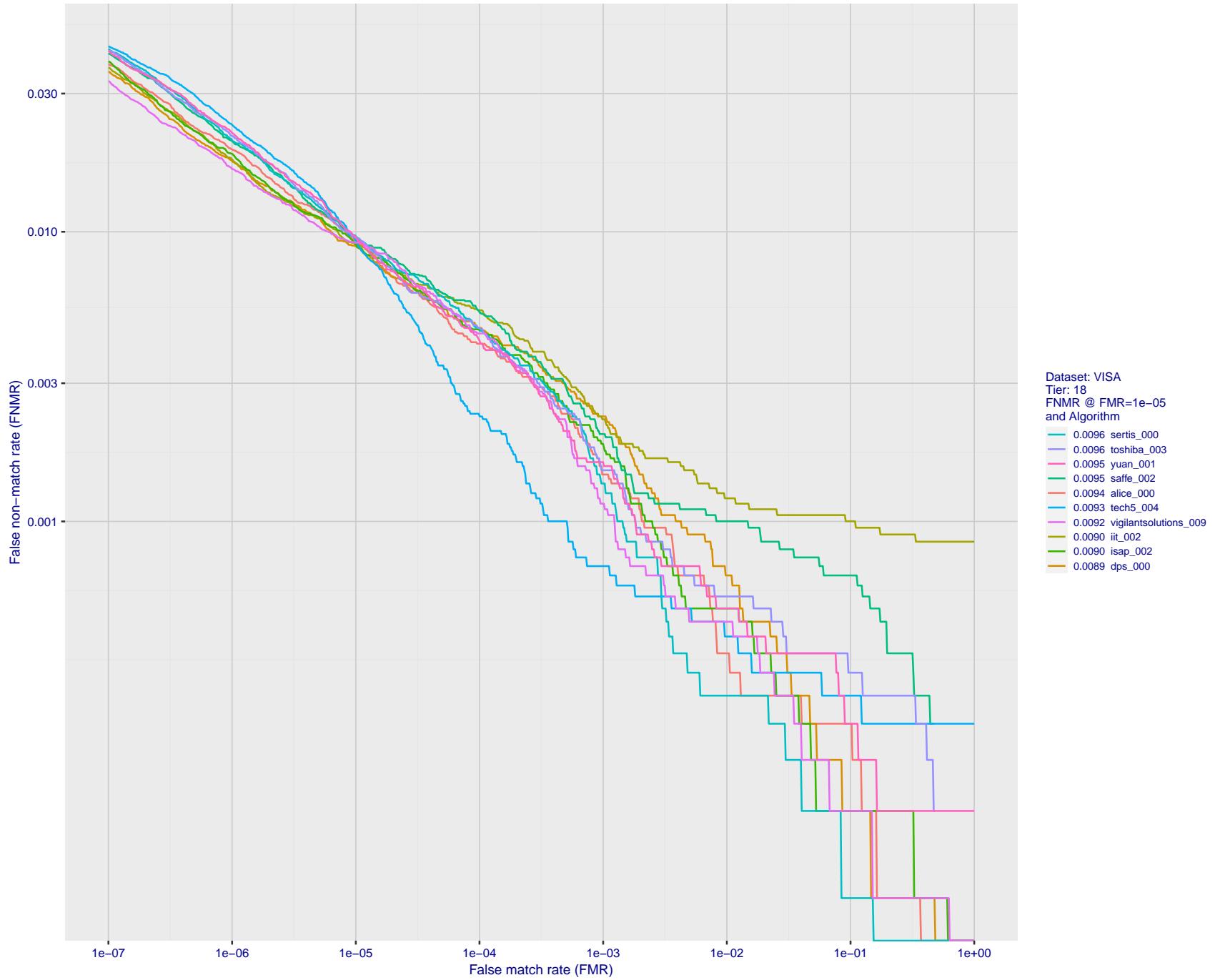


Figure 35: For the visa images, detection error tradeoff (DET) characteristics showing false non-match rate vs. false match rate plotted parametrically on threshold, T . The scales are logarithmic in order to show many decades of FMR.

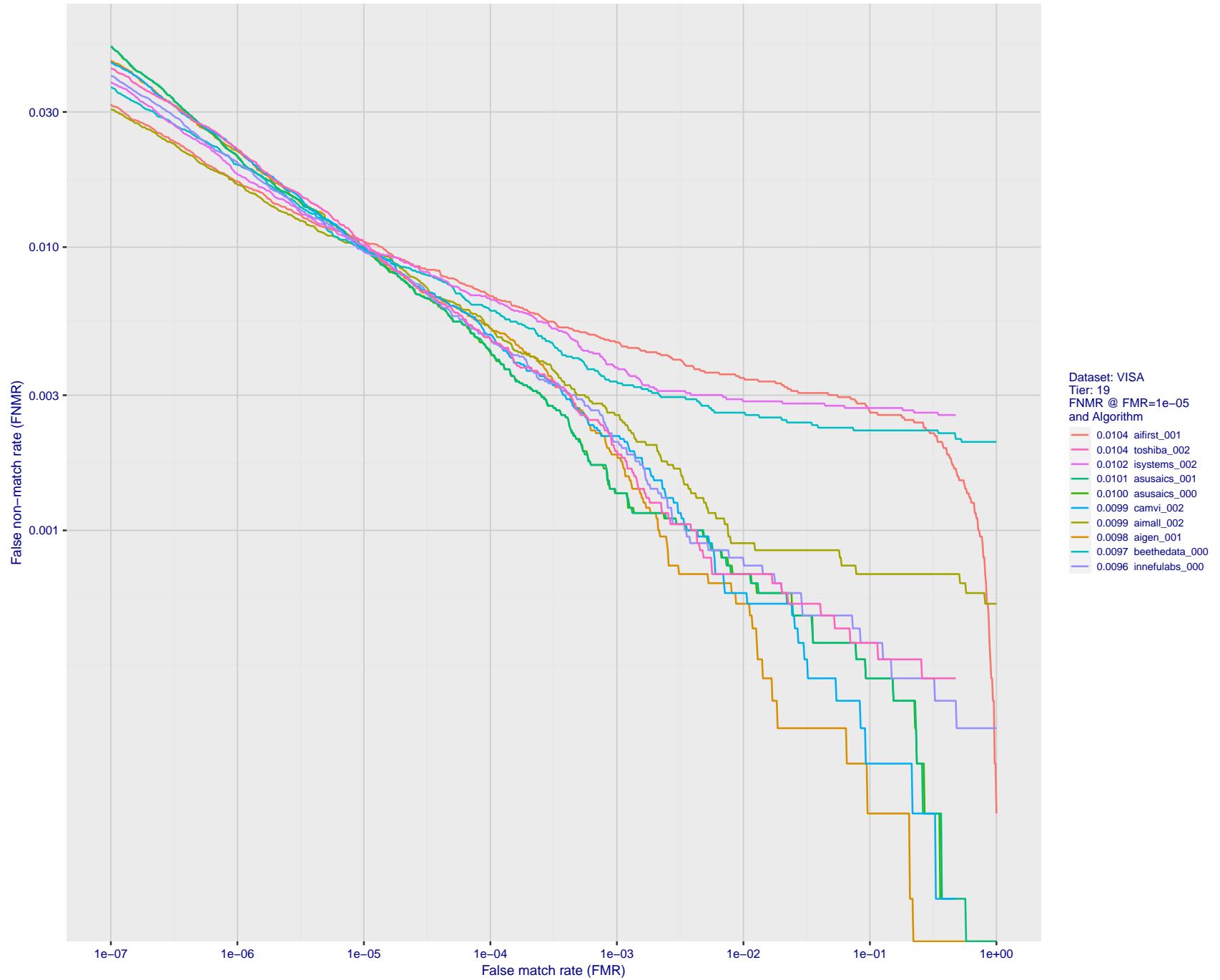


Figure 36: For the visa images, detection error tradeoff (DET) characteristics showing false non-match rate vs. false match rate plotted parametrically on threshold, T . The scales are logarithmic in order to show many decades of FMR.

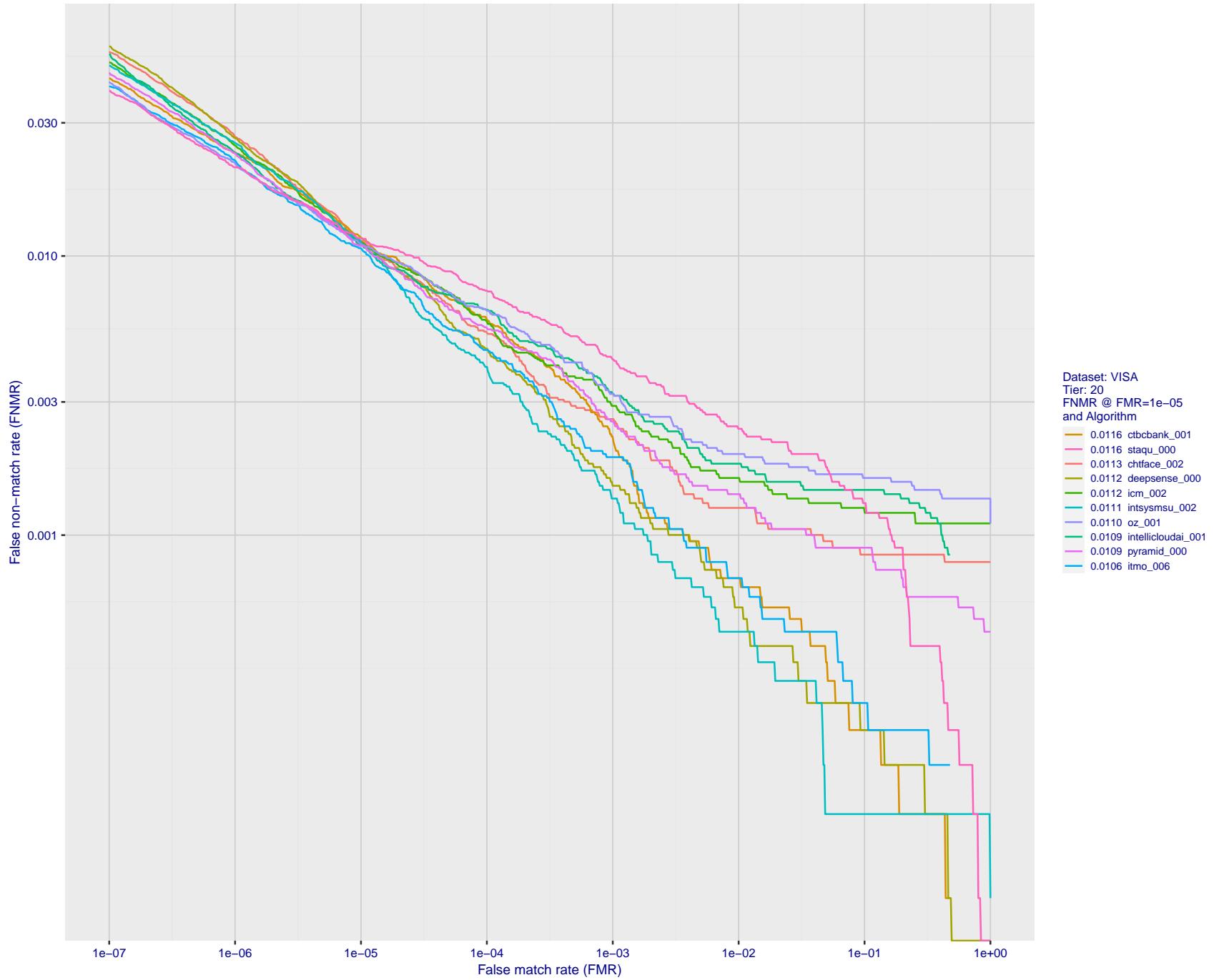


Figure 37: For the visa images, detection error tradeoff (DET) characteristics showing false non-match rate vs. false match rate plotted parametrically on threshold, T . The scales are logarithmic in order to show many decades of FMR.

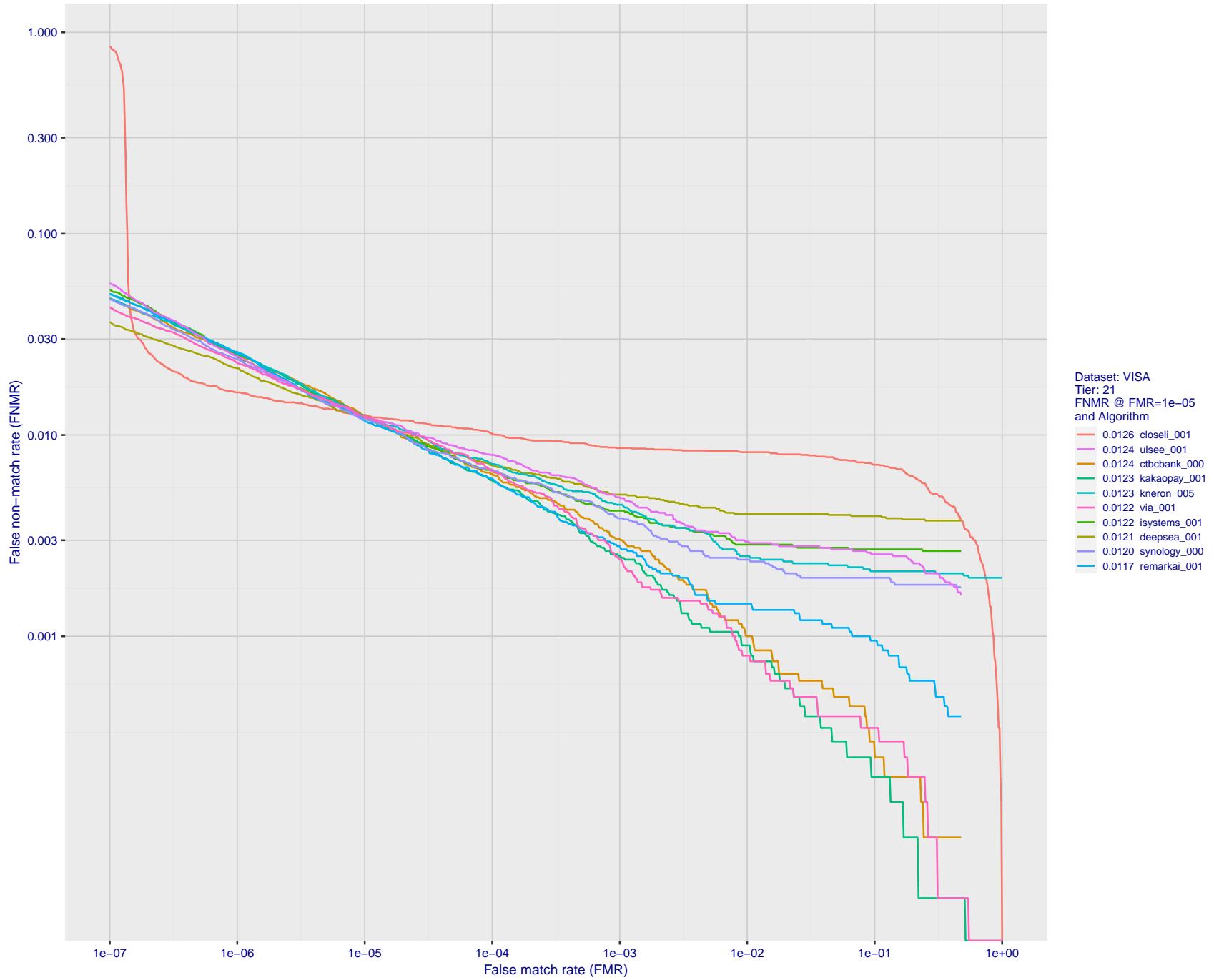


Figure 38: For the visa images, detection error tradeoff (DET) characteristics showing false non-match rate vs. false match rate plotted parametrically on threshold, T . The scales are logarithmic in order to show many decades of FMR.

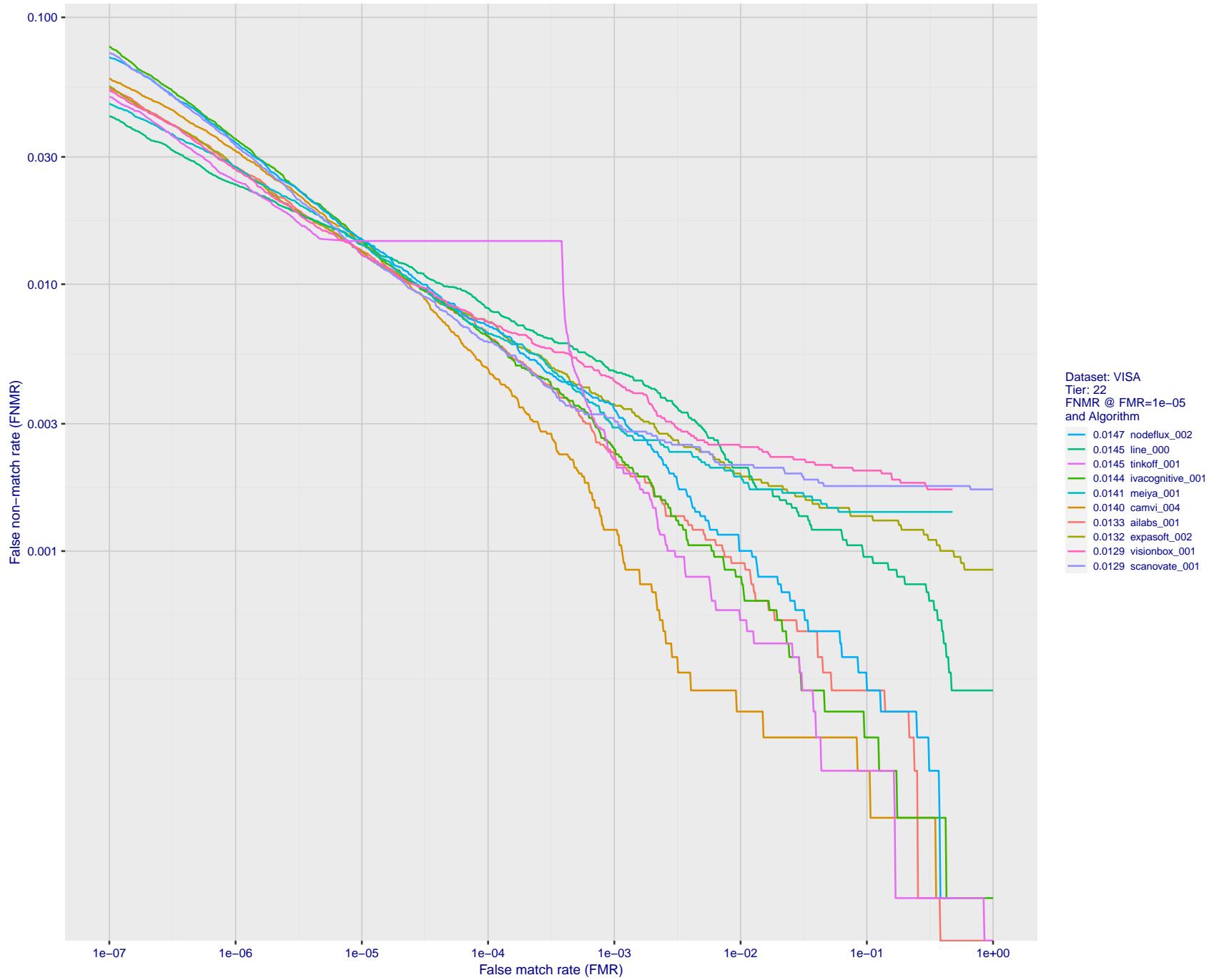


Figure 39: For the visa images, detection error tradeoff (DET) characteristics showing false non-match rate vs. false match rate plotted parametrically on threshold, T . The scales are logarithmic in order to show many decades of FMR.

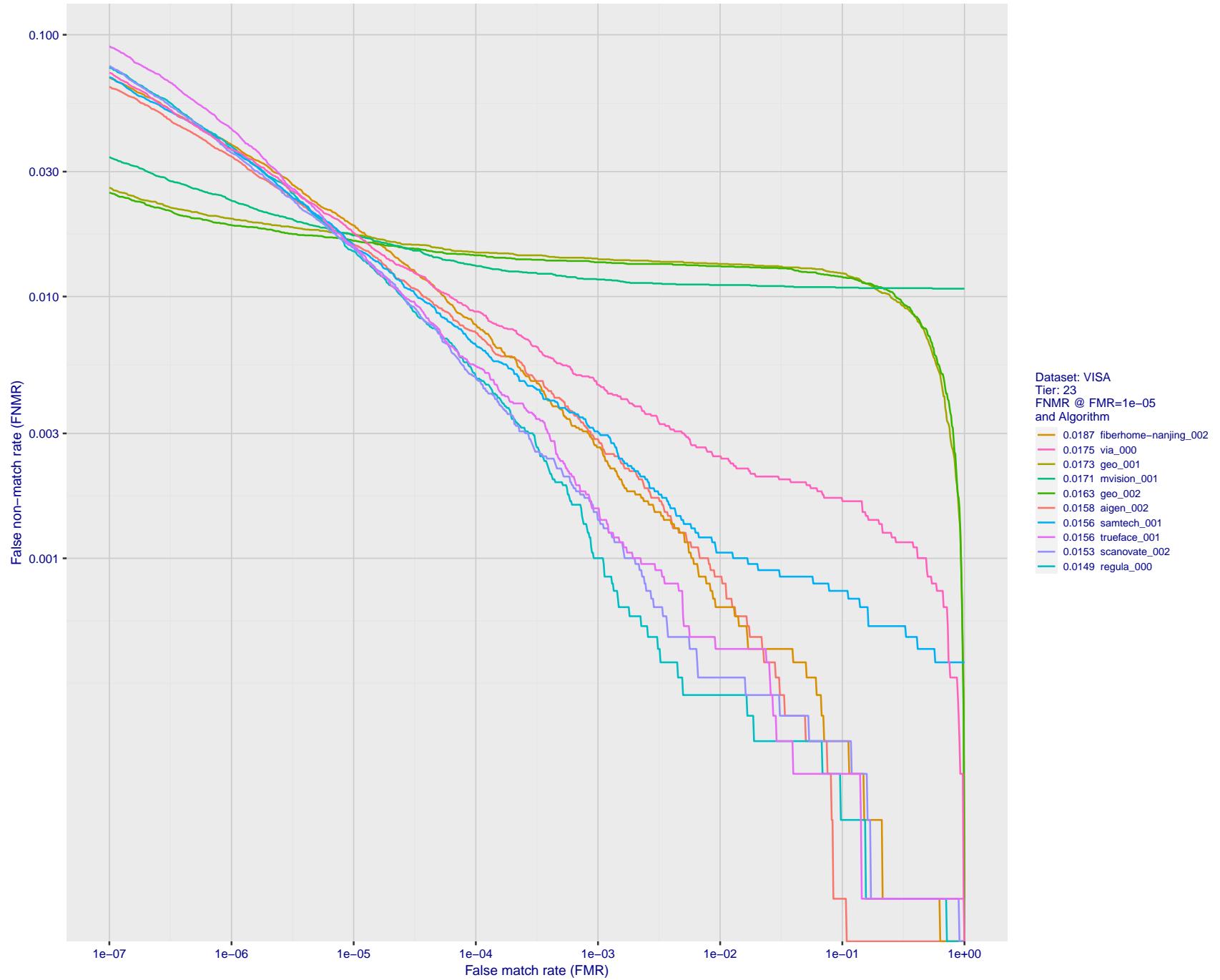


Figure 40: For the visa images, detection error tradeoff (DET) characteristics showing false non-match rate vs. false match rate plotted parametrically on threshold, T . The scales are logarithmic in order to show many decades of FMR.

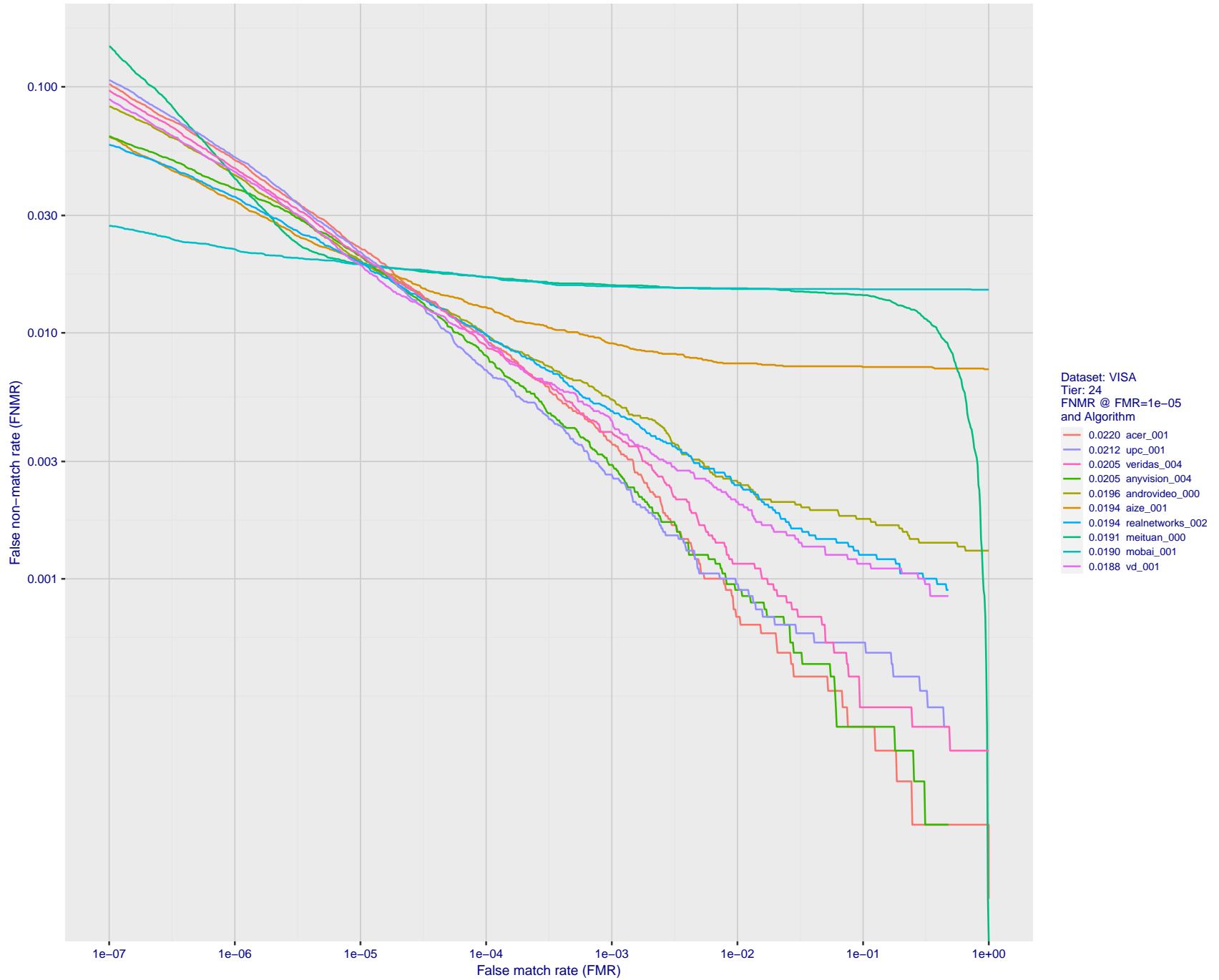


Figure 41: For the visa images, detection error tradeoff (DET) characteristics showing false non-match rate vs. false match rate plotted parametrically on threshold, T . The scales are logarithmic in order to show many decades of FMR.

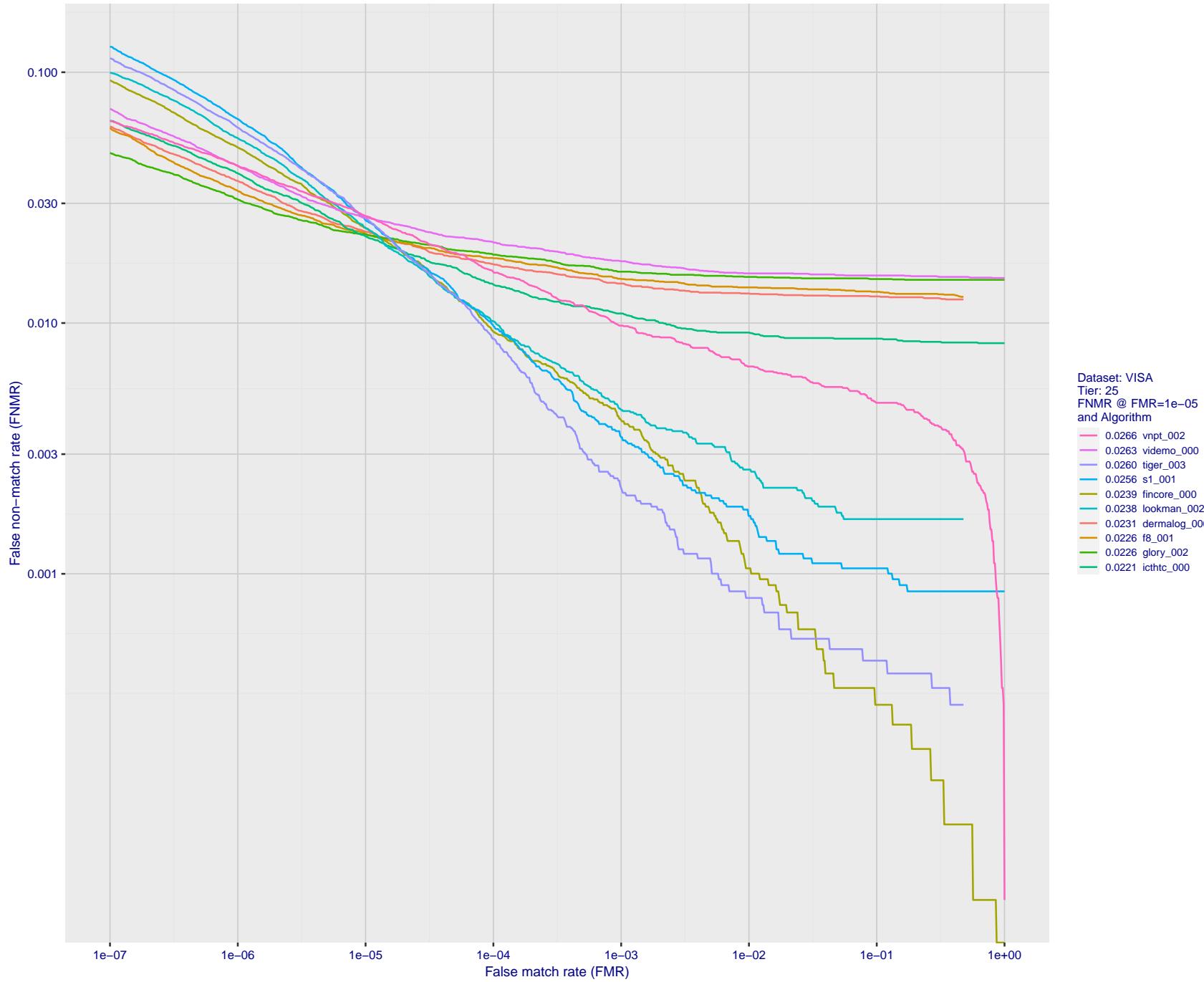


Figure 42: For the visa images, detection error tradeoff (DET) characteristics showing false non-match rate vs. false match rate plotted parametrically on threshold, T . The scales are logarithmic in order to show many decades of FMR.

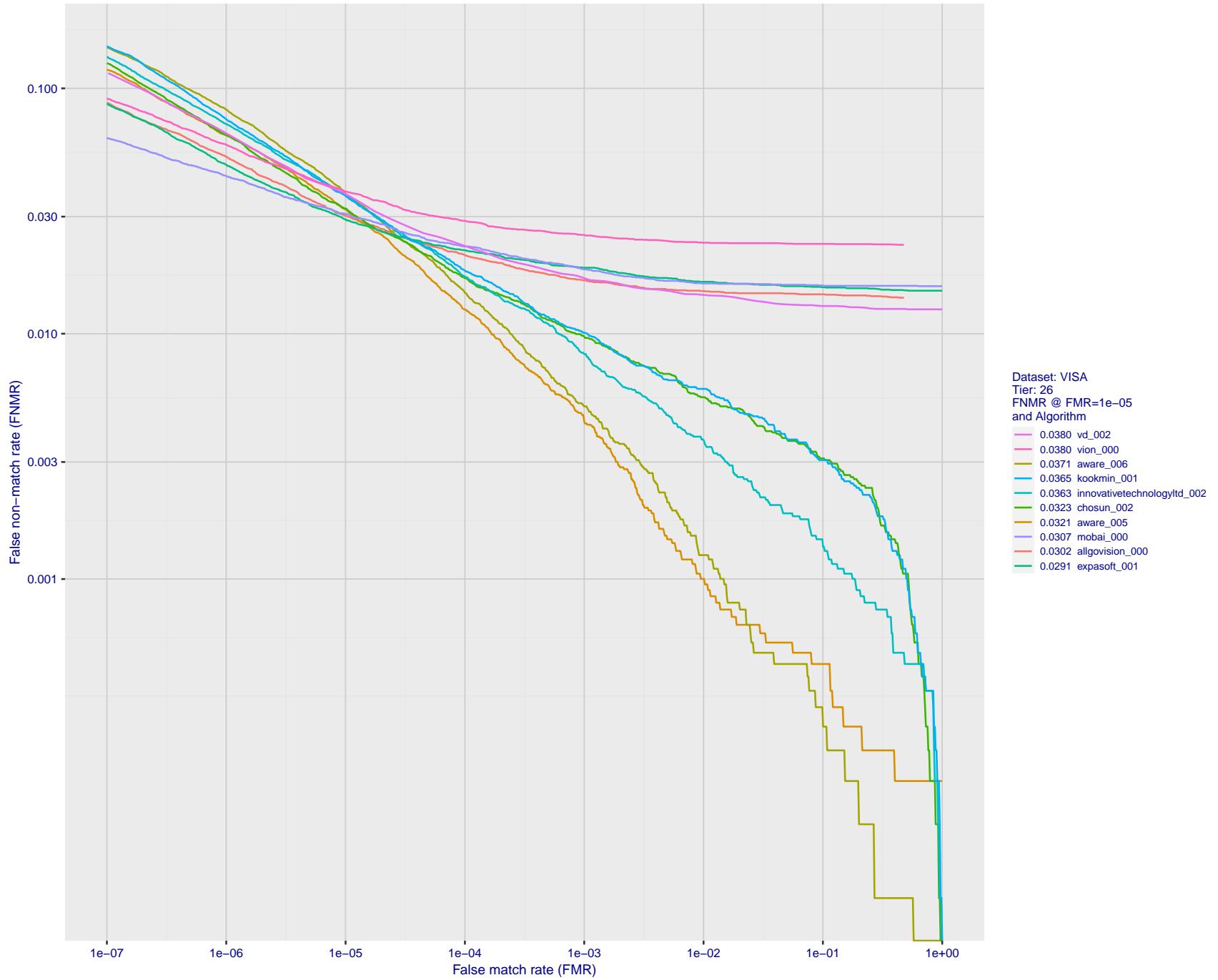


Figure 43: For the visa images, detection error tradeoff (DET) characteristics showing false non-match rate vs. false match rate plotted parametrically on threshold, T . The scales are logarithmic in order to show many decades of FMR.

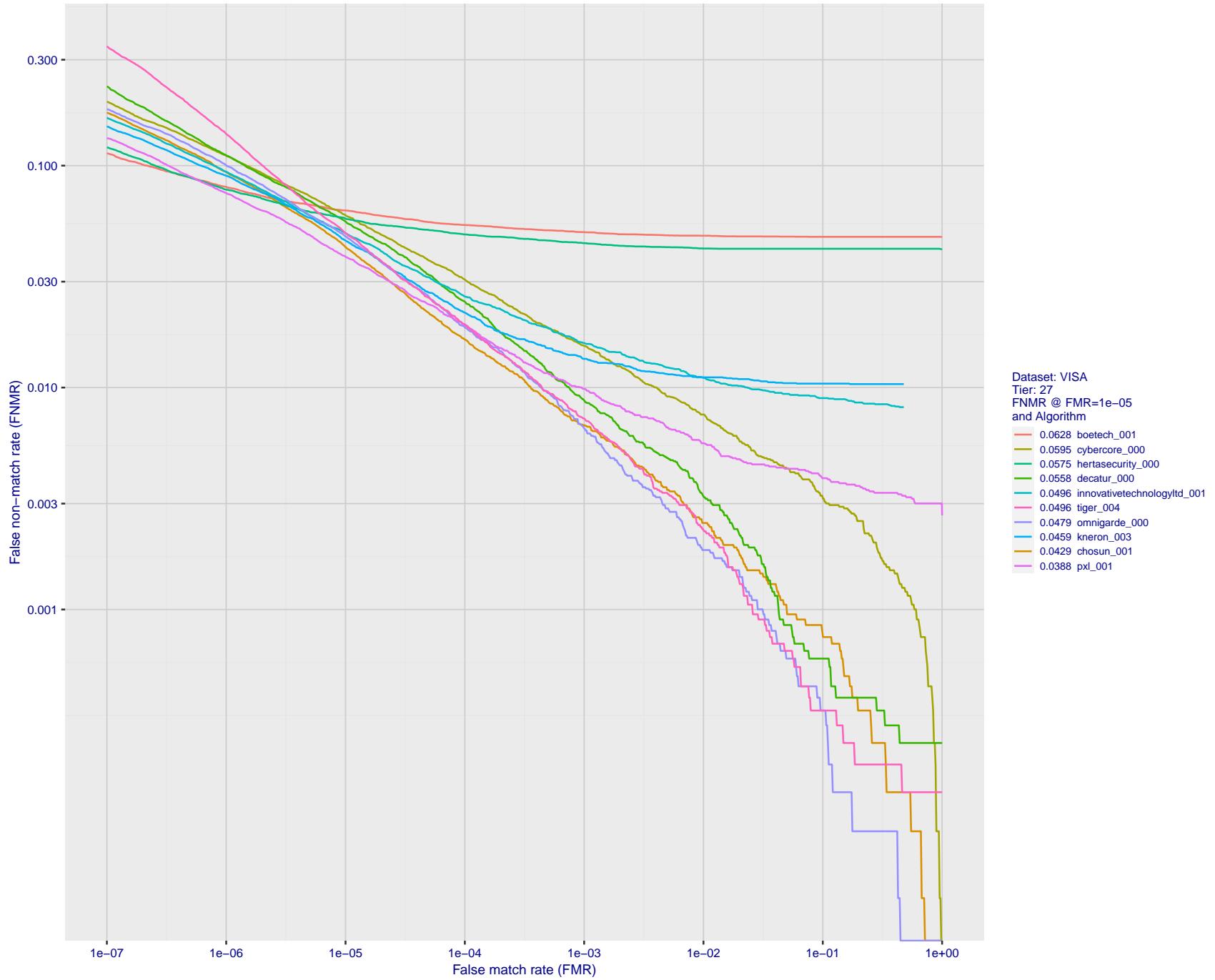


Figure 44: For the visa images, detection error tradeoff (DET) characteristics showing false non-match rate vs. false match rate plotted parametrically on threshold, T . The scales are logarithmic in order to show many decades of FMR.

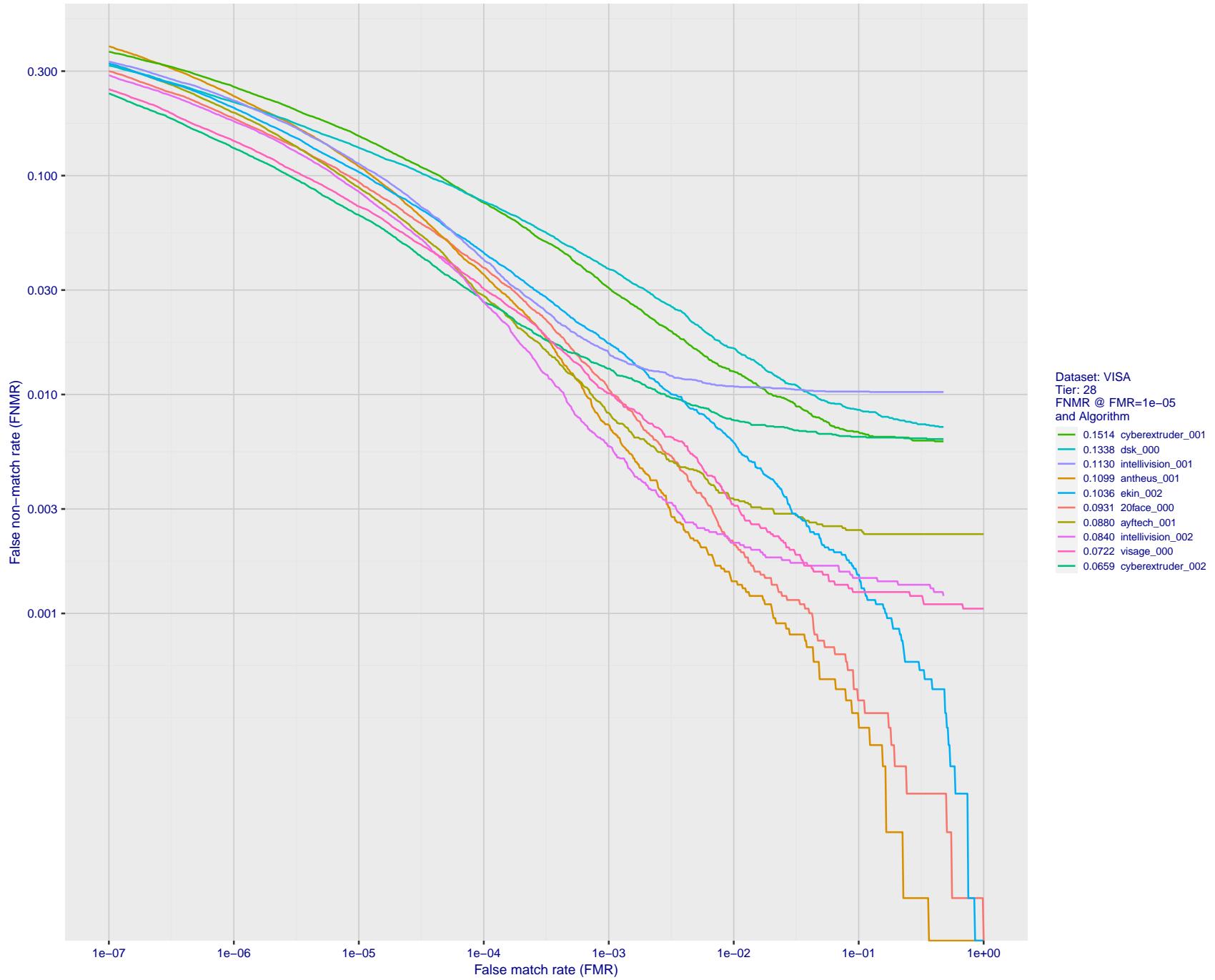


Figure 45: For the visa images, detection error tradeoff (DET) characteristics showing false non-match rate vs. false match rate plotted parametrically on threshold, T . The scales are logarithmic in order to show many decades of FMR.

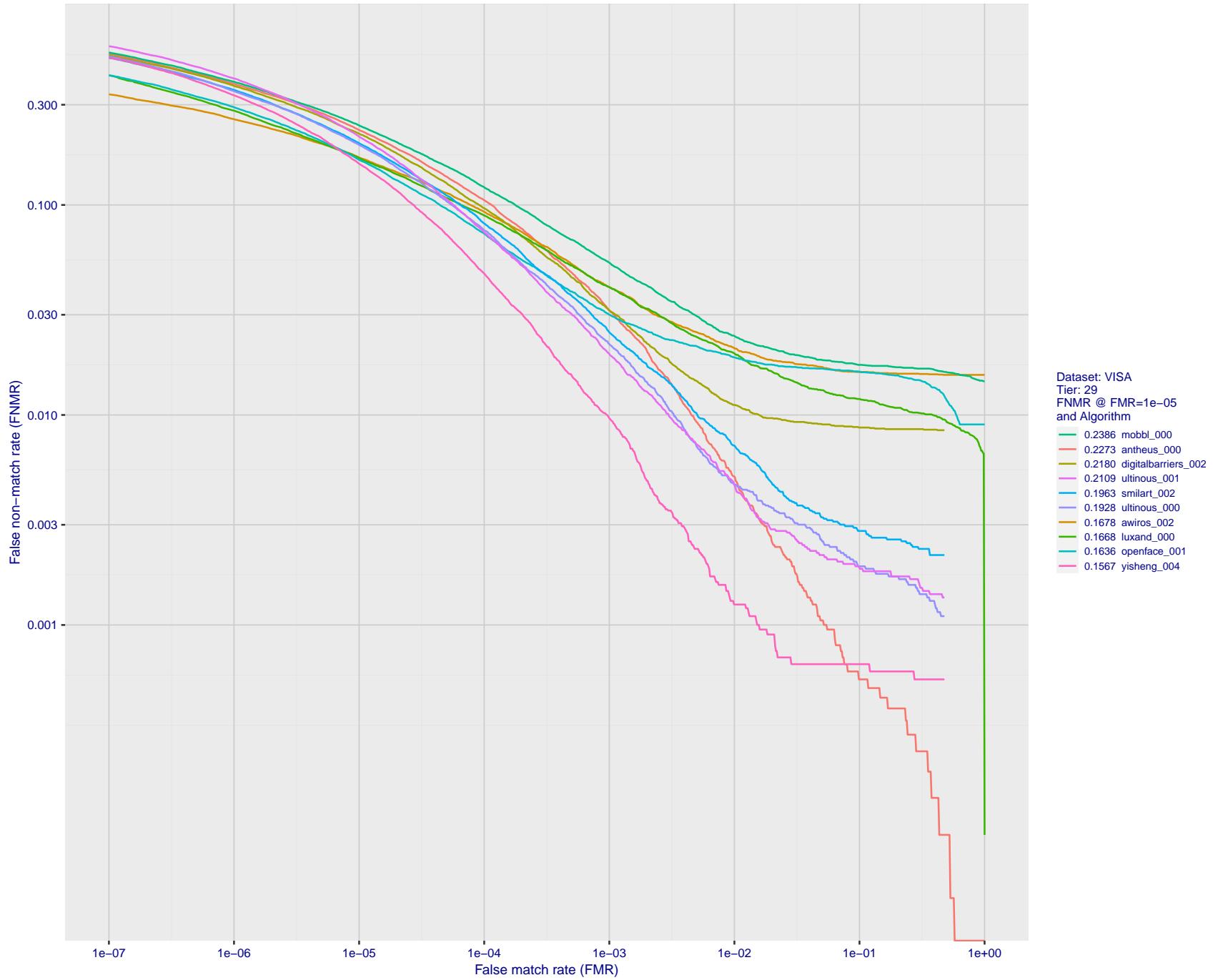


Figure 46: For the visa images, detection error tradeoff (DET) characteristics showing false non-match rate vs. false match rate plotted parametrically on threshold, T . The scales are logarithmic in order to show many decades of FMR.

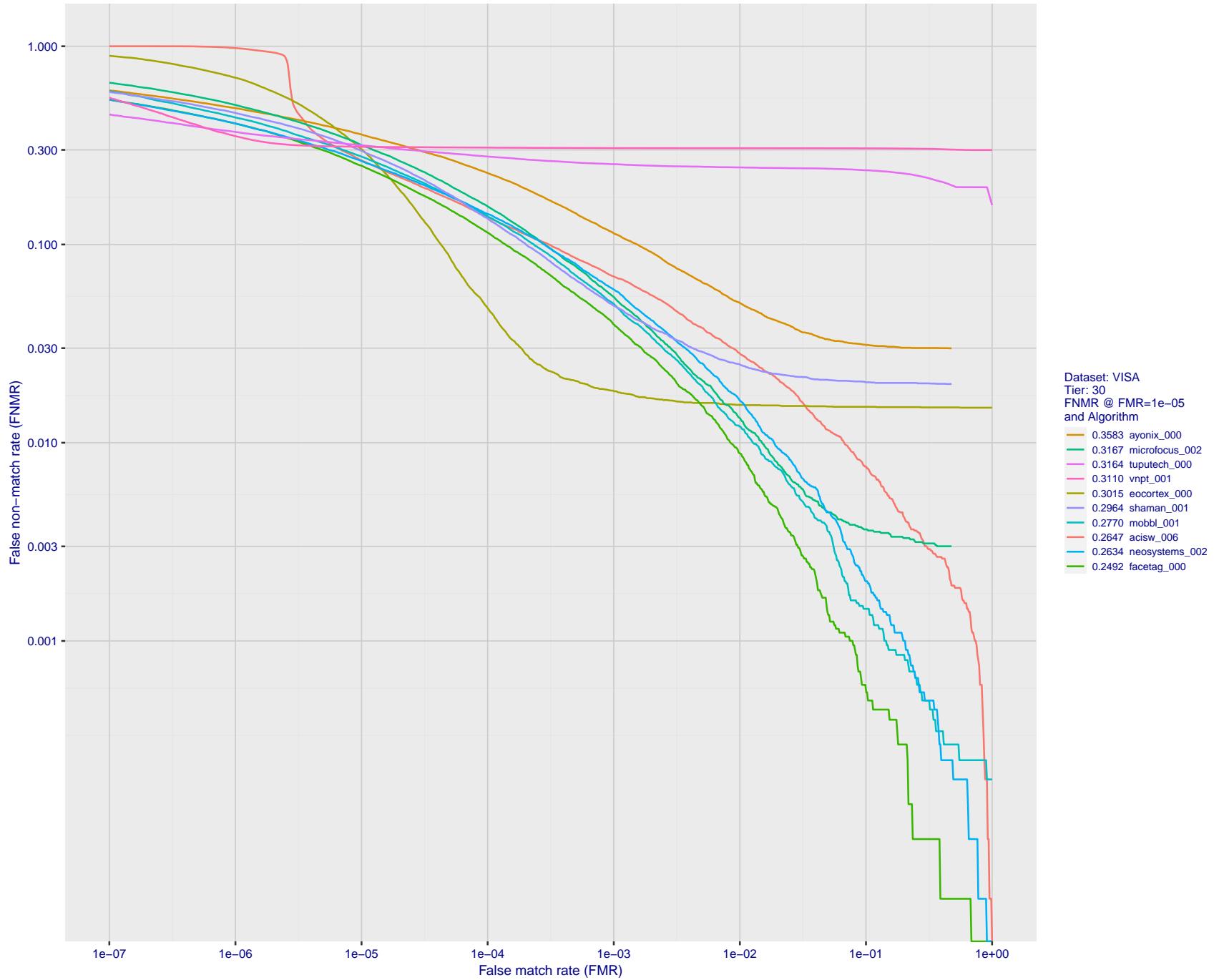


Figure 47: For the visa images, detection error tradeoff (DET) characteristics showing false non-match rate vs. false match rate plotted parametrically on threshold, T . The scales are logarithmic in order to show many decades of FMR.

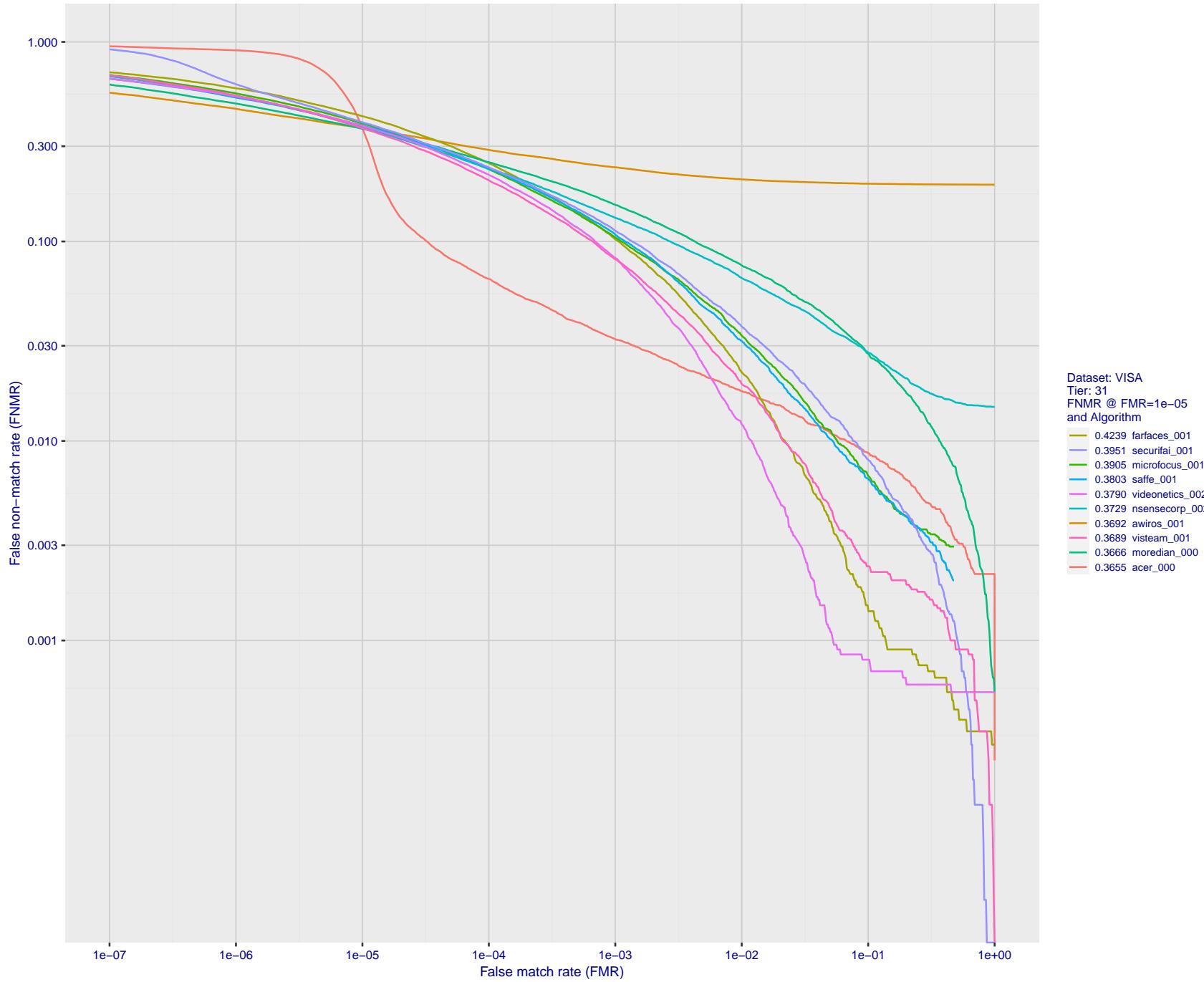


Figure 48: For the visa images, detection error tradeoff (DET) characteristics showing false non-match rate vs. false match rate plotted parametrically on threshold, T . The scales are logarithmic in order to show many decades of FMR.

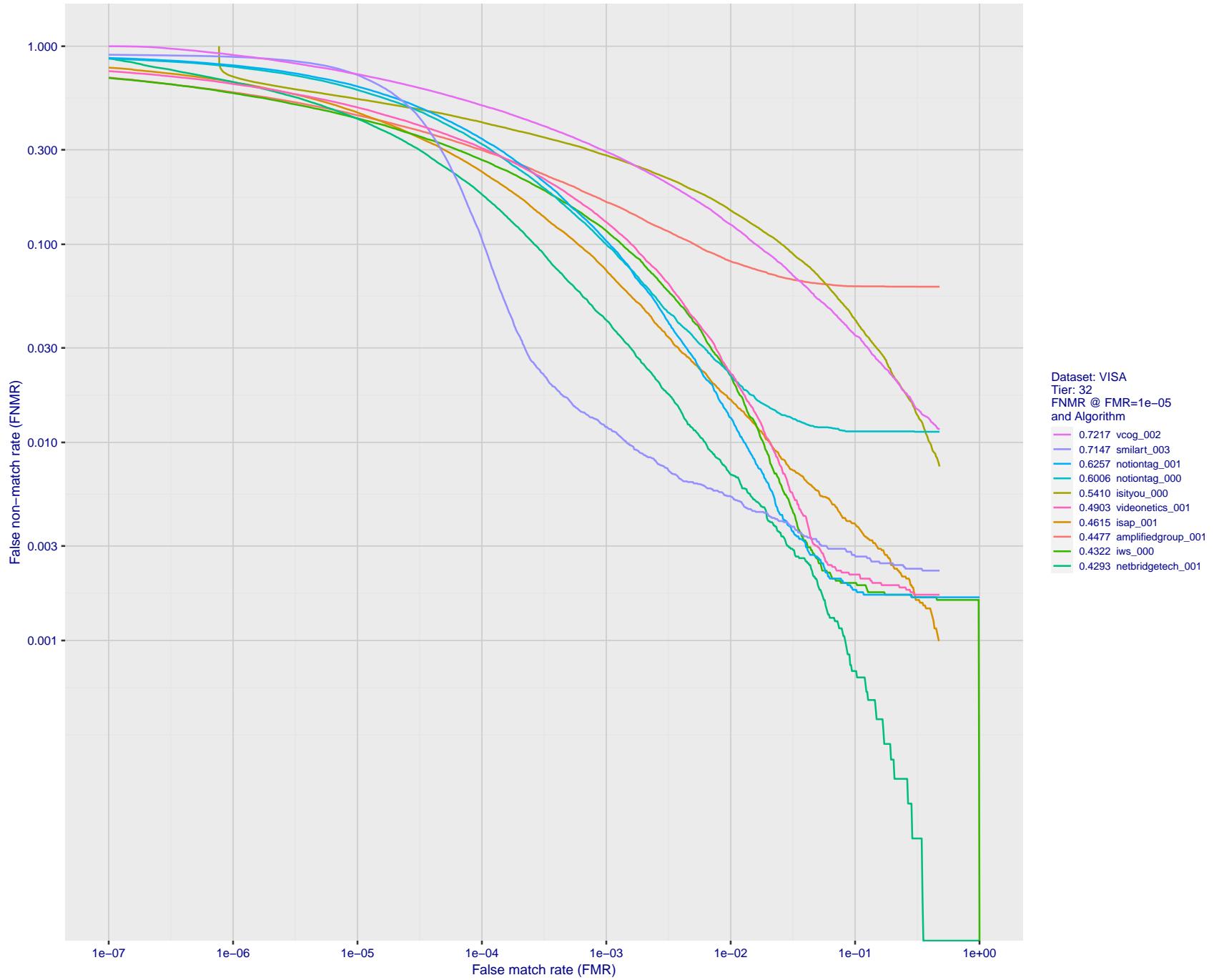


Figure 49: For the visa images, detection error tradeoff (DET) characteristics showing false non-match rate vs. false match rate plotted parametrically on threshold, T . The scales are logarithmic in order to show many decades of FMR.

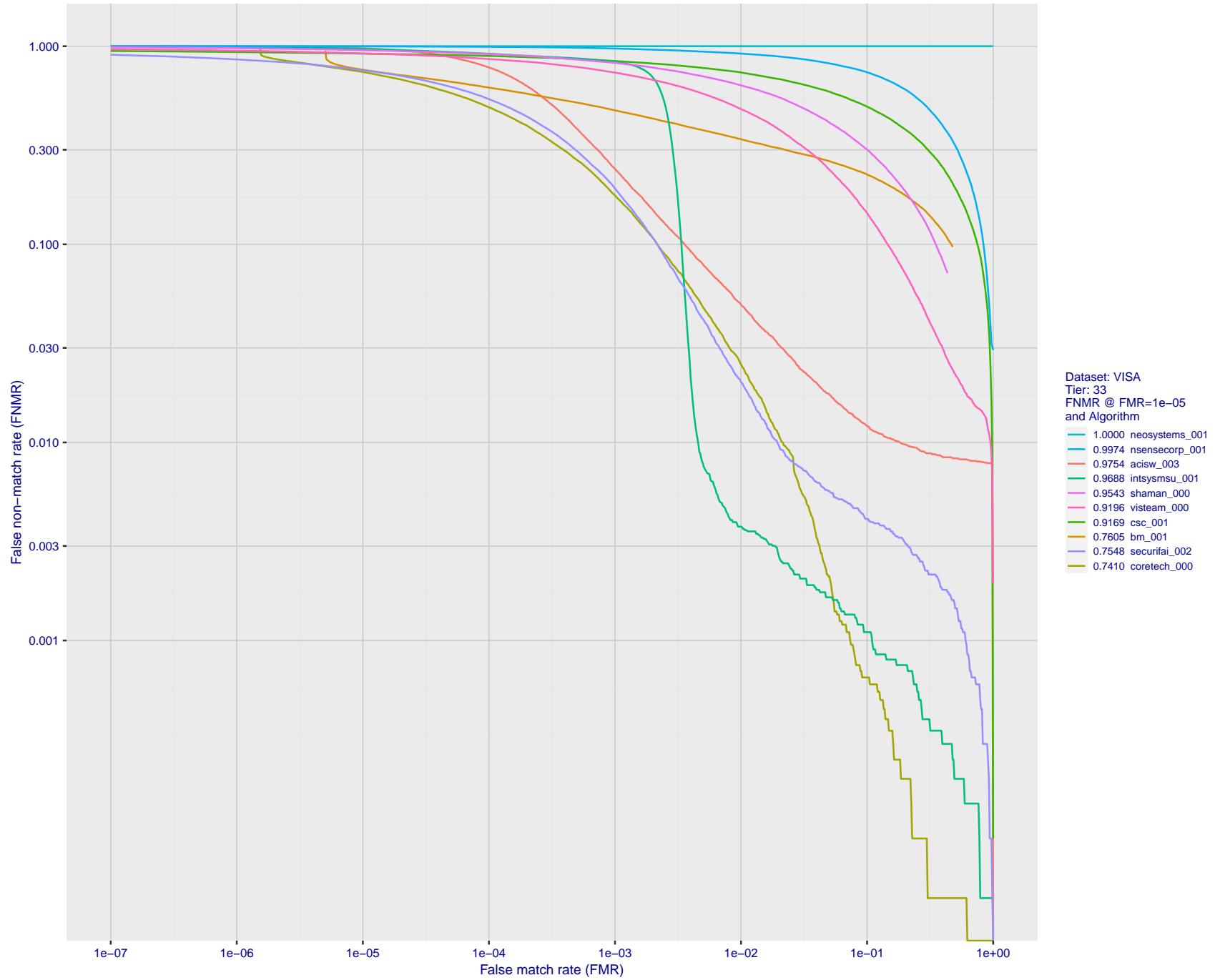


Figure 50: For the visa images, detection error tradeoff (DET) characteristics showing false non-match rate vs. false match rate plotted parametrically on threshold, T . The scales are logarithmic in order to show many decades of FMR.

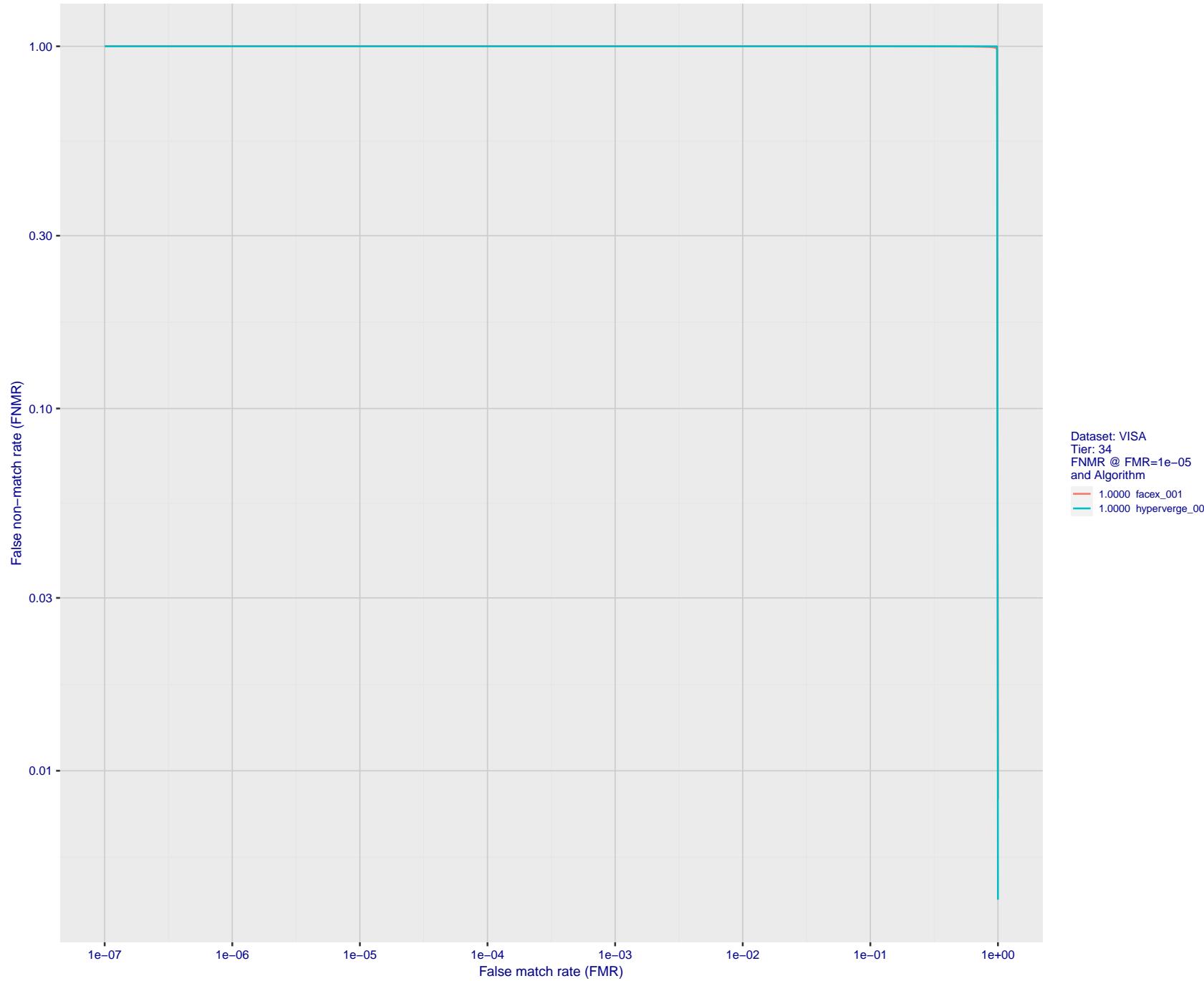


Figure 51: For the visa images, detection error tradeoff (DET) characteristics showing false non-match rate vs. false match rate plotted parametrically on threshold, T . The scales are logarithmic in order to show many decades of FMR.

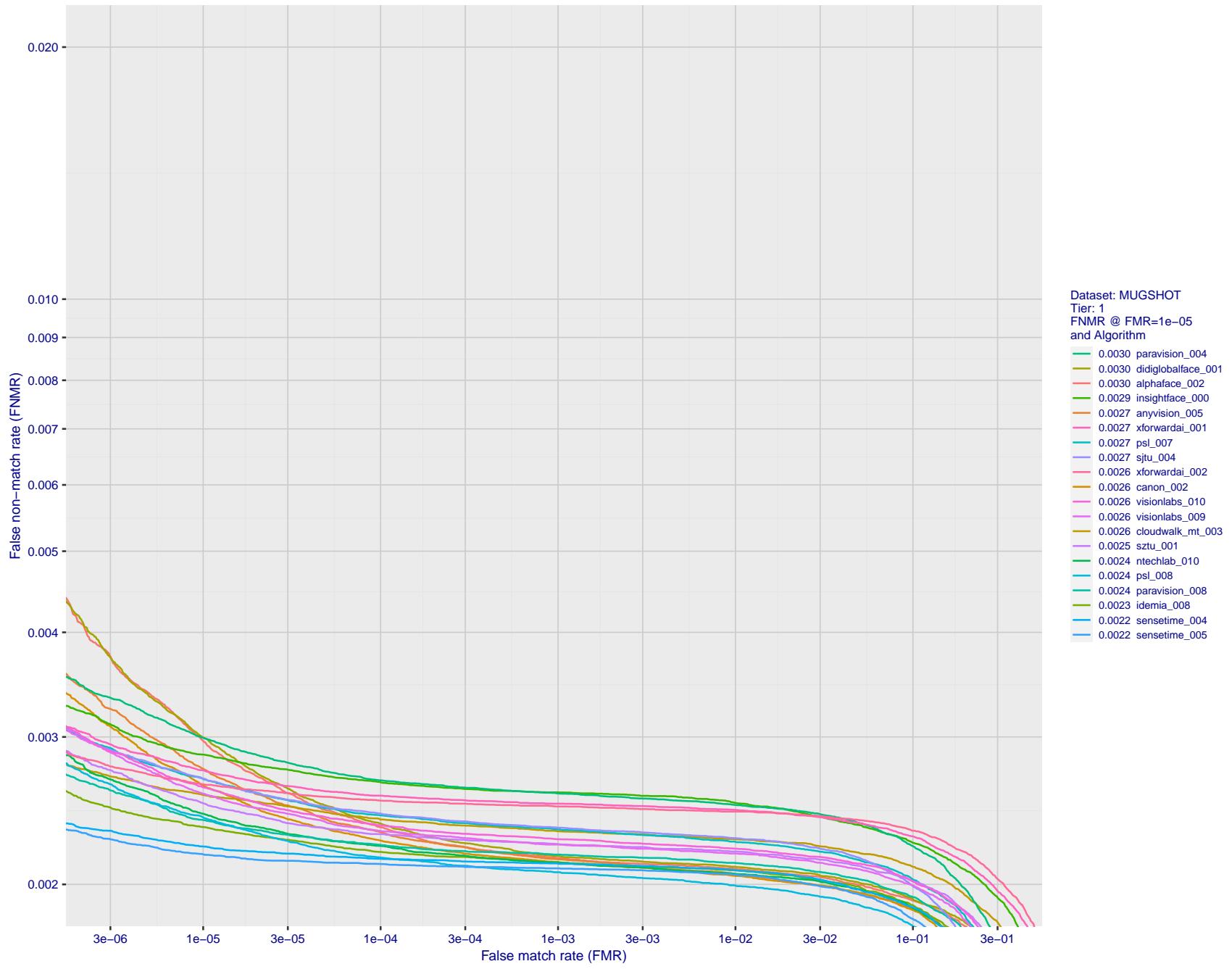


Figure 52: For the mugshot images, detection error tradeoff (DET) characteristics showing false non-match rate vs. false match rate plotted parametrically on threshold, T . The scales are logarithmic in order to show decades of FMR.

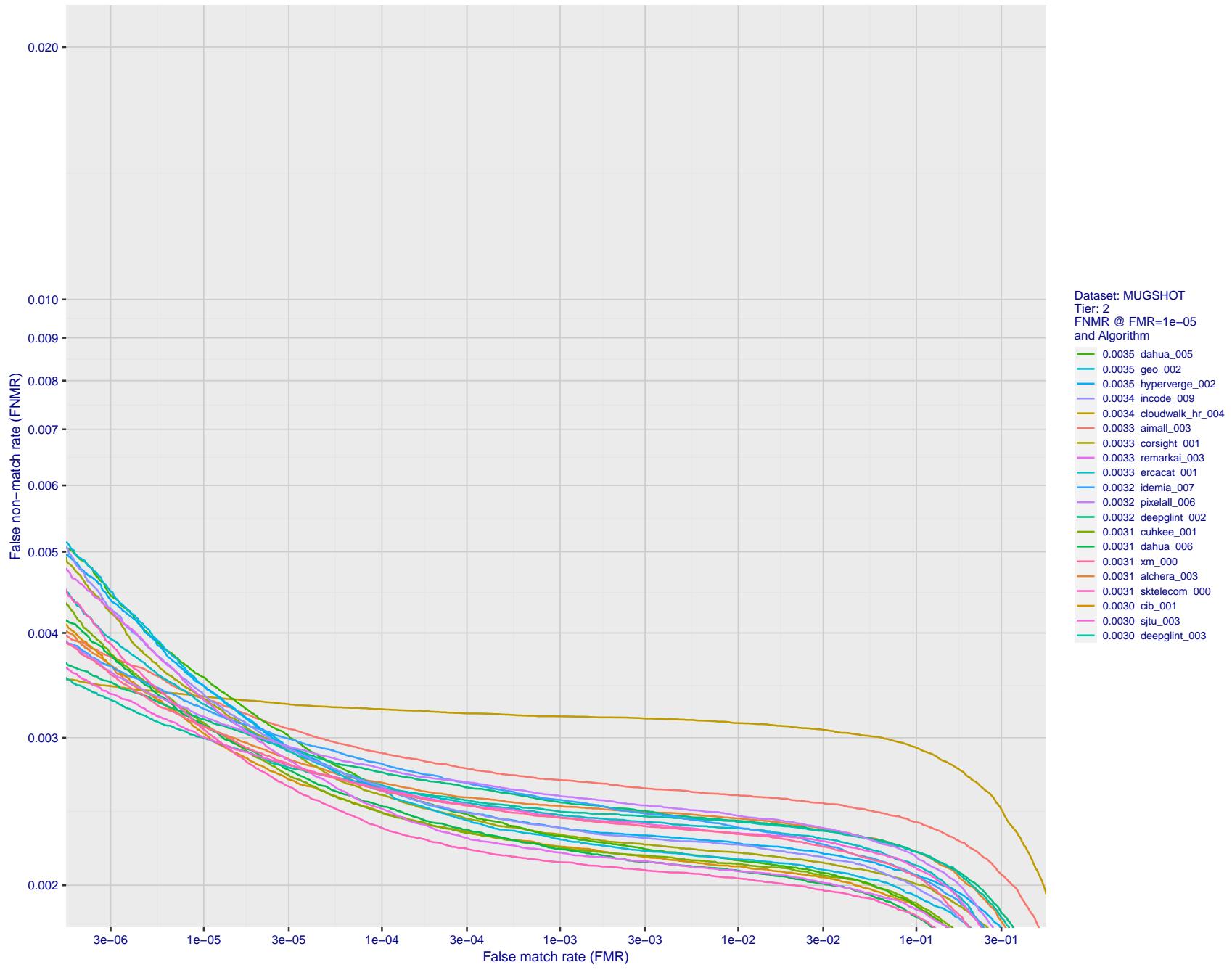


Figure 53: For the mugshot images, detection error tradeoff (DET) characteristics showing false non-match rate vs. false match rate plotted parametrically on threshold, T . The scales are logarithmic in order to show decades of FMR.

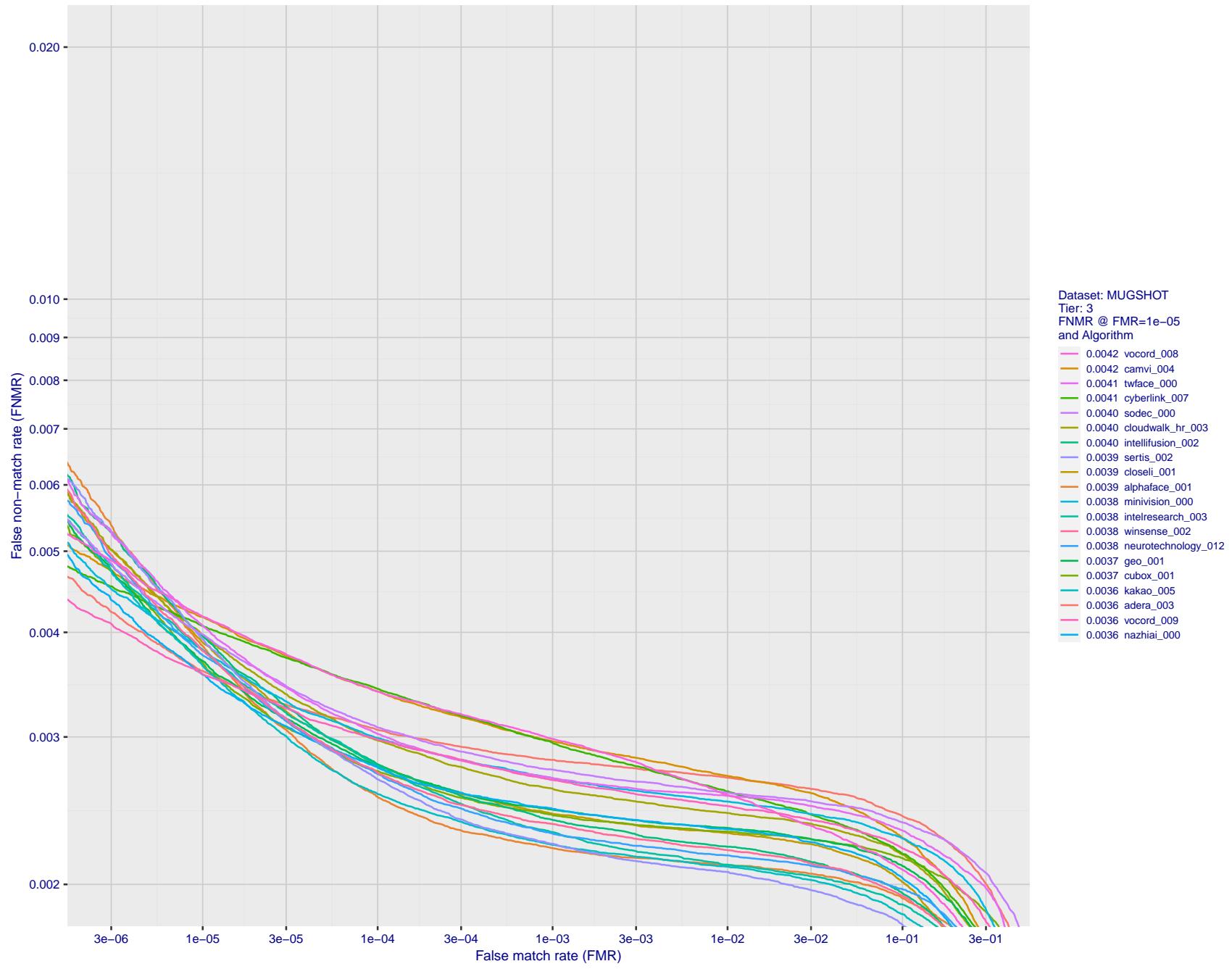


Figure 54: For the mugshot images, detection error tradeoff (DET) characteristics showing false non-match rate vs. false match rate plotted parametrically on threshold, T . The scales are logarithmic in order to show decades of FMR.

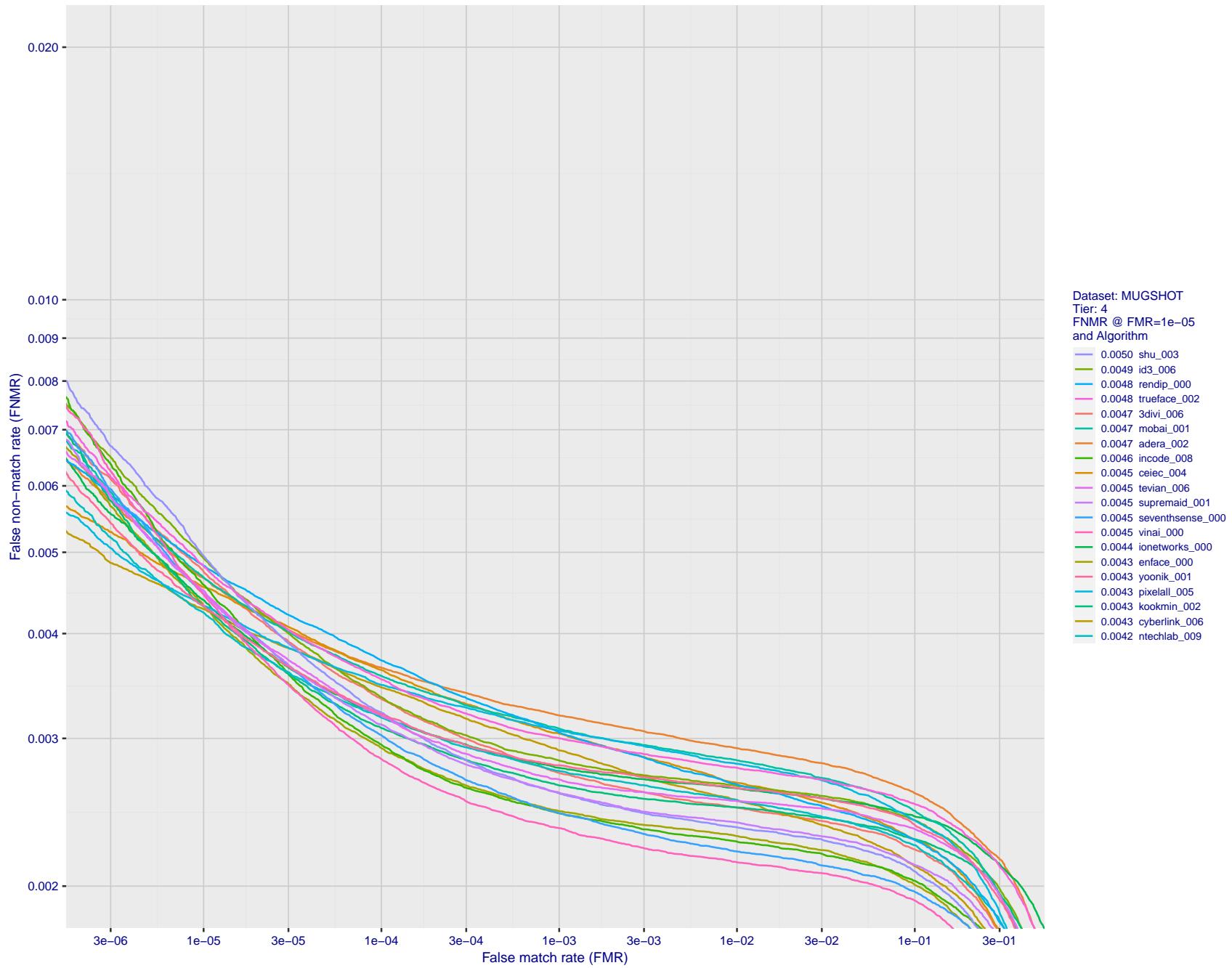


Figure 55: For the mugshot images, detection error tradeoff (DET) characteristics showing false non-match rate vs. false match rate plotted parametrically on threshold, T . The scales are logarithmic in order to show decades of FMR.

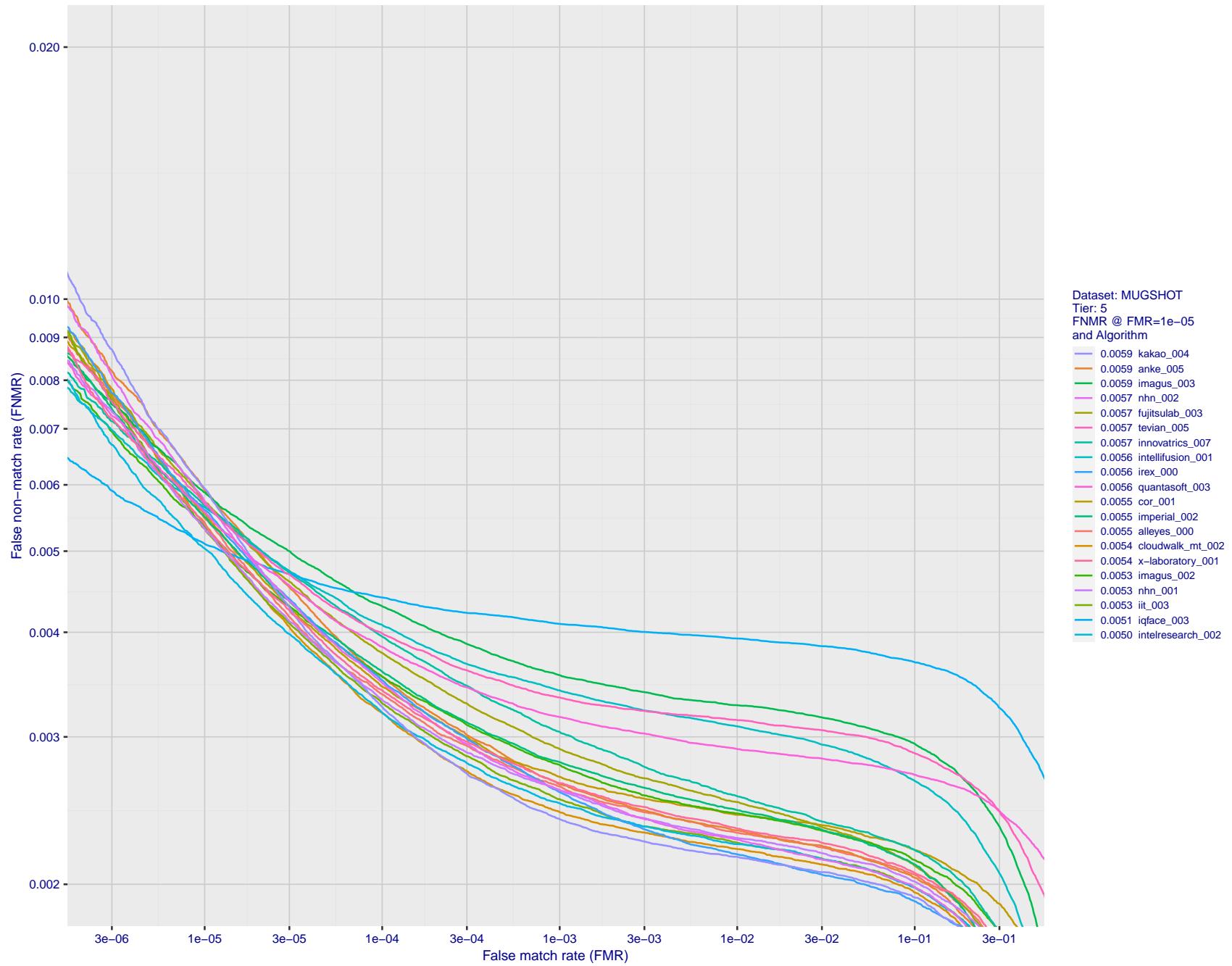
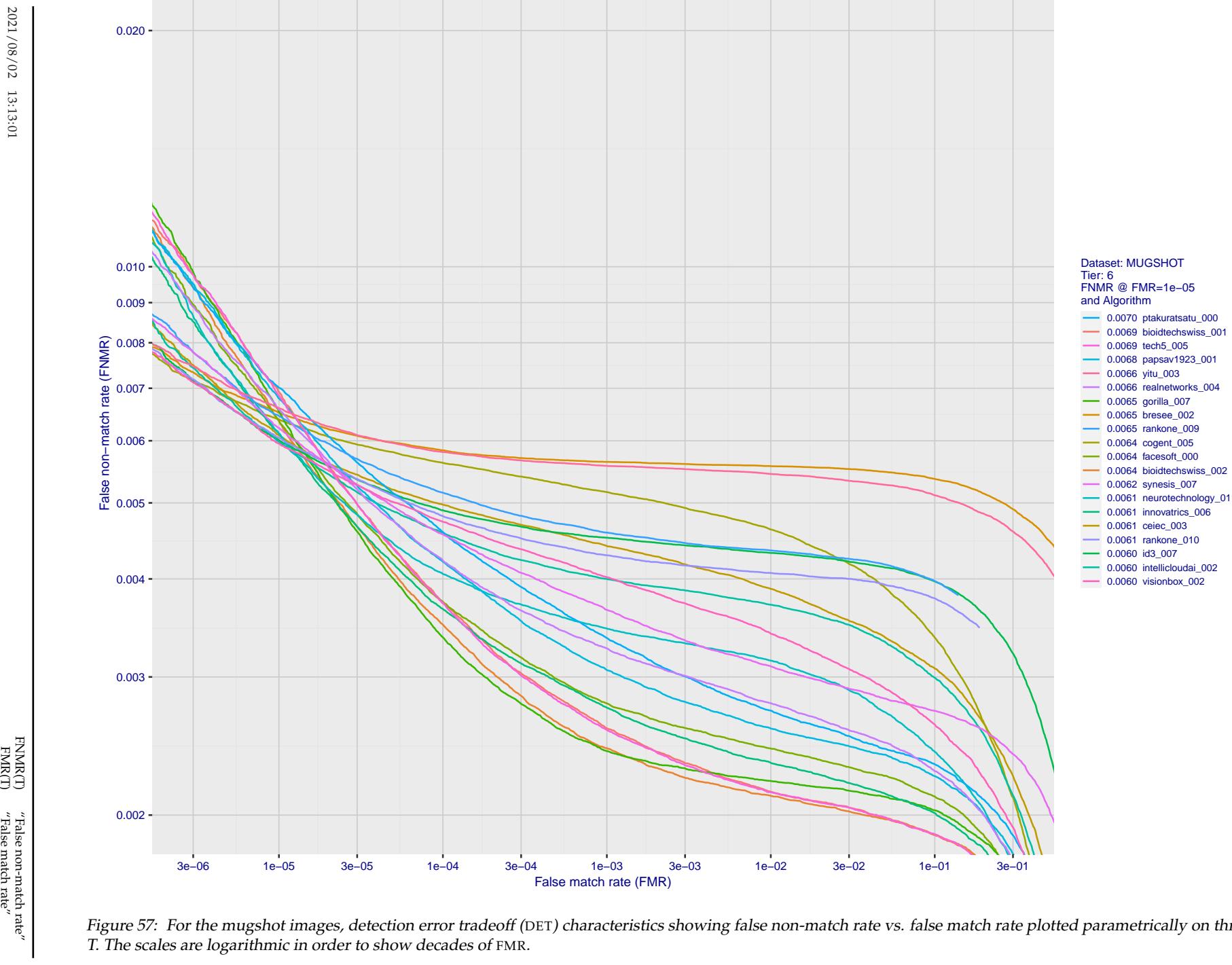


Figure 56: For the mugshot images, detection error tradeoff (DET) characteristics showing false non-match rate vs. false match rate plotted parametrically on threshold, T . The scales are logarithmic in order to show decades of FMR.



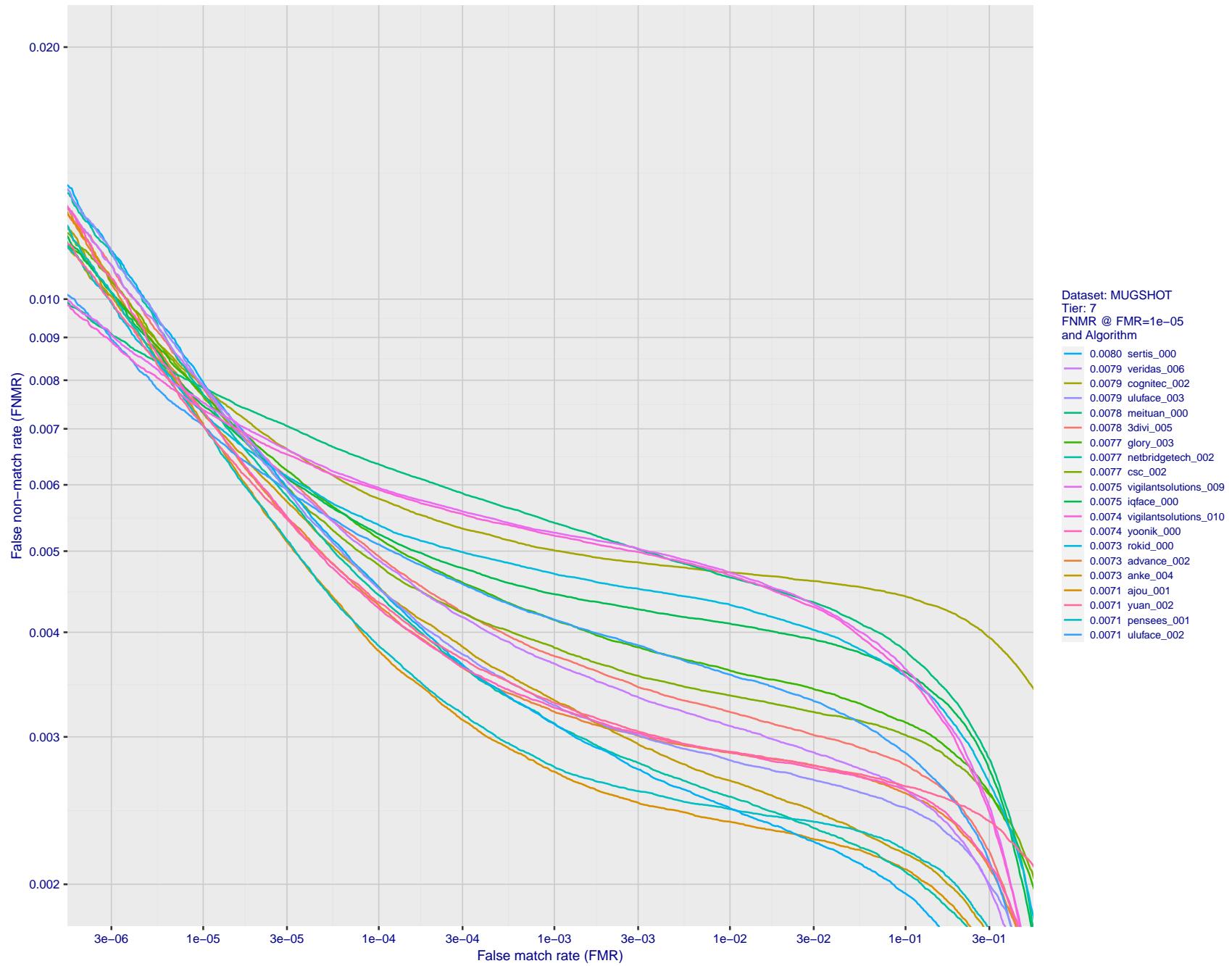


Figure 58: For the mugshot images, detection error tradeoff (DET) characteristics showing false non-match rate vs. false match rate plotted parametrically on threshold, T . The scales are logarithmic in order to show decades of FMR.

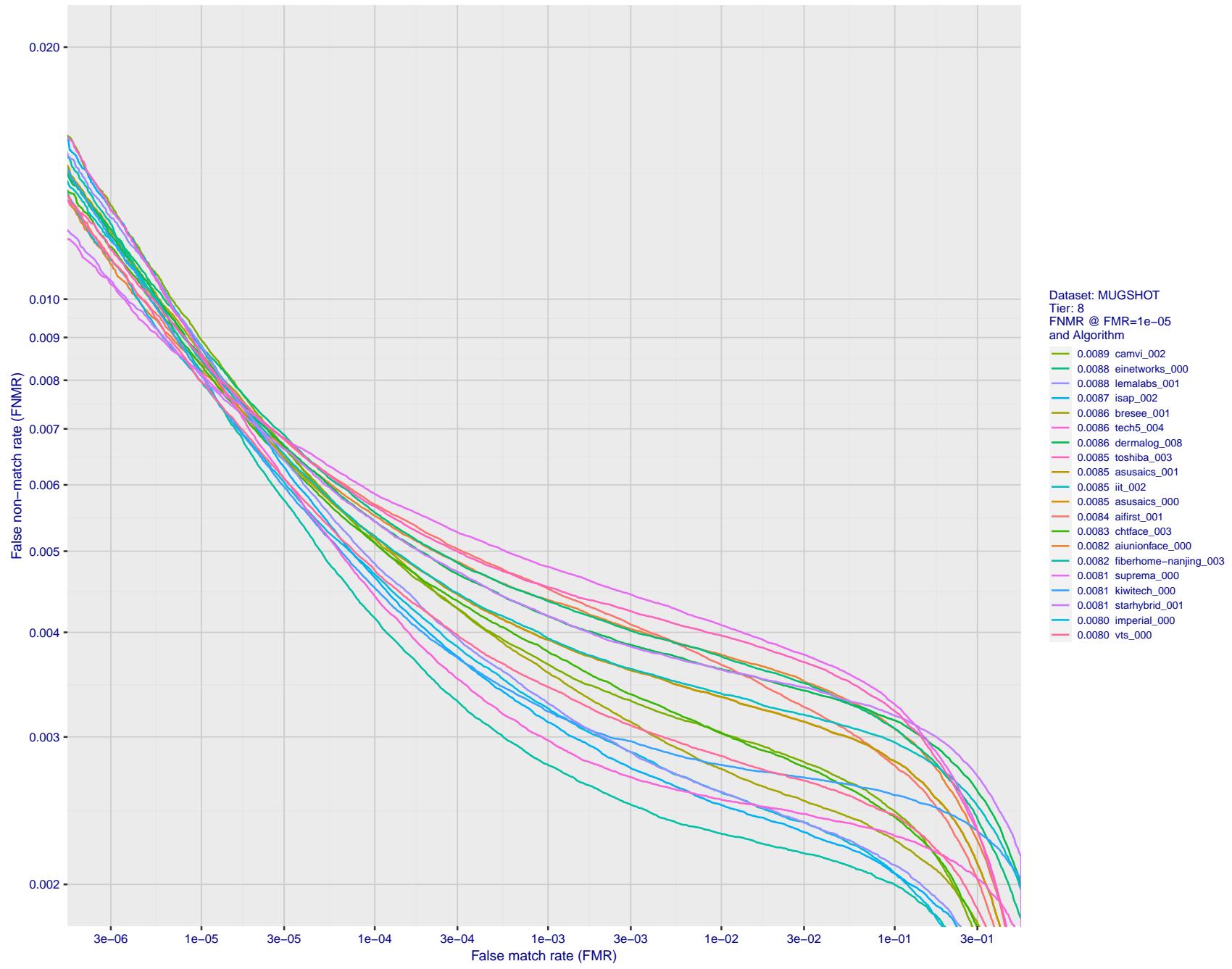
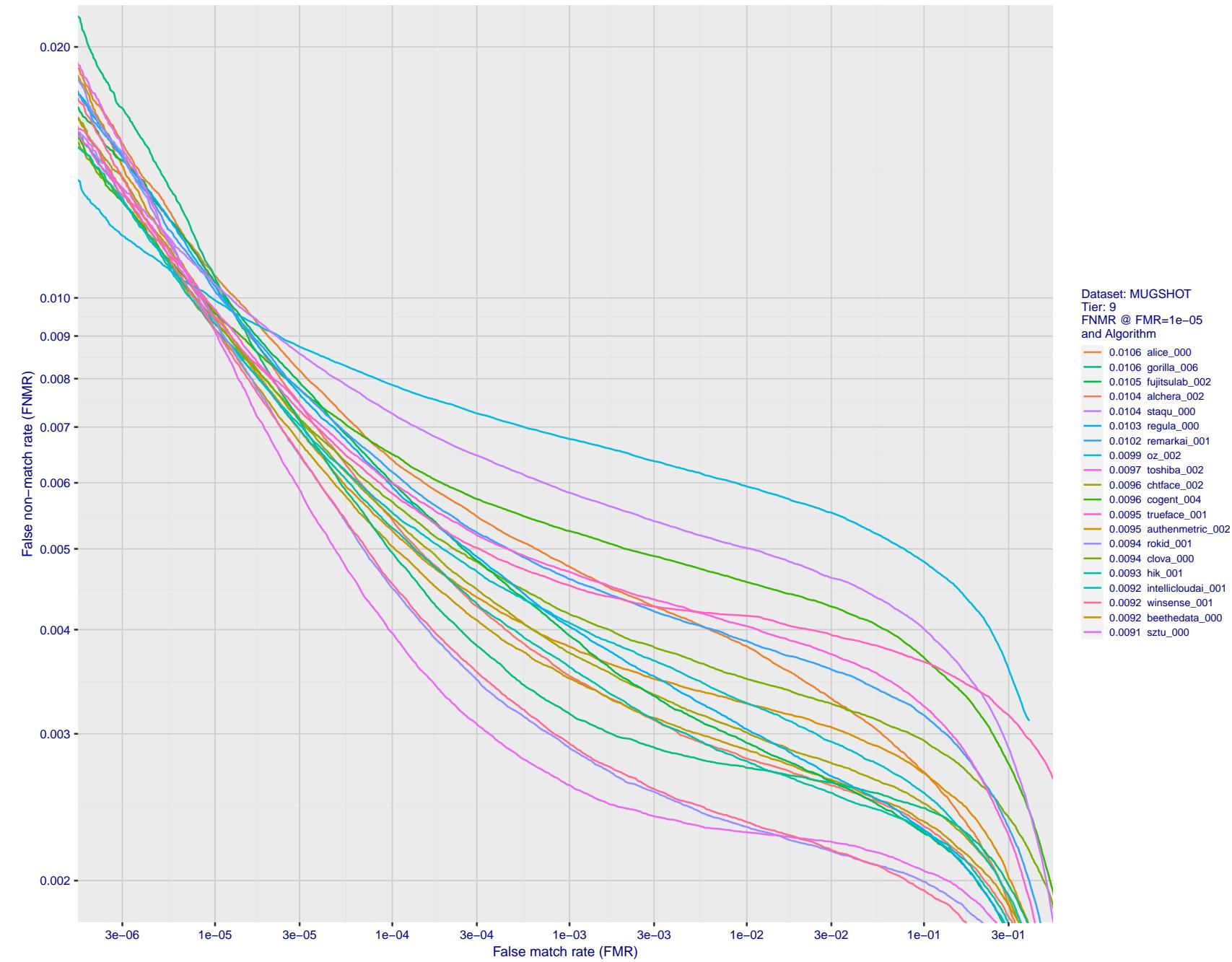


Figure 59: For the mugshot images, detection error tradeoff (DET) characteristics showing false non-match rate vs. false match rate plotted parametrically on threshold, T . The scales are logarithmic in order to show decades of FMR.



FNMR(T)
FMR(T)
"False non-match rate"
"False match rate"

Figure 60: For the mugshot images, detection error tradeoff (DET) characteristics showing false non-match rate vs. false match rate plotted parametrically on threshold, T . The scales are logarithmic in order to show decades of FMR.

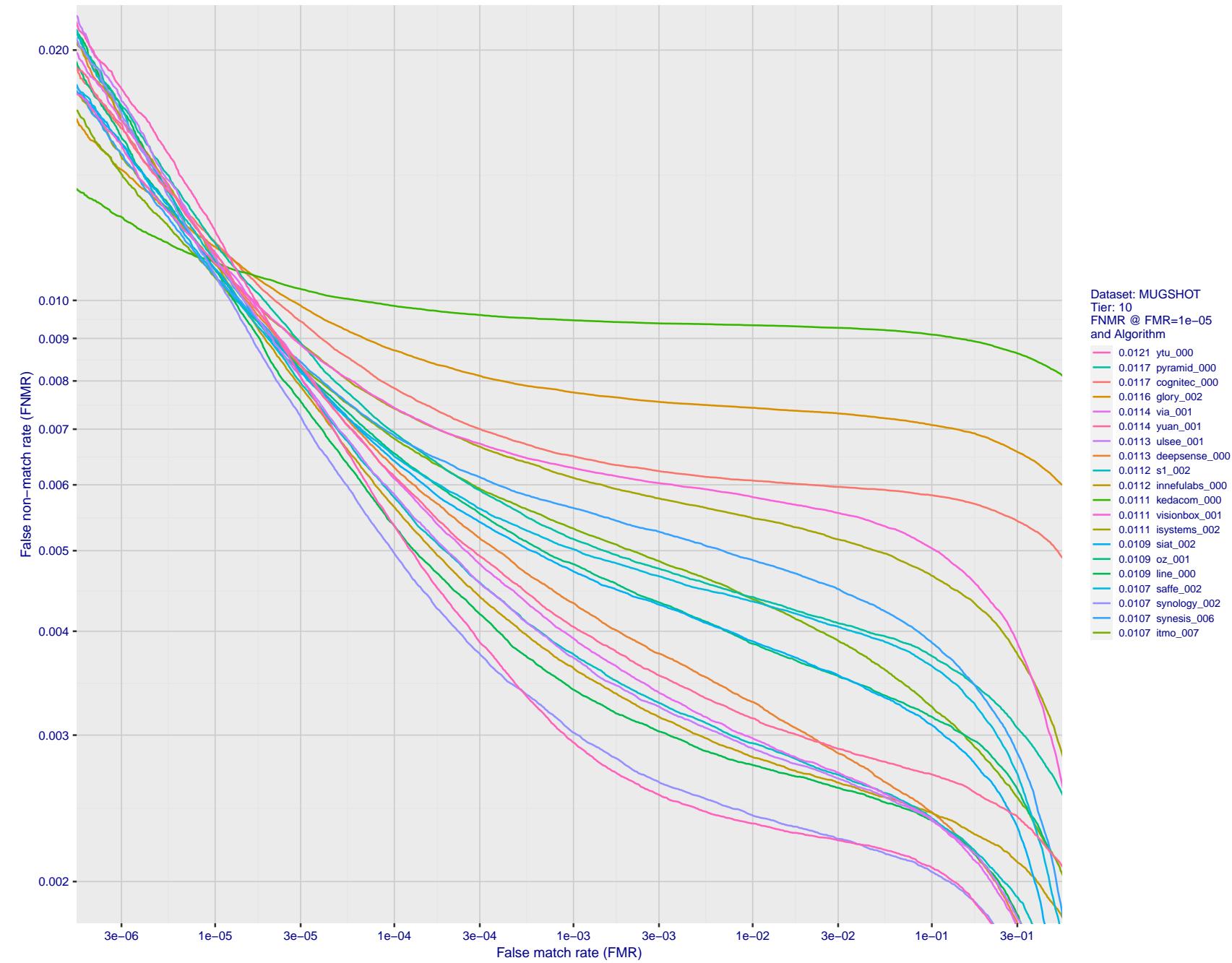


Figure 61: For the mugshot images, detection error tradeoff (DET) characteristics showing false non-match rate vs. false match rate plotted parametrically on threshold, T . The scales are logarithmic in order to show decades of FMR.

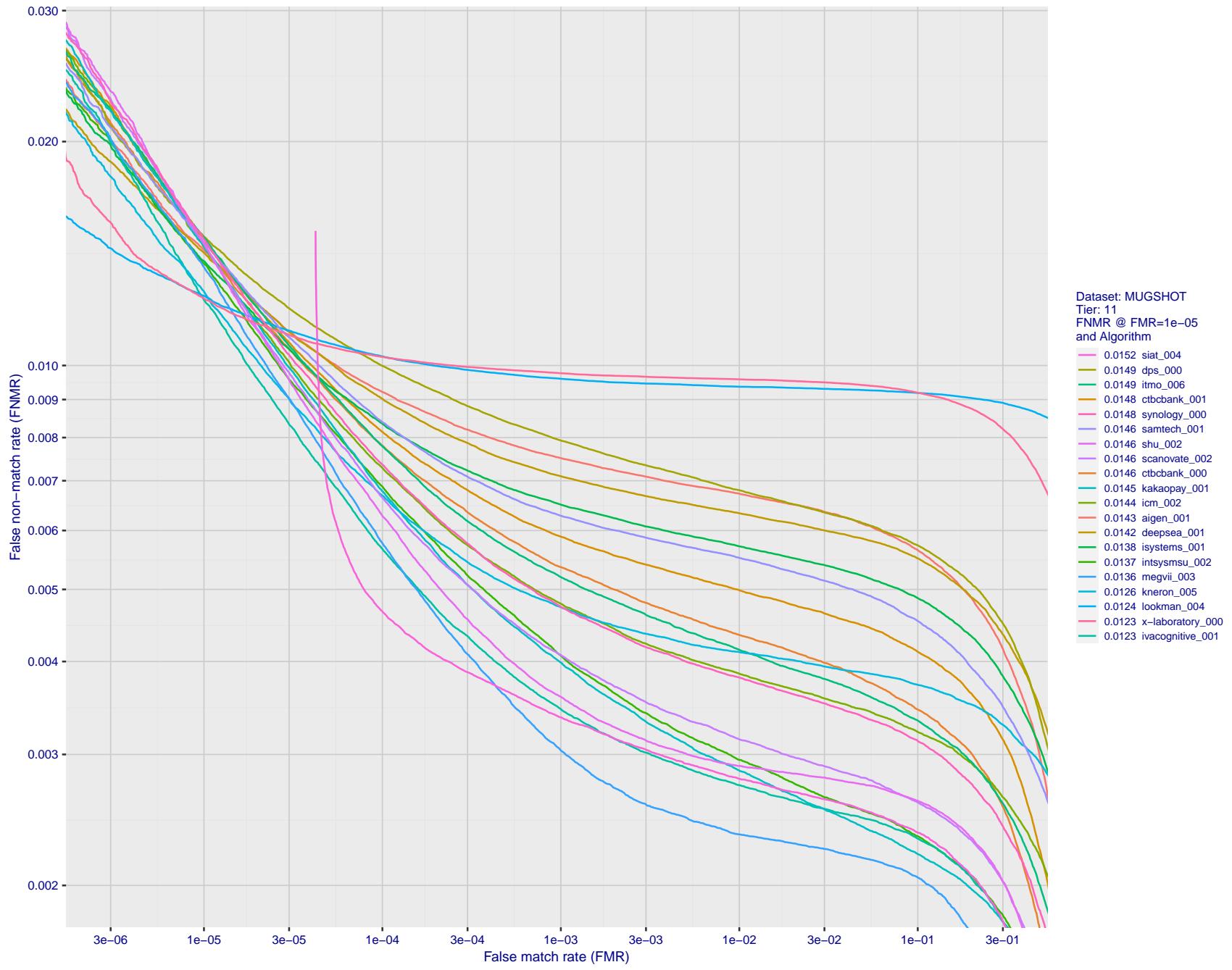


Figure 62: For the mugshot images, detection error tradeoff (DET) characteristics showing false non-match rate vs. false match rate plotted parametrically on threshold, T . The scales are logarithmic in order to show decades of FMR.

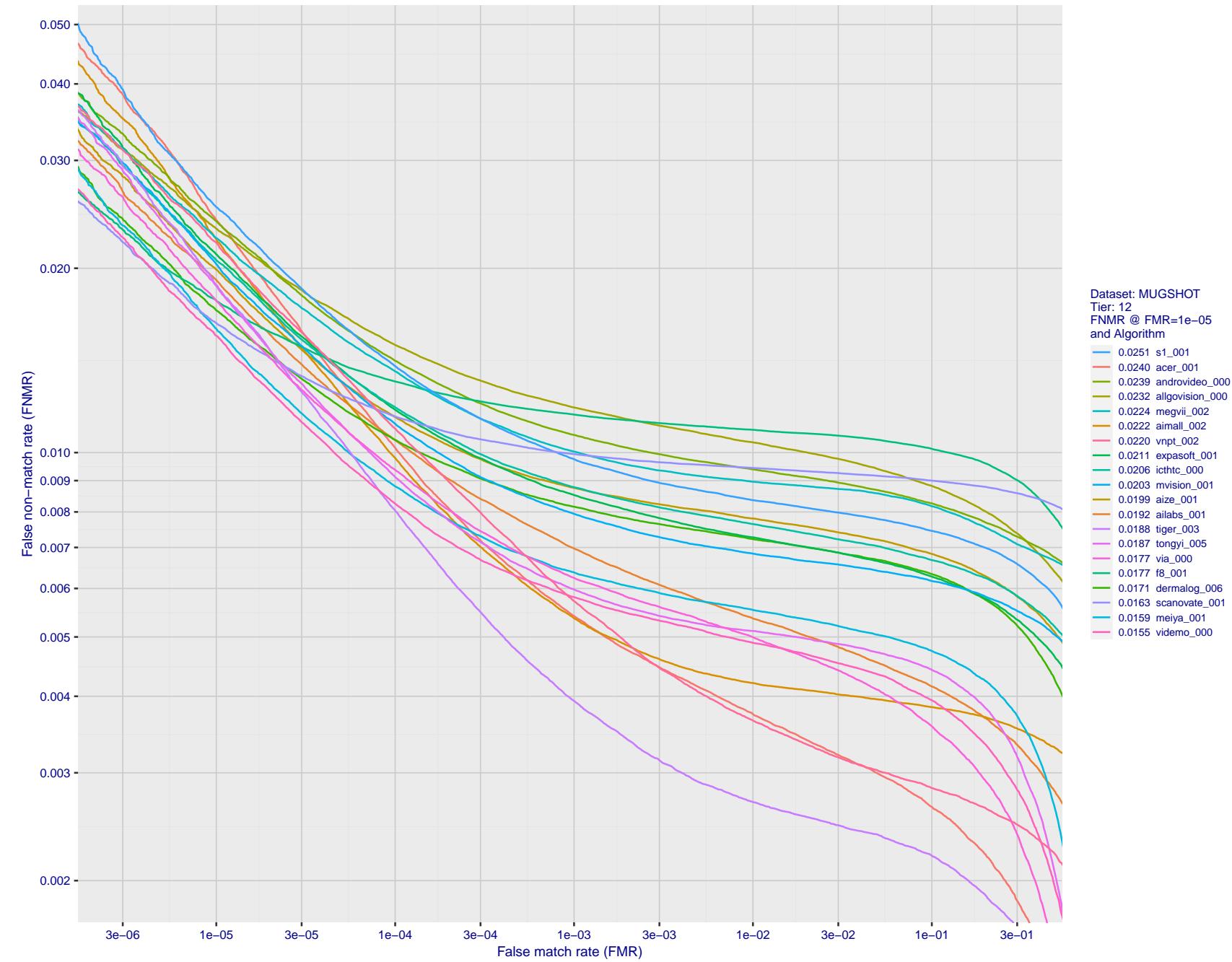


Figure 63: For the mugshot images, detection error tradeoff (DET) characteristics showing false non-match rate vs. false match rate plotted parametrically on threshold, T . The scales are logarithmic in order to show decades of FMR.

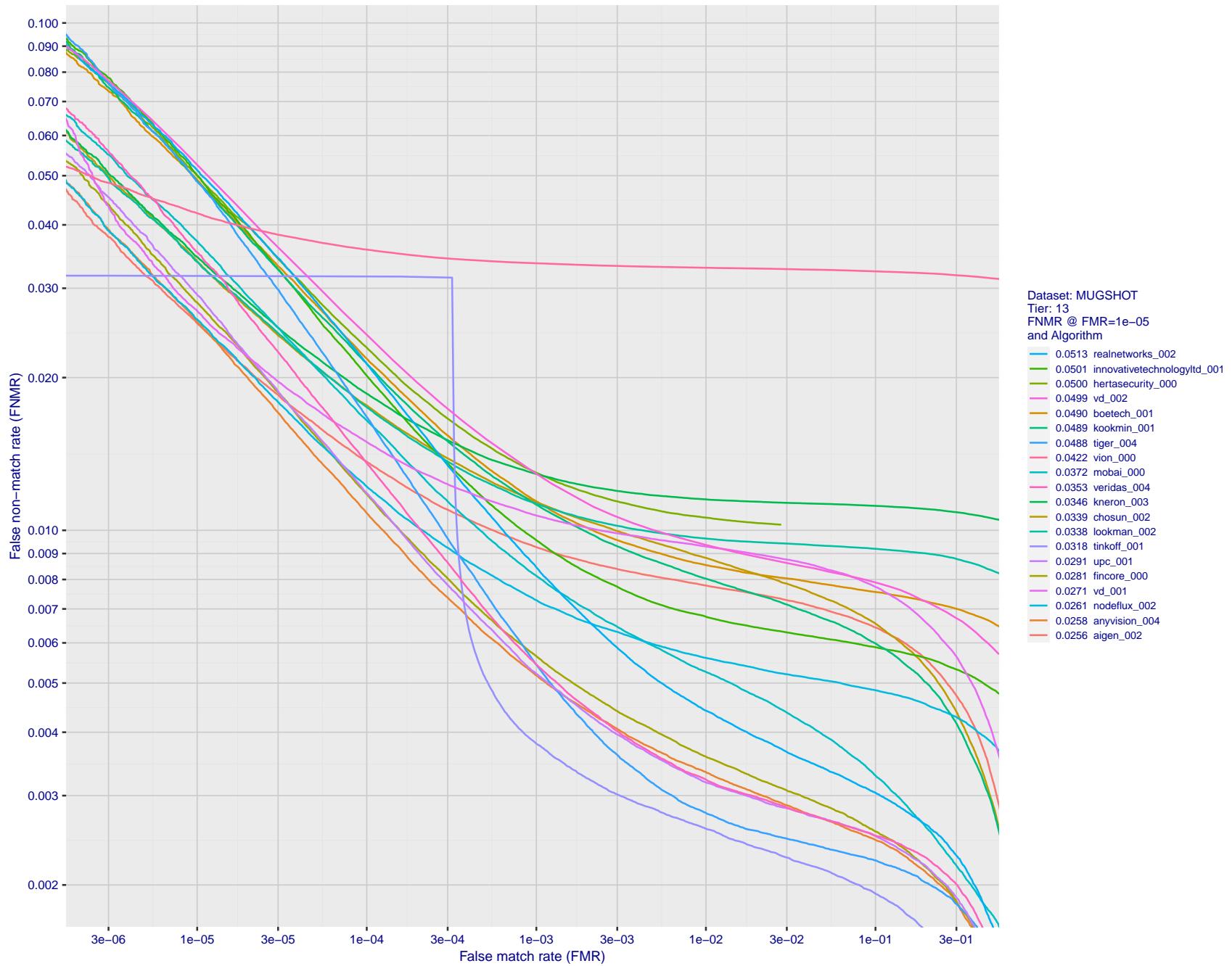


Figure 64: For the mugshot images, detection error tradeoff (DET) characteristics showing false non-match rate vs. false match rate plotted parametrically on threshold, T . The scales are logarithmic in order to show decades of FMR.

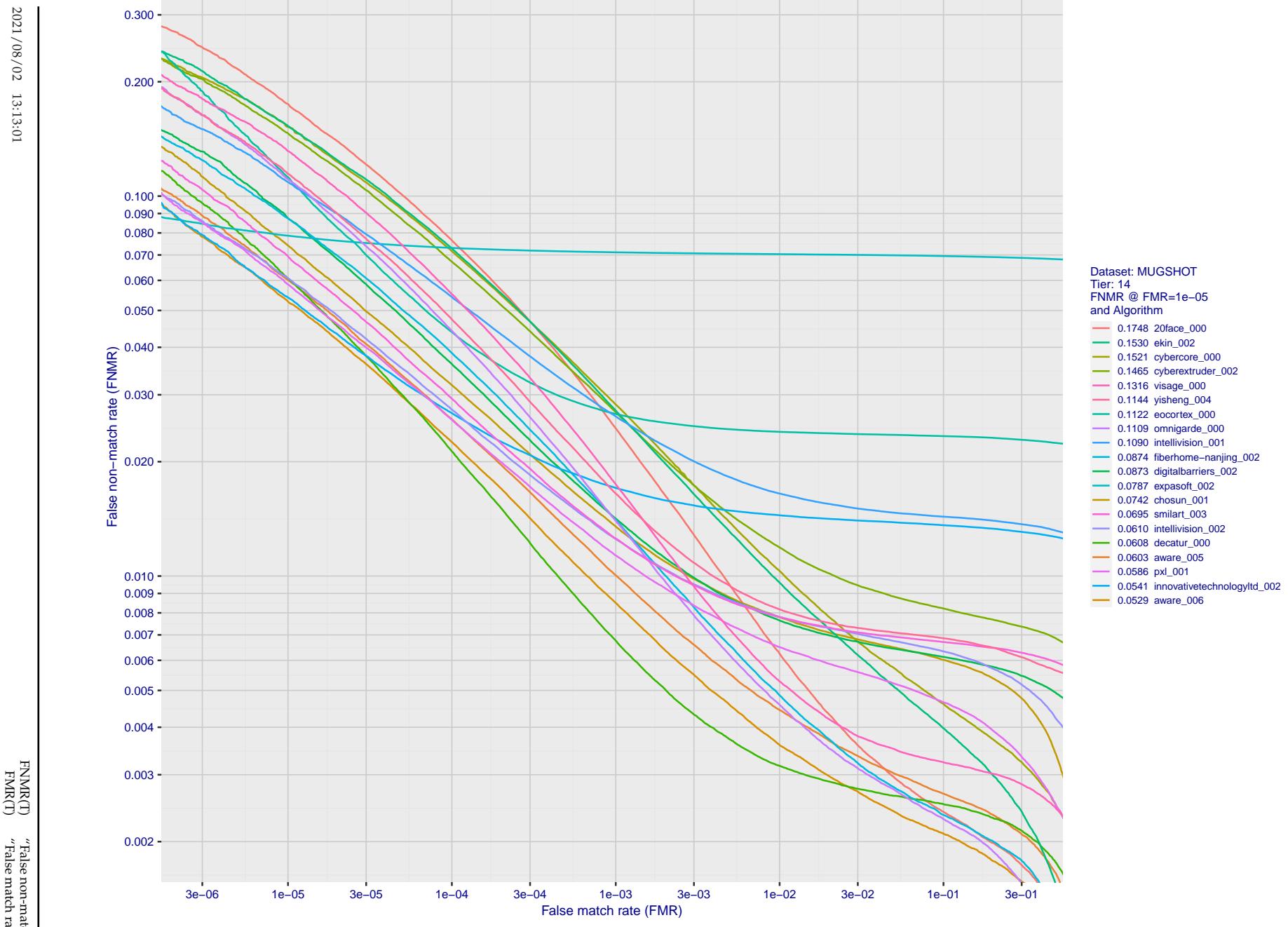


Figure 65: For the mugshot images, detection error tradeoff (DET) characteristics showing false non-match rate vs. false match rate plotted parametrically on threshold, T . The scales are logarithmic in order to show decades of FMR.

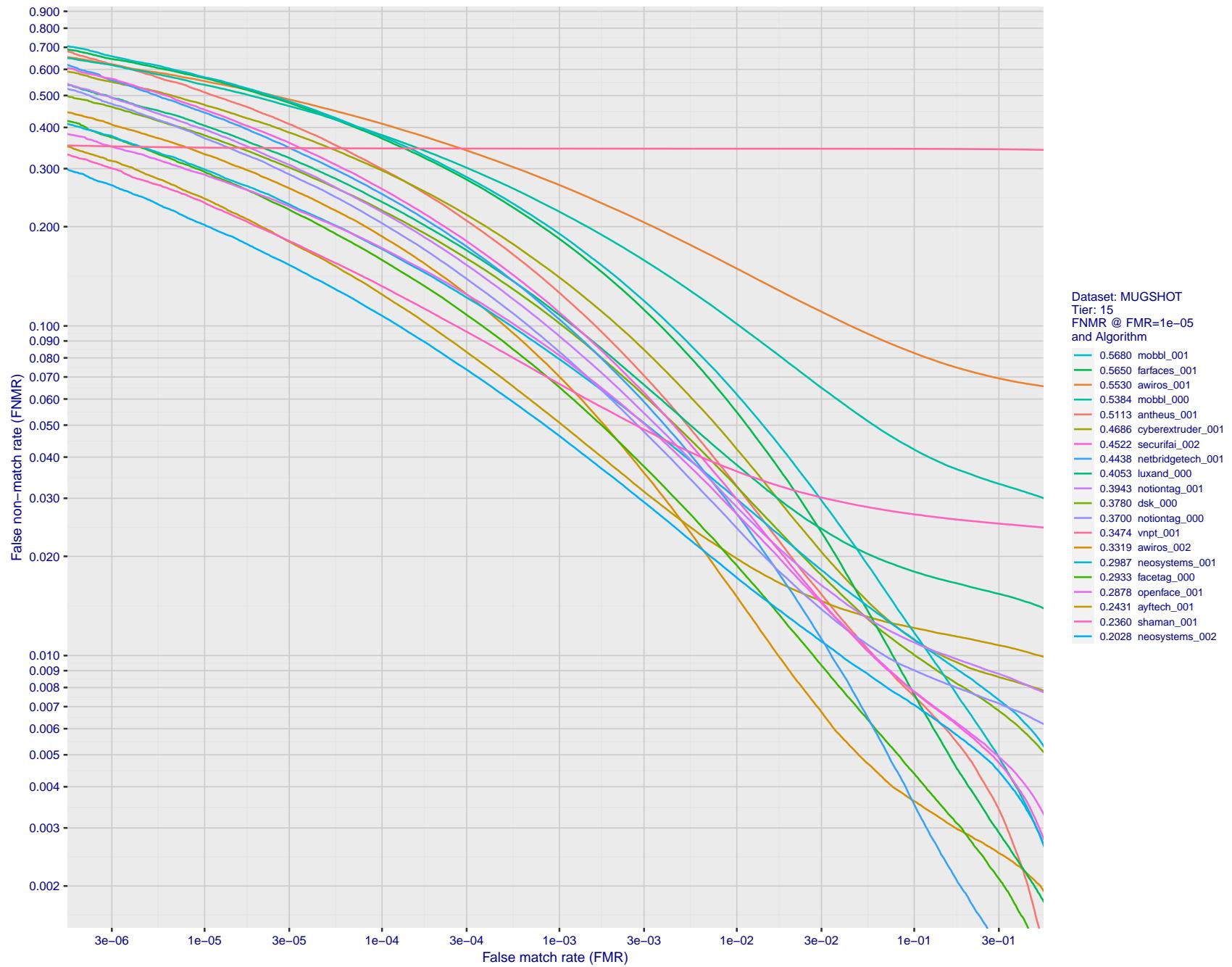


Figure 66: For the mugshot images, detection error tradeoff (DET) characteristics showing false non-match rate vs. false match rate plotted parametrically on threshold, T . The scales are logarithmic in order to show decades of FMR.

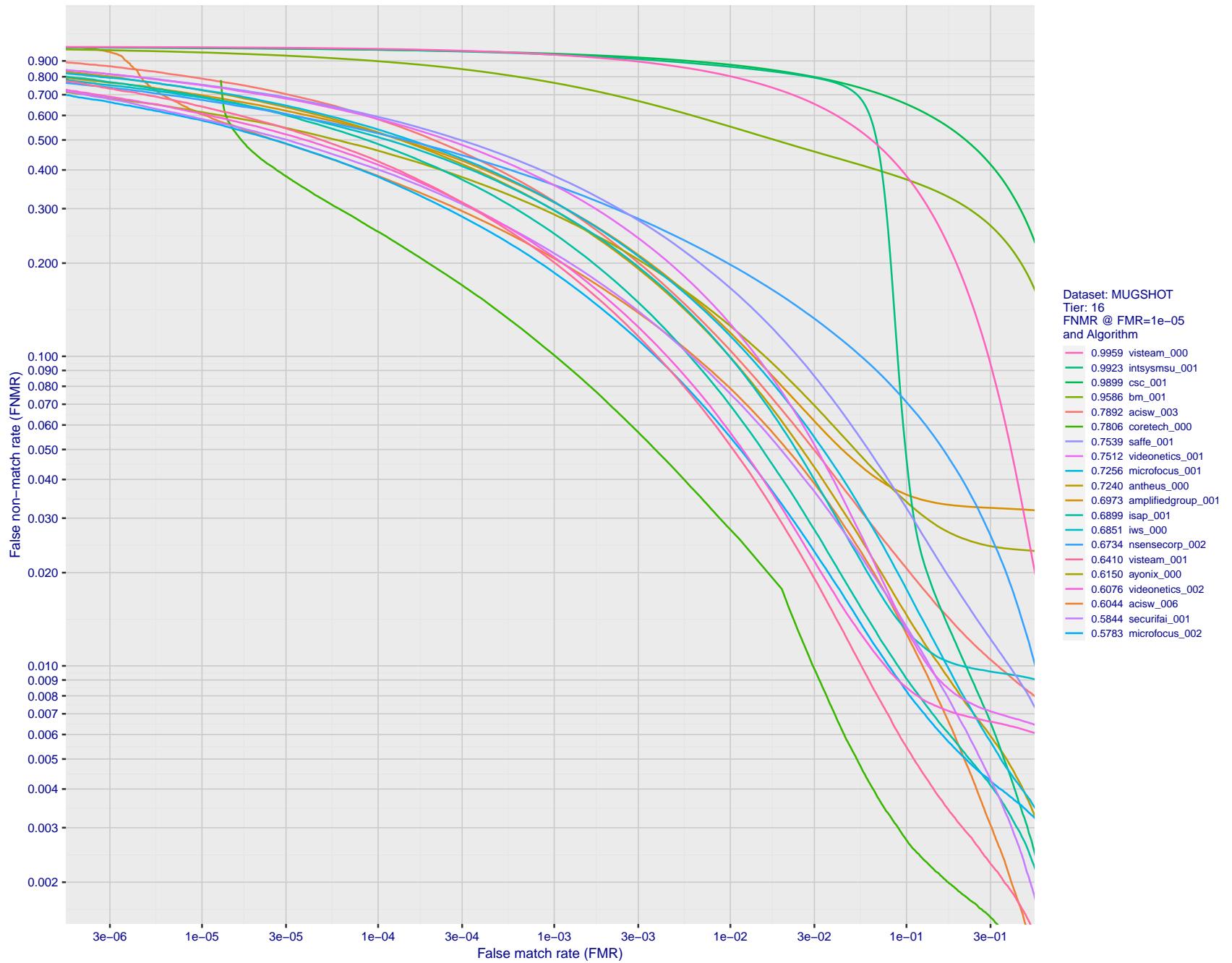


Figure 67: For the mugshot images, detection error tradeoff (DET) characteristics showing false non-match rate vs. false match rate plotted parametrically on threshold, T . The scales are logarithmic in order to show decades of FMR.

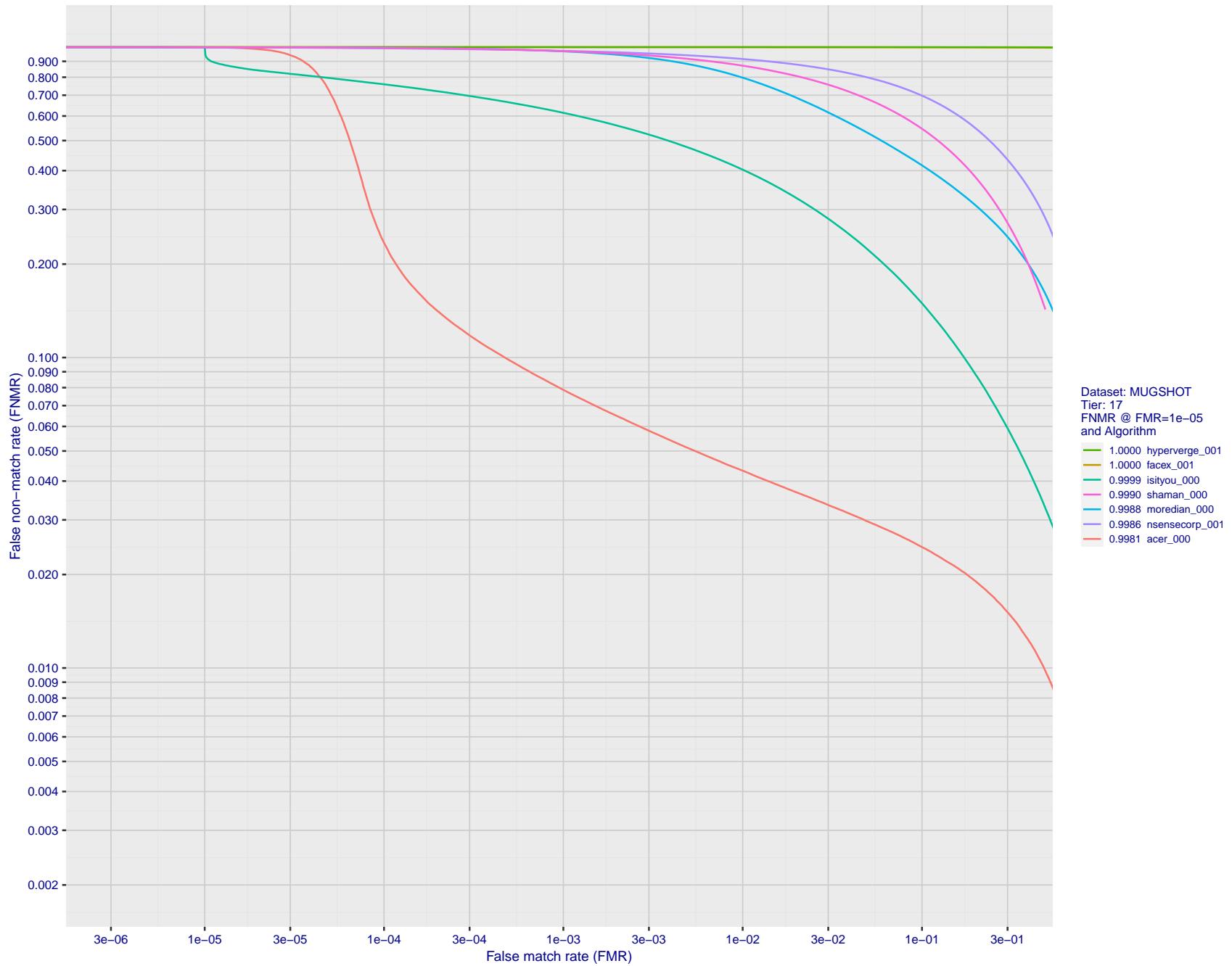


Figure 68: For the mugshot images, detection error tradeoff (DET) characteristics showing false non-match rate vs. false match rate plotted parametrically on threshold, T . The scales are logarithmic in order to show decades of FMR.

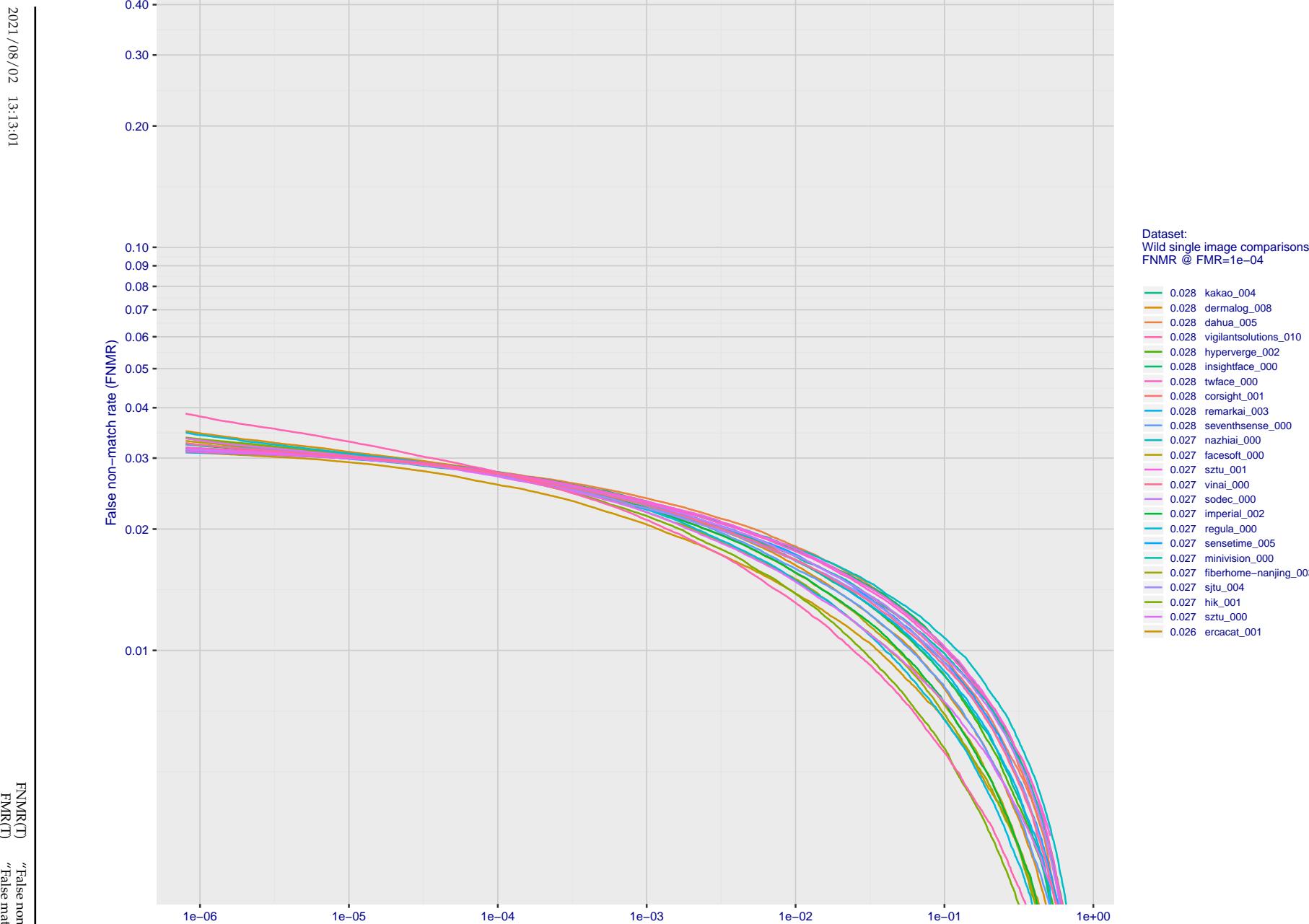


Figure 69: For the 2018 wild image comparisons, detection error tradeoff (DET) characteristics showing false non-match rate vs. false match rate plotted parametrically on threshold, T . The scales are logarithmic in order to show several decades of FMR.

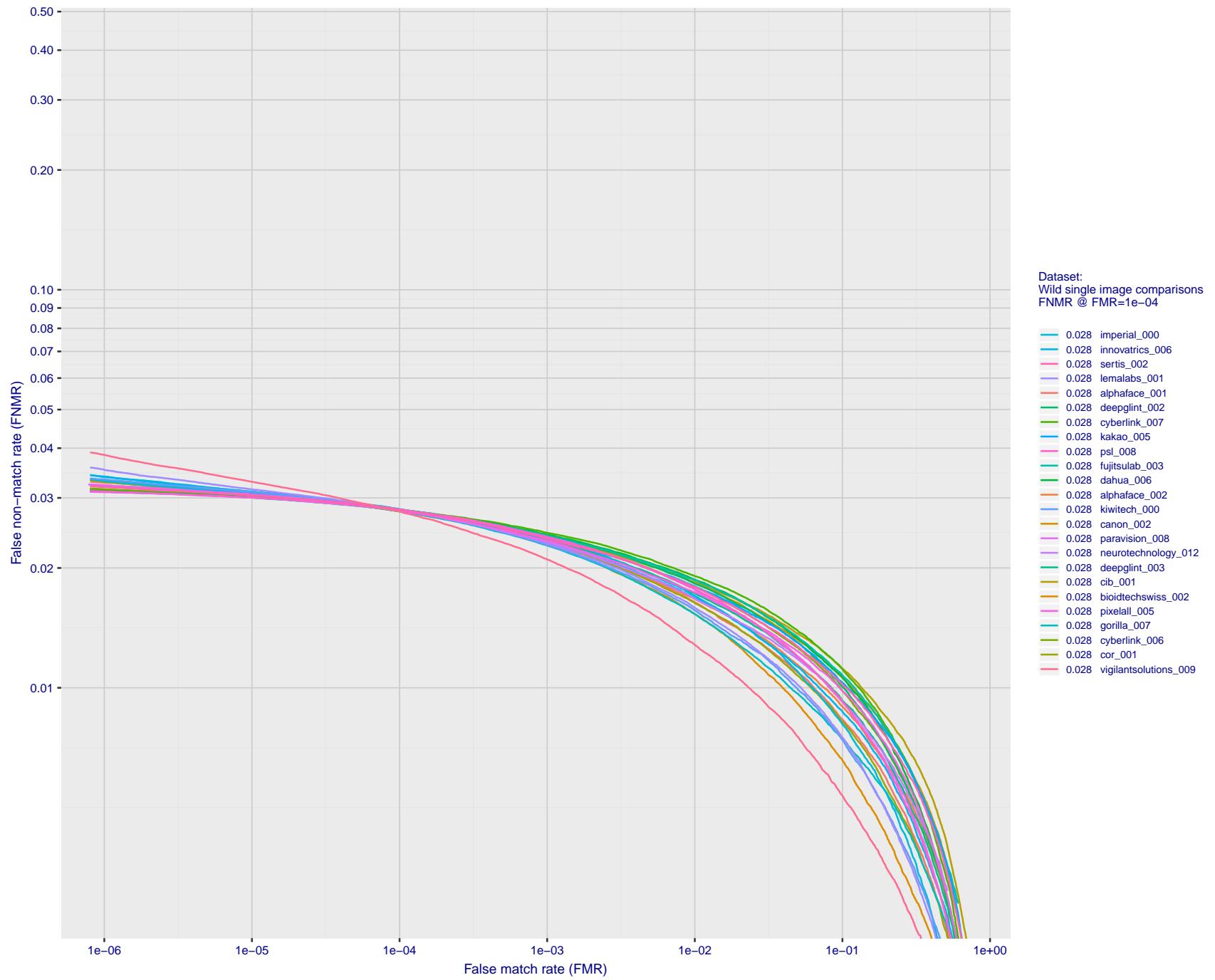


Figure 70: For the 2018 wild image comparisons, detection error tradeoff (DET) characteristics showing false non-match rate vs. false match rate plotted parametrically on threshold, T . The scales are logarithmic in order to show several decades of FMR.

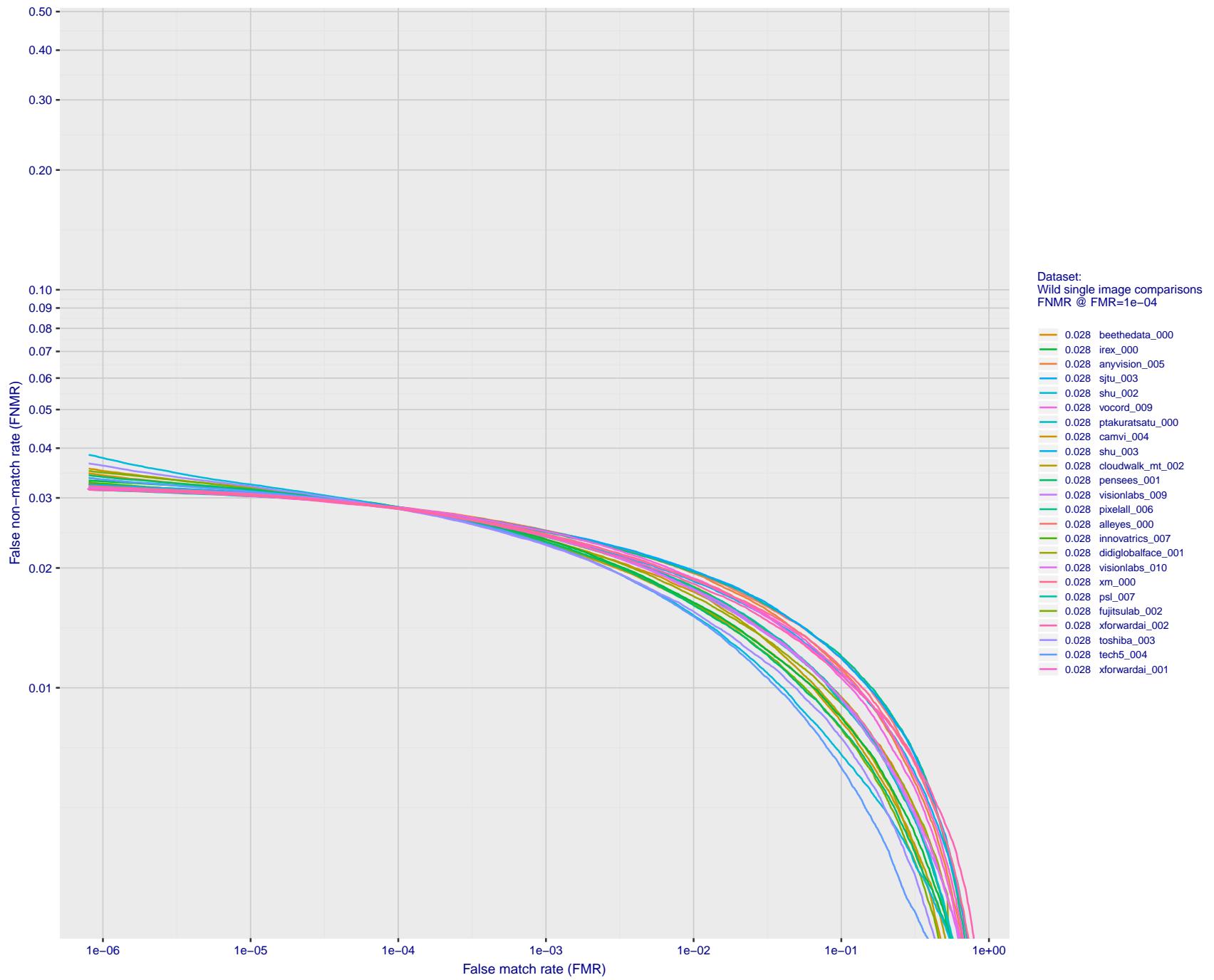


Figure 71: For the 2018 wild image comparisons, detection error tradeoff (DET) characteristics showing false non-match rate vs. false match rate plotted parametrically on threshold, T . The scales are logarithmic in order to show several decades of FMR.

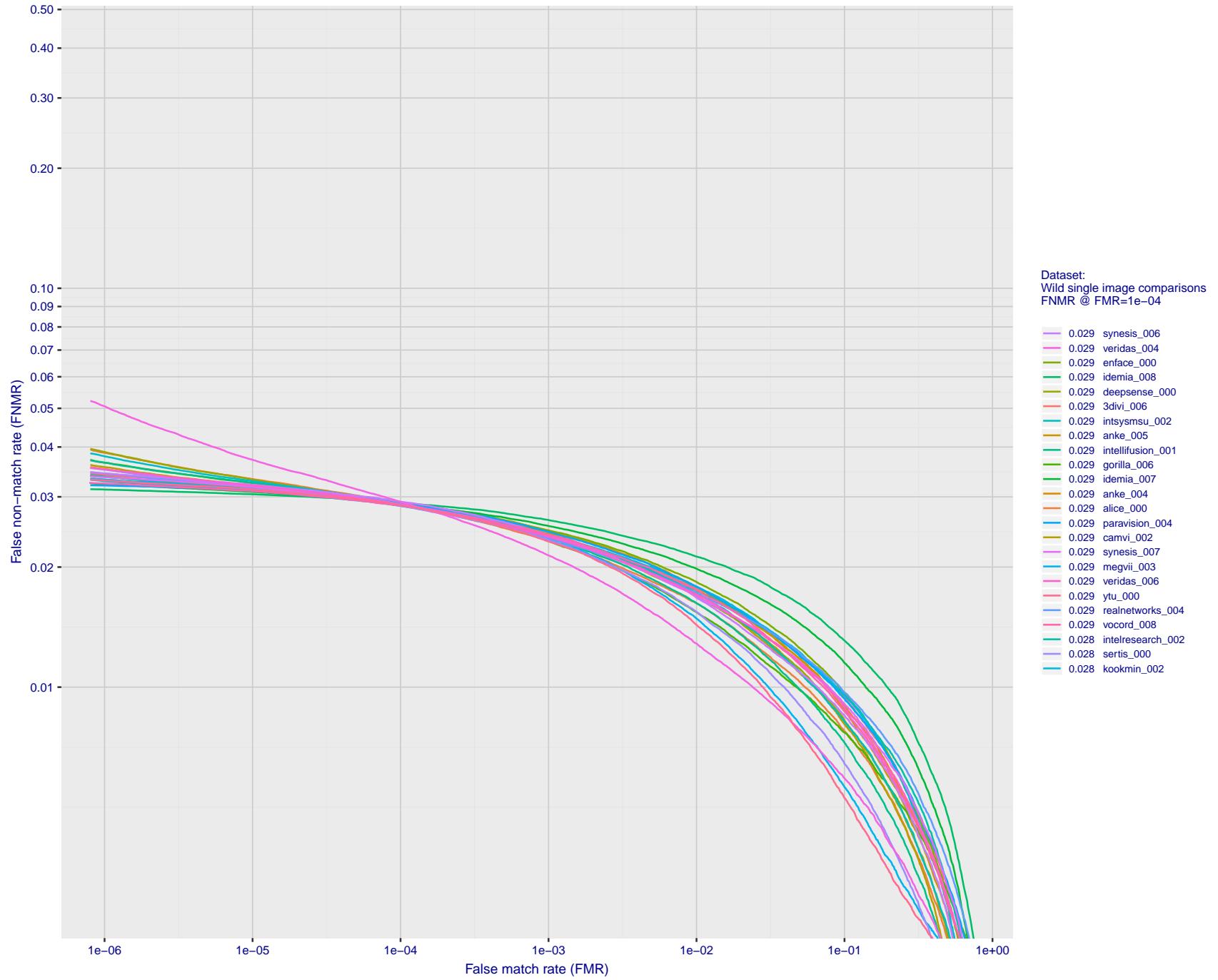


Figure 72: For the 2018 wild image comparisons, detection error tradeoff (DET) characteristics showing false non-match rate vs. false match rate plotted parametrically on threshold, T . The scales are logarithmic in order to show several decades of FMR.

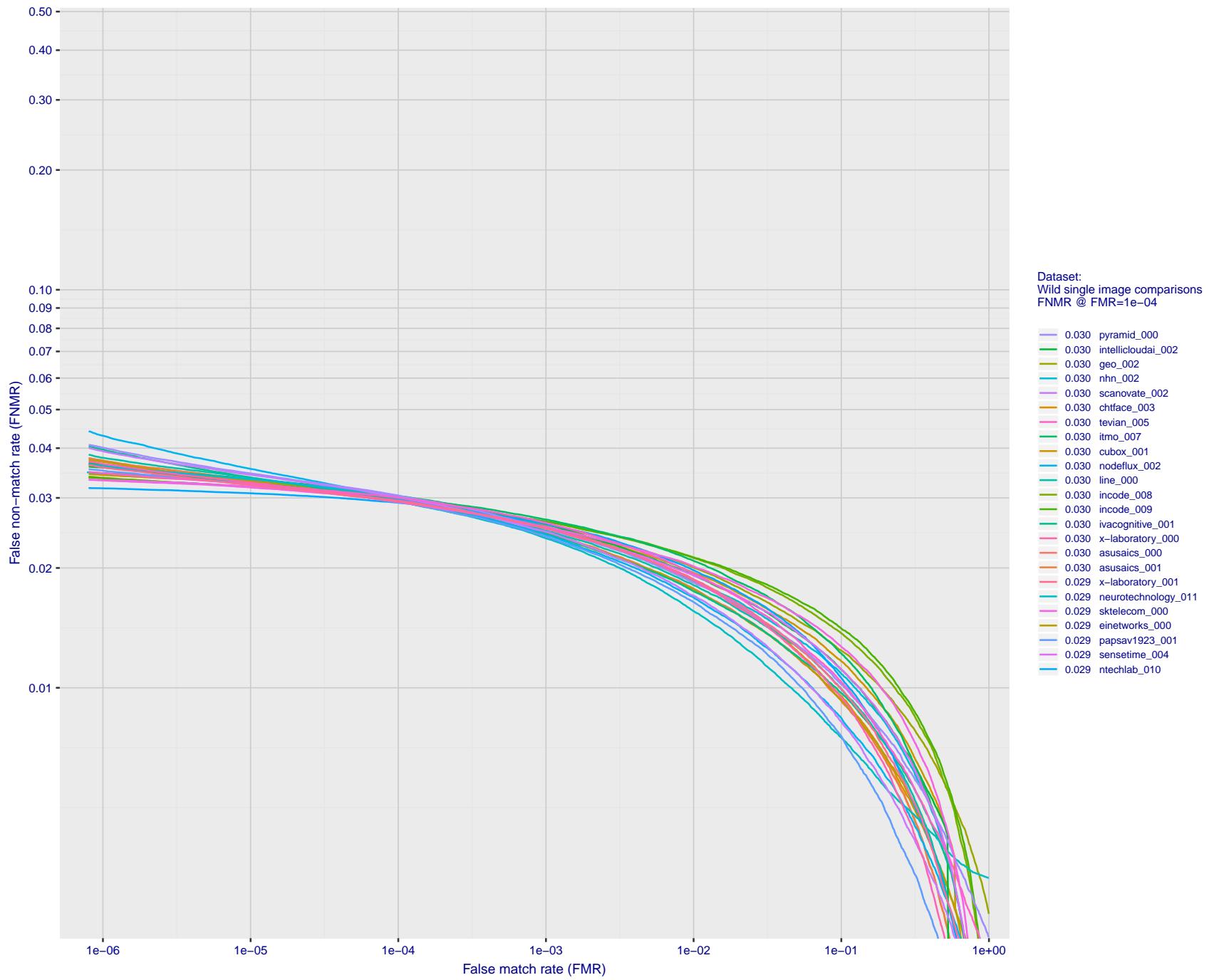


Figure 73: For the 2018 wild image comparisons, detection error tradeoff (DET) characteristics showing false non-match rate vs. false match rate plotted parametrically on threshold, T . The scales are logarithmic in order to show several decades of FMR.

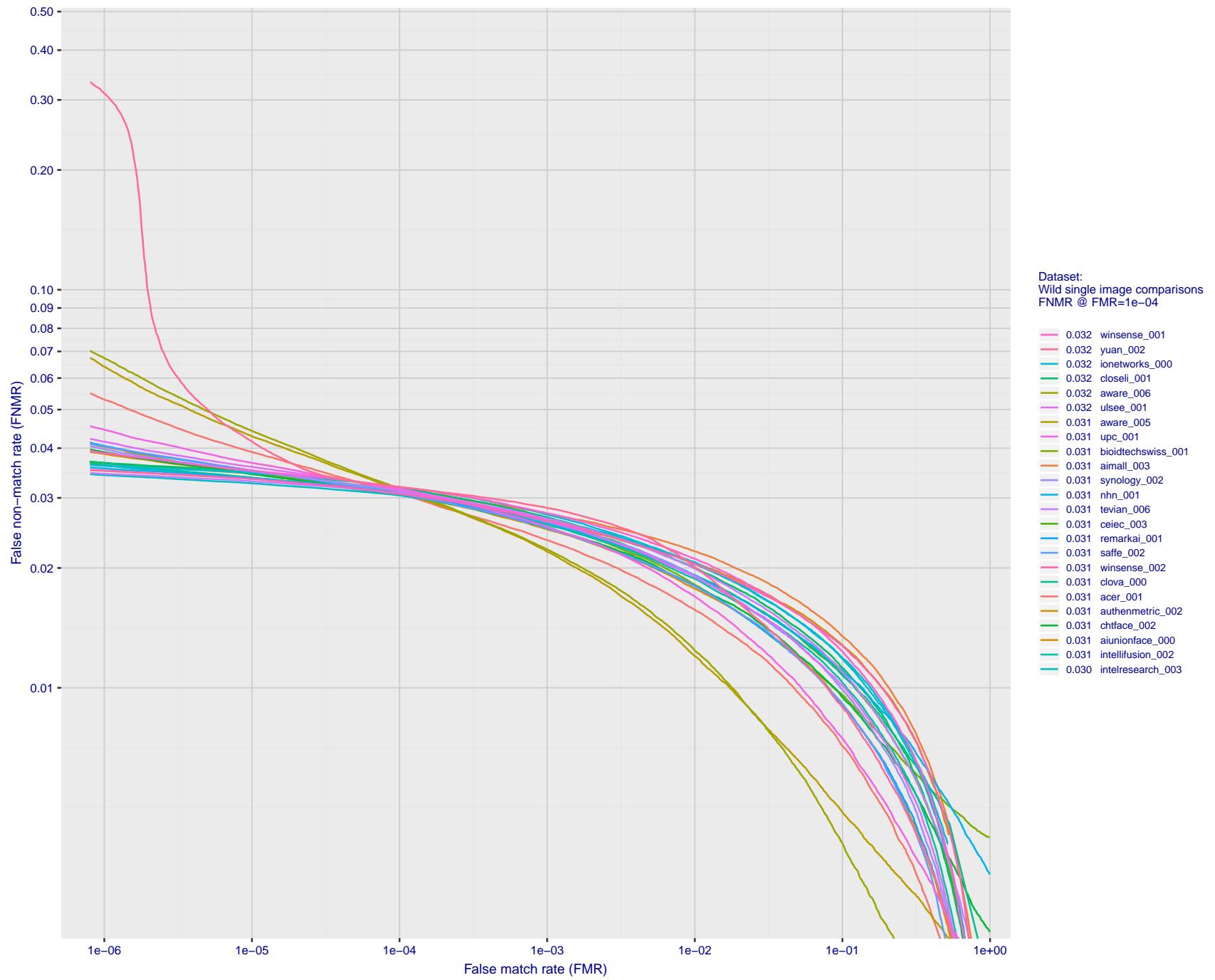


Figure 74: For the 2018 wild image comparisons, detection error tradeoff (DET) characteristics showing false non-match rate vs. false match rate plotted parametrically on threshold, T . The scales are logarithmic in order to show several decades of FMR.

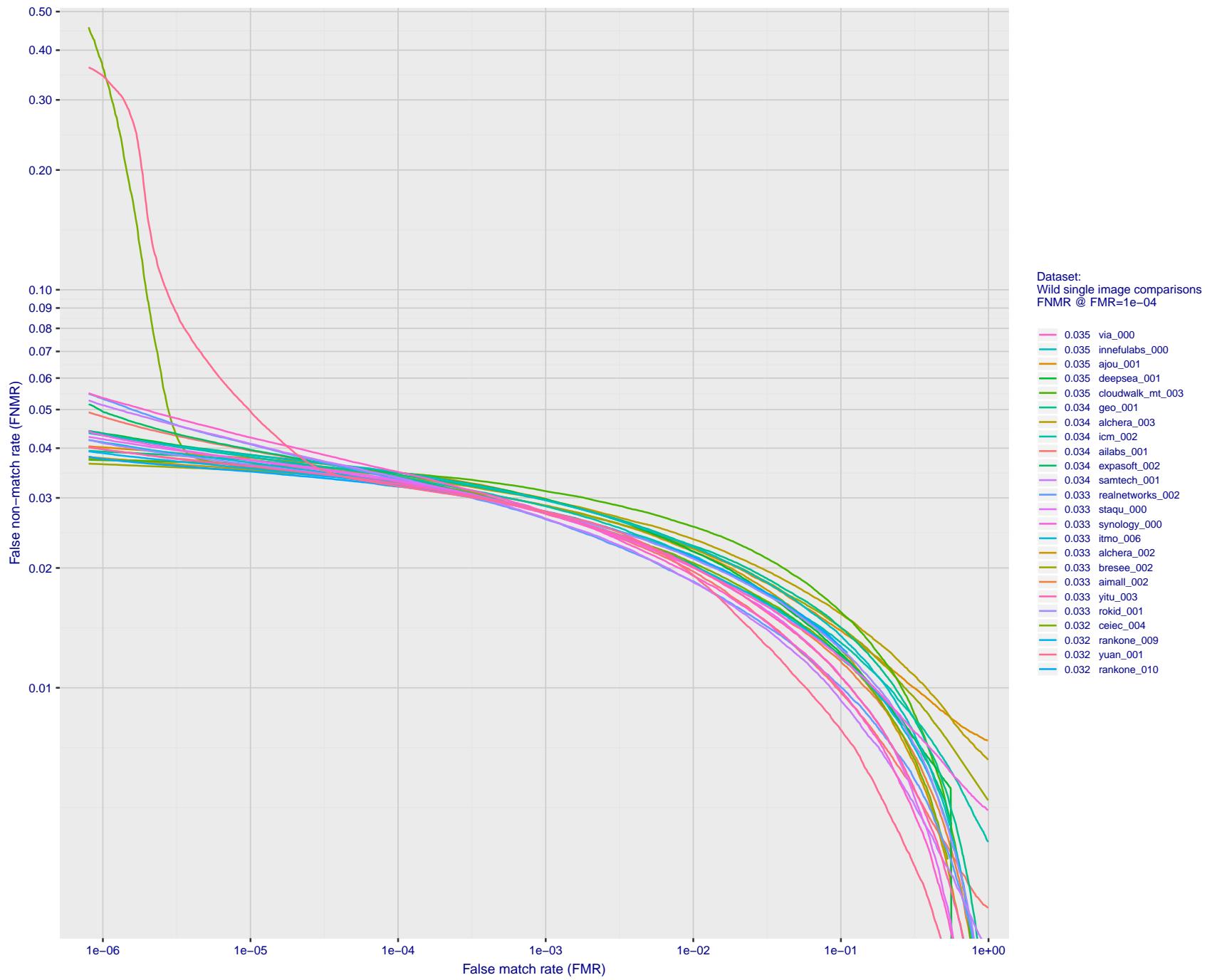


Figure 75: For the 2018 wild image comparisons, detection error tradeoff (DET) characteristics showing false non-match rate vs. false match rate plotted parametrically on threshold, T. The scales are logarithmic in order to show several decades of FMR.

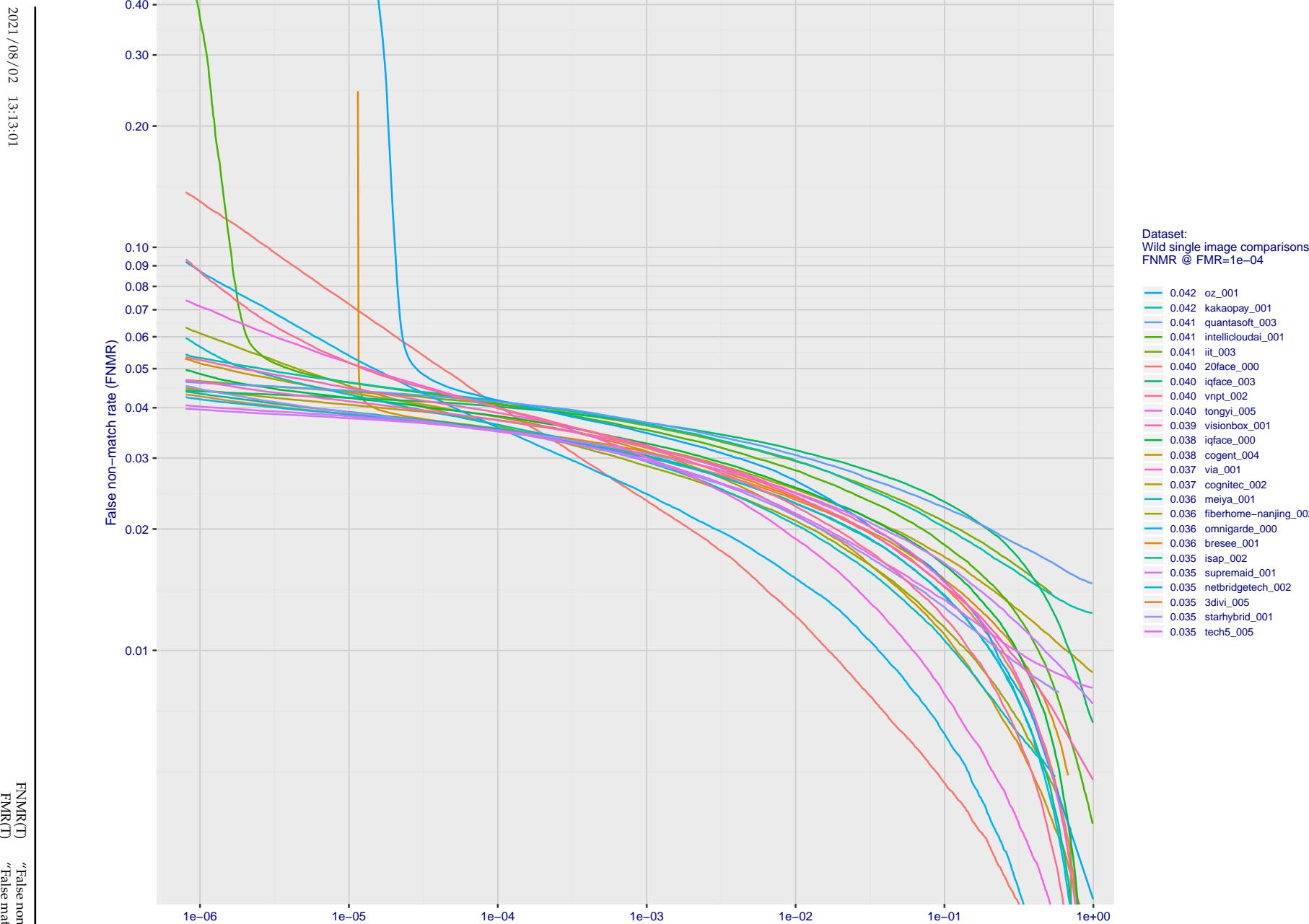


Figure 76: For the 2018 wild image comparisons, detection error tradeoff (DET) characteristics showing false non-match rate vs. false match rate plotted parametrically on threshold, T . The scales are logarithmic in order to show several decades of FMR.

2021/08/02 13:13:01

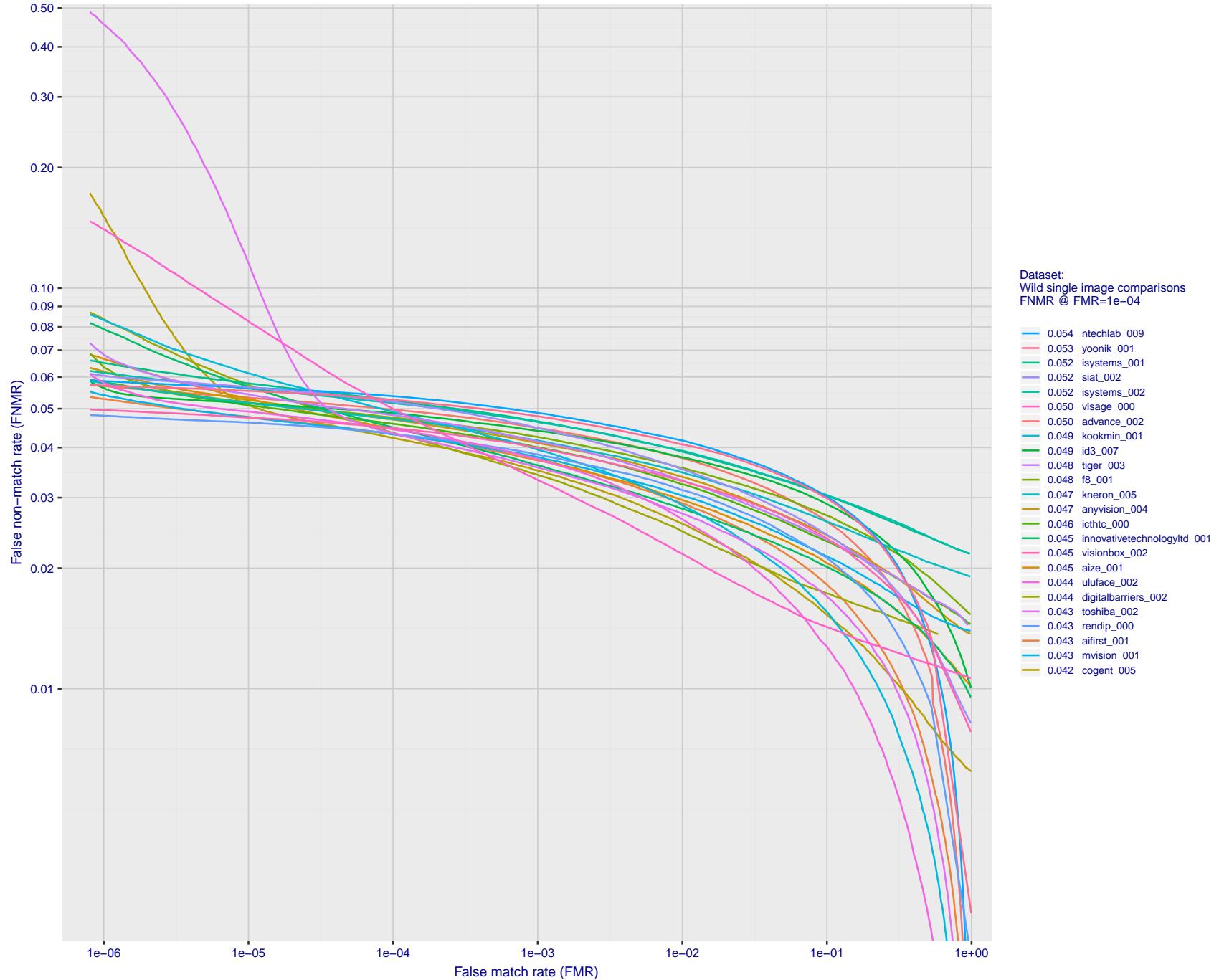


Figure 77: For the 2018 wild image comparisons, detection error tradeoff (DET) characteristics showing false non-match rate vs. false match rate plotted parametrically on threshold, T . The scales are logarithmic in order to show several decades of FMR.

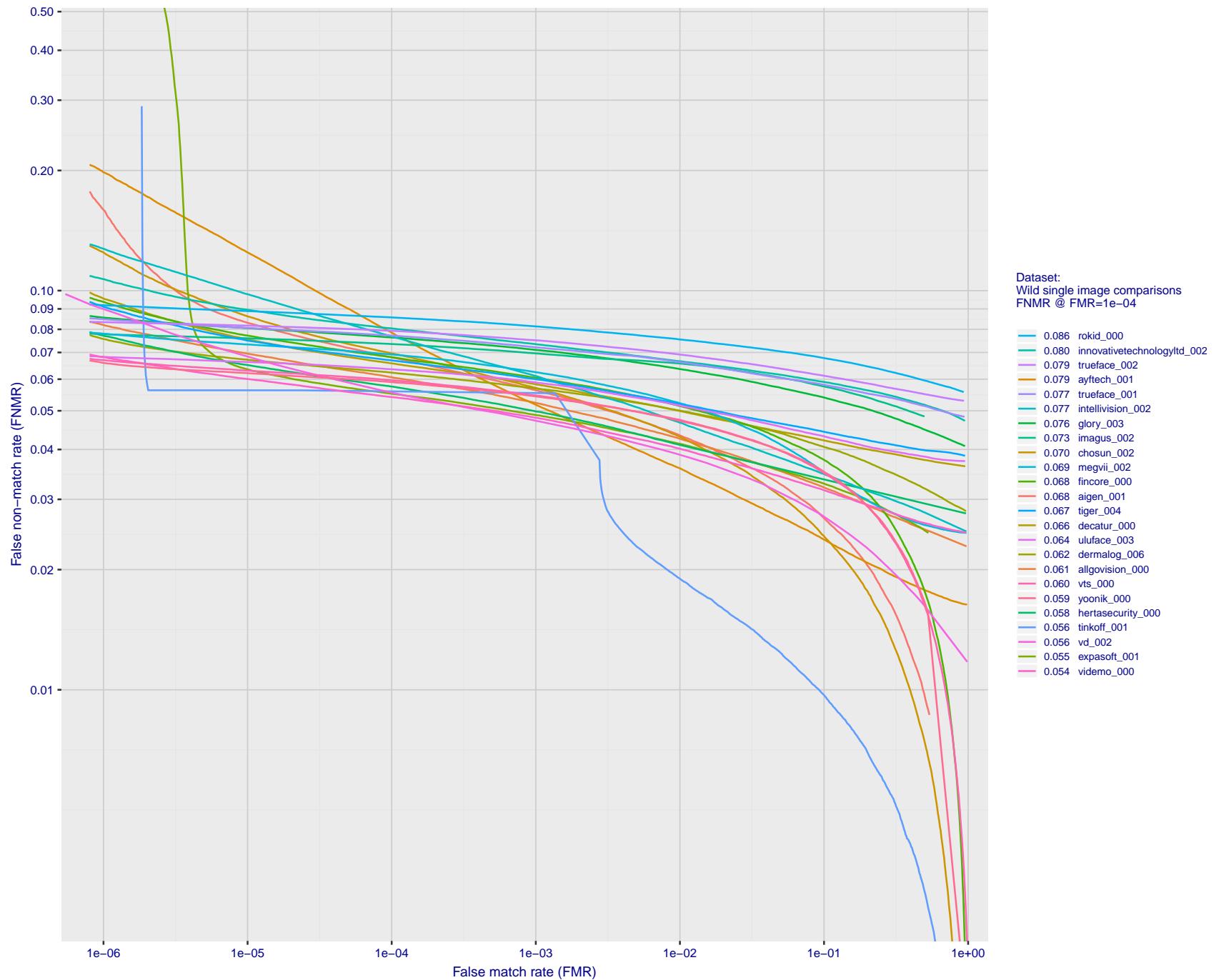


Figure 78: For the 2018 wild image comparisons, detection error tradeoff (DET) characteristics showing false non-match rate vs. false match rate plotted parametrically on threshold, T . The scales are logarithmic in order to show several decades of FMR.

2021/08/02 13:13:01

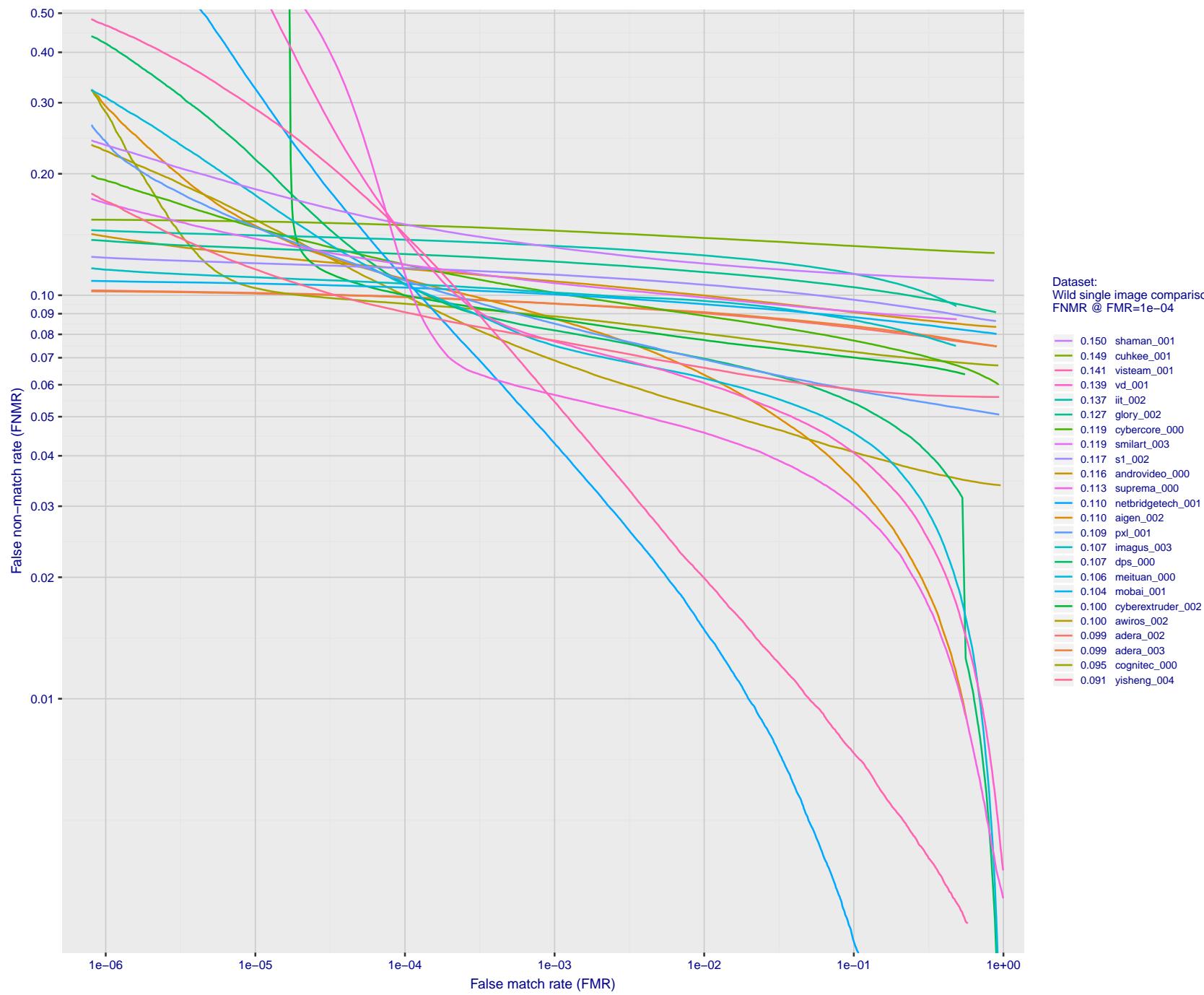


Figure 79: For the 2018 wild image comparisons, detection error tradeoff (DET) characteristics showing false non-match rate vs. false match rate plotted parametrically on threshold, T . The scales are logarithmic in order to show several decades of FMR.

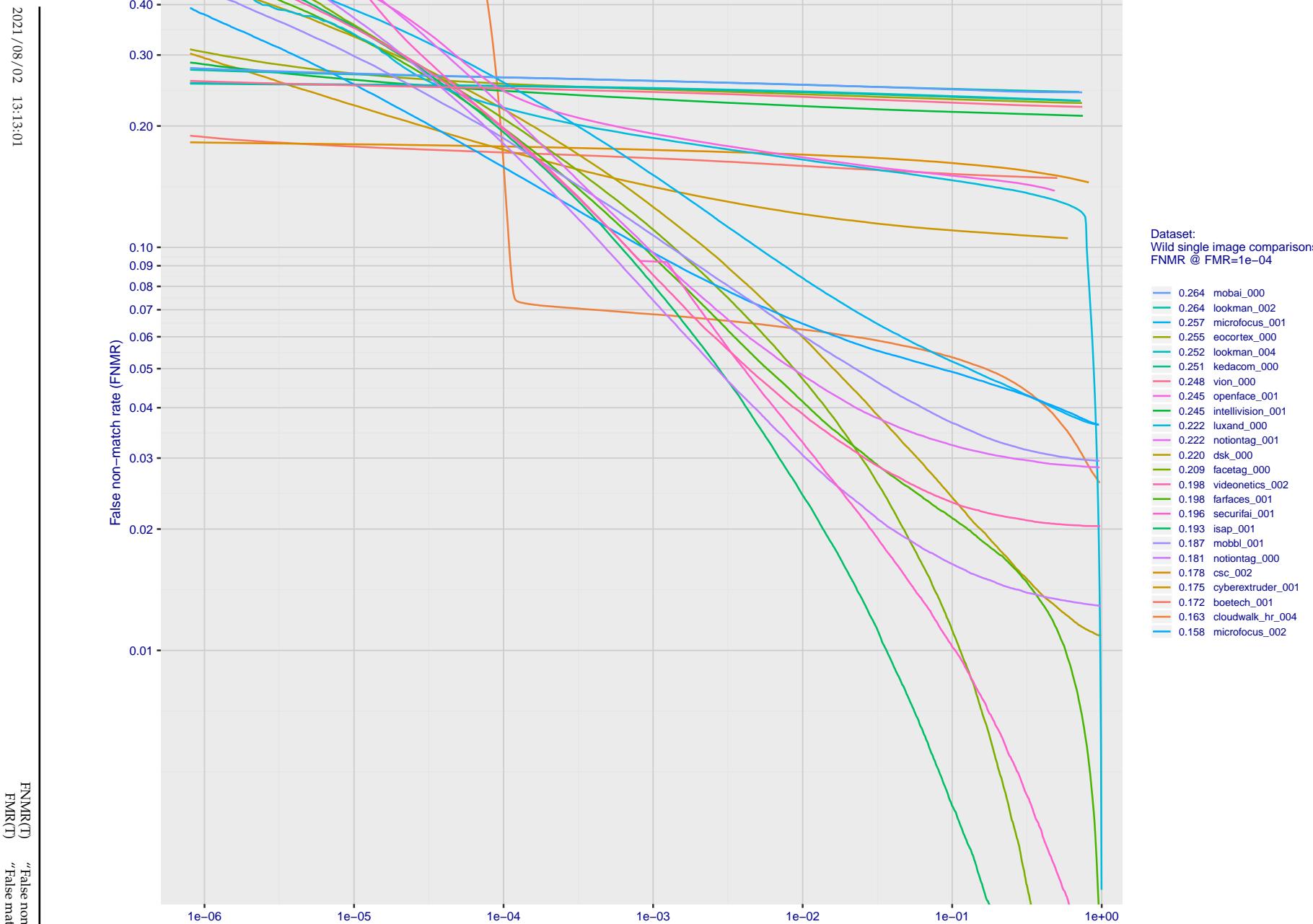


Figure 80: For the 2018 wild image comparisons, detection error tradeoff (DET) characteristics showing false non-match rate vs. false match rate plotted parametrically on threshold, T . The scales are logarithmic in order to show several decades of FMR.

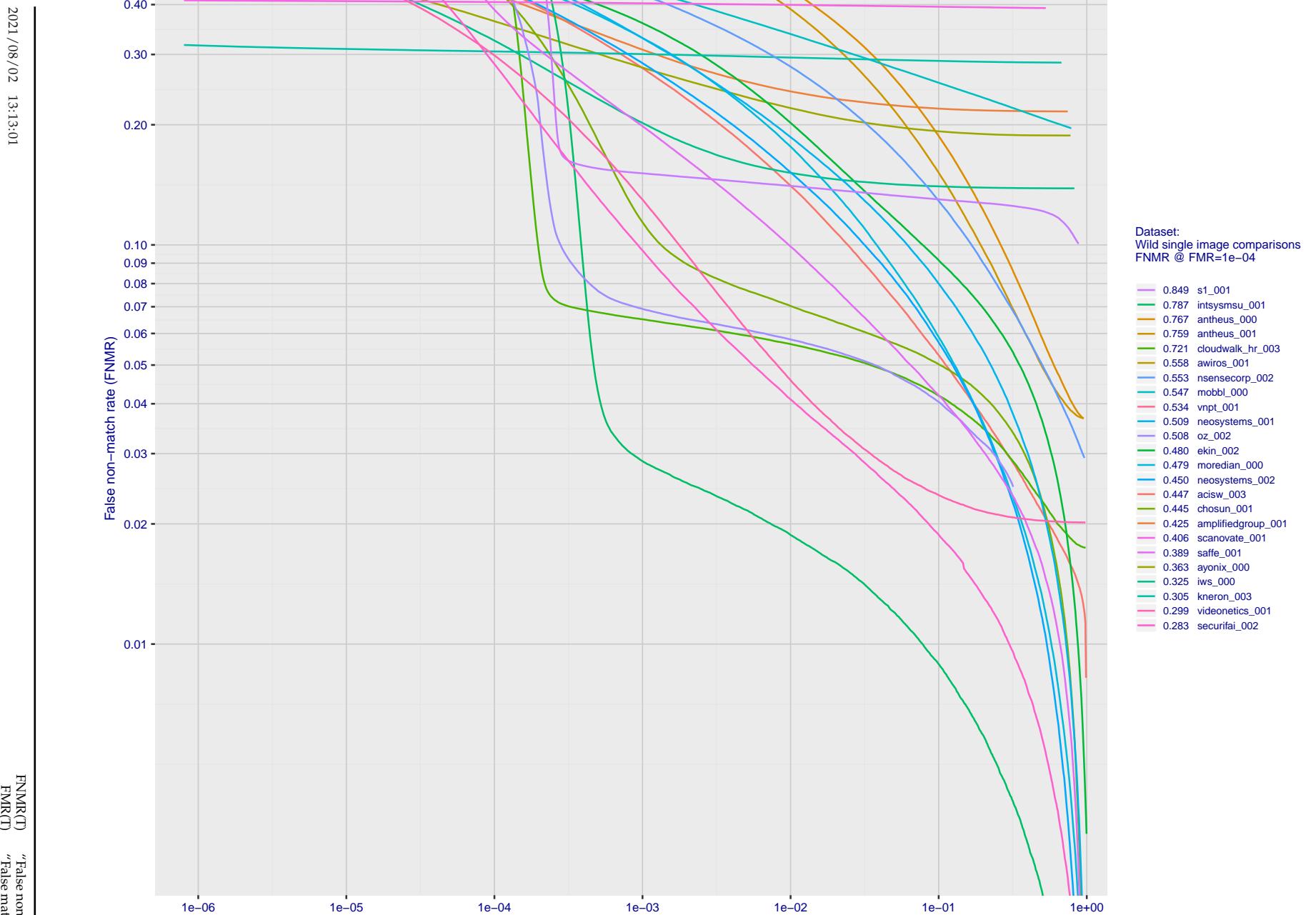


Figure 81: For the 2018 wild image comparisons, detection error tradeoff (DET) characteristics showing false non-match rate vs. false match rate plotted parametrically on threshold, T . The scales are logarithmic in order to show several decades of FMR.

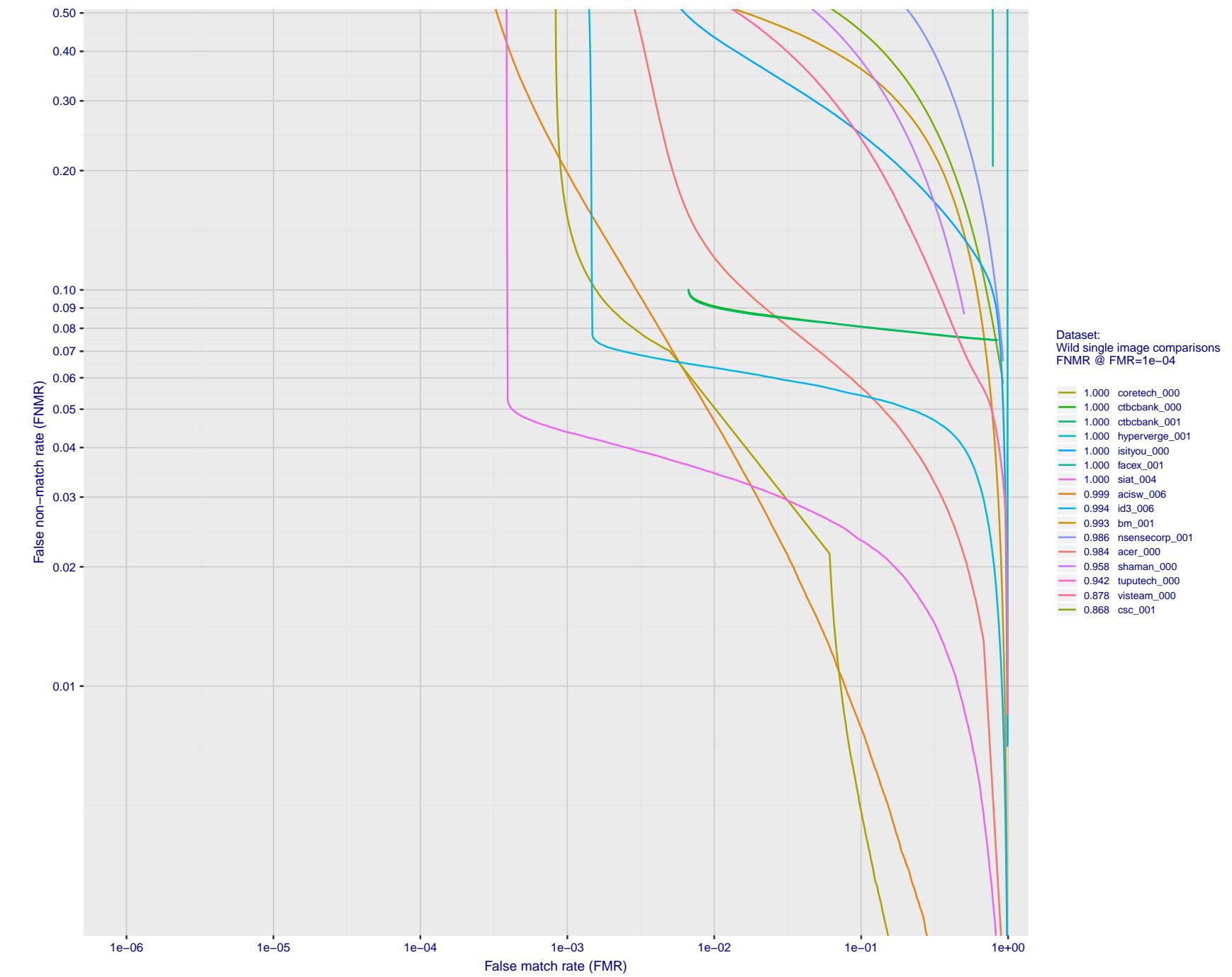


Figure 82: For the 2018 wild image comparisons, detection error tradeoff (DET) characteristics showing false non-match rate vs. false match rate plotted parametrically on threshold, T . The scales are logarithmic in order to show several decades of FMR.

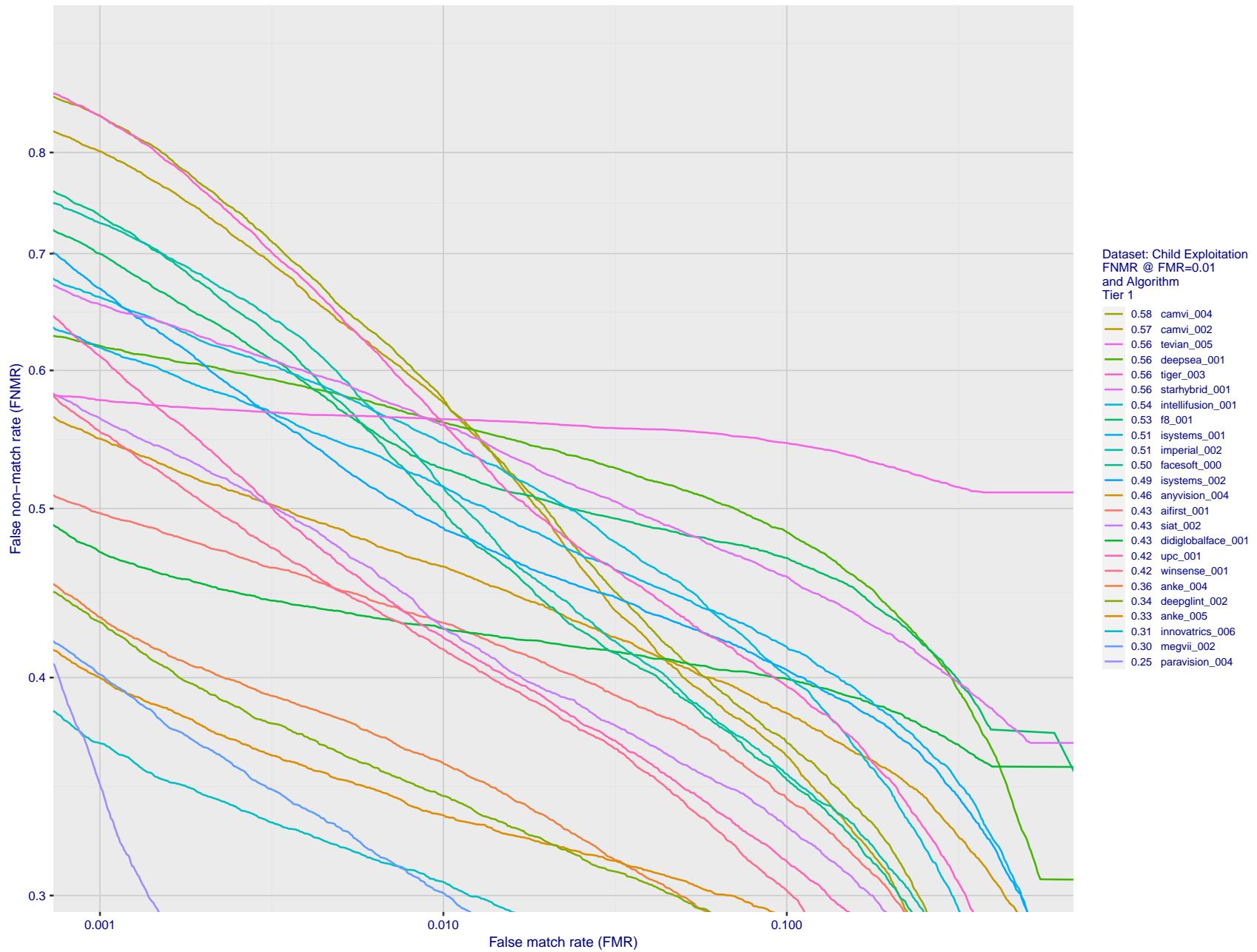


Figure 83: For child exploitation images, detection error tradeoff (DET) characteristics showing false non-match rate vs. false match rate plotted parametrically on threshold, T . The scales are logarithmic in order to show many decades of FMR. Accuracy is poor because many images have adverse quality characteristics, and because detection and enrollment fails.

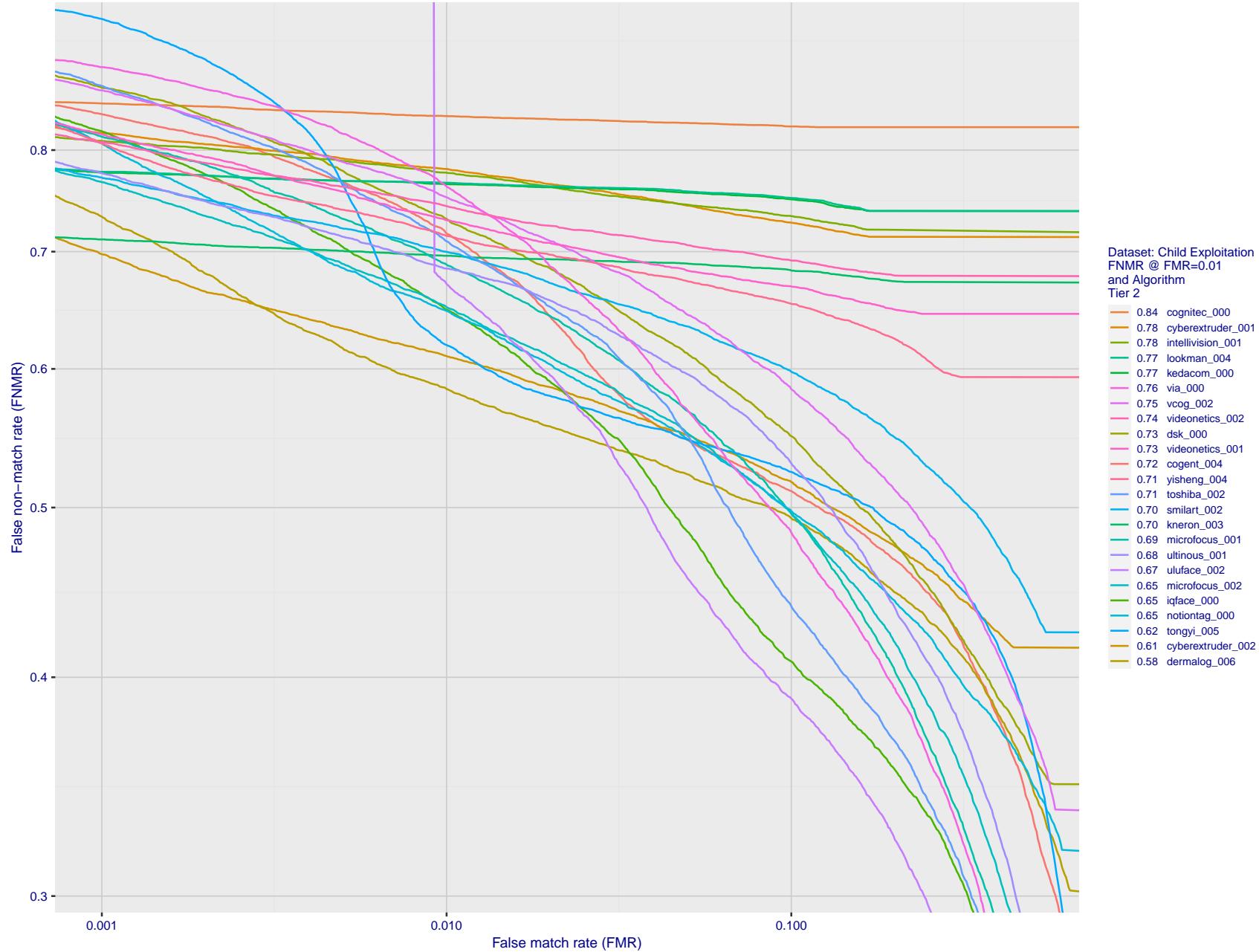


Figure 84: For child exploitation images, detection error tradeoff (DET) characteristics showing false non-match rate vs. false match rate plotted parametrically on threshold, T. The scales are logarithmic in order to show many decades of FMR. Accuracy is poor because many images have adverse quality characteristics, and because detection and enrollment fails.

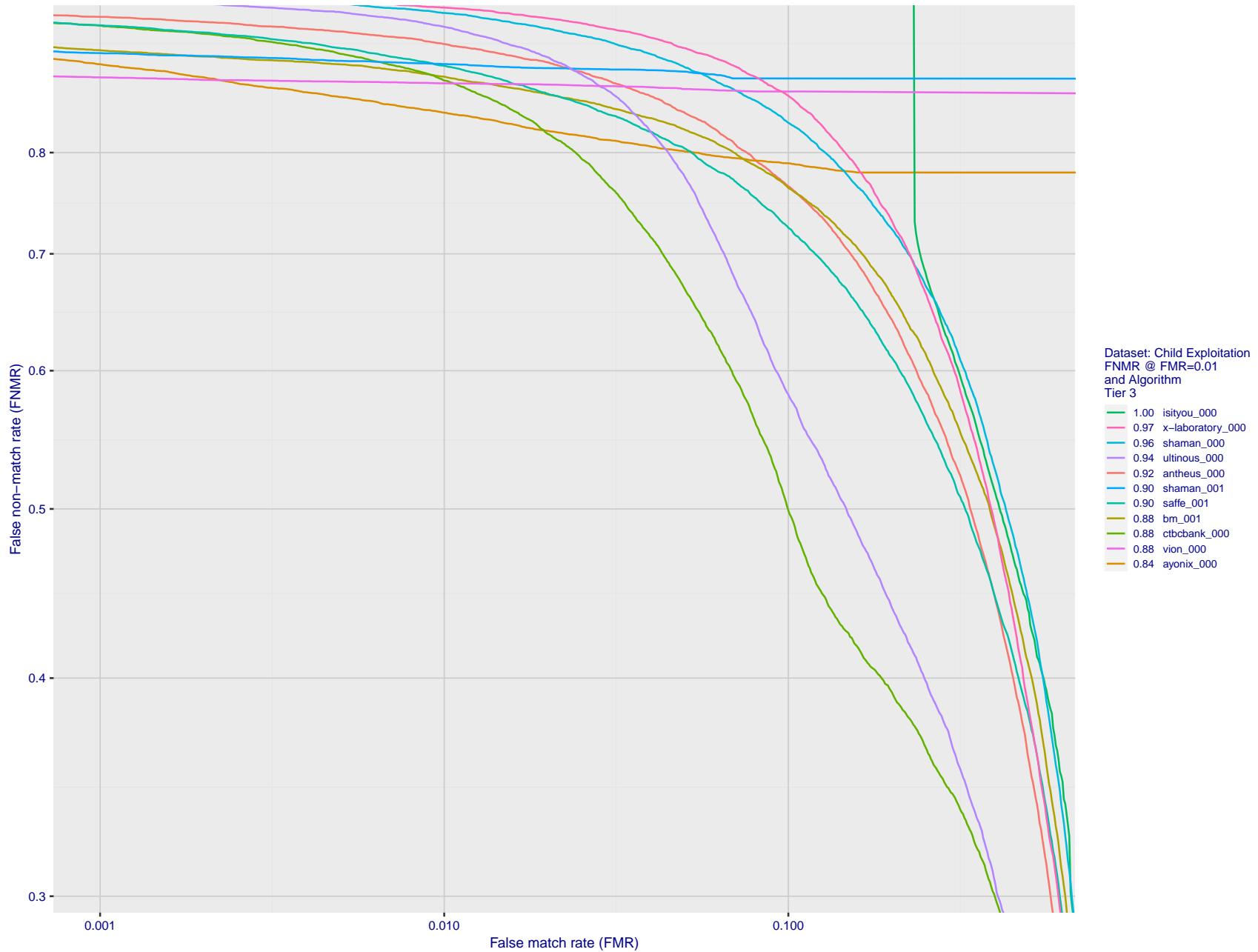


Figure 85: For child exploitation images, detection error tradeoff (DET) characteristics showing false non-match rate vs. false match rate plotted parametrically on threshold, T. The scales are logarithmic in order to show many decades of FMR. Accuracy is poor because many images have adverse quality characteristics, and because detection and enrollment fails.

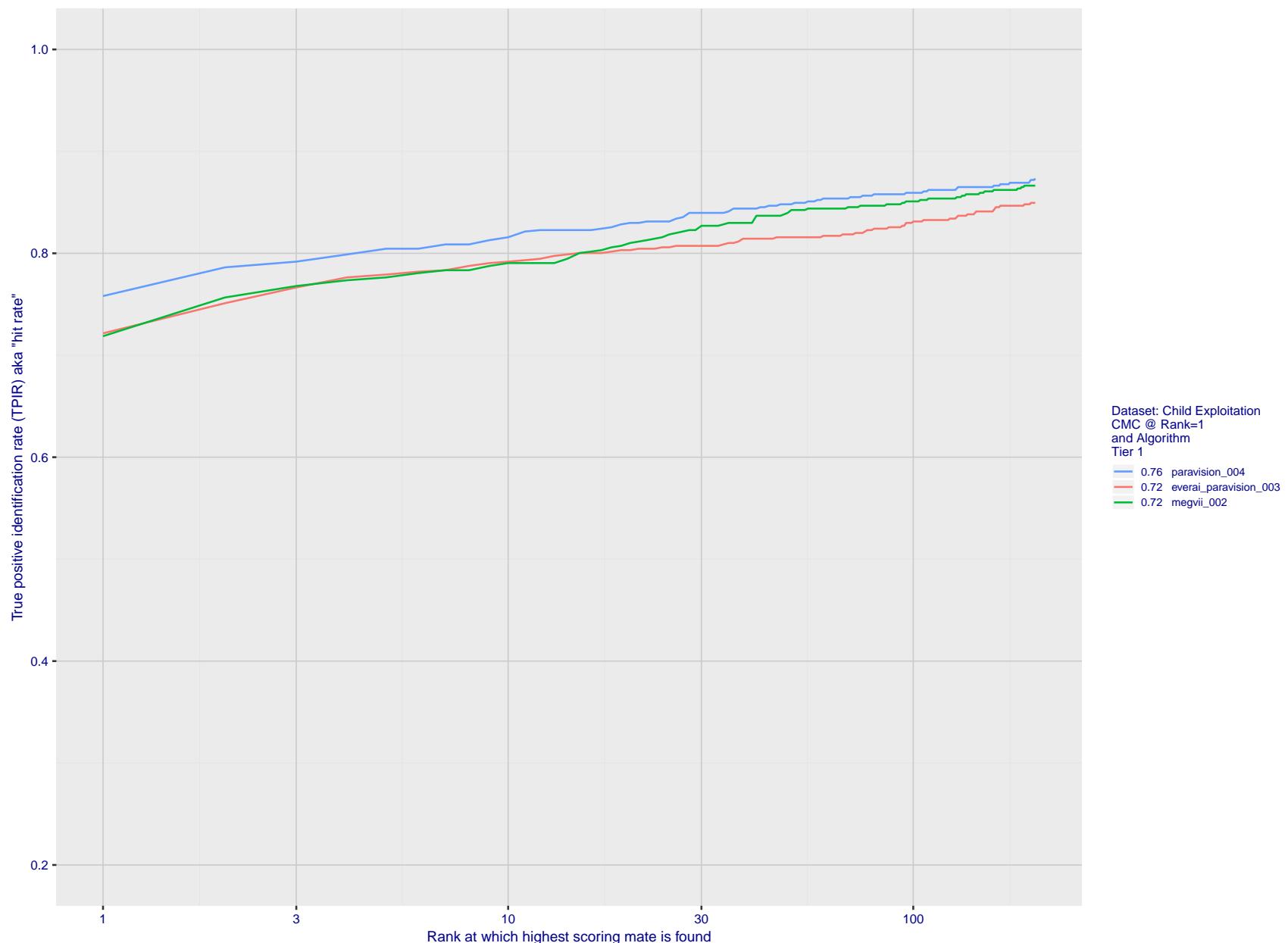


Figure 86: For child exploitation images, cumulative match characteristics (CMC) showing true positive identification rate vs. rank. This is simulation of a one-to-many search experiment - see discussion in section 3.2. The scales are logarithmic in order to show the effect of long candidate lists. Accuracy is poor but much improved relative to the 1:1 DETs of Fig. 85 because a search can succeed if any of a subject's several enrolled images matches the search image with a high score.

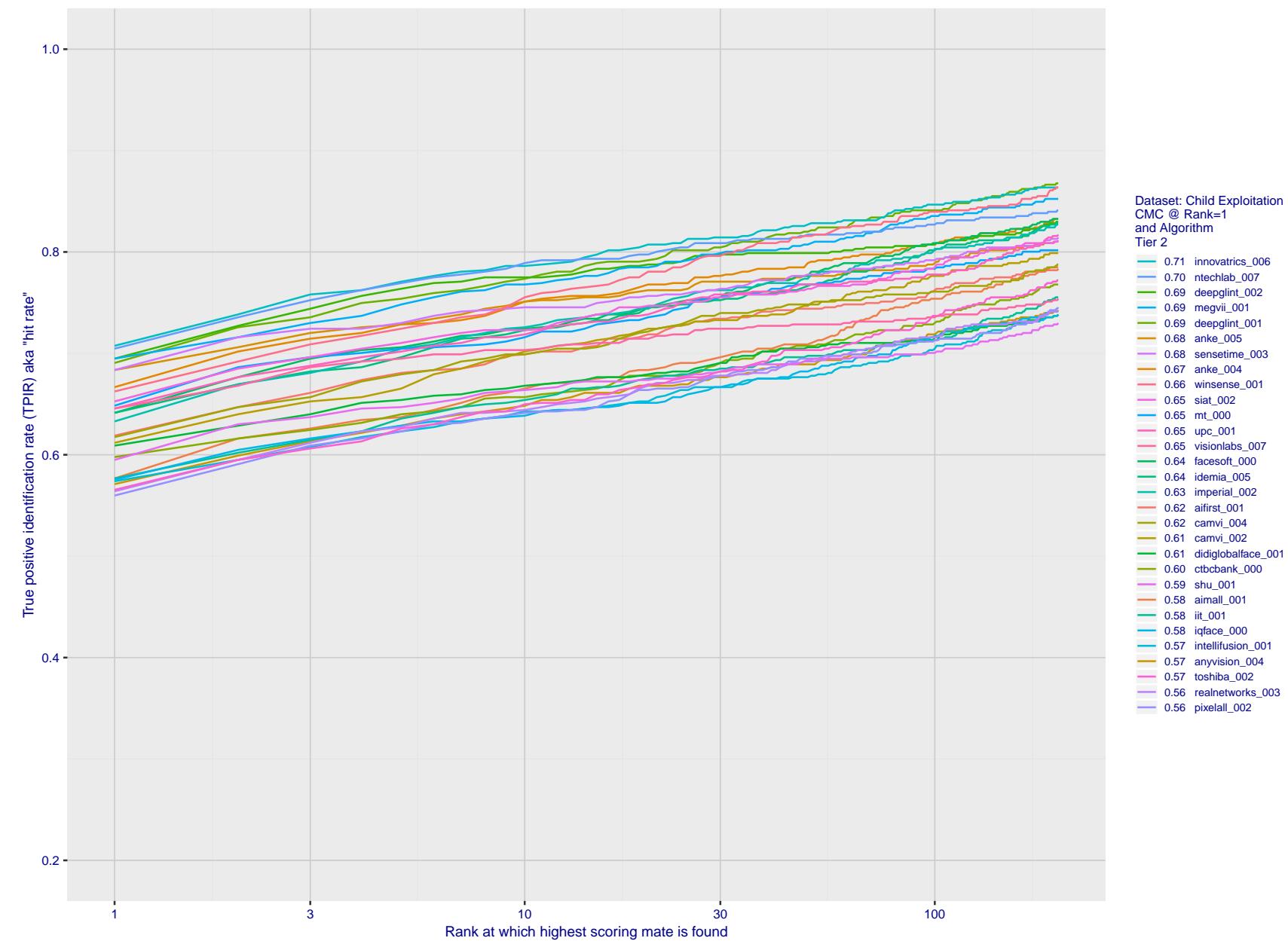


Figure 87: For child exploitation images, cumulative match characteristics (CMC) showing true positive identification rate vs. rank. This is simulation of a one-to-many search experiment - see discussion in section 3.2. The scales are logarithmic in order to show the effect of long candidate lists. Accuracy is poor but much improved relative to the 1:1 DETs of Fig. 85 because a search can succeed if any of a subject's several enrolled images matches the search image with a high score.

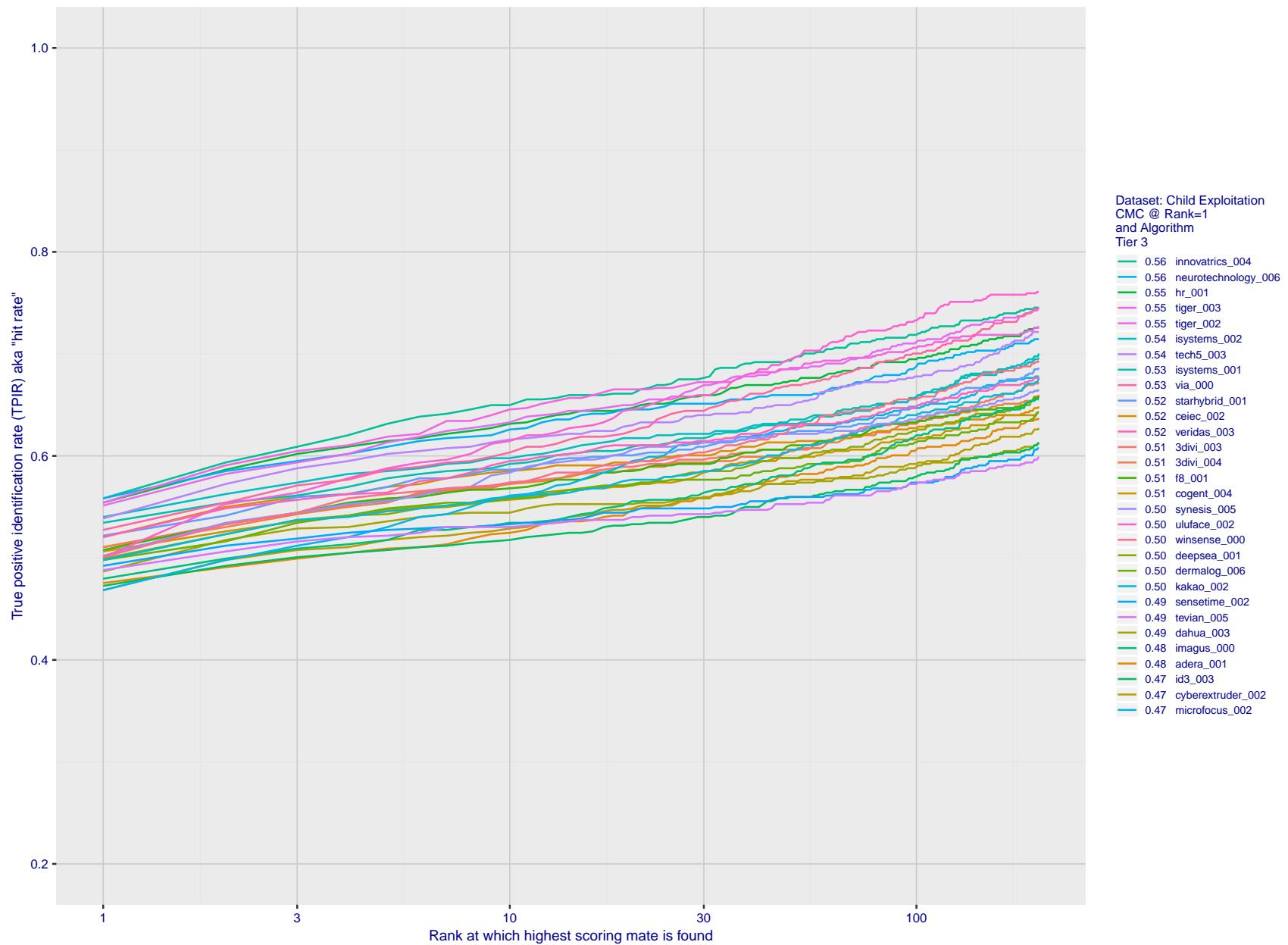


Figure 88: For child exploitation images, cumulative match characteristics (CMC) showing true positive identification rate vs. rank. This is simulation of a one-to-many search experiment - see discussion in section 3.2. The scales are logarithmic in order to show the effect of long candidate lists. Accuracy is poor but much improved relative to the 1:1 DETs of Fig. 85 because a search can succeed if any of a subject's several enrolled images matches the search image with a high score.

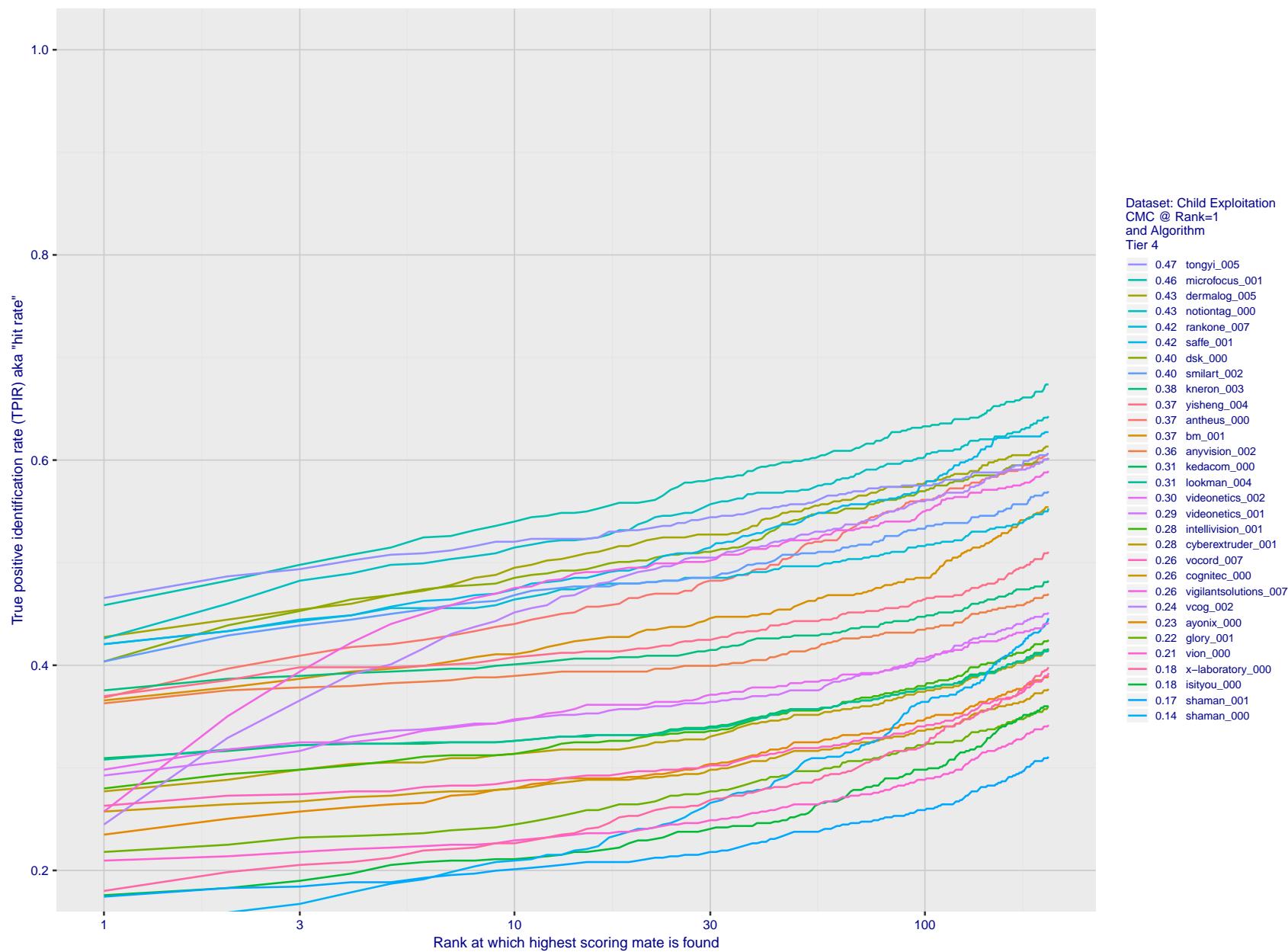


Figure 89: For child exploitation images, cumulative match characteristics (CMC) showing true positive identification rate vs. rank. This is simulation of a one-to-many search experiment - see discussion in section 3.2. The scales are logarithmic in order to show the effect of long candidate lists. Accuracy is poor but much improved relative to the 1:1 DETs of Fig. 85 because a search can succeed if any of a subject's several enrolled images matches the search image with a high score.

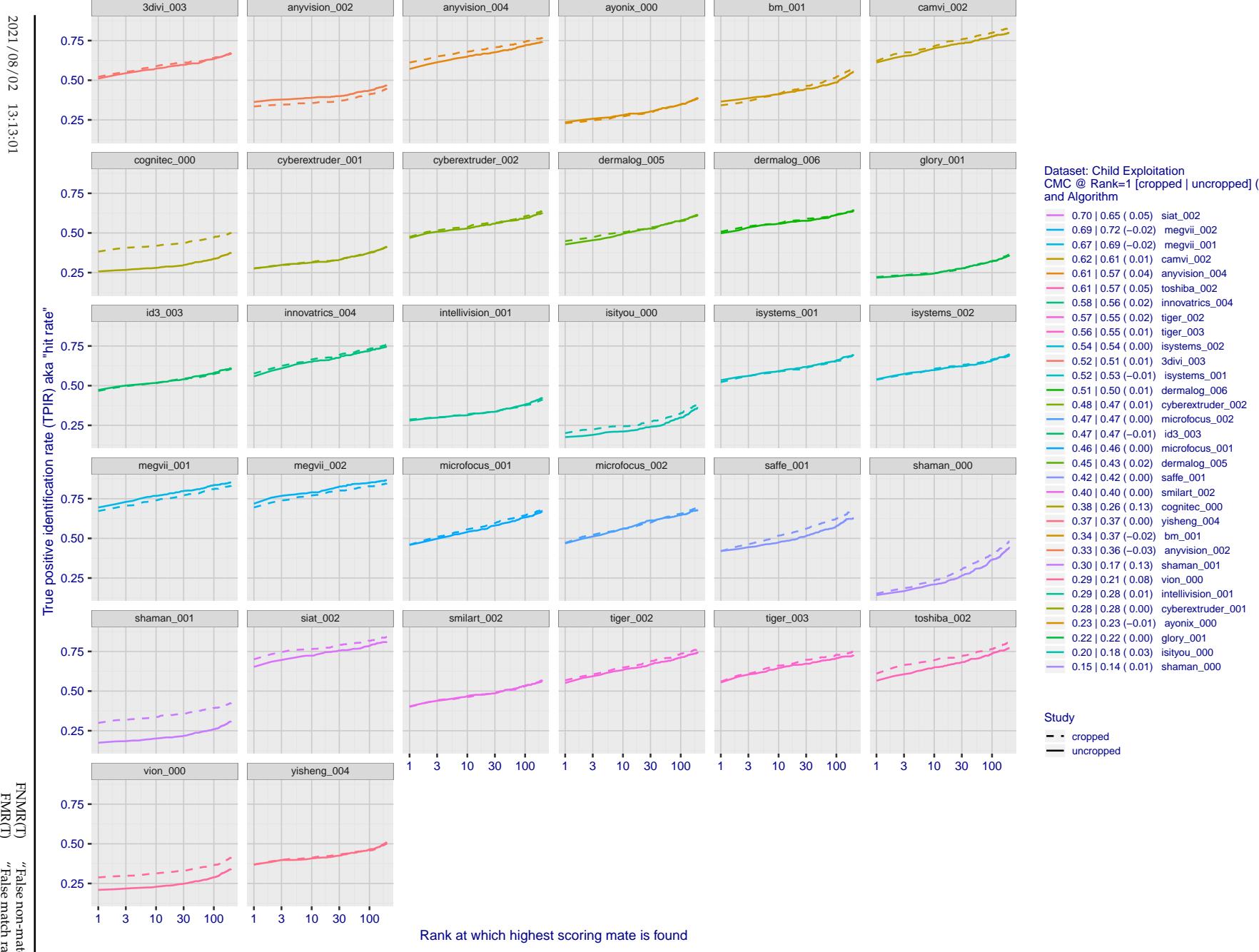


Figure 90: For child exploitation images, cumulative match characteristics (CMC) showing true positive identification rate vs. rank for two cases: 1. Whole image provided to the algorithm; 2. Human annotated rectangular region, cropped and provided to the algorithm. The difference between the traces is associated with detection of difficult faces, and fine localization.

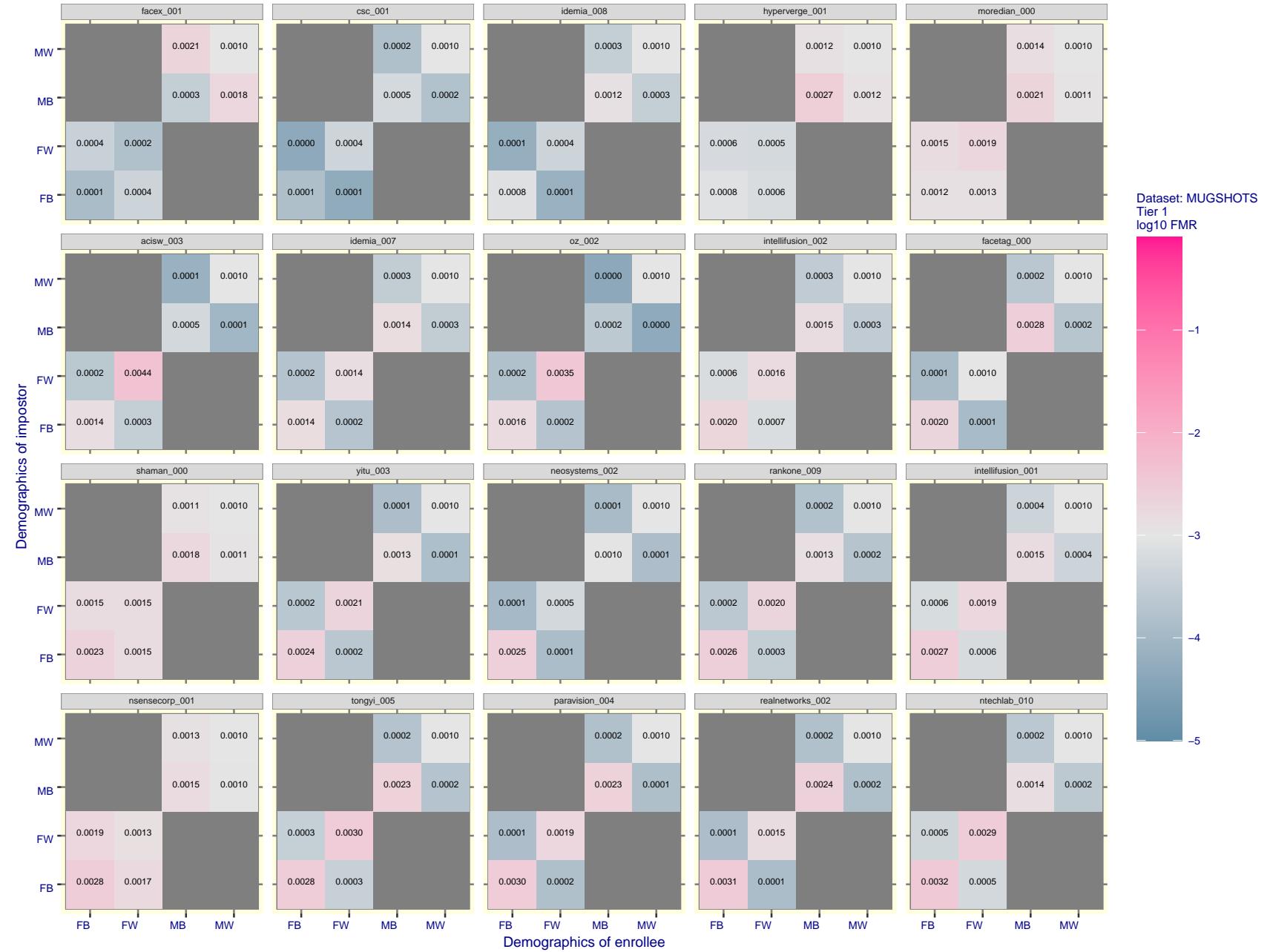


Figure 91: For the mugshot images, FMR for same-sex impostor pairs of images annotated with codes for black female, black male, white female, white male. The threshold is set for each algorithm to give FMR = 0.001 for white males which is the demographic that usually gives the lowest FMR. This means the top right box is the same color in all panels. The panels are sorted over multiple pages in order of FMR on black females, which is the demographic that usually gives the highest FMR.

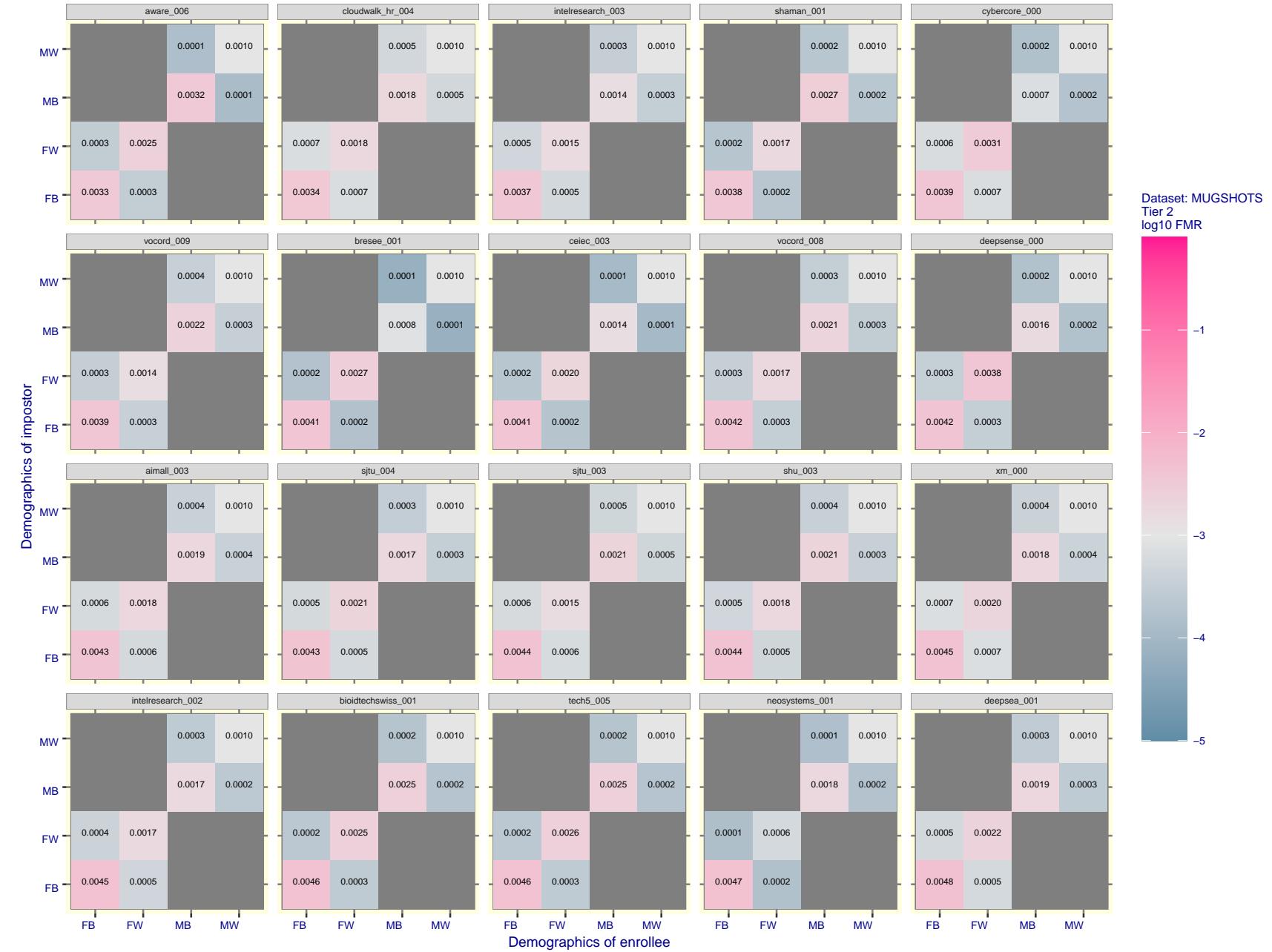


Figure 92: For the mugshot images, FMR for same-sex impostor pairs of images annotated with codes for black female, black male, white female, white male. The threshold is set for each algorithm to give $FMR = 0.001$ for white males which is the demographic that usually gives the lowest FMR. This means the top right box is the same color in all panels. The panels are sorted over multiple pages in order of FMR on black females, which is the demographic that usually gives the highest FMR.

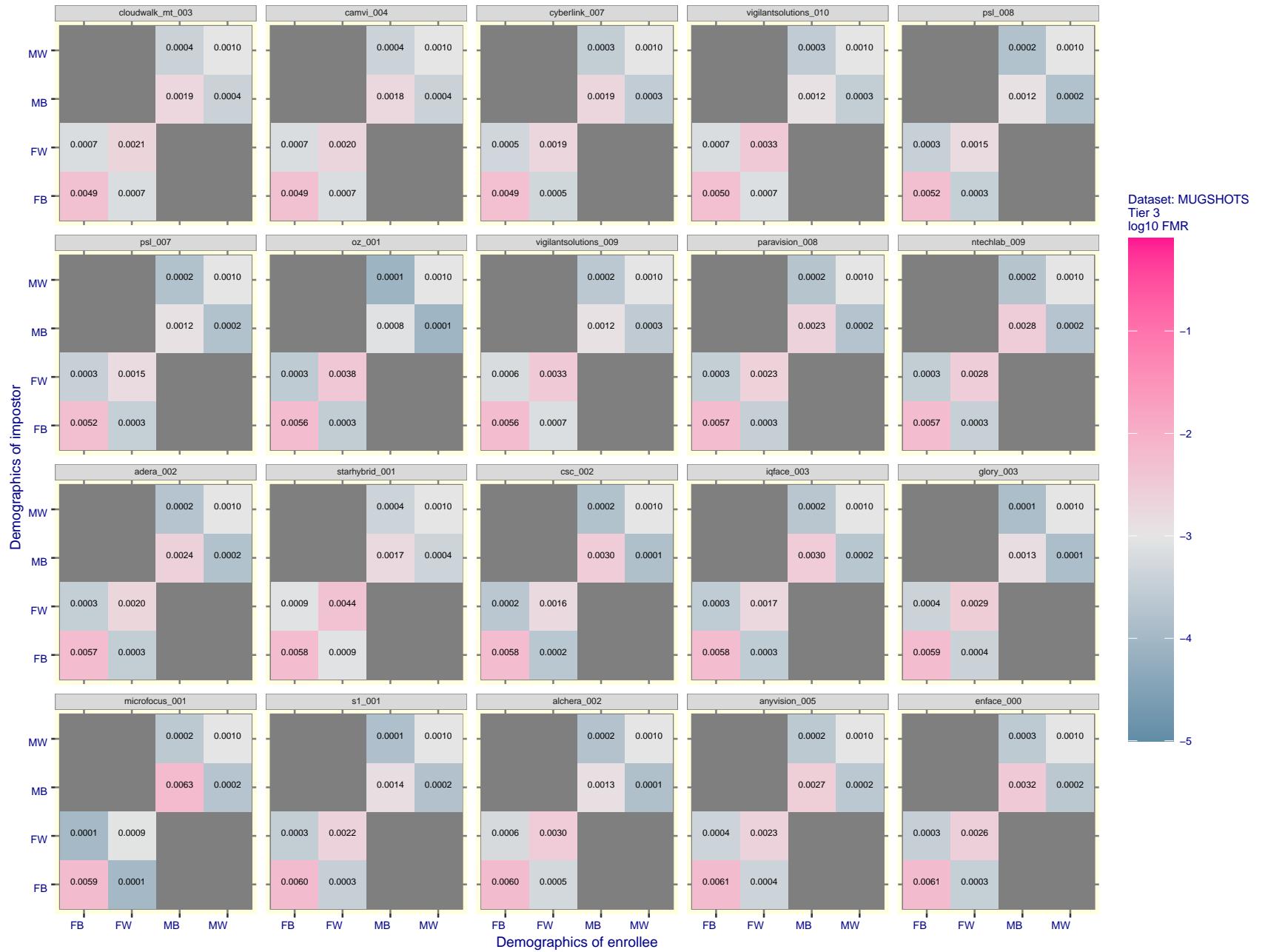


Figure 93: For the mugshot images, FMR for same-sex impostor pairs of images annotated with codes for black female, black male, white female, white male. The threshold is set for each algorithm to give FMR = 0.001 for white males which is the demographic that usually gives the lowest FMR. This means the top right box is the same color in all panels. The panels are sorted over multiple pages in order of FMR on black females, which is the demographic that usually gives the highest FMR.

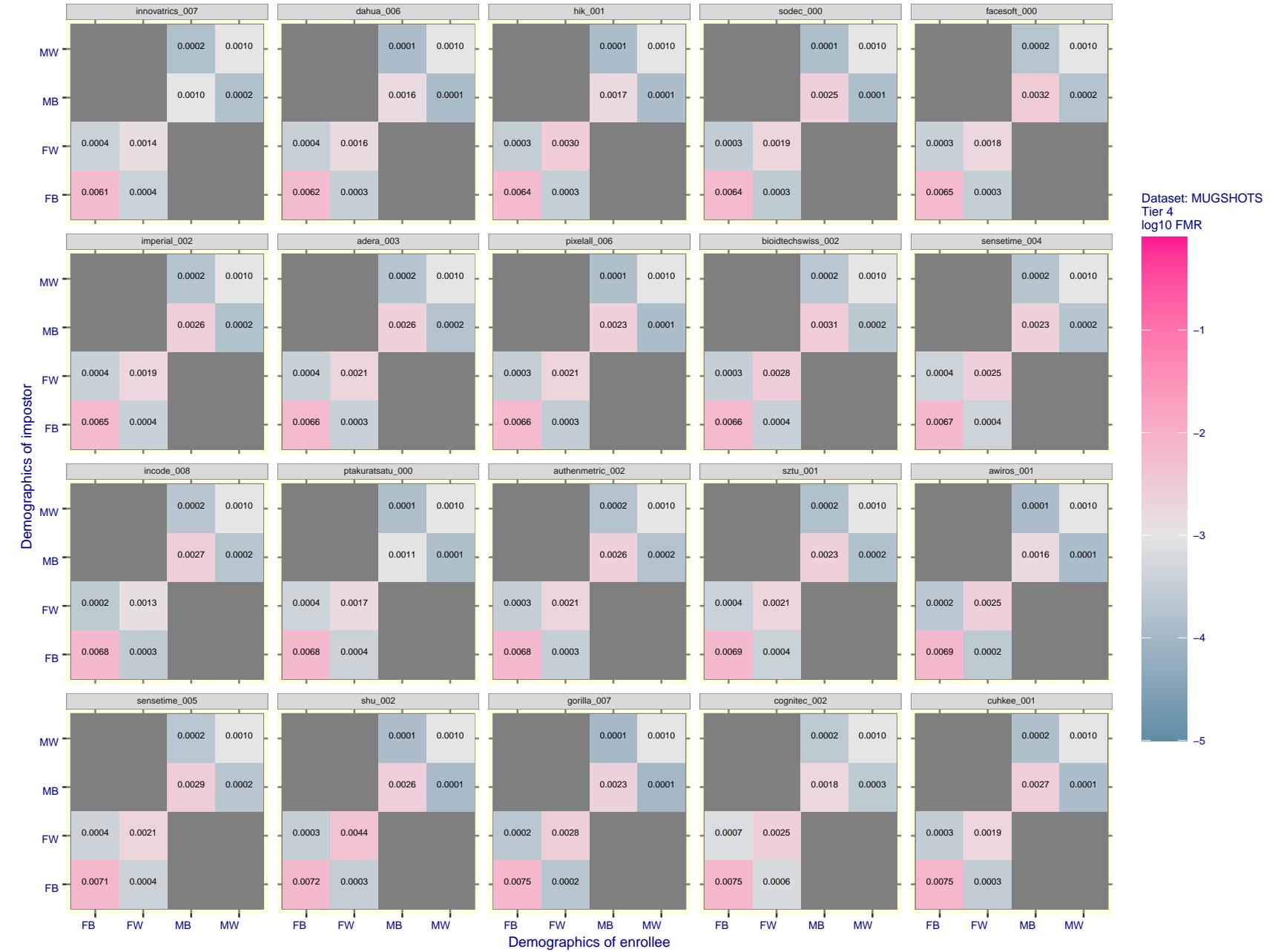


Figure 94: For the mugshot images, FMR for same-sex impostor pairs of images annotated with codes for black female, black male, white female, white male. The threshold is set for each algorithm to give $FMR = 0.001$ for white males which is the demographic that usually gives the lowest FMR. This means the top right box is the same color in all panels. The panels are sorted over multiple pages in order of FMR on black females, which is the demographic that usually gives the highest FMR.

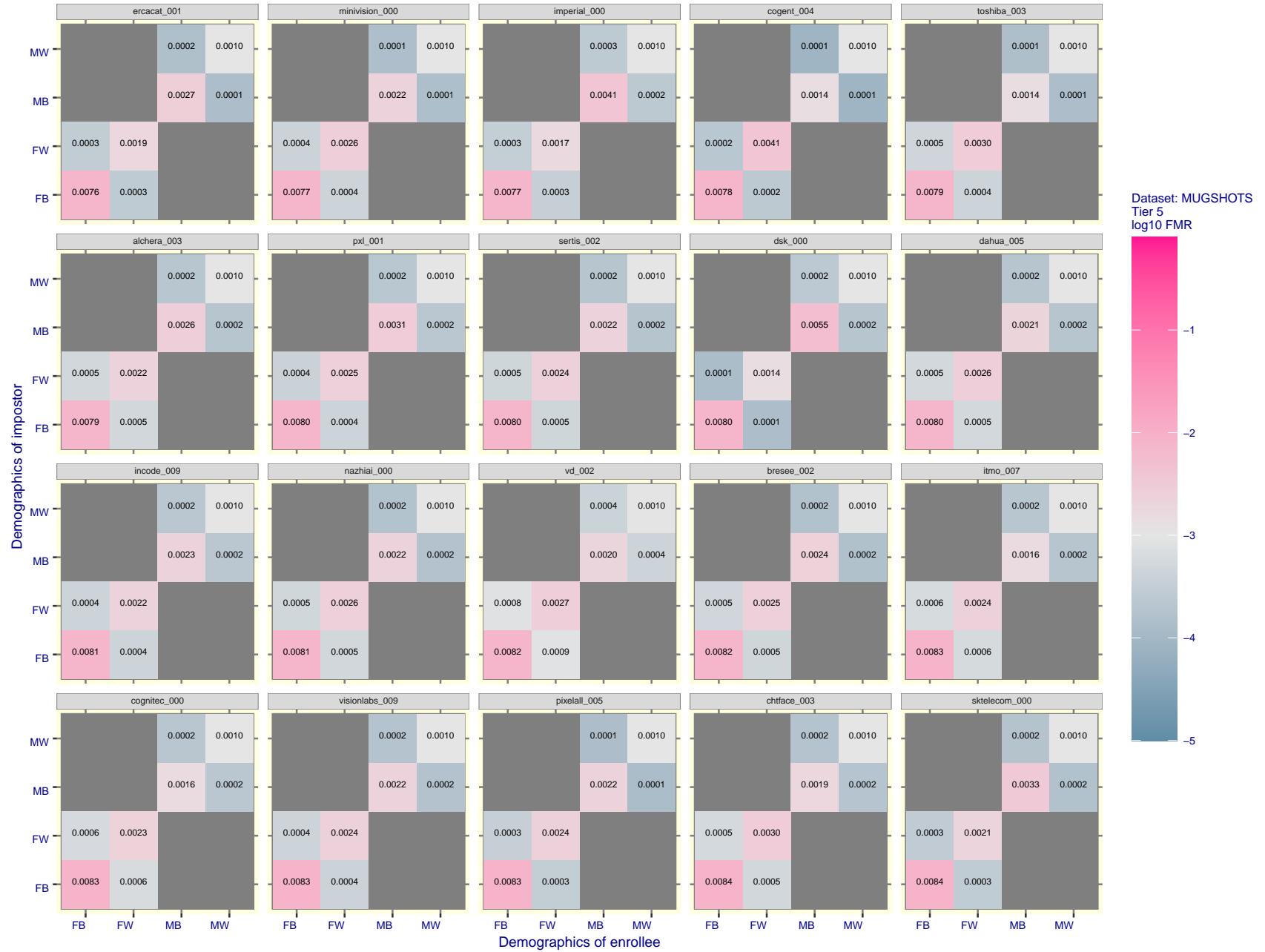


Figure 95: For the mugshot images, FMR for same-sex impostor pairs of images annotated with codes for black female, black male, white female, white male. The threshold is set for each algorithm to give $FMR = 0.001$ for white males which is the demographic that usually gives the lowest FMR. This means the top right box is the same color in all panels. The panels are sorted over multiple pages in order of FMR on black females, which is the demographic that usually gives the highest FMR.

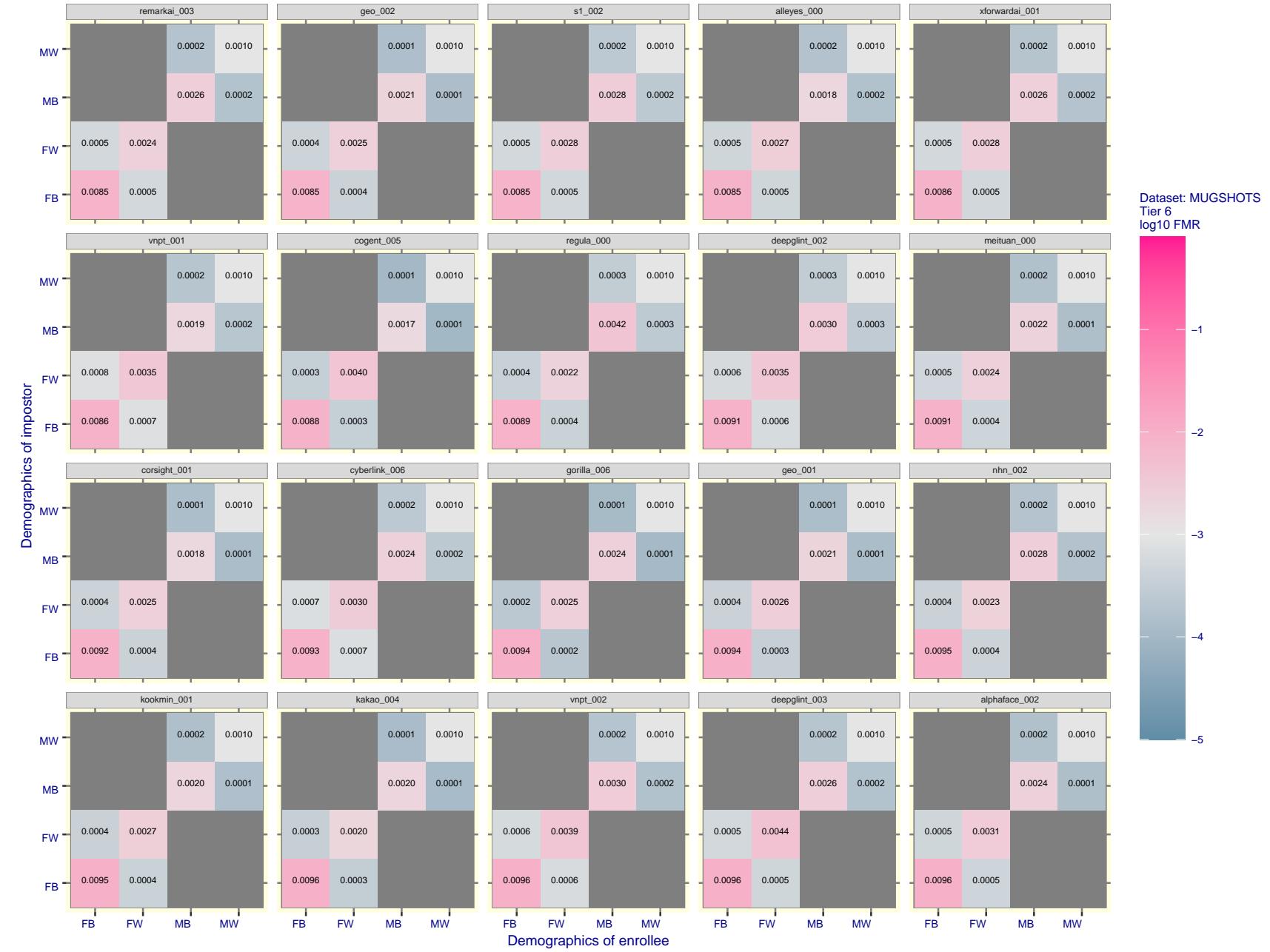


Figure 96: For the mugshot images, FMR for same-sex impostor pairs of images annotated with codes for black female, black male, white female, white male. The threshold is set for each algorithm to give FMR = 0.001 for white males which is the demographic that usually gives the lowest FMR. This means the top right box is the same color in all panels. The panels are sorted over multiple pages in order of FMR on black females, which is the demographic that usually gives the highest FMR.

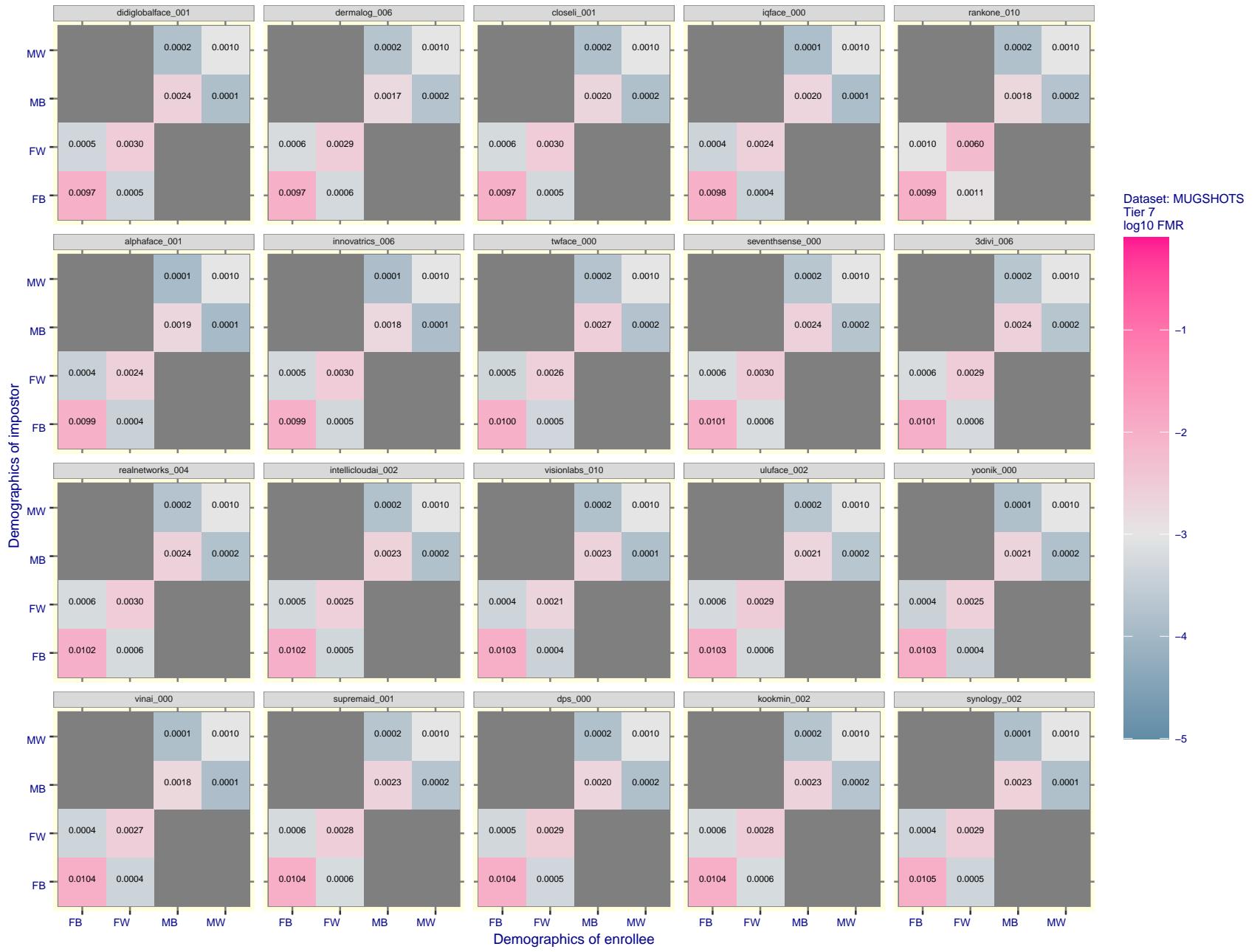
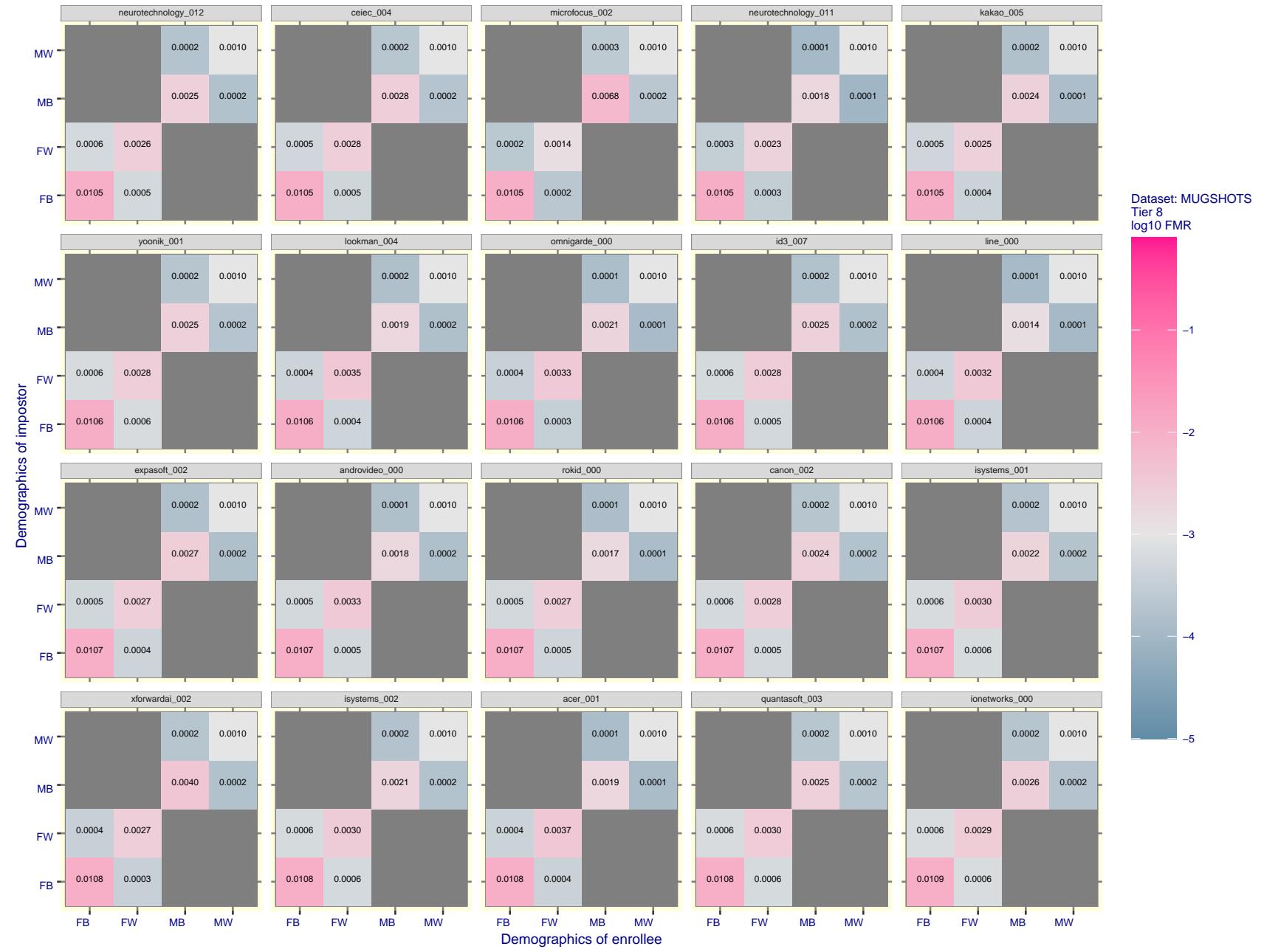


Figure 97: For the mugshot images, FMR for same-sex impostor pairs of images annotated with codes for black female, black male, white female, white male. The threshold is set for each algorithm to give $\text{FMR} = 0.001$ for white males which is the demographic that usually gives the lowest FMR. This means the top right box is the same color in all panels. The panels are sorted over multiple pages in order of FMR on black females, which is the demographic that usually gives the highest FMR.



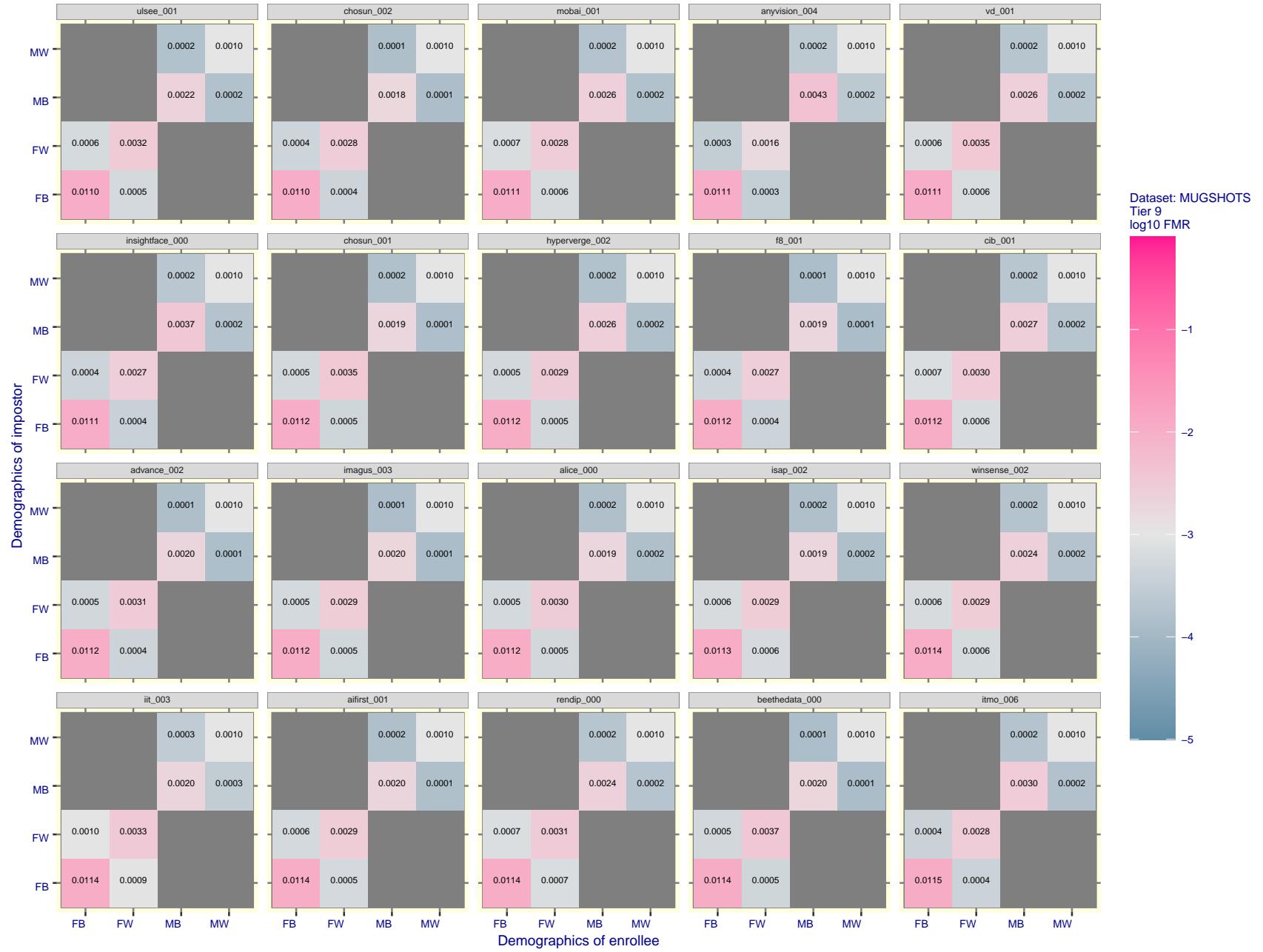


Figure 99: For the mugshot images, FMR for same-sex impostor pairs of images annotated with codes for black female, black male, white female, white male. The threshold is set for each algorithm to give $FMR = 0.001$ for white males which is the demographic that usually gives the lowest FMR. This means the top right box is the same color in all panels. The panels are sorted over multiple pages in order of FMR on black females, which is the demographic that usually gives the highest FMR.

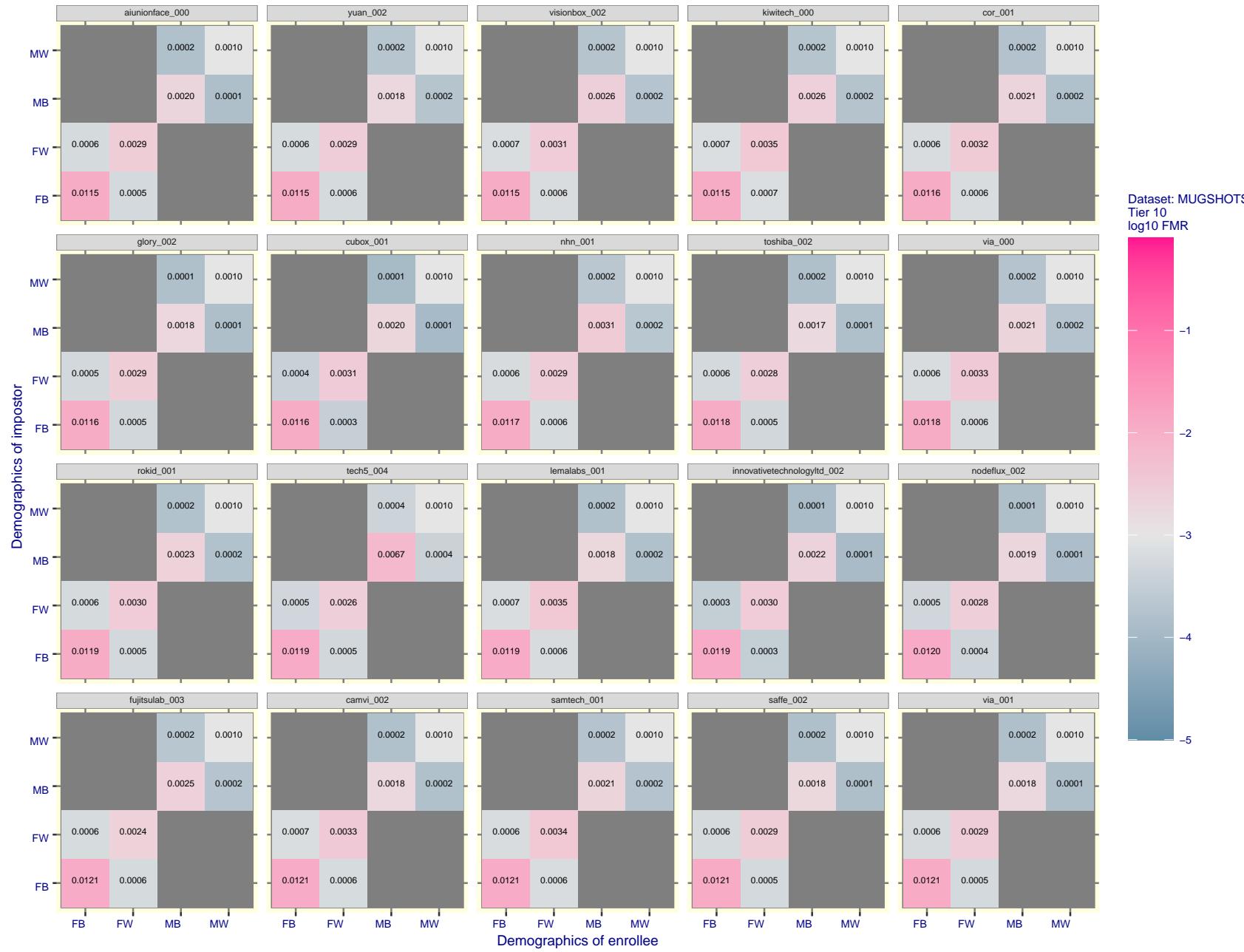


Figure 100: For the mugshot images, FMR for same-sex impostor pairs of images annotated with codes for black female, black male, white female, white male. The threshold is set for each algorithm to give FMR = 0.001 for white males which is the demographic that usually gives the lowest FMR. This means the top right box is the same color in all panels. The panels are sorted over multiple pages in order of FMR on black females, which is the demographic that usually gives the highest FMR.

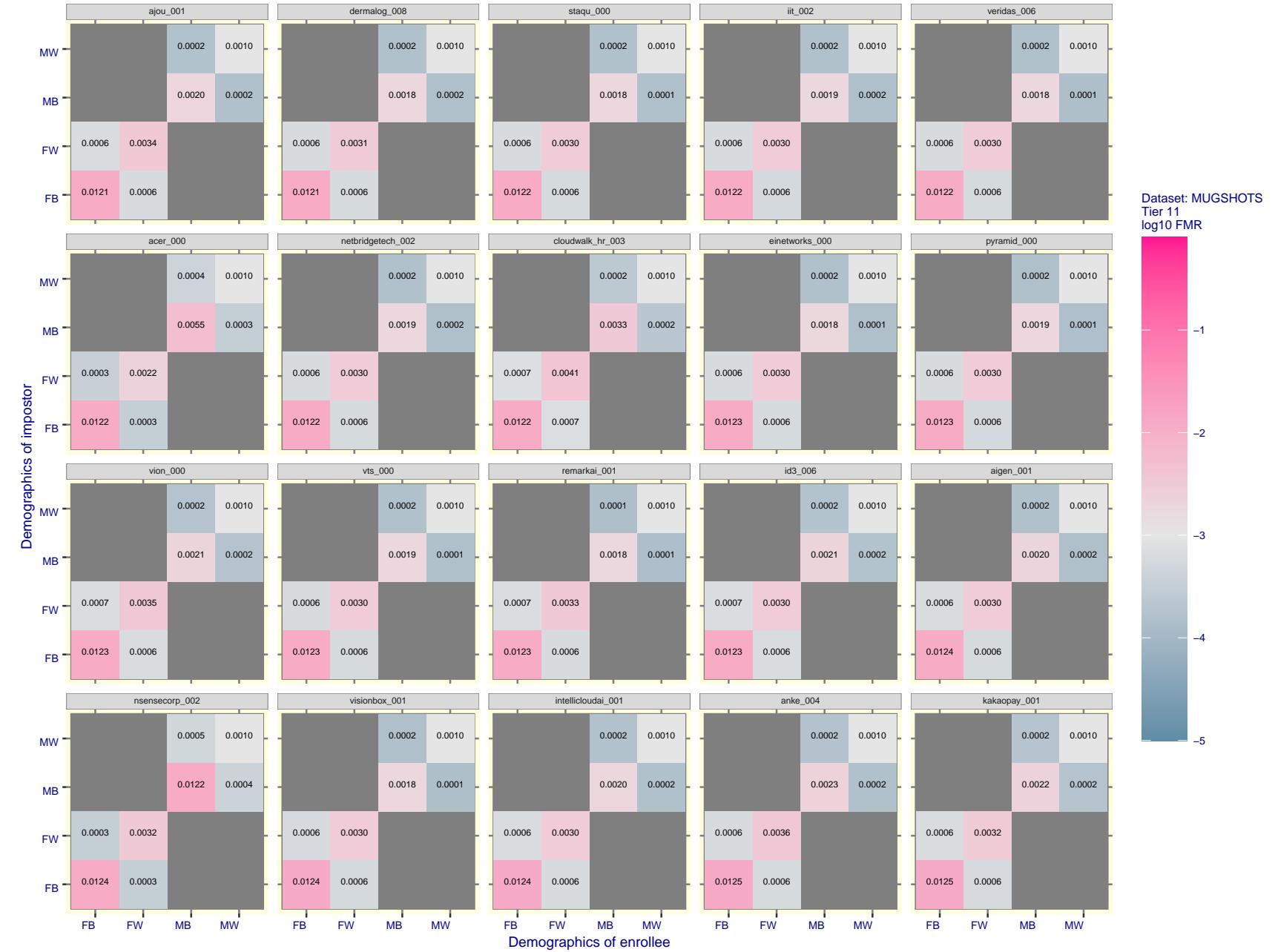


Figure 101: For the mugshot images, FMR for same-sex impostor pairs of images annotated with codes for black female, black male, white female, white male. The threshold is set for each algorithm to give FMR = 0.001 for white males which is the demographic that usually gives the lowest FMR. This means the top right box is the same color in all panels. The panels are sorted over multiple pages in order of FMR on black females, which is the demographic that usually gives the highest FMR.

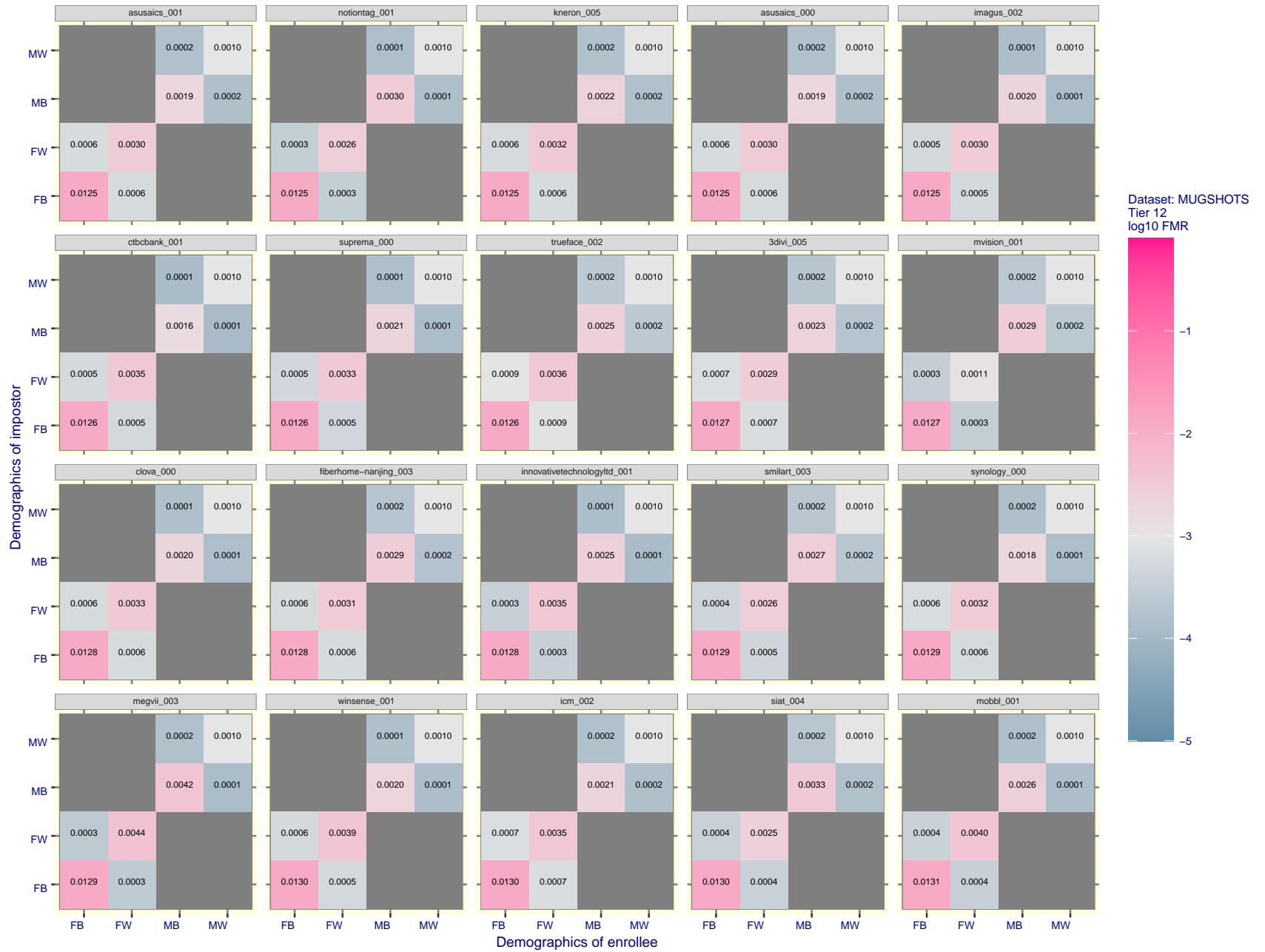


Figure 102: For the mugshot images, FMR for same-sex impostor pairs of images annotated with codes for black female, black male, white female, white male. The threshold is set for each algorithm to give FMR = 0.001 for white males which is the demographic that usually gives the lowest FMR. This means the top right box is the same color in all panels. The panels are sorted over multiple pages in order of FMR on black females, which is the demographic that usually gives the highest FMR.

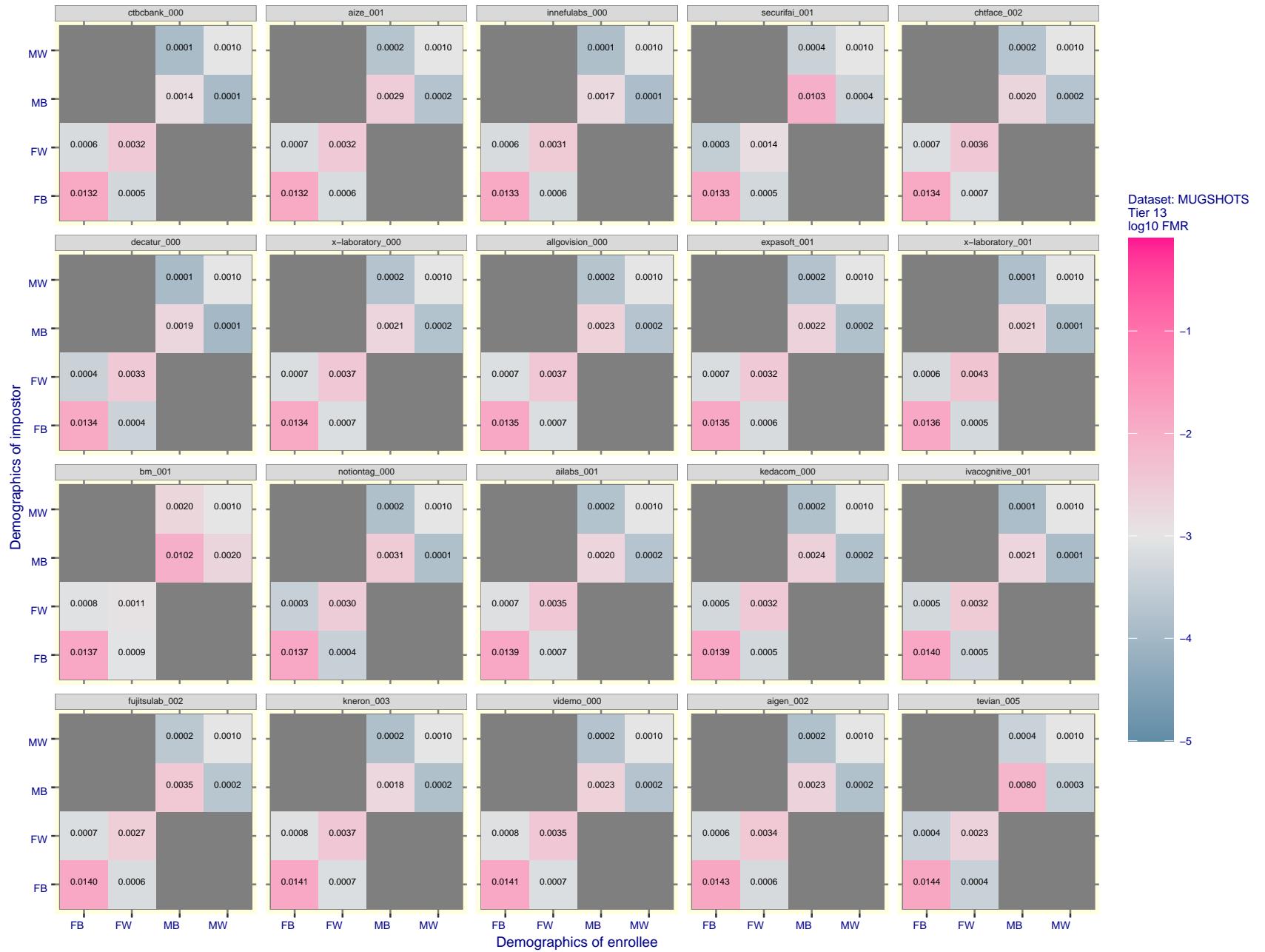


Figure 103: For the mugshot images, FMR for same-sex impostor pairs of images annotated with codes for black female, black male, white female, white male. The threshold is set for each algorithm to give FMR = 0.001 for white males which is the demographic that usually gives the lowest FMR. This means the top right box is the same color in all panels. The panels are sorted over multiple pages in order of FMR on black females, which is the demographic that usually gives the highest FMR.

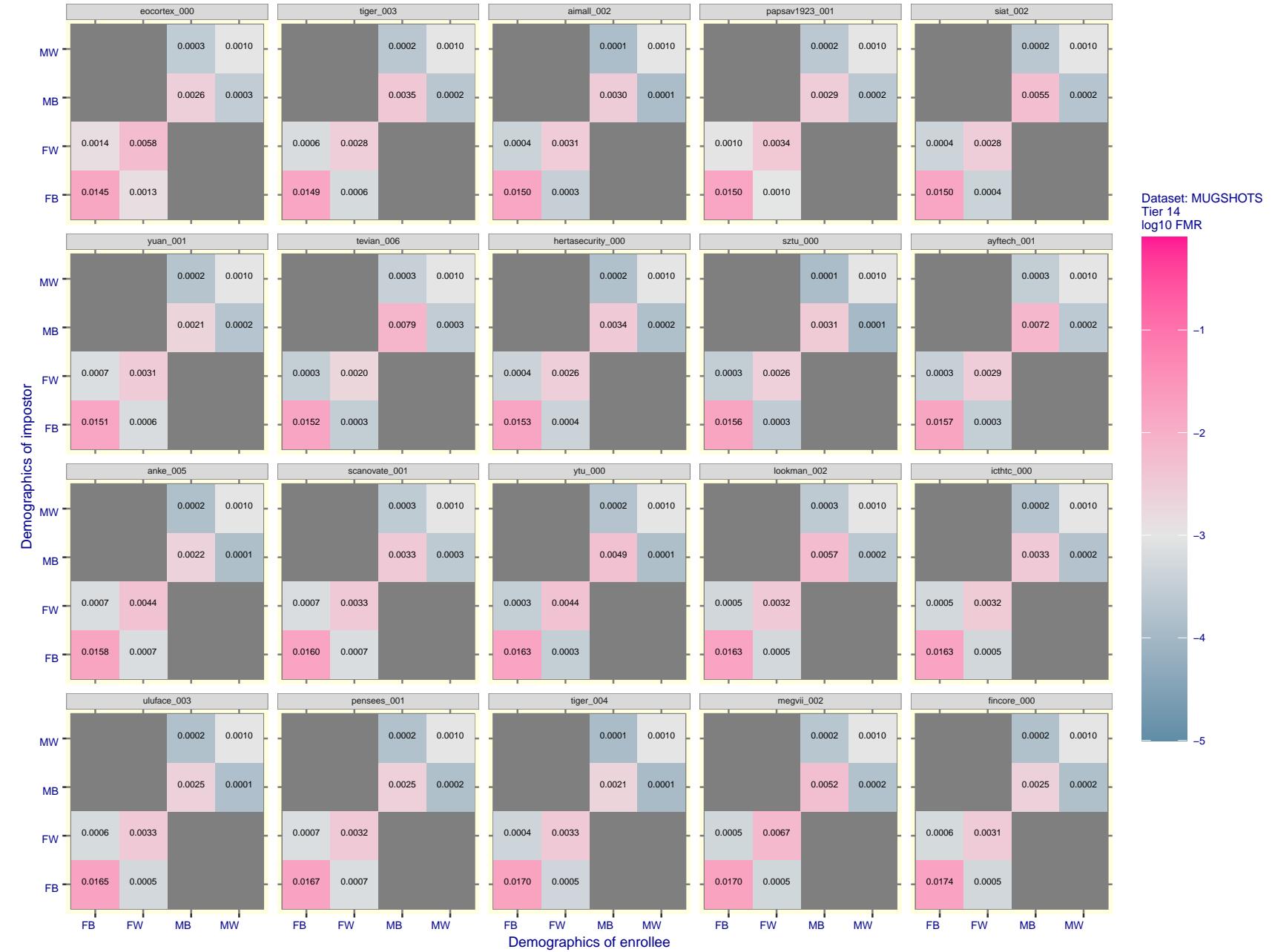


Figure 104: For the mugshot images, FMR for same-sex impostor pairs of images annotated with codes for black female, black male, white female, white male. The threshold is set for each algorithm to give FMR = 0.001 for white males which is the demographic that usually gives the lowest FMR. This means the top right box is the same color in all panels. The panels are sorted over multiple pages in order of FMR on black females, which is the demographic that usually gives the highest FMR.

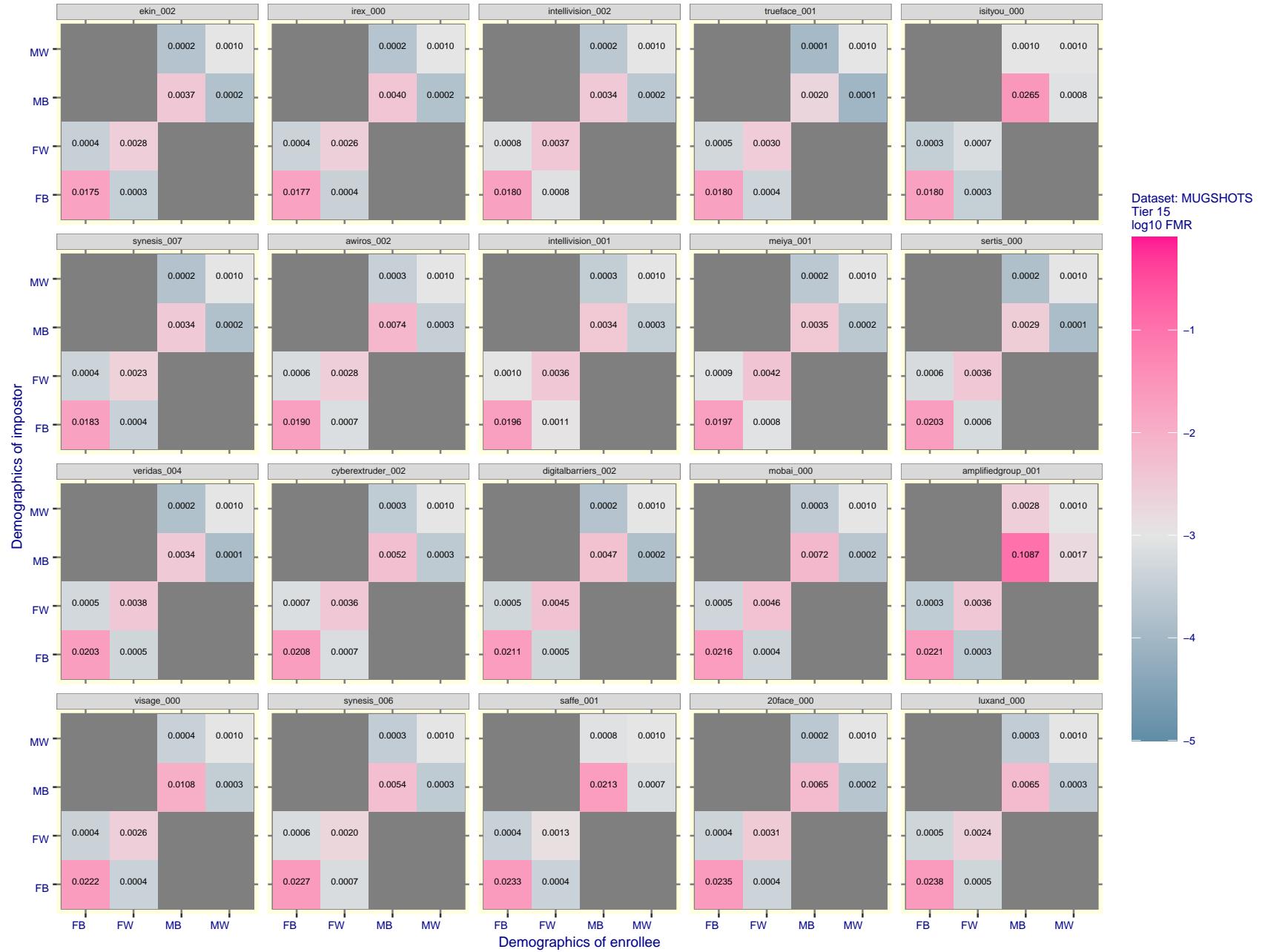


Figure 105: For the mugshot images, FMR for same-sex impostor pairs of images annotated with codes for black female, black male, white female, white male. The threshold is set for each algorithm to give FMR = 0.001 for white males which is the demographic that usually gives the lowest FMR. This means the top right box is the same color in all panels. The panels are sorted over multiple pages in order of FMR on black females, which is the demographic that usually gives the highest FMR.

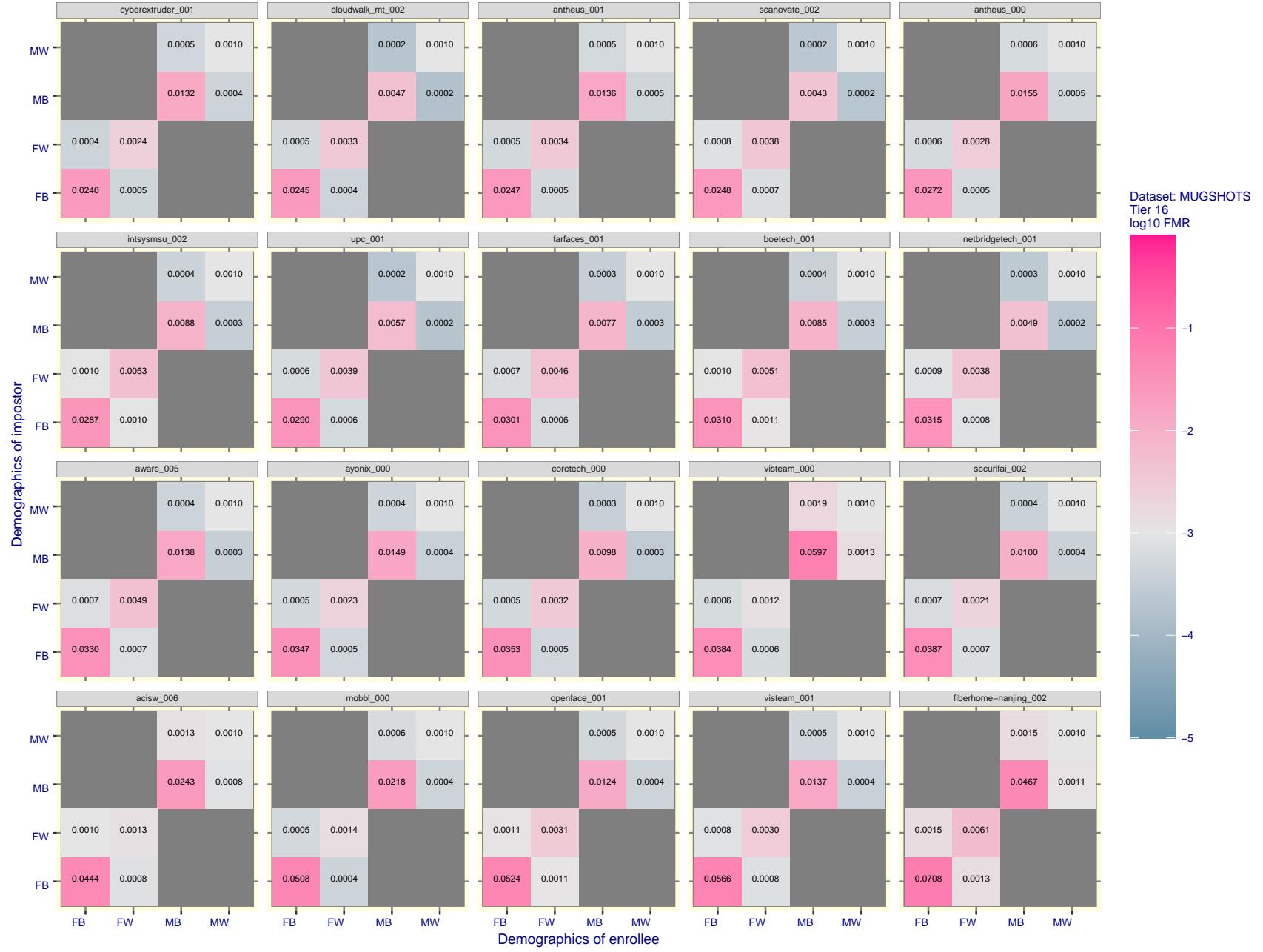


Figure 106: For the mugshot images, FMR for same-sex impostor pairs of images annotated with codes for black female, black male, white female, white male. The threshold is set for each algorithm to give FMR = 0.001 for white males which is the demographic that usually gives the lowest FMR. This means the top right box is the same color in all panels. The panels are sorted over multiple pages in order of FMR on black females, which is the demographic that usually gives the highest FMR.

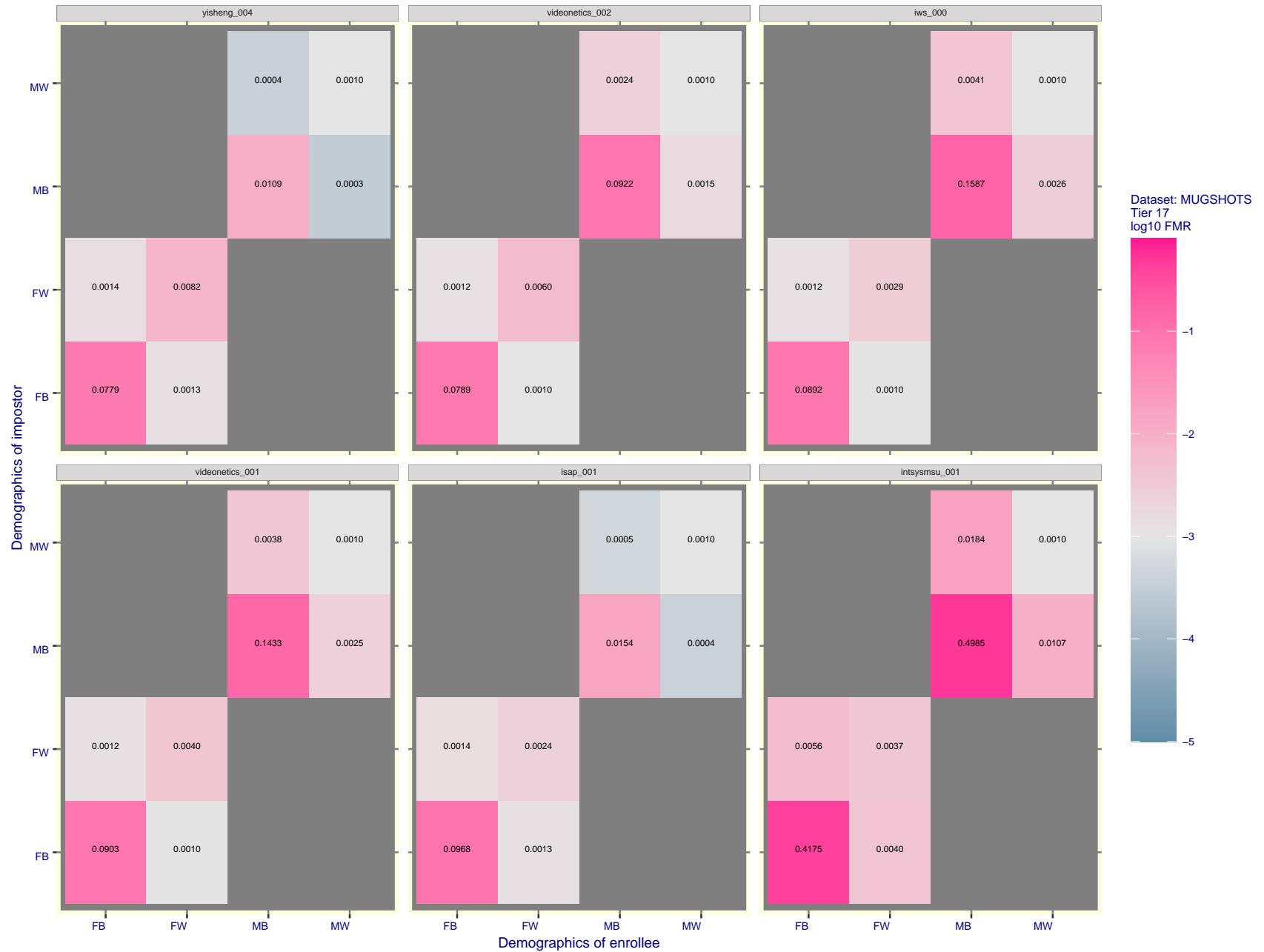


Figure 107: For the mugshot images, FMR for same-sex impostor pairs of images annotated with codes for black female, black male, white female, white male. The threshold is set for each algorithm to give $\text{FMR} = 0.001$ for white males which is the demographic that usually gives the lowest FMR. This means the top right box is the same color in all panels. The panels are sorted over multiple pages in order of FMR on black females, which is the demographic that usually gives the highest FMR.

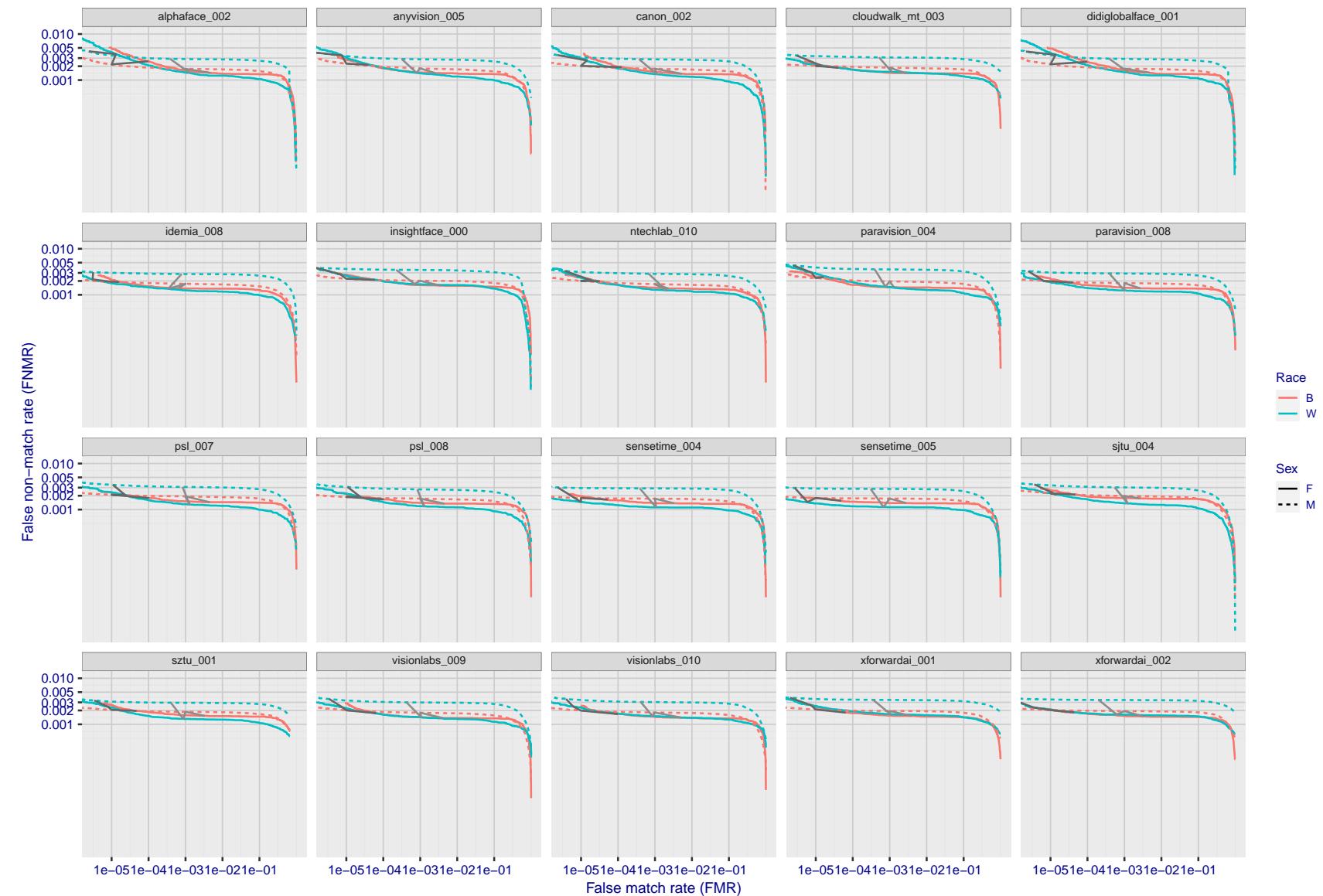


Figure 108: For the mugshot images, error tradeoff characteristics for white females, black females, black males and white males. The Z-shaped grey lines correspond to fixed thresholds, showing both FNMR and FMR vary at one T value. Note: Many of the plots will naively be read as saying women gives worse error rates than men because the solid traces lie above the dotted ones. However, this is misleading and incomplete: The grey lines show the traces reveal horizontal shifts. Thus for the cogent-003 algorithm FNMR for men is higher than for women at a fixed threshold but, at the same time, FMR is higher for women - see Figure 169. As access control systems almost always operate at a fixed threshold, the naive interpretation is incorrect.

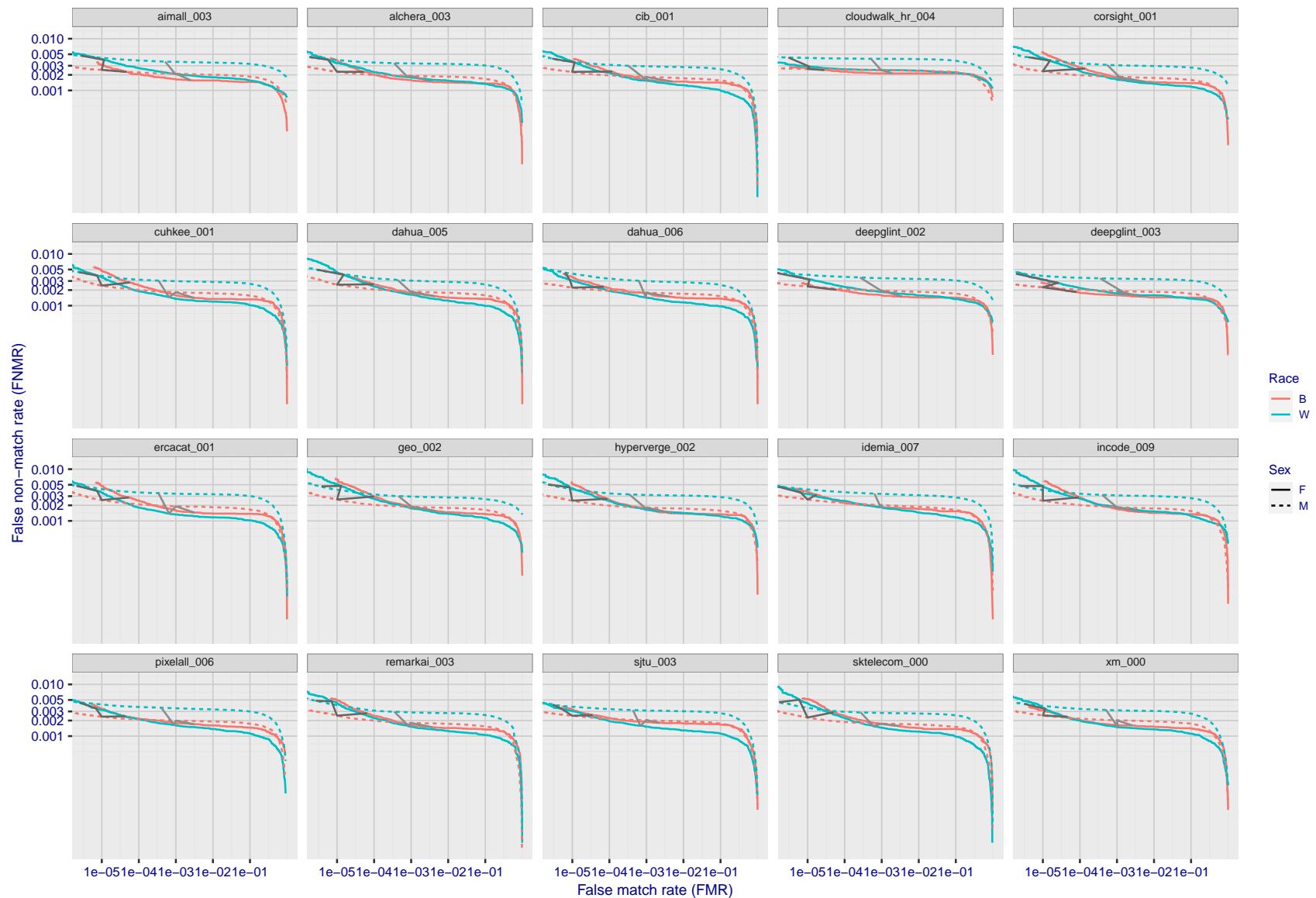


Figure 109: For the mugshot images, error tradeoff characteristics for white females, black females, black males and white males. The Z-shaped grey lines correspond to fixed thresholds, showing both FNMR and FMR vary at one T value. Note: Many of the plots will naively be read as saying women gives worse error rates than men because the solid traces lie above the dotted ones. However, this is misleading and incomplete: The grey lines show the traces reveal horizontal shifts. Thus for the cogent-003 algorithm FNMR for men is higher than for women at a fixed threshold but, at the same time, FMR is higher for women - see Figure 169. As access control systems almost always operate at a fixed threshold, the naive interpretation is incorrect.

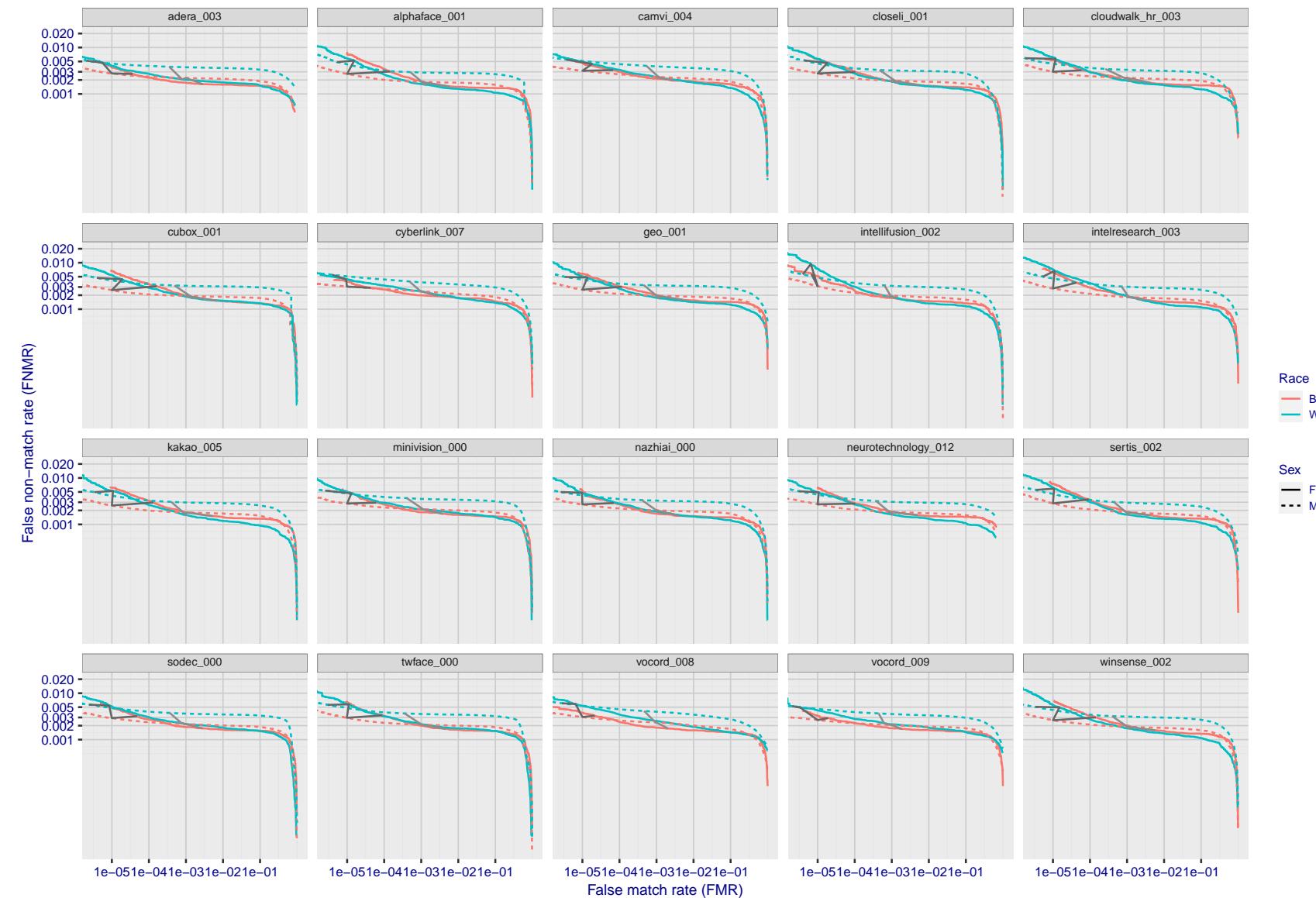


Figure 110: For the mugshot images, error tradeoff characteristics for white females, black females, black males and white males. The Z-shaped grey lines correspond to fixed thresholds, showing both FNMR and FMR vary at one T value. Note: Many of the plots will naively be read as saying women gives worse error rates than men because the solid traces lie above the dotted ones. However, this is misleading and incomplete: The grey lines show the traces reveal horizontal shifts. Thus for the cogent-003 algorithm FNMR for men is higher than for women at a fixed threshold but, at the same time, FMR is higher for women - see Figure 169. As access control systems almost always operate at a fixed threshold, the naive interpretation is incorrect.

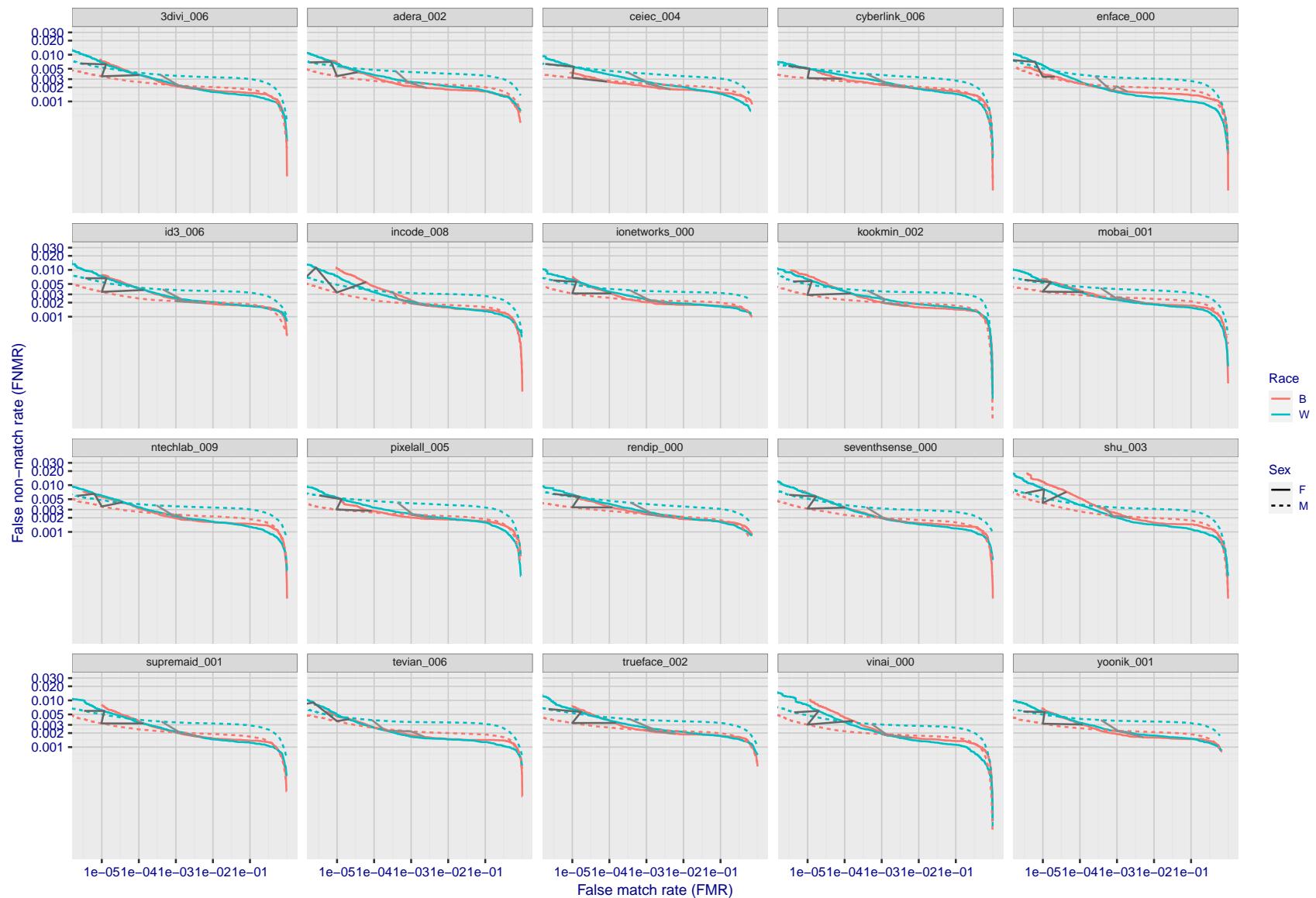


Figure 111: For the mugshot images, error tradeoff characteristics for white females, black females, black males and white males. The Z-shaped grey lines correspond to fixed thresholds, showing both FNMR and FMR vary at one T value. Note: Many of the plots will naively be read as saying women gives worse error rates than men because the solid traces lie above the dotted ones. However, this is misleading and incomplete: The grey lines show the traces reveal horizontal shifts. Thus for the cogent-003 algorithm FNMR for men is higher than for women at a fixed threshold but, at the same time, FMR is higher for women - see Figure 169. As access control systems almost always operate at a fixed threshold, the naive interpretation is incorrect.

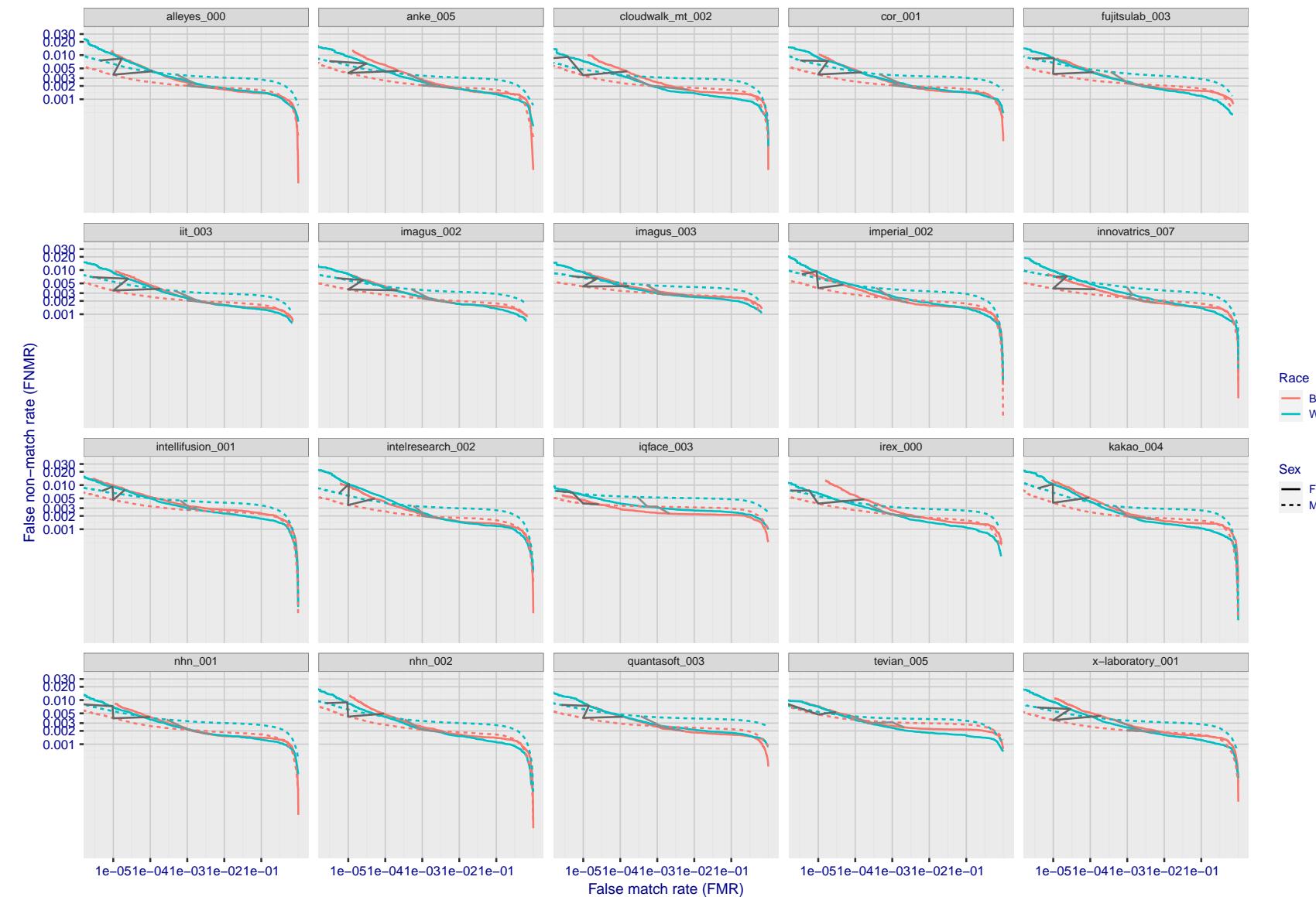


Figure 112: For the mugshot images, error tradeoff characteristics for white females, black females, black males and white males. The Z-shaped grey lines correspond to fixed thresholds, showing both FNMR and FMR vary at one T value. Note: Many of the plots will naively be read as saying women gives worse error rates than men because the solid traces lie above the dotted ones. However, this is misleading and incomplete: The grey lines show the traces reveal horizontal shifts. Thus for the cogent-003 algorithm FNMR for men is higher than for women at a fixed threshold but, at the same time, FMR is higher for women - see Figure 169. As access control systems almost always operate at a fixed threshold, the naive interpretation is incorrect.

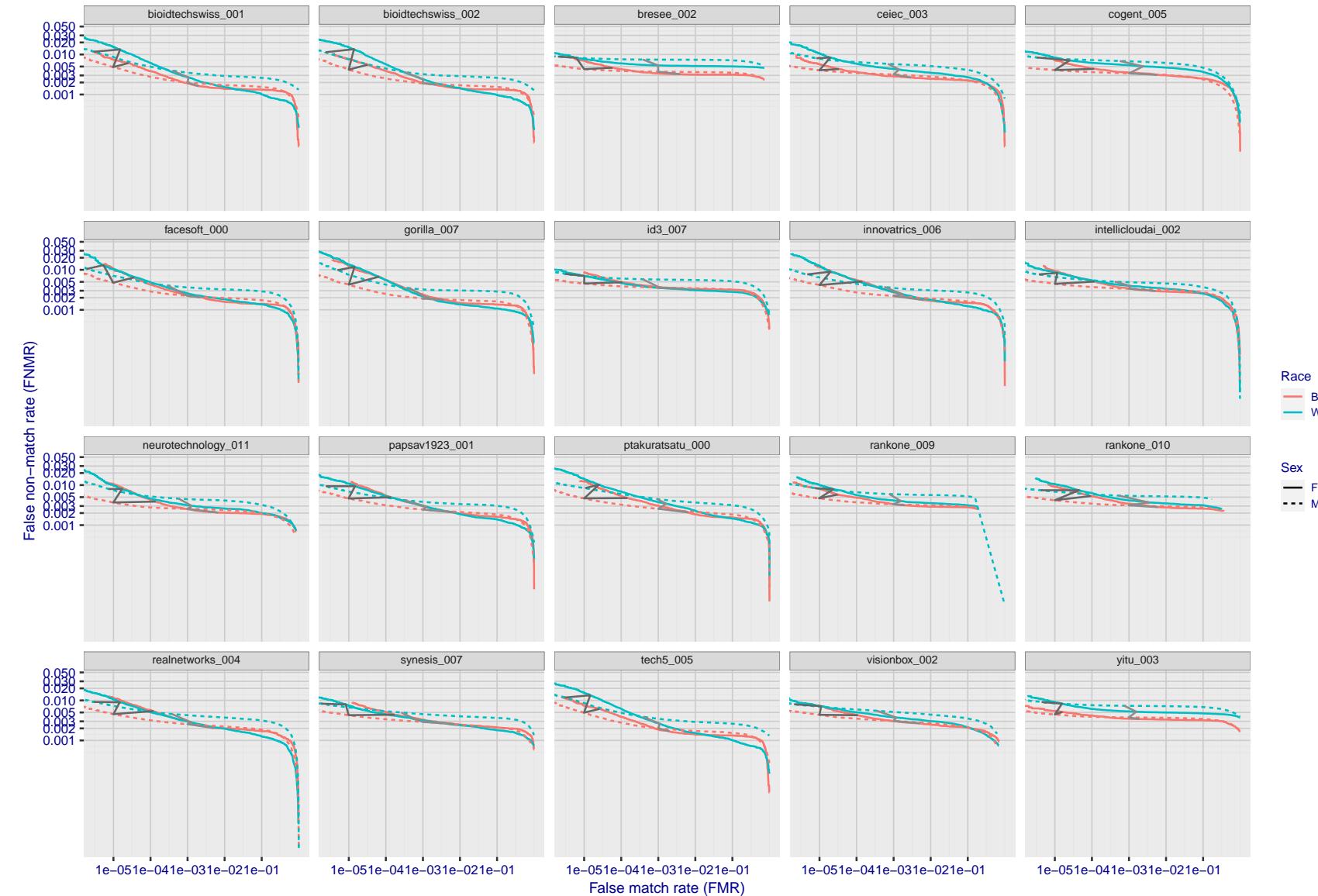


Figure 113: For the mugshot images, error tradeoff characteristics for white females, black females, black males and white males. The Z-shaped grey lines correspond to fixed thresholds, showing both FNMR and FMR vary at one T value. Note: Many of the plots will naively be read as saying women gives worse error rates than men because the solid traces lie above the dotted ones. However, this is misleading and incomplete: The grey lines show the traces reveal horizontal shifts. Thus for the cogent-003 algorithm FNMR for men is higher than for women at a fixed threshold but, at the same time, FMR is higher for women - see Figure 169. As access control systems almost always operate at a fixed threshold, the naive interpretation is incorrect.

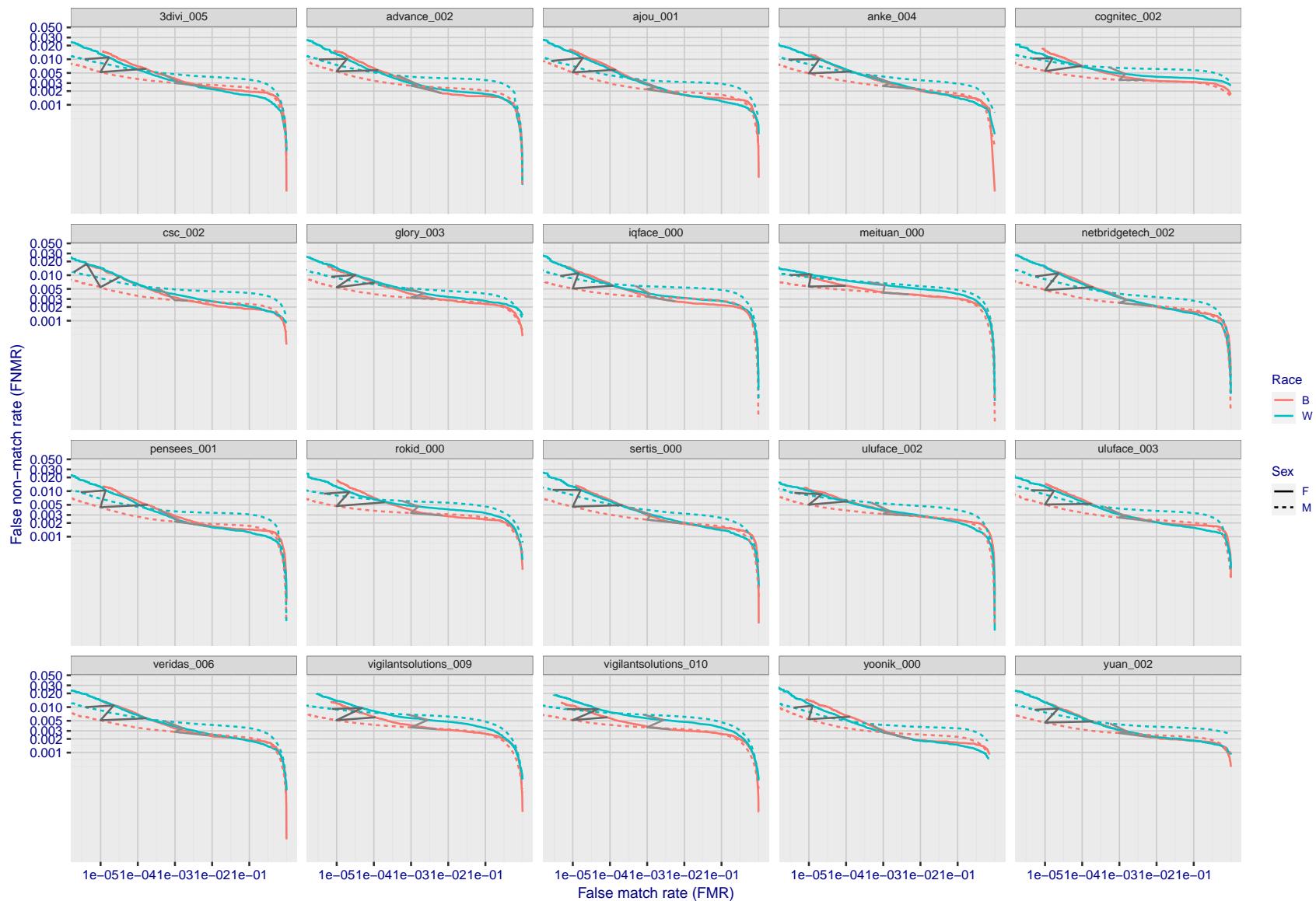


Figure 114: For the mugshot images, error tradeoff characteristics for white females, black females, black males and white males. The Z-shaped grey lines correspond to fixed thresholds, showing both FNMR and FMR vary at one T value. Note: Many of the plots will naively be read as saying women gives worse error rates than men because the solid traces lie above the dotted ones. However, this is misleading and incomplete: The grey lines show the traces reveal horizontal shifts. Thus for the cogent-003 algorithm FNMR for men is higher than for women at a fixed threshold but, at the same time, FMR is higher for women - see Figure 169. As access control systems almost always operate at a fixed threshold, the naive interpretation is incorrect.

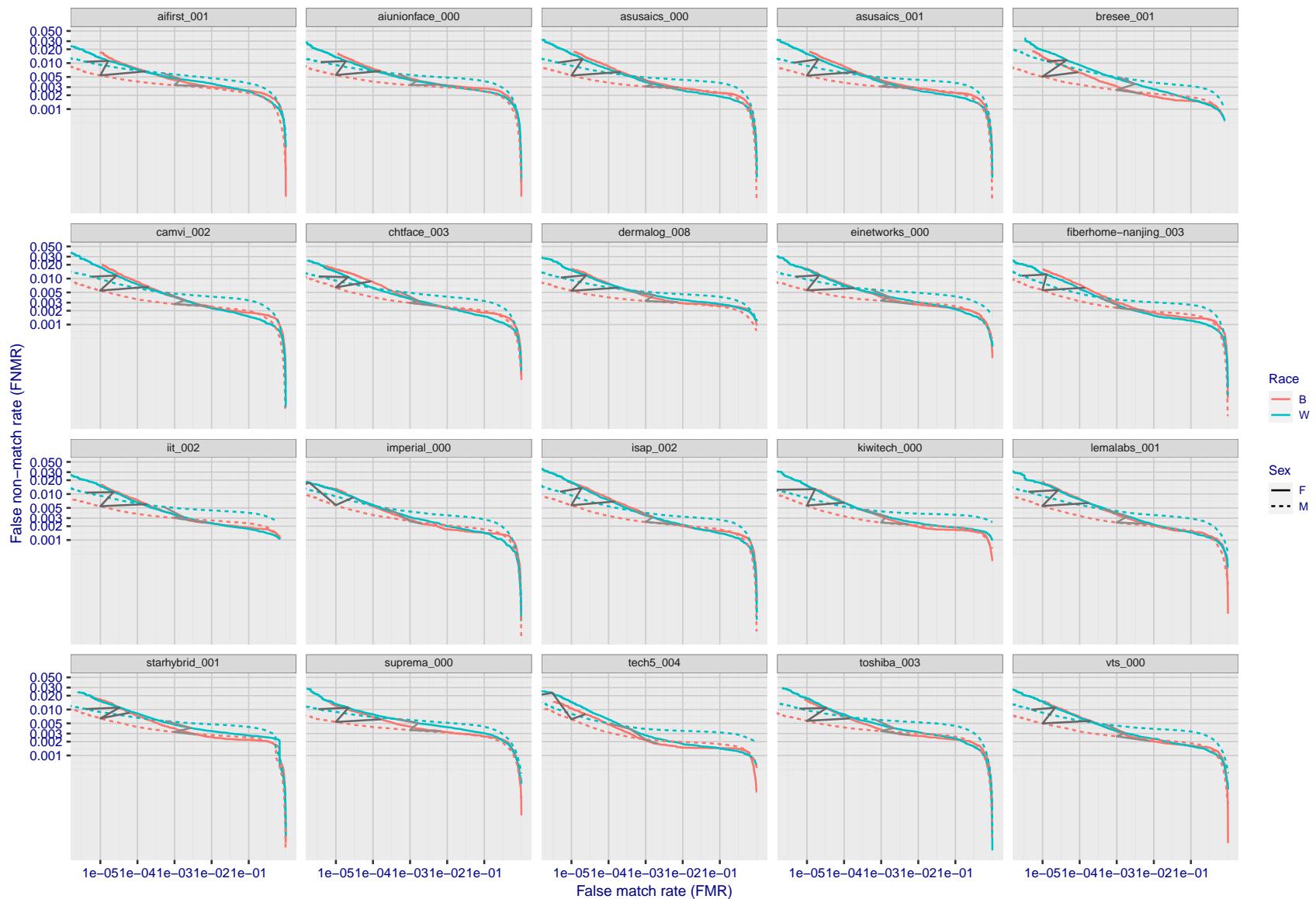


Figure 115: For the mugshot images, error tradeoff characteristics for white females, black females, black males and white males. The Z-shaped grey lines correspond to fixed thresholds, showing both FNMR and FMR vary at one T value. Note: Many of the plots will naively be read as saying women gives worse error rates than men because the solid traces lie above the dotted ones. However, this is misleading and incomplete: The grey lines show the traces reveal horizontal shifts. Thus for the cogent-003 algorithm FNMR for men is higher than for women at a fixed threshold but, at the same time, FMR is higher for women - see Figure 169. As access control systems almost always operate at a fixed threshold, the naive interpretation is incorrect.

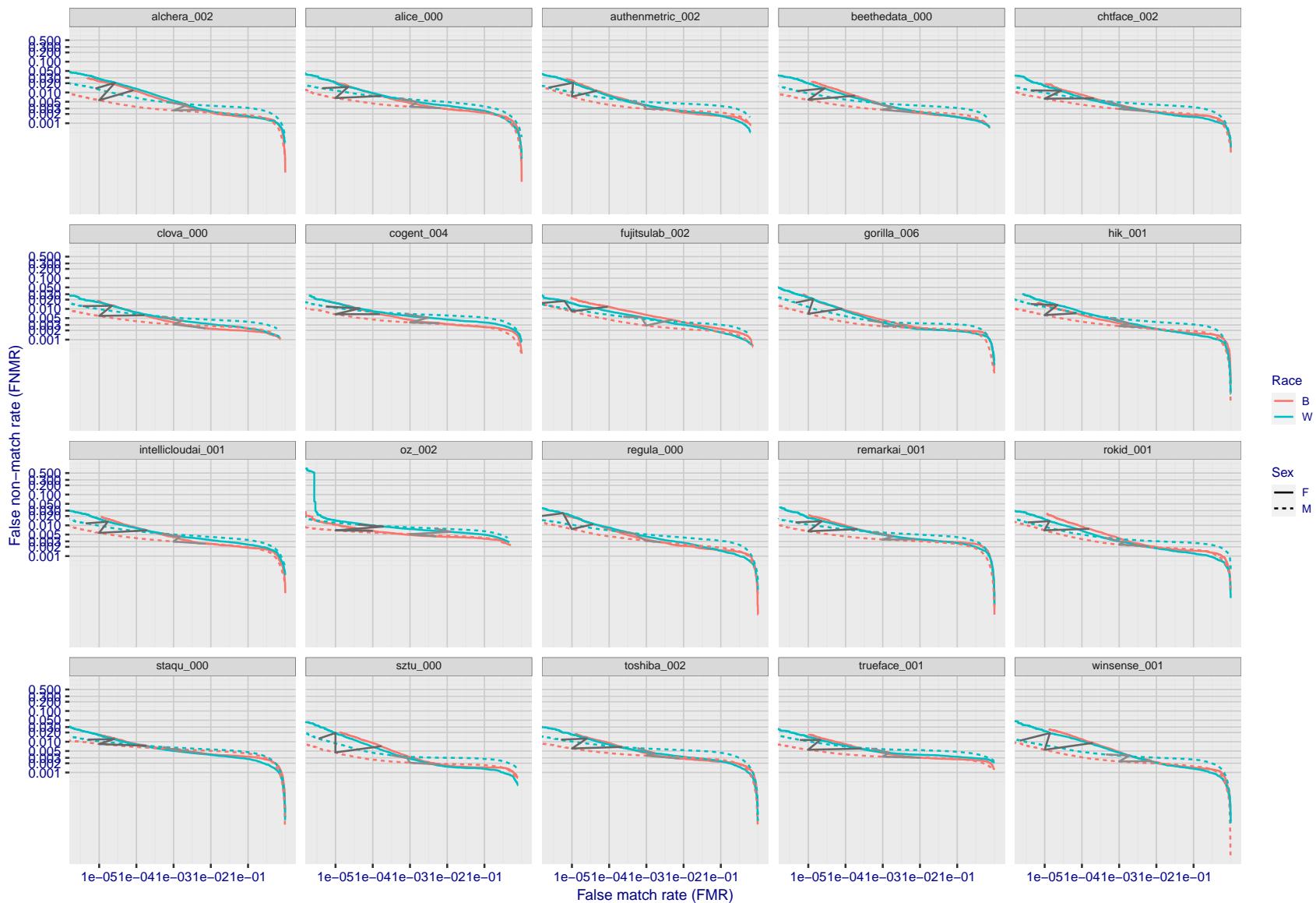


Figure 116: For the mugshot images, error tradeoff characteristics for white females, black females, black males and white males. The Z-shaped grey lines correspond to fixed thresholds, showing both FNMR and FMR vary at one T value. Note: Many of the plots will naively be read as saying women gives worse error rates than men because the solid traces lie above the dotted ones. However, this is misleading and incomplete: The grey lines show the traces reveal horizontal shifts. Thus for the cogent-003 algorithm FNMR for men is higher than for women at a fixed threshold but, at the same time, FMR is higher for women - see Figure 169. As access control systems almost always operate at a fixed threshold, the naive interpretation is incorrect.

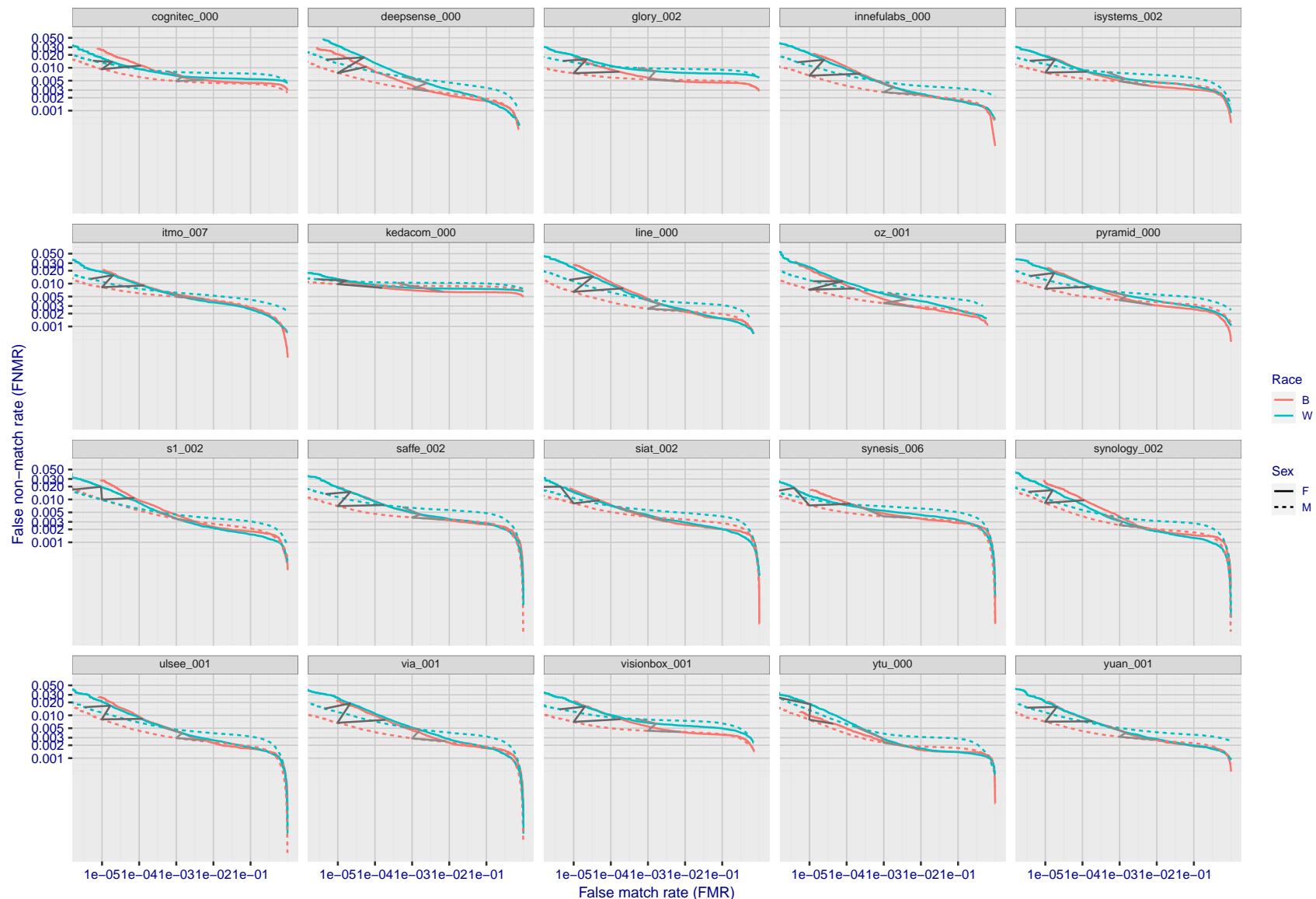


Figure 117: For the mugshot images, error tradeoff characteristics for white females, black females, black males and white males. The Z-shaped grey lines correspond to fixed thresholds, showing both FNMR and FMR vary at one T value. Note: Many of the plots will naively be read as saying women gives worse error rates than men because the solid traces lie above the dotted ones. However, this is misleading and incomplete: The grey lines show the traces reveal horizontal shifts. Thus for the cogent-003 algorithm FNMR for men is higher than for women at a fixed threshold but, at the same time, FMR is higher for women - see Figure 169. As access control systems almost always operate at a fixed threshold, the naive interpretation is incorrect.

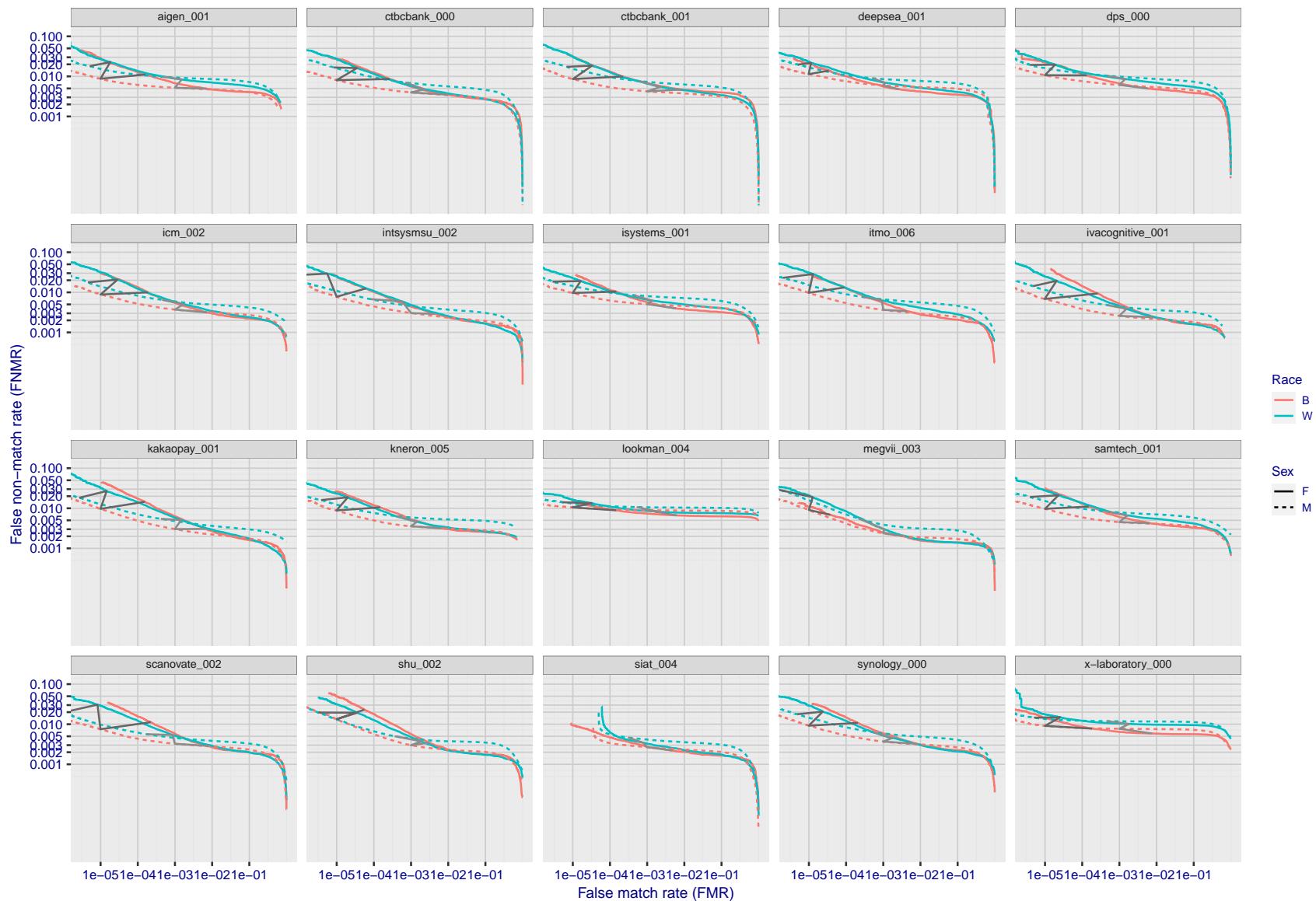


Figure 118: For the mugshot images, error tradeoff characteristics for white females, black females, black males and white males. The Z-shaped grey lines correspond to fixed thresholds, showing both FNMR and FMR vary at one T value. Note: Many of the plots will naively be read as saying women gives worse error rates than men because the solid traces lie above the dotted ones. However, this is misleading and incomplete: The grey lines show the traces reveal horizontal shifts. Thus for the cogent-003 algorithm FNMR for men is higher than for women at a fixed threshold but, at the same time, FMR is higher for women - see Figure 169. As access control systems almost always operate at a fixed threshold, the naive interpretation is incorrect.

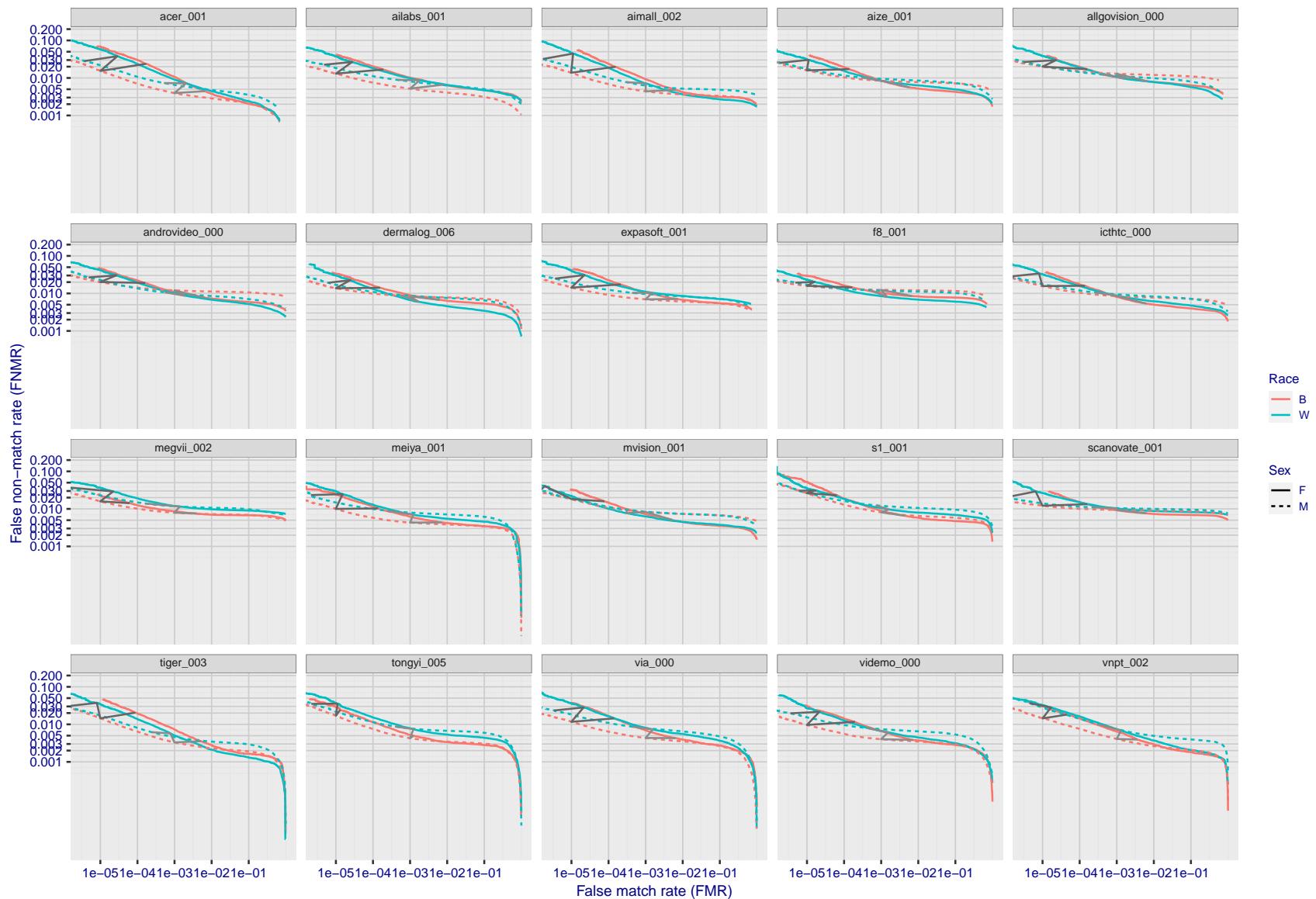


Figure 119: For the mugshot images, error tradeoff characteristics for white females, black females, black males and white males. The Z-shaped grey lines correspond to fixed thresholds, showing both FNMR and FMR vary at one T value. Note: Many of the plots will naively be read as saying women gives worse error rates than men because the solid traces lie above the dotted ones. However, this is misleading and incomplete: The grey lines show the traces reveal horizontal shifts. Thus for the cogent-003 algorithm FNMR for men is higher than for women at a fixed threshold but, at the same time, FMR is higher for women - see Figure 169. As access control systems almost always operate at a fixed threshold, the naive interpretation is incorrect.

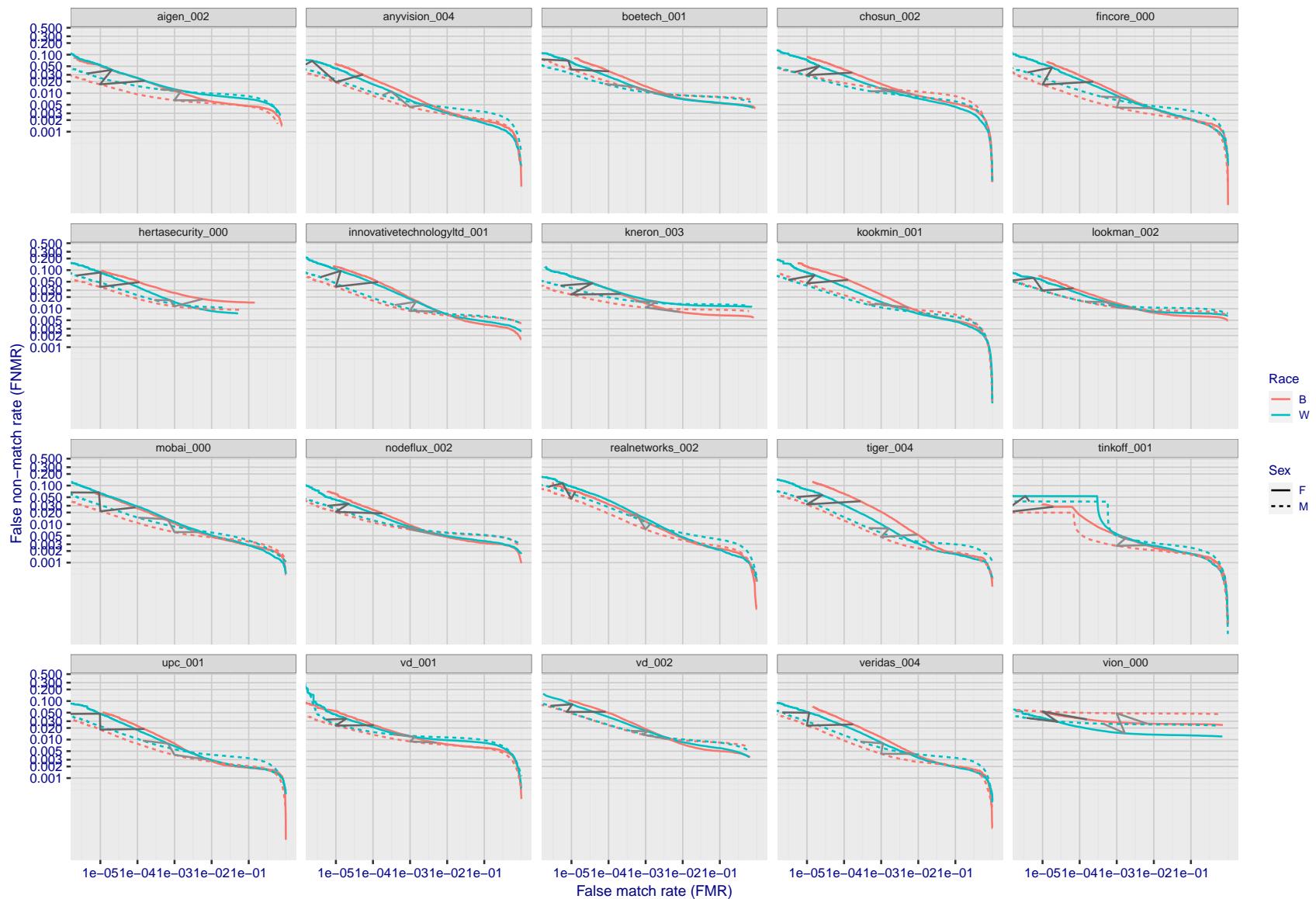


Figure 120: For the mugshot images, error tradeoff characteristics for white females, black females, black males and white males. The Z-shaped grey lines correspond to fixed thresholds, showing both FNMR and FMR vary at one T value. Note: Many of the plots will naively be read as saying women gives worse error rates than men because the solid traces lie above the dotted ones. However, this is misleading and incomplete: The grey lines show the traces reveal horizontal shifts. Thus for the cogent-003 algorithm FNMR for men is higher than for women at a fixed threshold but, at the same time, FMR is higher for women - see Figure 169. As access control systems almost always operate at a fixed threshold, the naive interpretation is incorrect.

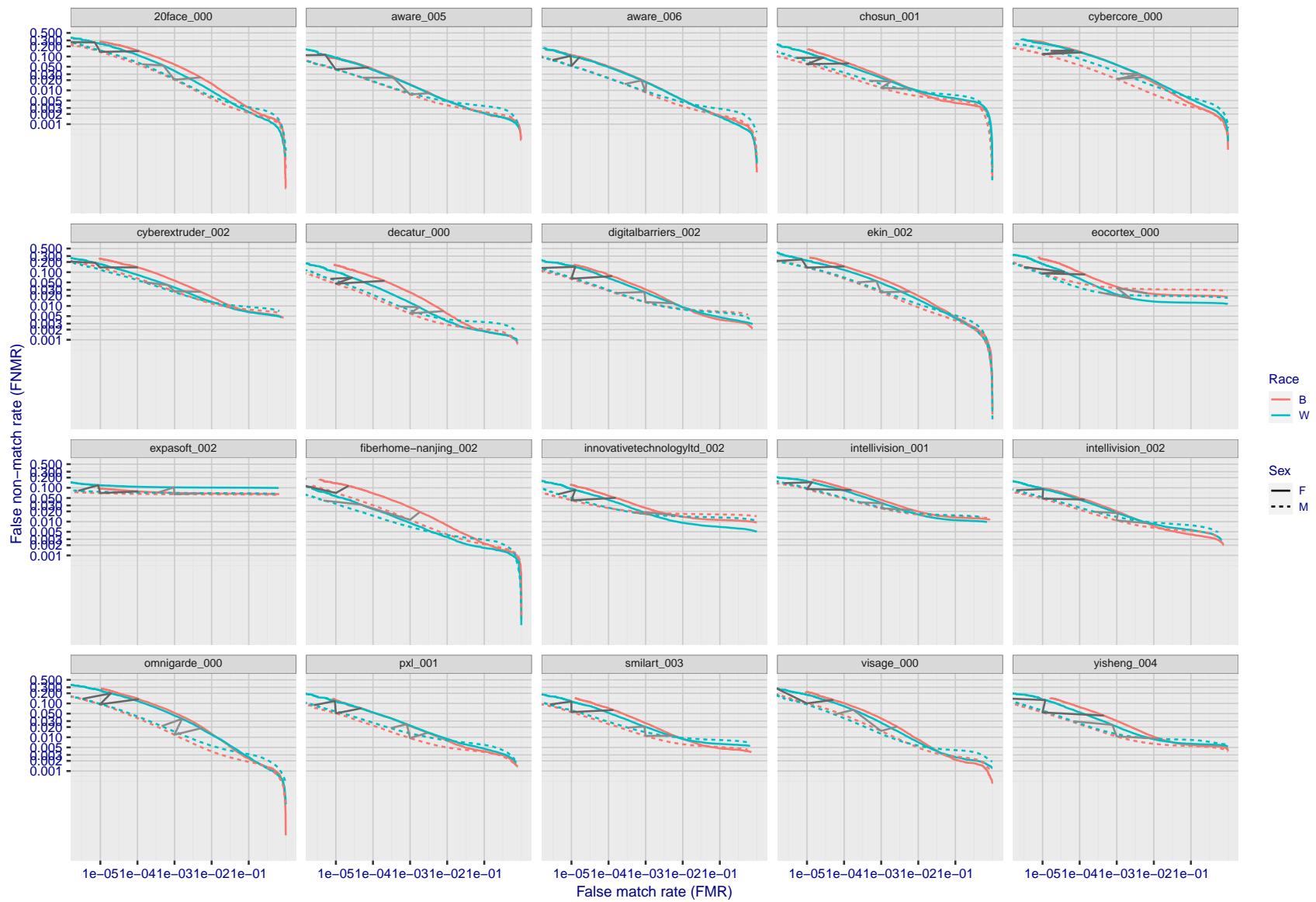


Figure 121: For the mugshot images, error tradeoff characteristics for white females, black females, black males and white males. The Z-shaped grey lines correspond to fixed thresholds, showing both FNMR and FMR vary at one T value. Note: Many of the plots will naively be read as saying women gives worse error rates than men because the solid traces lie above the dotted ones. However, this is misleading and incomplete: The grey lines show the traces reveal horizontal shifts. Thus for the cogent-003 algorithm FNMR for men is higher than for women at a fixed threshold but, at the same time, FMR is higher for women - see Figure 169. As access control systems almost always operate at a fixed threshold, the naive interpretation is incorrect.

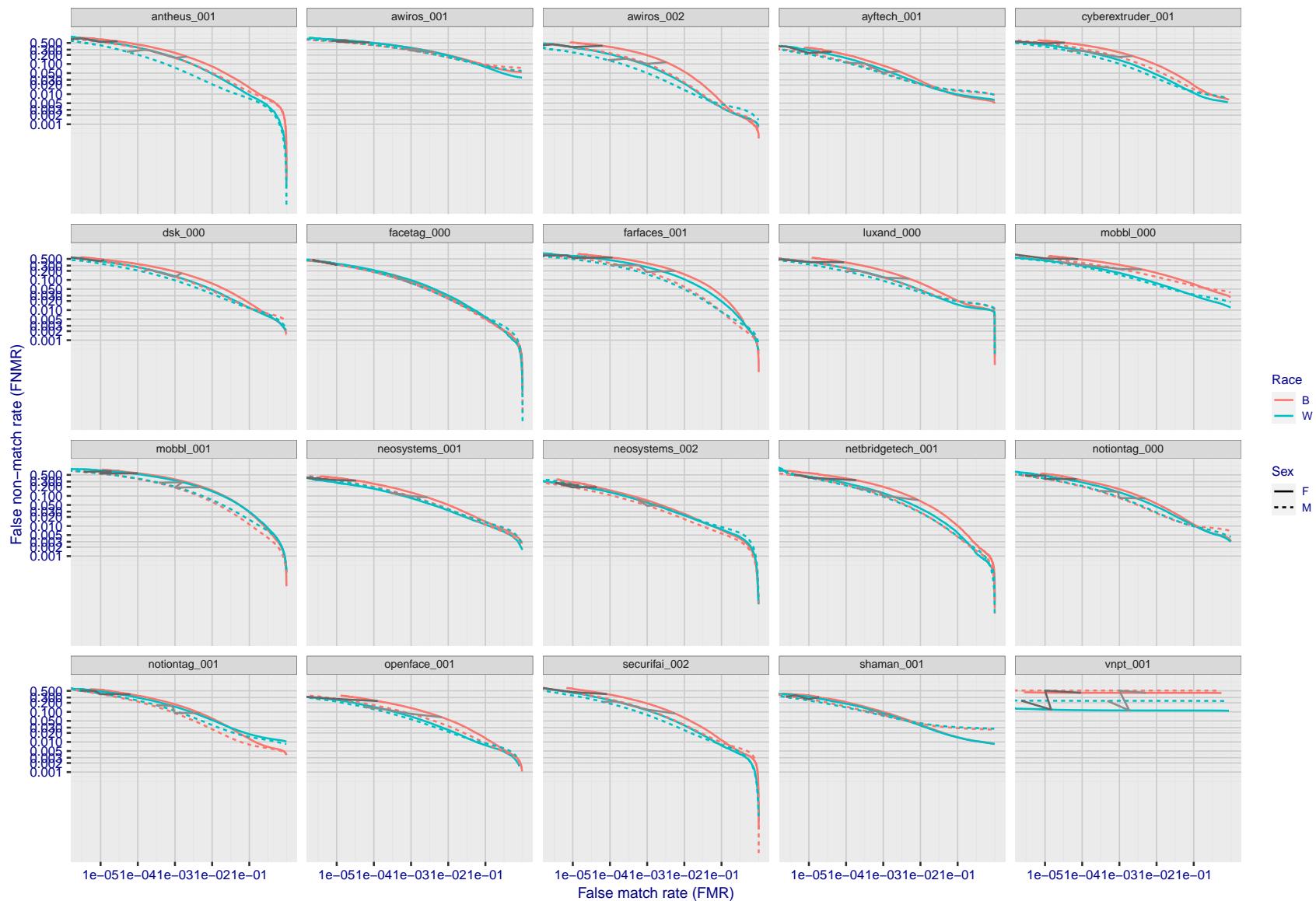


Figure 122: For the mugshot images, error tradeoff characteristics for white females, black females, black males and white males. The Z-shaped grey lines correspond to fixed thresholds, showing both FNMR and FMR vary at one T value. Note: Many of the plots will naively be read as saying women gives worse error rates than men because the solid traces lie above the dotted ones. However, this is misleading and incomplete: The grey lines show the traces reveal horizontal shifts. Thus for the cogent-003 algorithm FNMR for men is higher than for women at a fixed threshold but, at the same time, FMR is higher for women - see Figure 169. As access control systems almost always operate at a fixed threshold, the naive interpretation is incorrect.

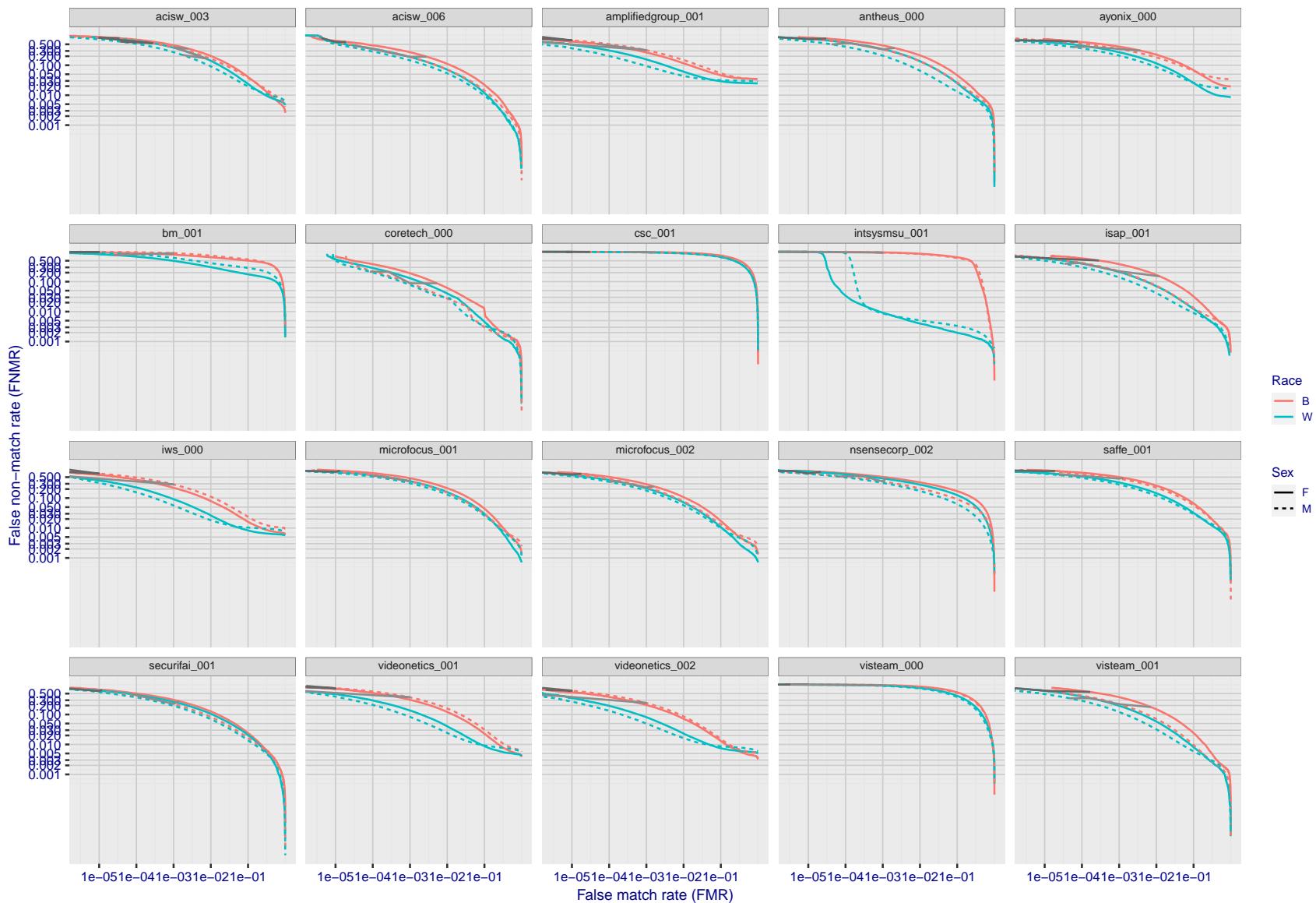


Figure 123: For the mugshot images, error tradeoff characteristics for white females, black females, black males and white males. The Z-shaped grey lines correspond to fixed thresholds, showing both FNMR and FMR vary at one T value. Note: Many of the plots will naively be read as saying women gives worse error rates than men because the solid traces lie above the dotted ones. However, this is misleading and incomplete: The grey lines show the traces reveal horizontal shifts. Thus for the cogent-003 algorithm FNMR for men is higher than for women at a fixed threshold but, at the same time, FMR is higher for women - see Figure 169. As access control systems almost always operate at a fixed threshold, the naive interpretation is incorrect.

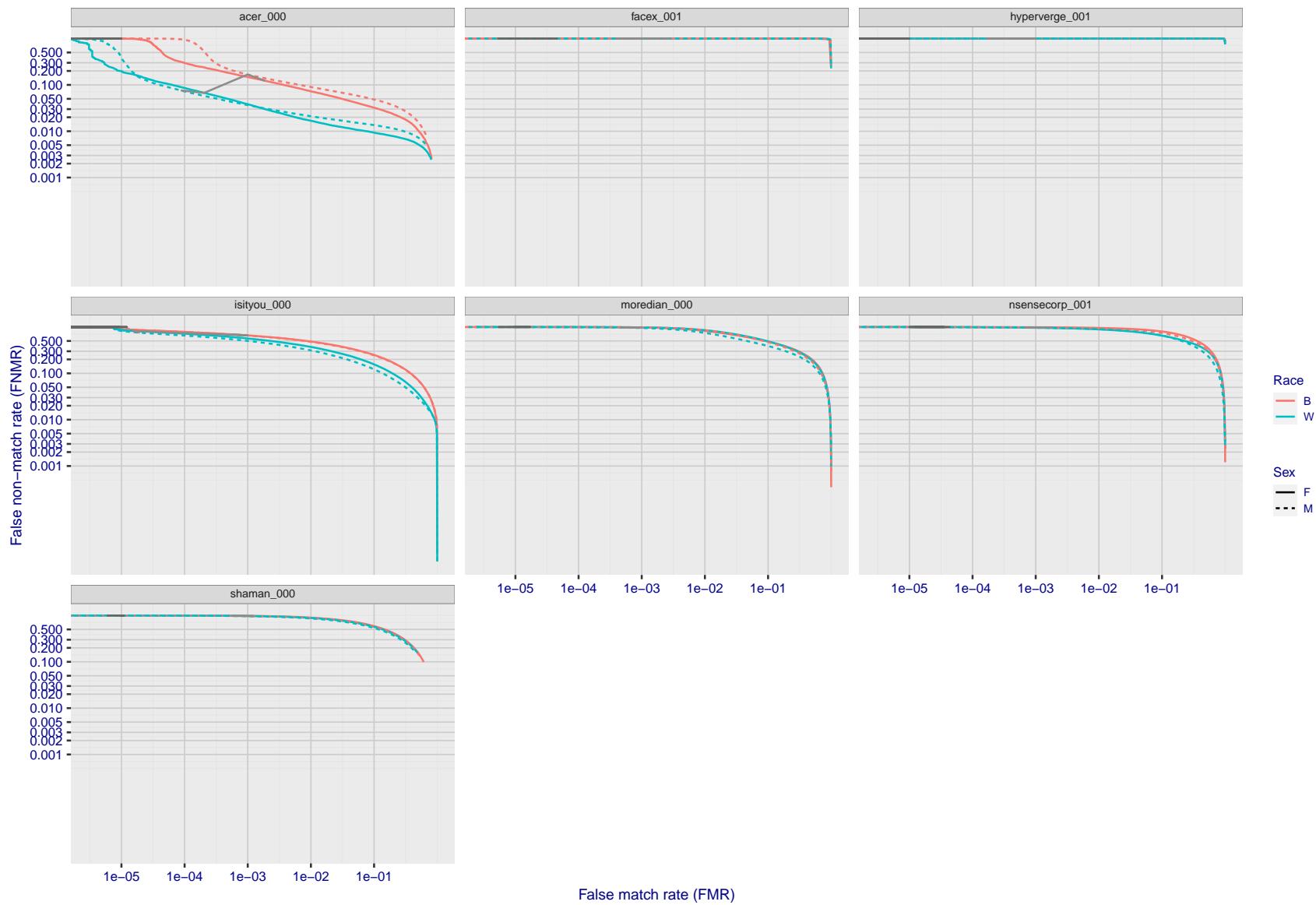


Figure 124: For the mugshot images, error tradeoff characteristics for white females, black females, black males and white males. The Z-shaped grey lines correspond to fixed thresholds, showing both FNMR and FMR vary at one T value. Note: Many of the plots will naively be read as saying women gives worse error rates than men because the solid traces lie above the dotted ones. However, this is misleading and incomplete: The grey lines show the traces reveal horizontal shifts. Thus for the cogent-003 algorithm FNMR for men is higher than for women at a fixed threshold but, at the same time, FMR is higher for women - see Figure 169. As access control systems almost always operate at a fixed threshold, the naive interpretation is incorrect.

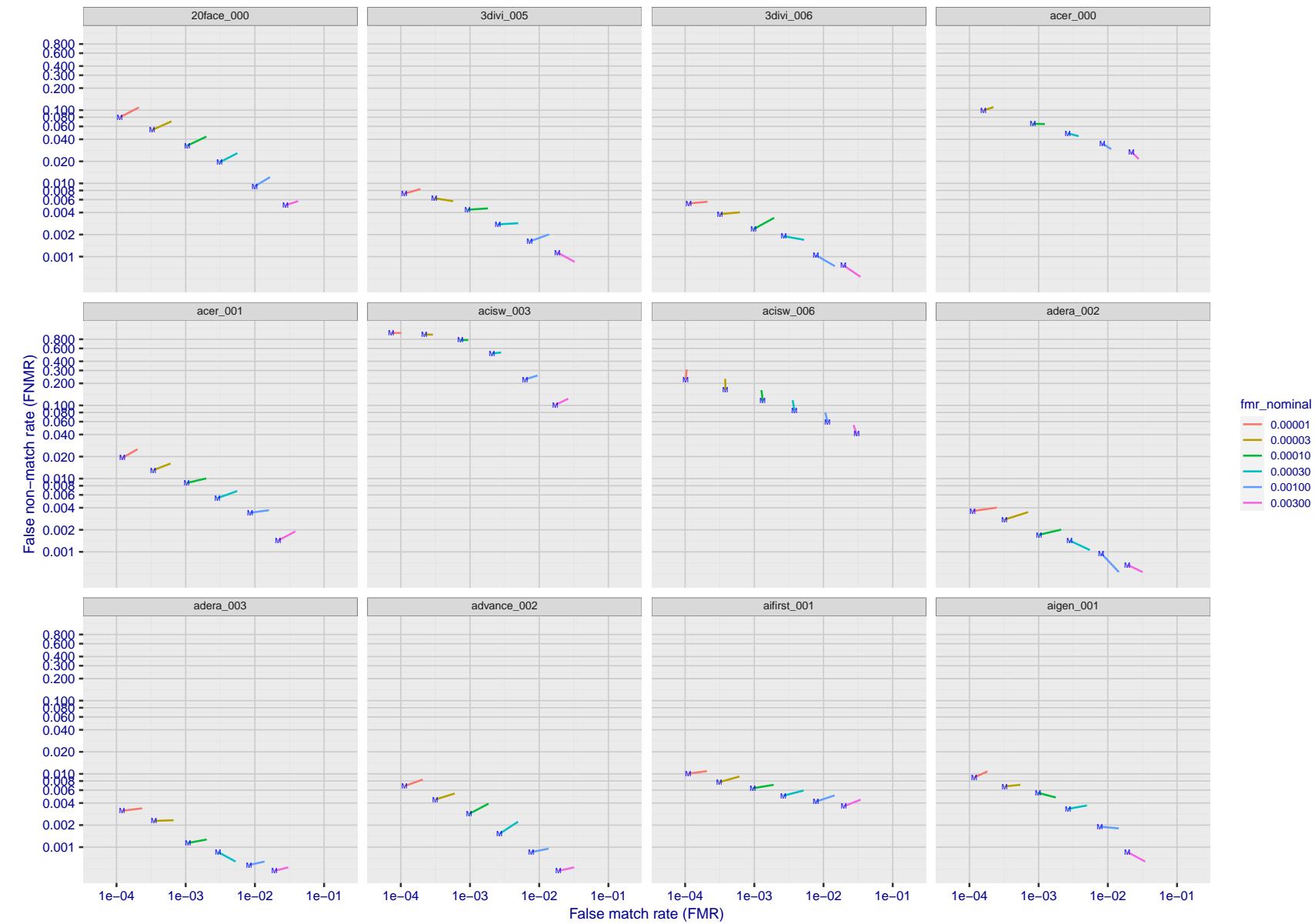


Figure 125: For the visa images, FNMR and FMR at six operating points along the DET characteristic. At each point a line is drawn between $(FMR, FNMR)_{MALE}$ and $(FMR, FNMR)_{FEMALE}$ showing how which sex has lower FMR and/or FNMR. The "M" label denotes male, the other end of the line corresponds to female. The six operating thresholds are selected to give the nominal false match rates given in the legend, and are computed over all impostor pairs regardless of age, sex, and place of birth. The plotted FMR values are broadly an order of magnitude larger than the nominal rates because FMR is computed over demographically-matched impostor pairs i.e individuals of the same sex, from the same geographic region (see section 3.6.1), and the same age group (see section 3.6.2).

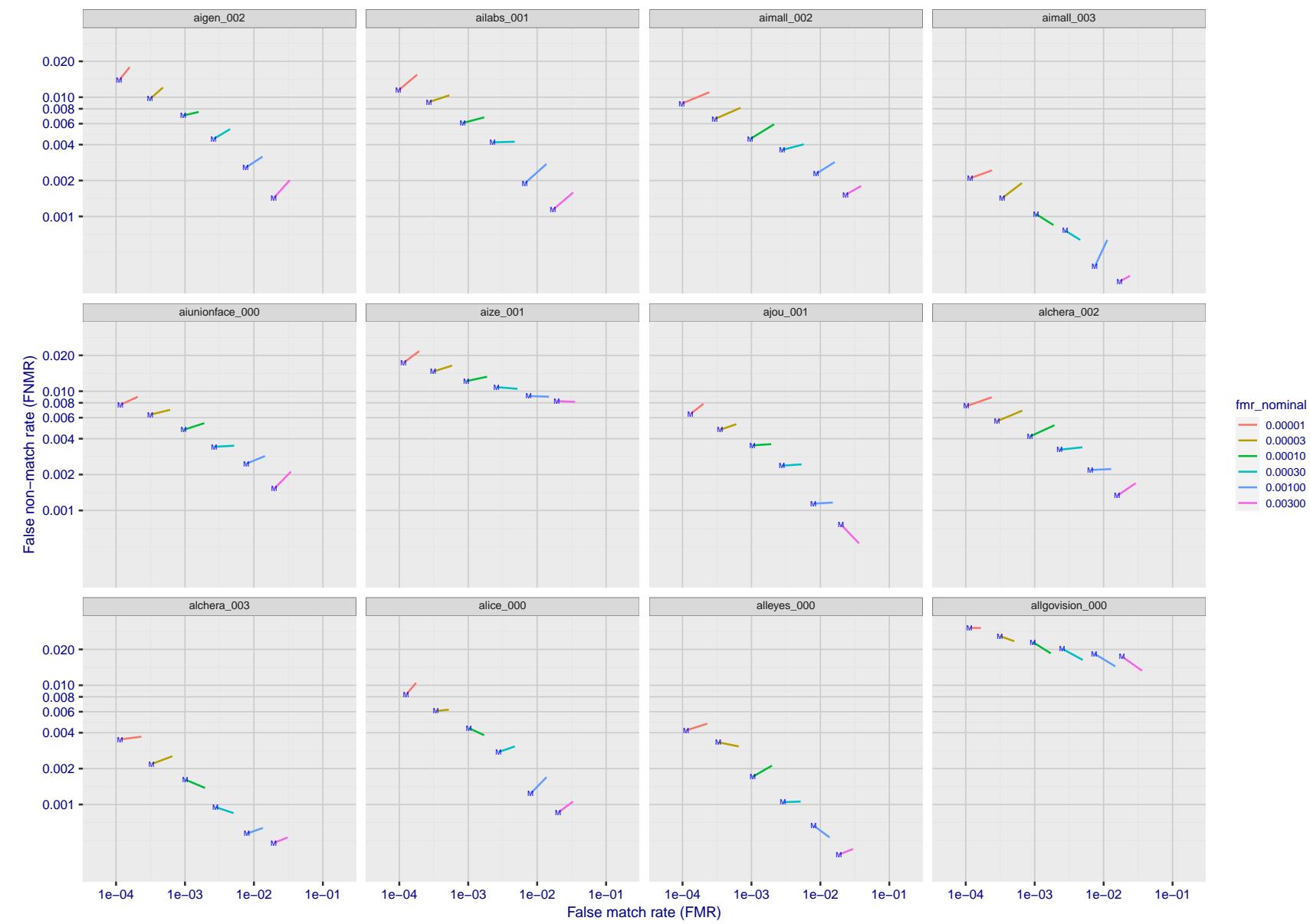


Figure 126: For the visa images, FNMR and FMR at six operating points along the DET characteristic. At each point a line is drawn between $(FMR, FNMR)_{MALE}$ and $(FMR, FNMR)_{FEMALE}$ showing how which sex has lower FMR and/or FNMR. The "M" label denotes male, the other end of the line corresponds to female. The six operating thresholds are selected to give the nominal false match rates given in the legend, and are computed over all impostor pairs regardless of age, sex, and place of birth. The plotted FMR values are broadly an order of magnitude larger than the nominal rates because FMR is computed over demographically-matched impostor pairs i.e individuals of the same sex, from the same geographic region (see section 3.6.1), and the same age group (see section 3.6.2).

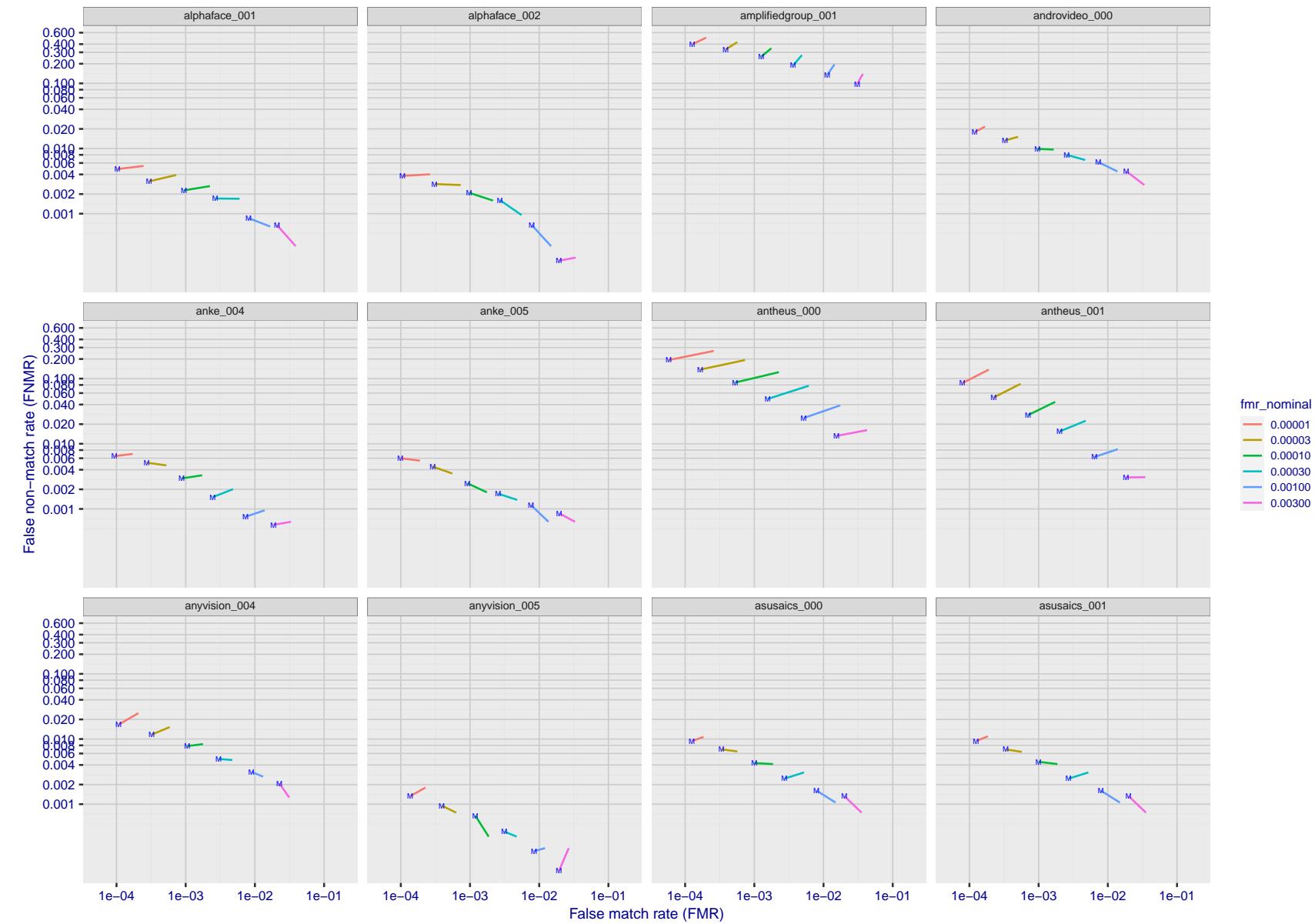


Figure 127: For the visa images, FNMR and FMR at six operating points along the DET characteristic. At each point a line is drawn between $(FMR, FNMR)_{MALE}$ and $(FMR, FNMR)_{FEMALE}$ showing how which sex has lower FMR and/or FNMR. The "M" label denotes male, the other end of the line corresponds to female. The six operating thresholds are selected to give the nominal false match rates given in the legend, and are computed over all impostor pairs regardless of age, sex, and place of birth. The plotted FMR values are broadly an order of magnitude larger than the nominal rates because FMR is computed over demographically-matched impostor pairs i.e individuals of the same sex, from the same geographic region (see section 3.6.1), and the same age group (see section 3.6.2).

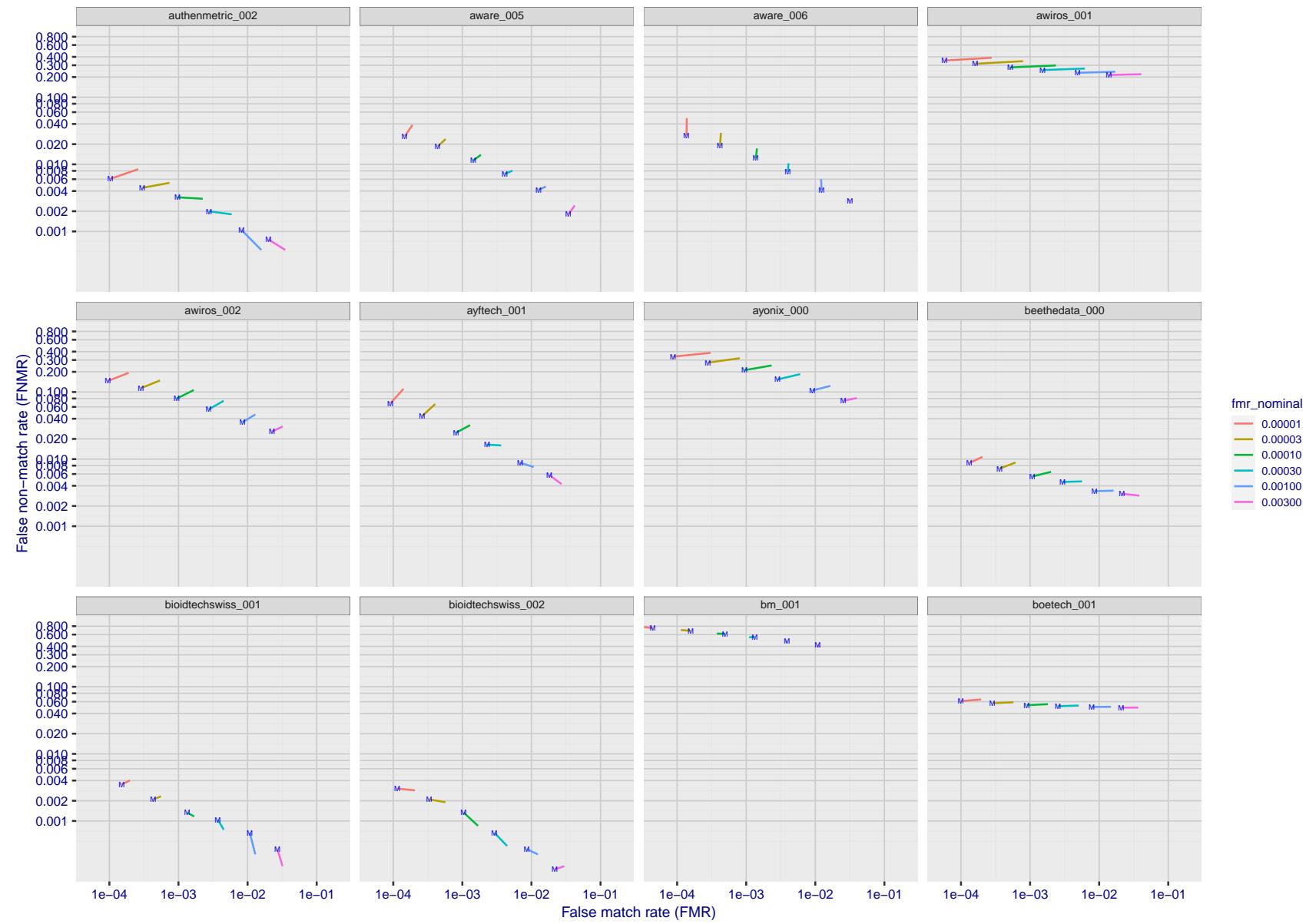


Figure 128: For the visa images, FNMR and FMR at six operating points along the DET characteristic. At each point a line is drawn between $(FMR, FNMR)_{MALE}$ and $(FMR, FNMR)_{FEMALE}$ showing how which sex has lower FMR and/or FNMR. The "M" label denotes male, the other end of the line corresponds to female. The six operating thresholds are selected to give the nominal false match rates given in the legend, and are computed over all impostor pairs regardless of age, sex, and place of birth. The plotted FMR values are broadly an order of magnitude larger than the nominal rates because FMR is computed over demographically-matched impostor pairs i.e individuals of the same sex, from the same geographic region (see section 3.6.1), and the same age group (see section 3.6.2).

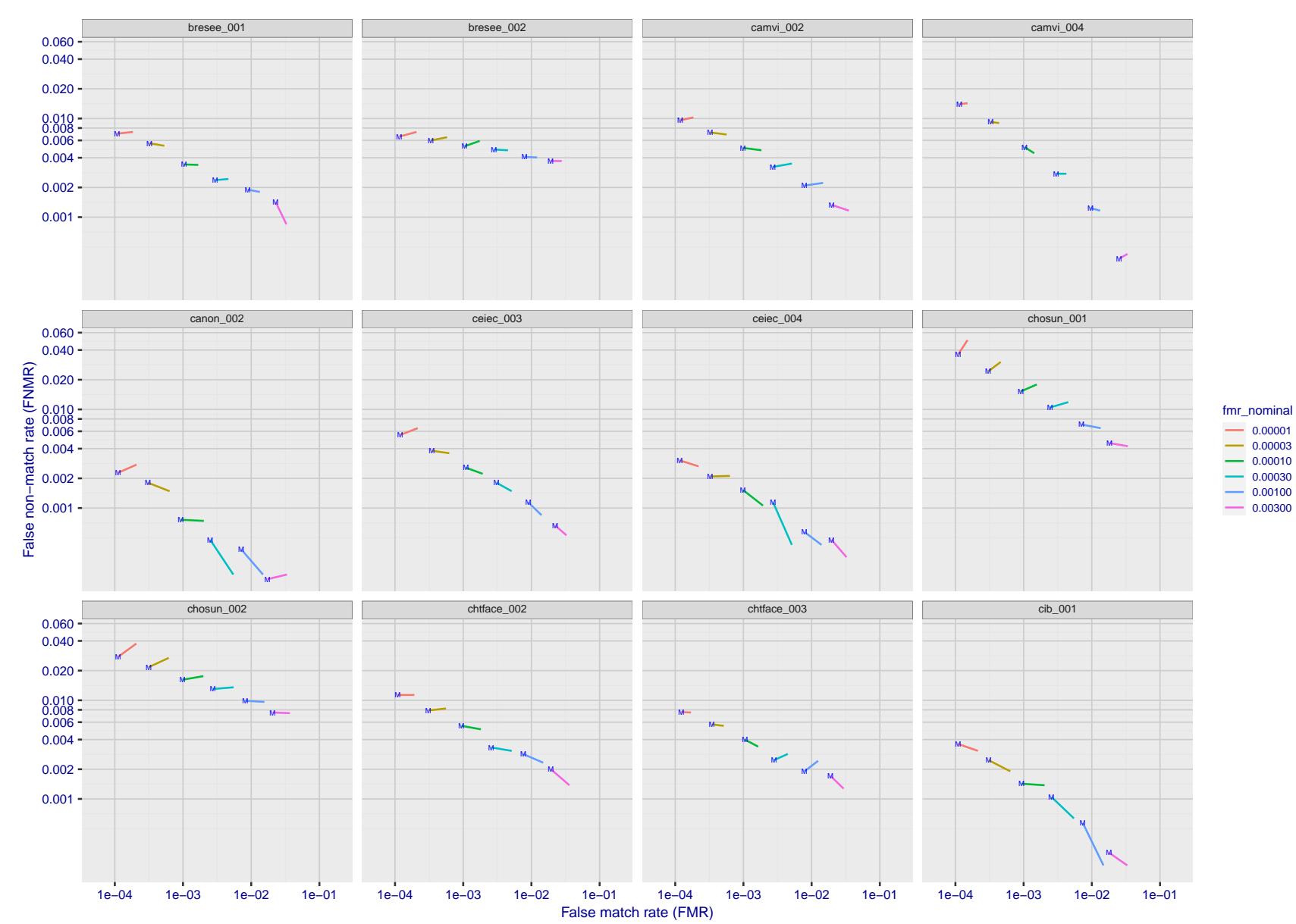


Figure 129: For the visa images, FNMR and FMR at six operating points along the DET characteristic. At each point a line is drawn between $(FMR, FNMR)_{MALE}$ and $(FMR, FNMR)_{FEMALE}$ showing how which sex has lower FMR and/or FNMR. The "M" label denotes male, the other end of the line corresponds to female. The six operating thresholds are selected to give the nominal false match rates given in the legend, and are computed over all impostor pairs regardless of age, sex, and place of birth. The plotted FMR values are broadly an order of magnitude larger than the nominal rates because FMR is computed over demographically-matched impostor pairs i.e individuals of the same sex, from the same geographic region (see section 3.6.1), and the same age group (see section 3.6.2).

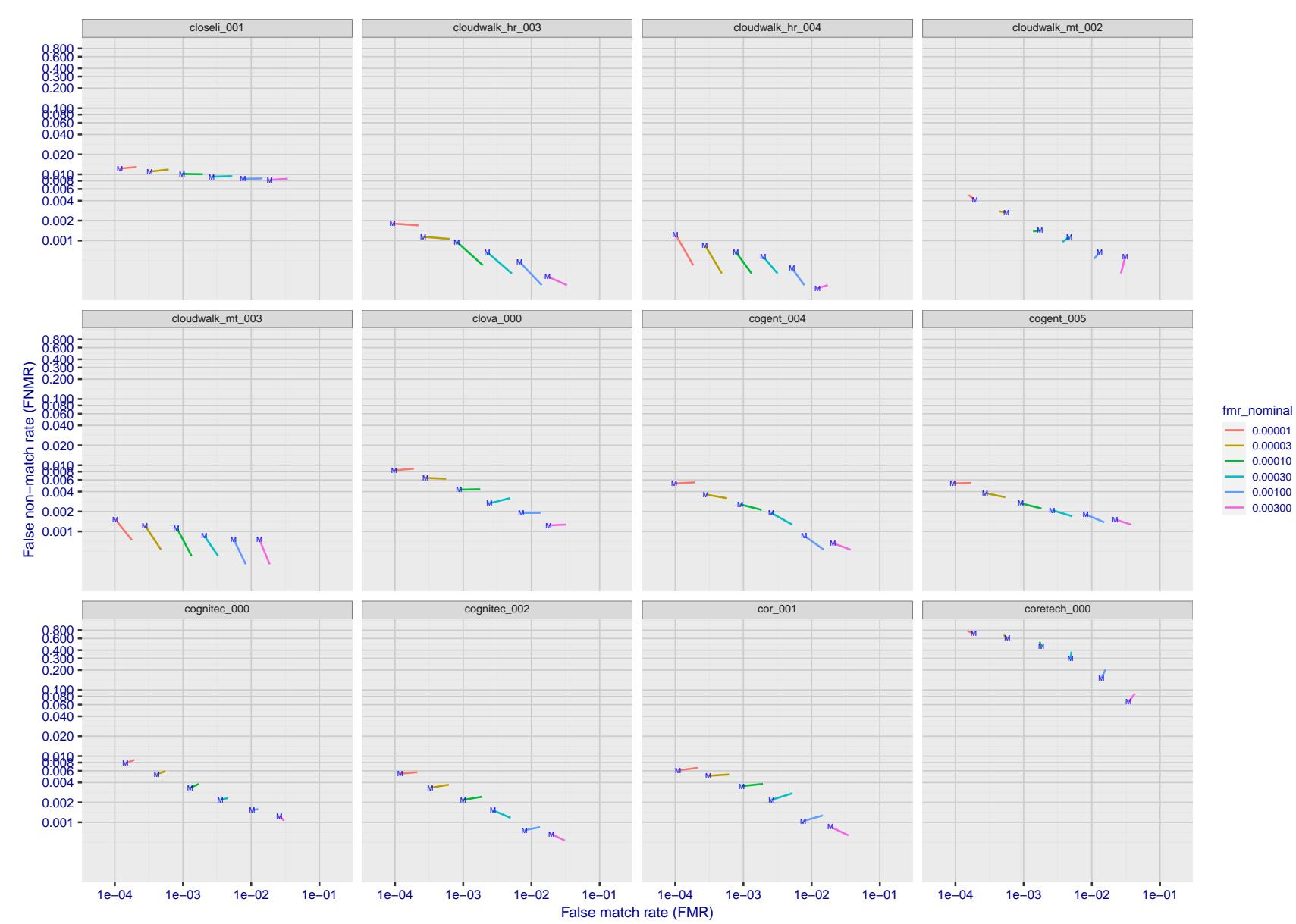


Figure 130: For the visa images, FNMR and FMR at six operating points along the DET characteristic. At each point a line is drawn between $(FMR, FNMR)_{MALE}$ and $(FMR, FNMR)_{FEMALE}$ showing how which sex has lower FMR and/or FNMR. The "M" label denotes male, the other end of the line corresponds to female. The six operating thresholds are selected to give the nominal false match rates given in the legend, and are computed over all impostor pairs regardless of age, sex, and place of birth. The plotted FMR values are broadly an order of magnitude larger than the nominal rates because FMR is computed over demographically-matched impostor pairs i.e individuals of the same sex, from the same geographic region (see section 3.6.1), and the same age group (see section 3.6.2).

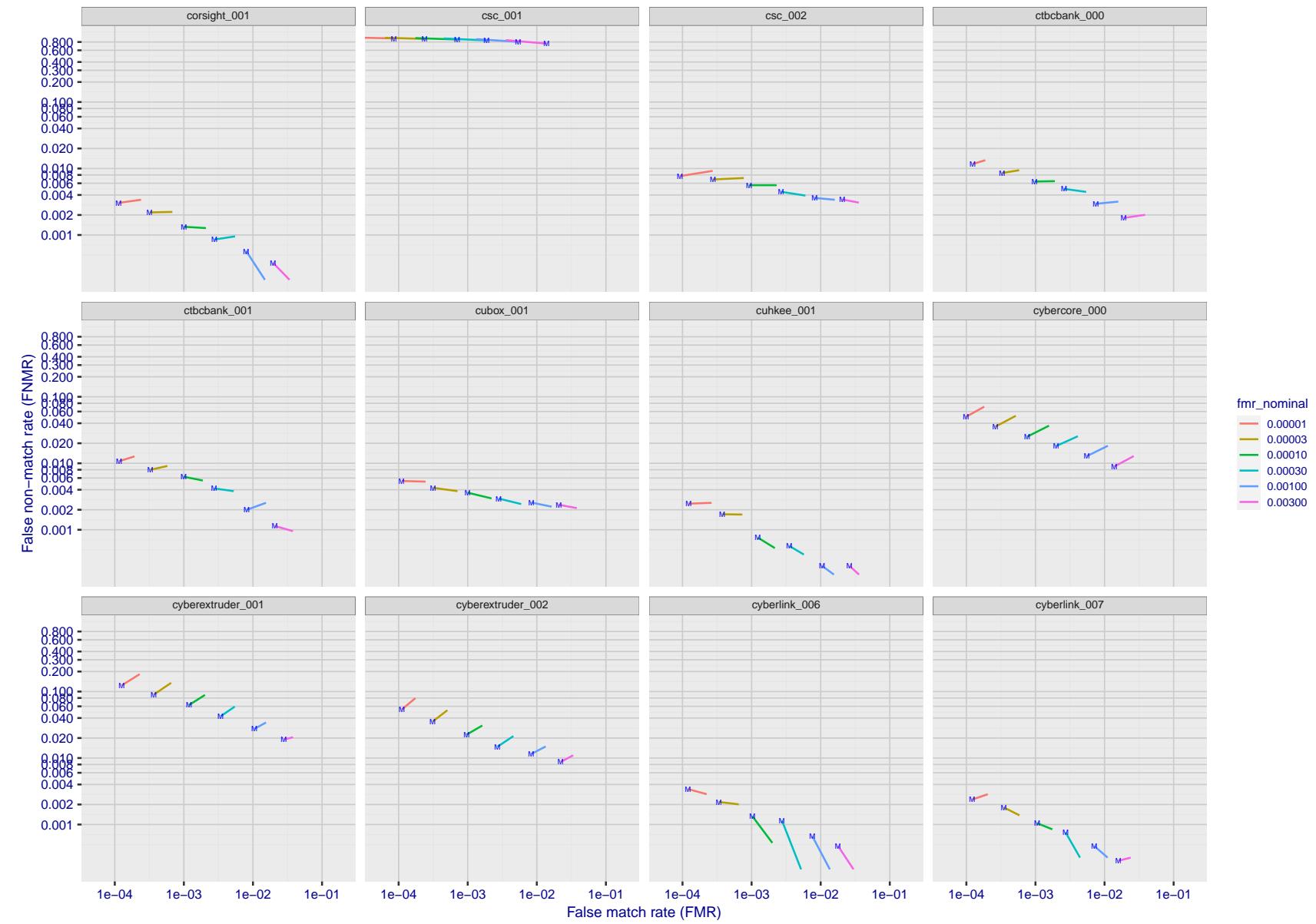


Figure 131: For the visa images, FNMR and FMR at six operating points along the DET characteristic. At each point a line is drawn between $(FMR, FNMR)_{MALE}$ and $(FMR, FNMR)_{FEMALE}$ showing how which sex has lower FMR and/or FNMR. The "M" label denotes male, the other end of the line corresponds to female. The six operating thresholds are selected to give the nominal false match rates given in the legend, and are computed over all impostor pairs regardless of age, sex, and place of birth. The plotted FMR values are broadly an order of magnitude larger than the nominal rates because FMR is computed over demographically-matched impostor pairs i.e individuals of the same sex, from the same geographic region (see section 3.6.1), and the same age group (see section 3.6.2).

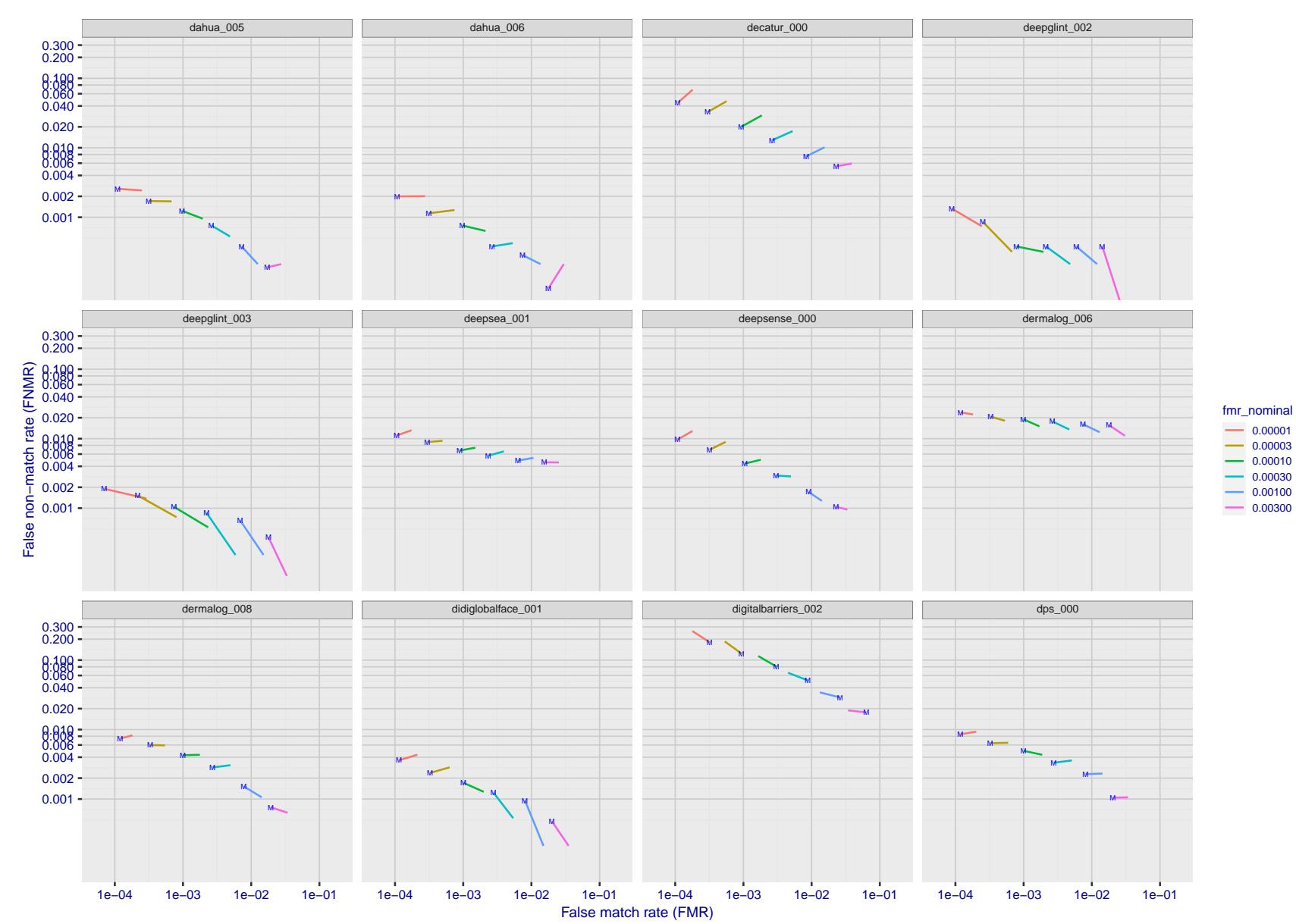


Figure 132: For the visa images, FNMR and FMR at six operating points along the DET characteristic. At each point a line is drawn between $(FMR, FNMR)_{MALE}$ and $(FMR, FNMR)_{FEMALE}$ showing how which sex has lower FMR and/or FNMR. The "M" label denotes male, the other end of the line corresponds to female. The six operating thresholds are selected to give the nominal false match rates given in the legend, and are computed over all impostor pairs regardless of age, sex, and place of birth. The plotted FMR values are broadly an order of magnitude larger than the nominal rates because FMR is computed over demographically-matched impostor pairs i.e individuals of the same sex, from the same geographic region (see section 3.6.1), and the same age group (see section 3.6.2).

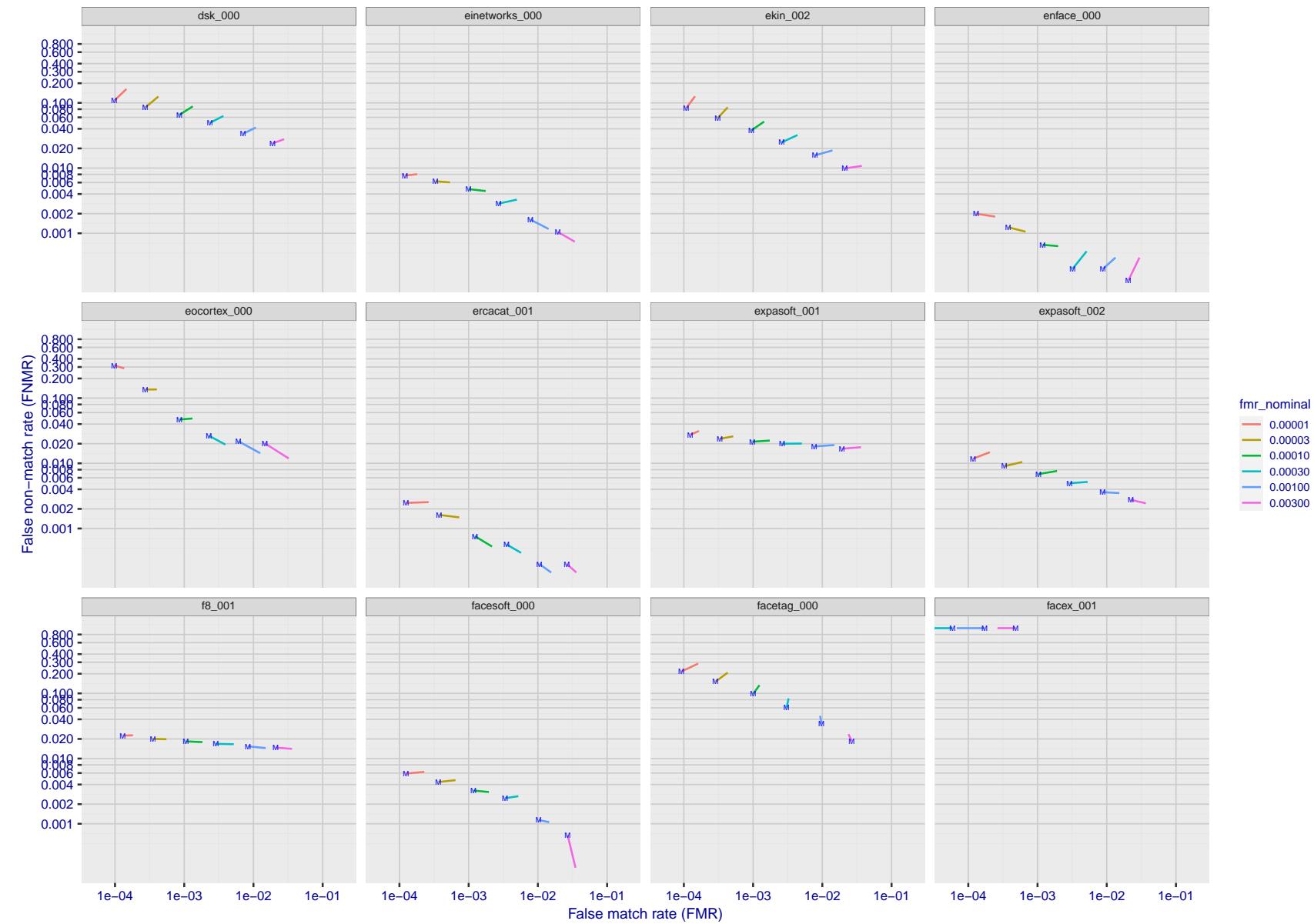


Figure 133: For the visa images, FNMR and FMR at six operating points along the DET characteristic. At each point a line is drawn between $(FMR, FNMR)_{MALE}$ and $(FMR, FNMR)_{FEMALE}$ showing how which sex has lower FMR and/or FNMR. The "M" label denotes male, the other end of the line corresponds to female. The six operating thresholds are selected to give the nominal false match rates given in the legend, and are computed over all impostor pairs regardless of age, sex, and place of birth. The plotted FMR values are broadly an order of magnitude larger than the nominal rates because FMR is computed over demographically-matched impostor pairs i.e individuals of the same sex, from the same geographic region (see section 3.6.1), and the same age group (see section 3.6.2).

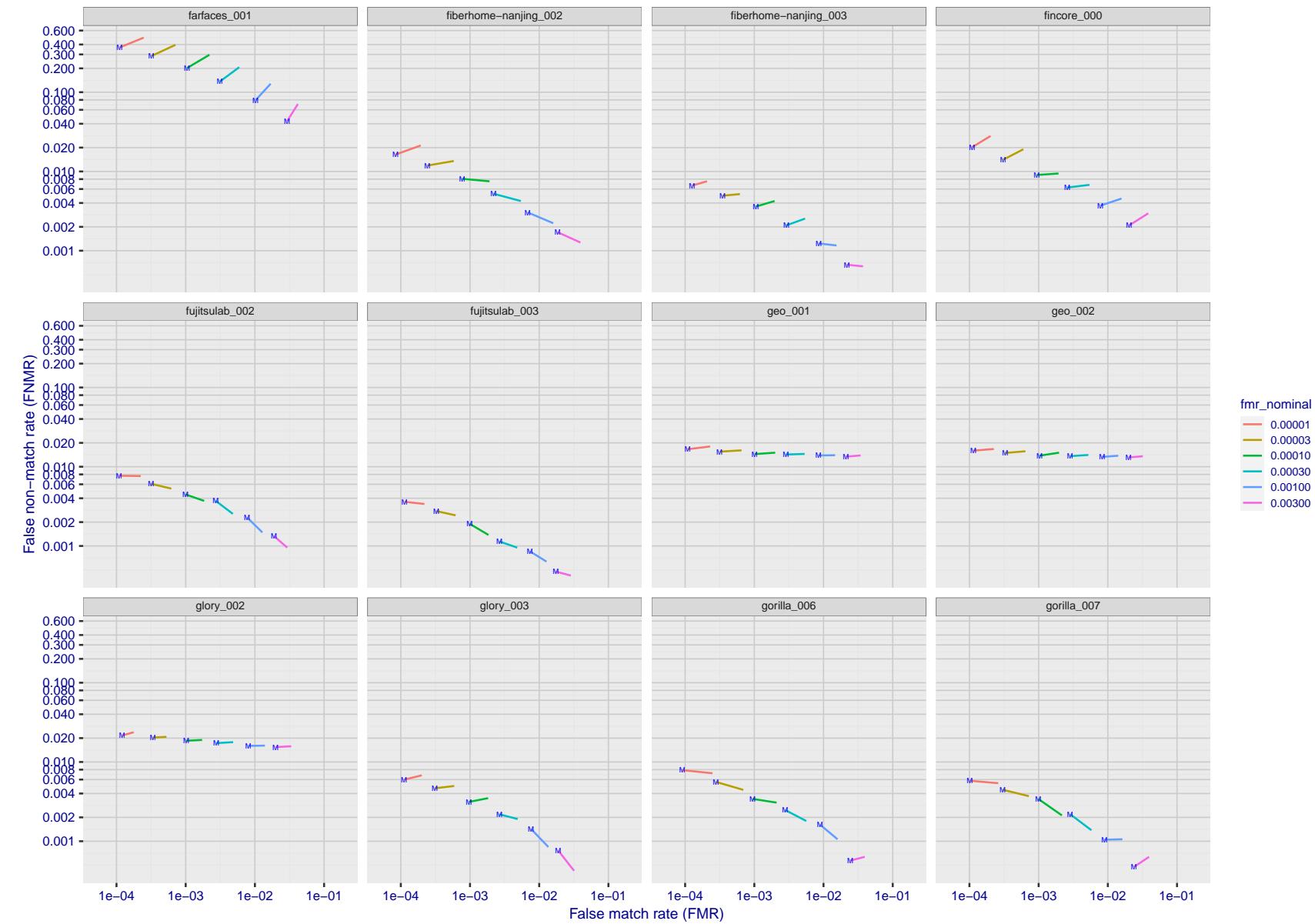


Figure 134: For the visa images, FNMR and FMR at six operating points along the DET characteristic. At each point a line is drawn between $(FMR, FNMR)_{MALE}$ and $(FMR, FNMR)_{FEMALE}$ showing how which sex has lower FMR and/or FNMR. The "M" label denotes male, the other end of the line corresponds to female. The six operating thresholds are selected to give the nominal false match rates given in the legend, and are computed over all impostor pairs regardless of age, sex, and place of birth. The plotted FMR values are broadly an order of magnitude larger than the nominal rates because FMR is computed over demographically-matched impostor pairs i.e individuals of the same sex, from the same geographic region (see section 3.6.1), and the same age group (see section 3.6.2).

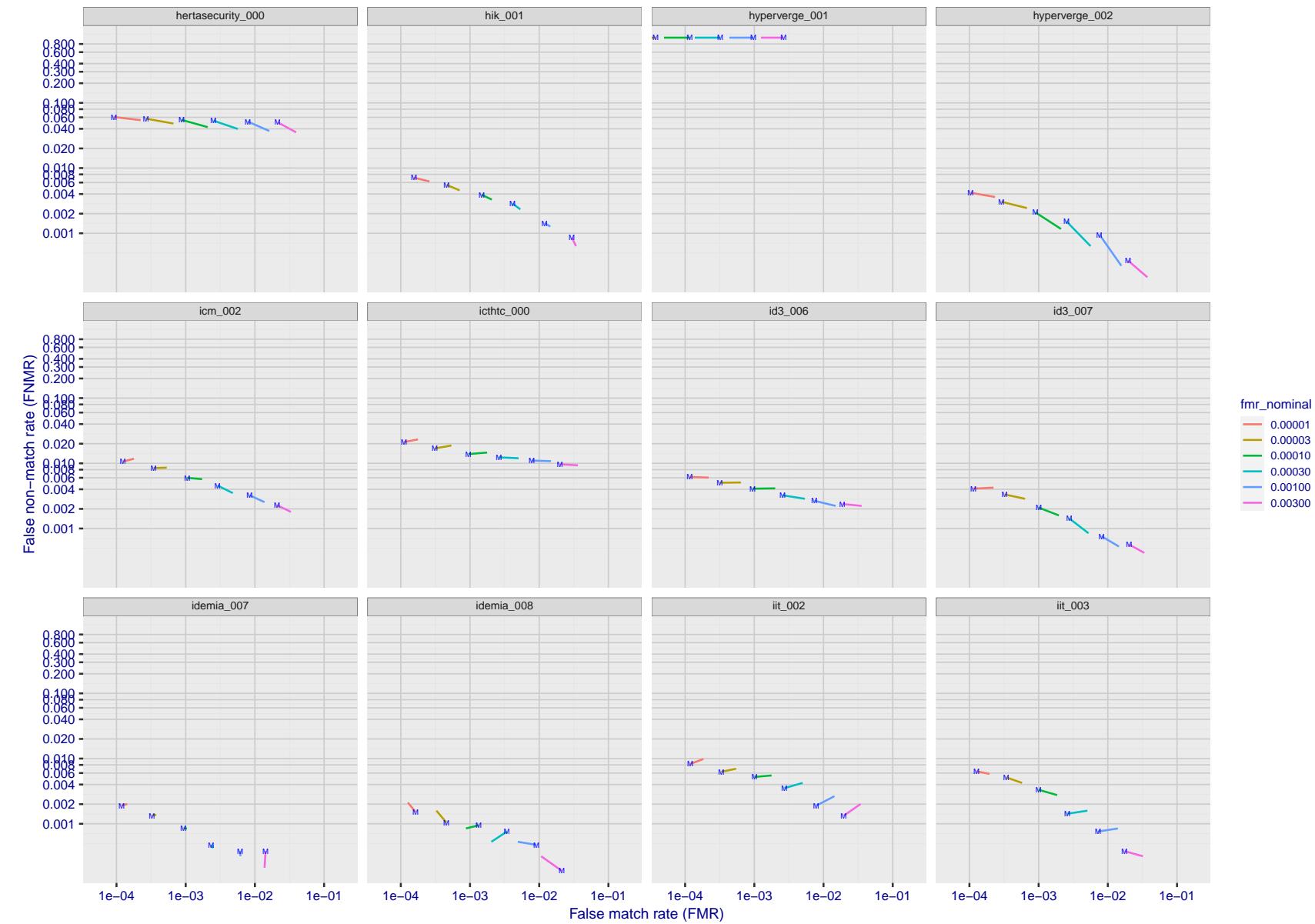


Figure 135: For the visa images, FNMR and FMR at six operating points along the DET characteristic. At each point a line is drawn between $(FMR, FNMR)_{MALE}$ and $(FMR, FNMR)_{FEMALE}$ showing how which sex has lower FMR and/or FNMR. The "M" label denotes male, the other end of the line corresponds to female. The six operating thresholds are selected to give the nominal false match rates given in the legend, and are computed over all impostor pairs regardless of age, sex, and place of birth. The plotted FMR values are broadly an order of magnitude larger than the nominal rates because FMR is computed over demographically-matched impostor pairs i.e individuals of the same sex, from the same geographic region (see section 3.6.1), and the same age group (see section 3.6.2).

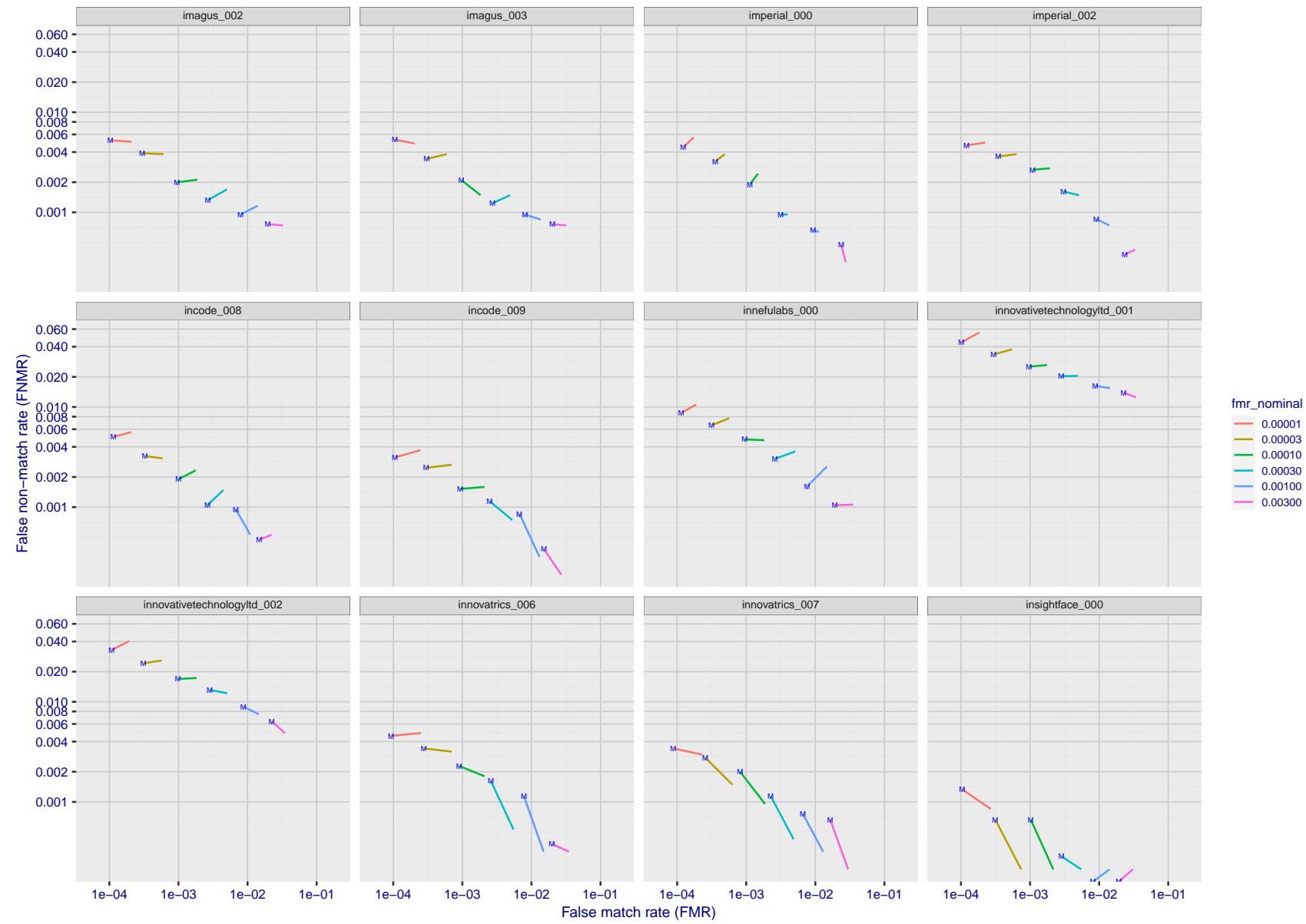


Figure 136: For the visa images, FNMR and FMR at six operating points along the DET characteristic. At each point a line is drawn between $(FMR, FNMR)_{MALE}$ and $(FMR, FNMR)_{FEMALE}$ showing how which sex has lower FMR and/or FNMR. The "M" label denotes male, the other end of the line corresponds to female. The six operating thresholds are selected to give the nominal false match rates given in the legend, and are computed over all impostor pairs regardless of age, sex, and place of birth. The plotted FMR values are broadly an order of magnitude larger than the nominal rates because FMR is computed over demographically-matched impostor pairs i.e individuals of the same sex, from the same geographic region (see section 3.6.1), and the same age group (see section 3.6.2).

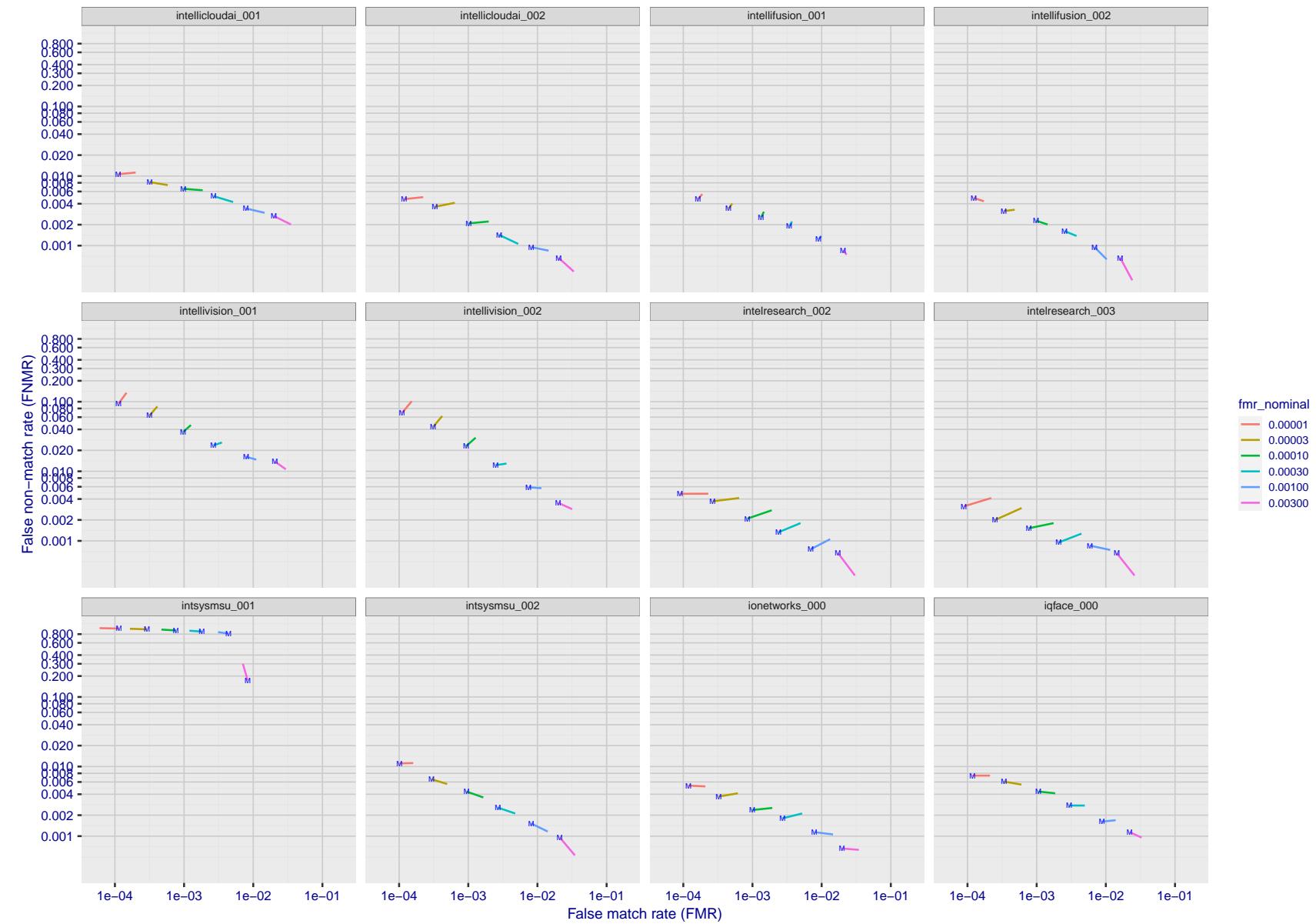


Figure 137: For the visa images, FNMR and FMR at six operating points along the DET characteristic. At each point a line is drawn between $(FMR, FNMR)_{MALE}$ and $(FMR, FNMR)_{FEMALE}$ showing how which sex has lower FMR and/or FNMR. The "M" label denotes male, the other end of the line corresponds to female. The six operating thresholds are selected to give the nominal false match rates given in the legend, and are computed over all impostor pairs regardless of age, sex, and place of birth. The plotted FMR values are broadly an order of magnitude larger than the nominal rates because FMR is computed over demographically-matched impostor pairs i.e individuals of the same sex, from the same geographic region (see section 3.6.1), and the same age group (see section 3.6.2).

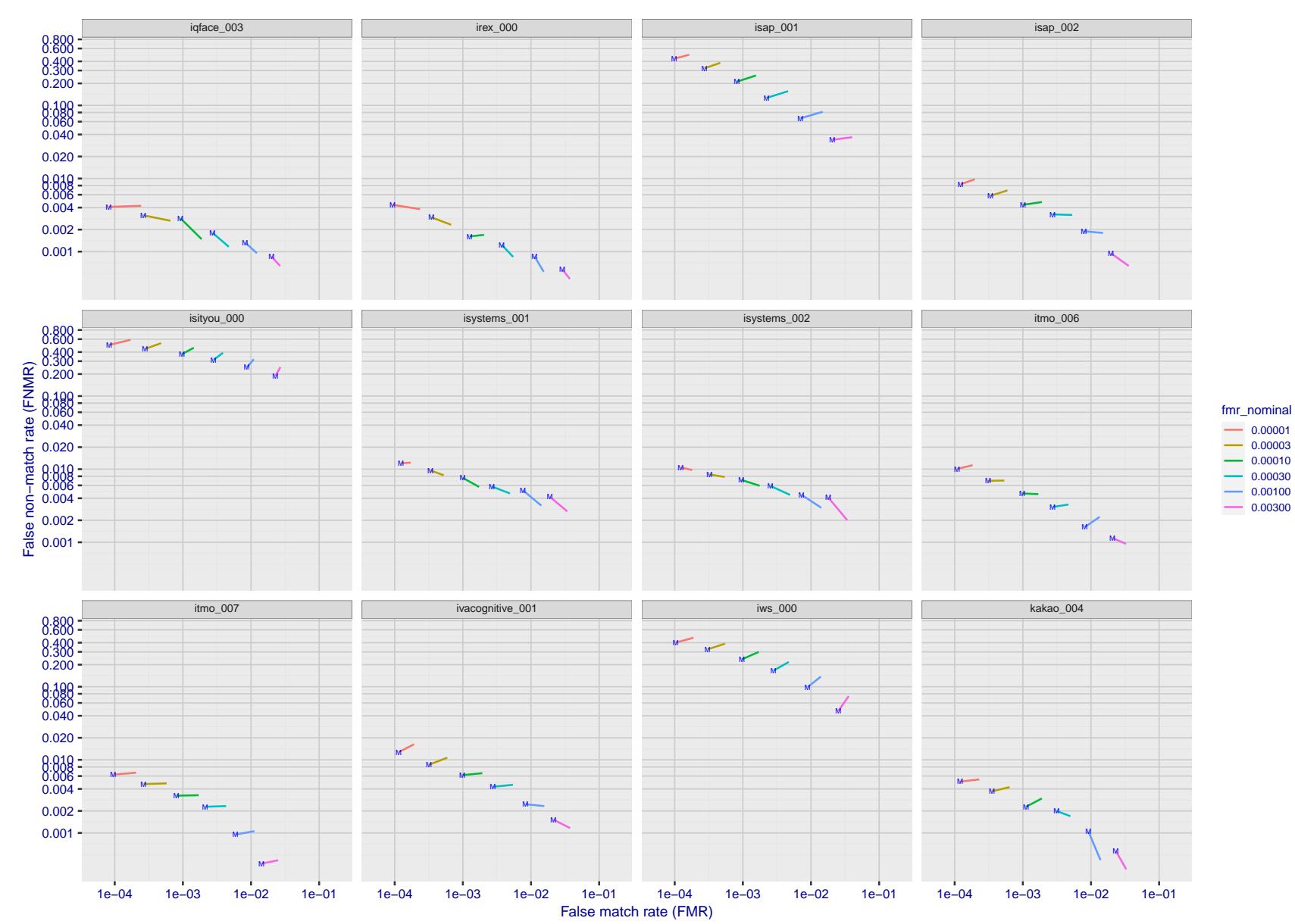


Figure 138: For the visa images, FNMR and FMR at six operating points along the DET characteristic. At each point a line is drawn between $(FMR, FNMR)_{MALE}$ and $(FMR, FNMR)_{FEMALE}$ showing how which sex has lower FMR and/or FNMR. The "M" label denotes male, the other end of the line corresponds to female. The six operating thresholds are selected to give the nominal false match rates given in the legend, and are computed over all impostor pairs regardless of age, sex, and place of birth. The plotted FMR values are broadly an order of magnitude larger than the nominal rates because FMR is computed over demographically-matched impostor pairs i.e individuals of the same sex, from the same geographic region (see section 3.6.1), and the same age group (see section 3.6.2).

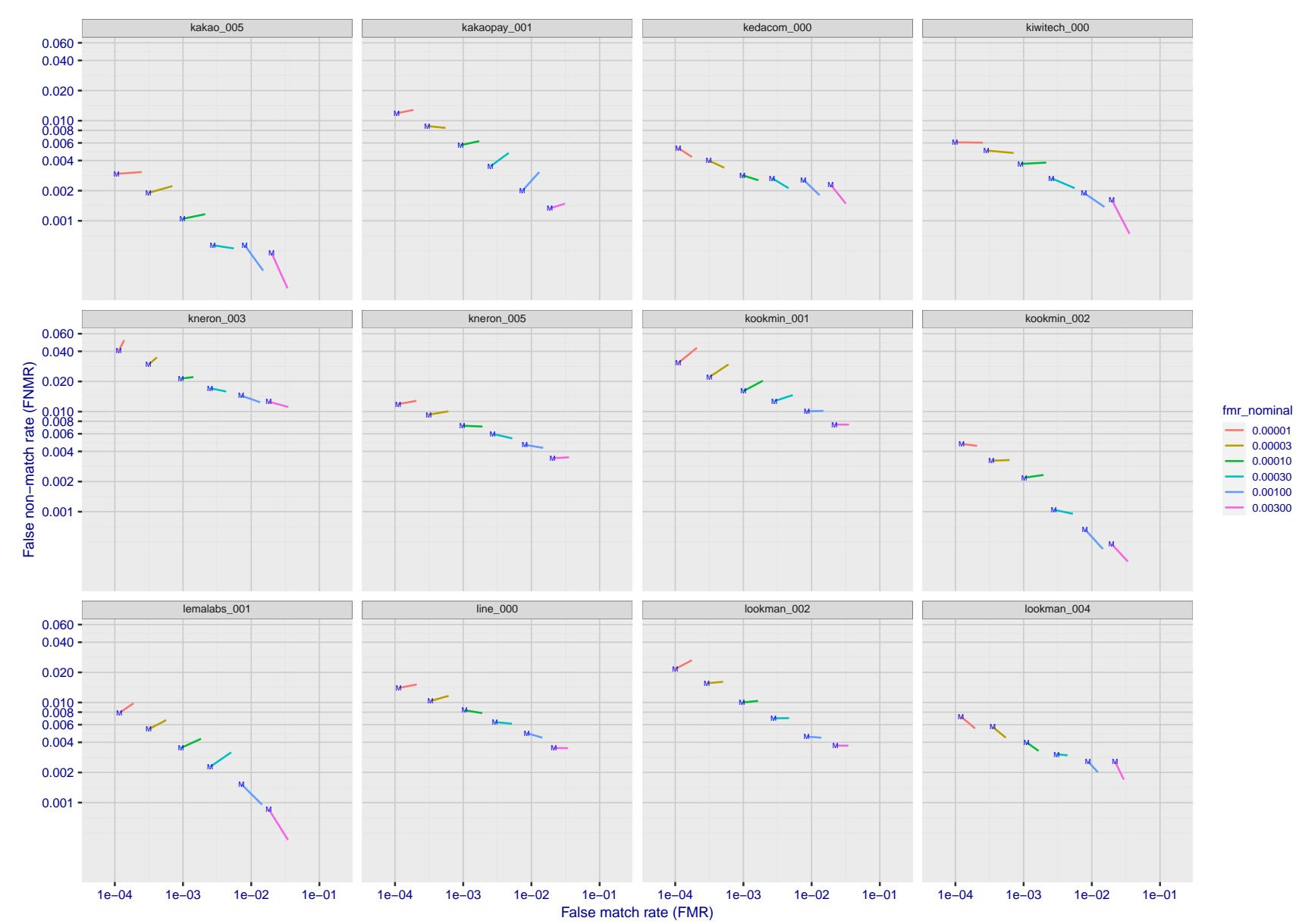


Figure 139: For the visa images, FNMR and FMR at six operating points along the DET characteristic. At each point a line is drawn between $(FMR, FNMR)_{MALE}$ and $(FMR, FNMR)_{FEMALE}$ showing how which sex has lower FMR and/or FNMR. The "M" label denotes male, the other end of the line corresponds to female. The six operating thresholds are selected to give the nominal false match rates given in the legend, and are computed over all impostor pairs regardless of age, sex, and place of birth. The plotted FMR values are broadly an order of magnitude larger than the nominal rates because FMR is computed over demographically-matched impostor pairs i.e individuals of the same sex, from the same geographic region (see section 3.6.1), and the same age group (see section 3.6.2).

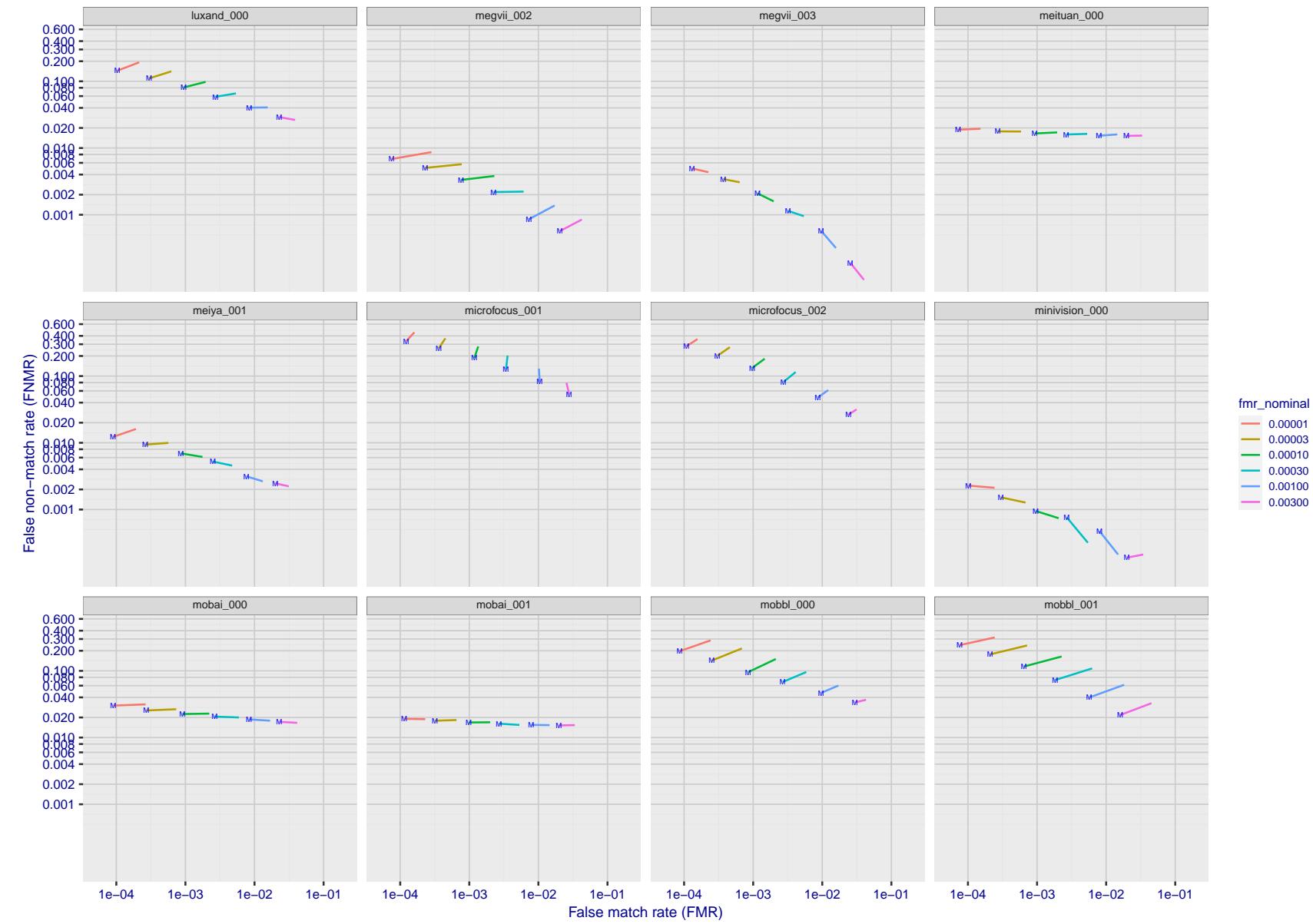


Figure 140: For the visa images, FNMR and FMR at six operating points along the DET characteristic. At each point a line is drawn between $(FMR, FNMR)_{MALE}$ and $(FMR, FNMR)_{FEMALE}$ showing how which sex has lower FMR and/or FNMR. The "M" label denotes male, the other end of the line corresponds to female. The six operating thresholds are selected to give the nominal false match rates given in the legend, and are computed over all impostor pairs regardless of age, sex, and place of birth. The plotted FMR values are broadly an order of magnitude larger than the nominal rates because FMR is computed over demographically-matched impostor pairs i.e individuals of the same sex, from the same geographic region (see section 3.6.1), and the same age group (see section 3.6.2).

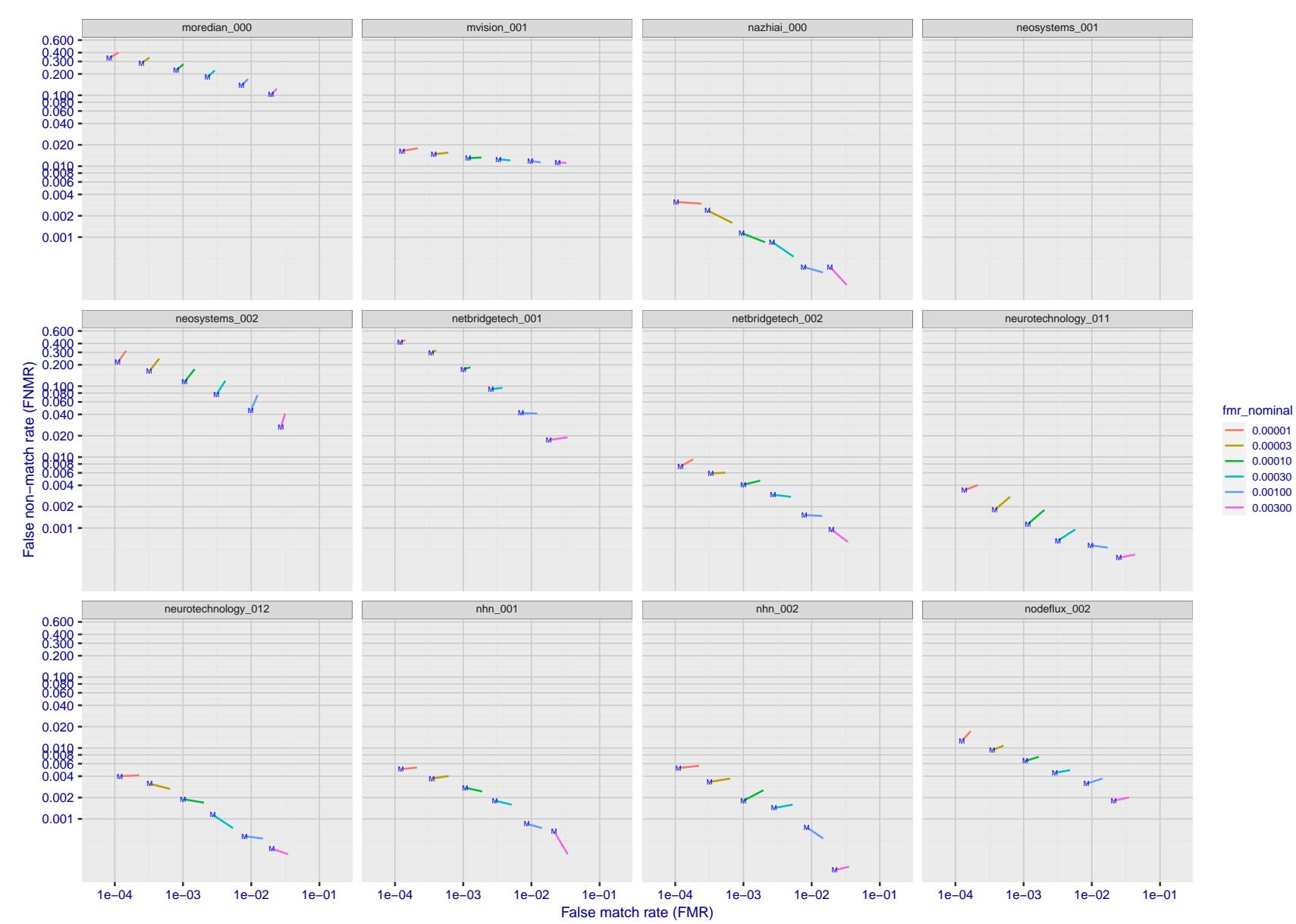


Figure 141: For the visa images, FNMR and FMR at six operating points along the DET characteristic. At each point a line is drawn between $(FMR, FNMR)_{MALE}$ and $(FMR, FNMR)_{FEMALE}$ showing how which sex has lower FMR and/or FNMR. The "M" label denotes male, the other end of the line corresponds to female. The six operating thresholds are selected to give the nominal false match rates given in the legend, and are computed over all impostor pairs regardless of age, sex, and place of birth. The plotted FMR values are broadly an order of magnitude larger than the nominal rates because FMR is computed over demographically-matched impostor pairs i.e individuals of the same sex, from the same geographic region (see section 3.6.1), and the same age group (see section 3.6.2).

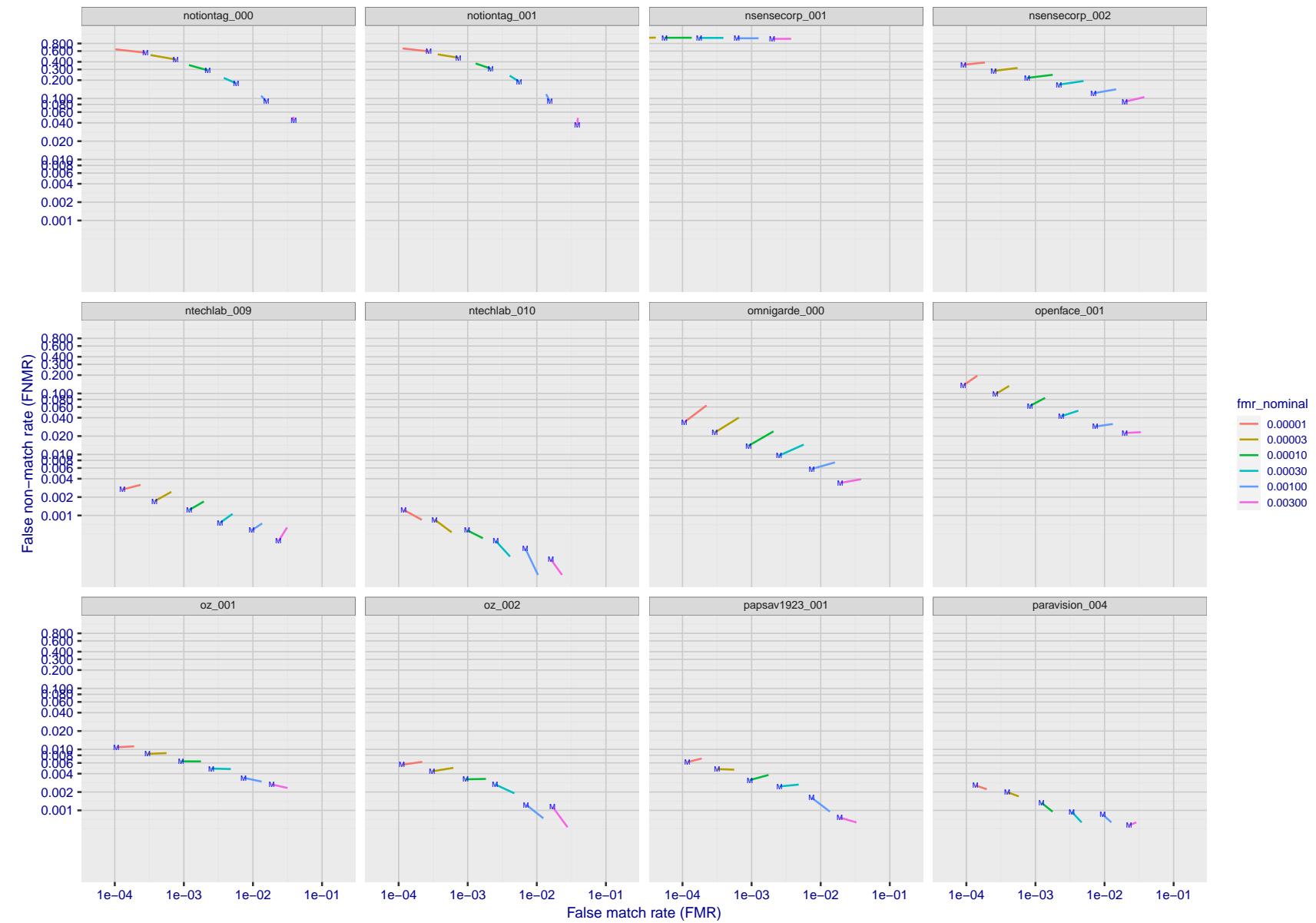


Figure 142: For the visa images, FNMR and FMR at six operating points along the DET characteristic. At each point a line is drawn between $(FMR, FNMR)_{MALE}$ and $(FMR, FNMR)_{FEMALE}$ showing how which sex has lower FMR and/or FNMR. The "M" label denotes male, the other end of the line corresponds to female. The six operating thresholds are selected to give the nominal false match rates given in the legend, and are computed over all impostor pairs regardless of age, sex, and place of birth. The plotted FMR values are broadly an order of magnitude larger than the nominal rates because FMR is computed over demographically-matched impostor pairs i.e individuals of the same sex, from the same geographic region (see section 3.6.1), and the same age group (see section 3.6.2).

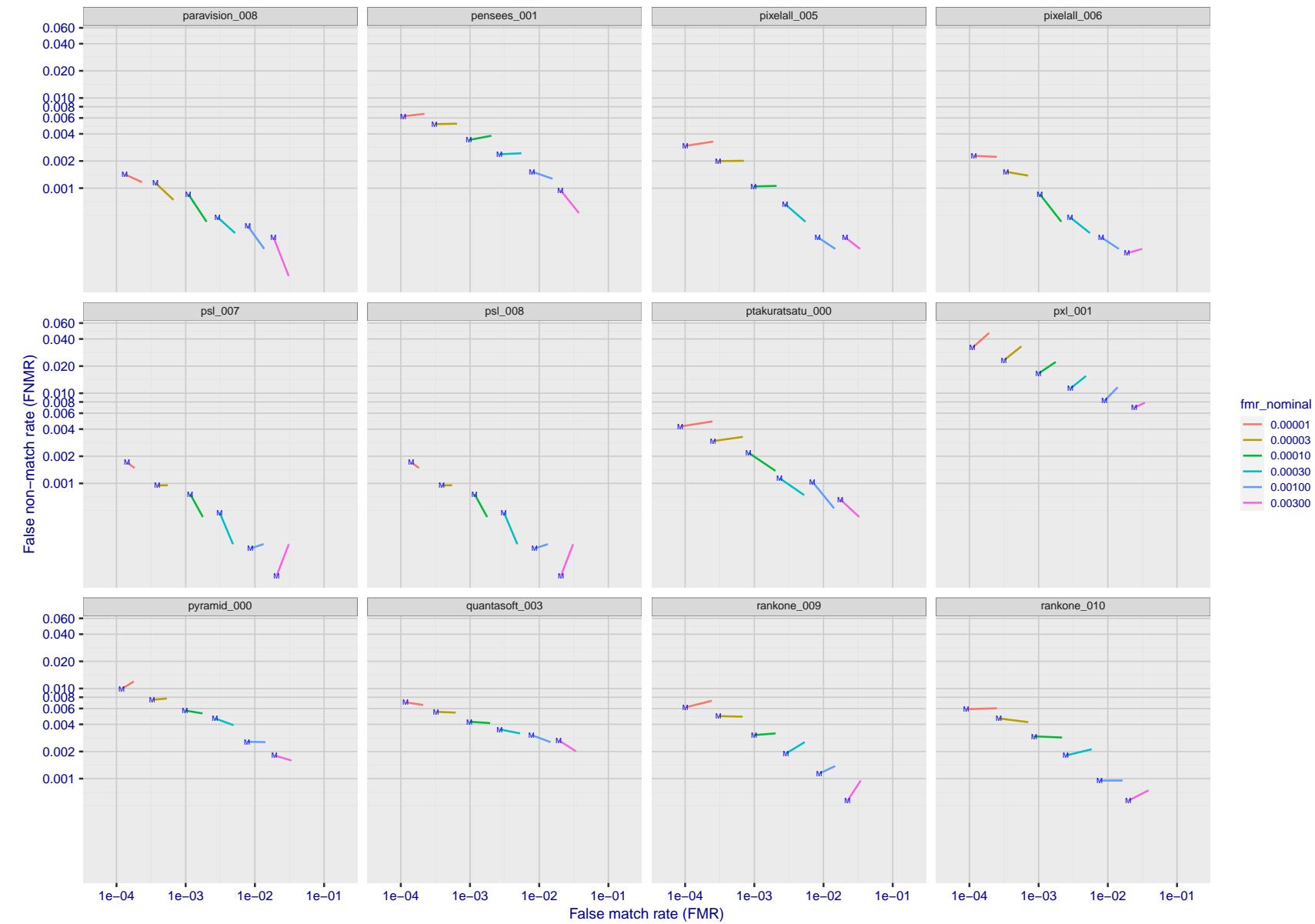


Figure 143: For the visa images, FNMR and FMR at six operating points along the DET characteristic. At each point a line is drawn between $(FMR, FNMR)_{MALE}$ and $(FMR, FNMR)_{FEMALE}$ showing how which sex has lower FMR and/or FNMR. The "M" label denotes male, the other end of the line corresponds to female. The six operating thresholds are selected to give the nominal false match rates given in the legend, and are computed over all impostor pairs regardless of age, sex, and place of birth. The plotted FMR values are broadly an order of magnitude larger than the nominal rates because FMR is computed over demographically-matched impostor pairs i.e individuals of the same sex, from the same geographic region (see section 3.6.1), and the same age group (see section 3.6.2).

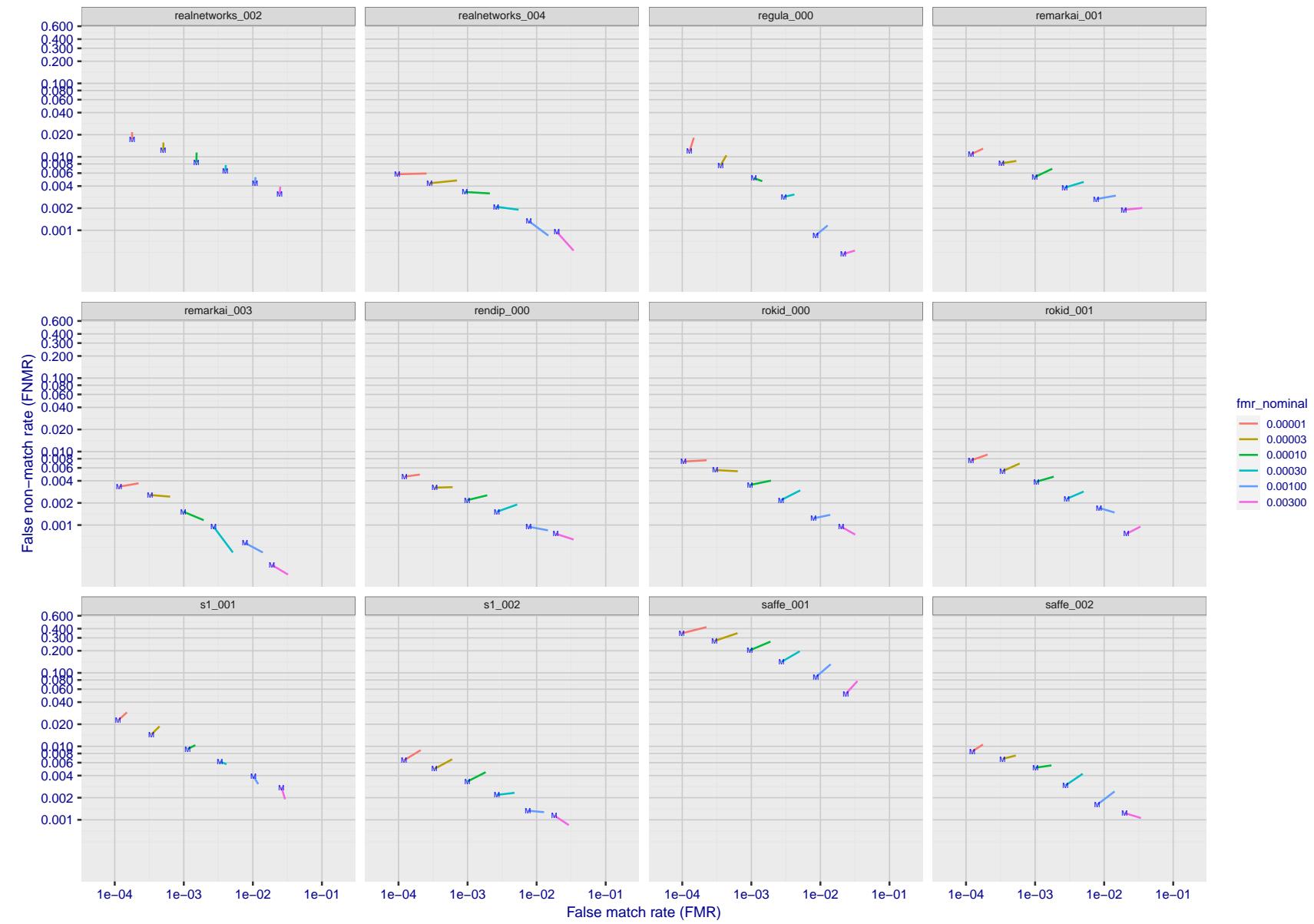


Figure 144: For the visa images, FNMR and FMR at six operating points along the DET characteristic. At each point a line is drawn between $(FMR, FNMR)_{MALE}$ and $(FMR, FNMR)_{FEMALE}$ showing how which sex has lower FMR and/or FNMR. The "M" label denotes male, the other end of the line corresponds to female. The six operating thresholds are selected to give the nominal false match rates given in the legend, and are computed over all impostor pairs regardless of age, sex, and place of birth. The plotted FMR values are broadly an order of magnitude larger than the nominal rates because FMR is computed over demographically-matched impostor pairs i.e individuals of the same sex, from the same geographic region (see section 3.6.1), and the same age group (see section 3.6.2).

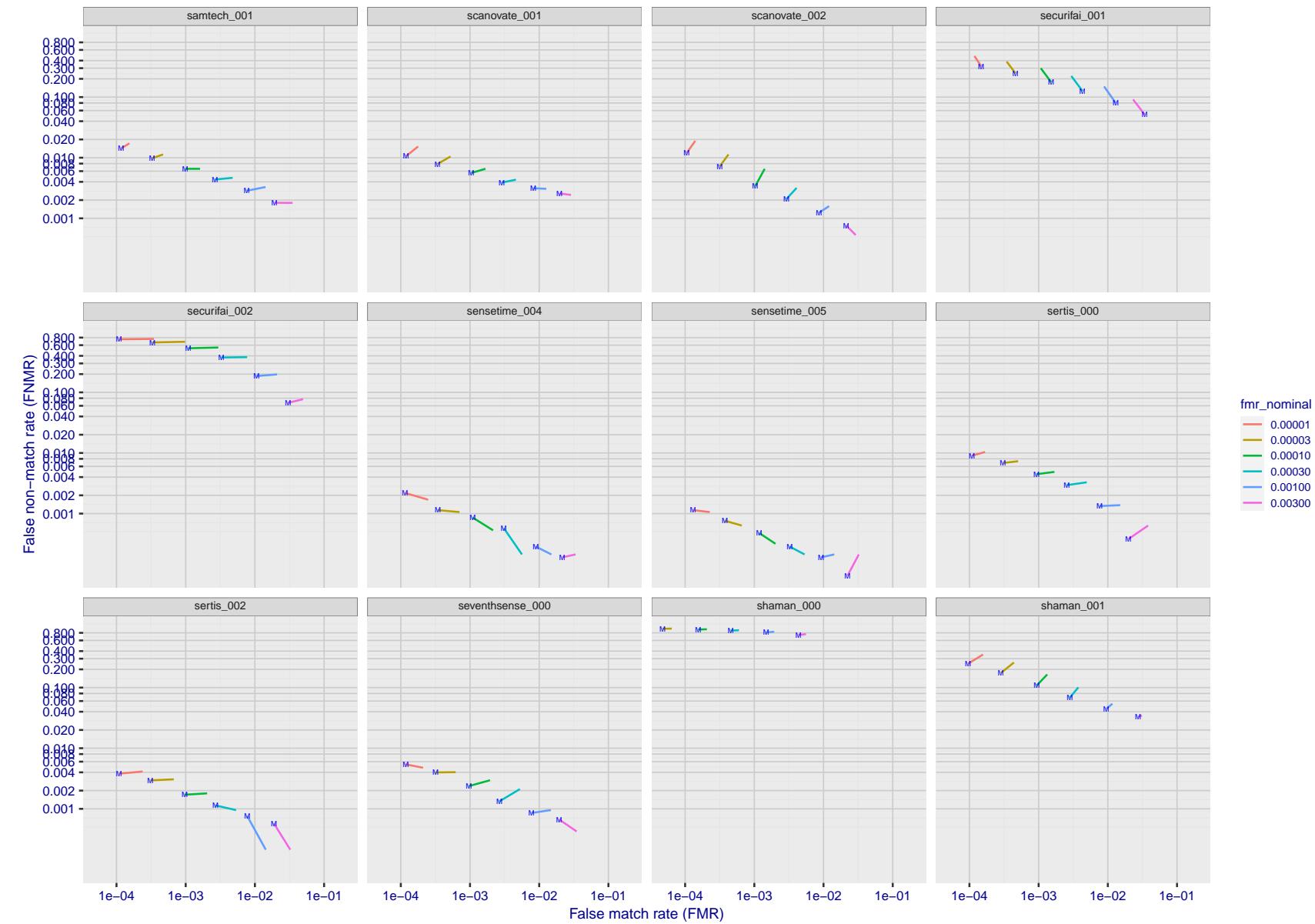


Figure 145: For the visa images, FNMR and FMR at six operating points along the DET characteristic. At each point a line is drawn between $(FMR, FNMR)_{MALE}$ and $(FMR, FNMR)_{FEMALE}$ showing how which sex has lower FMR and/or FNMR. The "M" label denotes male, the other end of the line corresponds to female. The six operating thresholds are selected to give the nominal false match rates given in the legend, and are computed over all impostor pairs regardless of age, sex, and place of birth. The plotted FMR values are broadly an order of magnitude larger than the nominal rates because FMR is computed over demographically-matched impostor pairs i.e individuals of the same sex, from the same geographic region (see section 3.6.1), and the same age group (see section 3.6.2).

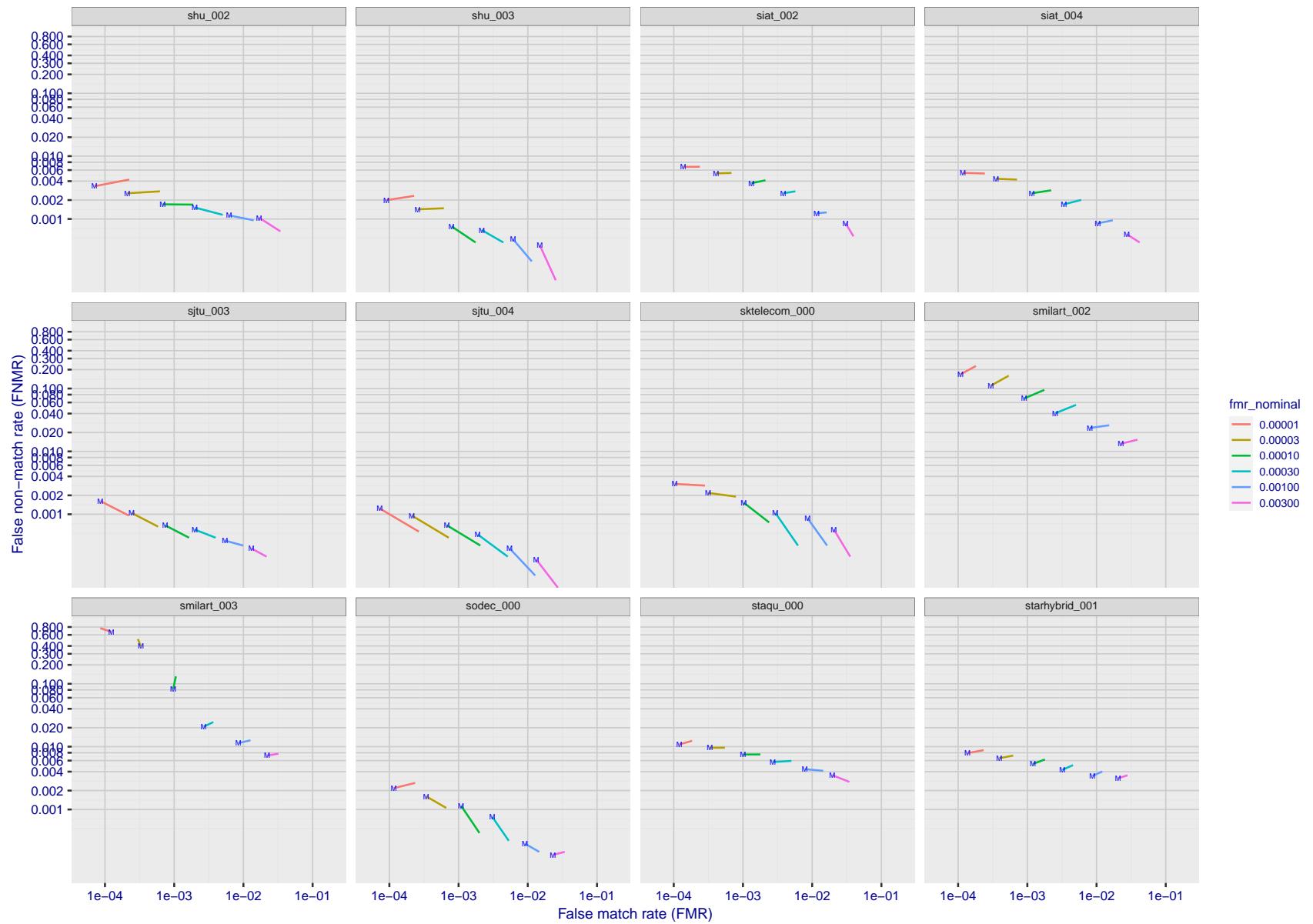


Figure 146: For the visa images, FNMR and FMR at six operating points along the DET characteristic. At each point a line is drawn between $(FMR, FNMR)_{MALE}$ and $(FMR, FNMR)_{FEMALE}$ showing how which sex has lower FMR and/or FNMR. The "M" label denotes male, the other end of the line corresponds to female. The six operating thresholds are selected to give the nominal false match rates given in the legend, and are computed over all impostor pairs regardless of age, sex, and place of birth. The plotted FMR values are broadly an order of magnitude larger than the nominal rates because FMR is computed over demographically-matched impostor pairs i.e individuals of the same sex, from the same geographic region (see section 3.6.1), and the same age group (see section 3.6.2).

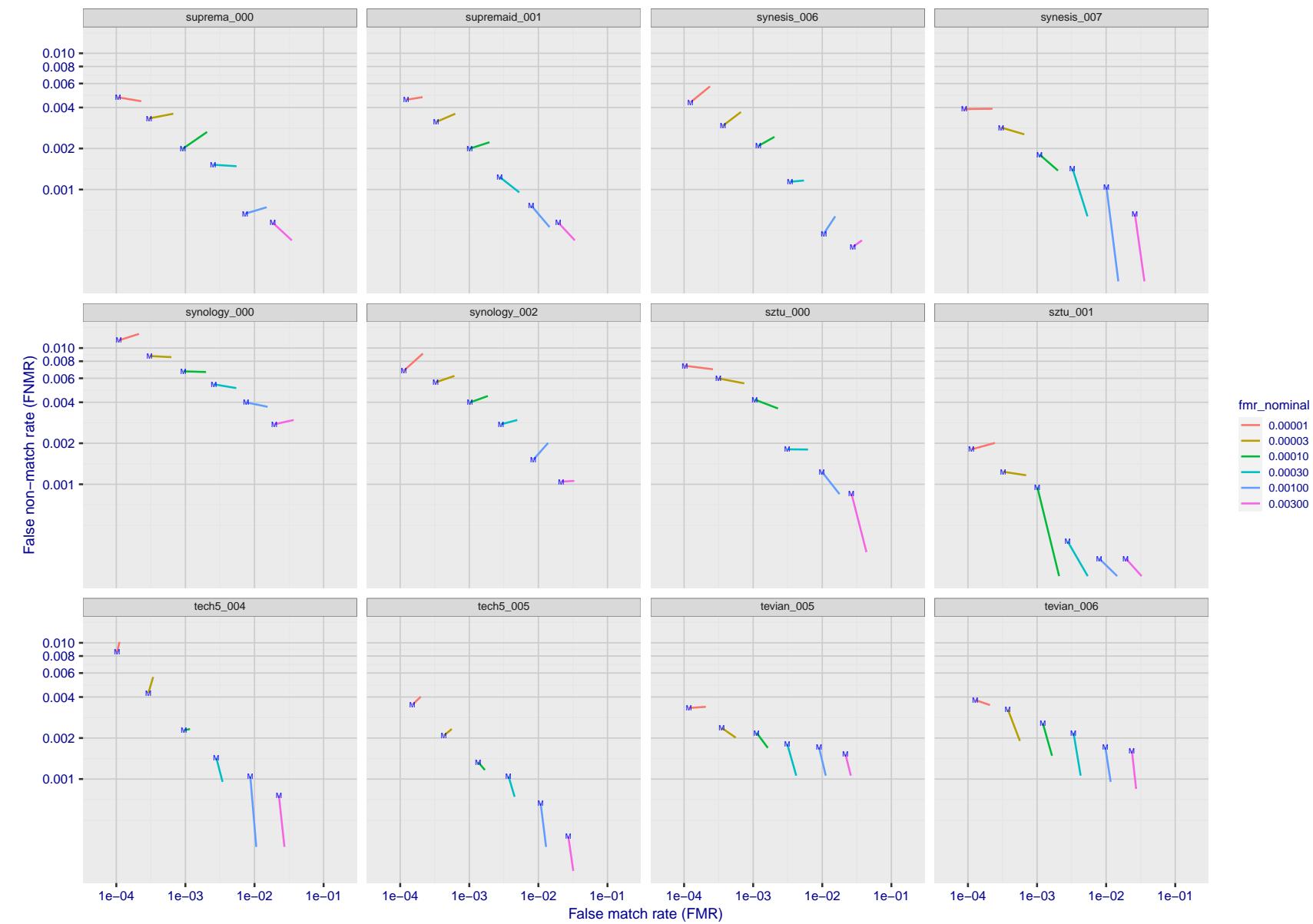


Figure 147: For the visa images, FNMR and FMR at six operating points along the DET characteristic. At each point a line is drawn between $(FMR, FNMR)_{MALE}$ and $(FMR, FNMR)_{FEMALE}$ showing how which sex has lower FMR and/or FNMR. The "M" label denotes male, the other end of the line corresponds to female. The six operating thresholds are selected to give the nominal false match rates given in the legend, and are computed over all impostor pairs regardless of age, sex, and place of birth. The plotted FMR values are broadly an order of magnitude larger than the nominal rates because FMR is computed over demographically-matched impostor pairs i.e individuals of the same sex, from the same geographic region (see section 3.6.1), and the same age group (see section 3.6.2).

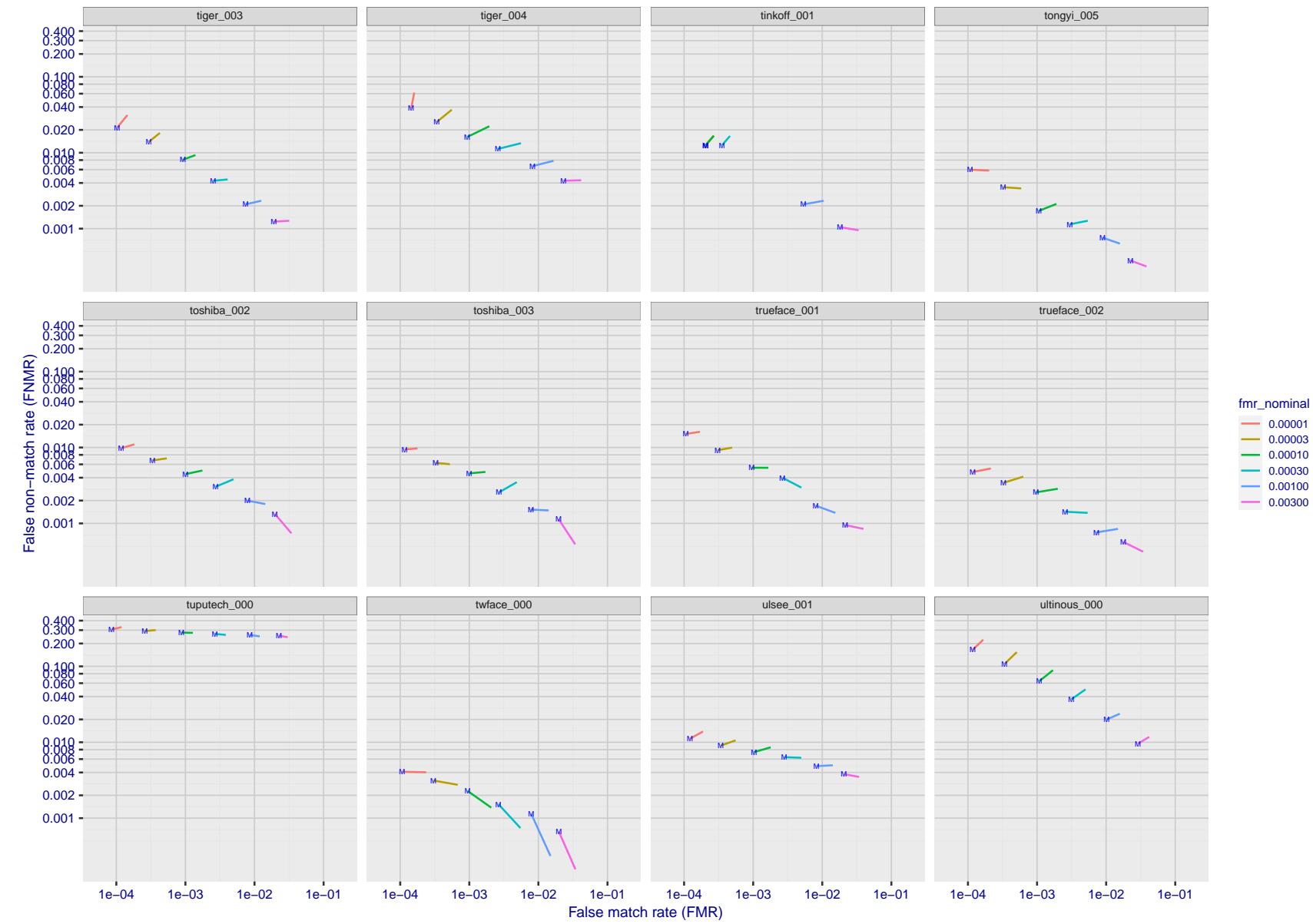


Figure 148: For the visa images, FNMR and FMR at six operating points along the DET characteristic. At each point a line is drawn between $(FMR, FNMR)_{MALE}$ and $(FMR, FNMR)_{FEMALE}$ showing how which sex has lower FMR and/or FNMR. The "M" label denotes male, the other end of the line corresponds to female. The six operating thresholds are selected to give the nominal false match rates given in the legend, and are computed over all impostor pairs regardless of age, sex, and place of birth. The plotted FMR values are broadly an order of magnitude larger than the nominal rates because FMR is computed over demographically-matched impostor pairs i.e individuals of the same sex, from the same geographic region (see section 3.6.1), and the same age group (see section 3.6.2).

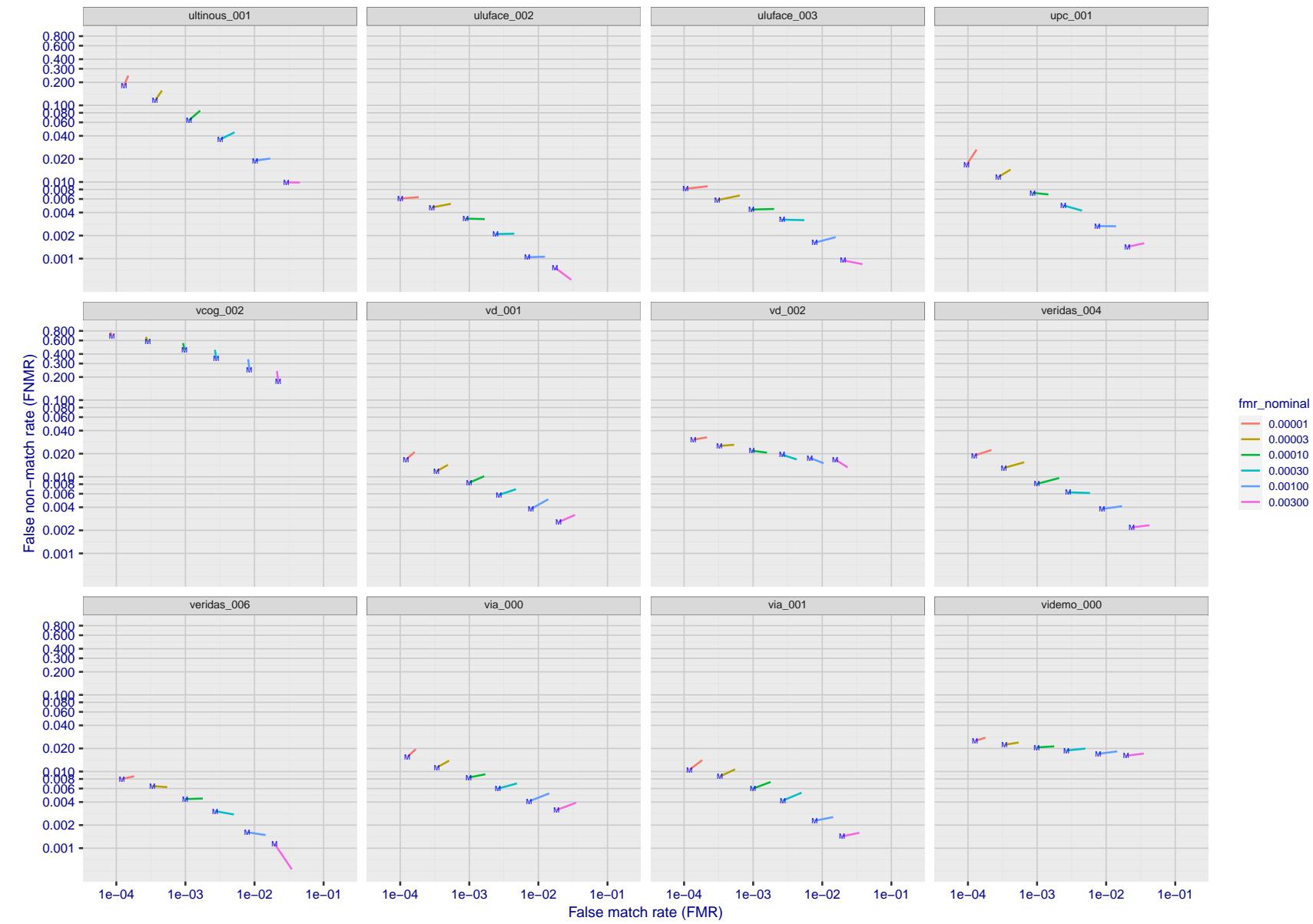


Figure 149: For the visa images, FNMR and FMR at six operating points along the DET characteristic. At each point a line is drawn between $(FMR, FNMR)_{MALE}$ and $(FMR, FNMR)_{FEMALE}$ showing how which sex has lower FMR and/or FNMR. The "M" label denotes male, the other end of the line corresponds to female. The six operating thresholds are selected to give the nominal false match rates given in the legend, and are computed over all impostor pairs regardless of age, sex, and place of birth. The plotted FMR values are broadly an order of magnitude larger than the nominal rates because FMR is computed over demographically-matched impostor pairs i.e individuals of the same sex, from the same geographic region (see section 3.6.1), and the same age group (see section 3.6.2).

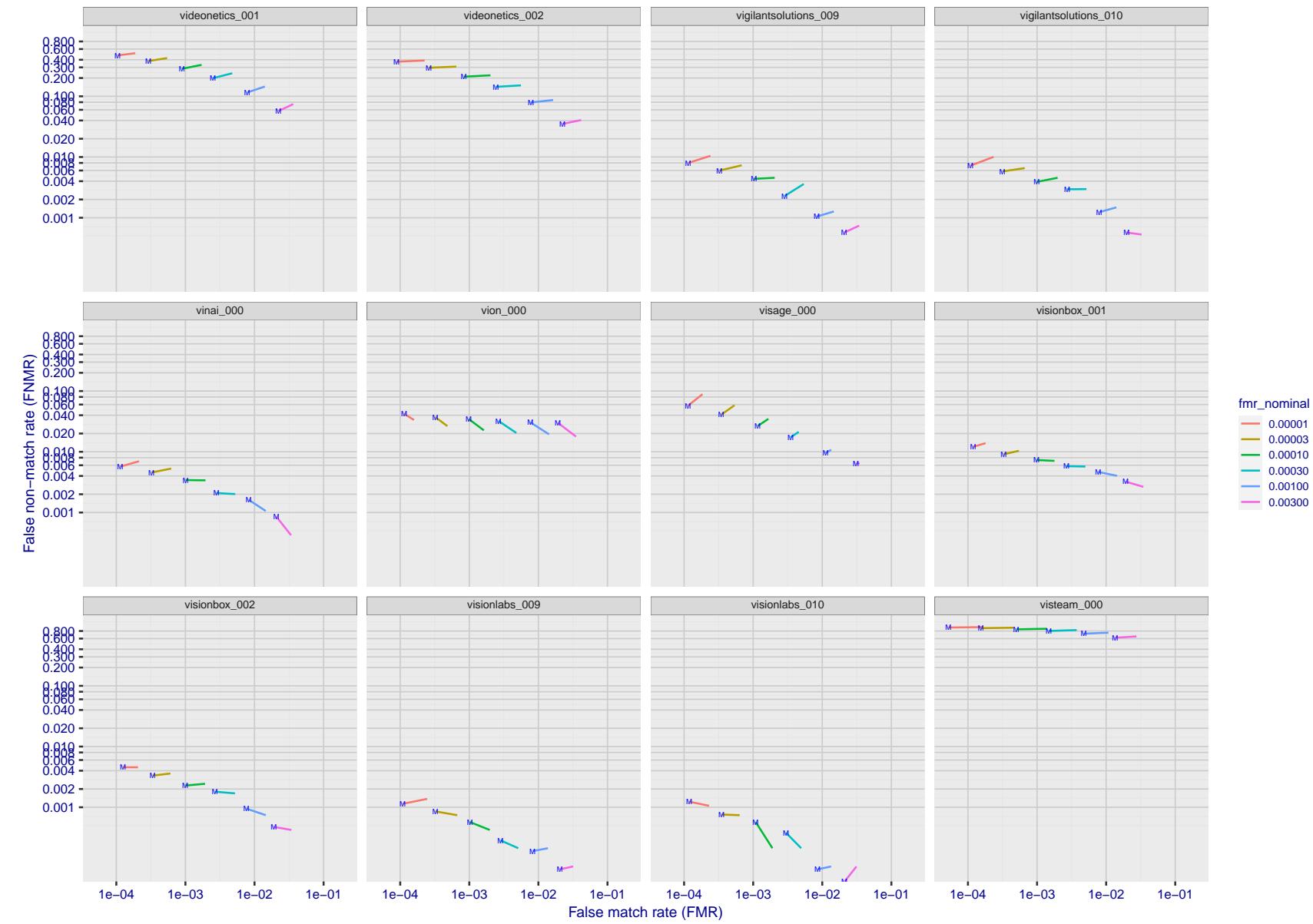


Figure 150: For the visa images, FNMR and FMR at six operating points along the DET characteristic. At each point a line is drawn between $(FMR, FNMR)_{MALE}$ and $(FMR, FNMR)_{FEMALE}$ showing how which sex has lower FMR and/or FNMR. The "M" label denotes male, the other end of the line corresponds to female. The six operating thresholds are selected to give the nominal false match rates given in the legend, and are computed over all impostor pairs regardless of age, sex, and place of birth. The plotted FMR values are broadly an order of magnitude larger than the nominal rates because FMR is computed over demographically-matched impostor pairs i.e individuals of the same sex, from the same geographic region (see section 3.6.1), and the same age group (see section 3.6.2).

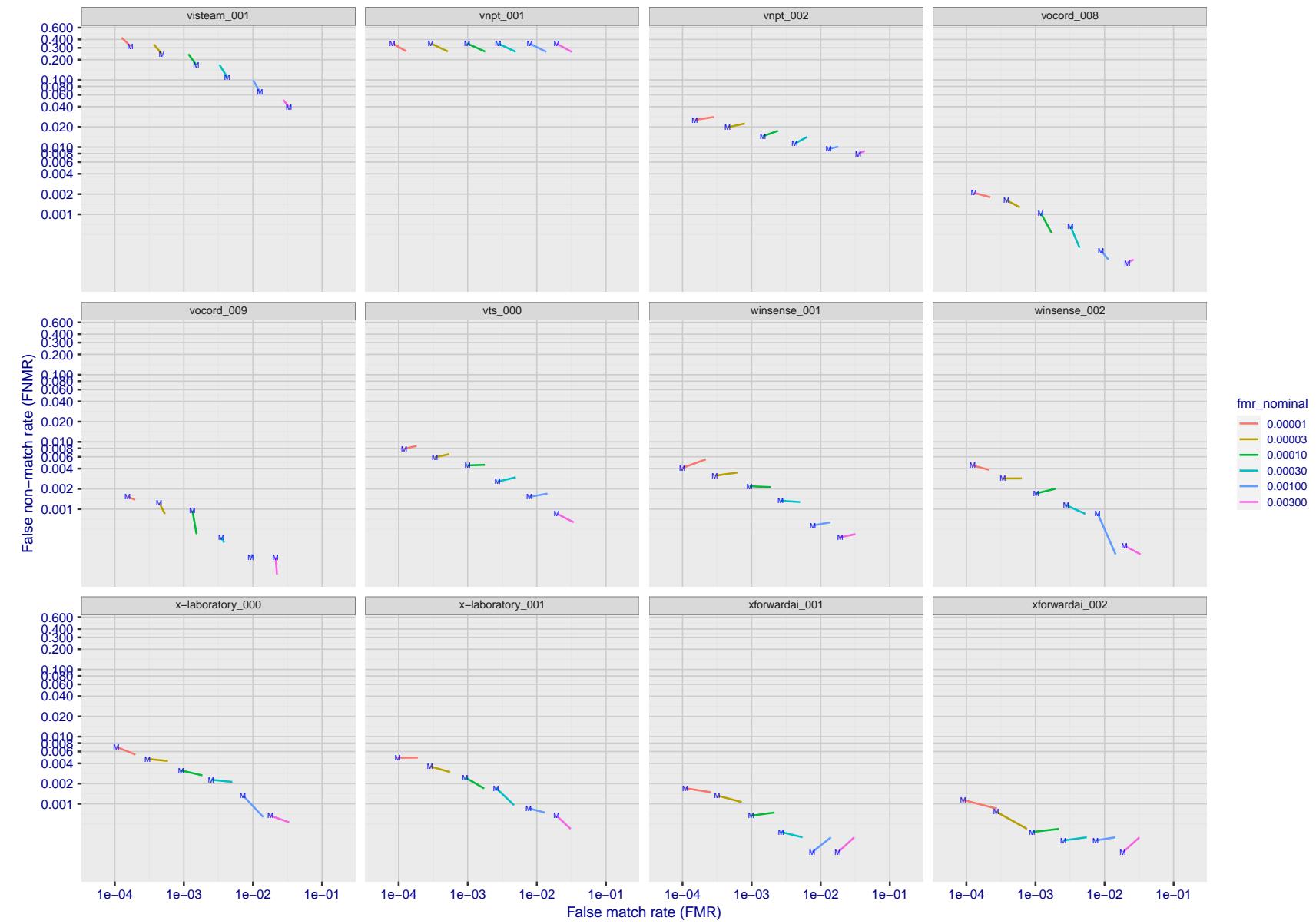


Figure 151: For the visa images, FNMR and FMR at six operating points along the DET characteristic. At each point a line is drawn between $(FMR, FNMR)_{MALE}$ and $(FMR, FNMR)_{FEMALE}$ showing how which sex has lower FMR and/or FNMR. The "M" label denotes male, the other end of the line corresponds to female. The six operating thresholds are selected to give the nominal false match rates given in the legend, and are computed over all impostor pairs regardless of age, sex, and place of birth. The plotted FMR values are broadly an order of magnitude larger than the nominal rates because FMR is computed over demographically-matched impostor pairs i.e individuals of the same sex, from the same geographic region (see section 3.6.1), and the same age group (see section 3.6.2).

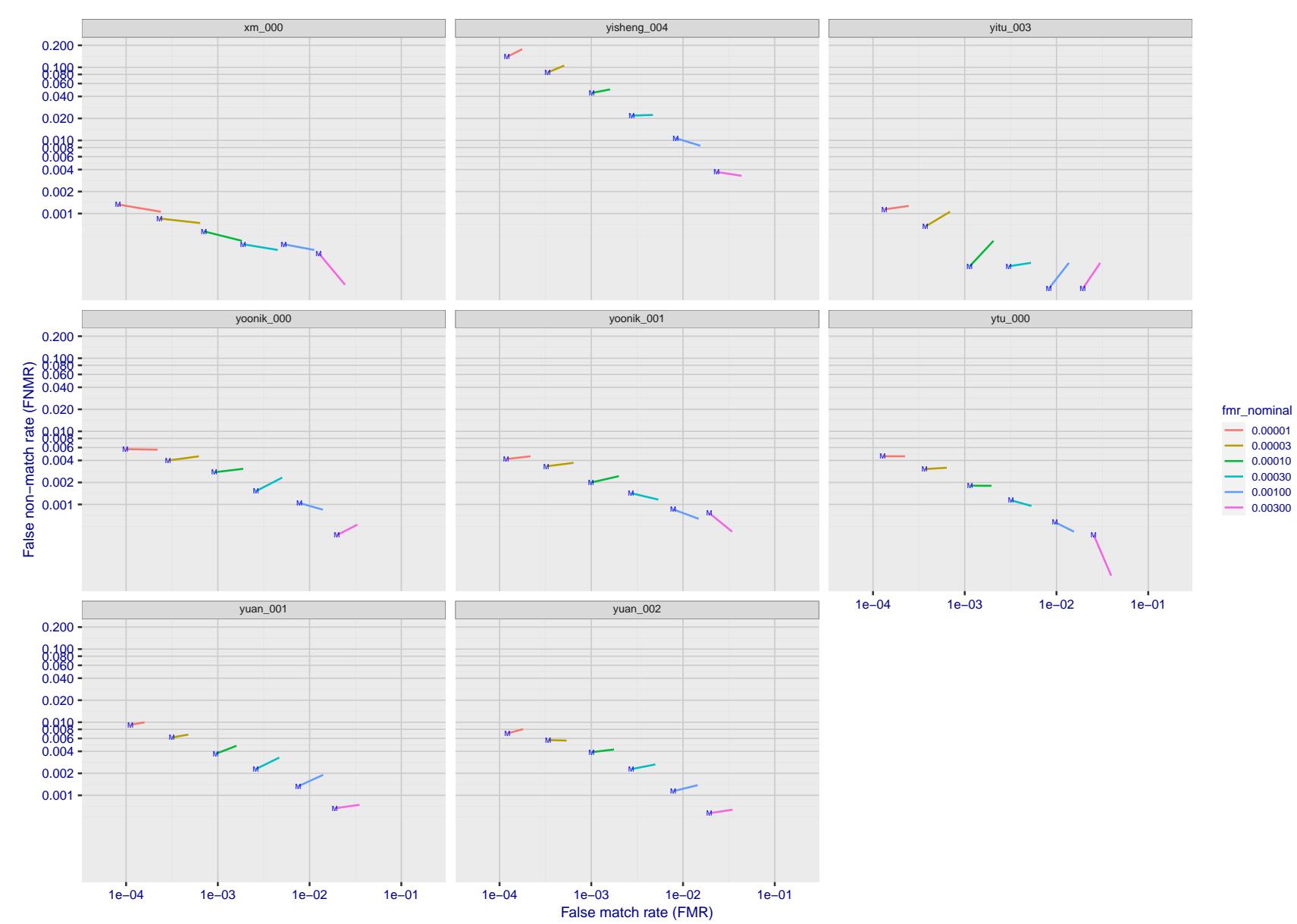


Figure 152: For the visa images, FNMR and FMR at six operating points along the DET characteristic. At each point a line is drawn between $(FMR, FNMR)_{MALE}$ and $(FMR, FNMR)_{FEMALE}$ showing how which sex has lower FMR and/or FNMR. The "M" label denotes male, the other end of the line corresponds to female. The six operating thresholds are selected to give the nominal false match rates given in the legend, and are computed over all impostor pairs regardless of age, sex, and place of birth. The plotted FMR values are broadly an order of magnitude larger than the nominal rates because FMR is computed over demographically-matched impostor pairs i.e individuals of the same sex, from the same geographic region (see section 3.6.1), and the same age group (see section 3.6.2).

2021/08/02 13:13:01

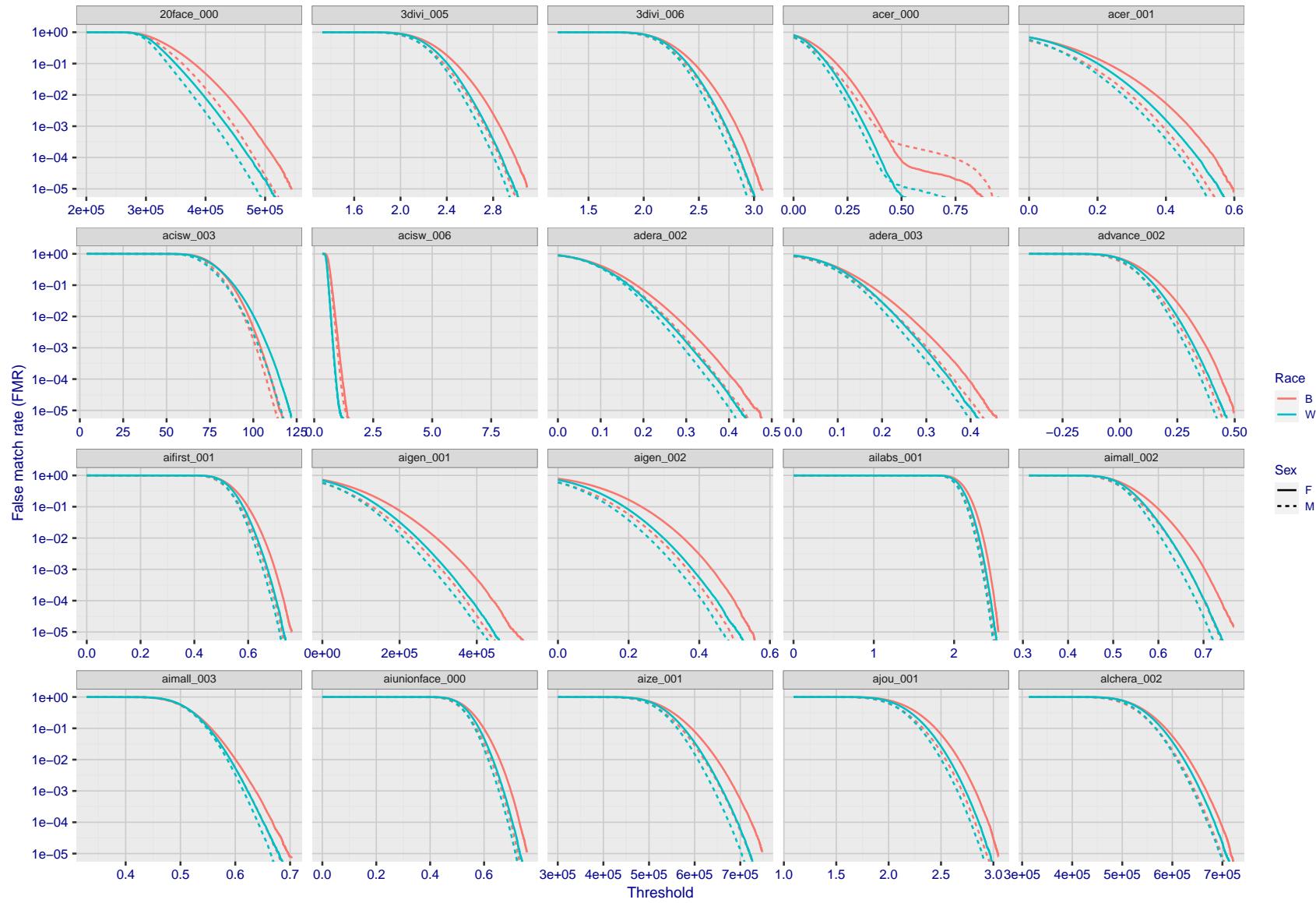


Figure 153: For the mugshot images, the false match calibration curves show false match rate vs. threshold. Separate curves appear for white females, black females, black males and white males.

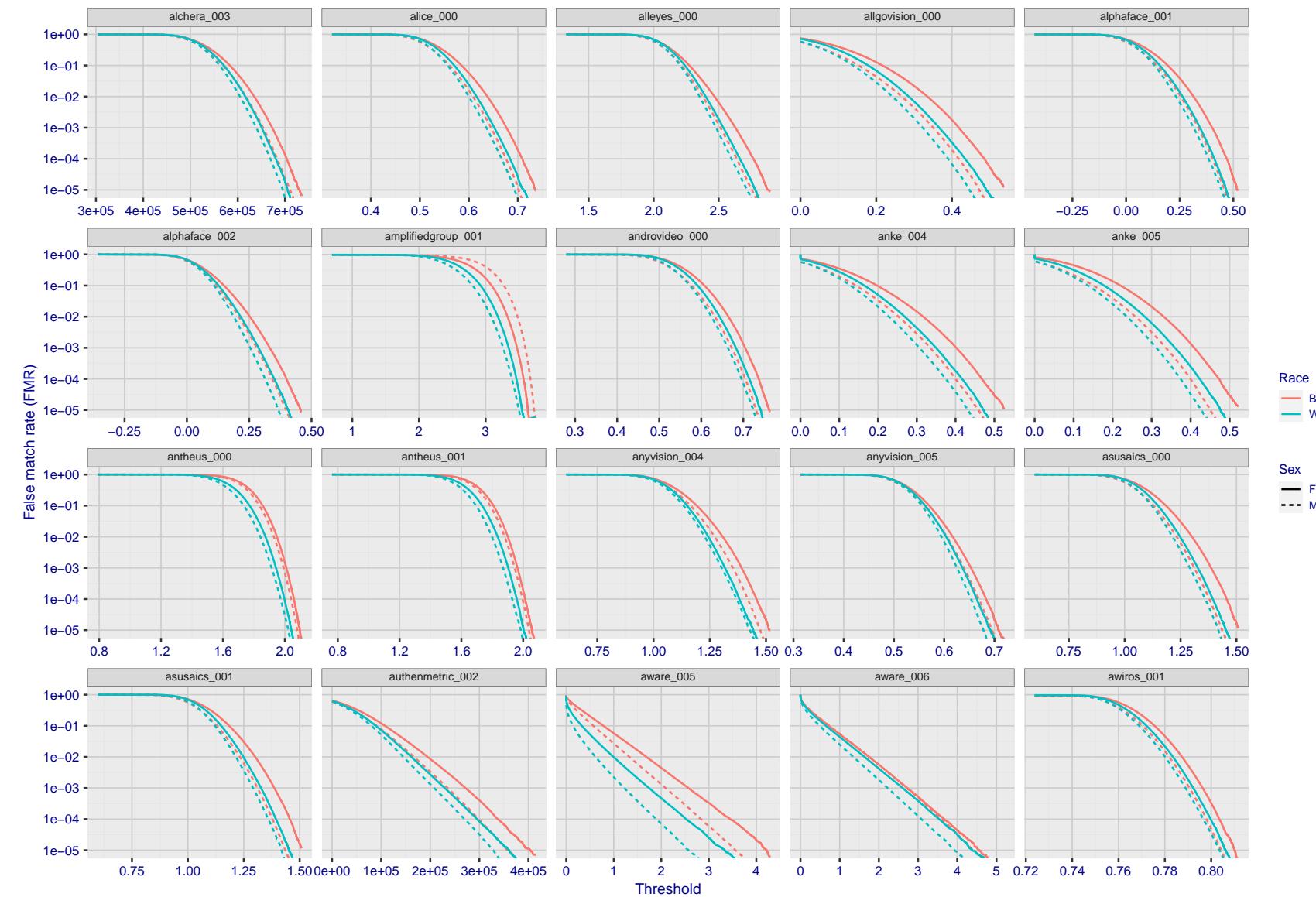


Figure 154: For the mugshot images, the false match calibration curves show false match rate vs. threshold. Separate curves appear for white females, black females, black males and white males.

2021/08/02 13:13:01

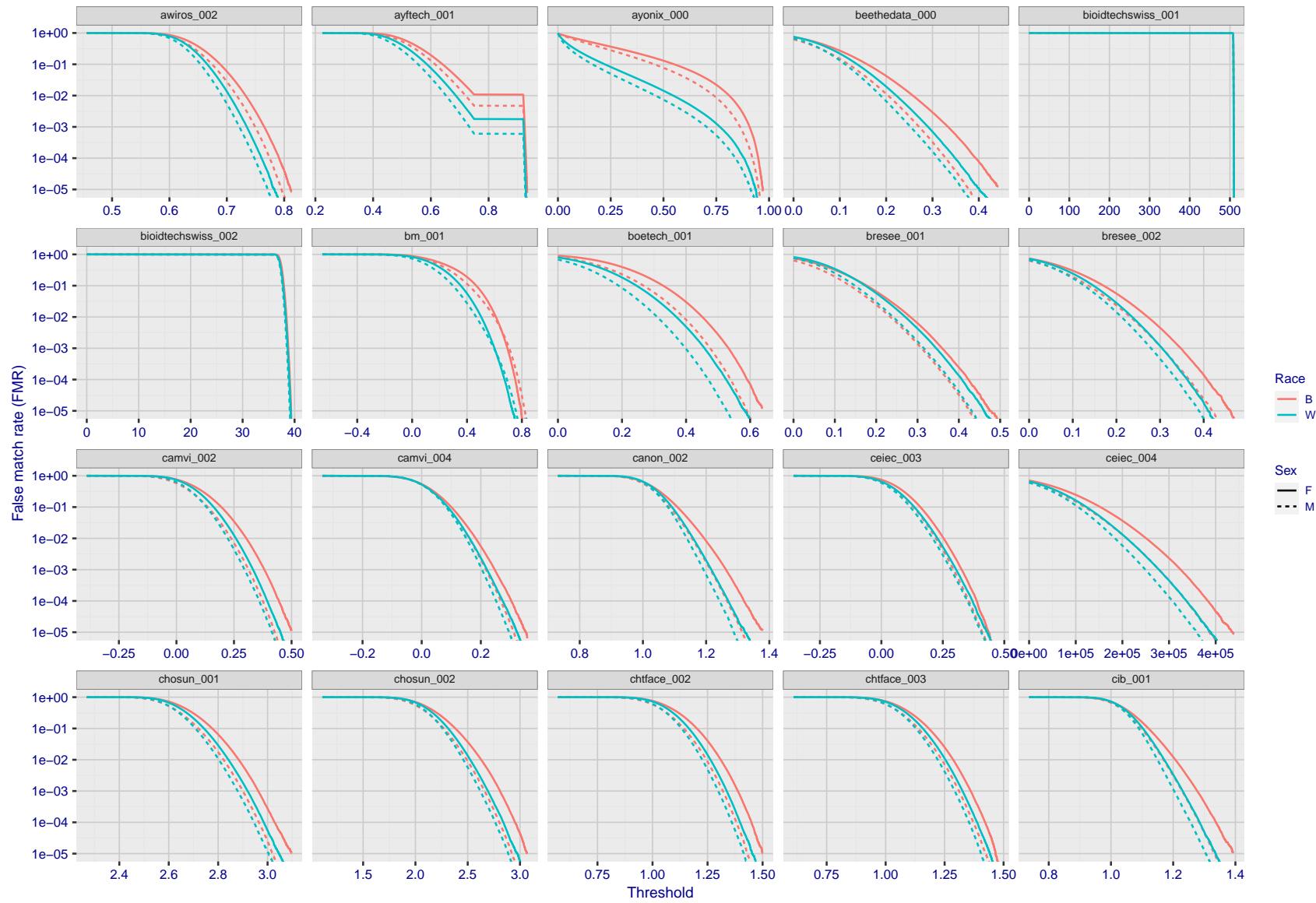


Figure 155: For the mugshot images, the false match calibration curves show false match rate vs. threshold. Separate curves appear for white females, black females, black males and white males.

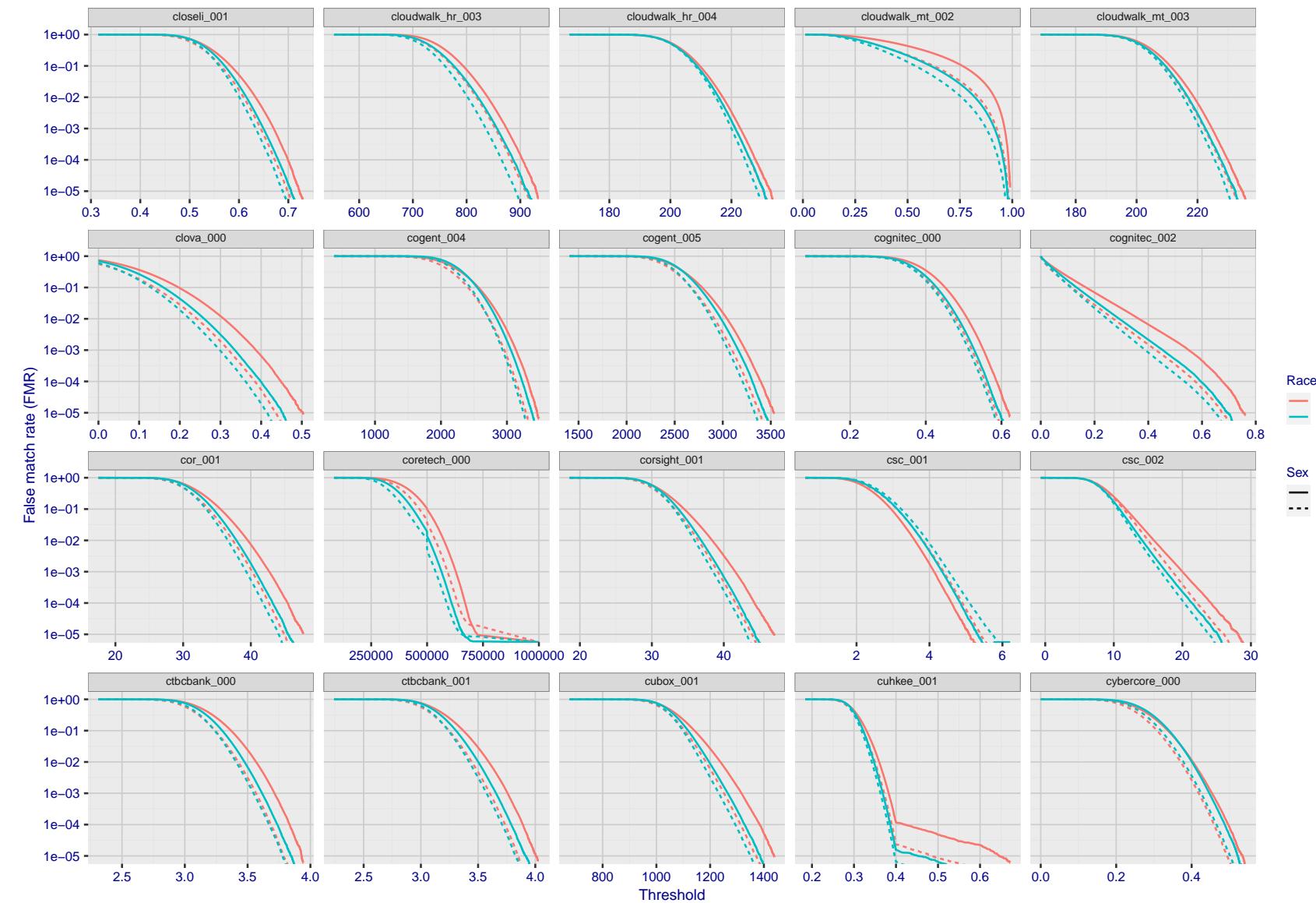


Figure 156: For the mugshot images, the false match calibration curves show false match rate vs. threshold. Separate curves appear for white females, black females, black males and white males.

2021/08/02 13:13:01

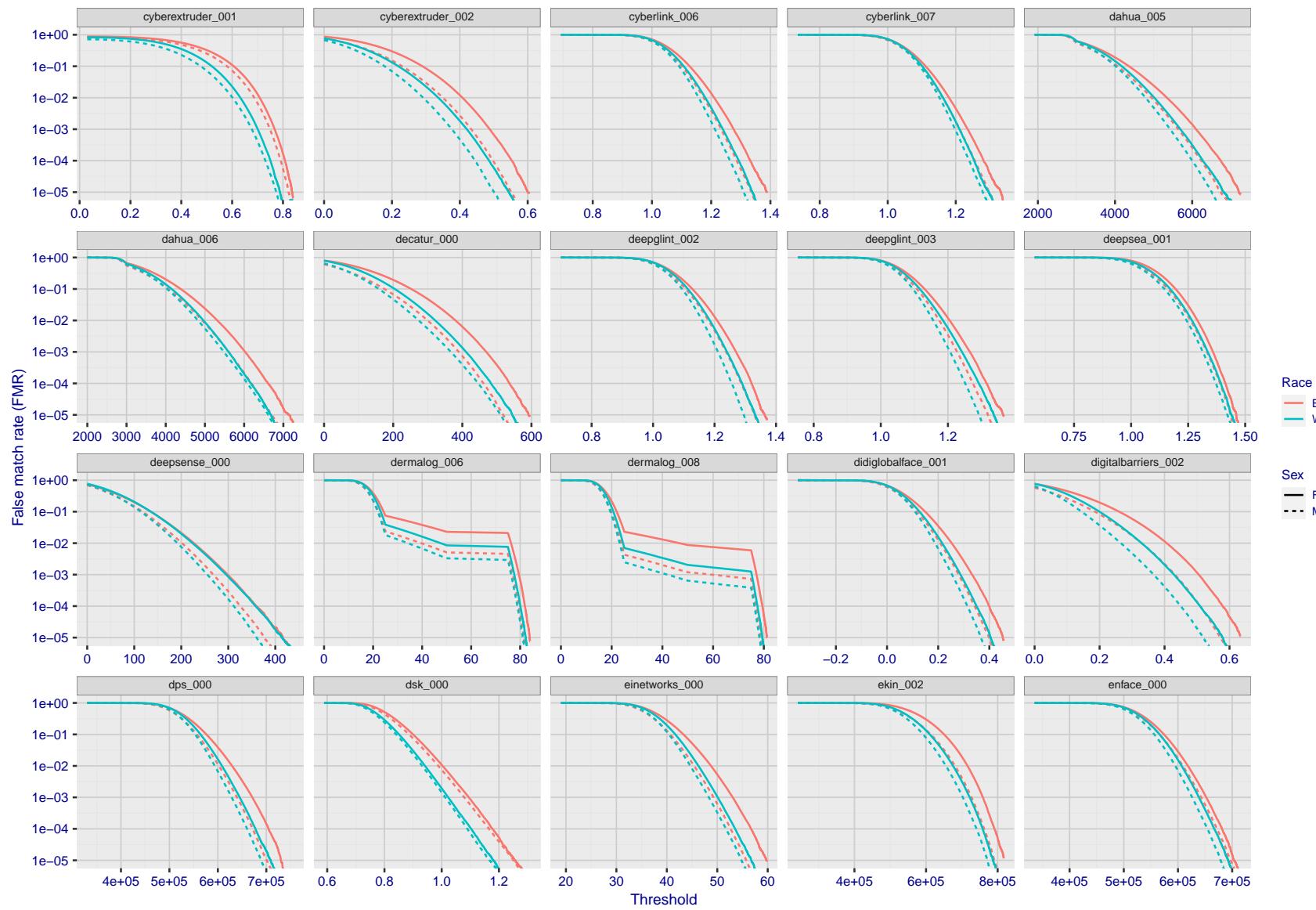


Figure 157: For the mugshot images, the false match calibration curves show false match rate vs. threshold. Separate curves appear for white females, black females, black males and white males.

FNMR(T)
"False non-match rate"
"False match rate"

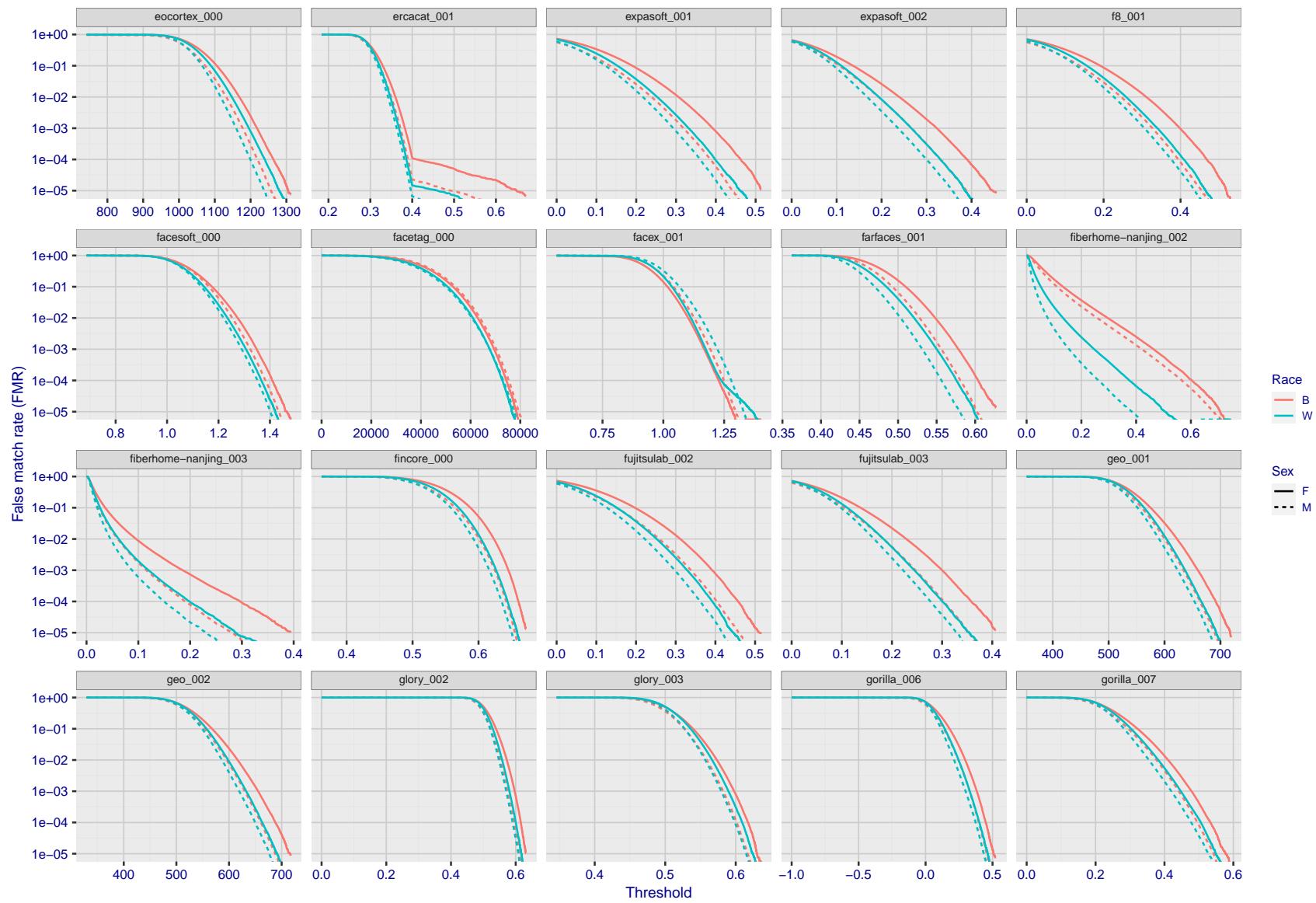


Figure 158: For the mugshot images, the false match calibration curves show false match rate vs. threshold. Separate curves appear for white females, black females, black males and white males.

2021/08/02 13:13:01

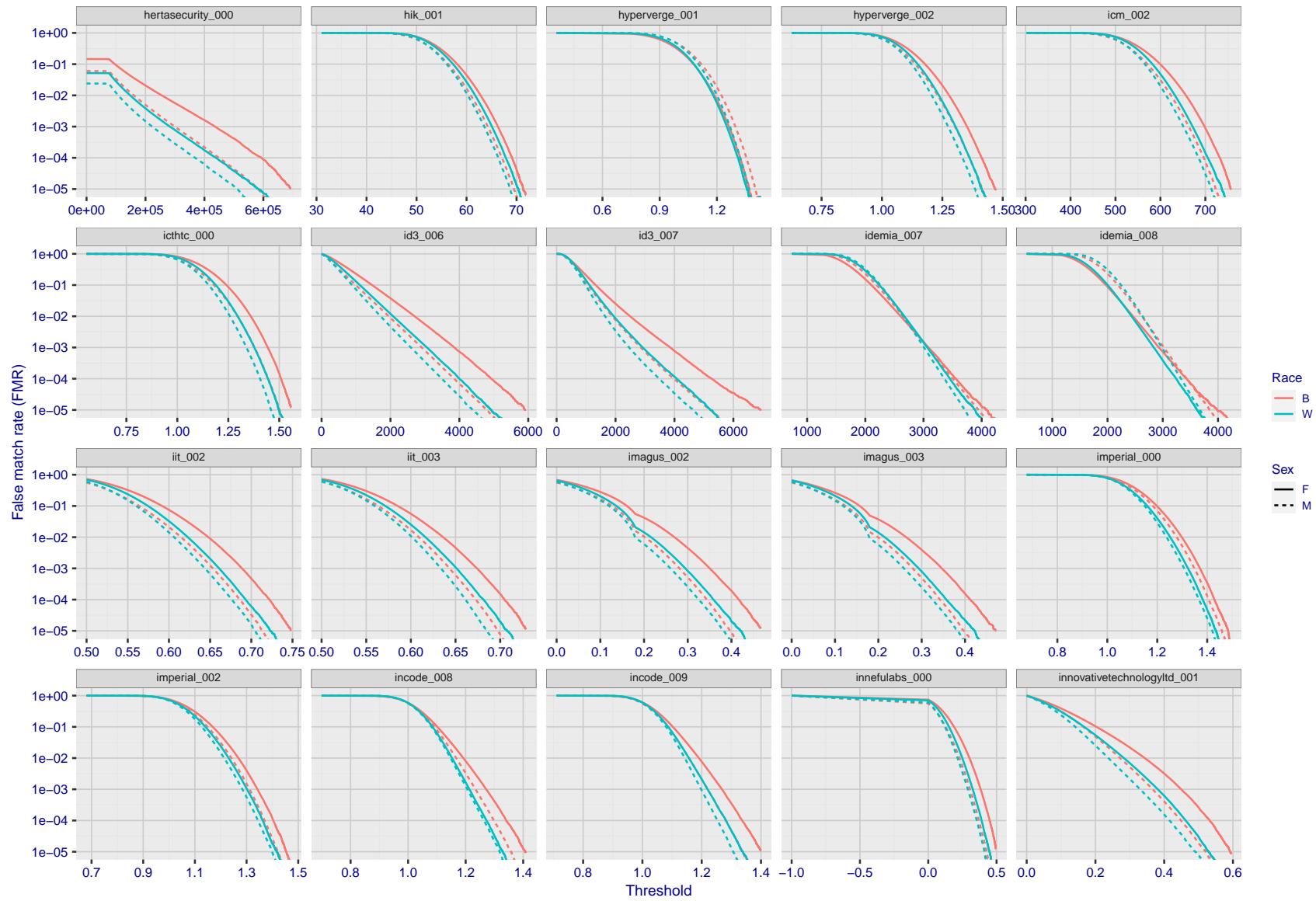


Figure 159: For the mugshot images, the false match calibration curves show false match rate vs. threshold. Separate curves appear for white females, black females, black males and white males.

2021/08/02 13:13:01

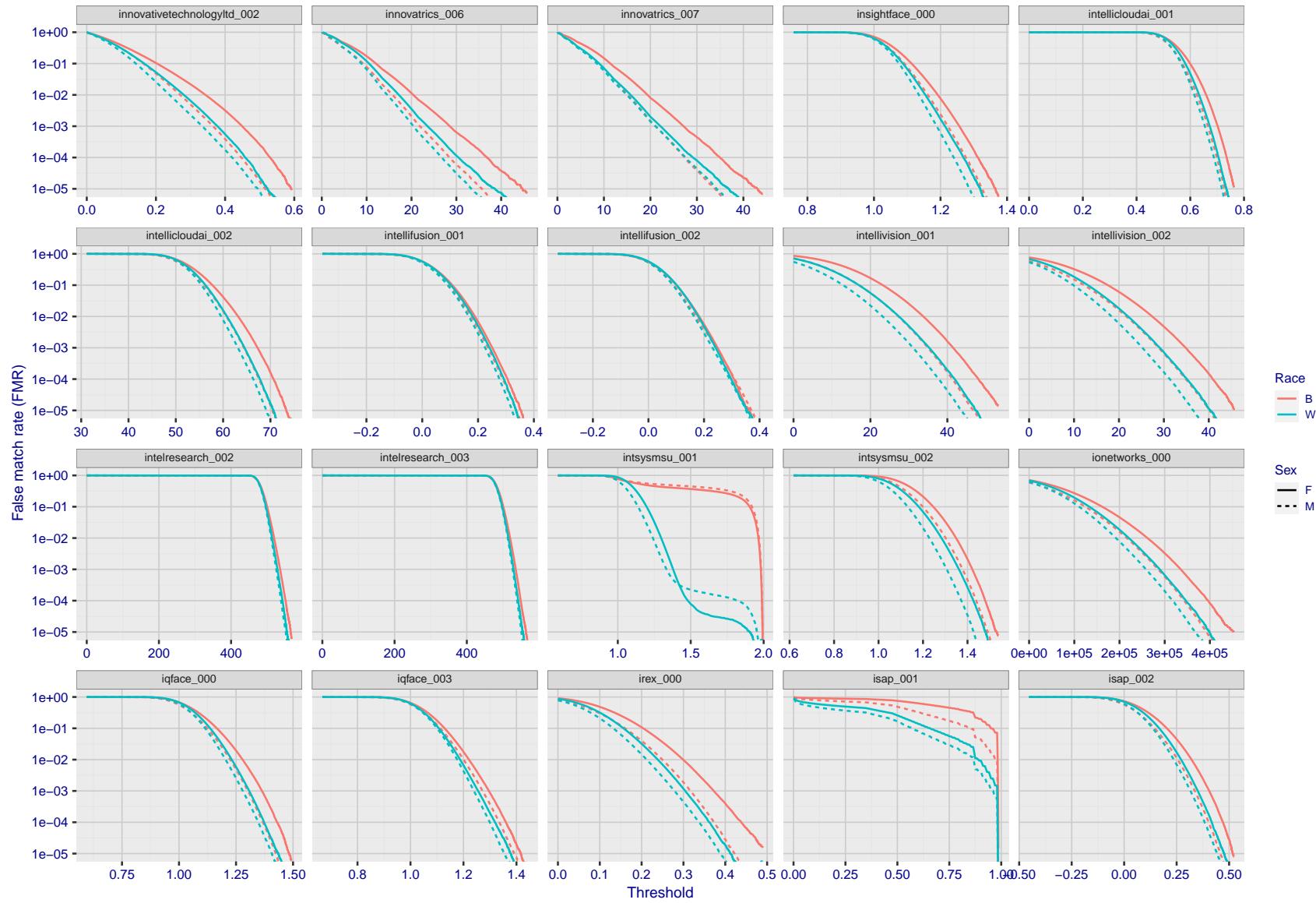


Figure 160: For the mugshot images, the false match calibration curves show false match rate vs. threshold. Separate curves appear for white females, black females, black males and white males.

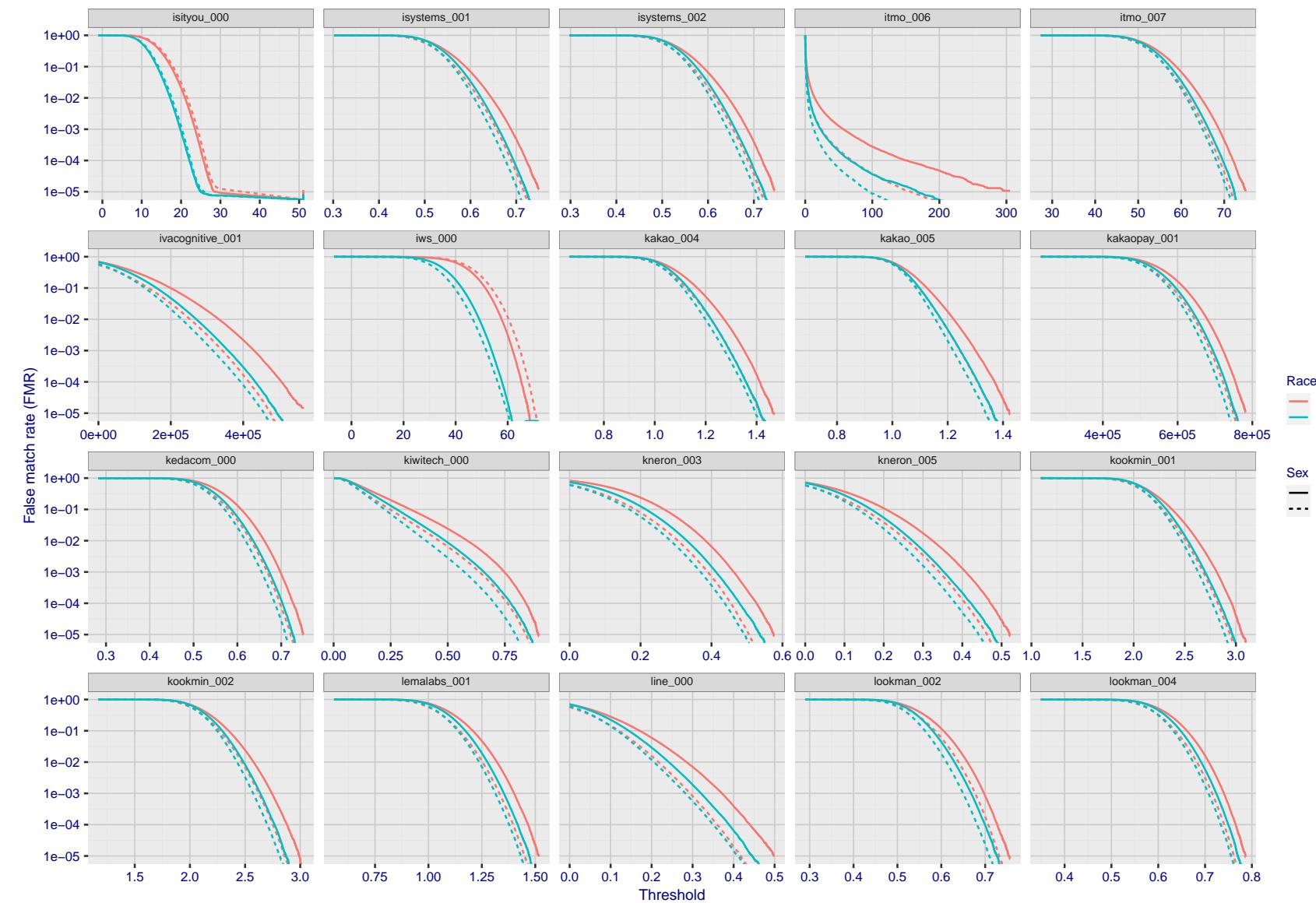


Figure 161: For the mugshot images, the false match calibration curves show false match rate vs. threshold. Separate curves appear for white females, black females, black males and white males.

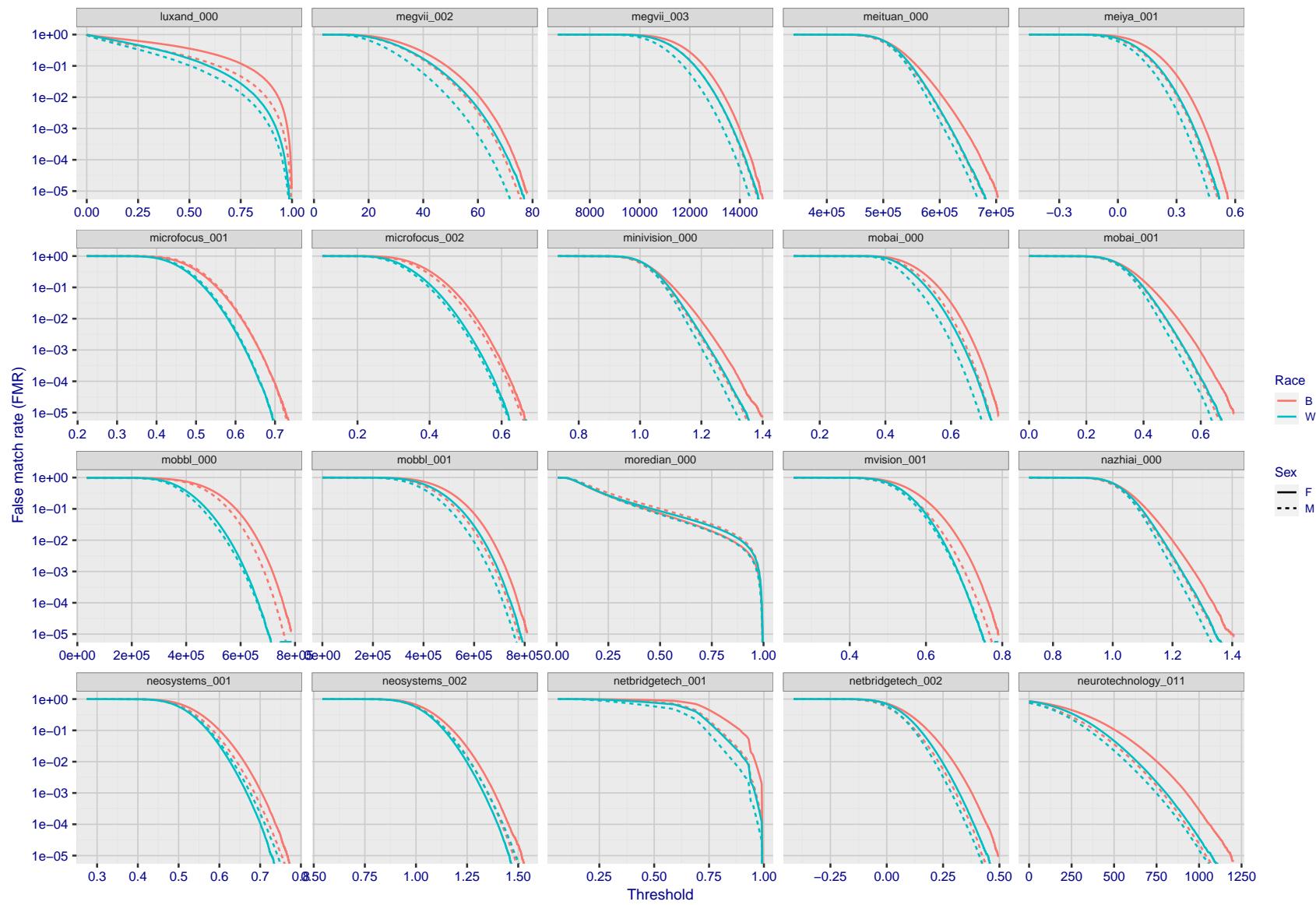


Figure 162: For the mugshot images, the false match calibration curves show false match rate vs. threshold. Separate curves appear for white females, black females, black males and white males.

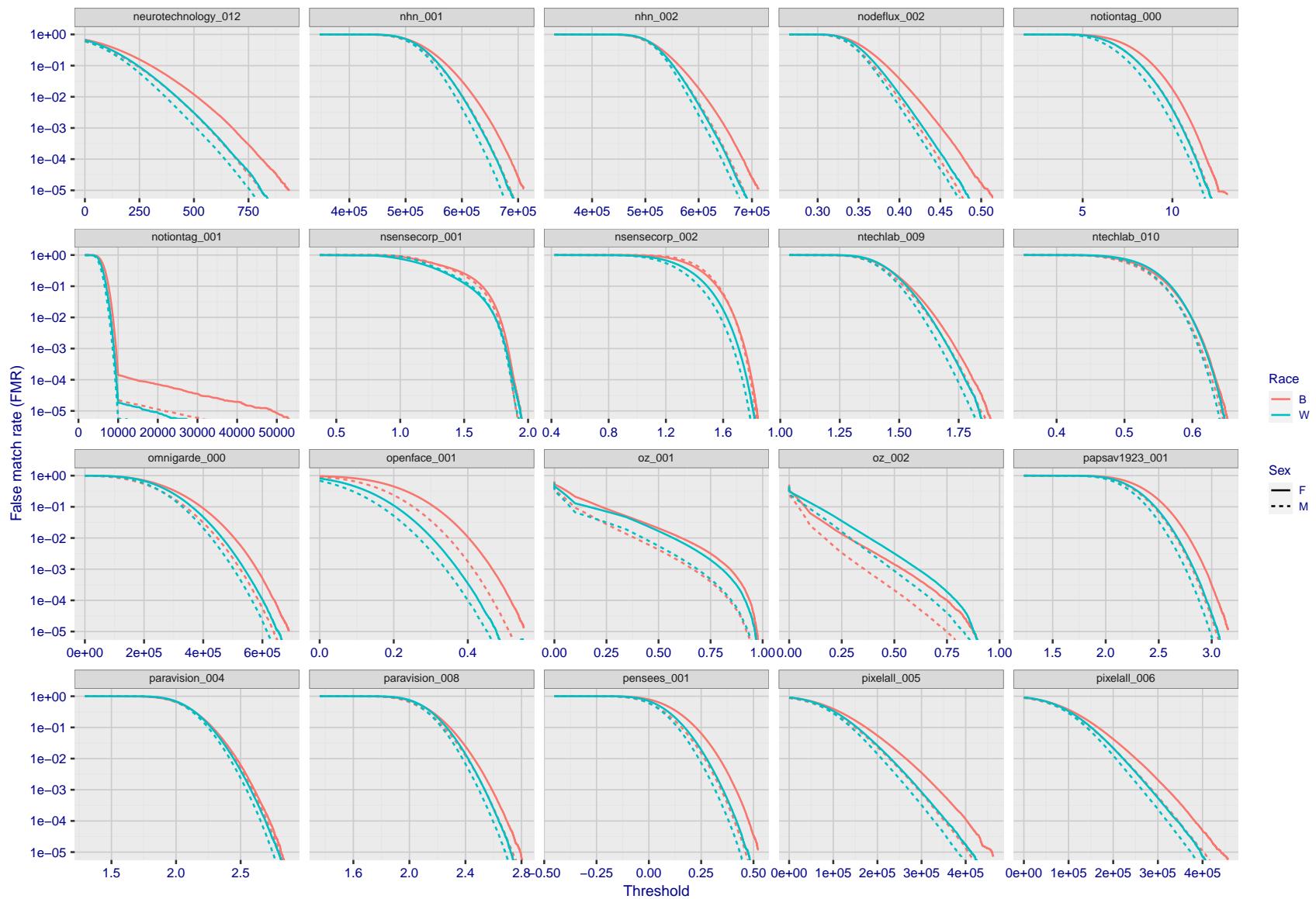


Figure 163: For the mugshot images, the false match calibration curves show false match rate vs. threshold. Separate curves appear for white females, black females, black males and white males.

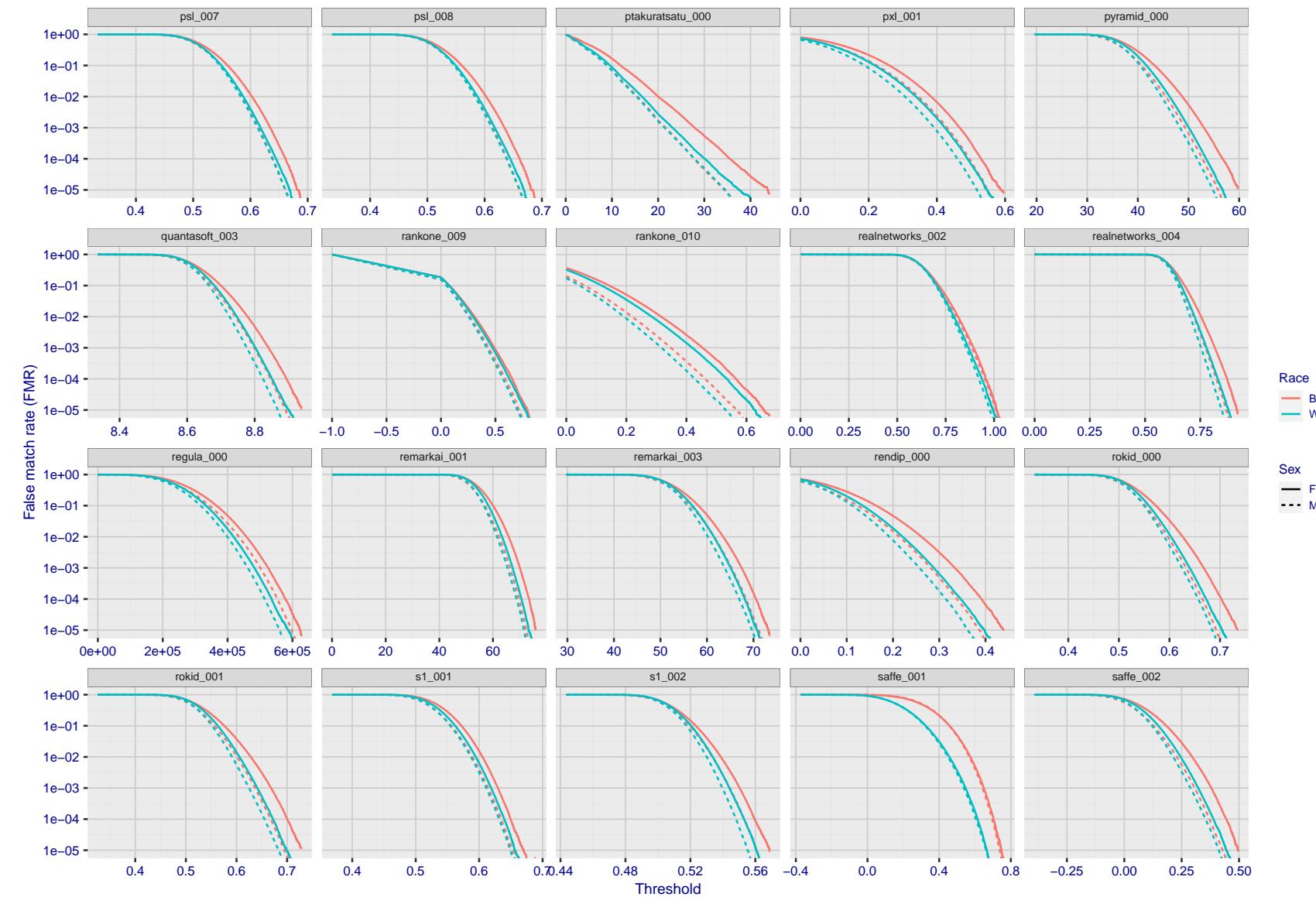


Figure 164: For the mugshot images, the false match calibration curves show false match rate vs. threshold. Separate curves appear for white females, black females, black males and white males.

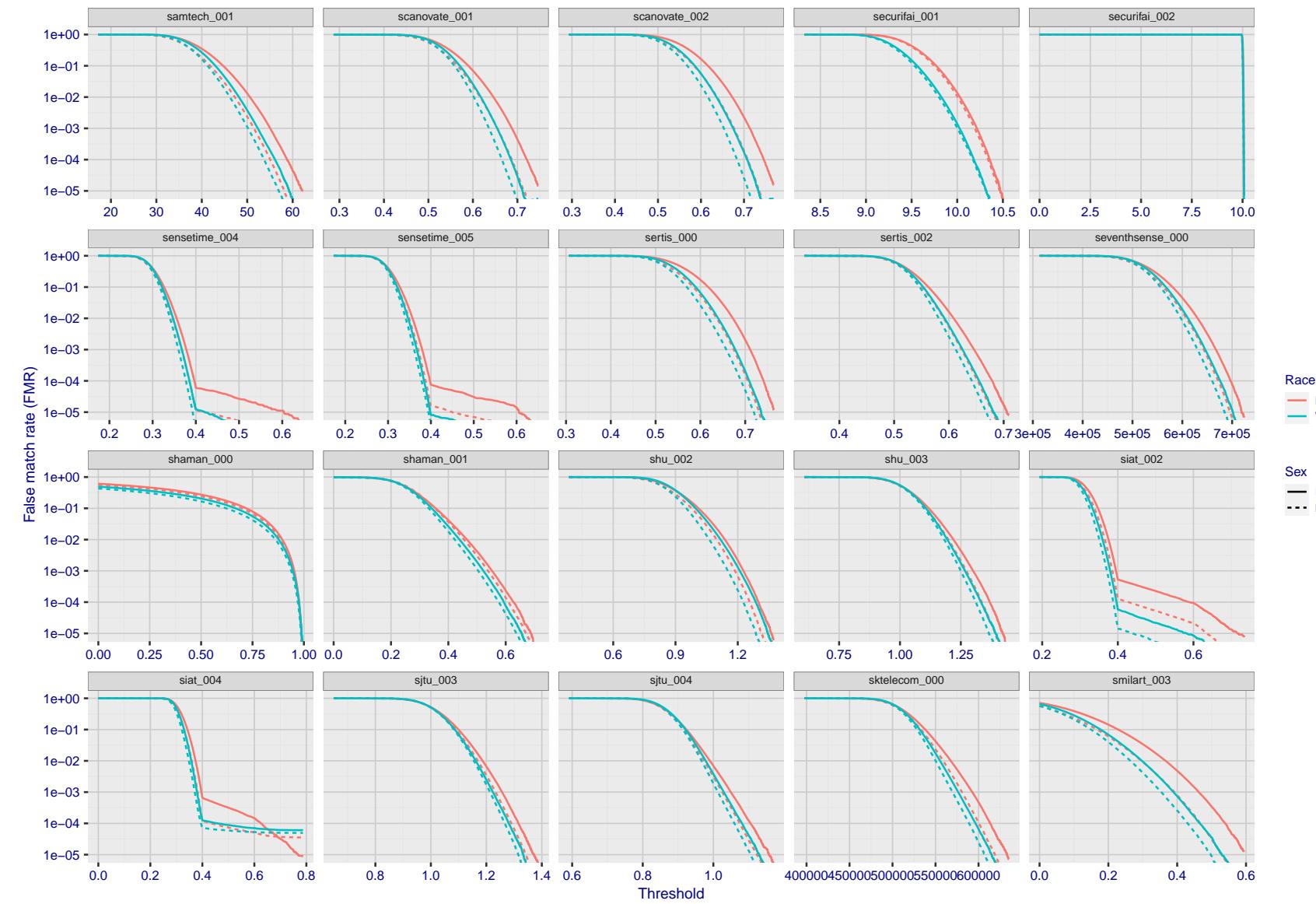


Figure 165: For the mugshot images, the false match calibration curves show false match rate vs. threshold. Separate curves appear for white females, black females, black males and white males.

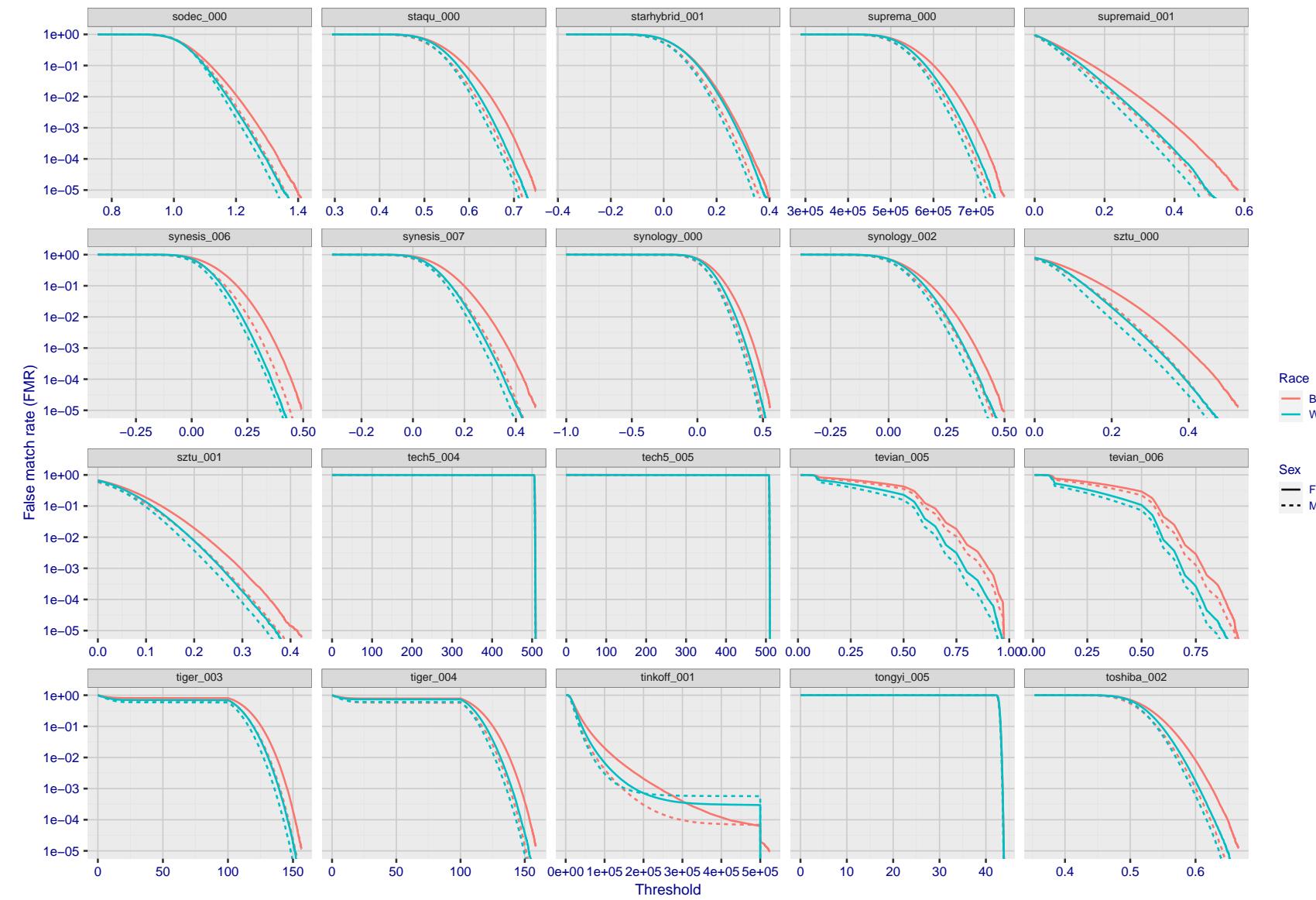


Figure 166: For the mugshot images, the false match calibration curves show false match rate vs. threshold. Separate curves appear for white females, black females, black males and white males.

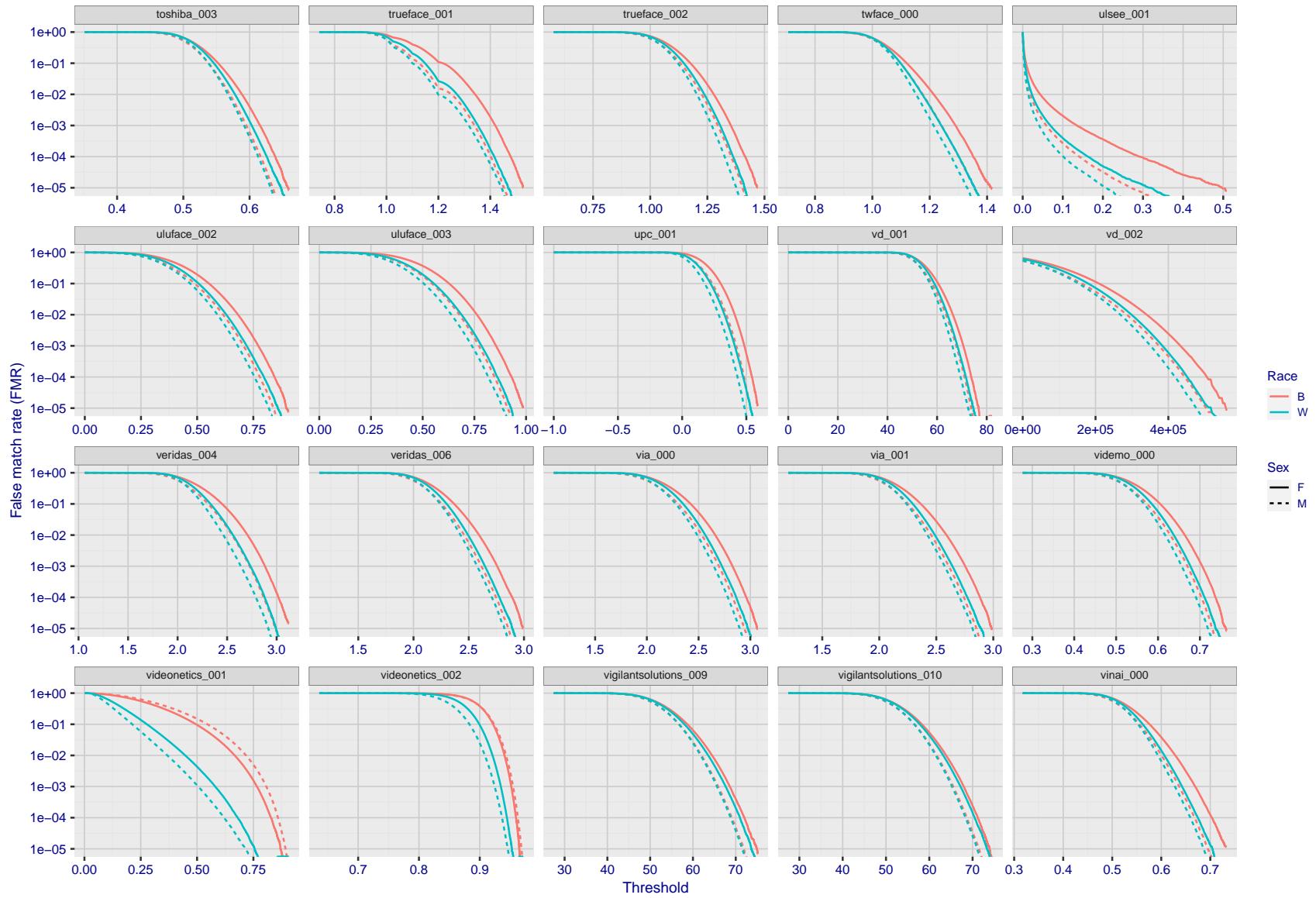


Figure 167: For the mugshot images, the false match calibration curves show false match rate vs. threshold. Separate curves appear for white females, black females, black males and white males.

2021/08/02 13:13:01

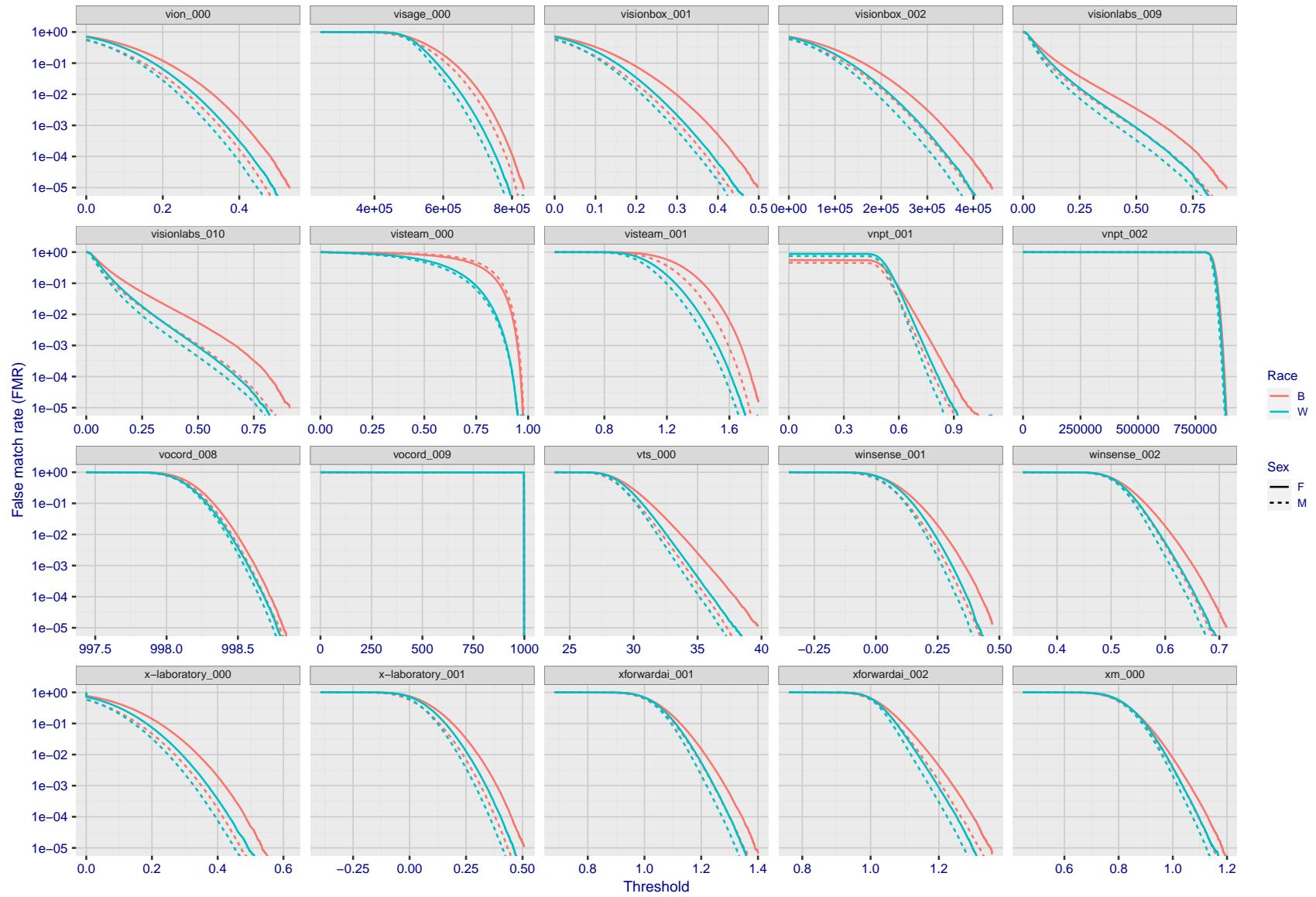


Figure 168: For the mugshot images, the false match calibration curves show false match rate vs. threshold. Separate curves appear for white females, black females, black males and white males.

FNMR(T)

"False non-match rate"

"False match rate"

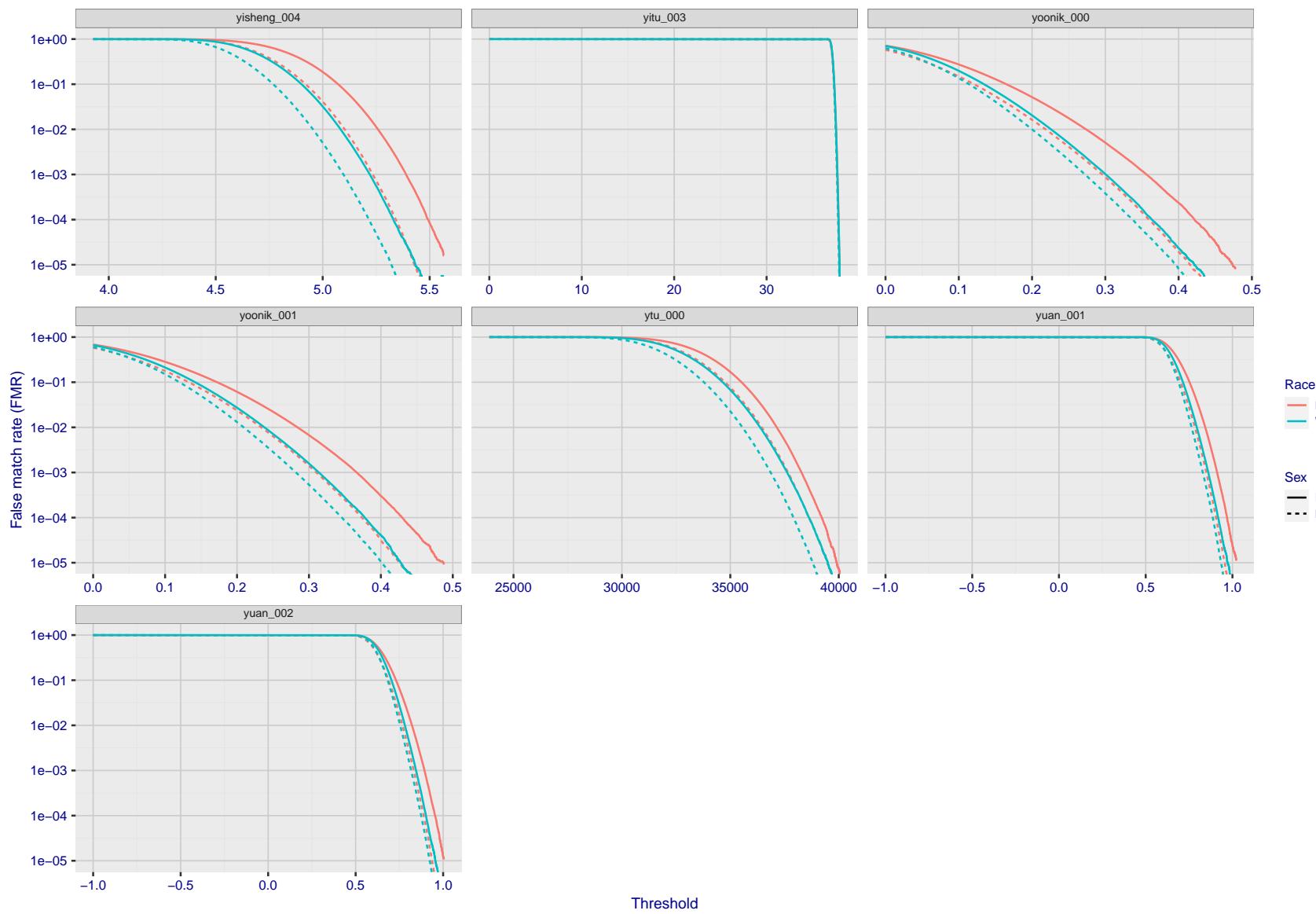


Figure 169: For the mugshot images, the false match calibration curves show false match rate vs. threshold. Separate curves appear for white females, black females, black males and white males.

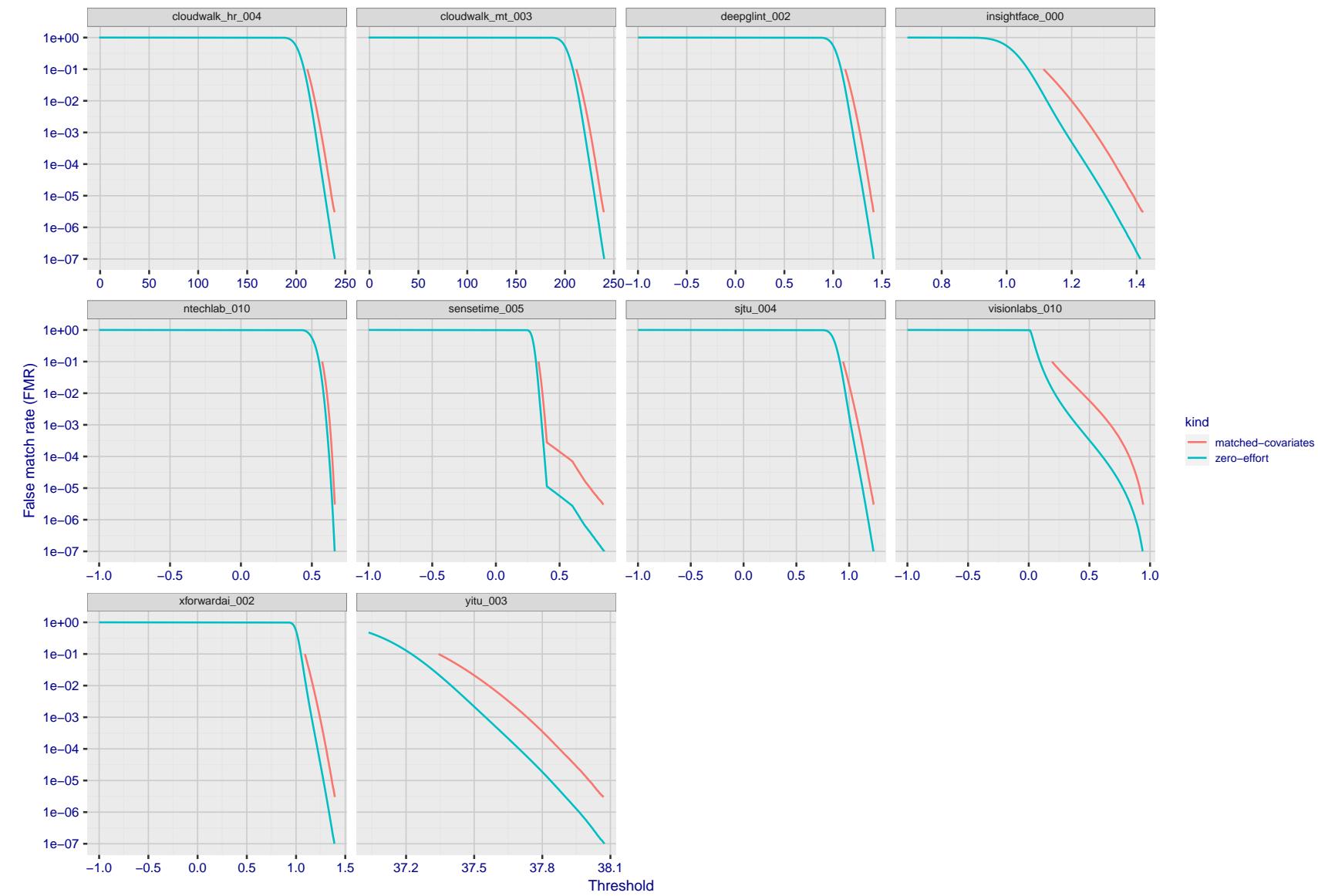


Figure 170: For the visa images, the false match calibration curves show FMR vs. threshold, T . The blue (lower) curves are for zero-effort impostors (i.e. comparing all images against all). The red (upper) curves are for persons of the same-sex, same-age, and same national-origin. This shows that FMR is underestimated (by a factor of 10 or more) by using a zero-effort impostor calculation to calibrate T . As shown later (sec. 3.6), FMR is higher for demographic-matched impostors.

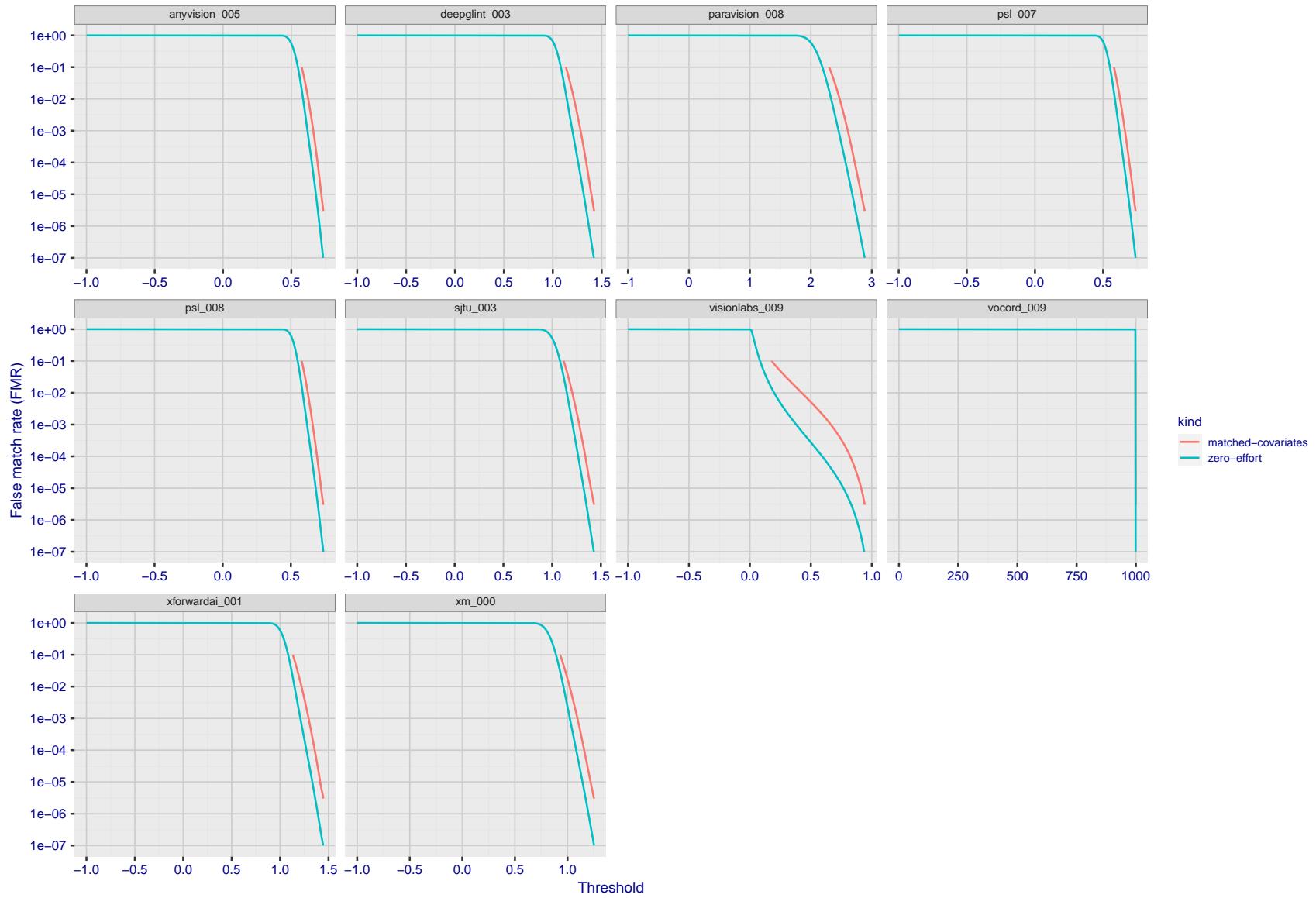


Figure 171: For the visa images, the false match calibration curves show FMR vs. threshold, T . The blue (lower) curves are for zero-effort impostors (i.e. comparing all images against all). The red (upper) curves are for persons of the same-sex, same-age, and same national-origin. This shows that FMR is underestimated (by a factor of 10 or more) by using a zero-effort impostor calculation to calibrate T . As shown later (sec. 3.6), FMR is higher for demographic-matched impostors.

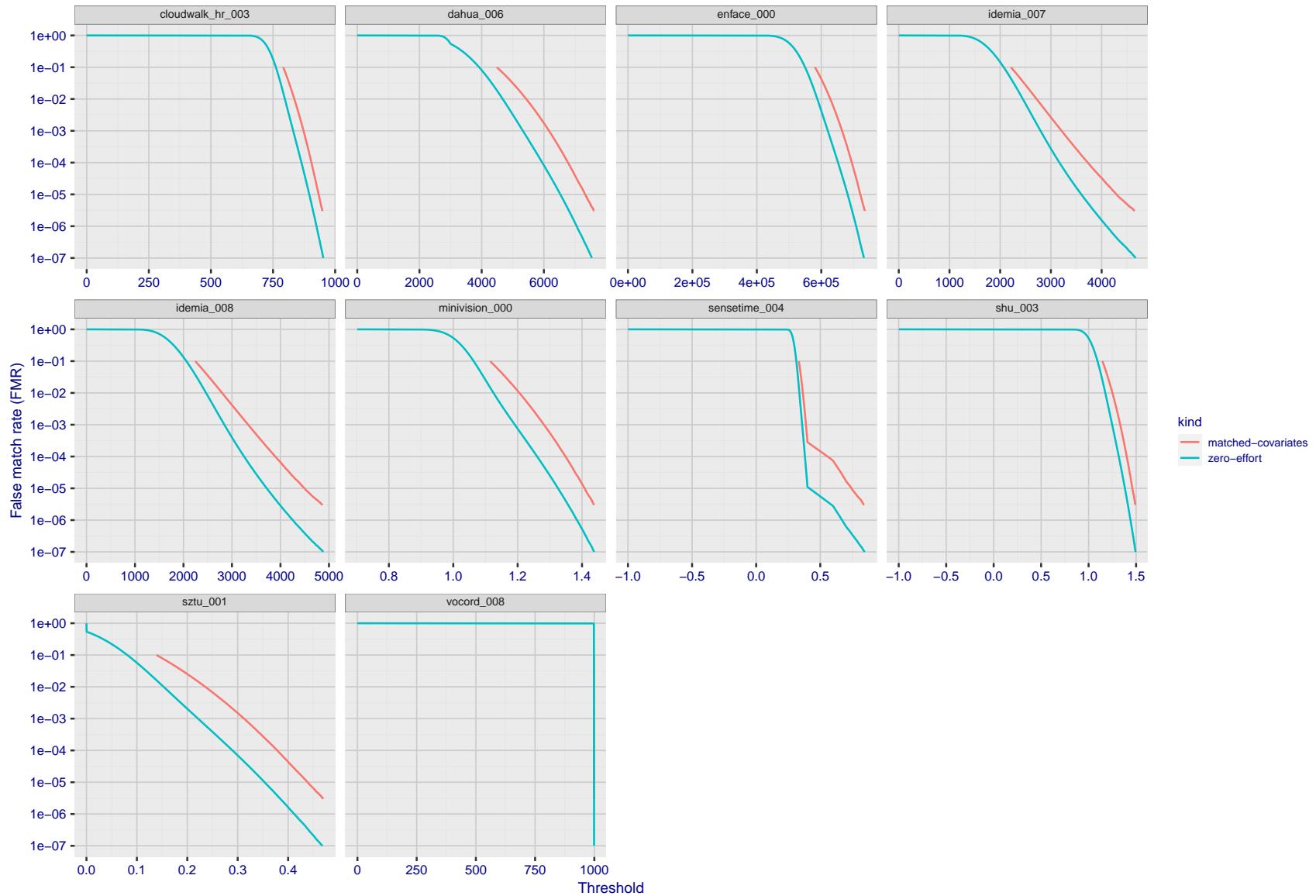


Figure 172: For the visa images, the false match calibration curves show FMR vs. threshold, T . The blue (lower) curves are for zero-effort impostors (i.e. comparing all images against all). The red (upper) curves are for persons of the same-sex, same-age, and same national-origin. This shows that FMR is underestimated (by a factor of 10 or more) by using a zero-effort impostor calculation to calibrate T . As shown later (sec. 3.6), FMR is higher for demographic-matched impostors.

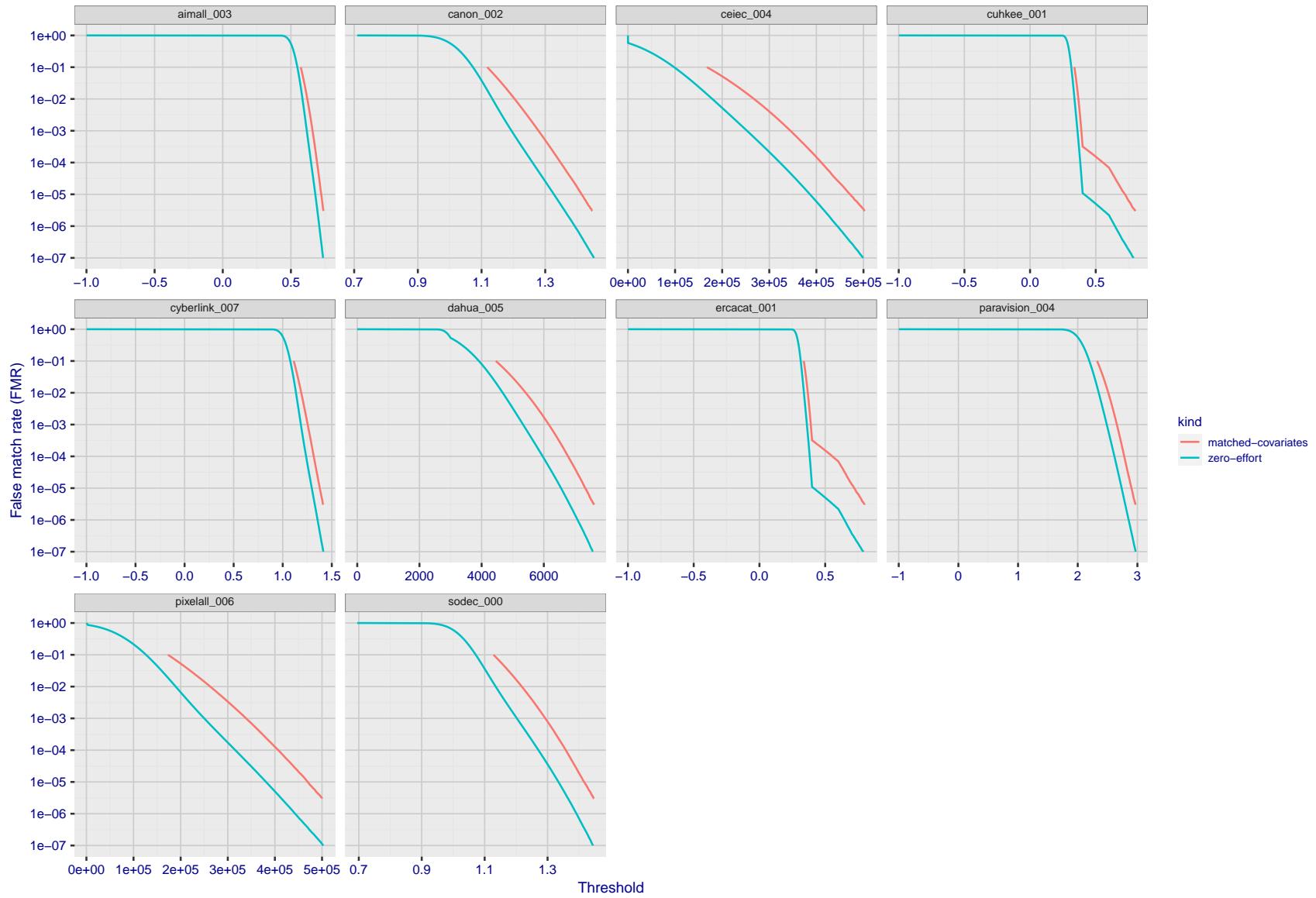


Figure 173: For the visa images, the false match calibration curves show FMR vs. threshold, T . The blue (lower) curves are for zero-effort impostors (i.e. comparing all images against all). The red (upper) curves are for persons of the same-sex, same-age, and same national-origin. This shows that FMR is underestimated (by a factor of 10 or more) by using a zero-effort impostor calculation to calibrate T . As shown later (sec. 3.6), FMR is higher for demographic-matched impostors.

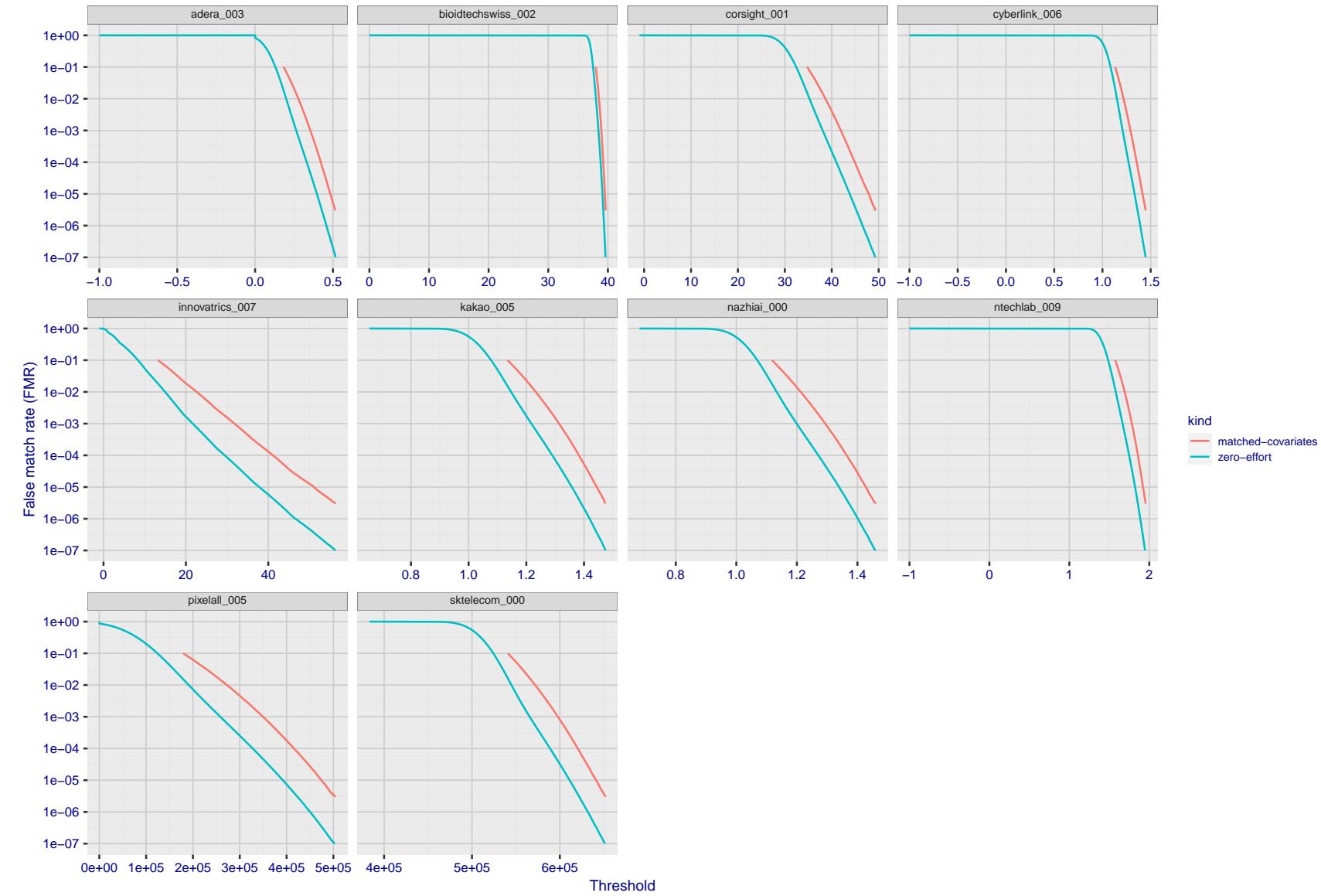


Figure 174: For the visa images, the false match calibration curves show FMR vs. threshold, T . The blue (lower) curves are for zero-effort impostors (i.e. comparing all images against all). The red (upper) curves are for persons of the same-sex, same-age, and same national-origin. This shows that FMR is underestimated (by a factor of 10 or more) by using a zero-effort impostor calculation to calibrate T . As shown later (sec. 3.6), FMR is higher for demographic-matched impostors.

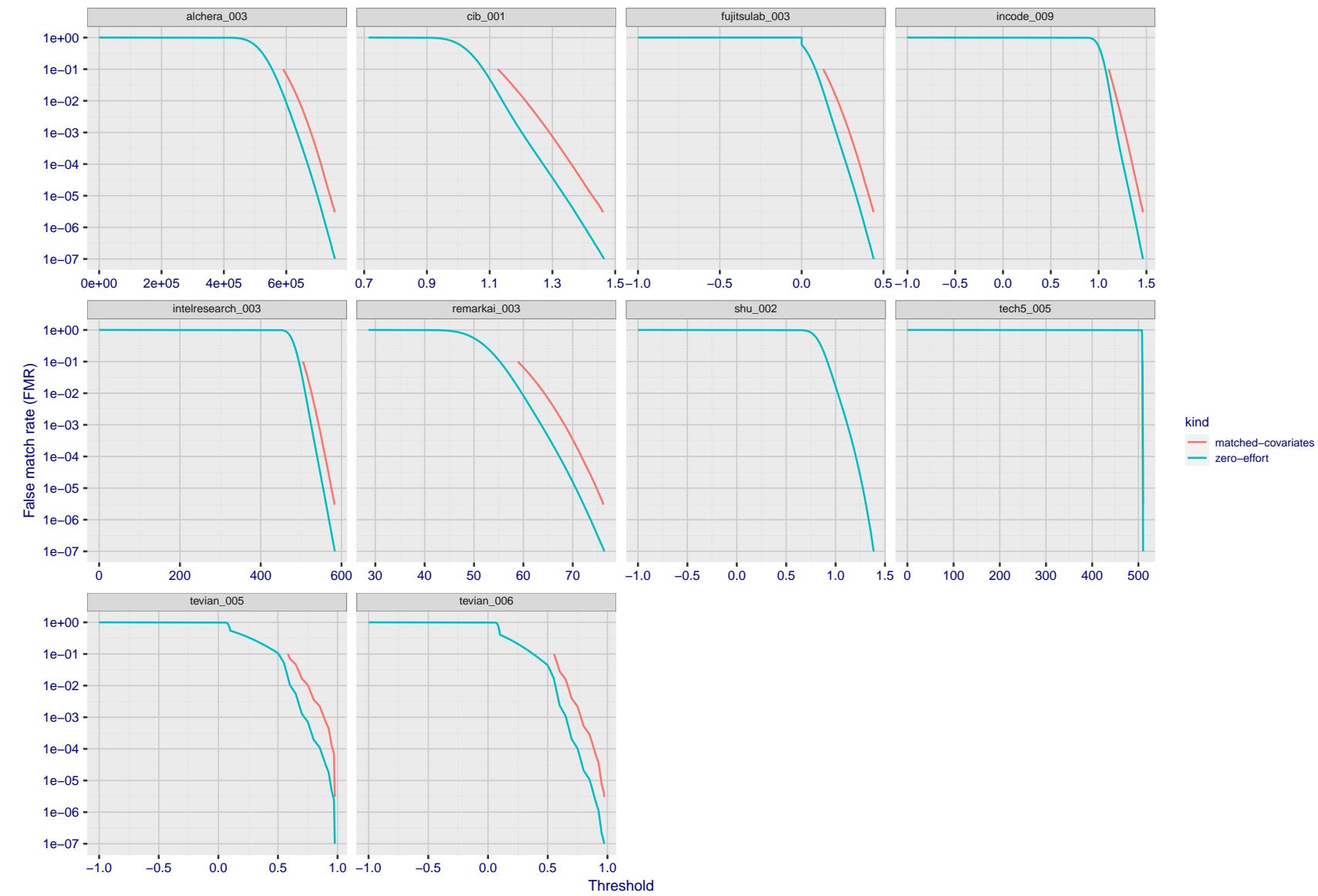


Figure 175: For the visa images, the false match calibration curves show FMR vs. threshold, T . The blue (lower) curves are for zero-effort impostors (i.e. comparing all images against all). The red (upper) curves are for persons of the same-sex, same-age, and same national-origin. This shows that FMR is underestimated (by a factor of 10 or more) by using a zero-effort impostor calculation to calibrate T . As shown later (sec. 3.6), FMR is higher for demographic-matched impostors.

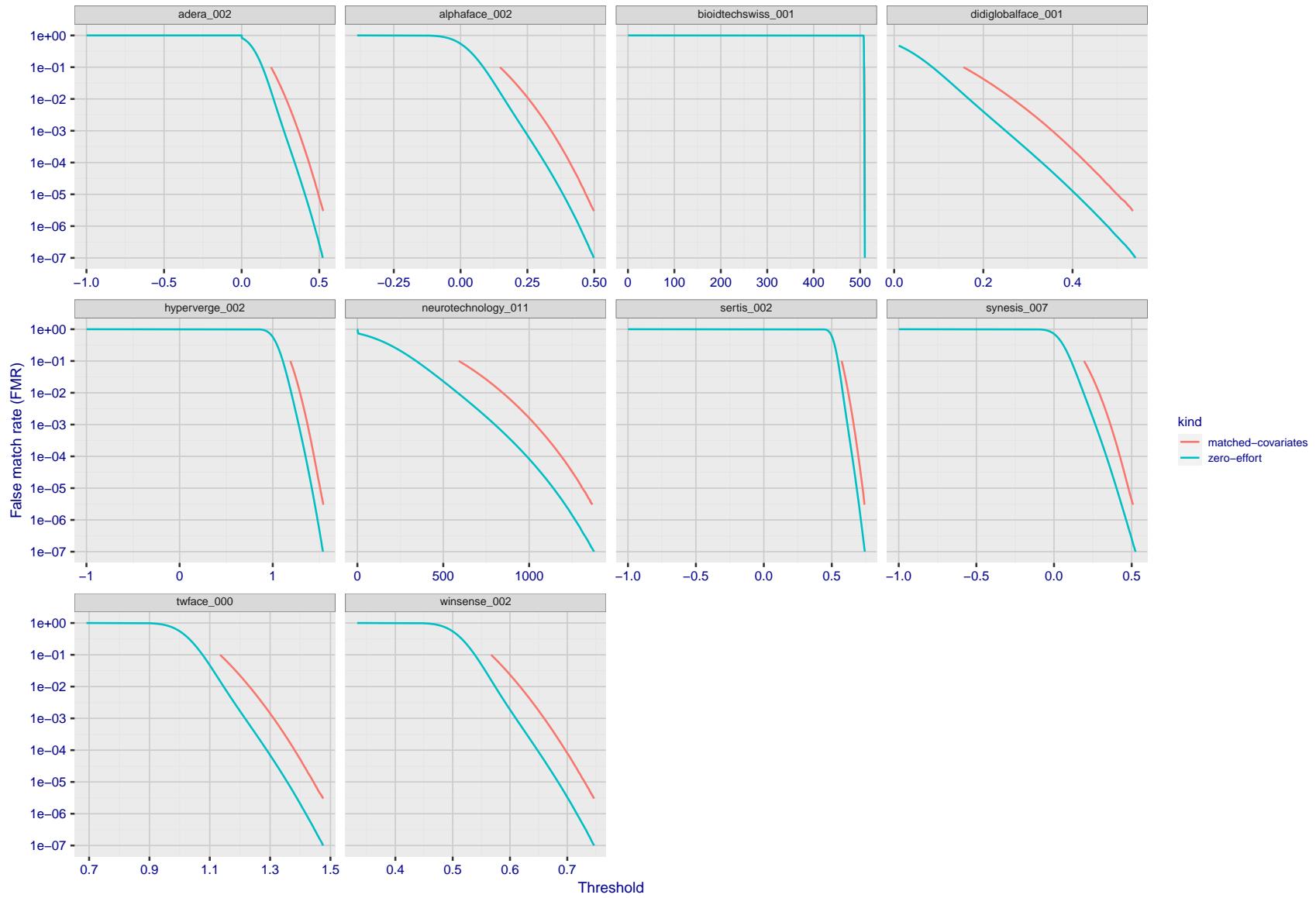


Figure 176: For the visa images, the false match calibration curves show FMR vs. threshold, T . The blue (lower) curves are for zero-effort impostors (i.e. comparing all images against all). The red (upper) curves are for persons of the same-sex, same-age, and same national-origin. This shows that FMR is underestimated (by a factor of 10 or more) by using a zero-effort impostor calculation to calibrate T . As shown later (sec. 3.6), FMR is higher for demographic-matched impostors.

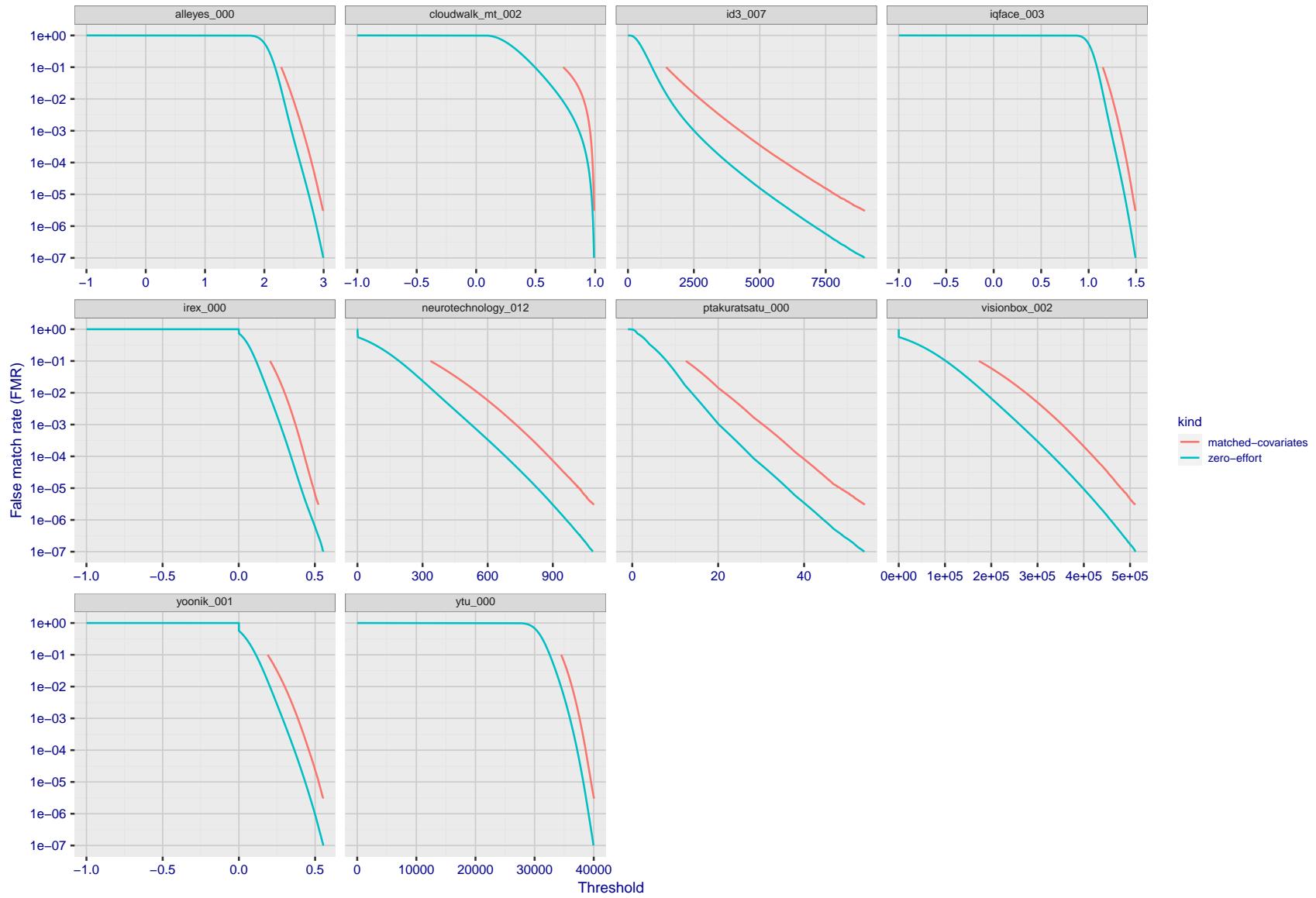


Figure 177: For the visa images, the false match calibration curves show FMR vs. threshold, T . The blue (lower) curves are for zero-effort impostors (i.e. comparing all images against all). The red (upper) curves are for persons of the same-sex, same-age, and same national-origin. This shows that FMR is underestimated (by a factor of 10 or more) by using a zero-effort impostor calculation to calibrate T . As shown later (sec. 3.6), FMR is higher for demographic-matched impostors.

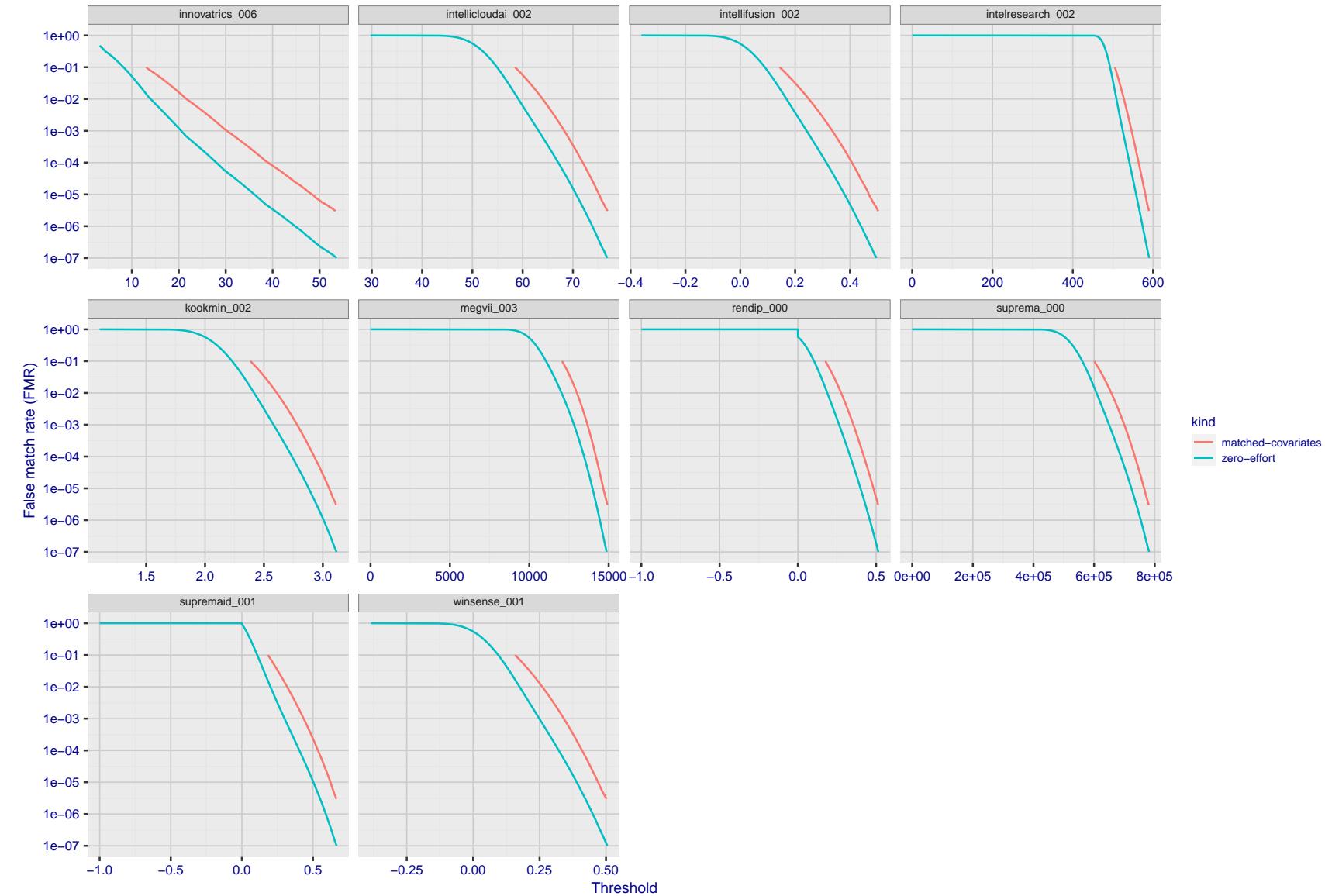


Figure 178: For the visa images, the false match calibration curves show FMR vs. threshold, T . The blue (lower) curves are for zero-effort impostors (i.e. comparing all images against all). The red (upper) curves are for persons of the same-sex, same-age, and same national-origin. This shows that FMR is underestimated (by a factor of 10 or more) by using a zero-effort impostor calculation to calibrate T . As shown later (sec. 3.6), FMR is higher for demographic-matched impostors.

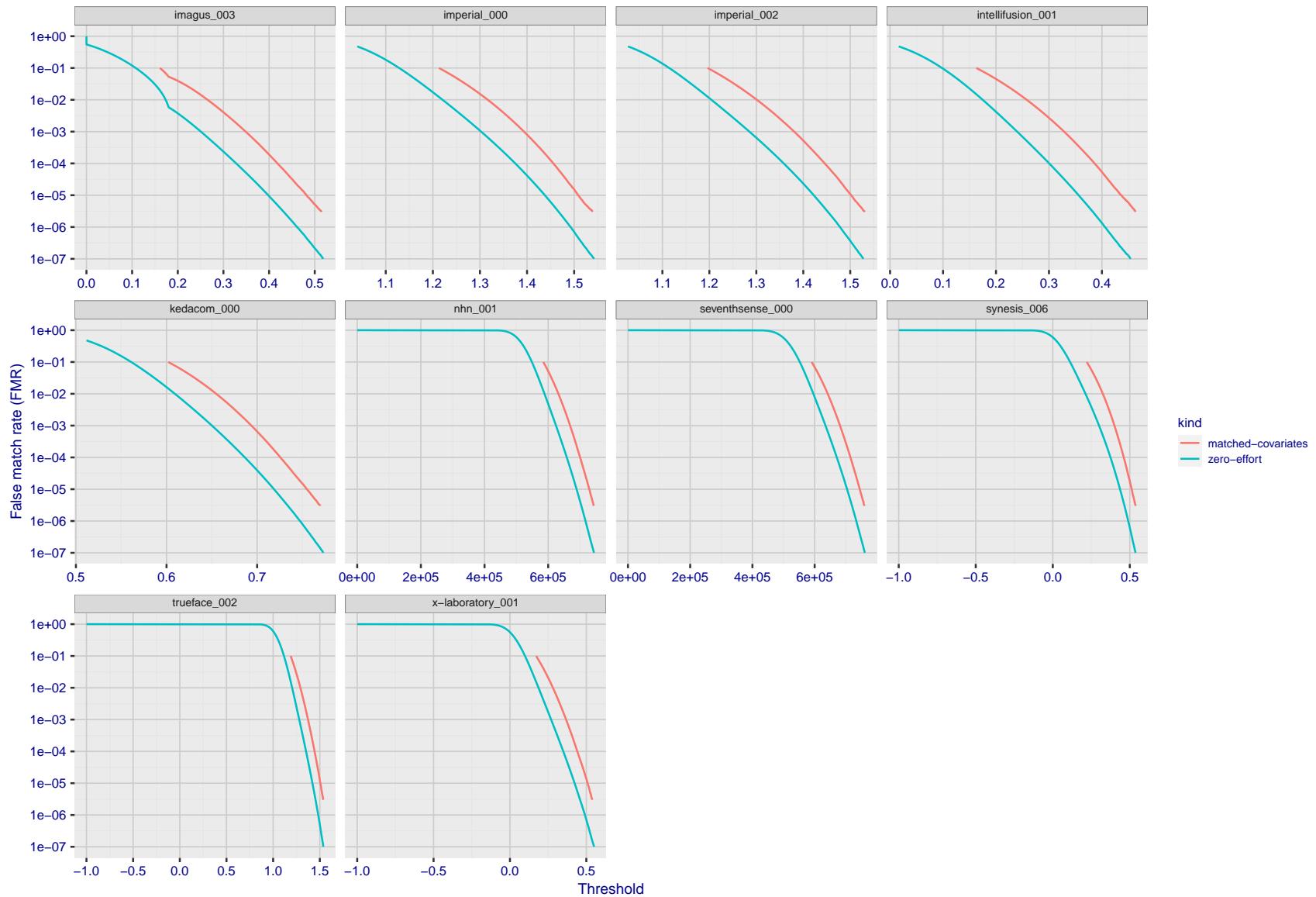


Figure 179: For the visa images, the false match calibration curves show FMR vs. threshold, T . The blue (lower) curves are for zero-effort impostors (i.e. comparing all images against all). The red (upper) curves are for persons of the same-sex, same-age, and same national-origin. This shows that FMR is underestimated (by a factor of 10 or more) by using a zero-effort impostor calculation to calibrate T . As shown later (sec. 3.6), FMR is higher for demographic-matched impostors.

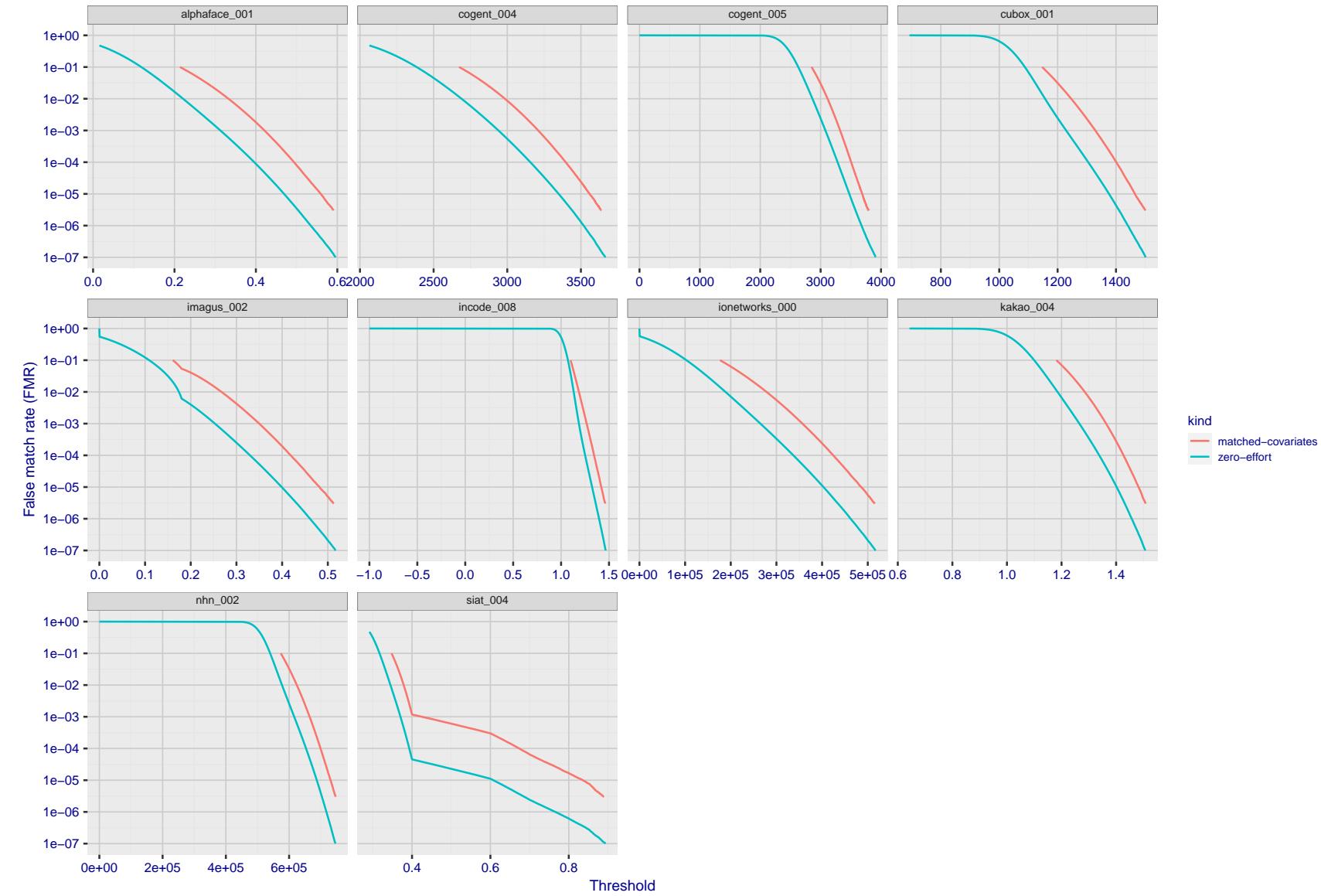


Figure 180: For the visa images, the false match calibration curves show FMR vs. threshold, T . The blue (lower) curves are for zero-effort impostors (i.e. comparing all images against all). The red (upper) curves are for persons of the same-sex, same-age, and same national-origin. This shows that FMR is underestimated (by a factor of 10 or more) by using a zero-effort impostor calculation to calibrate T . As shown later (sec. 3.6), FMR is higher for demographic-matched impostors.

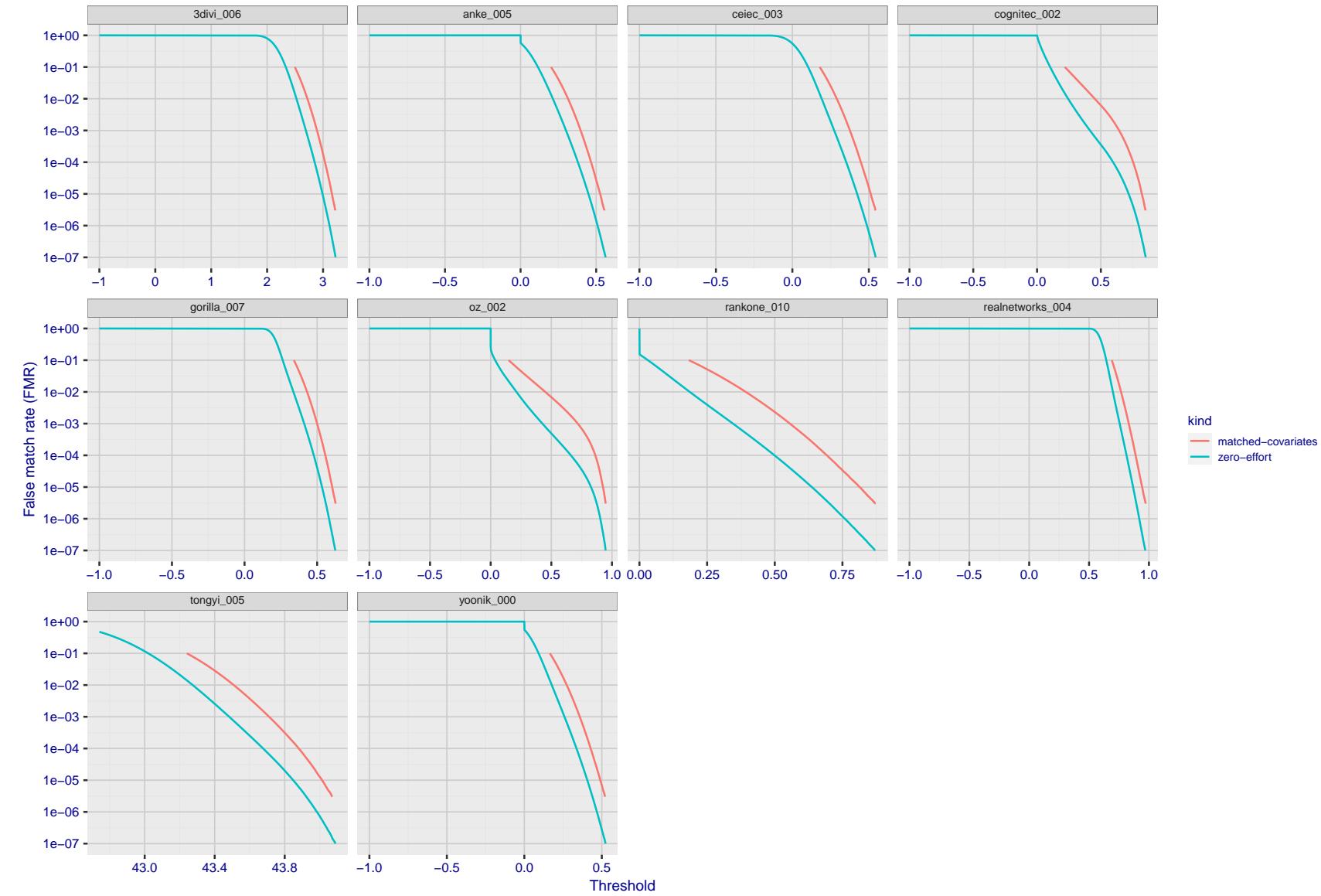


Figure 181: For the visa images, the false match calibration curves show FMR vs. threshold, T . The blue (lower) curves are for zero-effort impostors (i.e. comparing all images against all). The red (upper) curves are for persons of the same-sex, same-age, and same national-origin. This shows that FMR is underestimated (by a factor of 10 or more) by using a zero-effort impostor calculation to calibrate T . As shown later (sec. 3.6), FMR is higher for demographic-matched impostors.

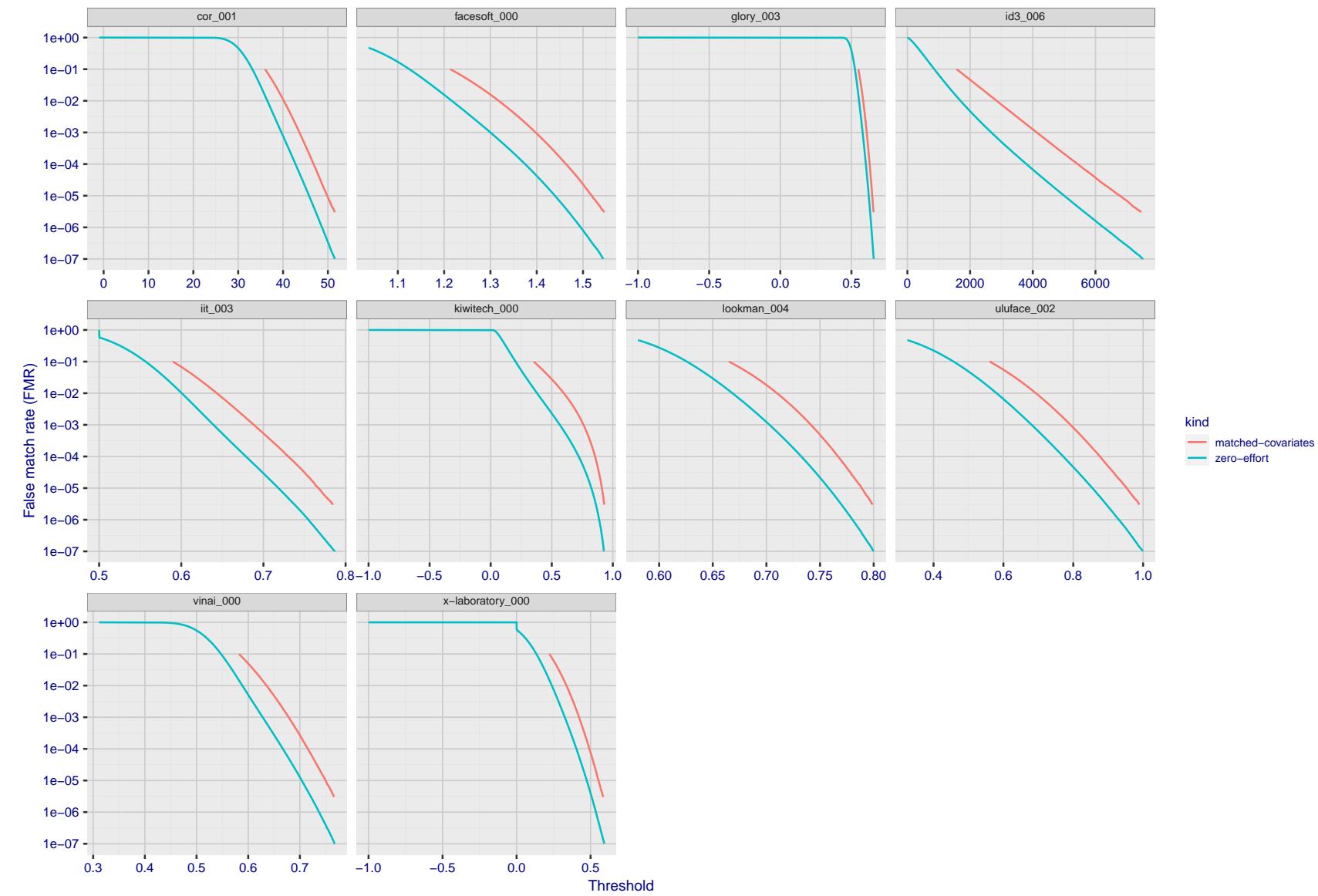


Figure 182: For the visa images, the false match calibration curves show FMR vs. threshold, T . The blue (lower) curves are for zero-effort impostors (i.e. comparing all images against all). The red (upper) curves are for persons of the same-sex, same-age, and same national-origin. This shows that FMR is underestimated (by a factor of 10 or more) by using a zero-effort impostor calculation to calibrate T . As shown later (sec. 3.6), FMR is higher for demographic-matched impostors.

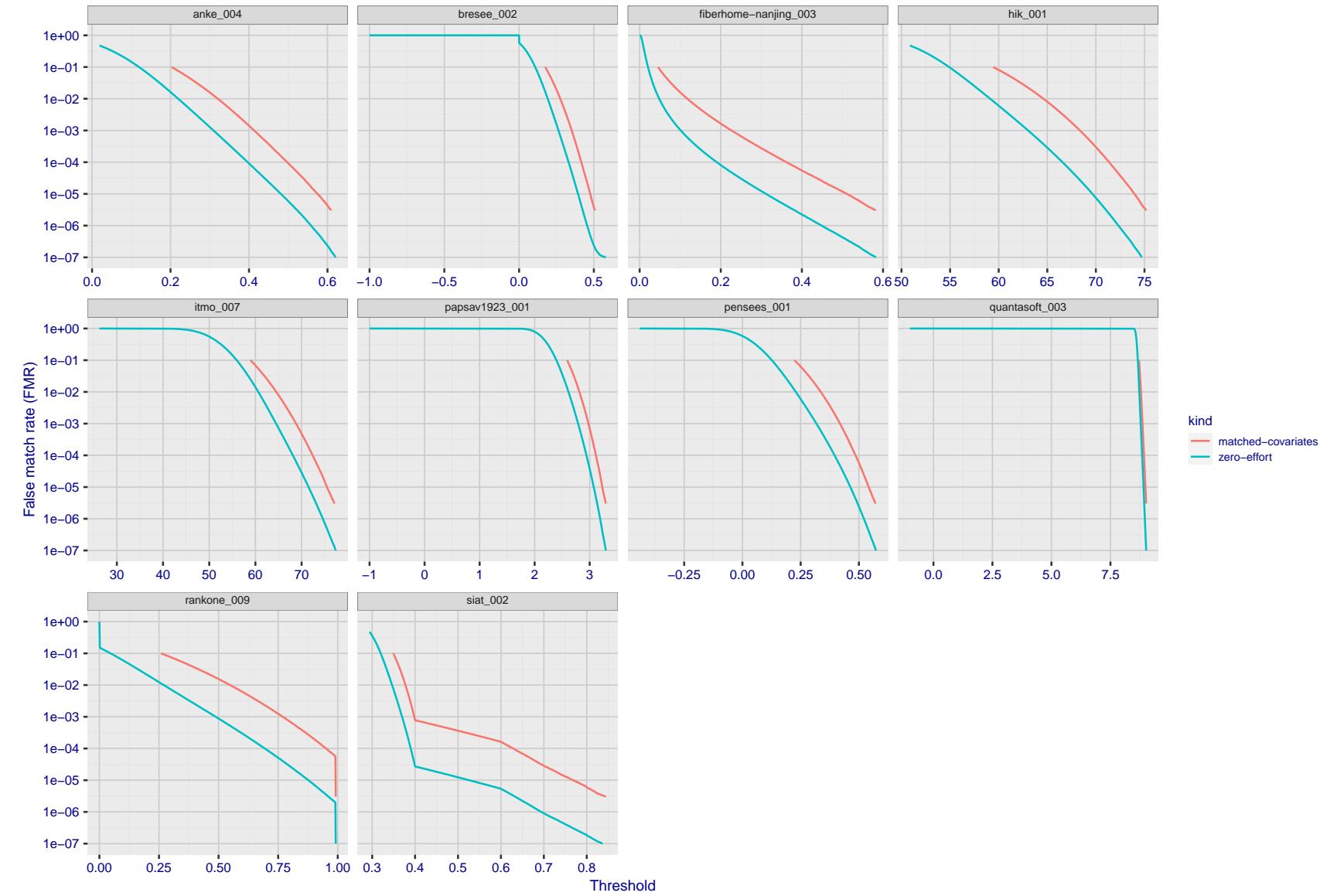


Figure 183: For the visa images, the false match calibration curves show FMR vs. threshold, T . The blue (lower) curves are for zero-effort impostors (i.e. comparing all images against all). The red (upper) curves are for persons of the same-sex, same-age, and same national-origin. This shows that FMR is underestimated (by a factor of 10 or more) by using a zero-effort impostor calculation to calibrate T . As shown later (sec. 3.6), FMR is higher for demographic-matched impostors.

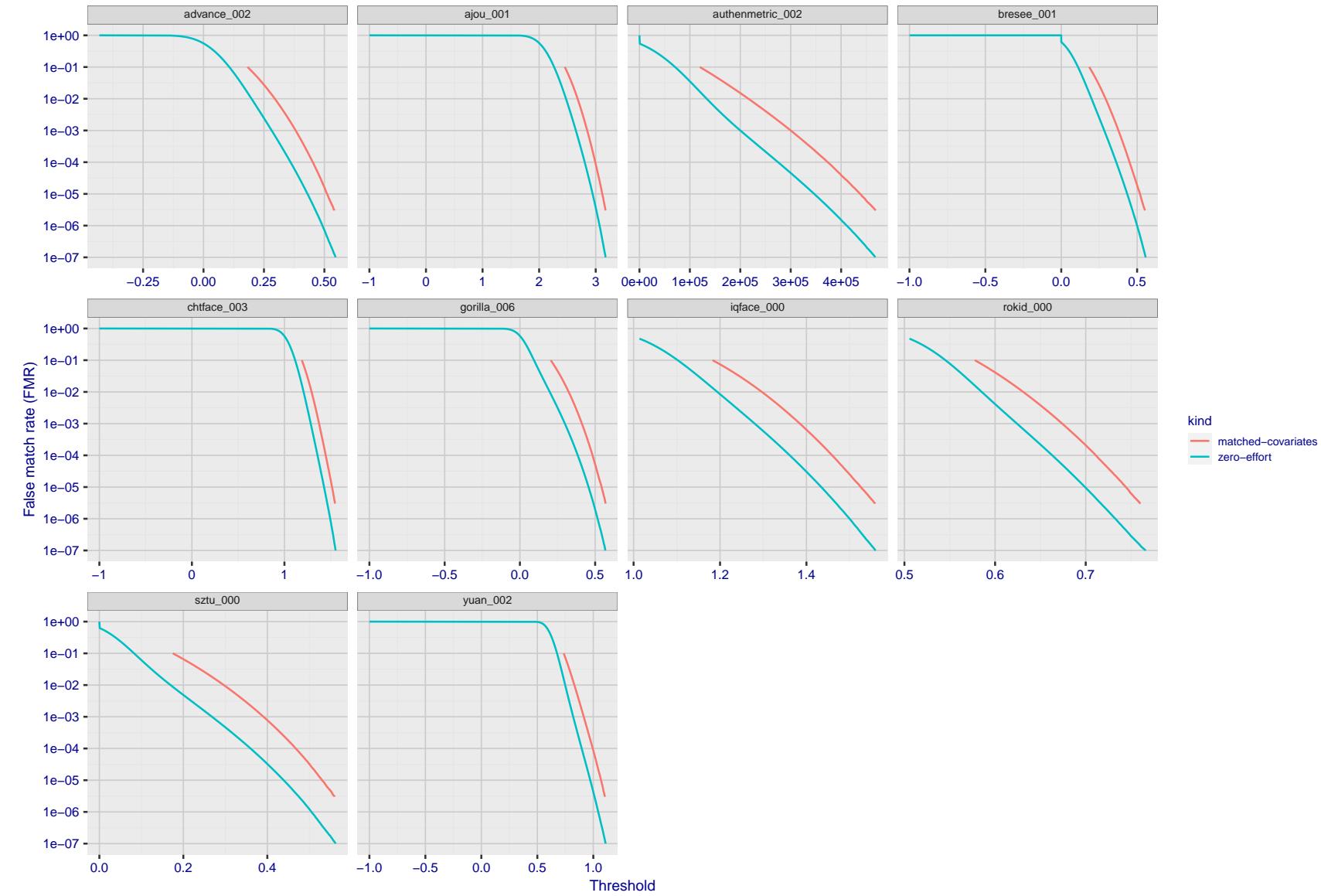


Figure 184: For the visa images, the false match calibration curves show FMR vs. threshold, T . The blue (lower) curves are for zero-effort impostors (i.e. comparing all images against all). The red (upper) curves are for persons of the same-sex, same-age, and same national-origin. This shows that FMR is underestimated (by a factor of 10 or more) by using a zero-effort impostor calculation to calibrate T . As shown later (sec. 3.6), FMR is higher for demographic-matched impostors.

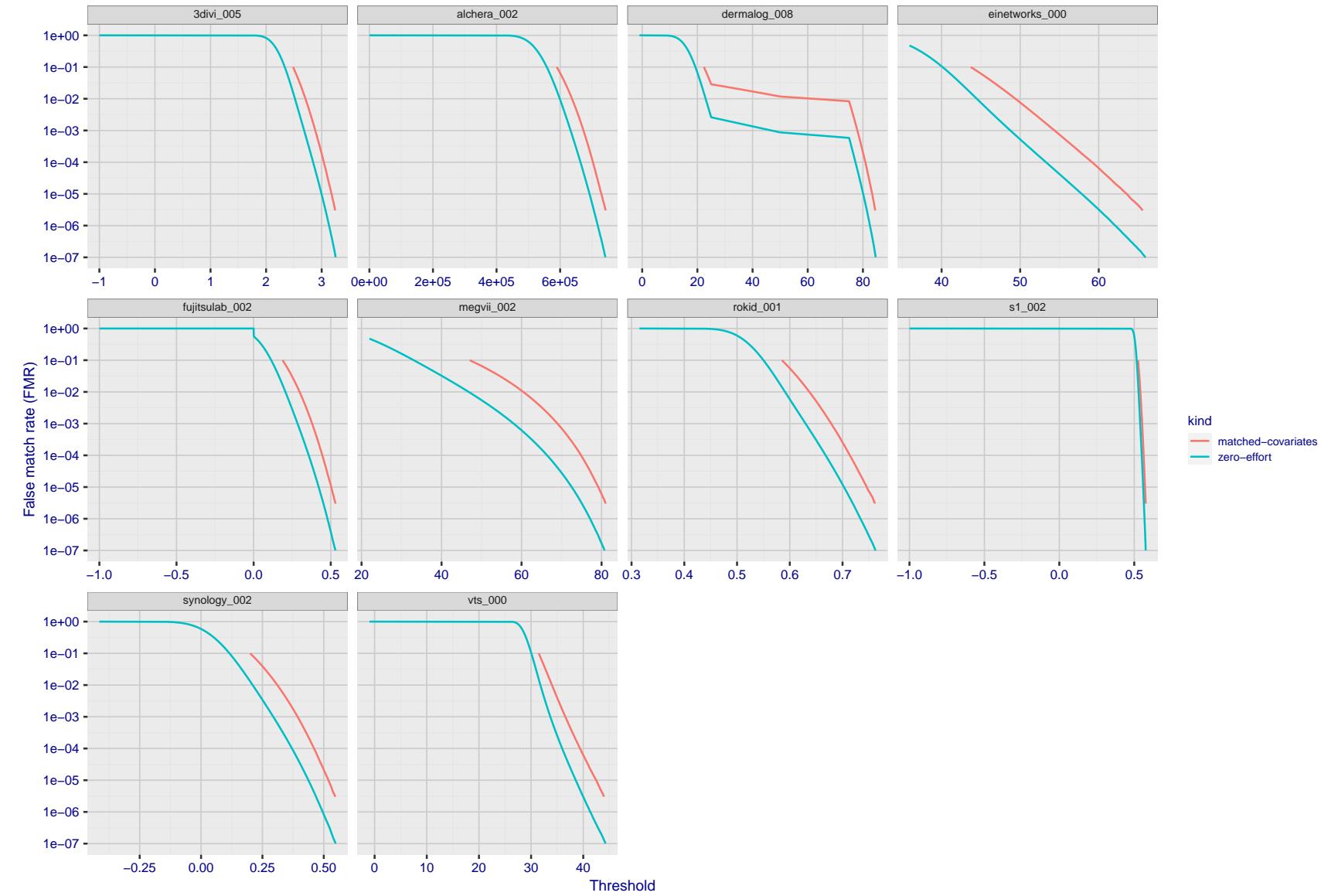


Figure 185: For the visa images, the false match calibration curves show FMR vs. threshold, T . The blue (lower) curves are for zero-effort impostors (i.e. comparing all images against all). The red (upper) curves are for persons of the same-sex, same-age, and same national-origin. This shows that FMR is underestimated (by a factor of 10 or more) by using a zero-effort impostor calculation to calibrate T . As shown later (sec. 3.6), FMR is higher for demographic-matched impostors.

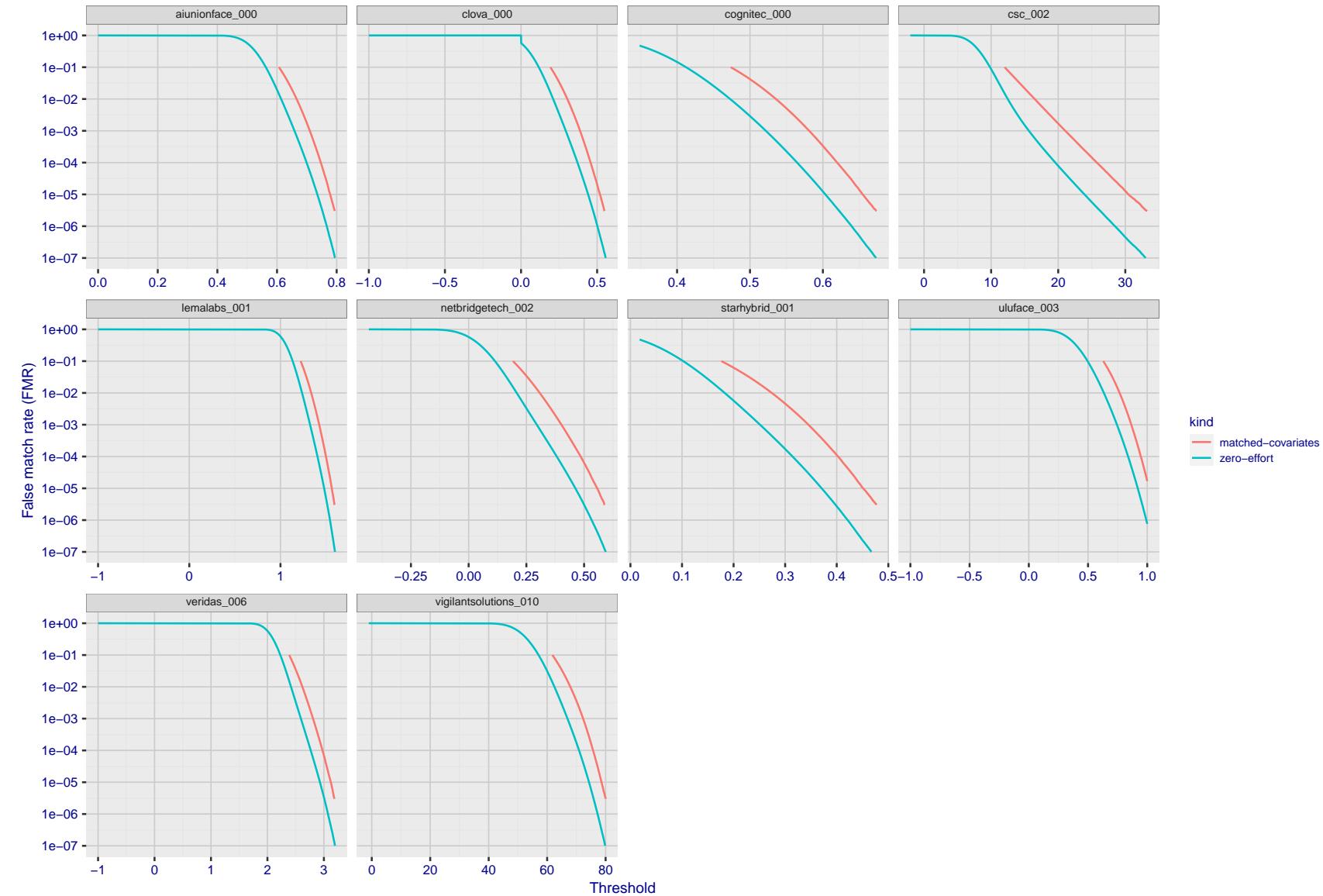


Figure 186: For the visa images, the false match calibration curves show FMR vs. threshold, T . The blue (lower) curves are for zero-effort impostors (i.e. comparing all images against all). The red (upper) curves are for persons of the same-sex, same-age, and same national-origin. This shows that FMR is underestimated (by a factor of 10 or more) by using a zero-effort impostor calculation to calibrate T . As shown later (sec. 3.6), FMR is higher for demographic-matched impostors.

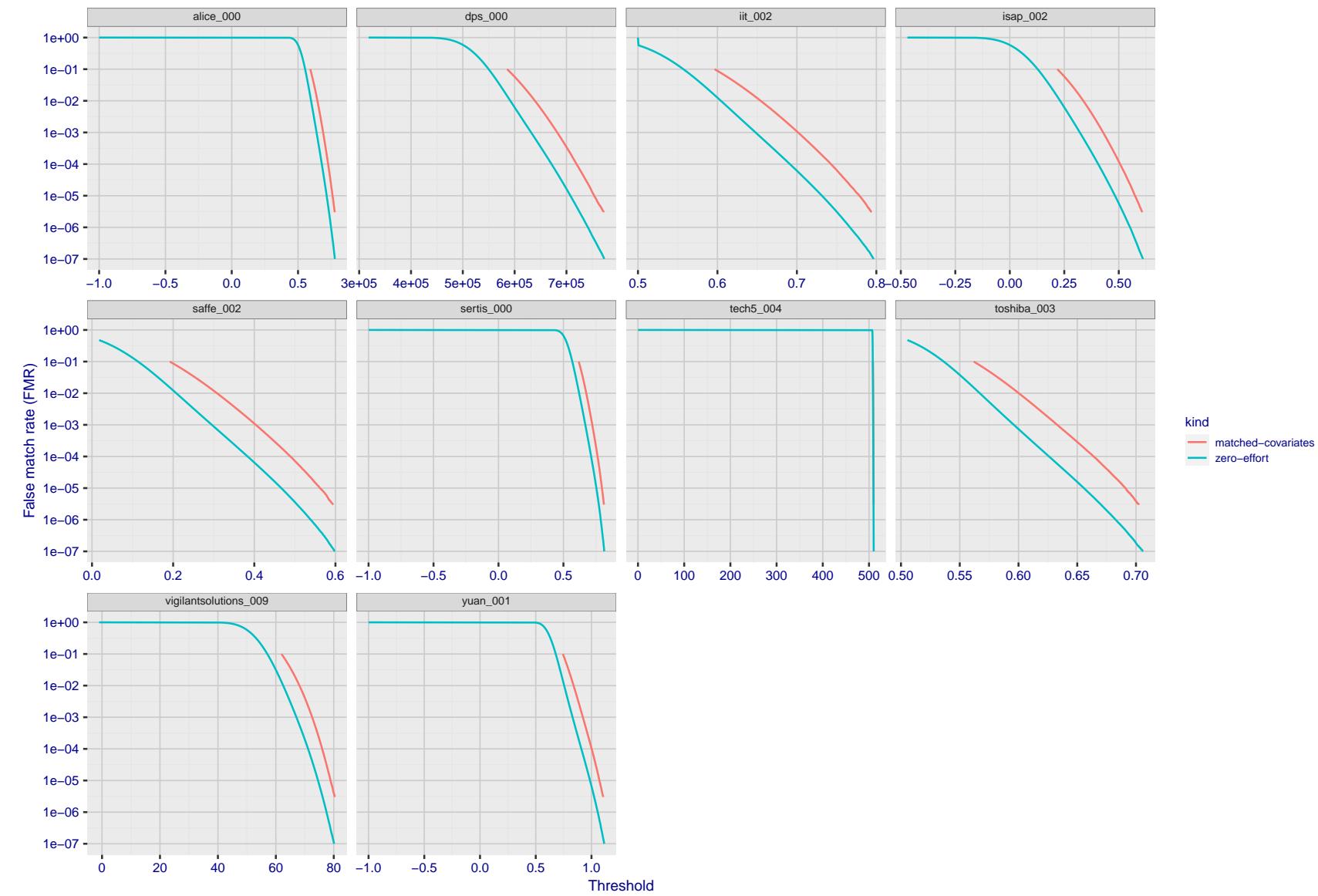


Figure 187: For the visa images, the false match calibration curves show FMR vs. threshold, T . The blue (lower) curves are for zero-effort impostors (i.e. comparing all images against all). The red (upper) curves are for persons of the same-sex, same-age, and same national-origin. This shows that FMR is underestimated (by a factor of 10 or more) by using a zero-effort impostor calculation to calibrate T . As shown later (sec. 3.6), FMR is higher for demographic-matched impostors.

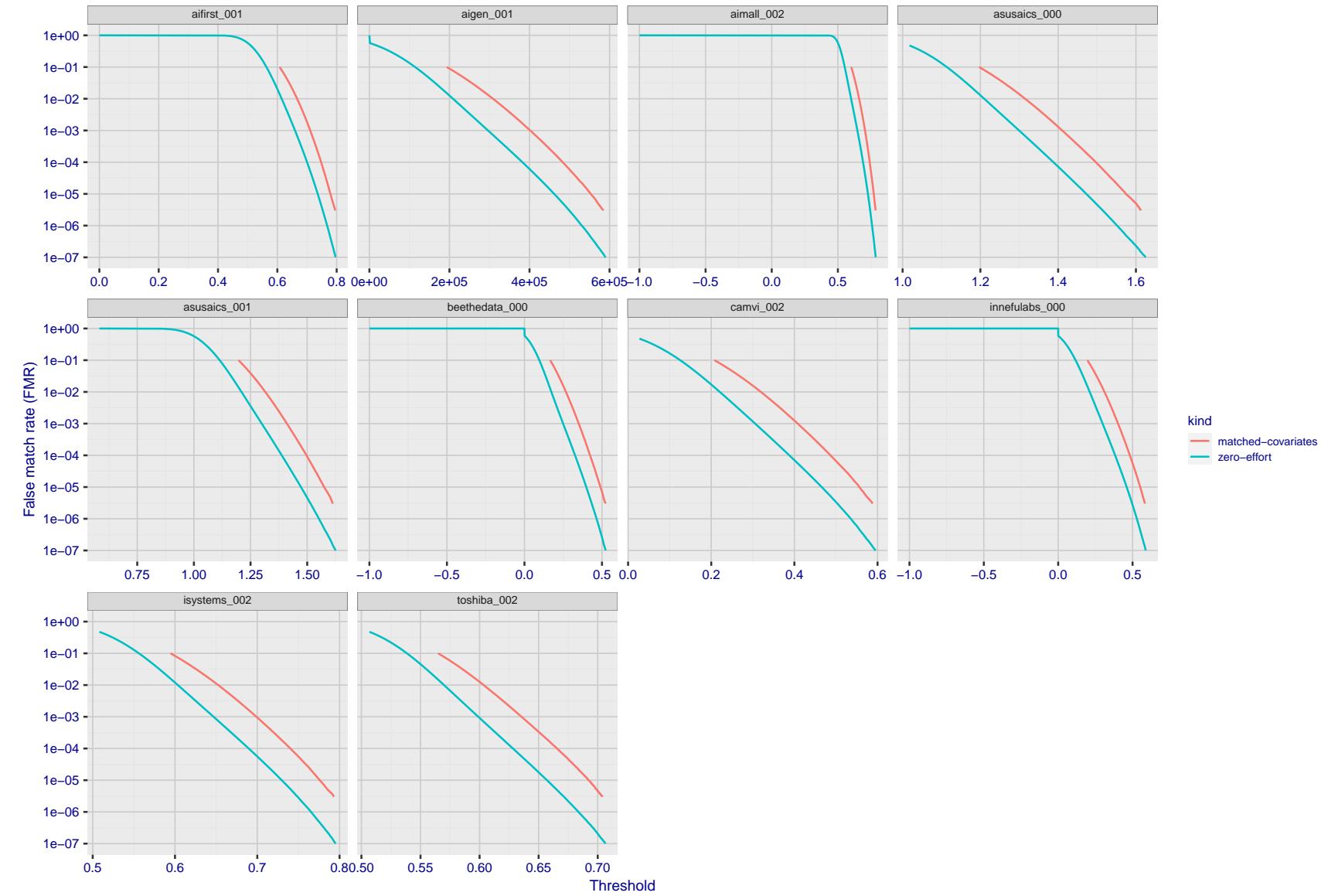


Figure 188: For the visa images, the false match calibration curves show FMR vs. threshold, T . The blue (lower) curves are for zero-effort impostors (i.e. comparing all images against all). The red (upper) curves are for persons of the same-sex, same-age, and same national-origin. This shows that FMR is underestimated (by a factor of 10 or more) by using a zero-effort impostor calculation to calibrate T . As shown later (sec. 3.6), FMR is higher for demographic-matched impostors.

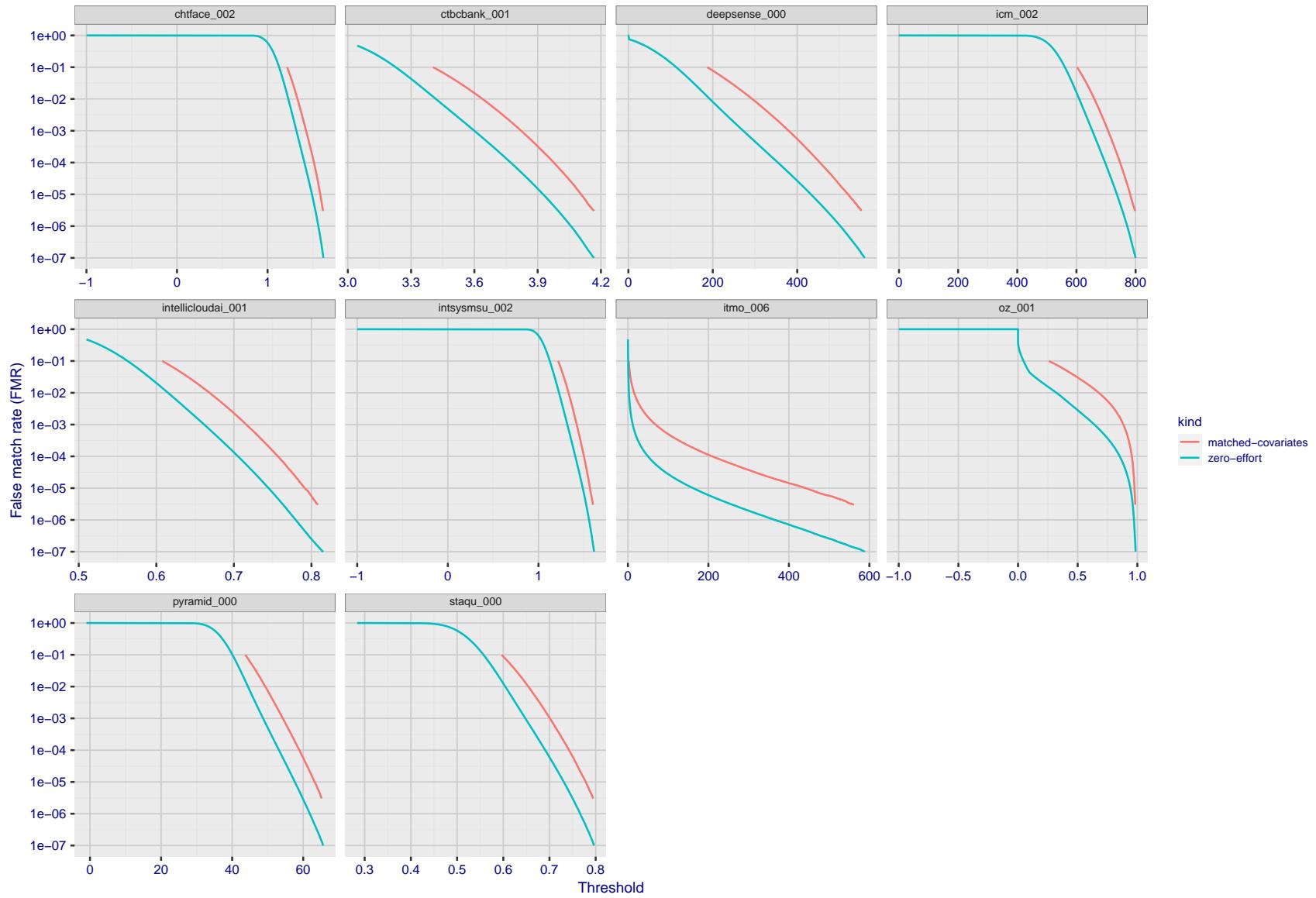


Figure 189: For the visa images, the false match calibration curves show FMR vs. threshold, T . The blue (lower) curves are for zero-effort impostors (i.e. comparing all images against all). The red (upper) curves are for persons of the same-sex, same-age, and same national-origin. This shows that FMR is underestimated (by a factor of 10 or more) by using a zero-effort impostor calculation to calibrate T . As shown later (sec. 3.6), FMR is higher for demographic-matched impostors.

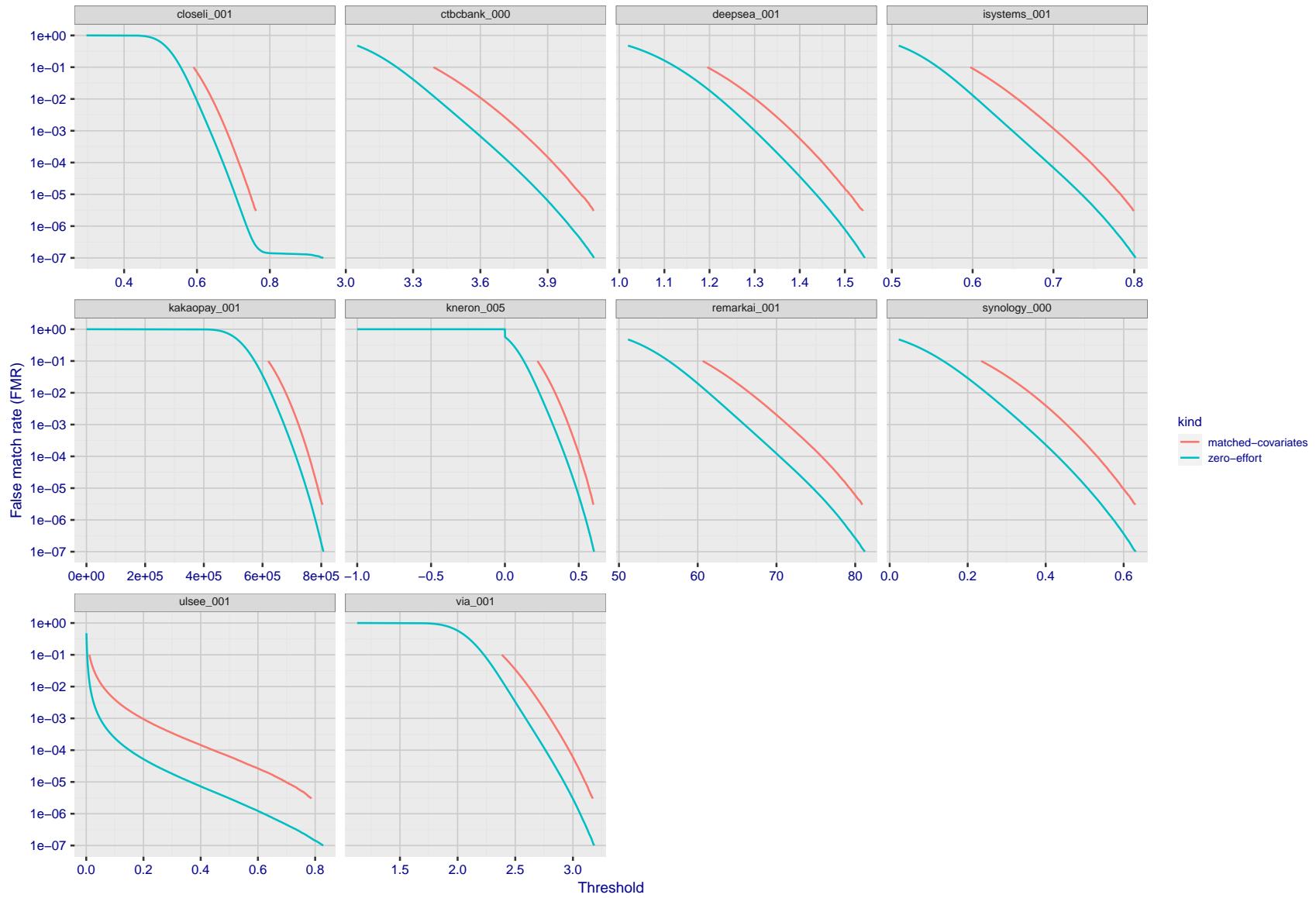


Figure 190: For the visa images, the false match calibration curves show FMR vs. threshold, T . The blue (lower) curves are for zero-effort impostors (i.e. comparing all images against all). The red (upper) curves are for persons of the same-sex, same-age, and same national-origin. This shows that FMR is underestimated (by a factor of 10 or more) by using a zero-effort impostor calculation to calibrate T . As shown later (sec. 3.6), FMR is higher for demographic-matched impostors.

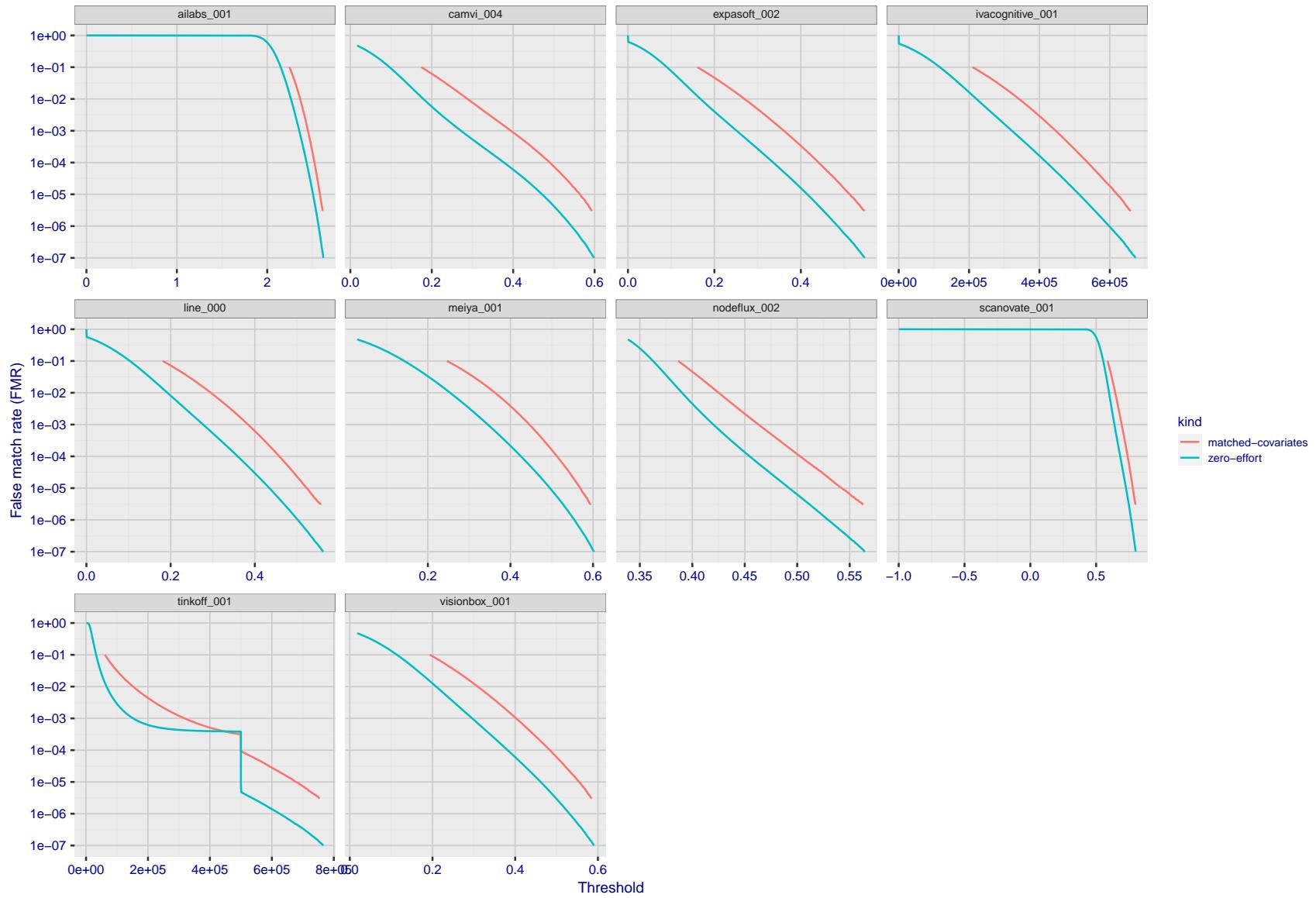


Figure 191: For the visa images, the false match calibration curves show FMR vs. threshold, T . The blue (lower) curves are for zero-effort impostors (i.e. comparing all images against all). The red (upper) curves are for persons of the same-sex, same-age, and same national-origin. This shows that FMR is underestimated (by a factor of 10 or more) by using a zero-effort impostor calculation to calibrate T . As shown later (sec. 3.6), FMR is higher for demographic-matched impostors.

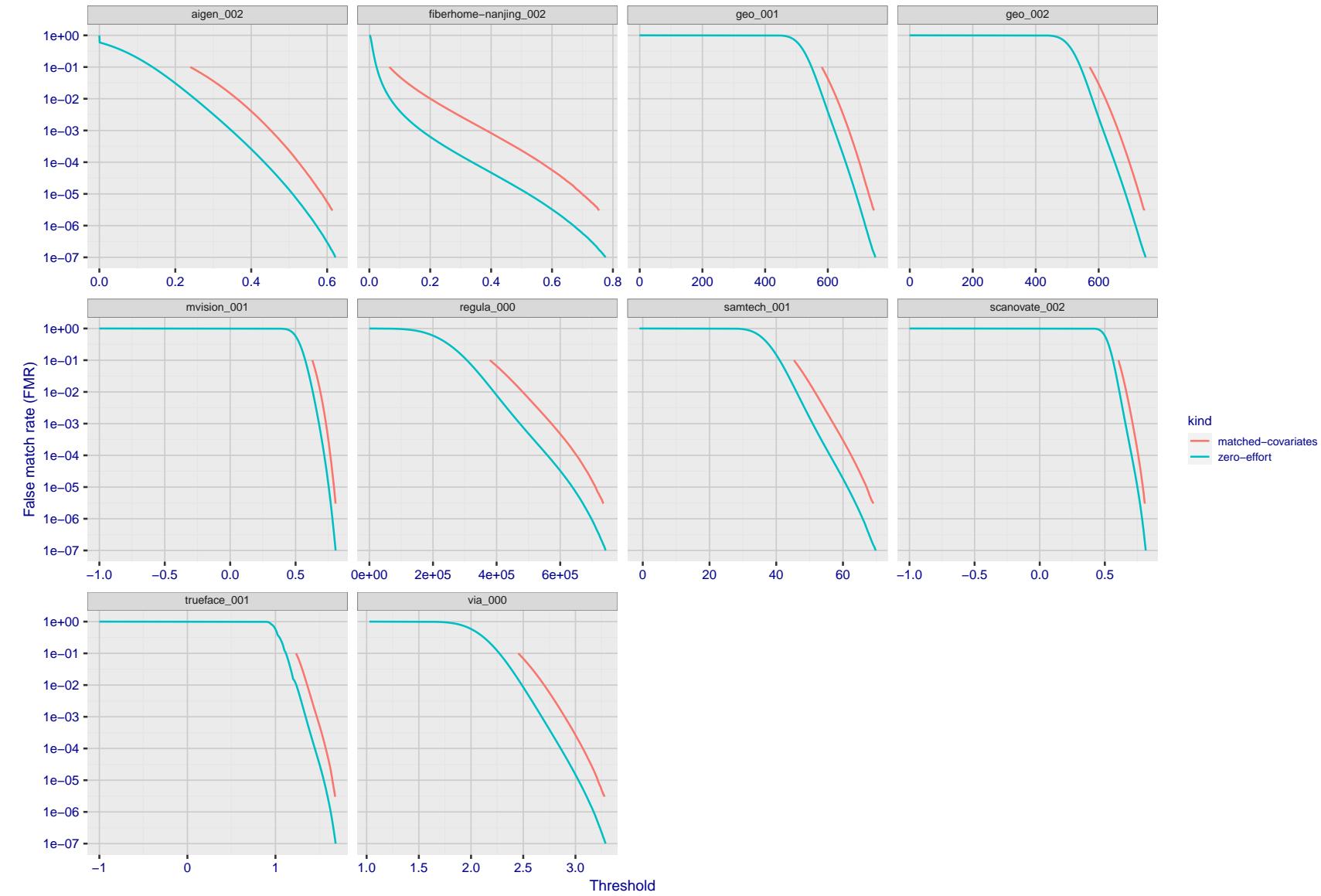


Figure 192: For the visa images, the false match calibration curves show FMR vs. threshold, T . The blue (lower) curves are for zero-effort impostors (i.e. comparing all images against all). The red (upper) curves are for persons of the same-sex, same-age, and same national-origin. This shows that FMR is underestimated (by a factor of 10 or more) by using a zero-effort impostor calculation to calibrate T . As shown later (sec. 3.6), FMR is higher for demographic-matched impostors.

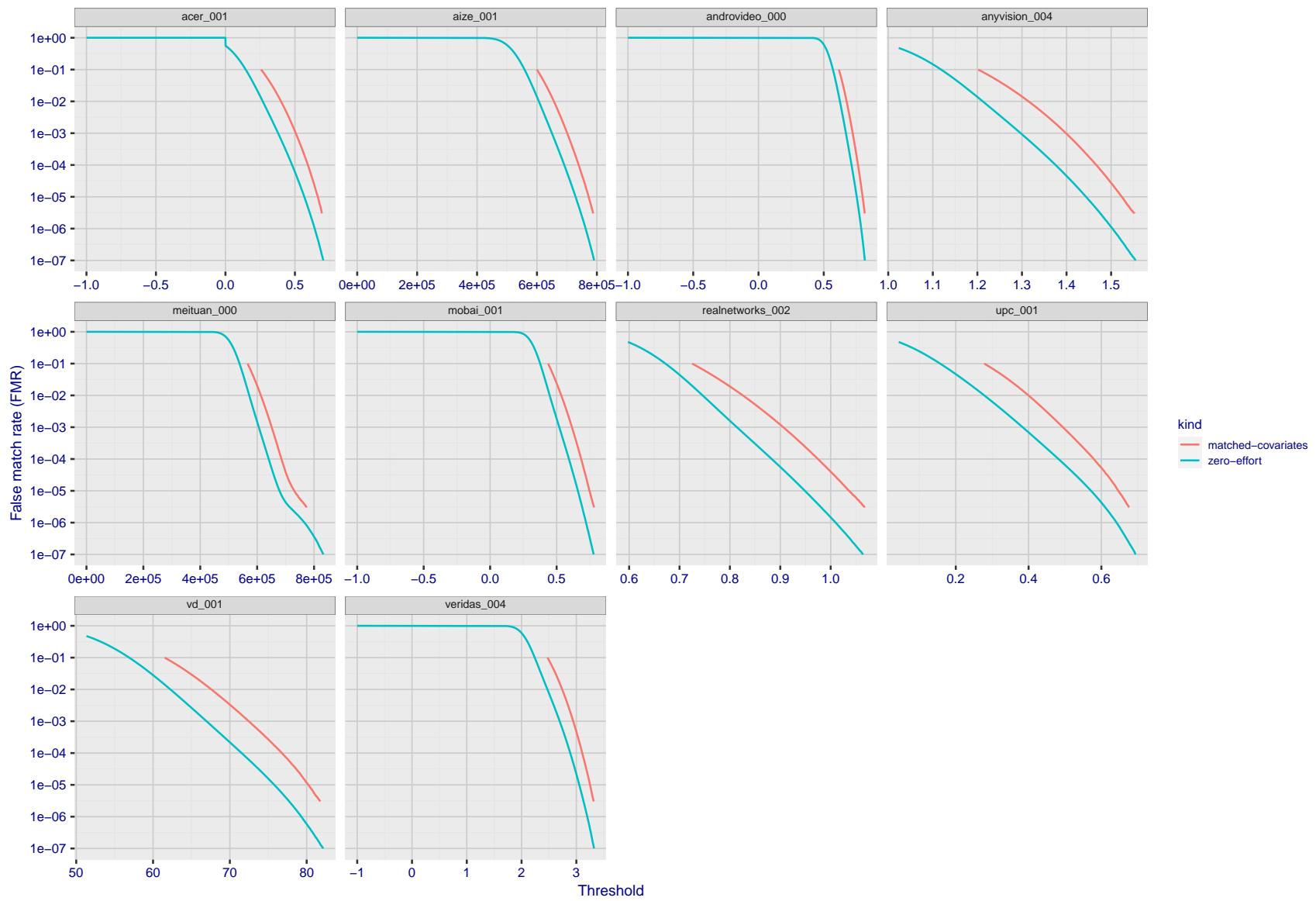


Figure 193: For the visa images, the false match calibration curves show FMR vs. threshold, T . The blue (lower) curves are for zero-effort impostors (i.e. comparing all images against all). The red (upper) curves are for persons of the same-sex, same-age, and same national-origin. This shows that FMR is underestimated (by a factor of 10 or more) by using a zero-effort impostor calculation to calibrate T . As shown later (sec. 3.6), FMR is higher for demographic-matched impostors.

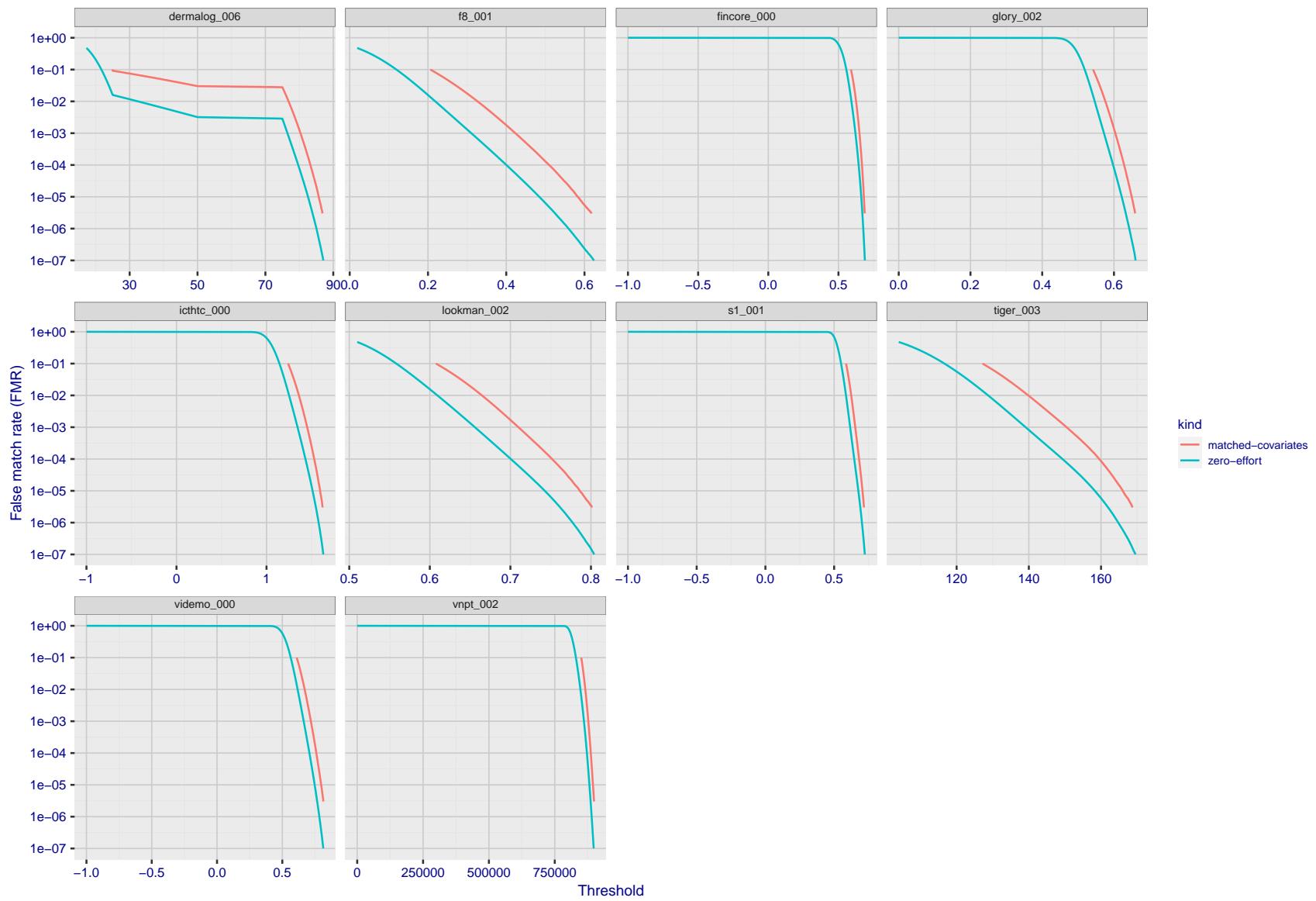


Figure 194: For the visa images, the false match calibration curves show FMR vs. threshold, T . The blue (lower) curves are for zero-effort impostors (i.e. comparing all images against all). The red (upper) curves are for persons of the same-sex, same-age, and same national-origin. This shows that FMR is underestimated (by a factor of 10 or more) by using a zero-effort impostor calculation to calibrate T . As shown later (sec. 3.6), FMR is higher for demographic-matched impostors.

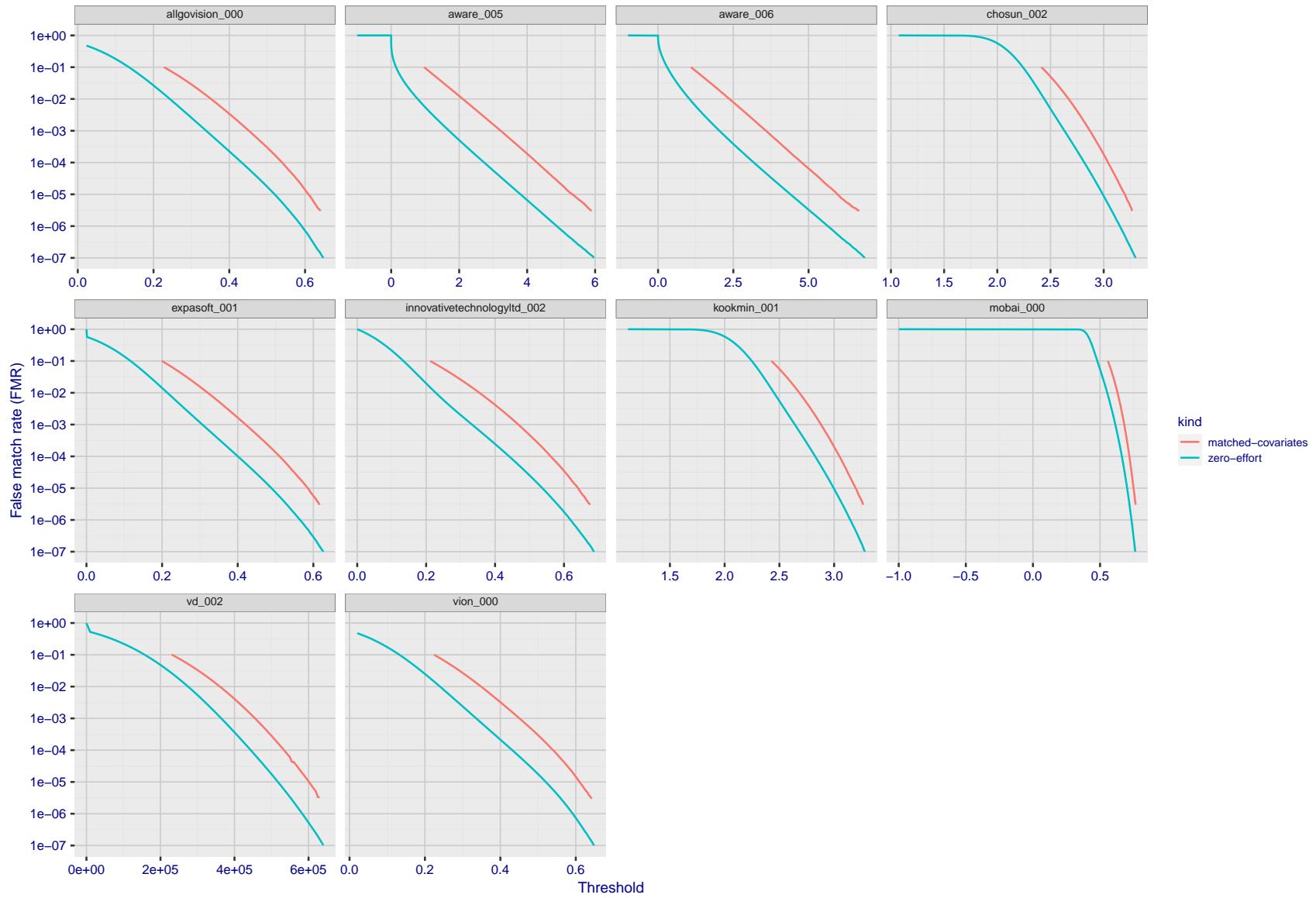


Figure 195: For the visa images, the false match calibration curves show FMR vs. threshold, T . The blue (lower) curves are for zero-effort impostors (i.e. comparing all images against all). The red (upper) curves are for persons of the same-sex, same-age, and same national-origin. This shows that FMR is underestimated (by a factor of 10 or more) by using a zero-effort impostor calculation to calibrate T . As shown later (sec. 3.6), FMR is higher for demographic-matched impostors.

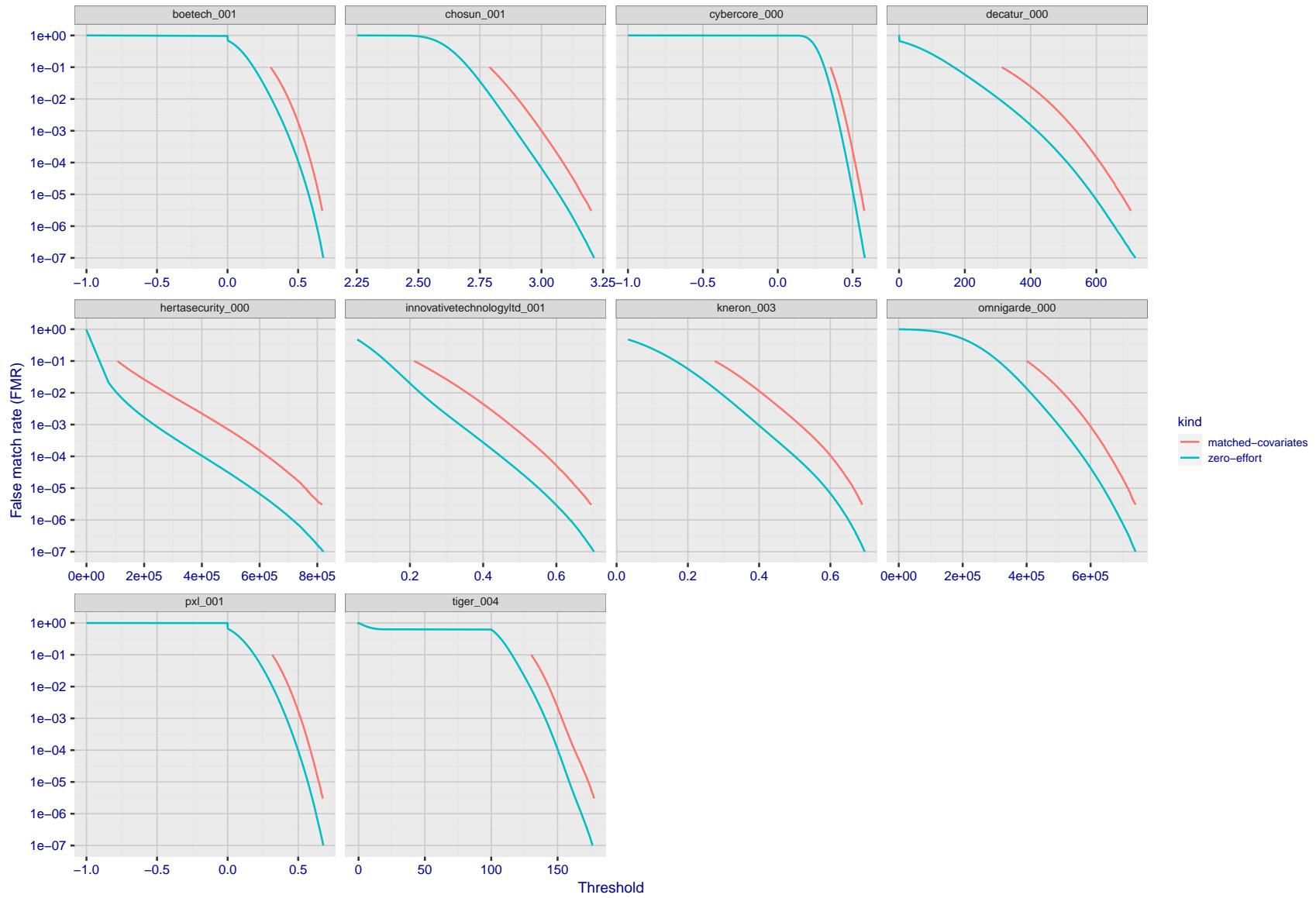


Figure 196: For the visa images, the false match calibration curves show FMR vs. threshold, T . The blue (lower) curves are for zero-effort impostors (i.e. comparing all images against all). The red (upper) curves are for persons of the same-sex, same-age, and same national-origin. This shows that FMR is underestimated (by a factor of 10 or more) by using a zero-effort impostor calculation to calibrate T . As shown later (sec. 3.6), FMR is higher for demographic-matched impostors.

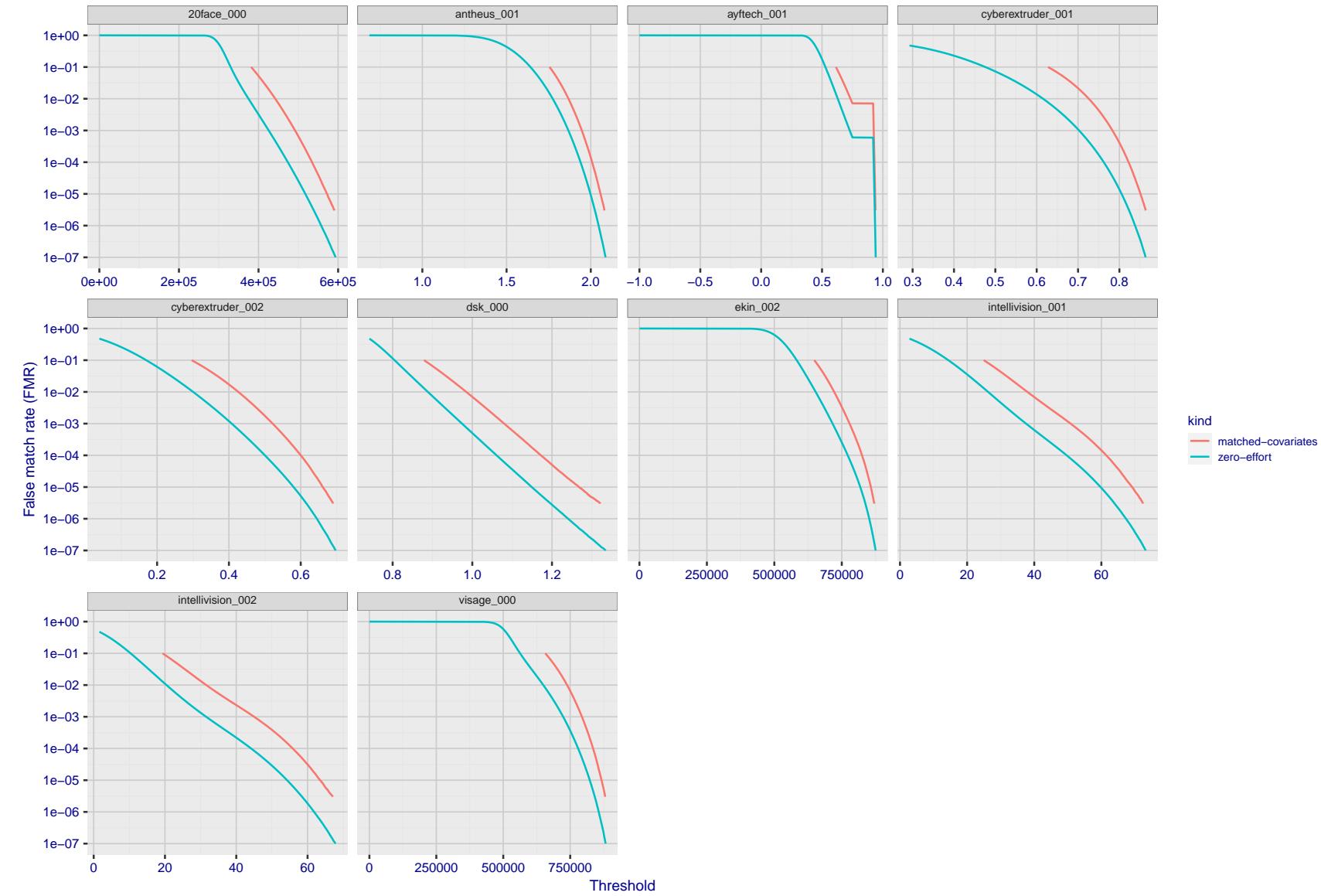


Figure 197: For the visa images, the false match calibration curves show FMR vs. threshold, T . The blue (lower) curves are for zero-effort impostors (i.e. comparing all images against all). The red (upper) curves are for persons of the same-sex, same-age, and same national-origin. This shows that FMR is underestimated (by a factor of 10 or more) by using a zero-effort impostor calculation to calibrate T . As shown later (sec. 3.6), FMR is higher for demographic-matched impostors.

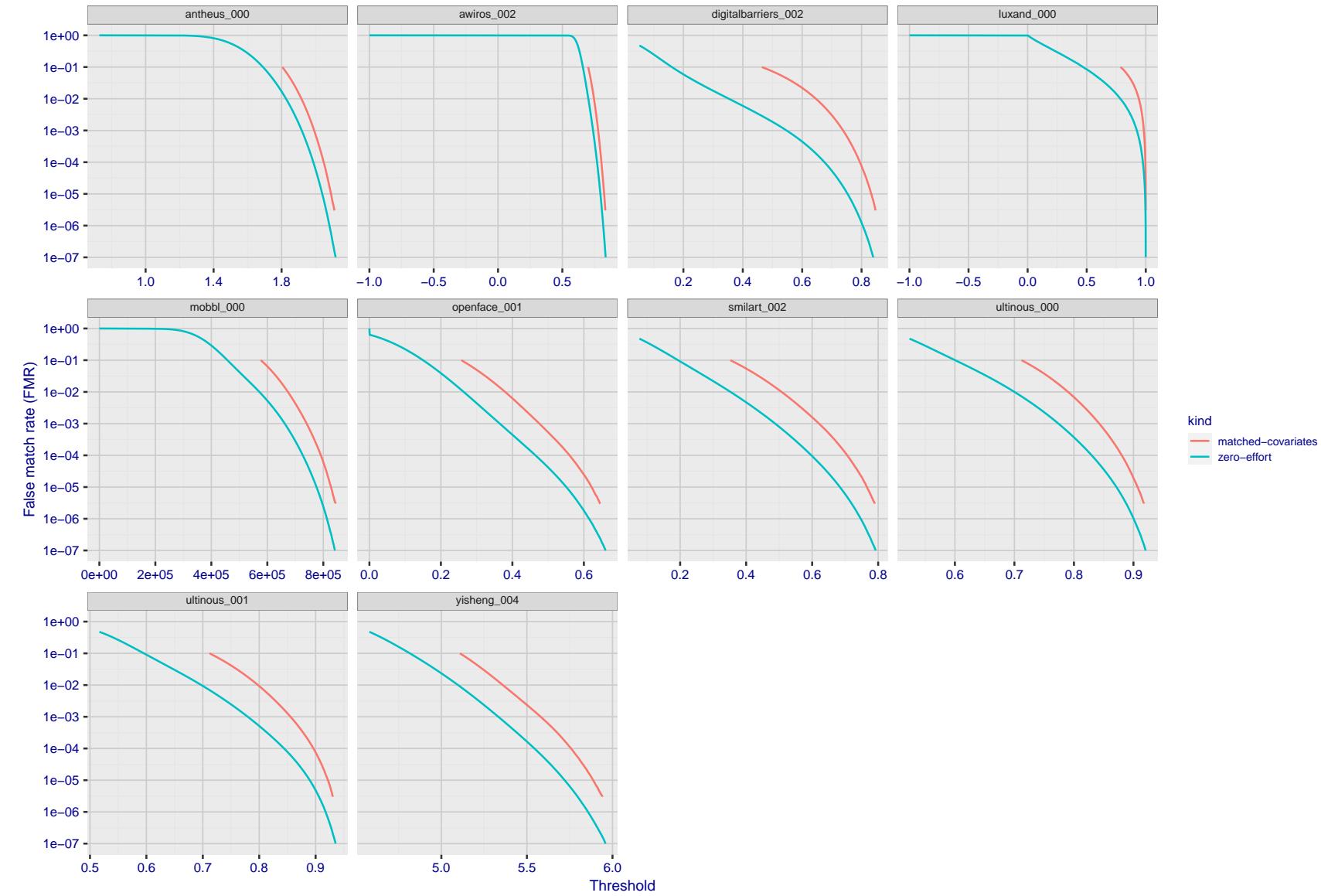


Figure 198: For the visa images, the false match calibration curves show FMR vs. threshold, T . The blue (lower) curves are for zero-effort impostors (i.e. comparing all images against all). The red (upper) curves are for persons of the same-sex, same-age, and same national-origin. This shows that FMR is underestimated (by a factor of 10 or more) by using a zero-effort impostor calculation to calibrate T . As shown later (sec. 3.6), FMR is higher for demographic-matched impostors.

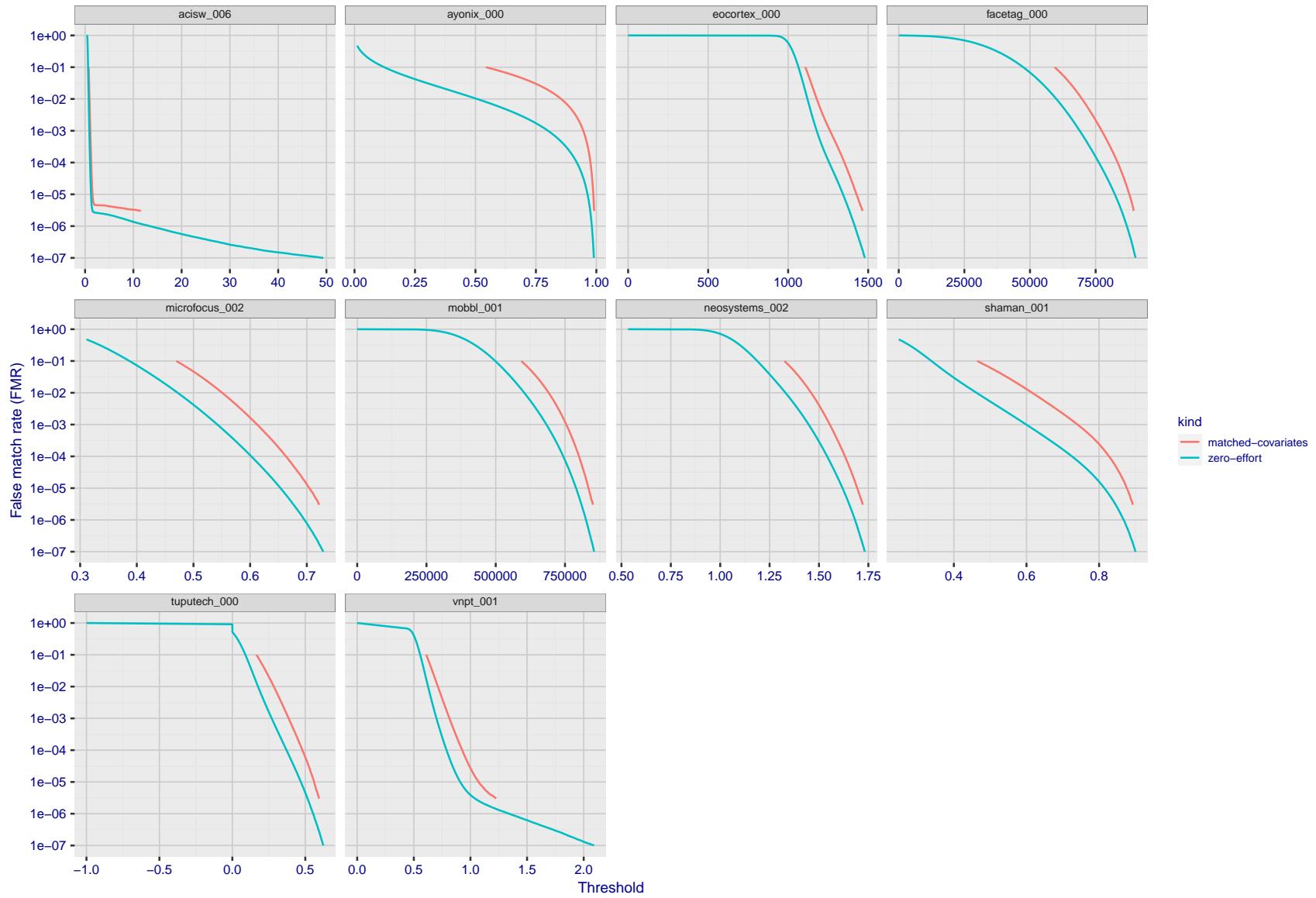


Figure 199: For the visa images, the false match calibration curves show FMR vs. threshold, T . The blue (lower) curves are for zero-effort impostors (i.e. comparing all images against all). The red (upper) curves are for persons of the same-sex, same-age, and same national-origin. This shows that FMR is underestimated (by a factor of 10 or more) by using a zero-effort impostor calculation to calibrate T . As shown later (sec. 3.6), FMR is higher for demographic-matched impostors.

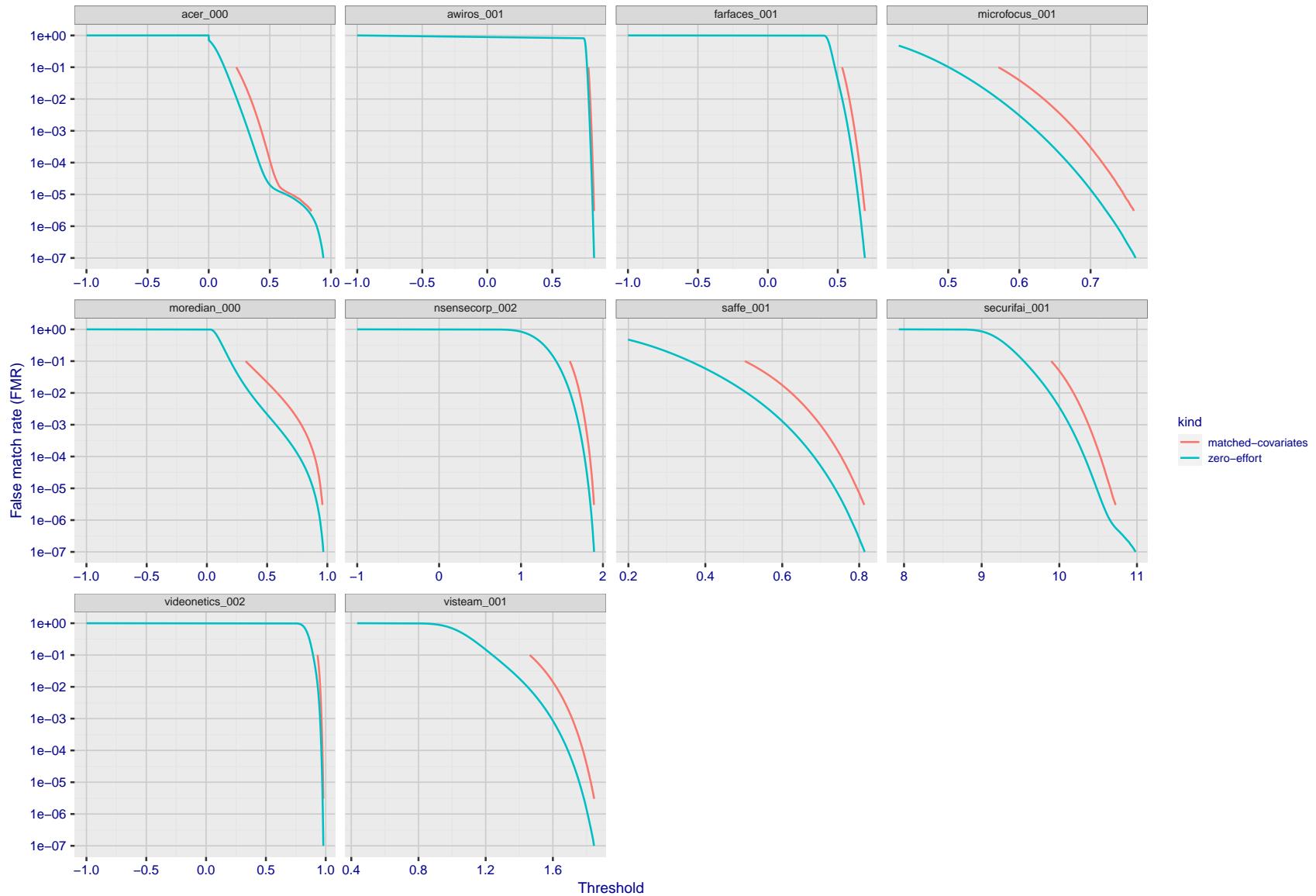


Figure 200: For the visa images, the false match calibration curves show FMR vs. threshold, T . The blue (lower) curves are for zero-effort impostors (i.e. comparing all images against all). The red (upper) curves are for persons of the same-sex, same-age, and same national-origin. This shows that FMR is underestimated (by a factor of 10 or more) by using a zero-effort impostor calculation to calibrate T . As shown later (sec. 3.6), FMR is higher for demographic-matched impostors.

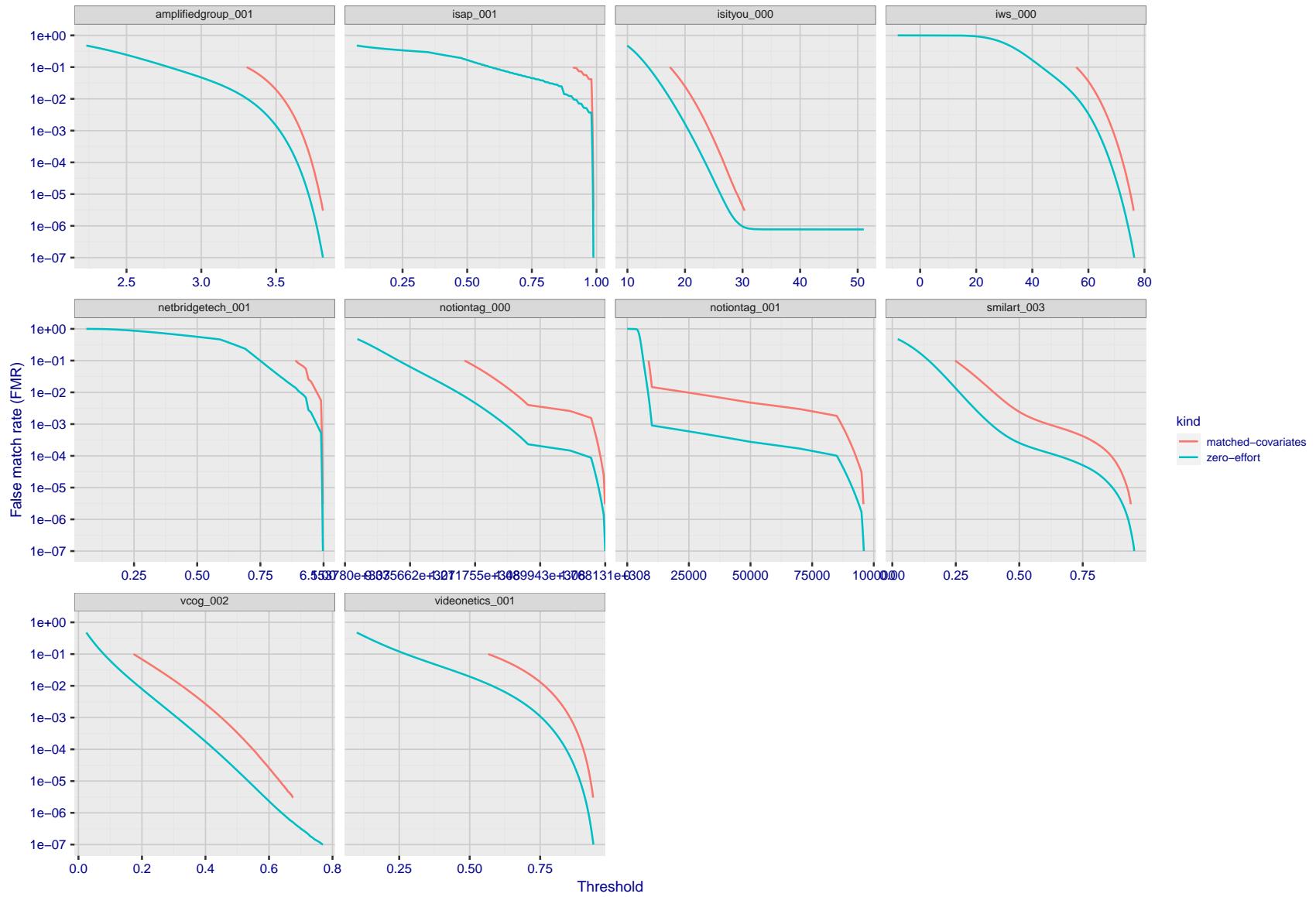


Figure 201: For the visa images, the false match calibration curves show FMR vs. threshold, T . The blue (lower) curves are for zero-effort impostors (i.e. comparing all images against all). The red (upper) curves are for persons of the same-sex, same-age, and same national-origin. This shows that FMR is underestimated (by a factor of 10 or more) by using a zero-effort impostor calculation to calibrate T . As shown later (sec. 3.6), FMR is higher for demographic-matched impostors.

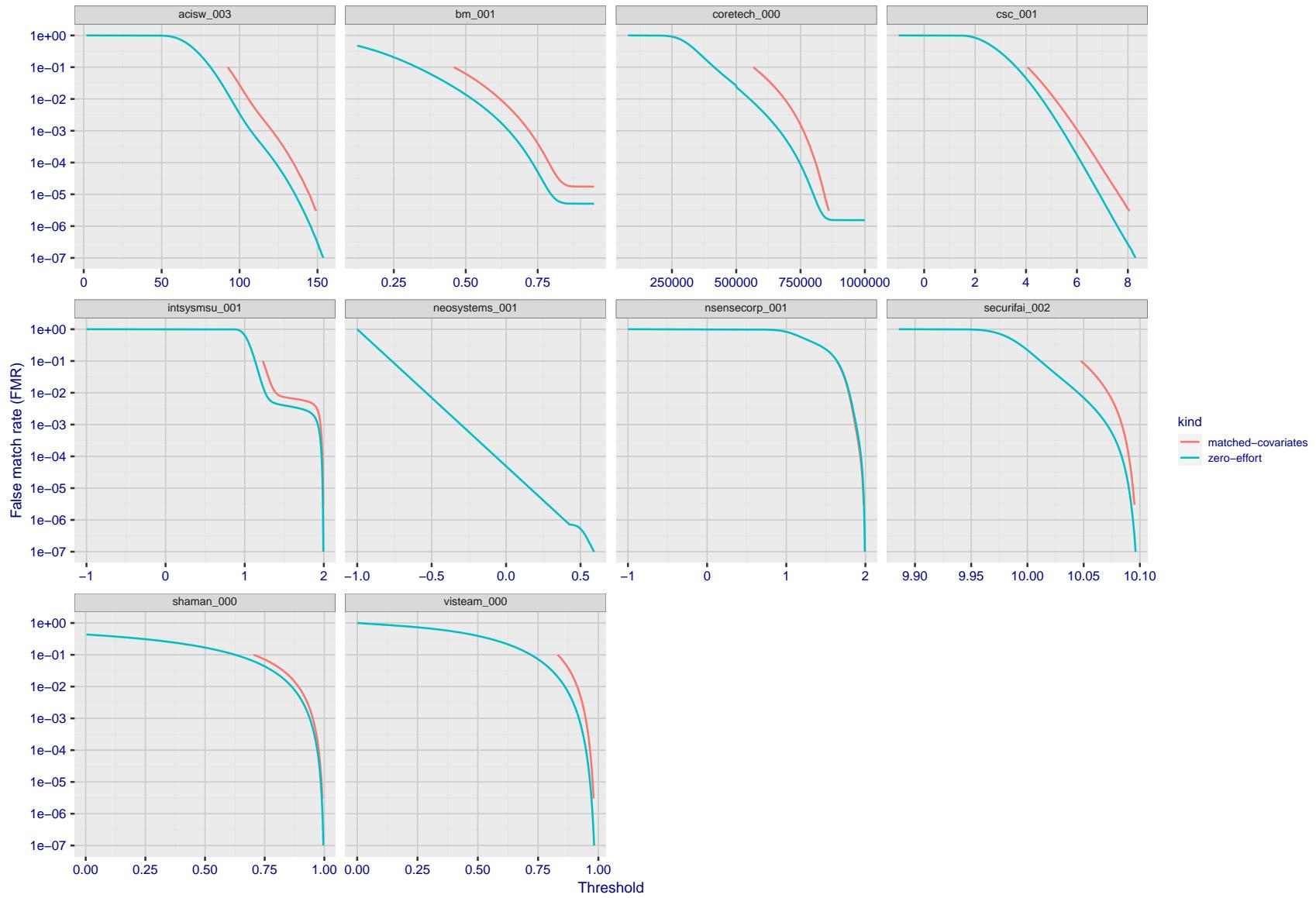


Figure 202: For the visa images, the false match calibration curves show FMR vs. threshold, T . The blue (lower) curves are for zero-effort impostors (i.e. comparing all images against all). The red (upper) curves are for persons of the same-sex, same-age, and same national-origin. This shows that FMR is underestimated (by a factor of 10 or more) by using a zero-effort impostor calculation to calibrate T . As shown later (sec. 3.6), FMR is higher for demographic-matched impostors.

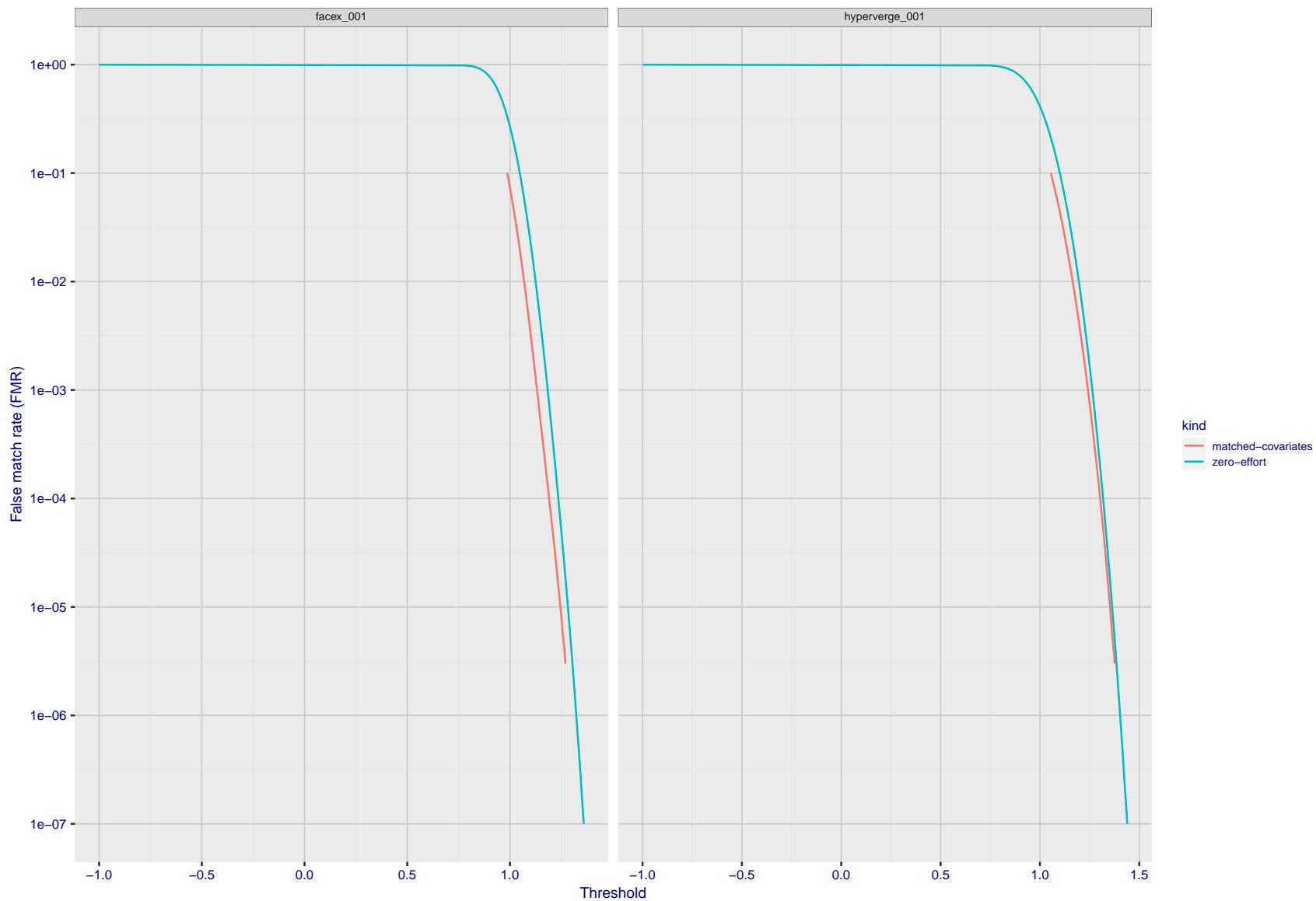


Figure 203: For the visa images, the false match calibration curves show FMR vs. threshold, T . The blue (lower) curves are for zero-effort impostors (i.e. comparing all images against all). The red (upper) curves are for persons of the same-sex, same-age, and same national-origin. This shows that FMR is underestimated (by a factor of 10 or more) by using a zero-effort impostor calculation to calibrate T . As shown later (sec. 3.6), FMR is higher for demographic-matched impostors.

3.5 Genuine distribution stability

3.5.1 Effect of birth place on the genuine distribution

Background: Both skin tone and bone structure vary geographically. Prior studies have reported variations in FNMR and FMR.

Goal: To measure false non-match rate (FNMR) variation with country of birth.

Methods: Thresholds are determined that give $FMR = \{0.001, 0.0001\}$ over the entire impostor set. Then FNMR is measured over 1000 bootstrap replications of the genuine scores. Only those countries with at least 140 individuals are included in the analysis.

Results: Figure 231 shows FNMR by country of birth for the two thresholds.

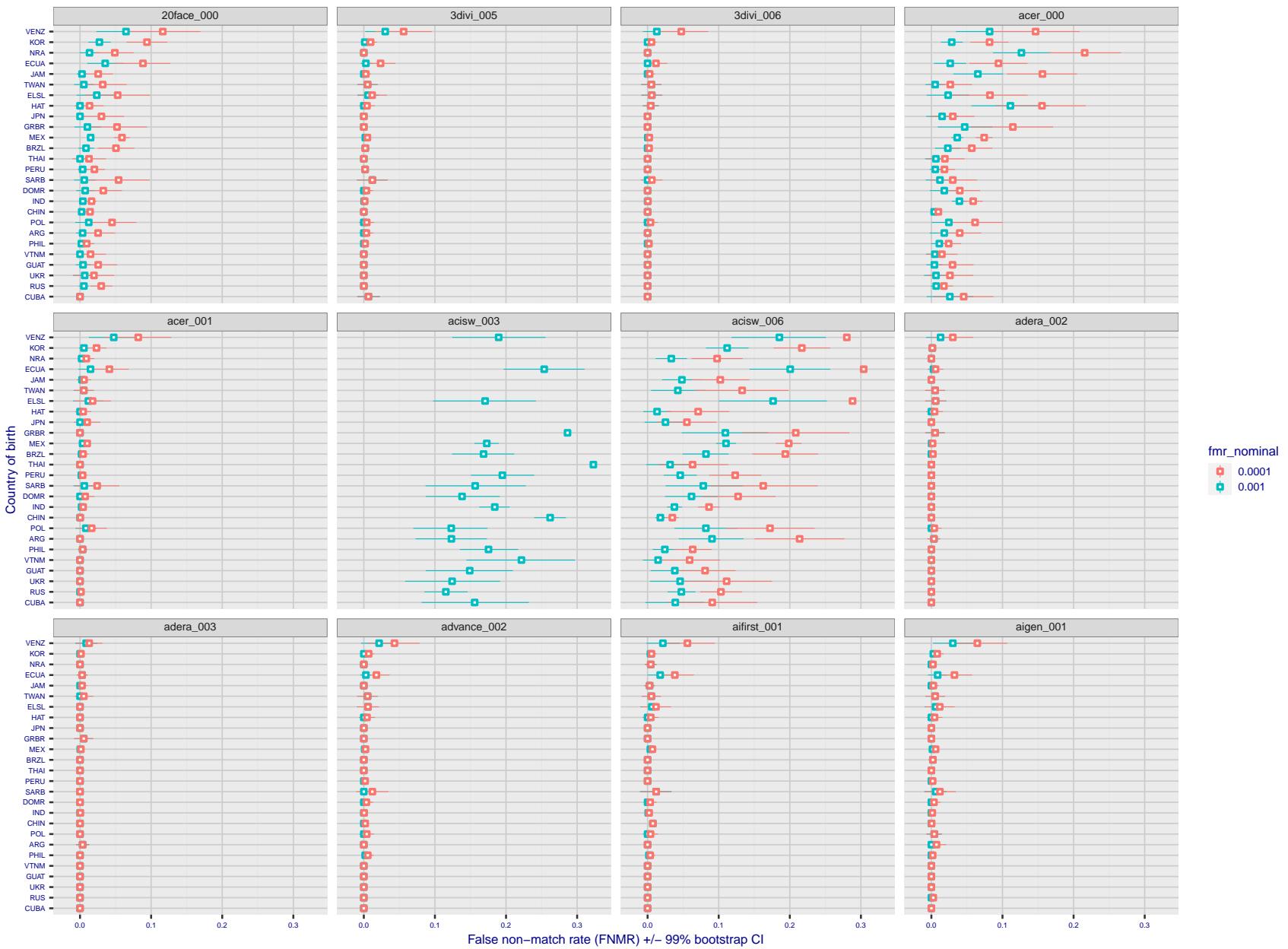


Figure 204: For the visa images, the dots show FNMR by country of birth for two globally set operating thresholds corresponding to $FMR = \{0.001, 0.0001\}$ computed over all on the order of 10^{10} impostor scores. The FMR in each bin will vary also - see subsequent impostor heatmaps in sec. 3.6.1. The figures shows an order of magnitude variation in FNMR across country of birth; these effects are likely due quality variations, then demographics like age and race. The error rates in some cases are zero, and in others the DET is flat so the error rates at the two thresholds are identical. The lines span 1% and 99% of bootstrap replicated FNMR estimates.

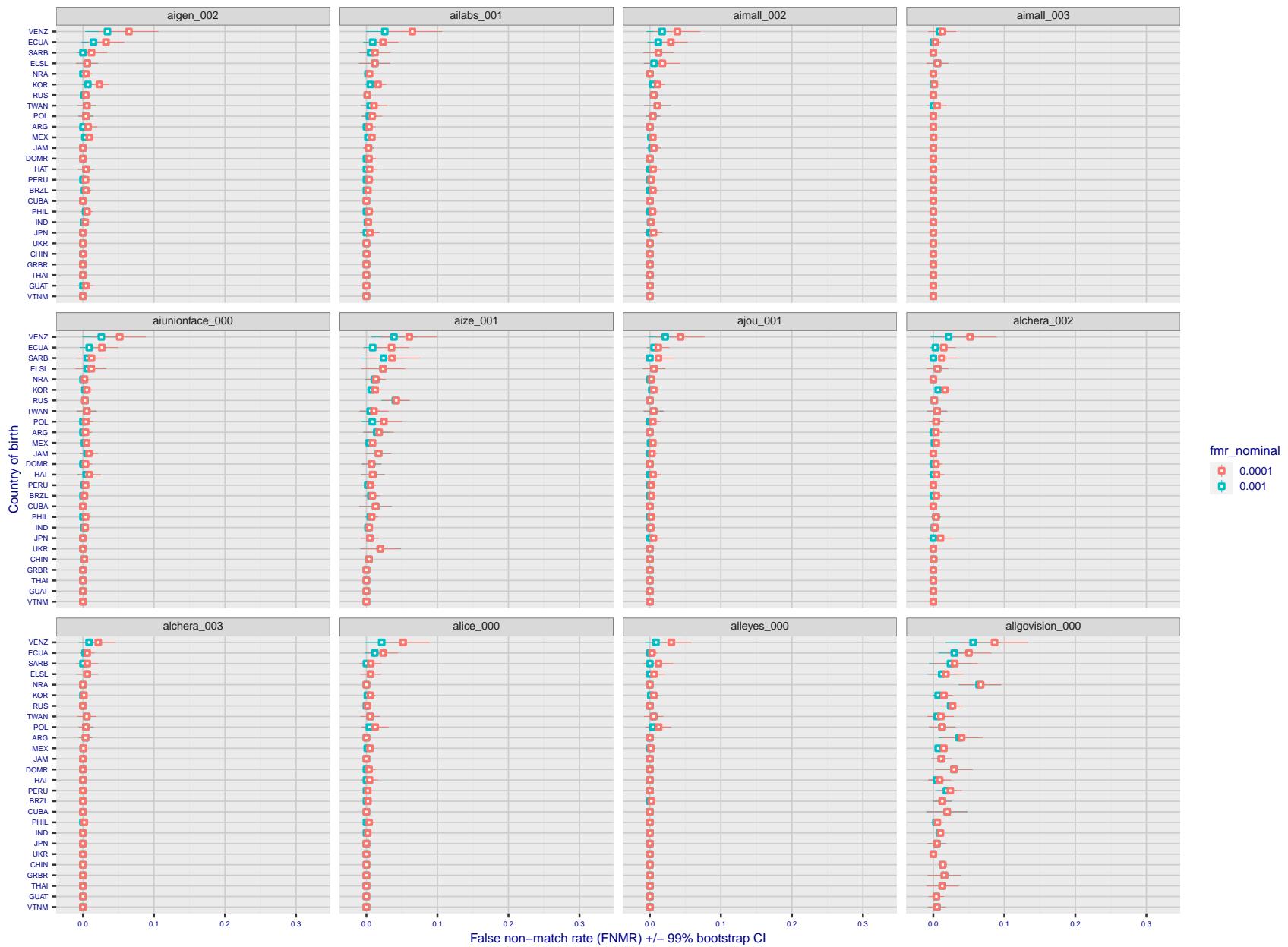


Figure 205: For the visa images, the dots show FNMR by country of birth for two globally set operating thresholds corresponding to $FMR = \{0.001, 0.0001\}$ computed over all on the order of 10^{10} impostor scores. The FMR in each bin will vary also - see subsequent impostor heatmaps in sec. 3.6.1. The figures shows an order of magnitude variation in FNMR across country of birth; these effects are likely due quality variations, then demographics like age and race. The error rates in some cases are zero, and in others the DET is flat so the error rates at the two thresholds are identical. The lines span 1% and 99% of bootstrap replicated FNMR estimates.

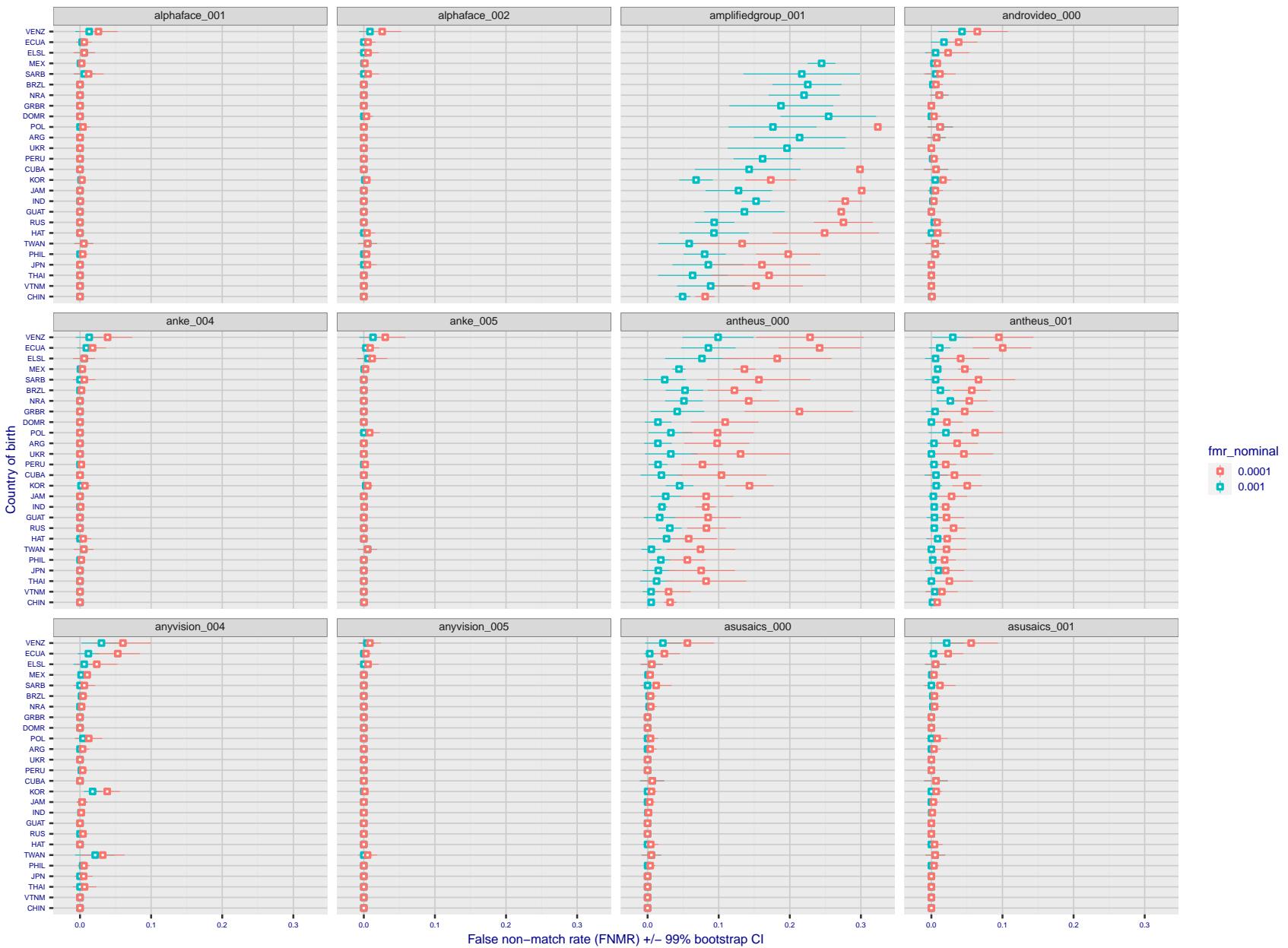


Figure 206: For the visa images, the dots show FNMR by country of birth for two globally set operating thresholds corresponding to $FMR = \{0.001, 0.0001\}$ computed over all on the order of 10^{10} impostor scores. The FMR in each bin will vary also - see subsequent impostor heatmaps in sec. 3.6.1. The figures shows an order of magnitude variation in FNMR across country of birth; these effects are likely due quality variations, then demographics like age and race. The error rates in some cases are zero, and in others the DET is flat so the error rates at the two thresholds are identical. The lines span 1% and 99% of bootstrap replicated FNMR estimates.

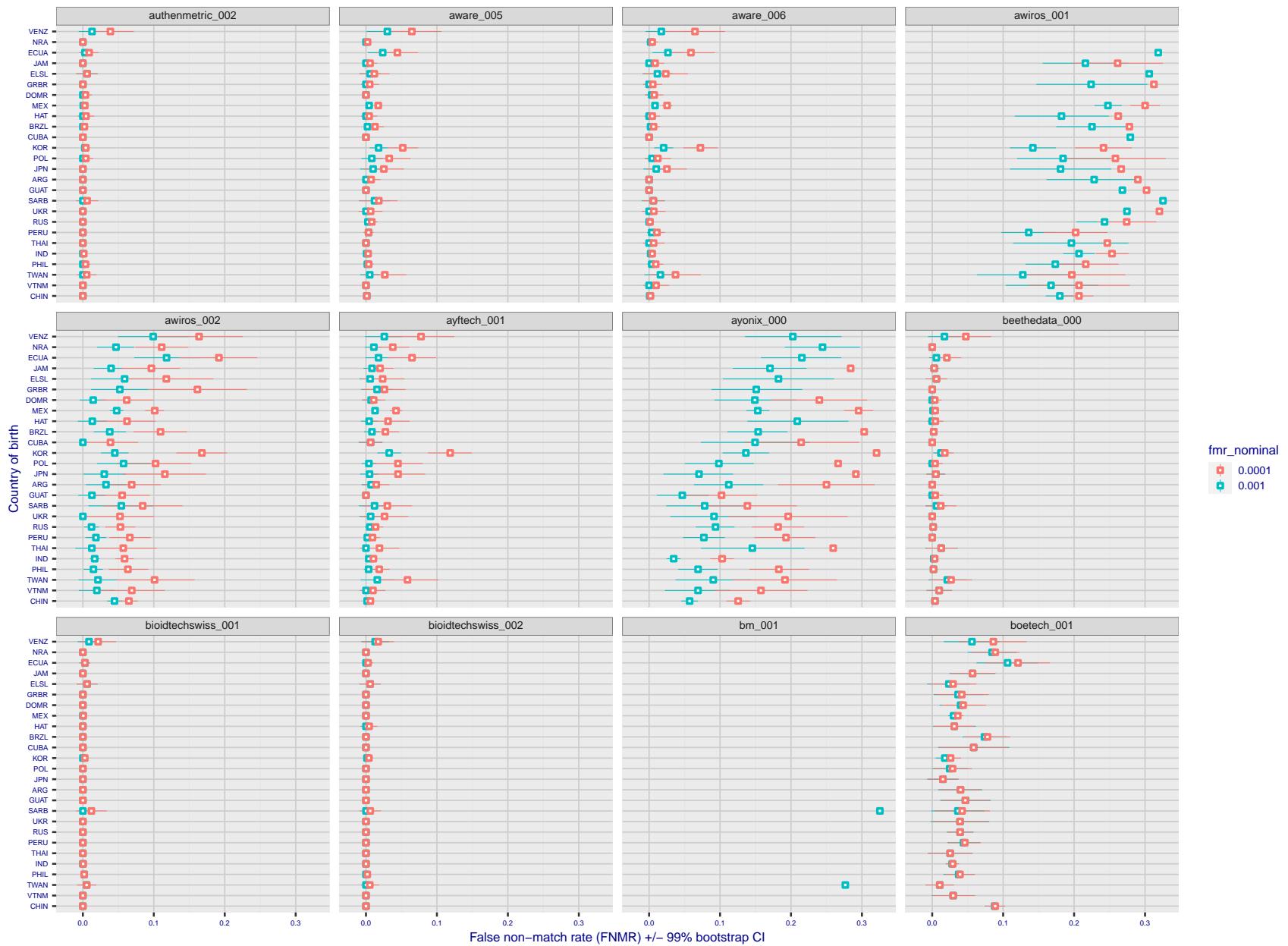


Figure 207: For the visa images, the dots show FNMR by country of birth for two globally set operating thresholds corresponding to $FMR = \{0.001, 0.0001\}$ computed over all on the order of 10^{10} impostor scores. The FMR in each bin will vary also - see subsequent impostor heatmaps in sec. 3.6.1. The figures shows an order of magnitude variation in FNMR across country of birth; these effects are likely due quality variations, then demographics like age and race. The error rates in some cases are zero, and in others the DET is flat so the error rates at the two thresholds are identical. The lines span 1% and 99% of bootstrap replicated FNMR estimates.

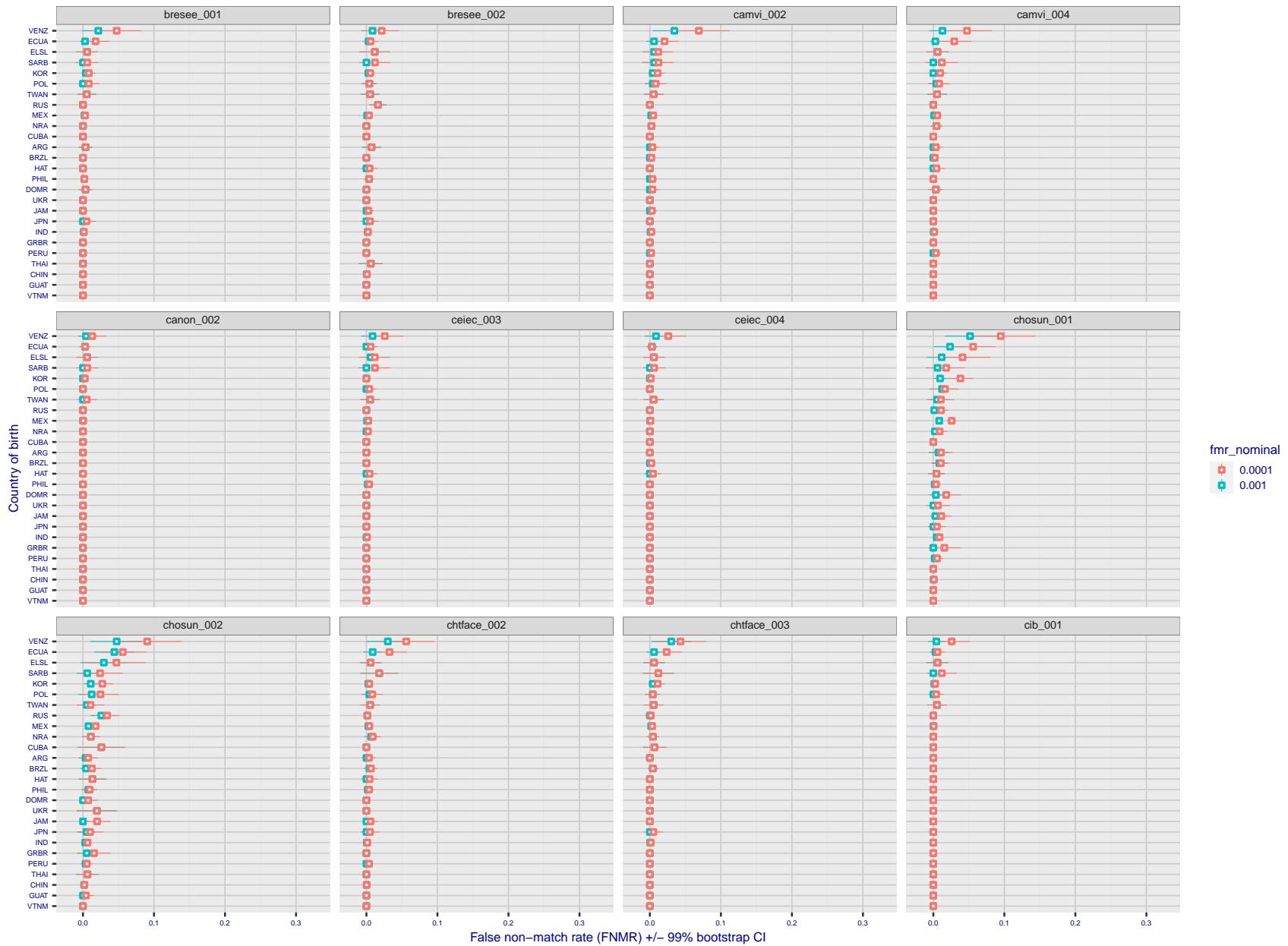


Figure 208: For the visa images, the dots show FNMR by country of birth for two globally set operating thresholds corresponding to $FMR = \{0.001, 0.0001\}$ computed over all on the order of 10^{10} impostor scores. The FMR in each bin will vary also - see subsequent impostor heatmaps in sec. 3.6.1. The figures shows an order of magnitude variation in FNMR across country of birth; these effects are likely due quality variations, then demographics like age and race. The error rates in some cases are zero, and in others the DET is flat so the error rates at the two thresholds are identical. The lines span 1% and 99% of bootstrap replicated FNMR estimates.

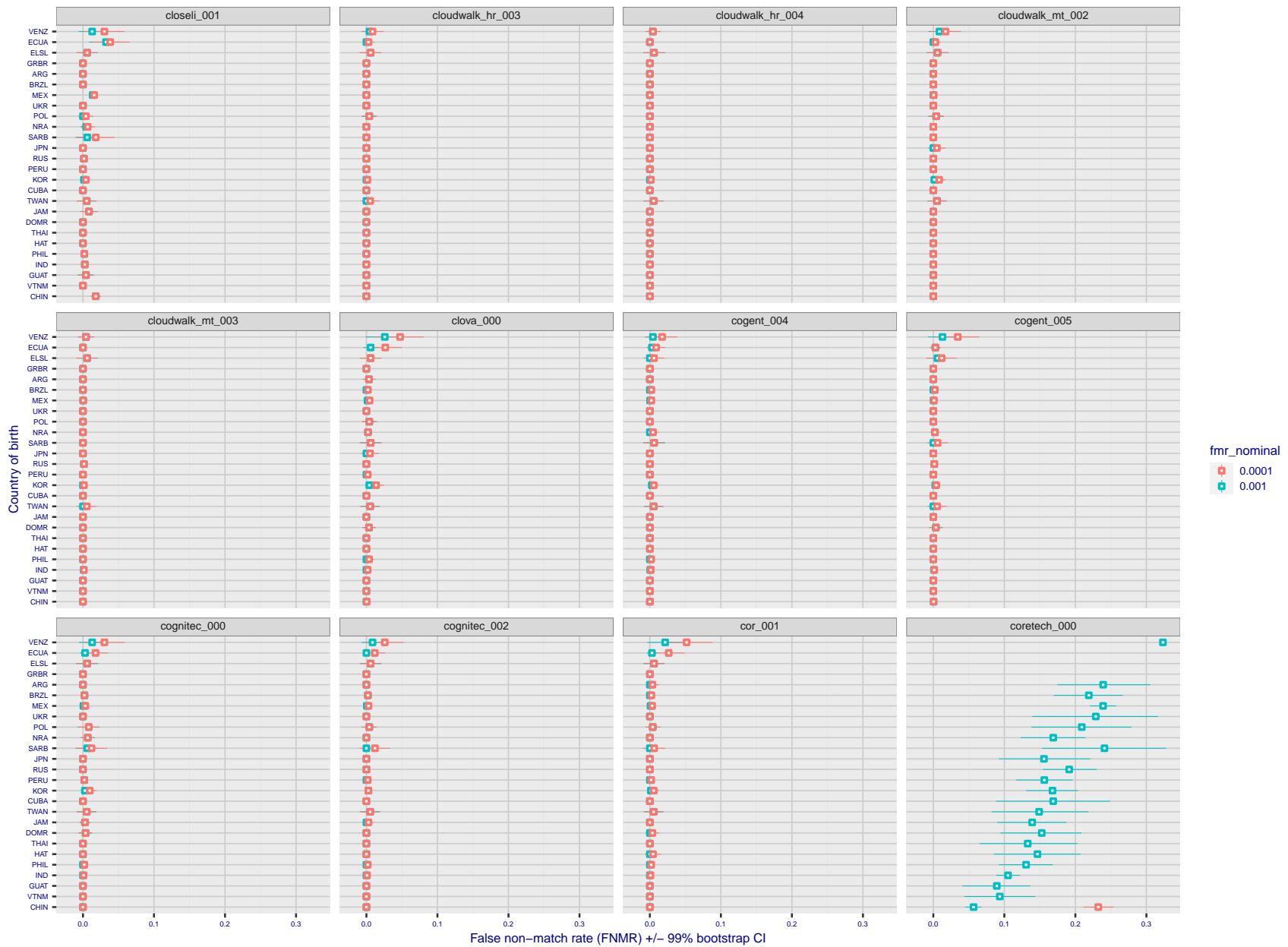


Figure 209: For the visa images, the dots show FNMR by country of birth for two globally set operating thresholds corresponding to $FMR = \{0.001, 0.0001\}$ computed over all on the order of 10^{10} impostor scores. The FMR in each bin will vary also - see subsequent impostor heatmaps in sec. 3.6.1. The figures shows an order of magnitude variation in FNMR across country of birth; these effects are likely due quality variations, then demographics like age and race. The error rates in some cases are zero, and in others the DET is flat so the error rates at the two thresholds are identical. The lines span 1% and 99% of bootstrap replicated FNMR estimates.

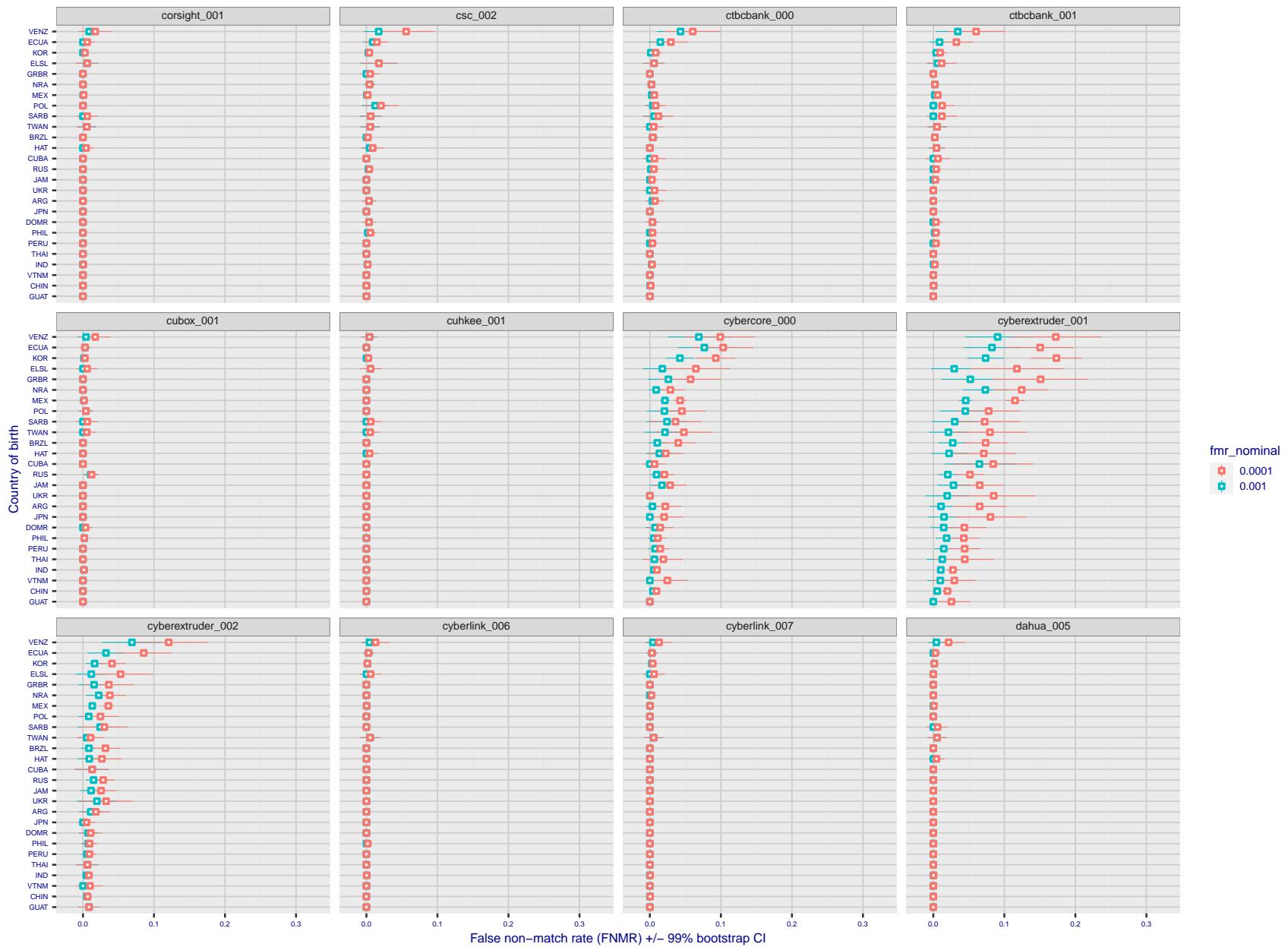


Figure 210: For the visa images, the dots show FNMR by country of birth for two globally set operating thresholds corresponding to $FMR = \{0.001, 0.0001\}$ computed over all on the order of 10^{10} impostor scores. The FMR in each bin will vary also - see subsequent impostor heatmaps in sec. 3.6.1. The figures shows an order of magnitude variation in FNMR across country of birth; these effects are likely due quality variations, then demographics like age and race. The error rates in some cases are zero, and in others the DET is flat so the error rates at the two thresholds are identical. The lines span 1% and 99% of bootstrap replicated FNMR estimates.

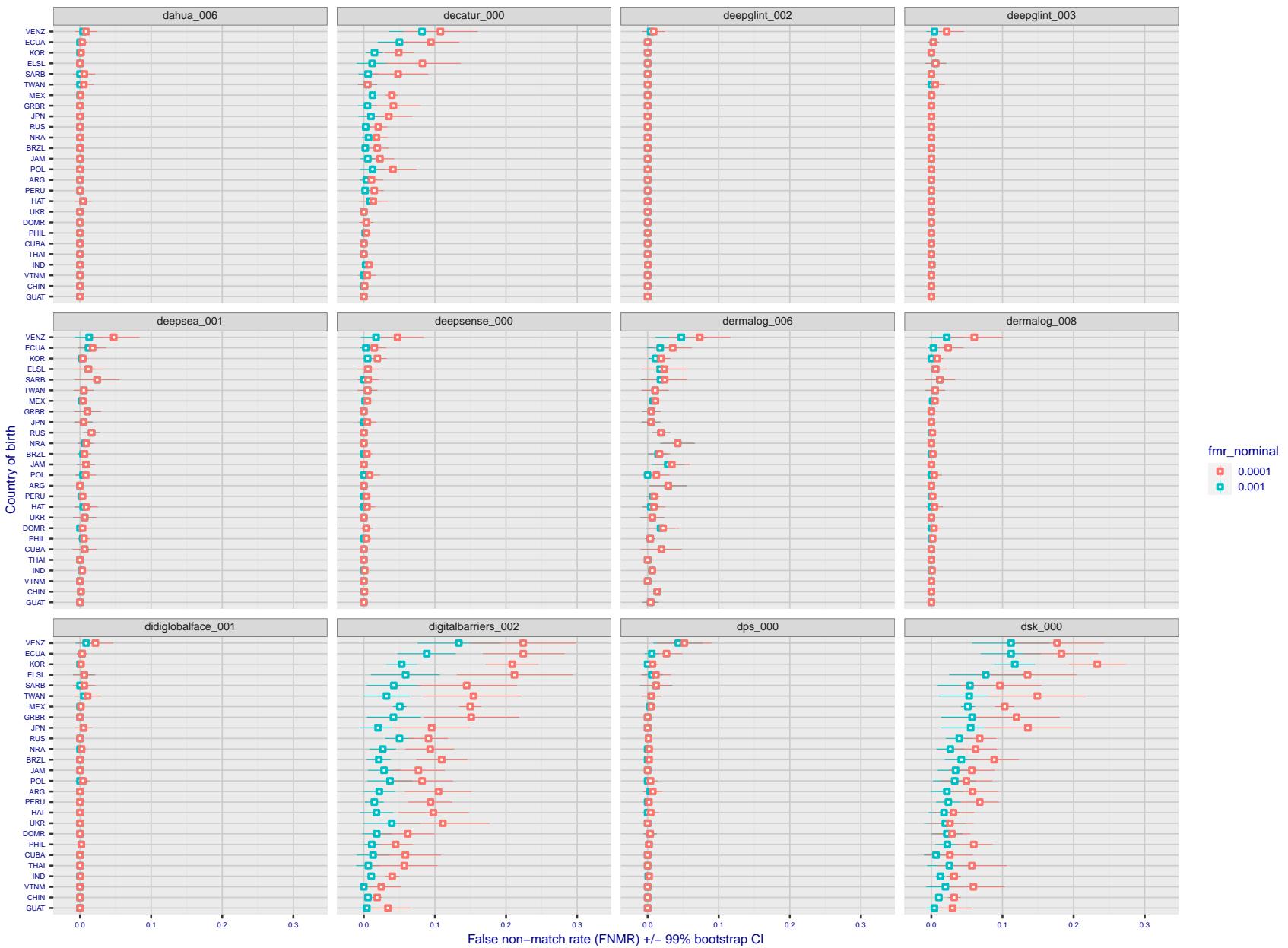


Figure 211: For the visa images, the dots show FNMR by country of birth for two globally set operating thresholds corresponding to $FMR = \{0.001, 0.0001\}$ computed over all on the order of 10^{10} impostor scores. The FMR in each bin will vary also - see subsequent impostor heatmaps in sec. 3.6.1. The figures shows an order of magnitude variation in FNMR across country of birth; these effects are likely due quality variations, then demographics like age and race. The error rates in some cases are zero, and in others the DET is flat so the error rates at the two thresholds are identical. The lines span 1% and 99% of bootstrap replicated FNMR estimates.

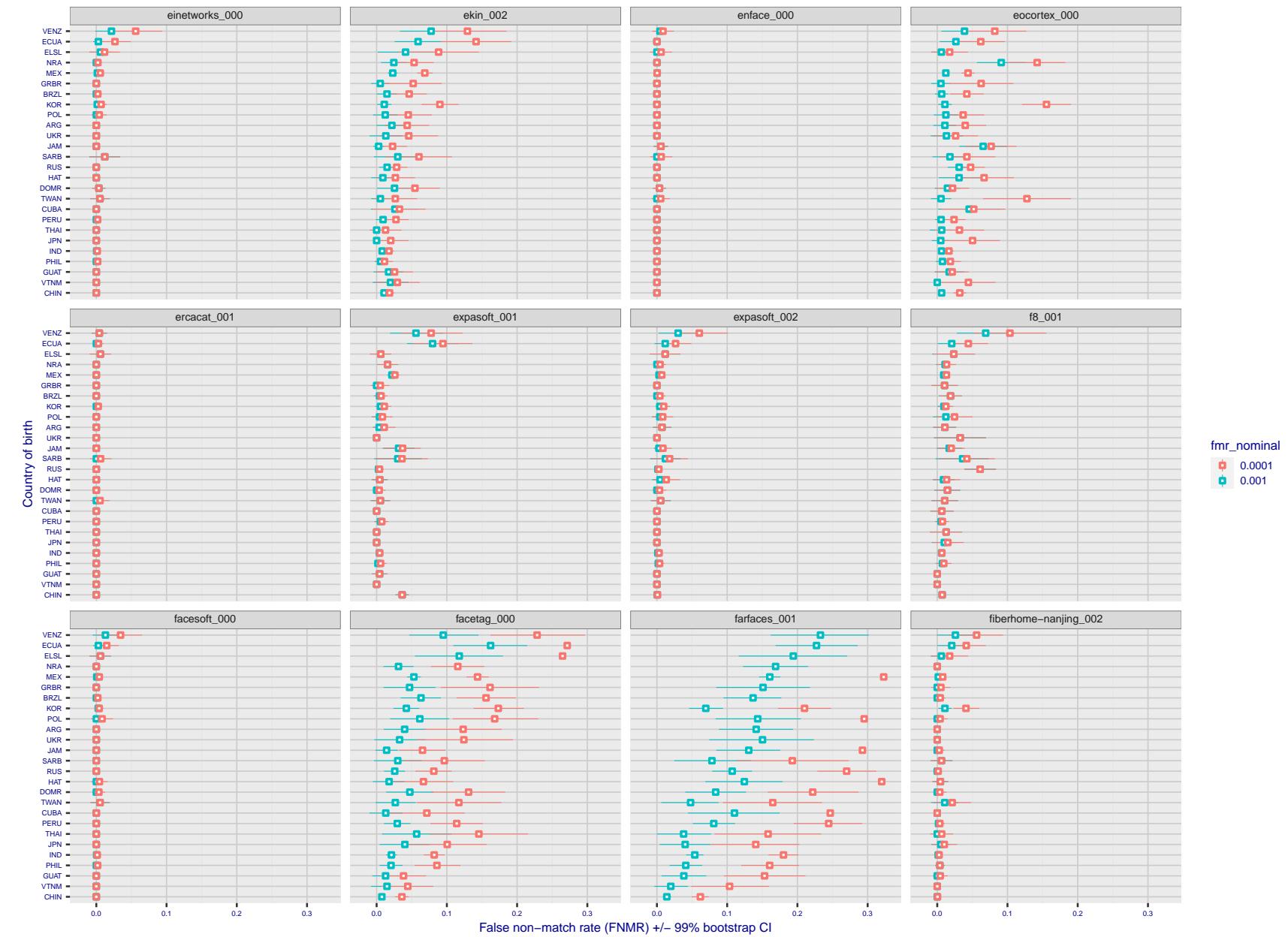


Figure 212: For the visa images, the dots show FNMR by country of birth for two globally set operating thresholds corresponding to $FMR = \{0.001, 0.0001\}$ computed over all on the order of 10^{10} impostor scores. The FMR in each bin will vary also - see subsequent impostor heatmaps in sec. 3.6.1. The figures shows an order of magnitude variation in FNMR across country of birth; these effects are likely due quality variations, then demographics like age and race. The error rates in some cases are zero, and in others the DET is flat so the error rates at the two thresholds are identical. The lines span 1% and 99% of bootstrap replicated FNMR estimates.

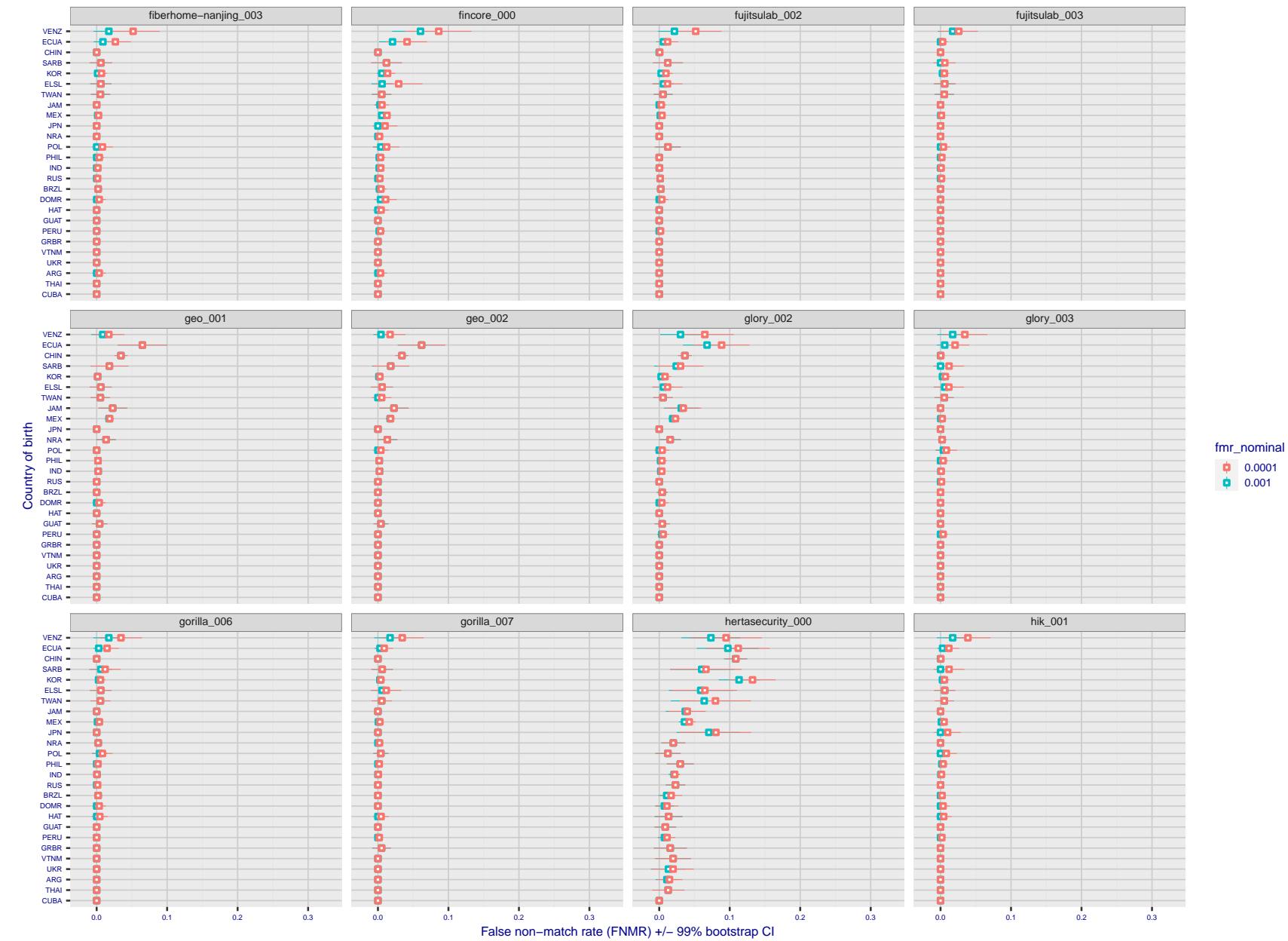


Figure 213: For the visa images, the dots show FNMR by country of birth for two globally set operating thresholds corresponding to $FMR = \{0.001, 0.0001\}$ computed over all on the order of 10^{10} impostor scores. The FMR in each bin will vary also - see subsequent impostor heatmaps in sec. 3.6.1. The figures shows an order of magnitude variation in FNMR across country of birth; these effects are likely due quality variations, then demographics like age and race. The error rates in some cases are zero, and in others the DET is flat so the error rates at the two thresholds are identical. The lines span 1% and 99% of bootstrap replicated FNMR estimates.

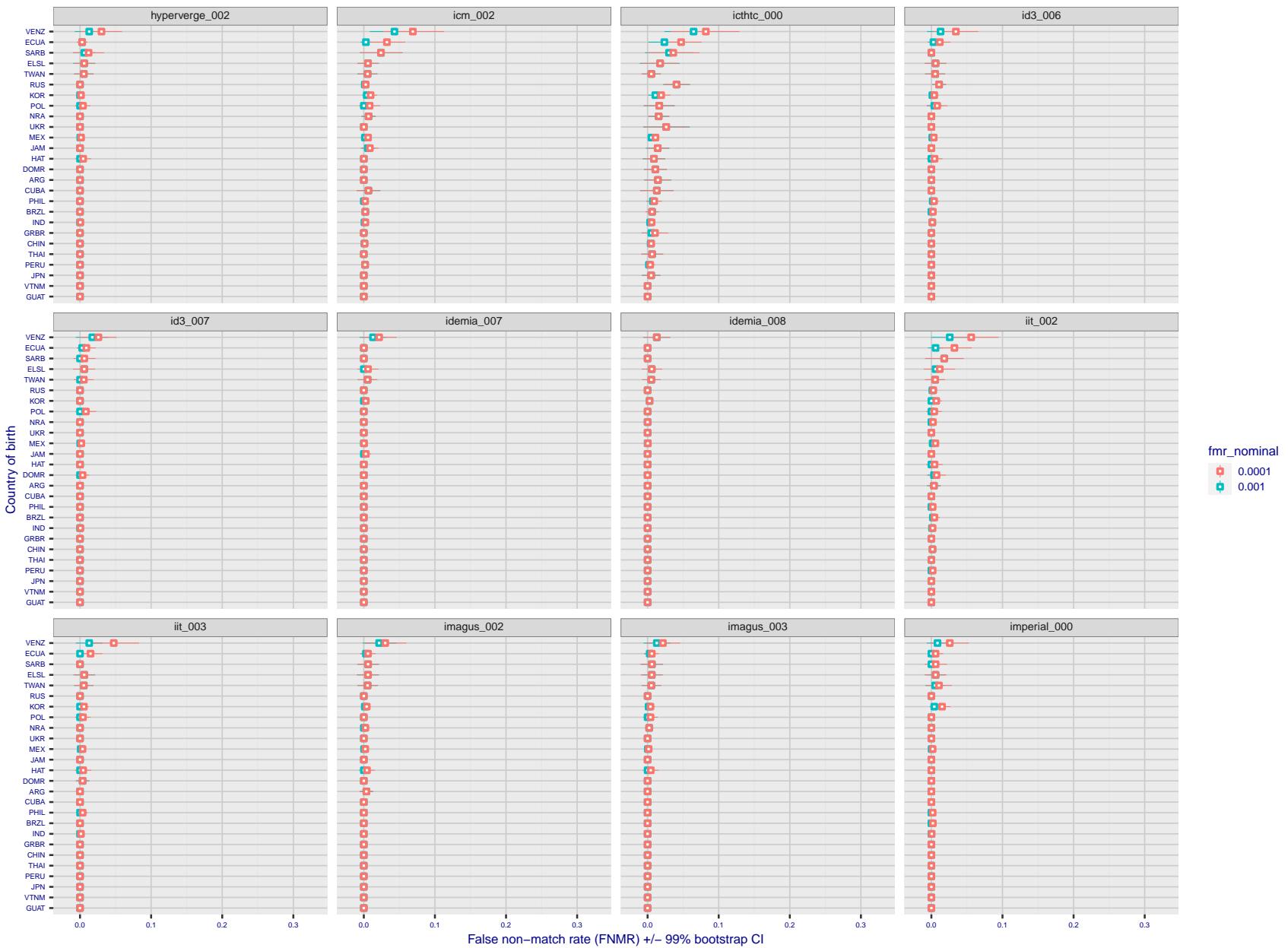


Figure 214: For the visa images, the dots show FNMR by country of birth for two globally set operating thresholds corresponding to $FMR = \{0.001, 0.0001\}$ computed over all on the order of 10^{10} impostor scores. The FMR in each bin will vary also - see subsequent impostor heatmaps in sec. 3.6.1. The figures shows an order of magnitude variation in FNMR across country of birth; these effects are likely due quality variations, then demographics like age and race. The error rates in some cases are zero, and in others the DET is flat so the error rates at the two thresholds are identical. The lines span 1% and 99% of bootstrap replicated FNMR estimates.

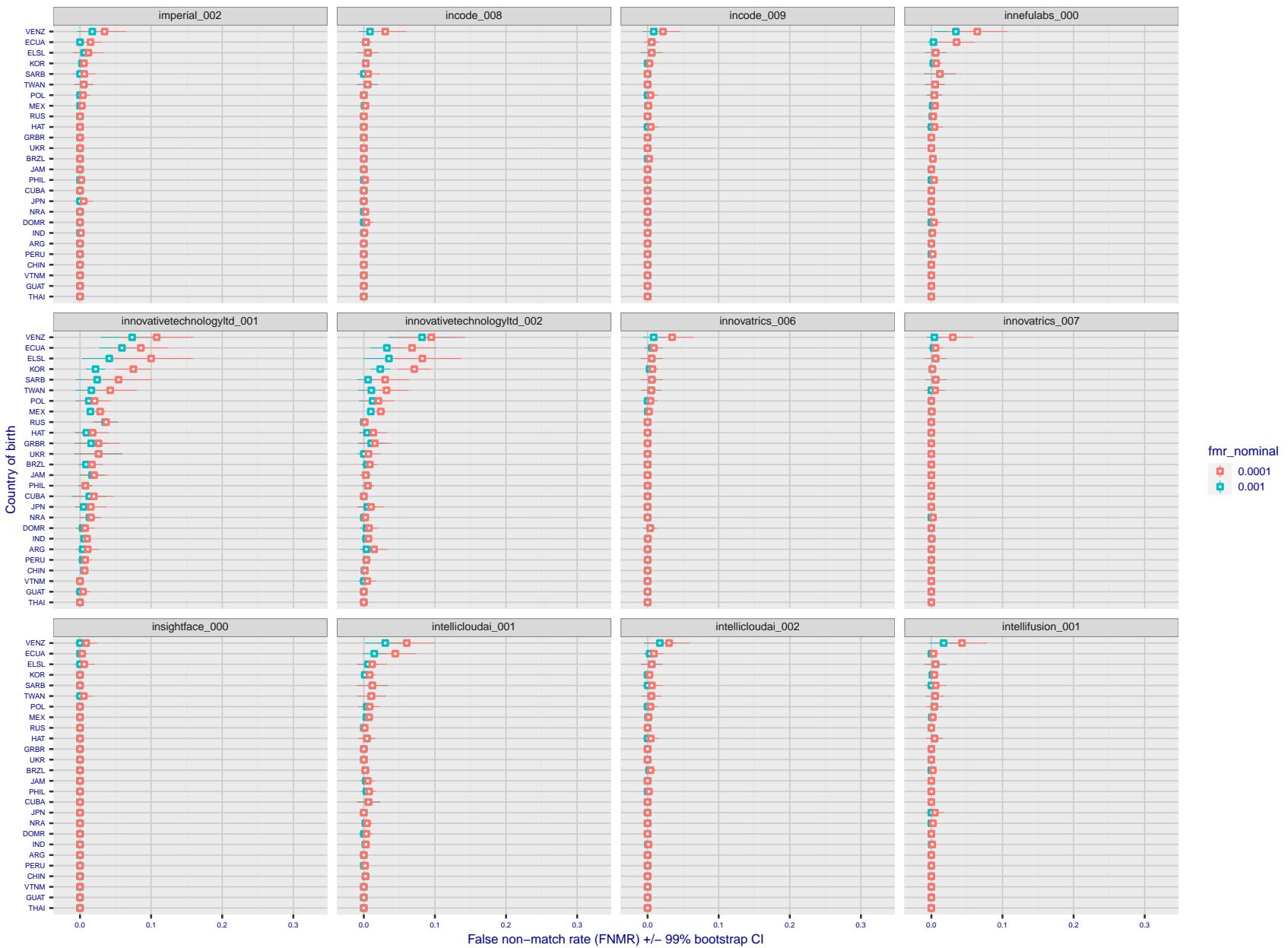


Figure 215: For the visa images, the dots show FNMR by country of birth for two globally set operating thresholds corresponding to $FMR = \{0.001, 0.0001\}$ computed over all on the order of 10^{10} impostor scores. The FMR in each bin will vary also - see subsequent impostor heatmaps in sec. 3.6.1. The figures shows an order of magnitude variation in FNMR across country of birth; these effects are likely due quality variations, then demographics like age and race. The error rates in some cases are zero, and in others the DET is flat so the error rates at the two thresholds are identical. The lines span 1% and 99% of bootstrap replicated FNMR estimates.

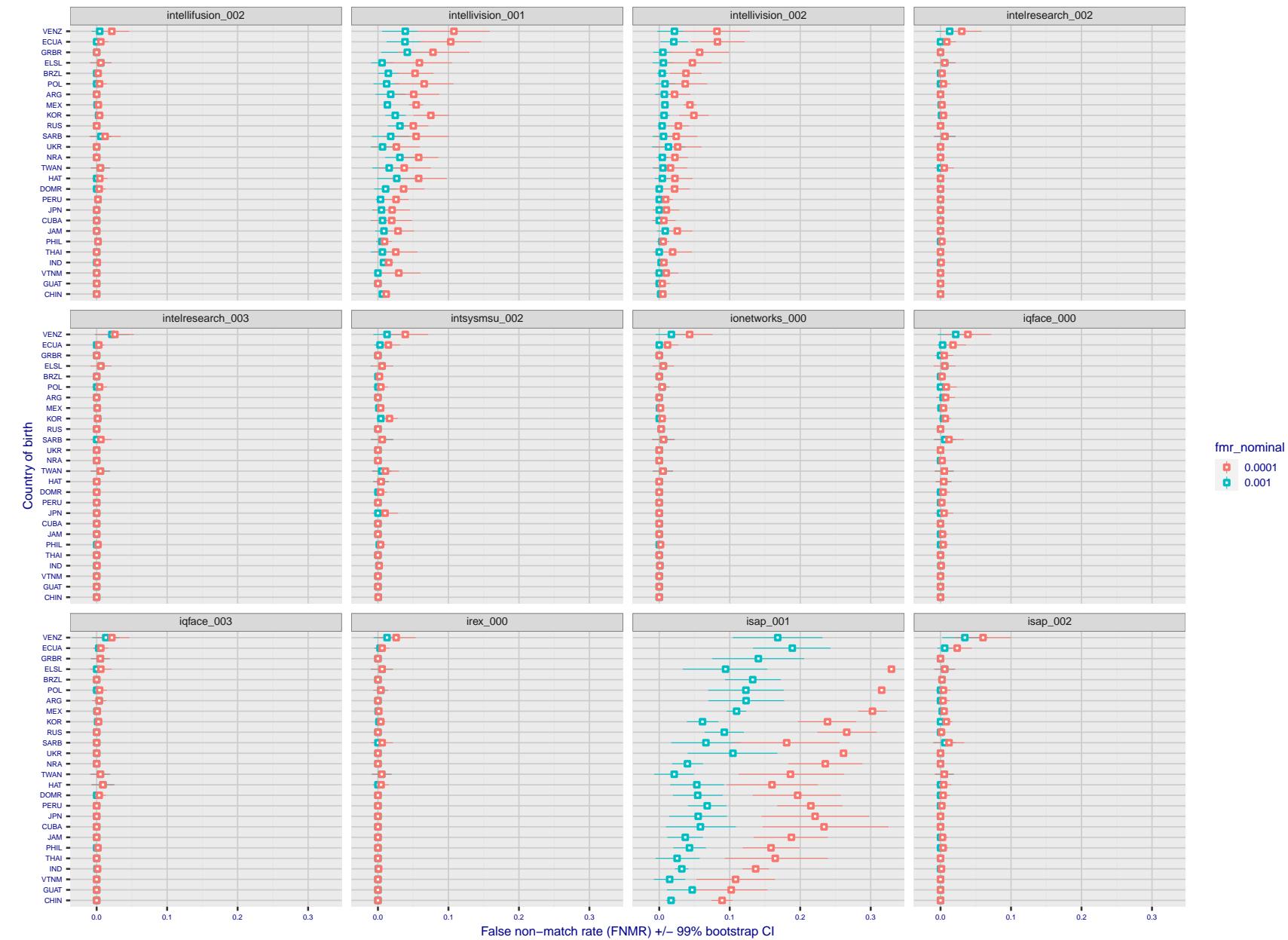


Figure 216: For the visa images, the dots show FNMR by country of birth for two globally set operating thresholds corresponding to $FMR = \{0.001, 0.0001\}$ computed over all on the order of 10^{10} impostor scores. The FMR in each bin will vary also - see subsequent impostor heatmaps in sec. 3.6.1. The figures shows an order of magnitude variation in FNMR across country of birth; these effects are likely due quality variations, then demographics like age and race. The error rates in some cases are zero, and in others the DET is flat so the error rates at the two thresholds are identical. The lines span 1% and 99% of bootstrap replicated FNMR estimates.

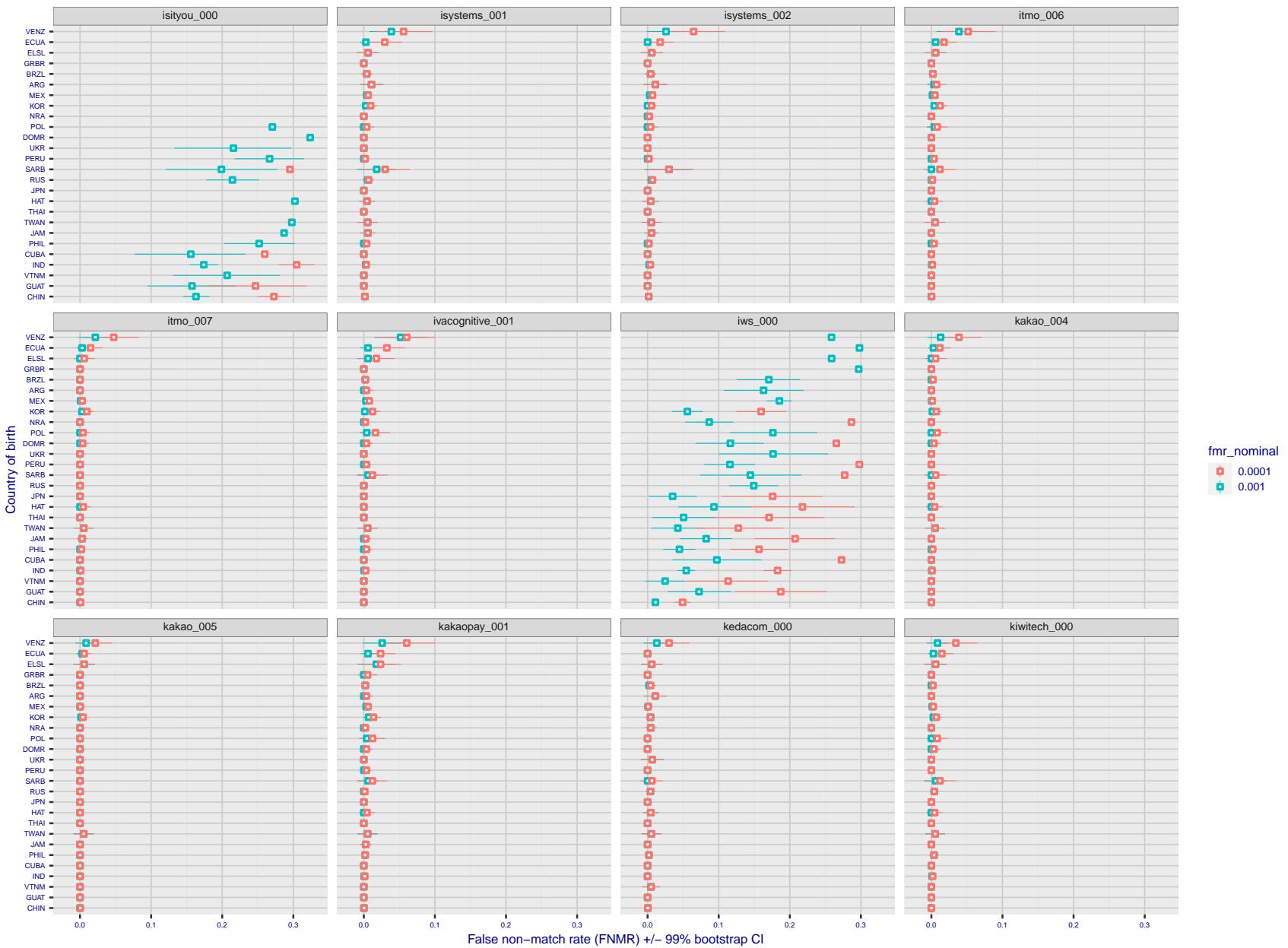


Figure 217: For the visa images, the dots show FNMR by country of birth for two globally set operating thresholds corresponding to $FMR = \{0.001, 0.0001\}$ computed over all on the order of 10^{10} impostor scores. The FMR in each bin will vary also - see subsequent impostor heatmaps in sec. 3.6.1. The figures shows an order of magnitude variation in FNMR across country of birth; these effects are likely due quality variations, then demographics like age and race. The error rates in some cases are zero, and in others the DET is flat so the error rates at the two thresholds are identical. The lines span 1% and 99% of bootstrap replicated FNMR estimates.

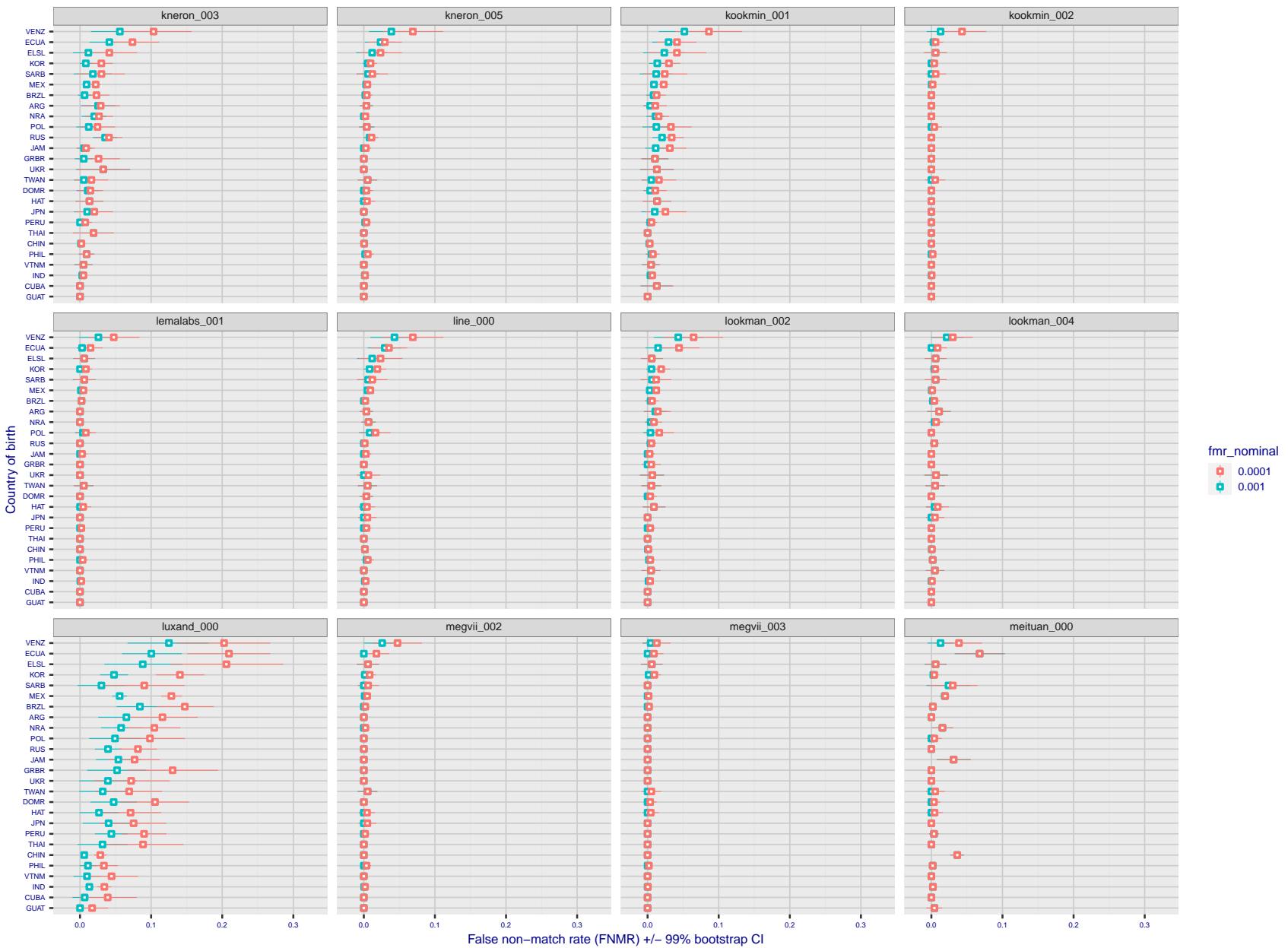


Figure 218: For the visa images, the dots show FNMR by country of birth for two globally set operating thresholds corresponding to $FMR = \{0.001, 0.0001\}$ computed over all on the order of 10^{10} impostor scores. The FMR in each bin will vary also - see subsequent impostor heatmaps in sec. 3.6.1. The figures shows an order of magnitude variation in FNMR across country of birth; these effects are likely due quality variations, then demographics like age and race. The error rates in some cases are zero, and in others the DET is flat so the error rates at the two thresholds are identical. The lines span 1% and 99% of bootstrap replicated FNMR estimates.

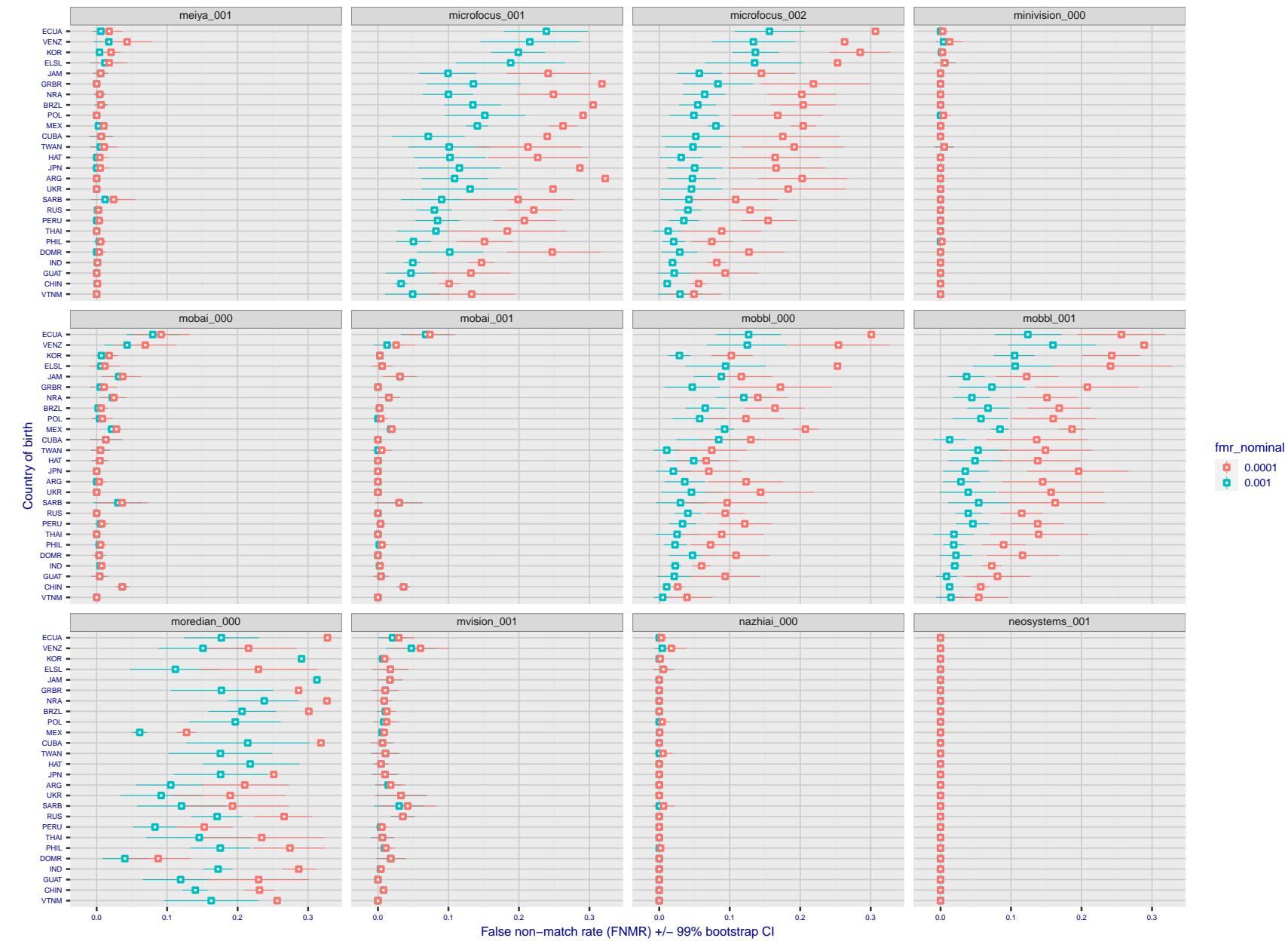


Figure 219: For the visa images, the dots show FNMR by country of birth for two globally set operating thresholds corresponding to $FMR = \{0.001, 0.0001\}$ computed over all on the order of 10^{10} impostor scores. The FMR in each bin will vary also - see subsequent impostor heatmaps in sec. 3.6.1. The figures shows an order of magnitude variation in FNMR across country of birth; these effects are likely due quality variations, then demographics like age and race. The error rates in some cases are zero, and in others the DET is flat so the error rates at the two thresholds are identical. The lines span 1% and 99% of bootstrap replicated FNMR estimates.

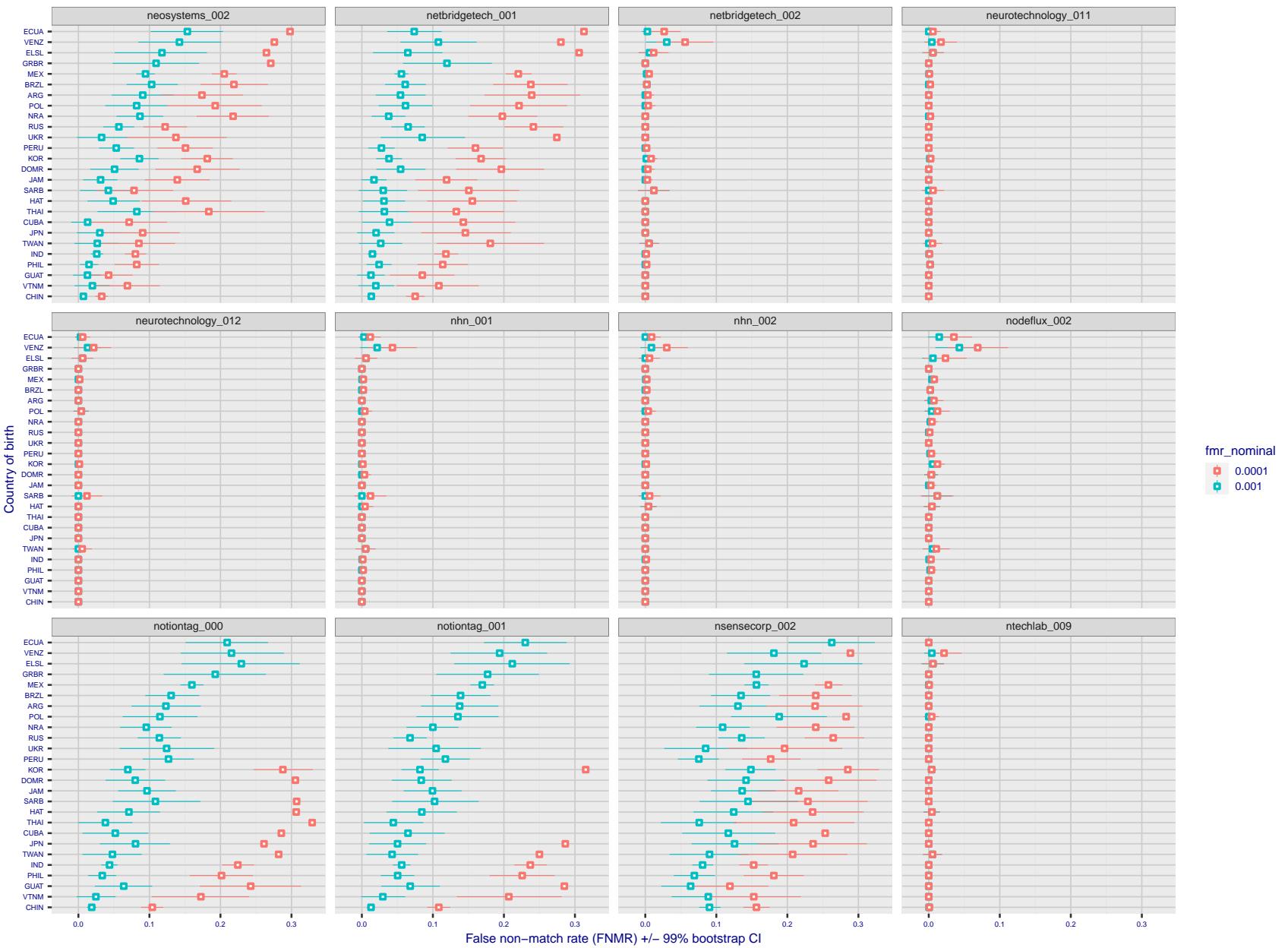


Figure 220: For the visa images, the dots show FNMR by country of birth for two globally set operating thresholds corresponding to $FMR = \{0.001, 0.0001\}$ computed over all on the order of 10^{10} impostor scores. The FMR in each bin will vary also - see subsequent impostor heatmaps in sec. 3.6.1. The figures shows an order of magnitude variation in FNMR across country of birth; these effects are likely due quality variations, then demographics like age and race. The error rates in some cases are zero, and in others the DET is flat so the error rates at the two thresholds are identical. The lines span 1% and 99% of bootstrap replicated FNMR estimates.

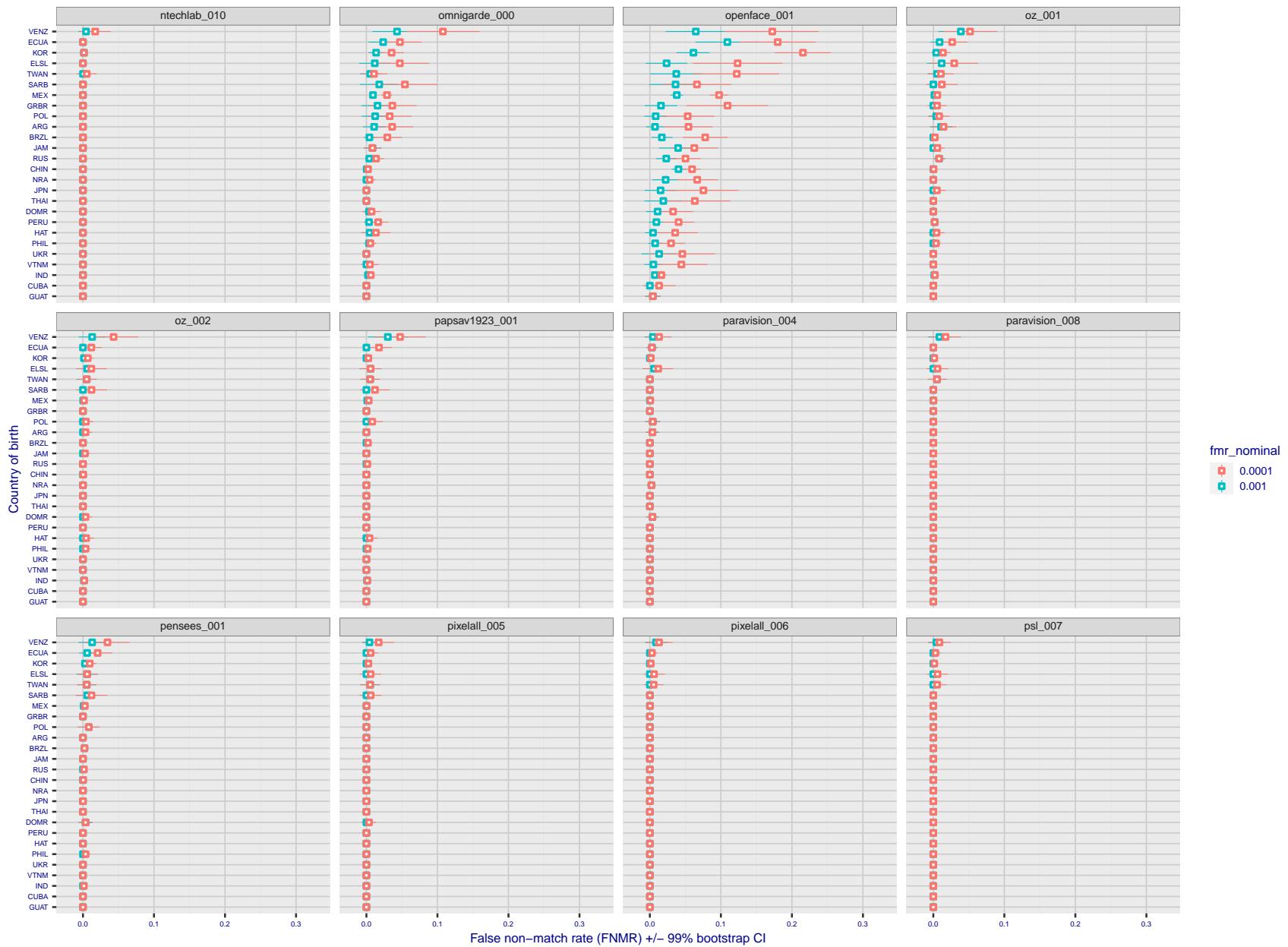


Figure 221: For the visa images, the dots show FNMR by country of birth for two globally set operating thresholds corresponding to $FMR = \{0.001, 0.0001\}$ computed over all on the order of 10^{10} impostor scores. The FMR in each bin will vary also - see subsequent impostor heatmaps in sec. 3.6.1. The figures shows an order of magnitude variation in FNMR across country of birth; these effects are likely due quality variations, then demographics like age and race. The error rates in some cases are zero, and in others the DET is flat so the error rates at the two thresholds are identical. The lines span 1% and 99% of bootstrap replicated FNMR estimates.

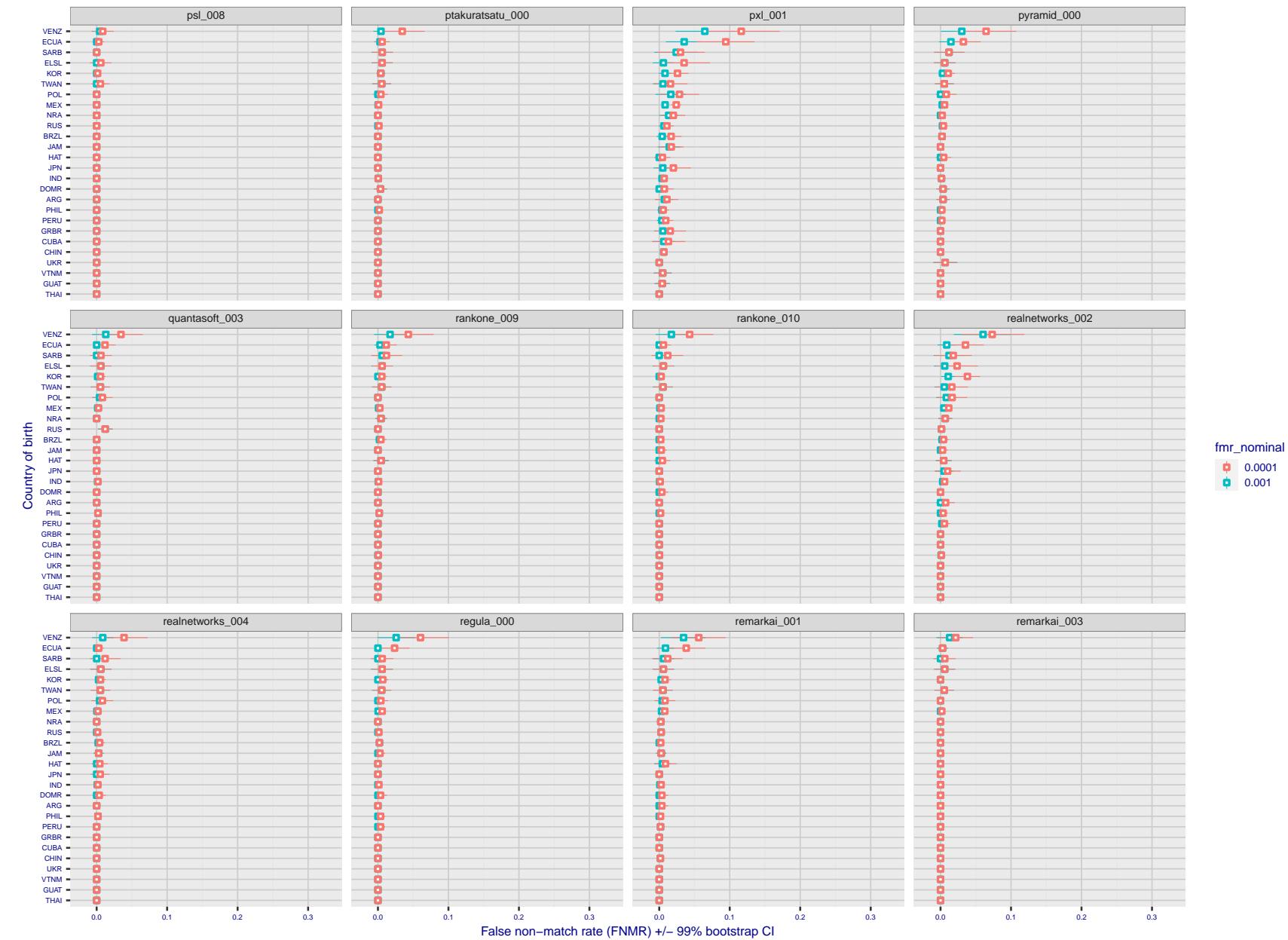


Figure 222: For the visa images, the dots show FNMR by country of birth for two globally set operating thresholds corresponding to $FMR = \{0.001, 0.0001\}$ computed over all on the order of 10^{10} impostor scores. The FMR in each bin will vary also - see subsequent impostor heatmaps in sec. 3.6.1. The figures shows an order of magnitude variation in FNMR across country of birth; these effects are likely due quality variations, then demographics like age and race. The error rates in some cases are zero, and in others the DET is flat so the error rates at the two thresholds are identical. The lines span 1% and 99% of bootstrap replicated FNMR estimates.

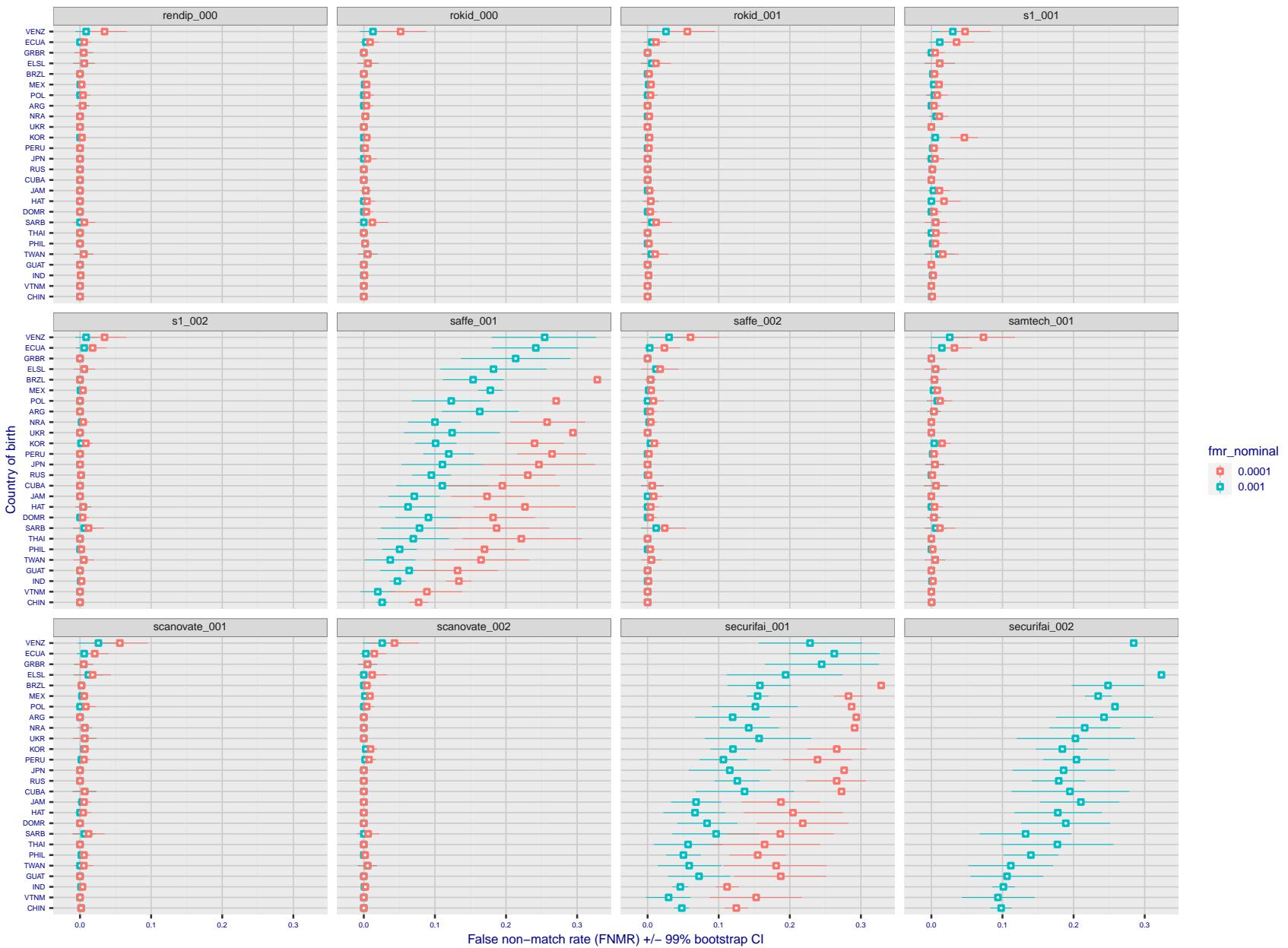


Figure 223: For the visa images, the dots show FNMR by country of birth for two globally set operating thresholds corresponding to $FMR = \{0.001, 0.0001\}$ computed over all on the order of 10^{10} impostor scores. The FMR in each bin will vary also - see subsequent impostor heatmaps in sec. 3.6.1. The figures shows an order of magnitude variation in FNMR across country of birth; these effects are likely due quality variations, then demographics like age and race. The error rates in some cases are zero, and in others the DET is flat so the error rates at the two thresholds are identical. The lines span 1% and 99% of bootstrap replicated FNMR estimates.

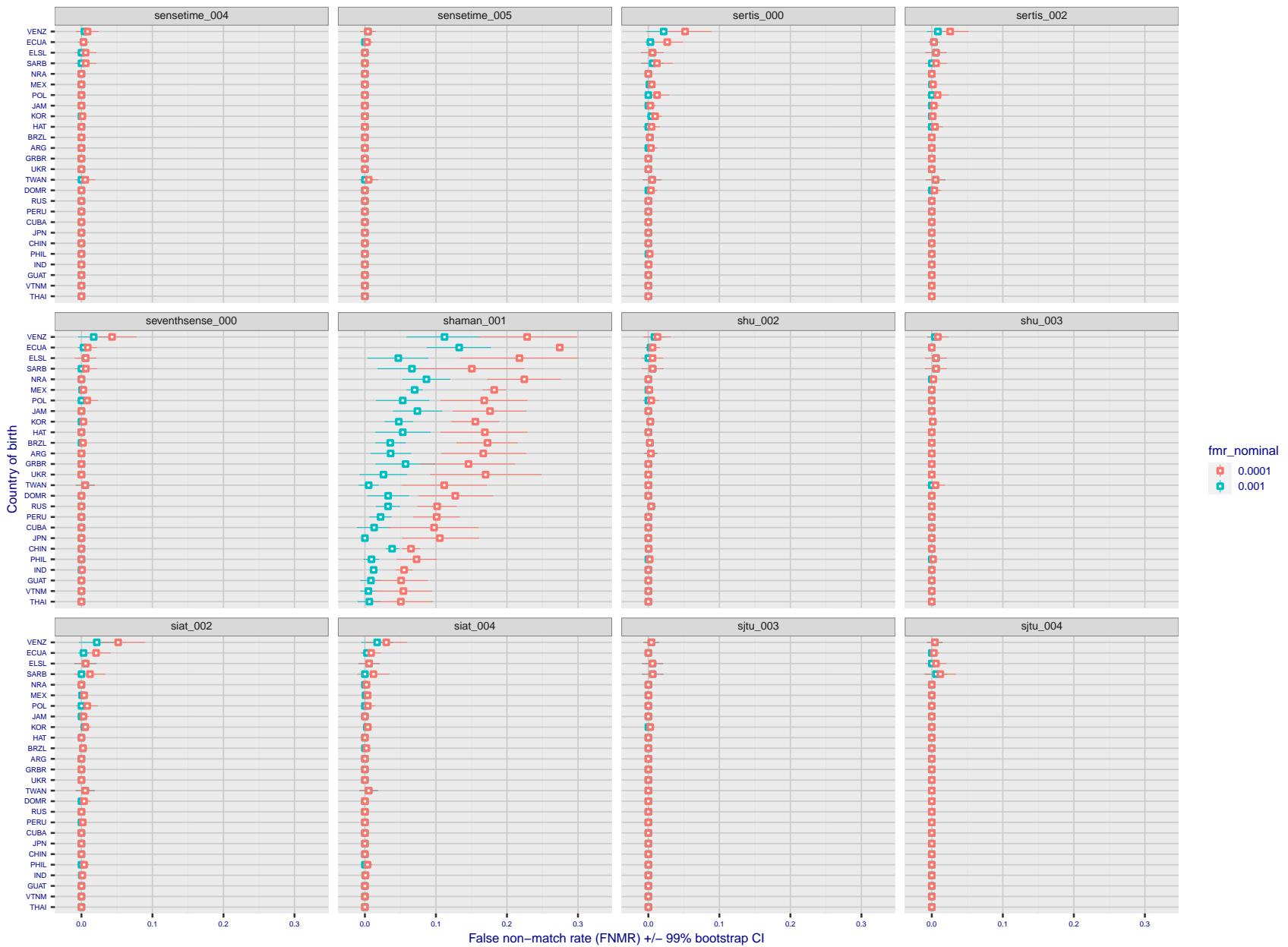


Figure 224: For the visa images, the dots show FNMR by country of birth for two globally set operating thresholds corresponding to $FMR = \{0.001, 0.0001\}$ computed over all on the order of 10^{10} impostor scores. The FMR in each bin will vary also - see subsequent impostor heatmaps in sec. 3.6.1. The figures shows an order of magnitude variation in FNMR across country of birth; these effects are likely due quality variations, then demographics like age and race. The error rates in some cases are zero, and in others the DET is flat so the error rates at the two thresholds are identical. The lines span 1% and 99% of bootstrap replicated FNMR estimates.

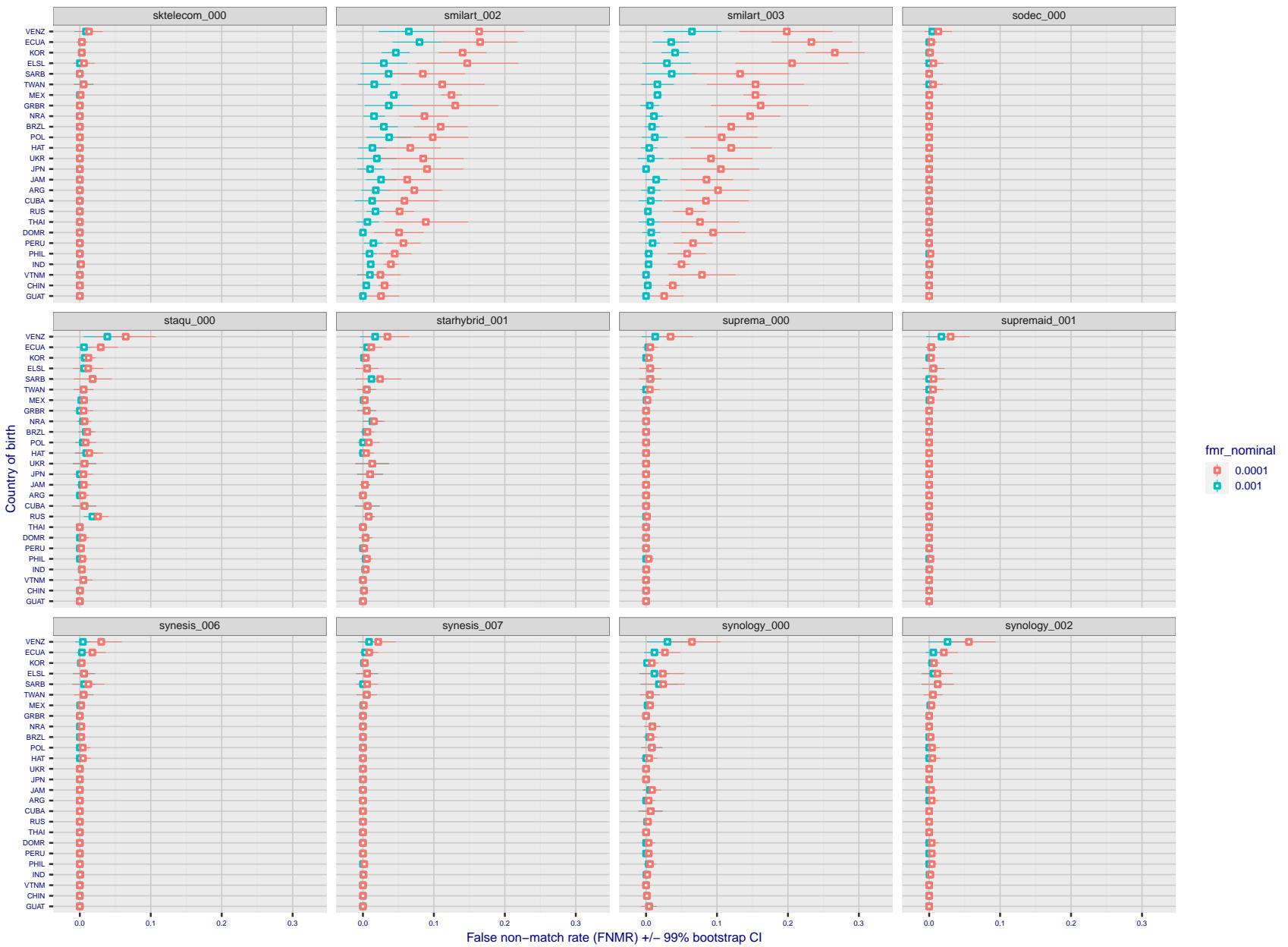


Figure 225: For the visa images, the dots show FNMR by country of birth for two globally set operating thresholds corresponding to $FMR = \{0.001, 0.0001\}$ computed over all on the order of 10^{10} impostor scores. The FMR in each bin will vary also - see subsequent impostor heatmaps in sec. 3.6.1. The figures shows an order of magnitude variation in FNMR across country of birth; these effects are likely due quality variations, then demographics like age and race. The error rates in some cases are zero, and in others the DET is flat so the error rates at the two thresholds are identical. The lines span 1% and 99% of bootstrap replicated FNMR estimates.

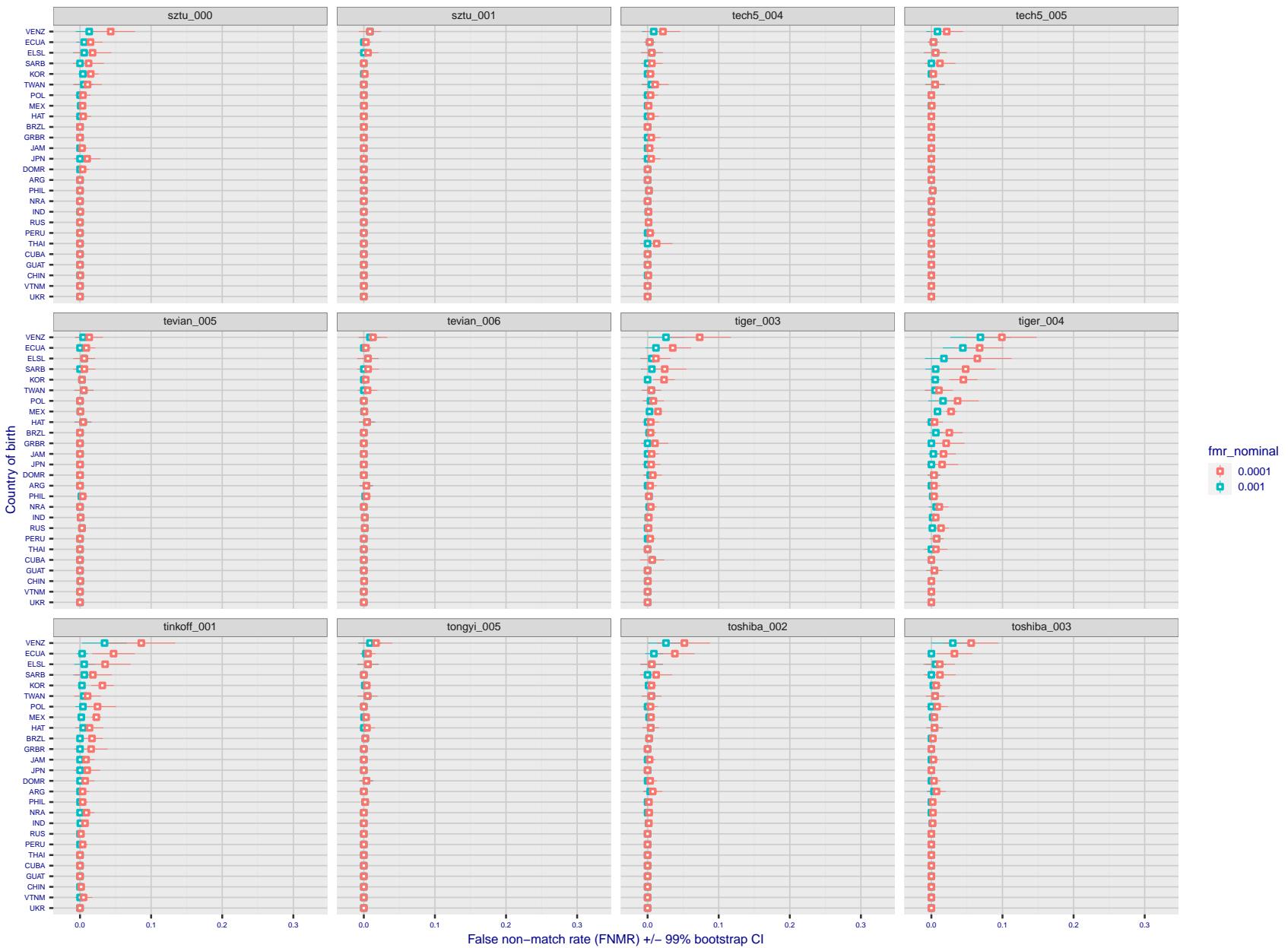


Figure 226: For the visa images, the dots show FNMR by country of birth for two globally set operating thresholds corresponding to $FMR = \{0.001, 0.0001\}$ computed over all on the order of 10^{10} impostor scores. The FMR in each bin will vary also - see subsequent impostor heatmaps in sec. 3.6.1. The figures shows an order of magnitude variation in FNMR across country of birth; these effects are likely due quality variations, then demographics like age and race. The error rates in some cases are zero, and in others the DET is flat so the error rates at the two thresholds are identical. The lines span 1% and 99% of bootstrap replicated FNMR estimates.

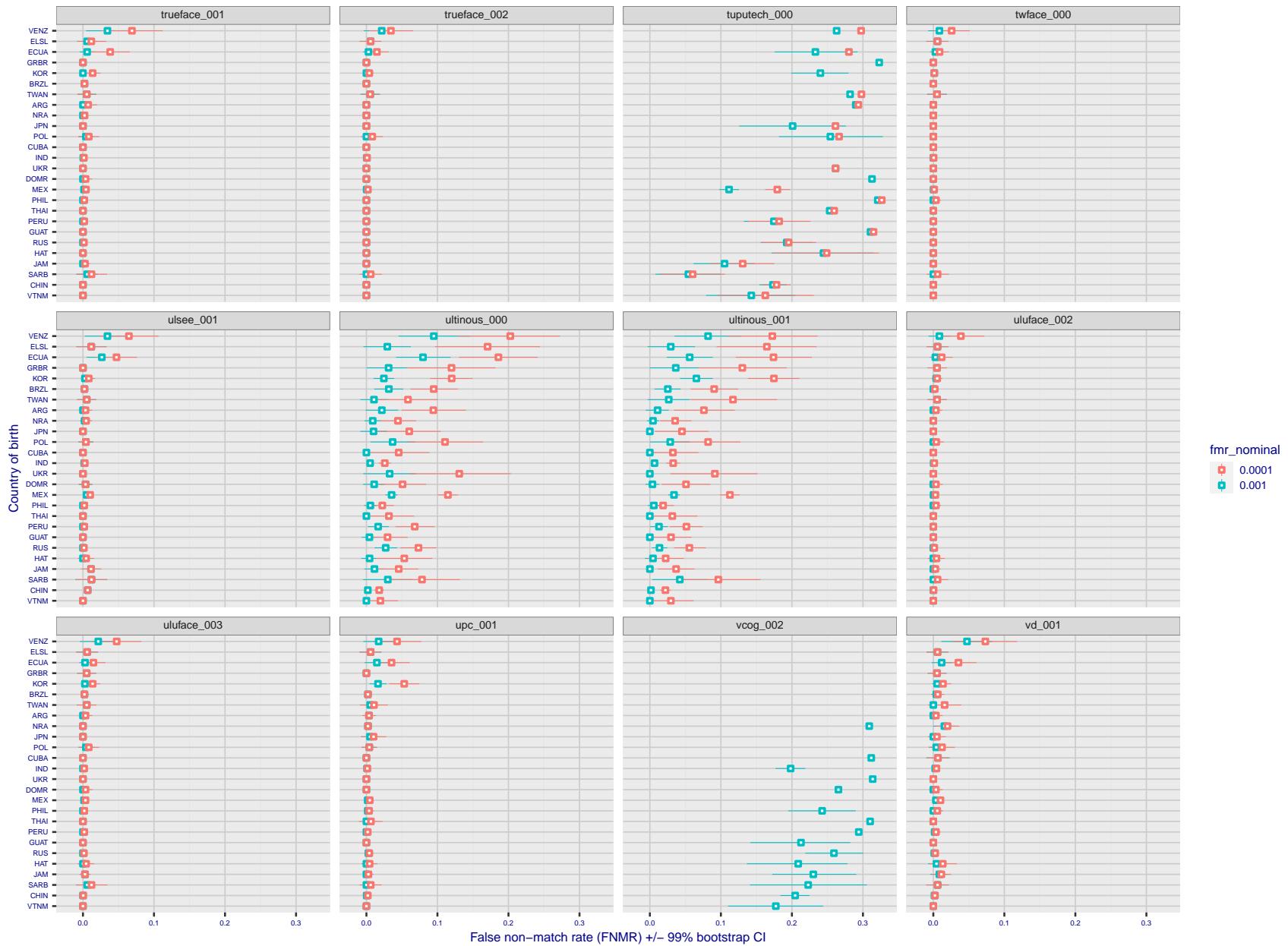


Figure 227: For the visa images, the dots show FNMR by country of birth for two globally set operating thresholds corresponding to $FMR = \{0.001, 0.0001\}$ computed over all on the order of 10^{10} impostor scores. The FMR in each bin will vary also - see subsequent impostor heatmaps in sec. 3.6.1. The figures shows an order of magnitude variation in FNMR across country of birth; these effects are likely due quality variations, then demographics like age and race. The error rates in some cases are zero, and in others the DET is flat so the error rates at the two thresholds are identical. The lines span 1% and 99% of bootstrap replicated FNMR estimates.

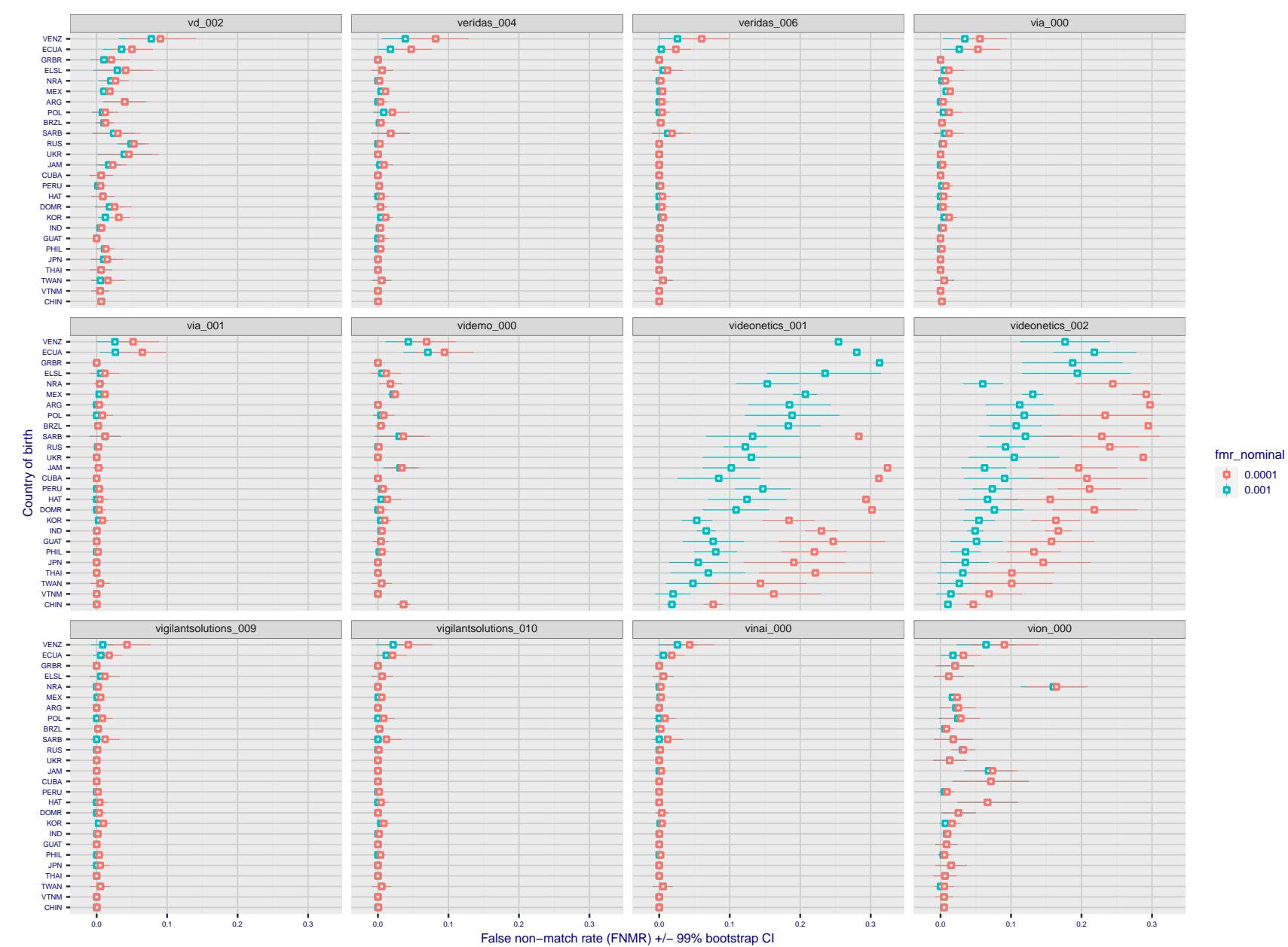


Figure 228: For the visa images, the dots show FNMR by country of birth for two globally set operating thresholds corresponding to $FMR = \{0.001, 0.0001\}$ computed over all on the order of 10^{10} impostor scores. The FMR in each bin will vary also - see subsequent impostor heatmaps in sec. 3.6.1. The figures shows an order of magnitude variation in FNMR across country of birth; these effects are likely due quality variations, then demographics like age and race. The error rates in some cases are zero, and in others the DET is flat so the error rates at the two thresholds are identical. The lines span 1% and 99% of bootstrap replicated FNMR estimates.

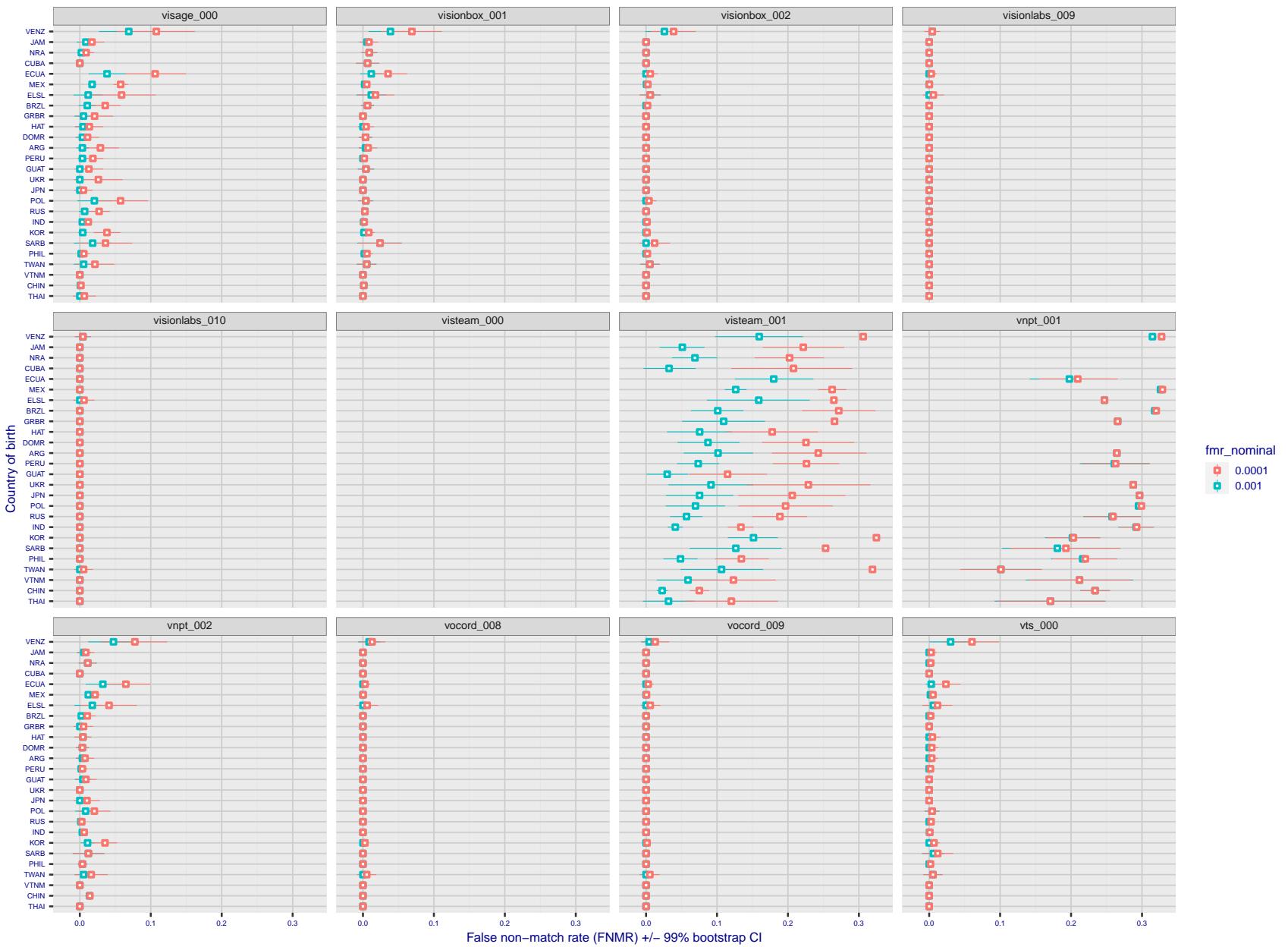


Figure 229: For the visa images, the dots show FNMR by country of birth for two globally set operating thresholds corresponding to $FMR = \{0.001, 0.0001\}$ computed over all on the order of 10^{10} impostor scores. The FMR in each bin will vary also - see subsequent impostor heatmaps in sec. 3.6.1. The figures shows an order of magnitude variation in FNMR across country of birth; these effects are likely due quality variations, then demographics like age and race. The error rates in some cases are zero, and in others the DET is flat so the error rates at the two thresholds are identical. The lines span 1% and 99% of bootstrap replicated FNMR estimates.

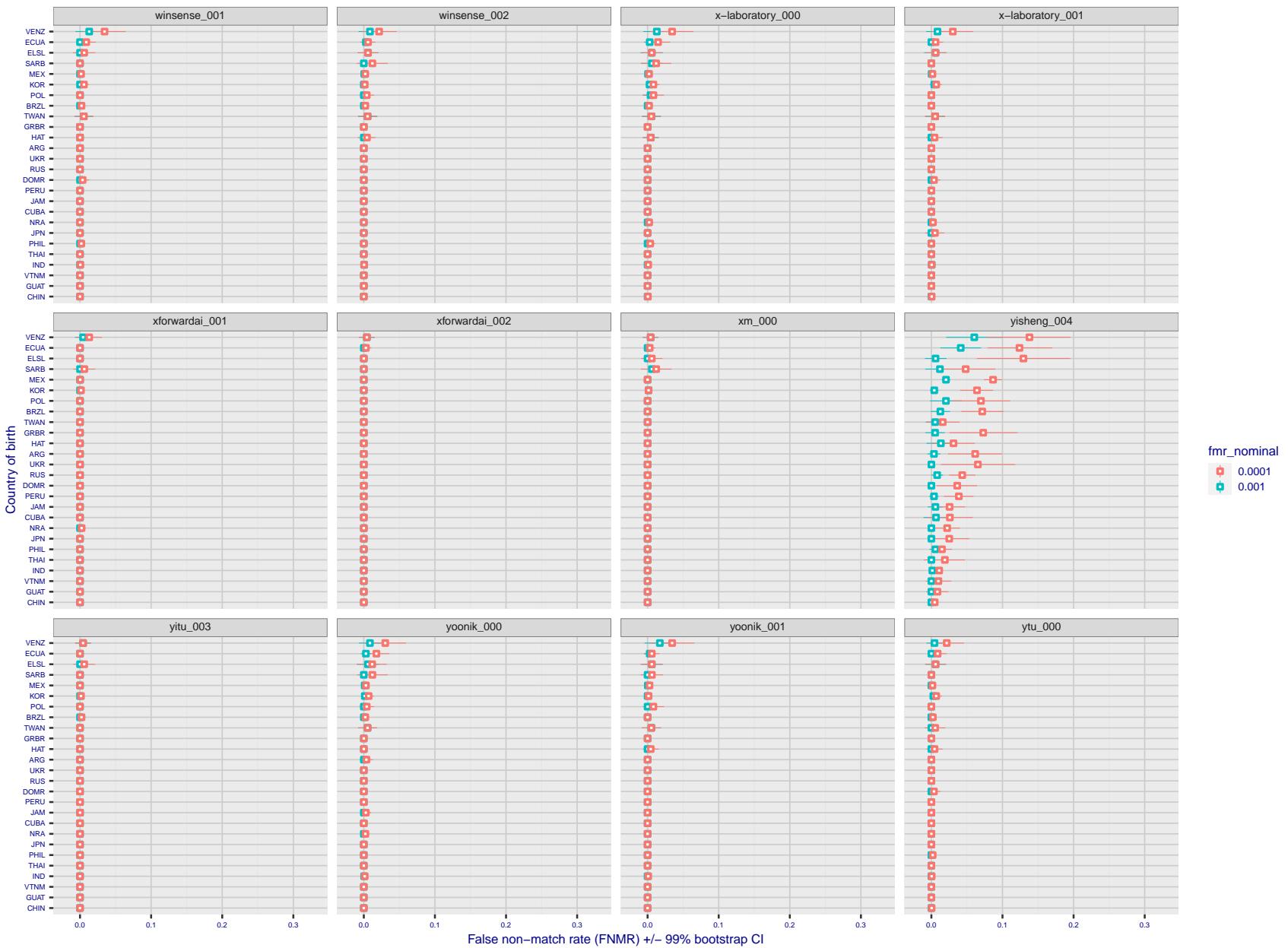


Figure 230: For the visa images, the dots show FNMR by country of birth for two globally set operating thresholds corresponding to $FMR = \{0.001, 0.0001\}$ computed over all on the order of 10^{10} impostor scores. The FMR in each bin will vary also - see subsequent impostor heatmaps in sec. 3.6.1. The figures shows an order of magnitude variation in FNMR across country of birth; these effects are likely due quality variations, then demographics like age and race. The error rates in some cases are zero, and in others the DET is flat so the error rates at the two thresholds are identical. The lines span 1% and 99% of bootstrap replicated FNMR estimates.

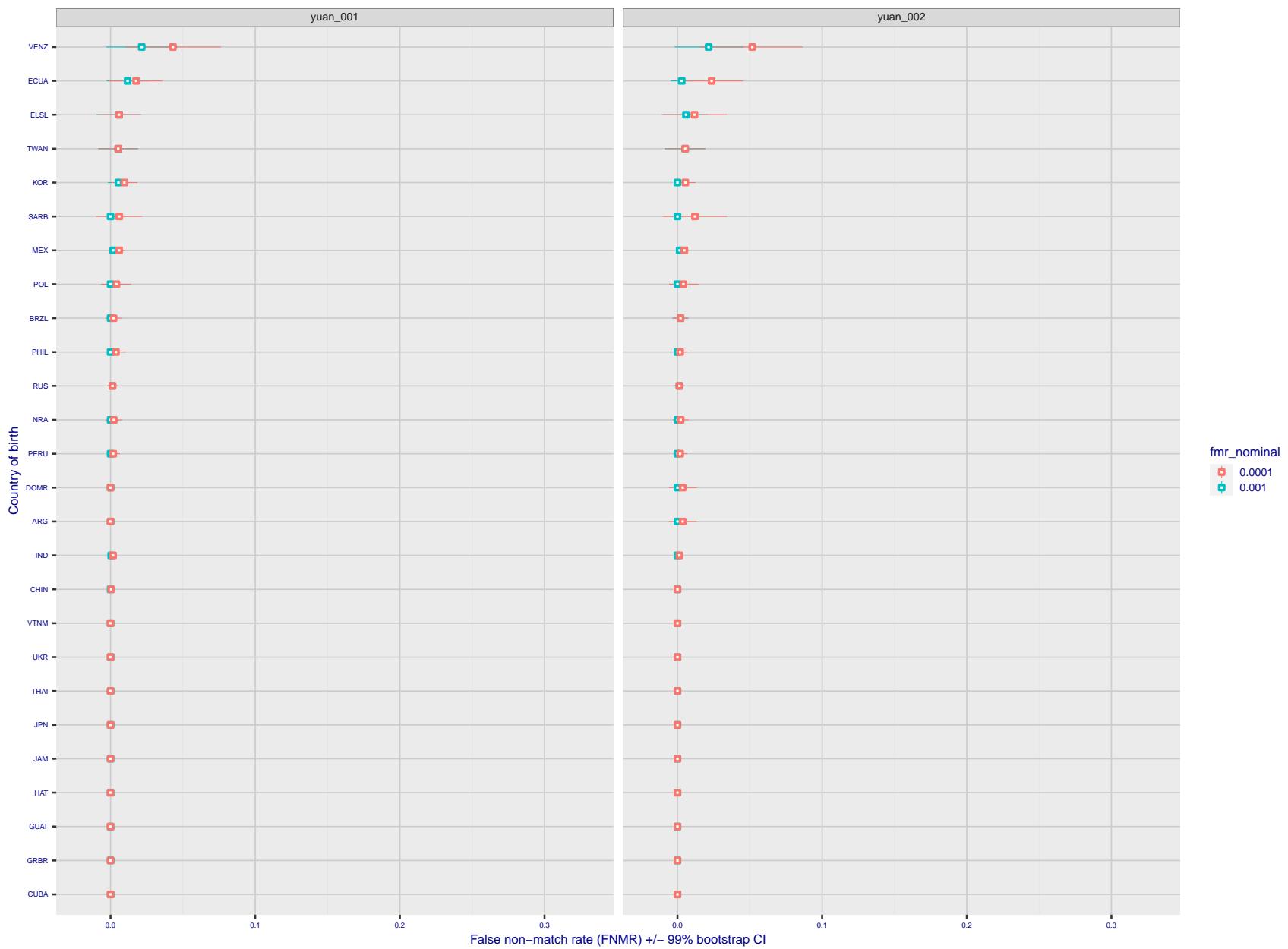


Figure 231: For the visa images, the dots show FNMR by country of birth for two globally set operating thresholds corresponding to $FMR = \{0.001, 0.0001\}$ computed over all on the order of 10^{10} impostor scores. The FMR in each bin will vary also - see subsequent impostor heatmaps in sec. 3.6.1. The figures shows an order of magnitude variation in FNMR across country of birth; these effects are likely due quality variations, then demographics like age and race. The error rates in some cases are zero, and in others the DET is flat so the error rates at the two thresholds are identical. The lines span 1% and 99% of bootstrap replicated FNMR estimates.

Caveats: The results may not relate to subject-specific properties. Instead they could reflect image-specific quality differences, which could occur due to collection protocol or software processing variations.

3.5.2 Effect of ageing

Background: Faces change appearance throughout life. This change gradually reduces similarity of a new image to an earlier image. Face recognition algorithms give reduced similarity scores and more frequent false rejections.

Goal: To quantify false non-match rates (FNMR) as a function of elapsed time in an adult population.

Methods: Using the mugshot images, a threshold is set to give FMR = 0.00001 over the entire impostor set. Then FNMR is measured over 1000 bootstrap replications of the genuine scores.

Results: For the visa images, Figure 251 shows how false non-match rates for genuine users, as a function of age group.

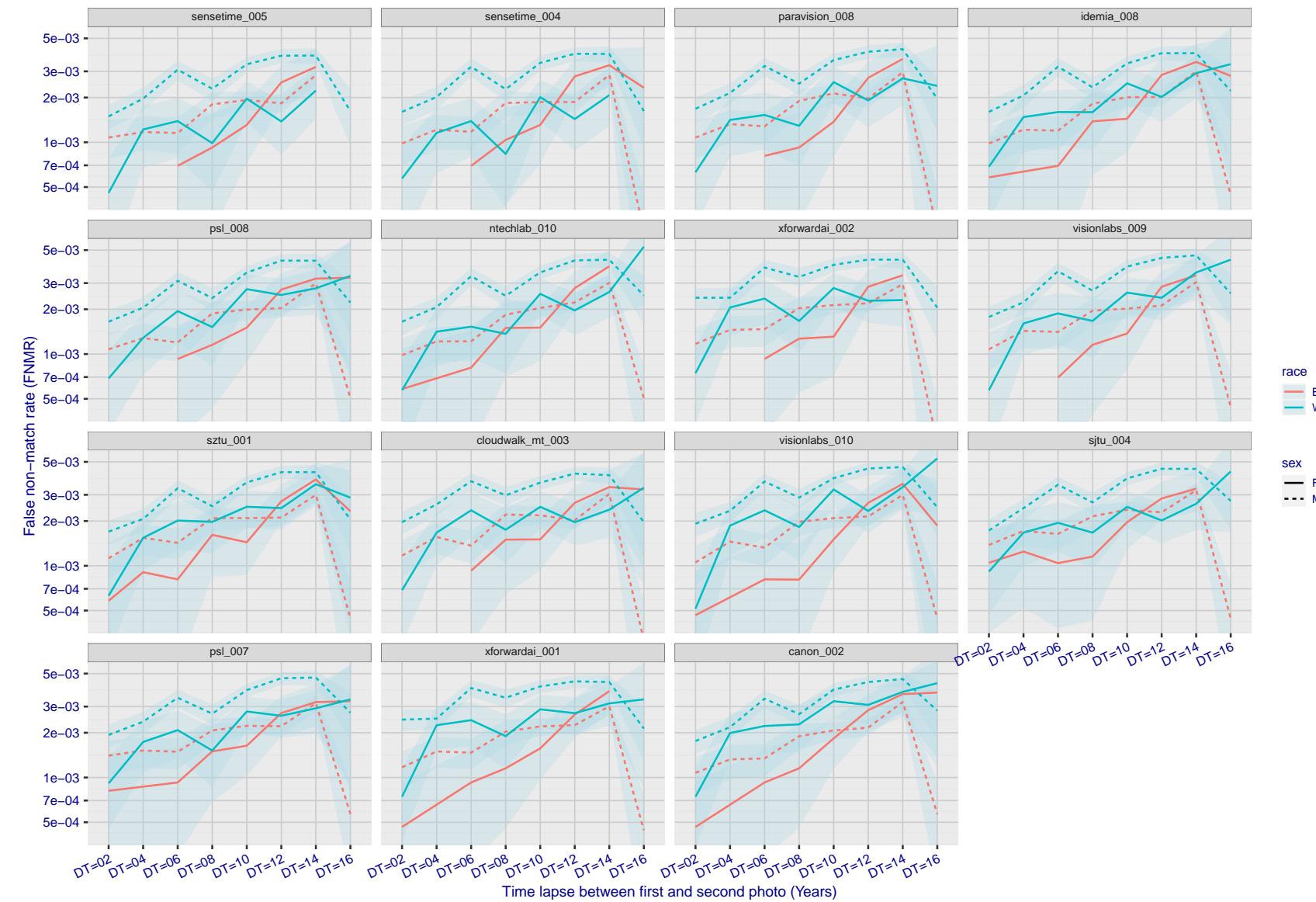


Figure 232: For the mugshot images, FNMR as a function of elapsed time between initial enrollment and second verification images. The panels appear most accurate first, and vertical scale changes on each page. The four traces correspond to images annotated with codes for black female, black male, white female, white male. The threshold is fixed for each algorithm to give $FMR = 0.00001$ over all (10^8) impostor comparisons. For short time-lapses, the most accurate algorithms give very few errors ($FNMR < 0.001$) so that the uncertainty estimates are high.

2021/08/02 13:13:01

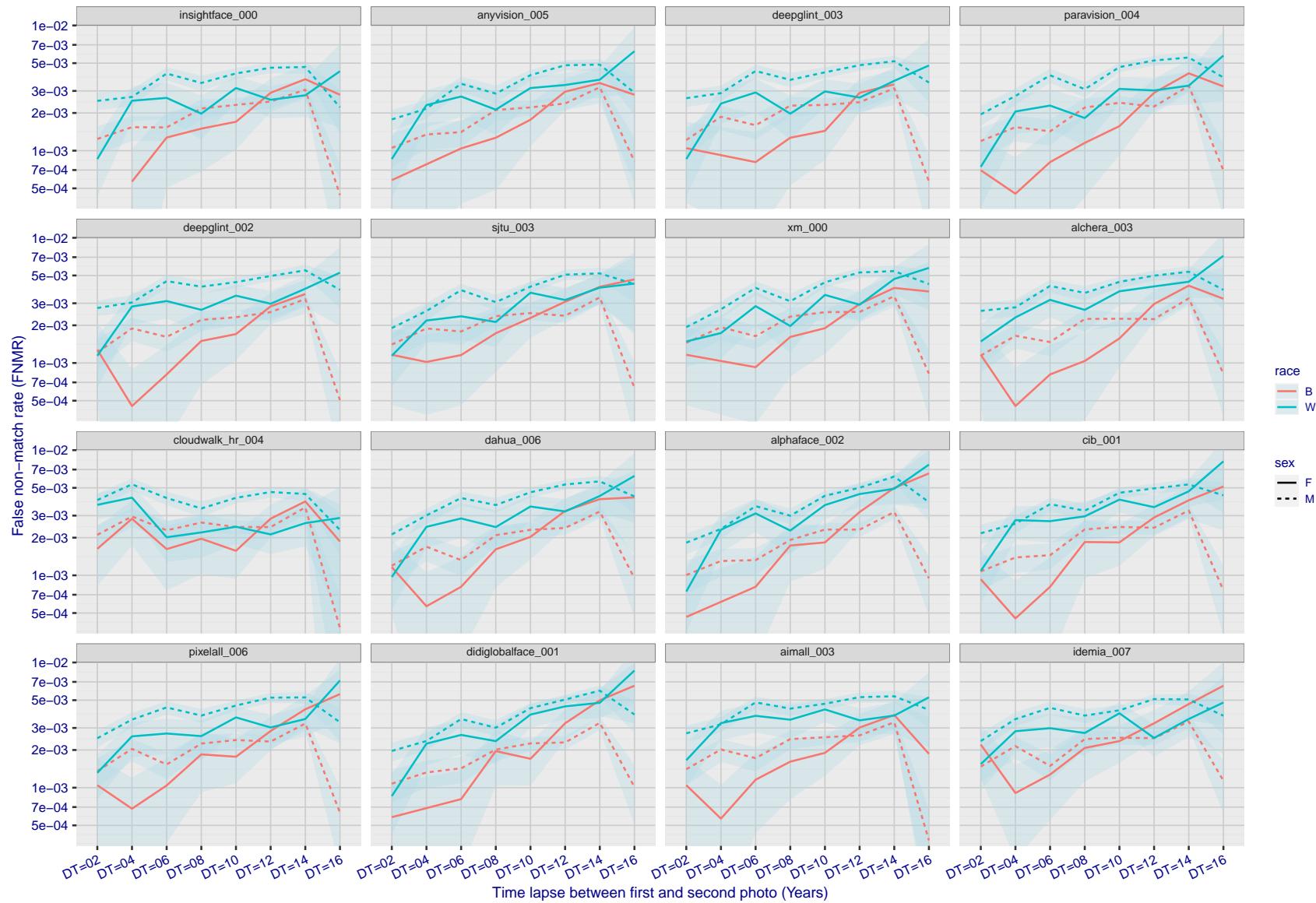


Figure 233: For the mugshot images, FNMR as a function of elapsed time between initial enrollment and second verification images. The panels appear most accurate first, and vertical scale changes on each page. The four traces correspond to images annotated with codes for black female, black male, white female, white male. The threshold is fixed for each algorithm to give FMR = 0.00001 over all (10^8) impostor comparisons. For short time-lapses, the most accurate algorithms give very few errors (FNMR < 0.001) so that the uncertainty estimates are high.

FNMR(T)
FMR(T)
"False match rate"
"False non-match rate"

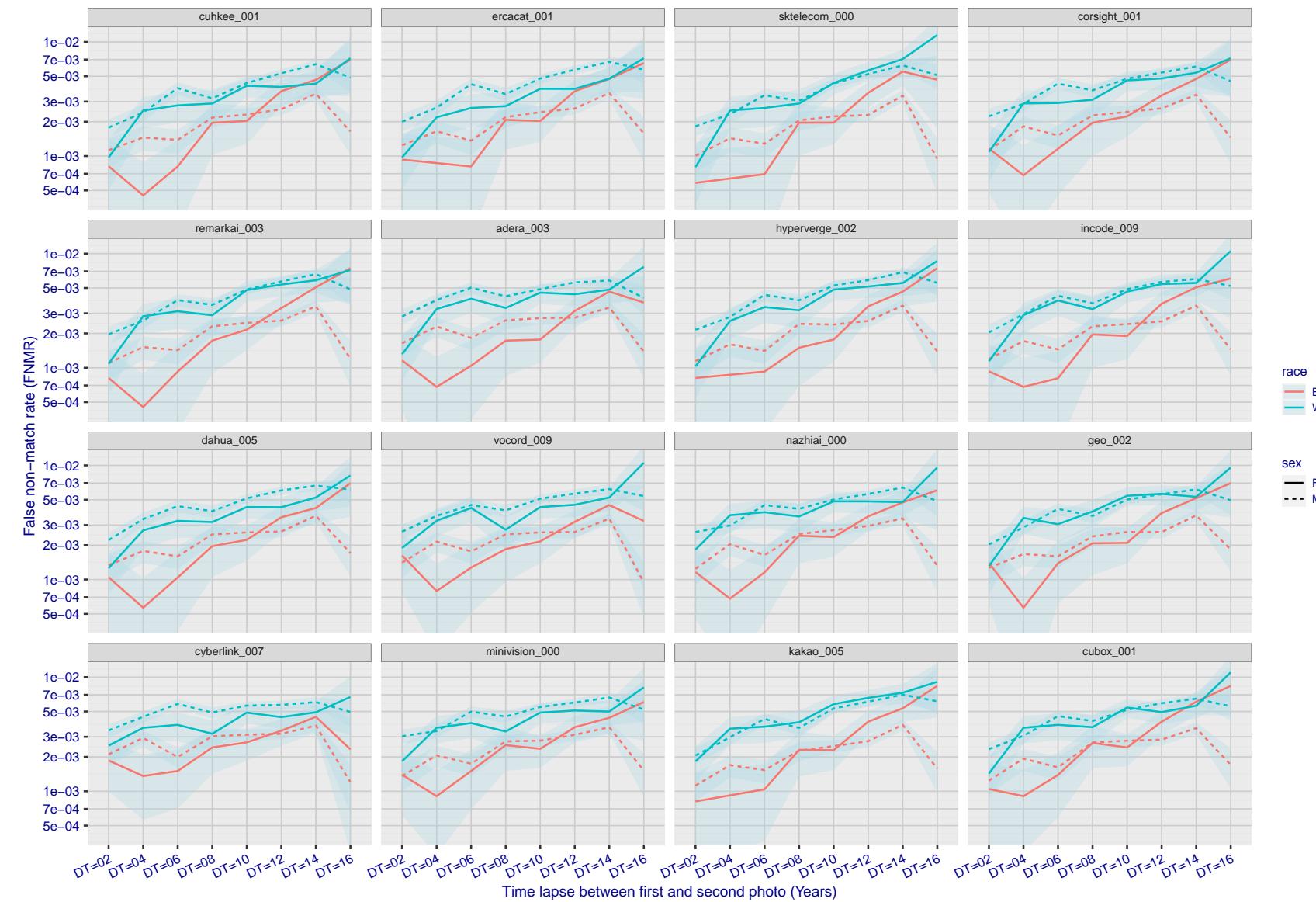


Figure 234: For the mugshot images, FNMR as a function of elapsed time between initial enrollment and second verification images. The panels appear most accurate first, and vertical scale changes on each page. The four traces correspond to images annotated with codes for black female, black male, white female, white male. The threshold is fixed for each algorithm to give $FMR = 0.00001$ over all (10^8) impostor comparisons. For short time-lapses, the most accurate algorithms give very few errors ($FNMR < 0.001$) so that the uncertainty estimates are high.

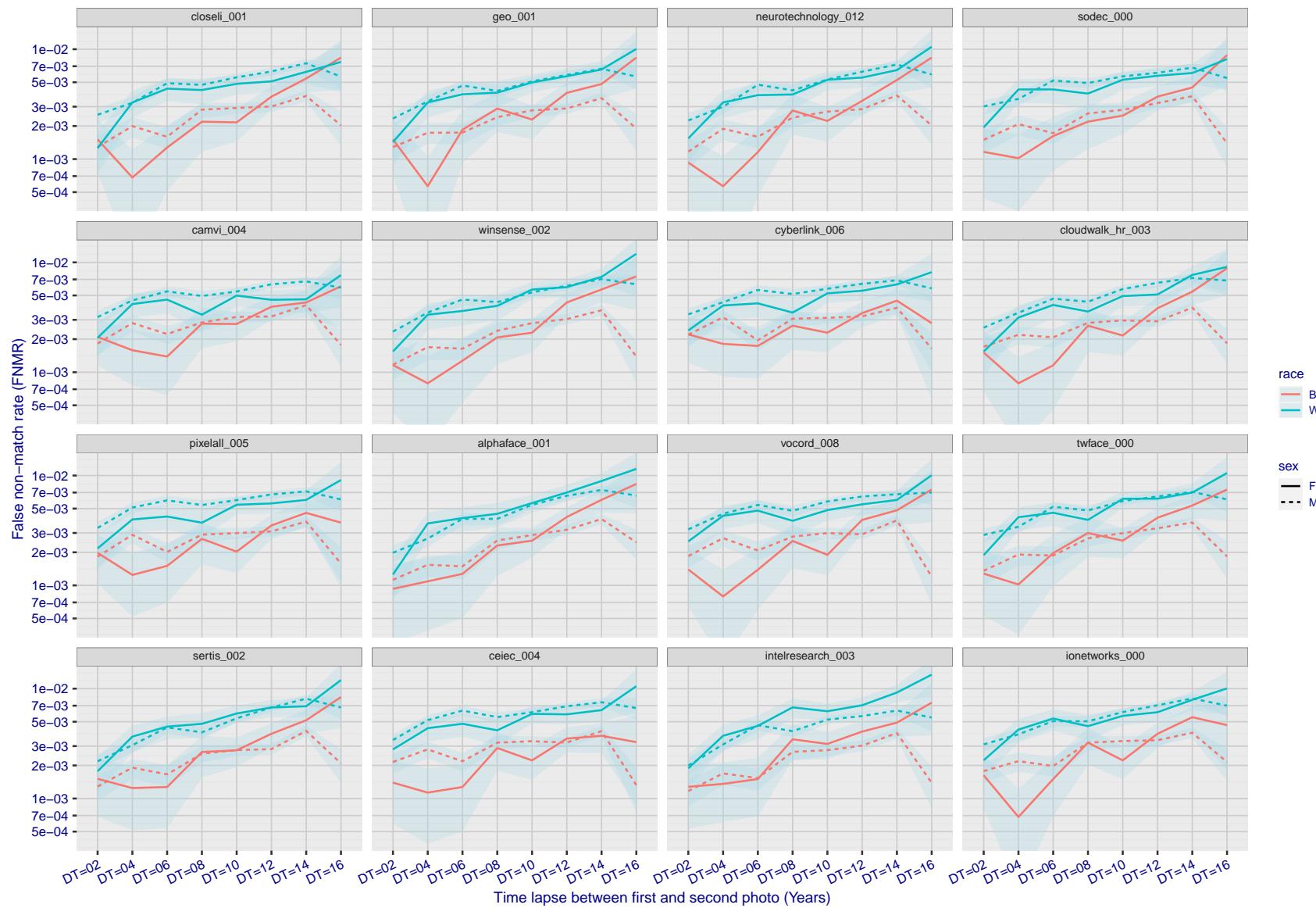


Figure 235: For the mugshot images, FNMR as a function of elapsed time between initial enrollment and second verification images. The panels appear most accurate first, and vertical scale changes on each page. The four traces correspond to images annotated with codes for black female, black male, white female, white male. The threshold is fixed for each algorithm to give $FMR = 0.00001$ over all (10^8) impostor comparisons. For short time-lapses, the most accurate algorithms give very few errors ($FNMR < 0.001$) so that the uncertainty estimates are high.

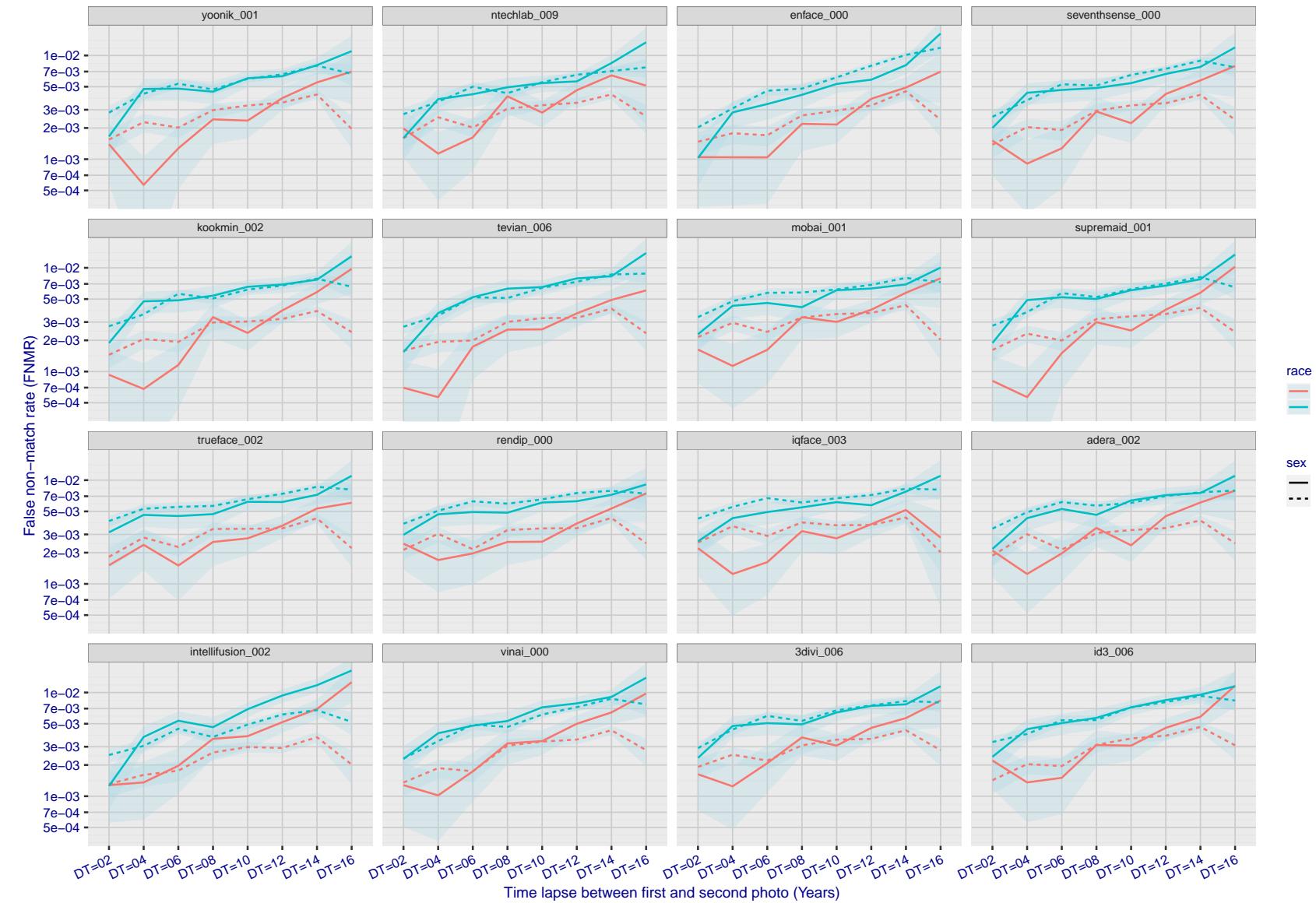


Figure 236: For the mugshot images, FNMR as a function of elapsed time between initial enrollment and second verification images. The panels appear most accurate first, and vertical scale changes on each page. The four traces correspond to images annotated with codes for black female, black male, white female, white male. The threshold is fixed for each algorithm to give $FMR = 0.00001$ over all (10^8) impostor comparisons. For short time-lapses, the most accurate algorithms give very few errors ($FNMR < 0.001$) so that the uncertainty estimates are high.

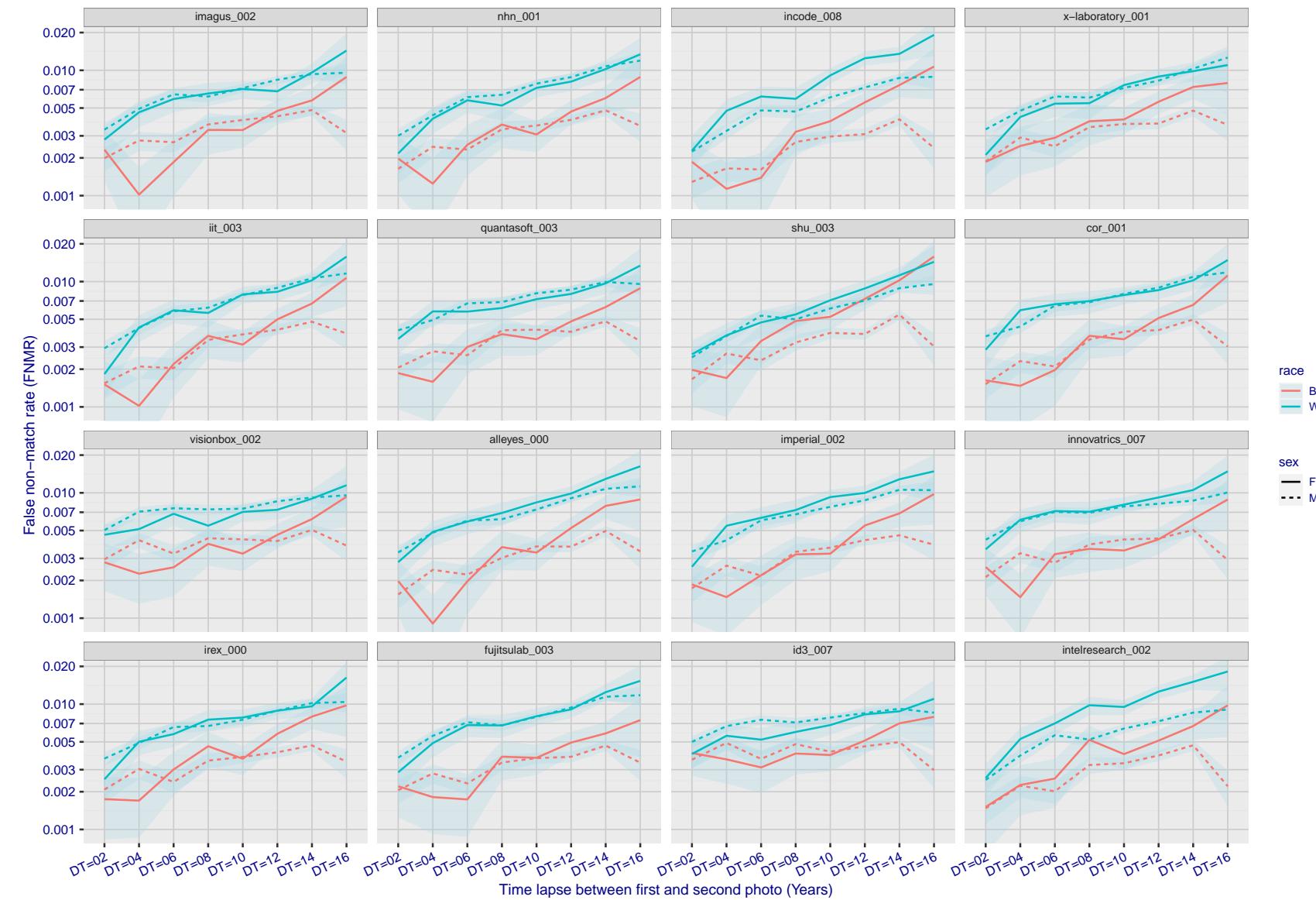


Figure 237: For the mugshot images, FNMR as a function of elapsed time between initial enrollment and second verification images. The panels appear most accurate first, and vertical scale changes on each page. The four traces correspond to images annotated with codes for black female, black male, white female, white male. The threshold is fixed for each algorithm to give FMR = 0.00001 over all (10^8) impostor comparisons. For short time-lapses, the most accurate algorithms give very few errors (FNMR < 0.001) so that the uncertainty estimates are high.

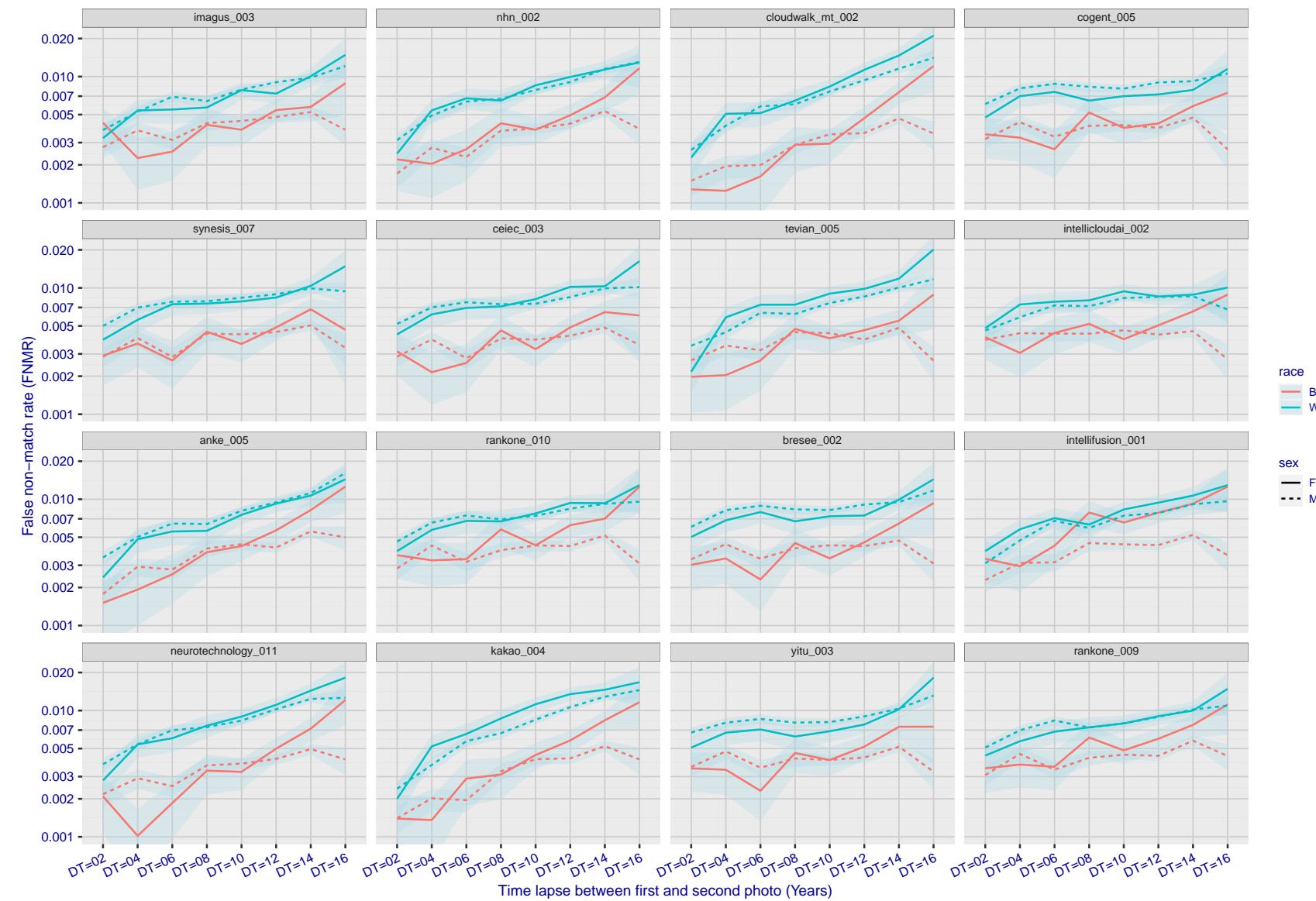


Figure 238: For the mugshot images, FNMR as a function of elapsed time between initial enrollment and second verification images. The panels appear most accurate first, and vertical scale changes on each page. The four traces correspond to images annotated with codes for black female, black male, white female, white male. The threshold is fixed for each algorithm to give FMR = 0.00001 over all (10^8) impostor comparisons. For short time-lapses, the most accurate algorithms give very few errors (FNMR < 0.001) so that the uncertainty estimates are high.

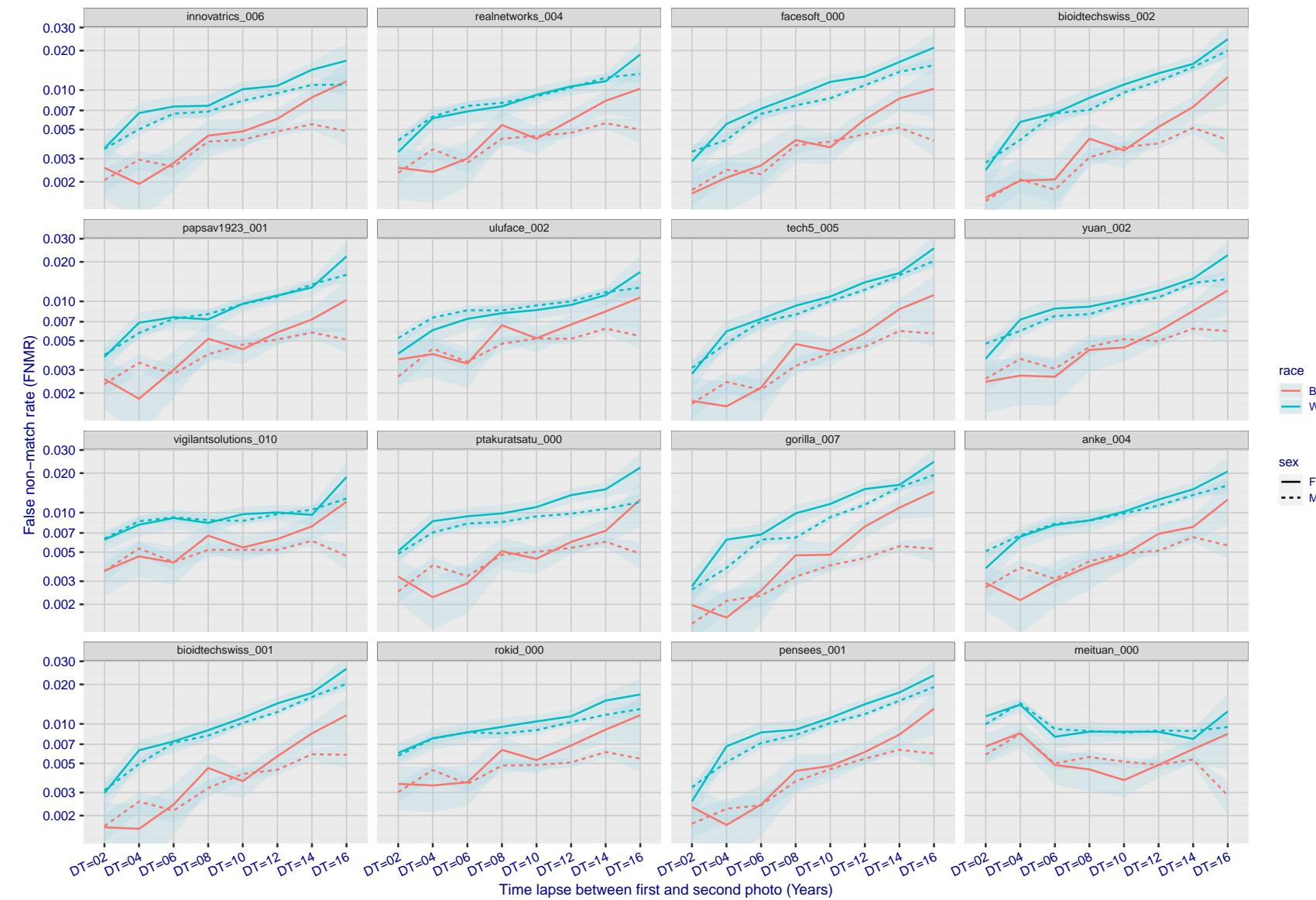


Figure 239: For the mugshot images, FNMR as a function of elapsed time between initial enrollment and second verification images. The panels appear most accurate first, and vertical scale changes on each page. The four traces correspond to images annotated with codes for black female, black male, white female, white male. The threshold is fixed for each algorithm to give FMR = 0.00001 over all (10^8) impostor comparisons. For short time-lapses, the most accurate algorithms give very few errors (FNMR < 0.001) so that the uncertainty estimates are high.

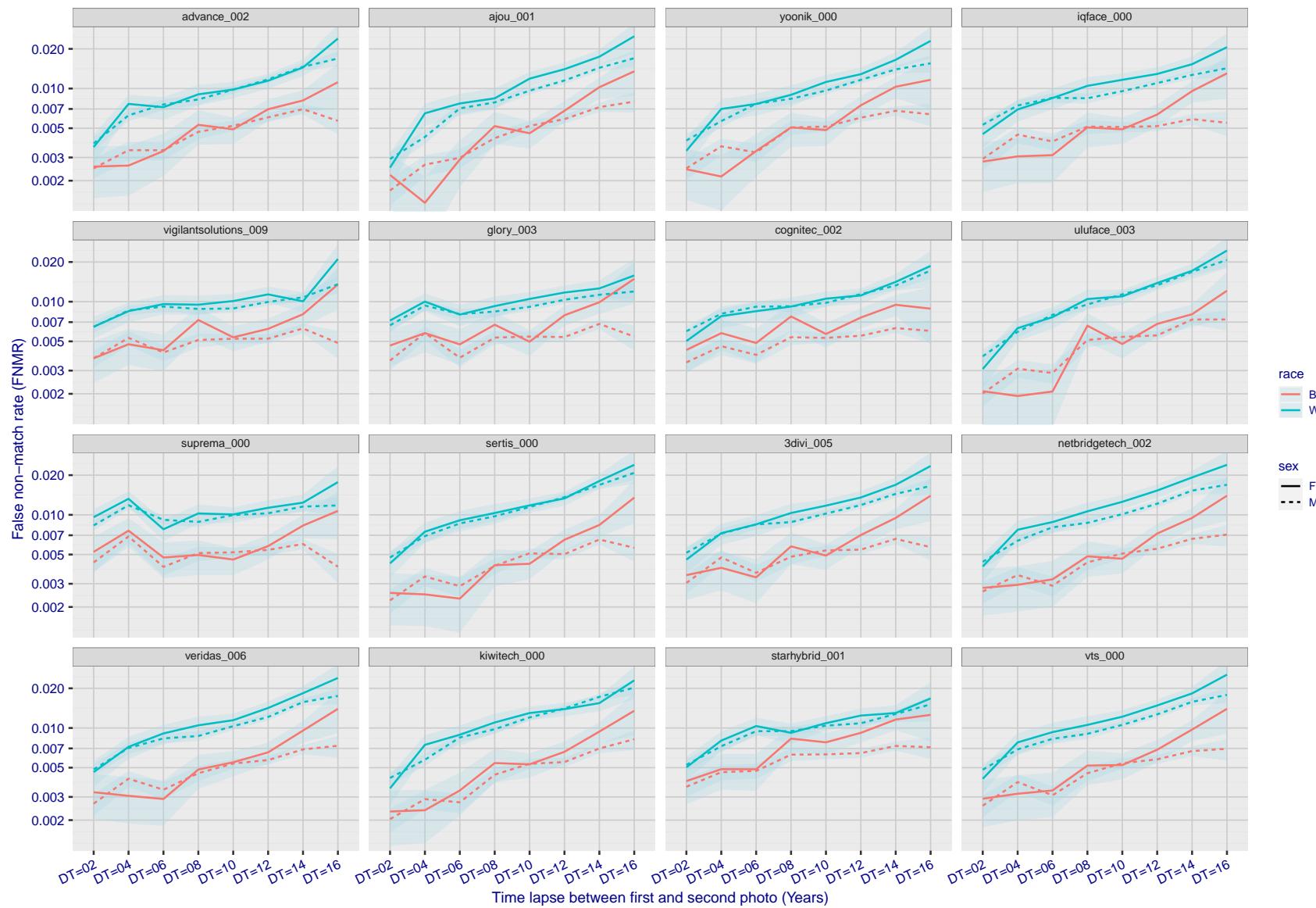


Figure 240: For the mugshot images, FNMR as a function of elapsed time between initial enrollment and second verification images. The panels appear most accurate first, and vertical scale changes on each page. The four traces correspond to images annotated with codes for black female, black male, white female, white male. The threshold is fixed for each algorithm to give $FMR = 0.00001$ over all (10^8) impostor comparisons. For short time-lapses, the most accurate algorithms give very few errors ($FNMR < 0.001$) so that the uncertainty estimates are high.

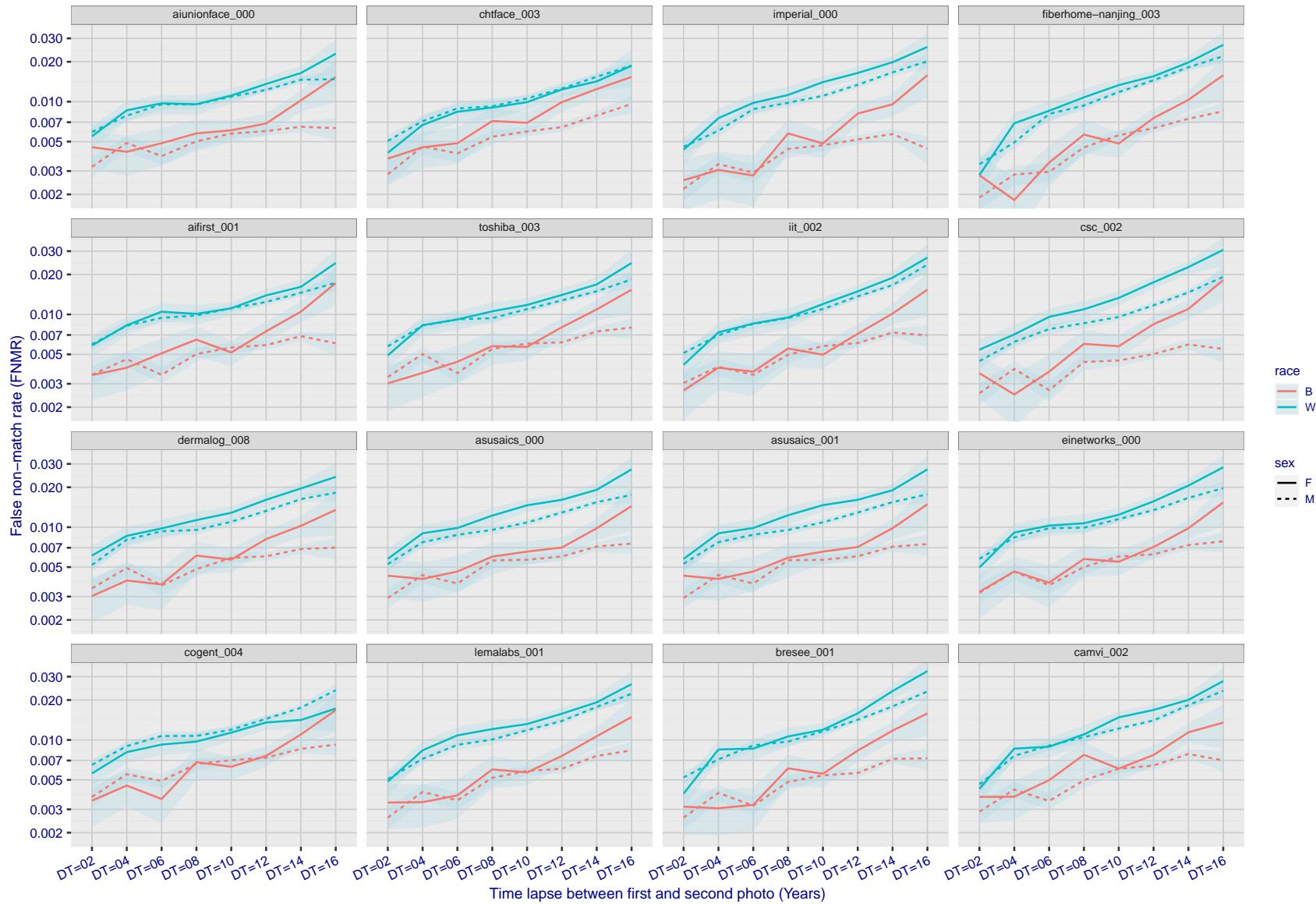


Figure 241: For the mugshot images, FNMR as a function of elapsed time between initial enrollment and second verification images. The panels appear most accurate first, and vertical scale changes on each page. The four traces correspond to images annotated with codes for black female, black male, white female, white male. The threshold is fixed for each algorithm to give FMR = 0.00001 over all (10^8) impostor comparisons. For short time-lapses, the most accurate algorithms give very few errors (FNMR < 0.001) so that the uncertainty estimates are high.

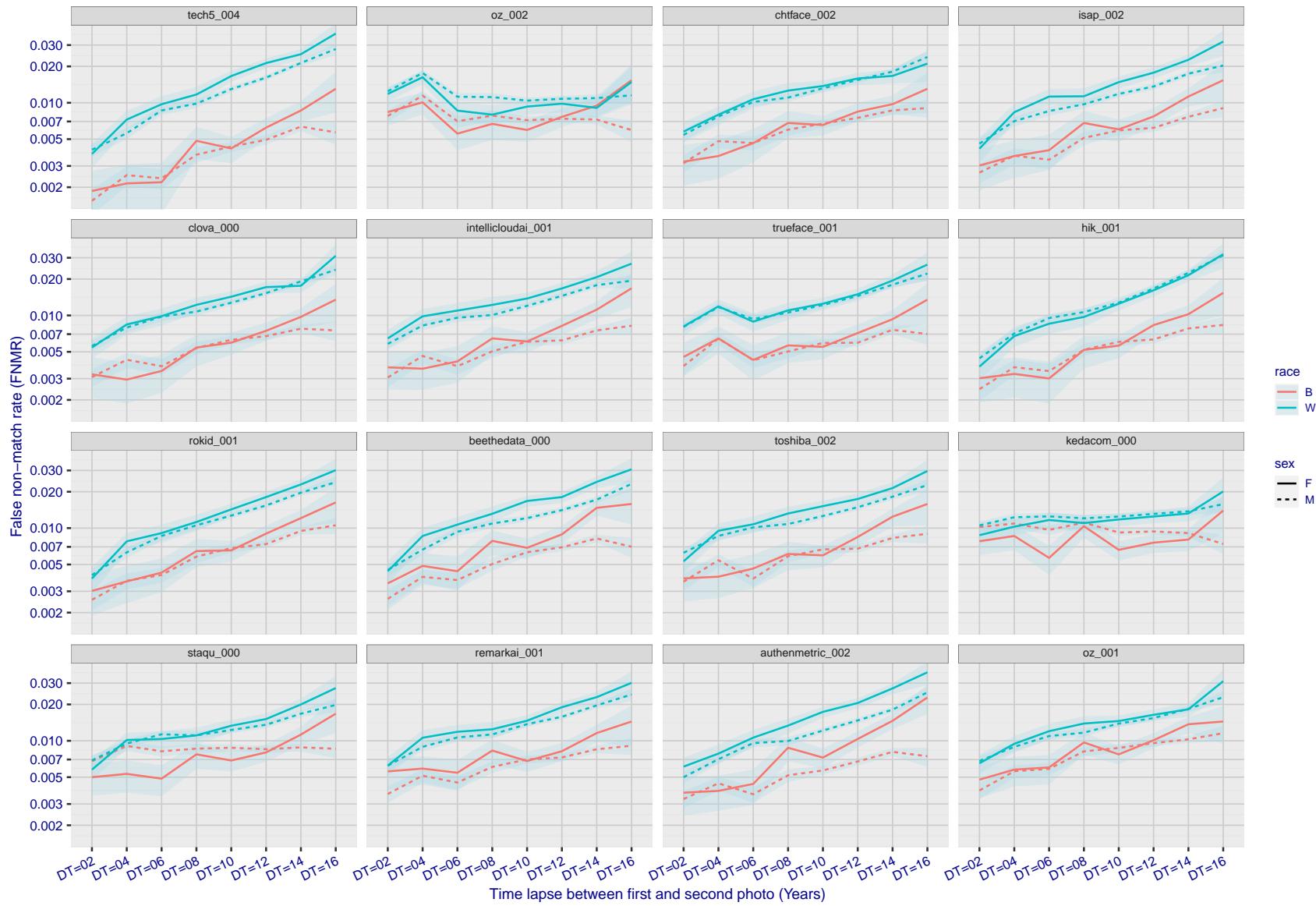


Figure 242: For the mugshot images, FNMR as a function of elapsed time between initial enrollment and second verification images. The panels appear most accurate first, and vertical scale changes on each page. The four traces correspond to images annotated with codes for black female, black male, white female, white male. The threshold is fixed for each algorithm to give $FMR = 0.00001$ over all (10^8) impostor comparisons. For short time-lapses, the most accurate algorithms give very few errors ($FNMR < 0.001$) so that the uncertainty estimates are high.

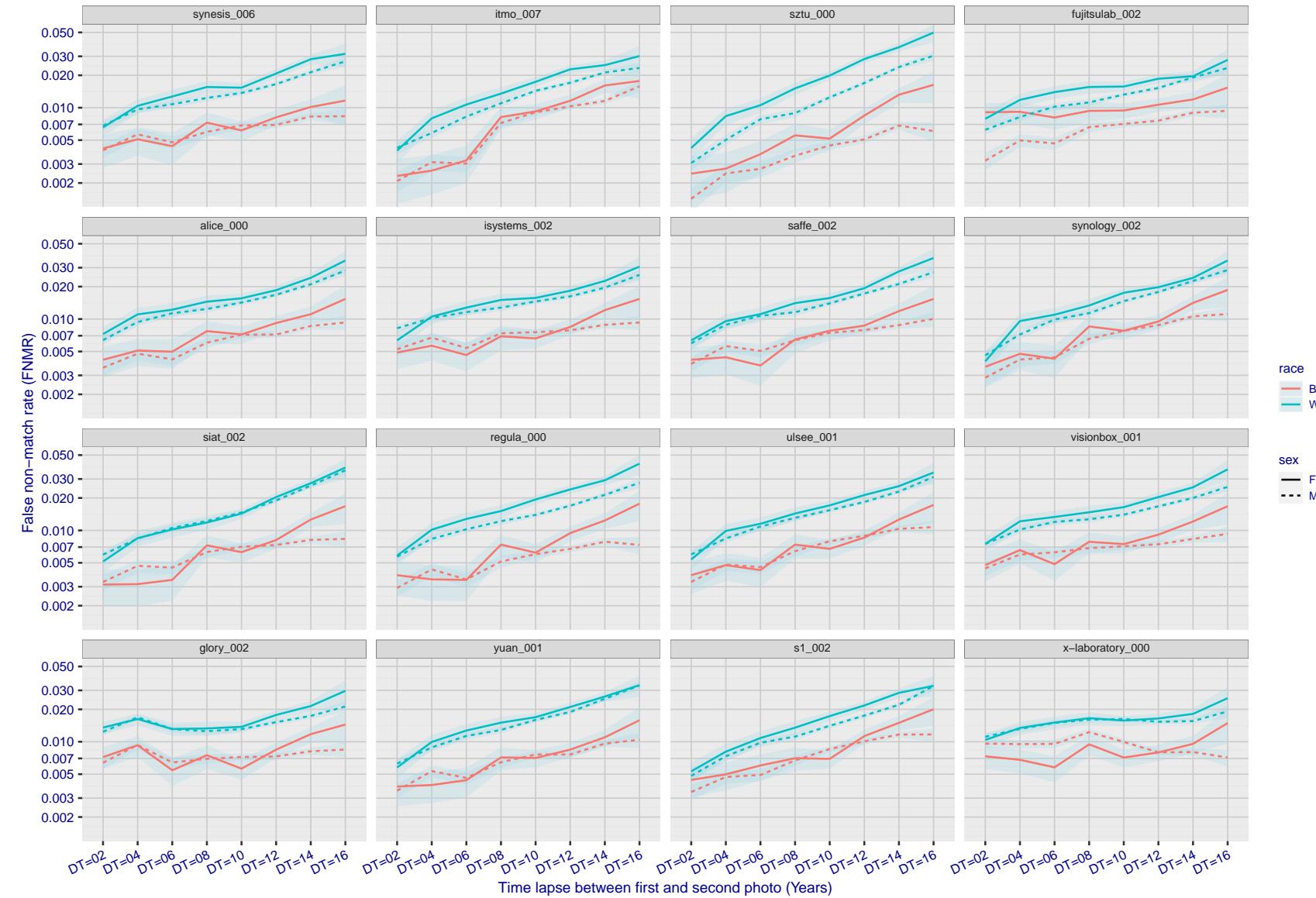


Figure 243: For the mugshot images, FNMR as a function of elapsed time between initial enrollment and second verification images. The panels appear most accurate first, and vertical scale changes on each page. The four traces correspond to images annotated with codes for black female, black male, white female, white male. The threshold is fixed for each algorithm to give $FMR = 0.00001$ over all (10^8) impostor comparisons. For short time-lapses, the most accurate algorithms give very few errors ($FNMR < 0.001$) so that the uncertainty estimates are high.

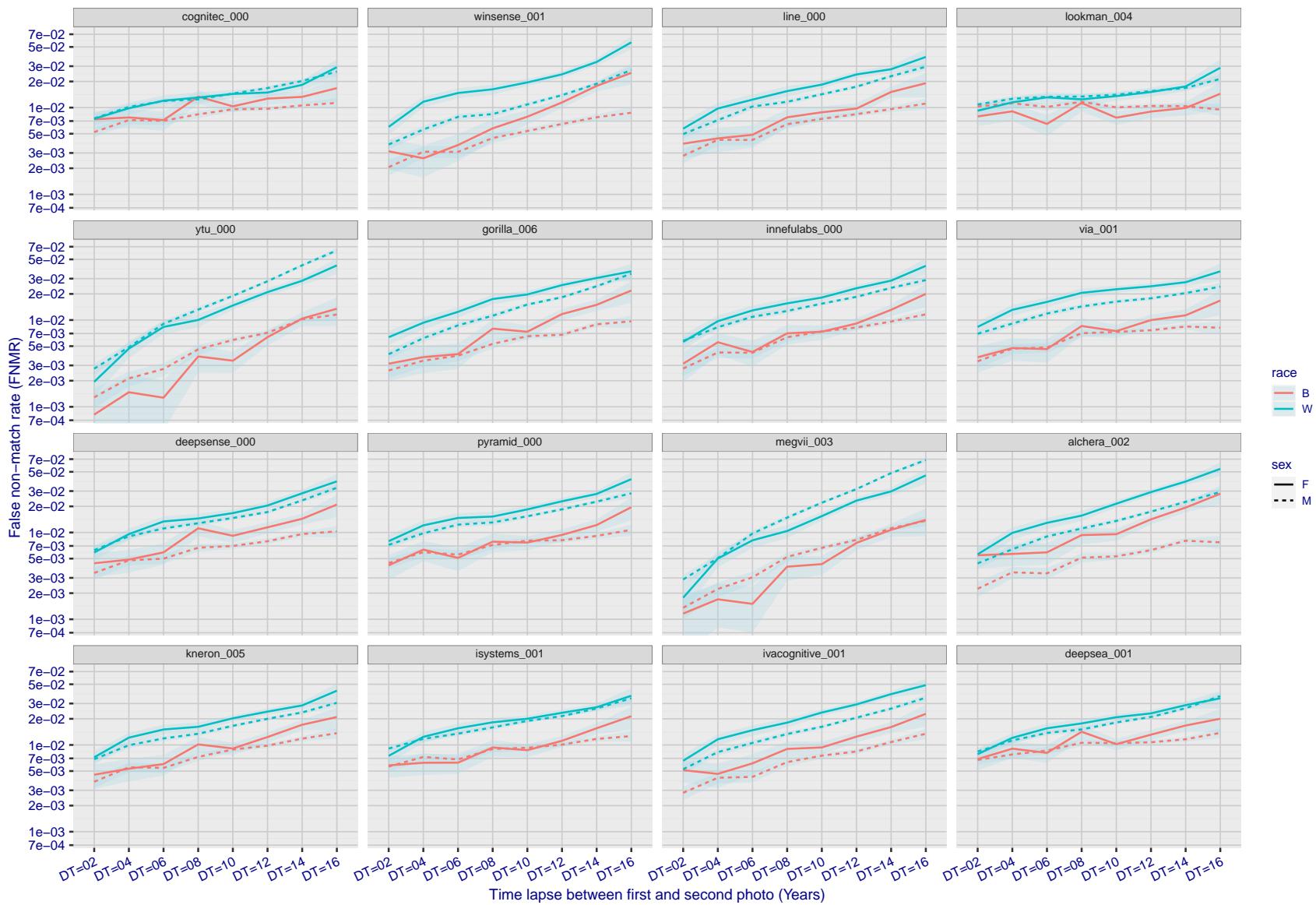


Figure 244: For the mugshot images, FNMR as a function of elapsed time between initial enrollment and second verification images. The panels appear most accurate first, and vertical scale changes on each page. The four traces correspond to images annotated with codes for black female, black male, white female, white male. The threshold is fixed for each algorithm to give $FMR = 0.00001$ over all (10^8) impostor comparisons. For short time-lapses, the most accurate algorithms give very few errors ($FNMR < 0.001$) so that the uncertainty estimates are high.

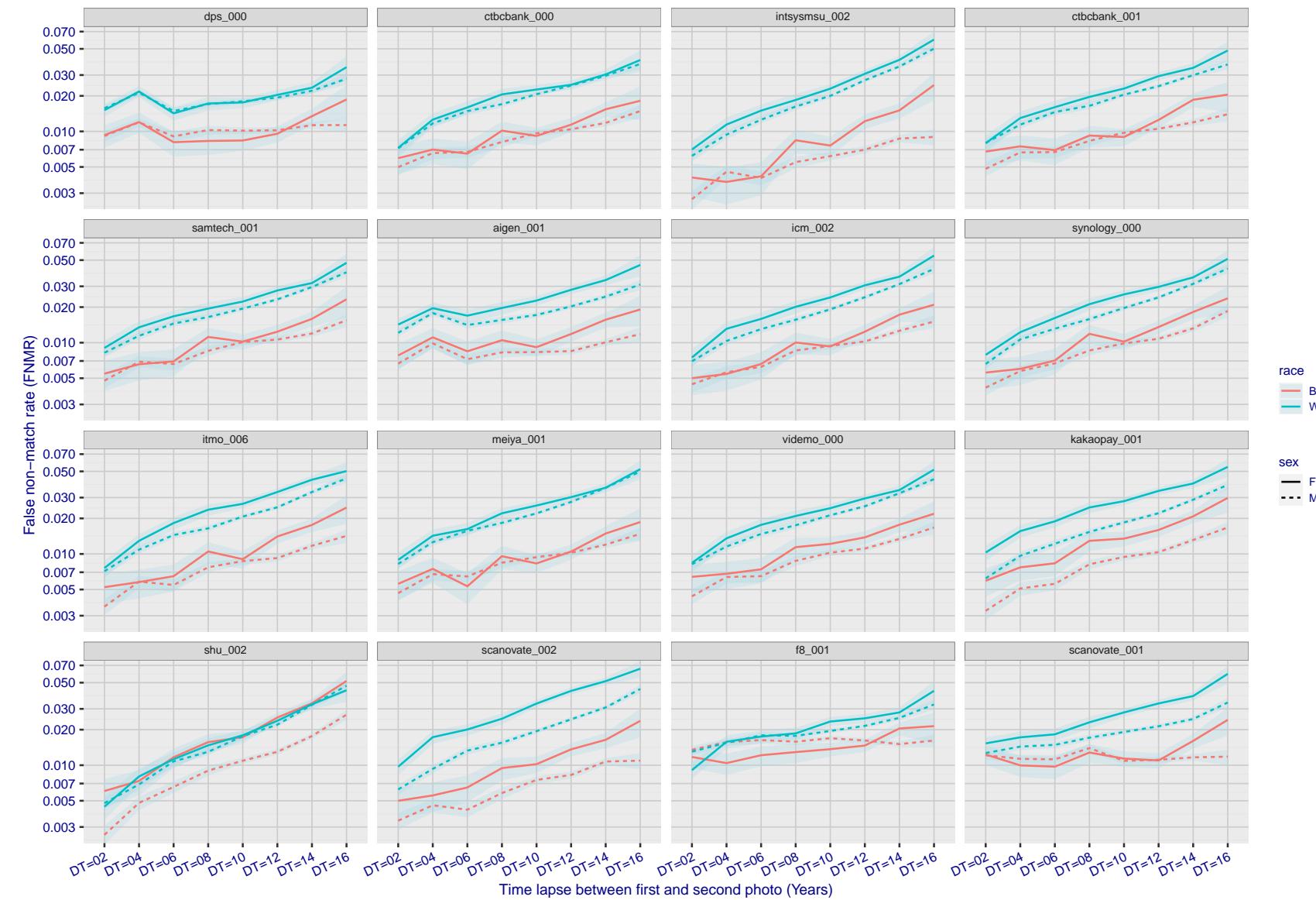


Figure 245: For the mugshot images, FNMR as a function of elapsed time between initial enrollment and second verification images. The panels appear most accurate first, and vertical scale changes on each page. The four traces correspond to images annotated with codes for black female, black male, white female, white male. The threshold is fixed for each algorithm to give FMR = 0.00001 over all (10^8) impostor comparisons. For short time-lapses, the most accurate algorithms give very few errors (FNMR < 0.001) so that the uncertainty estimates are high.

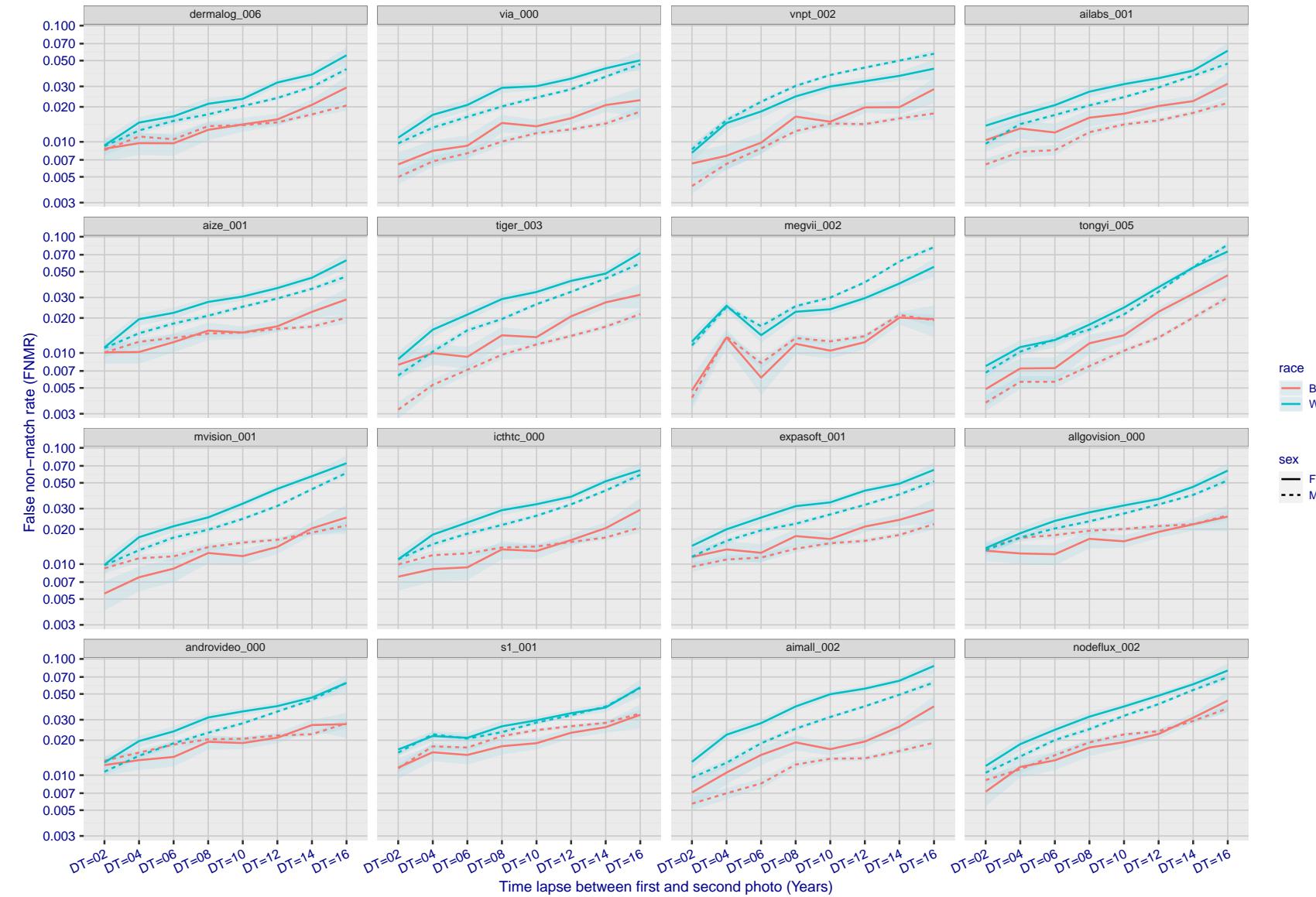


Figure 246: For the mugshot images, FNMR as a function of elapsed time between initial enrollment and second verification images. The panels appear most accurate first, and vertical scale changes on each page. The four traces correspond to images annotated with codes for black female, black male, white female, white male. The threshold is fixed for each algorithm to give FMR = 0.00001 over all (10^8) impostor comparisons. For short time-lapses, the most accurate algorithms give very few errors (FNMR < 0.001) so that the uncertainty estimates are high.

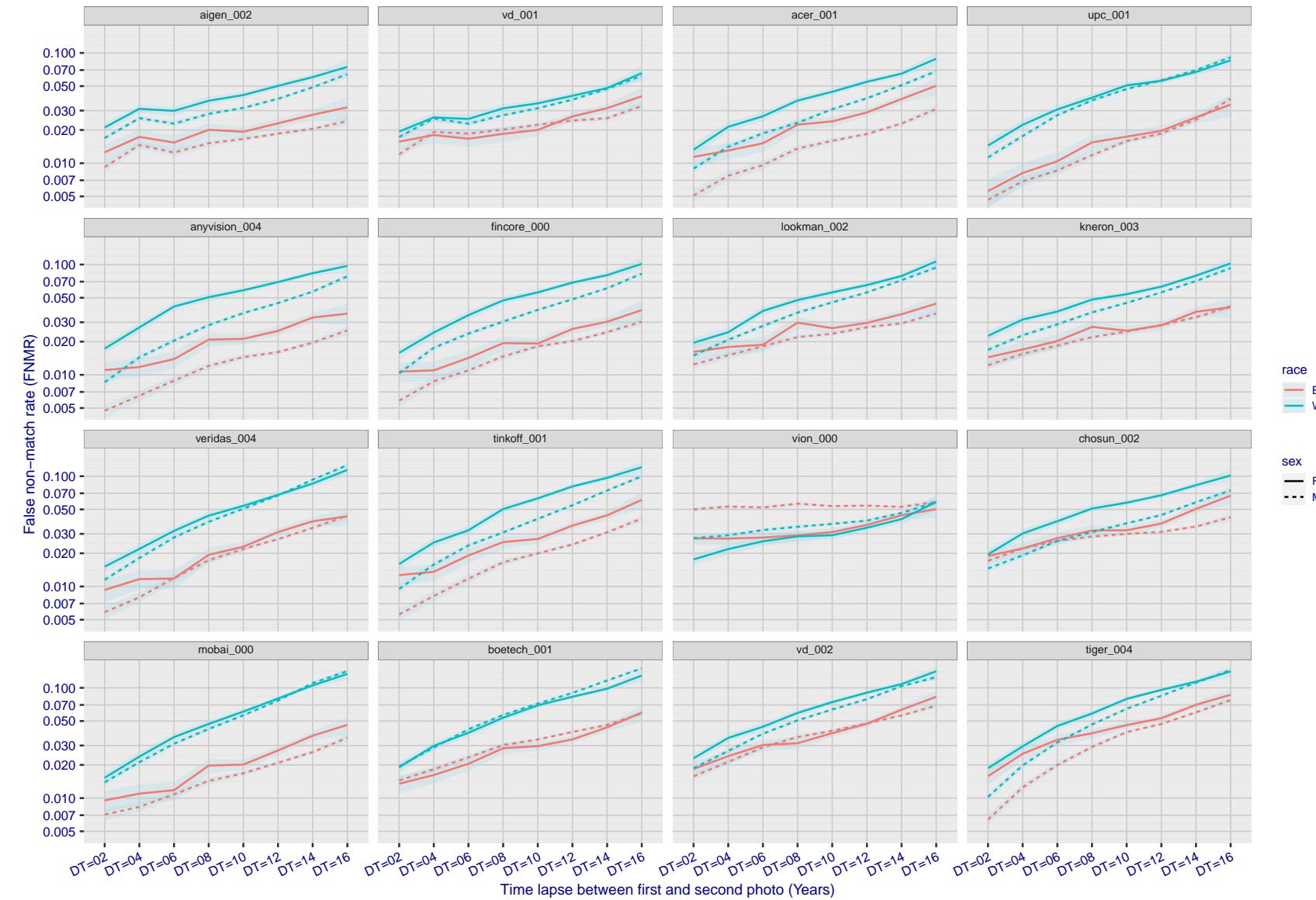


Figure 247: For the mugshot images, FNMR as a function of elapsed time between initial enrollment and second verification images. The panels appear most accurate first, and vertical scale changes on each page. The four traces correspond to images annotated with codes for black female, black male, white female, white male. The threshold is fixed for each algorithm to give FMR = 0.00001 over all (10^8) impostor comparisons. For short time-lapses, the most accurate algorithms give very few errors (FNMR < 0.001) so that the uncertainty estimates are high.

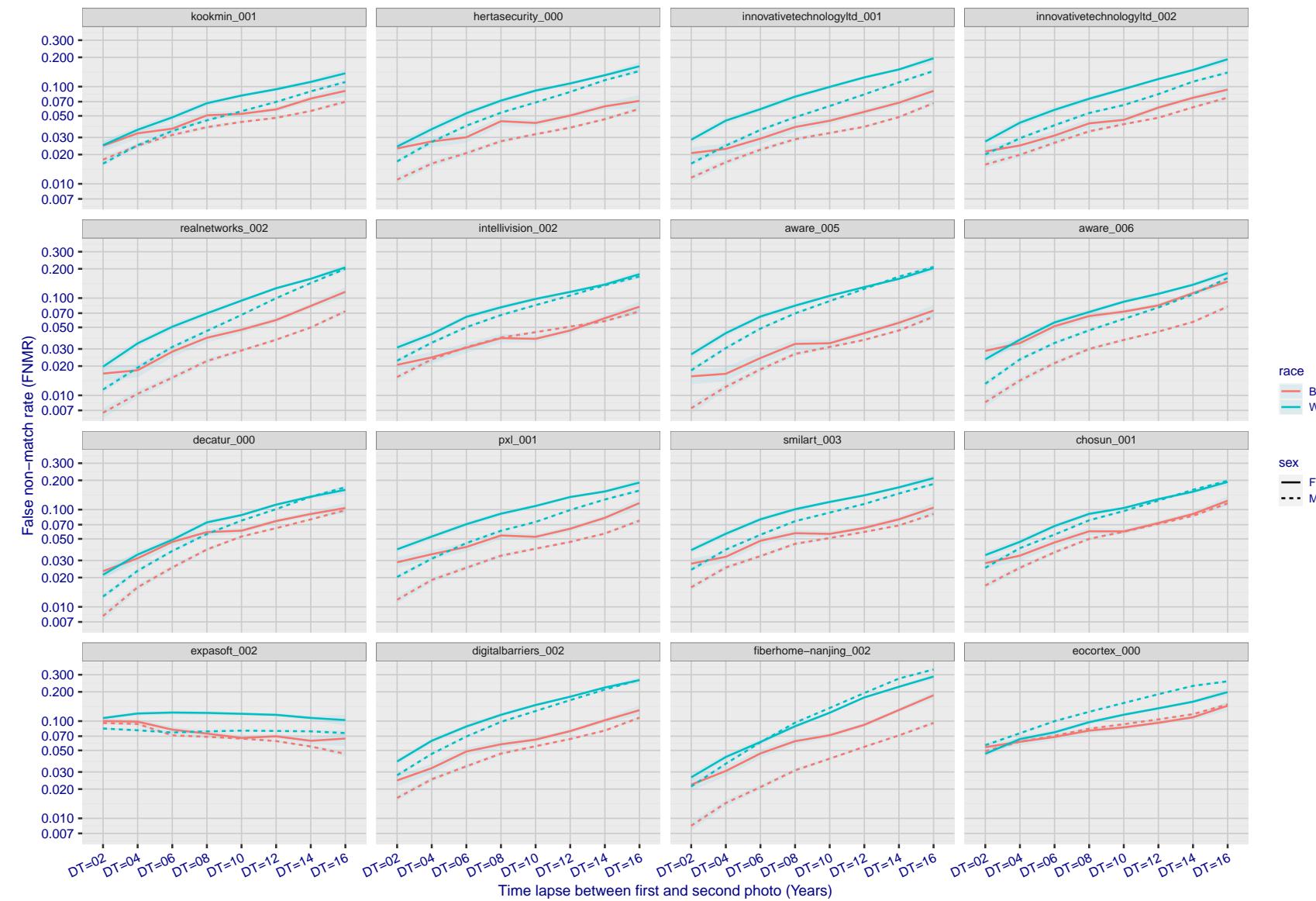


Figure 248: For the mugshot images, FNMR as a function of elapsed time between initial enrollment and second verification images. The panels appear most accurate first, and vertical scale changes on each page. The four traces correspond to images annotated with codes for black female, black male, white female, white male. The threshold is fixed for each algorithm to give FMR = 0.00001 over all (10^8) impostor comparisons. For short time-lapses, the most accurate algorithms give very few errors (FNMR < 0.001) so that the uncertainty estimates are high.

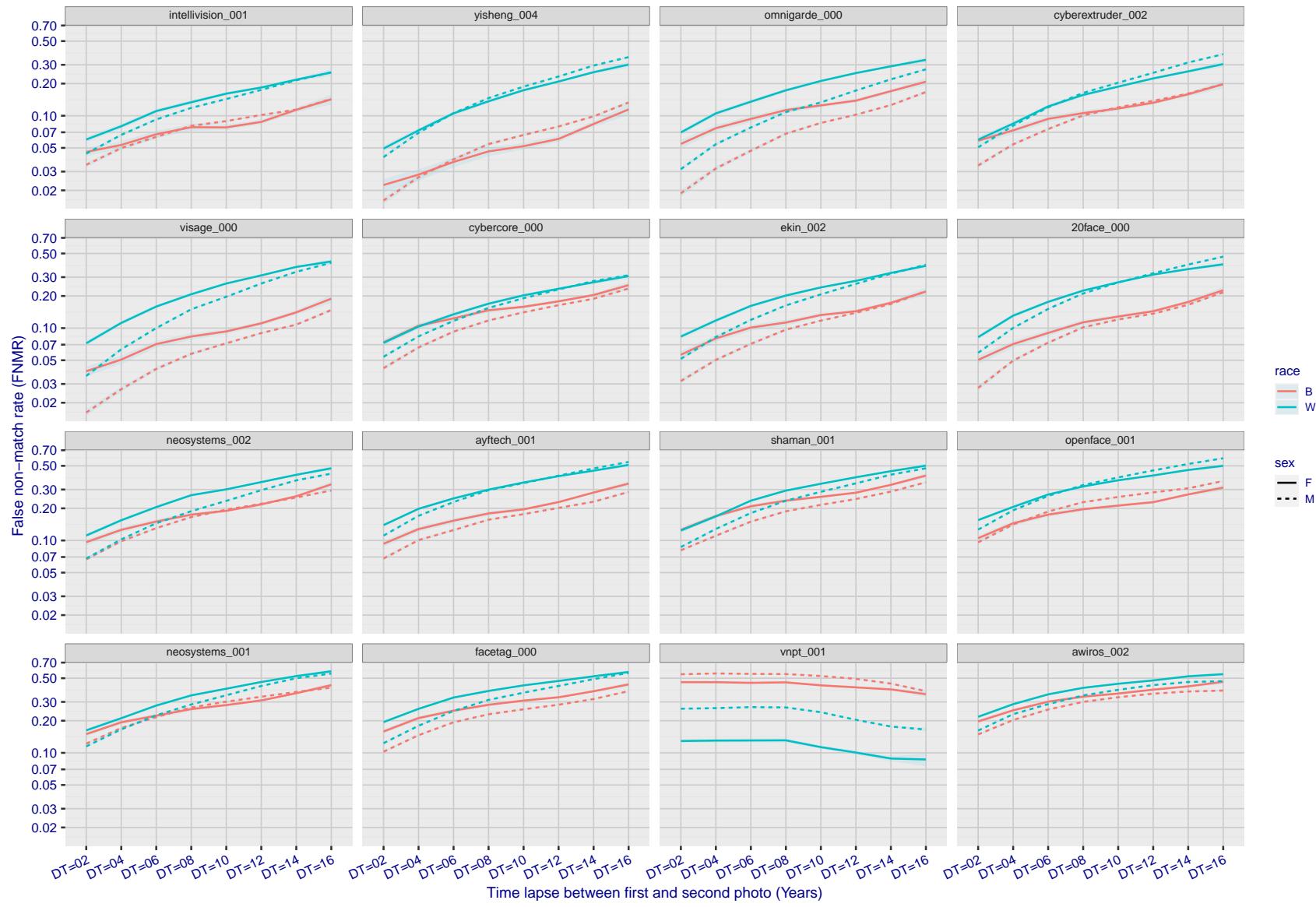


Figure 249: For the mugshot images, FNMR as a function of elapsed time between initial enrollment and second verification images. The panels appear most accurate first, and vertical scale changes on each page. The four traces correspond to images annotated with codes for black female, black male, white female, white male. The threshold is fixed for each algorithm to give FMR = 0.00001 over all (10^8) impostor comparisons. For short time-lapses, the most accurate algorithms give very few errors (FNMR < 0.001) so that the uncertainty estimates are high.

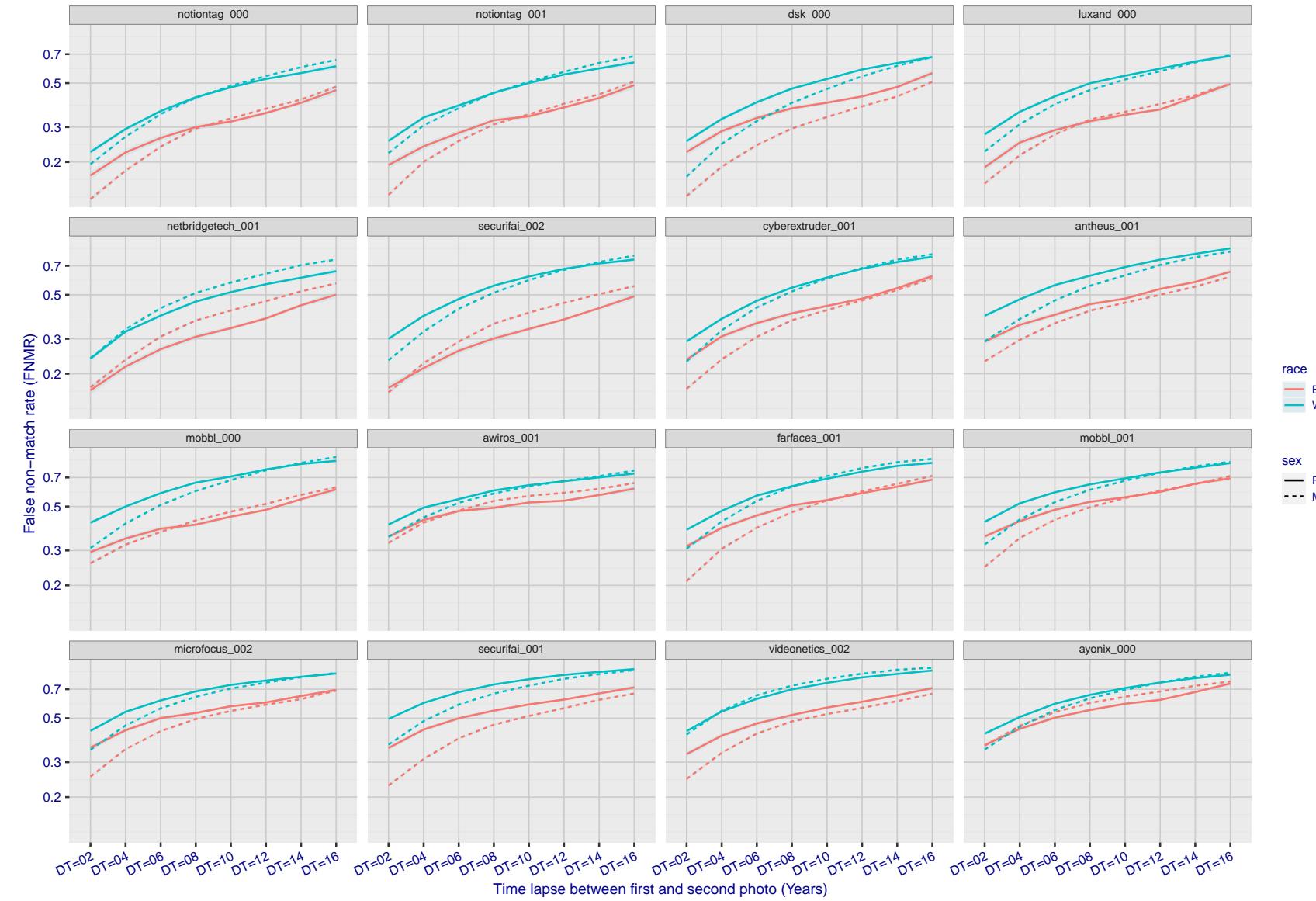


Figure 250: For the mugshot images, FNMR as a function of elapsed time between initial enrollment and second verification images. The panels appear most accurate first, and vertical scale changes on each page. The four traces correspond to images annotated with codes for black female, black male, white female, white male. The threshold is fixed for each algorithm to give FMR = 0.00001 over all (10^8) impostor comparisons. For short time-lapses, the most accurate algorithms give very few errors (FNMR < 0.001) so that the uncertainty estimates are high.

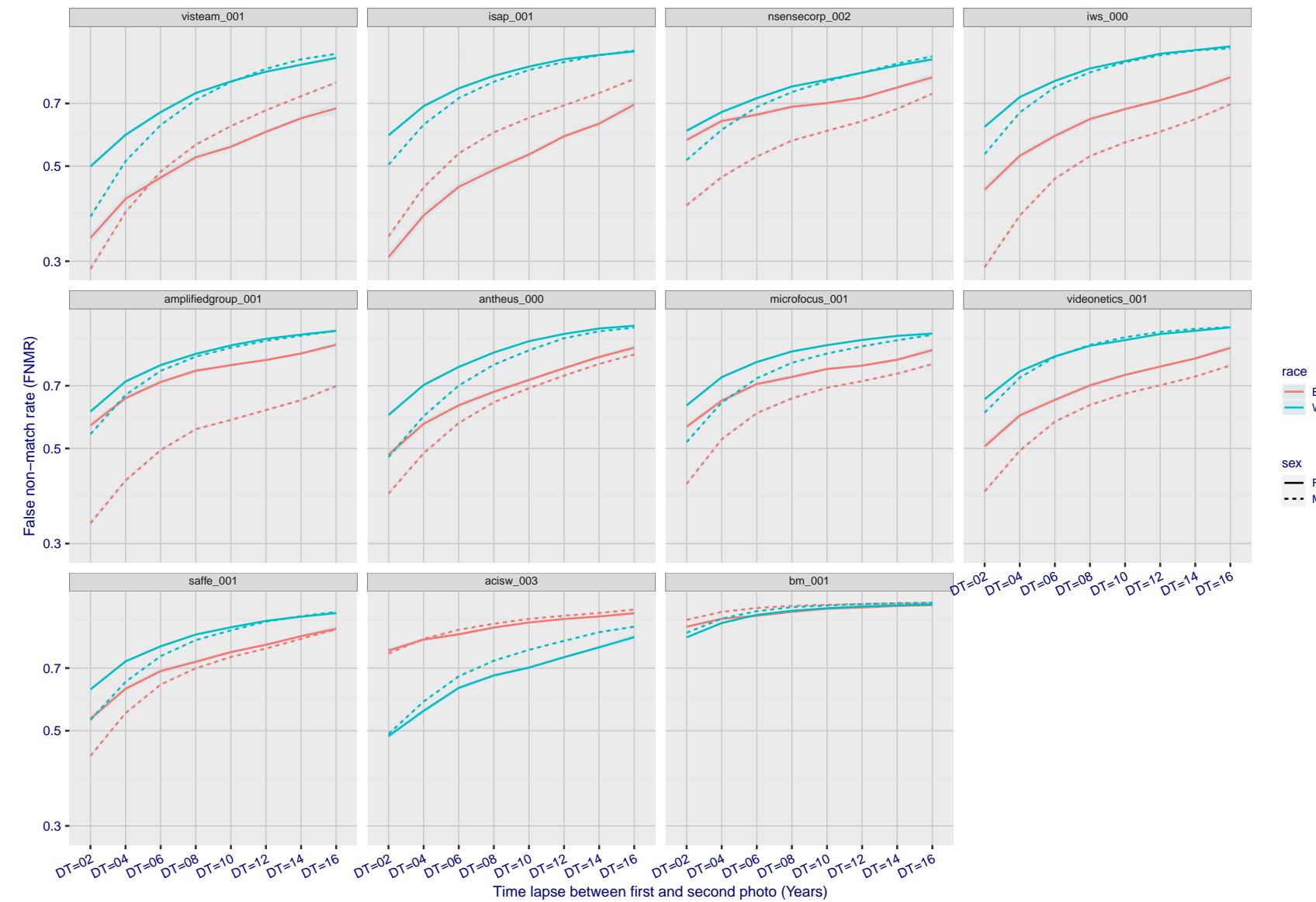


Figure 251: For the mugshot images, FNMR as a function of elapsed time between initial enrollment and second verification images. The panels appear most accurate first, and vertical scale changes on each page. The four traces correspond to images annotated with codes for black female, black male, white female, white male. The threshold is fixed for each algorithm to give FMR = 0.00001 over all (10^8) impostor comparisons. For short time-lapses, the most accurate algorithms give very few errors (FNMR < 0.001) so that the uncertainty estimates are high.

3.5.3 Effect of age on genuine subjects

Background: Faces change appearance throughout life. Face recognition algorithms have previously been reported to give better accuracy on older individuals (See NIST IR 8009).

Goal: To quantify false non-match rates (FNMR) as a function of age, without an ageing component.

Methods: Using the visa images, which span fewer than five years, thresholds are determined that give FMR = 0.001 and 0.0001 over the entire impostor set. Then FNMR is measured over 1000 bootstrap replications of the genuine scores.

Results: For the visa images, Figure 279 shows how false non-match rates for genuine users, as a function of age group.

The notable aspects are:

- ▷ Younger subjects give considerably higher FNMR. This is likely due to rapid growth and change in facial appearance.
- ▷ FNMR trends down throughout life. The last bin, AGE > 72, contains fewer than 140 mated pairs, and may be affected by small sample size.

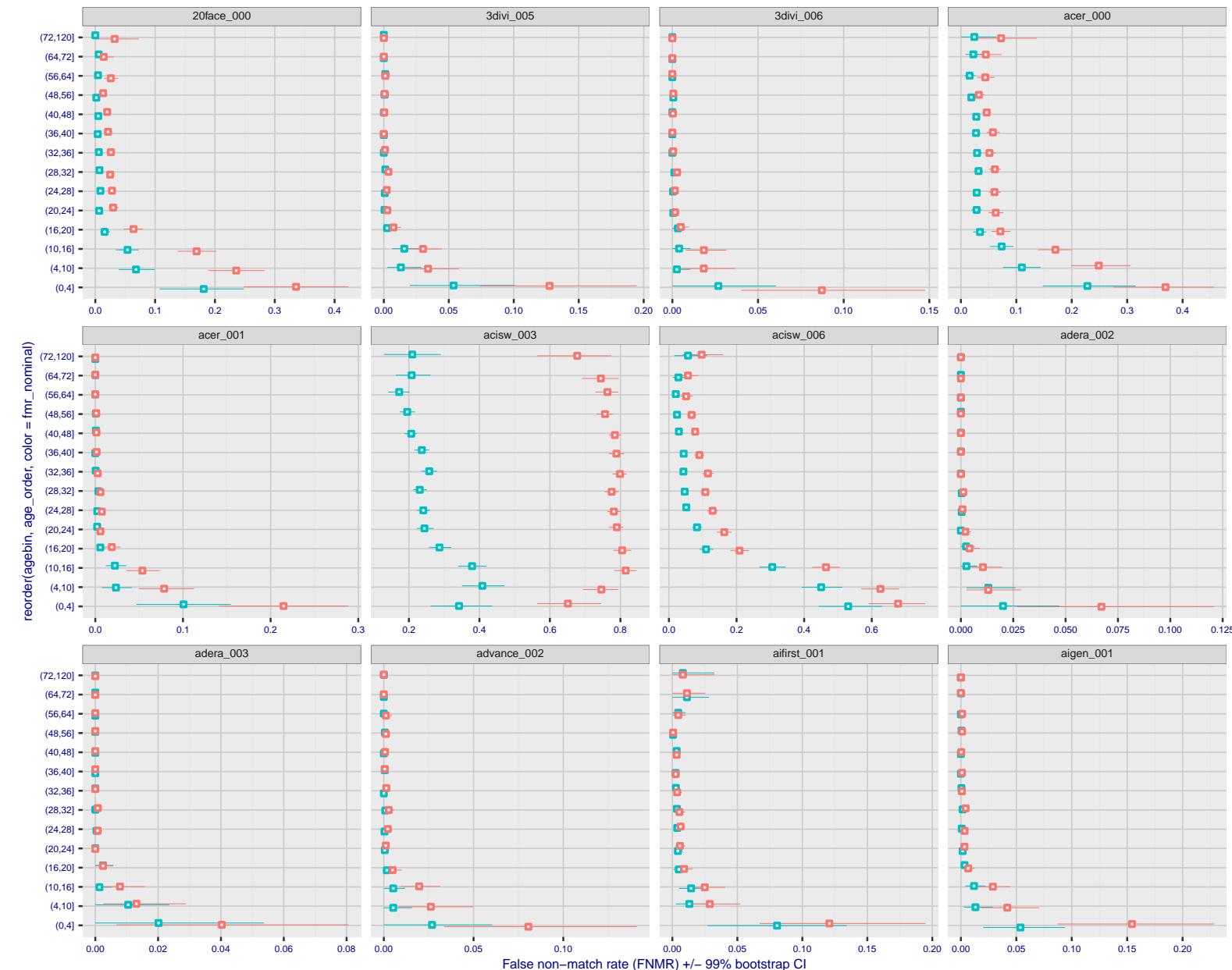


Figure 252: For the visa images, the dots show FNMR by age group for two operating thresholds corresponding to $FMR = \{0.001, 0.0001\}$ computed over all on the order of 10^{10} impostor scores. The FMR in each bin will vary also - see subsequent impostor heatmaps in sec. 3.6.2. Given a pair of face images taken at different times, we assign the comparison to the bin that is the arithmetic average of the subject's ages. This plot shows only the effect of age, not ageing. The number of comparisons in each bin is generally in the thousands, however the first and last bins are computed over 149 and 124 respectively. The error rates in some (adult) cases are zero, and in others the DET is flat so the error rates at the two thresholds are identical. The lines span 1% and 99% of bootstrap replicated FNMR estimates.

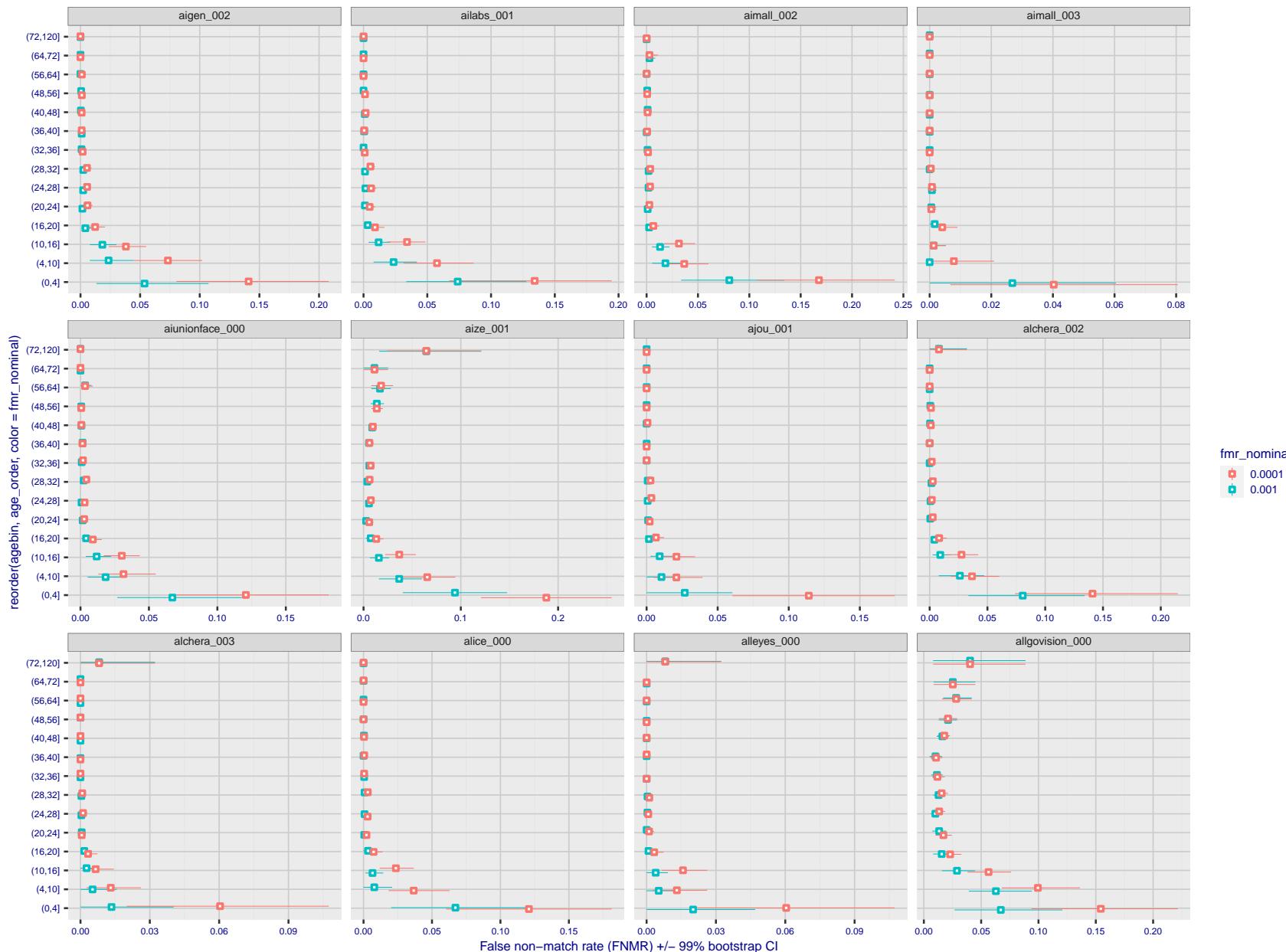


Figure 253: For the visa images, the dots show FNMR by age group for two operating thresholds corresponding to $FMR = \{0.001, 0.0001\}$ computed over all on the order of 10^{10} impostor scores. The FMR in each bin will vary also - see subsequent impostor heatmaps in sec. 3.6.2. Given a pair of face images taken at different times, we assign the comparison to the bin that is the arithmetic average of the subject's ages. This plot shows only the effect of age, not ageing. The number of comparisons in each bin is generally in the thousands, however the first and last bins are computed over 149 and 124 respectively. The error rates in some (adult) cases are zero, and in others the DET is flat so the error rates at the two thresholds are identical. The lines span 1% and 99% of bootstrap replicated FNMR estimates.

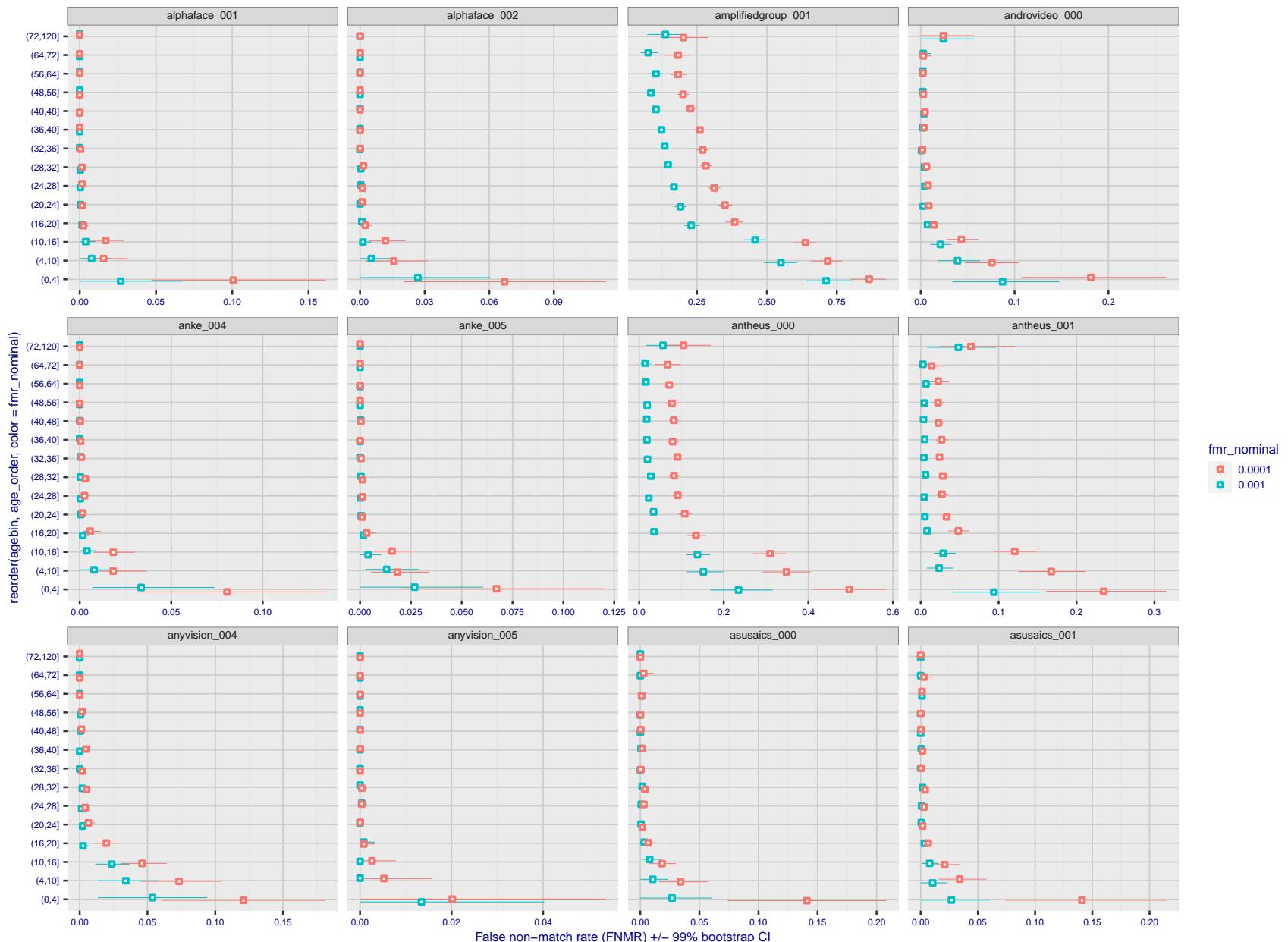


Figure 254: For the visa images, the dots show FNMR by age group for two operating thresholds corresponding to $FMR = \{0.001, 0.0001\}$ computed over all on the order of 10^{10} impostor scores. The FMR in each bin will vary also - see subsequent impostor heatmaps in sec. 3.6.2. Given a pair of face images taken at different times, we assign the comparison to the bin that is the arithmetic average of the subject's ages. This plot shows only the effect of age, not ageing. The number of comparisons in each bin is generally in the thousands, however the first and last bins are computed over 149 and 124 respectively. The error rates in some (adult) cases are zero, and in others the DET is flat so the error rates at the two thresholds are identical. The lines span 1% and 99% of bootstrap replicated FNMR estimates.



Figure 255: For the visa images, the dots show FNMR by age group for two operating thresholds corresponding to $FMR = \{0.001, 0.0001\}$ computed over all on the order of 10^{10} impostor scores. The FMR in each bin will vary also - see subsequent impostor heatmaps in sec. 3.6.2. Given a pair of face images taken at different times, we assign the comparison to the bin that is the arithmetic average of the subject's ages. This plot shows only the effect of age, not ageing. The number of comparisons in each bin is generally in the thousands, however the first and last bins are computed over 149 and 124 respectively. The error rates in some (adult) cases are zero, and in others the DET is flat so the error rates at the two thresholds are identical. The lines span 1% and 99% of bootstrap replicated FNMR estimates.



Figure 256: For the visa images, the dots show FNMR by age group for two operating thresholds corresponding to $FMR = \{0.001, 0.0001\}$ computed over all on the order of 10^{10} impostor scores. The FMR in each bin will vary also - see subsequent impostor heatmaps in sec. 3.6.2. Given a pair of face images taken at different times, we assign the comparison to the bin that is the arithmetic average of the subject's ages. This plot shows only the effect of age, not ageing. The number of comparisons in each bin is generally in the thousands, however the first and last bins are computed over 149 and 124 respectively. The error rates in some (adult) cases are zero, and in others the DET is flat so the error rates at the two thresholds are identical. The lines span 1% and 99% of bootstrap replicated FNMR estimates.

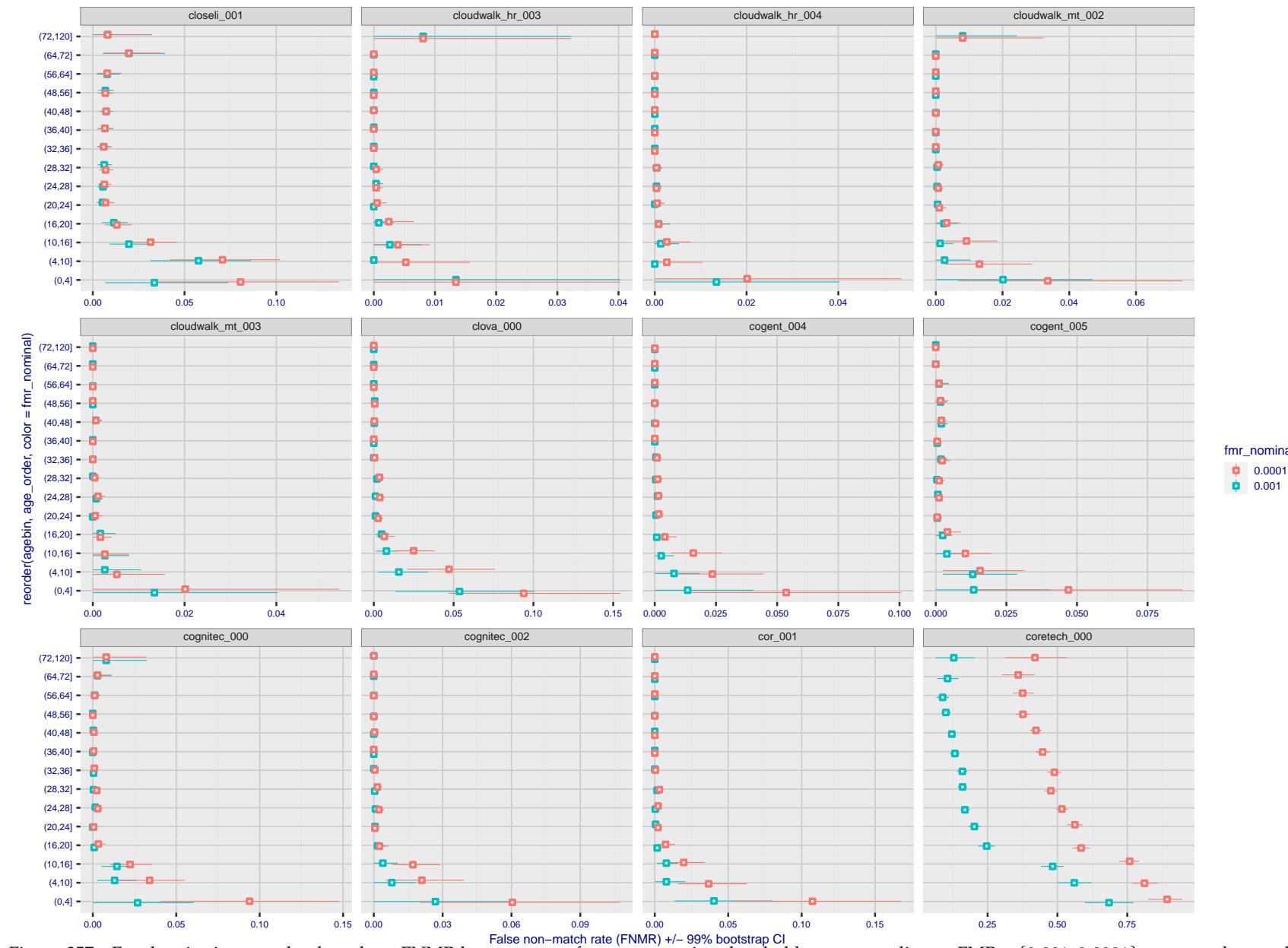


Figure 257: For the visa images, the dots show FNMR by age group for two operating thresholds corresponding to $FMR = \{0.001, 0.0001\}$ computed over all on the order of 10^{10} impostor scores. The FMR in each bin will vary also - see subsequent impostor heatmaps in sec. 3.6.2. Given a pair of face images taken at different times, we assign the comparison to the bin that is the arithmetic average of the subject's ages. This plot shows only the effect of age, not ageing. The number of comparisons in each bin is generally in the thousands, however the first and last bins are computed over 149 and 124 respectively. The error rates in some (adult) cases are zero, and in others the DET is flat so the error rates at the two thresholds are identical. The lines span 1% and 99% of bootstrap replicated FNMR estimates.

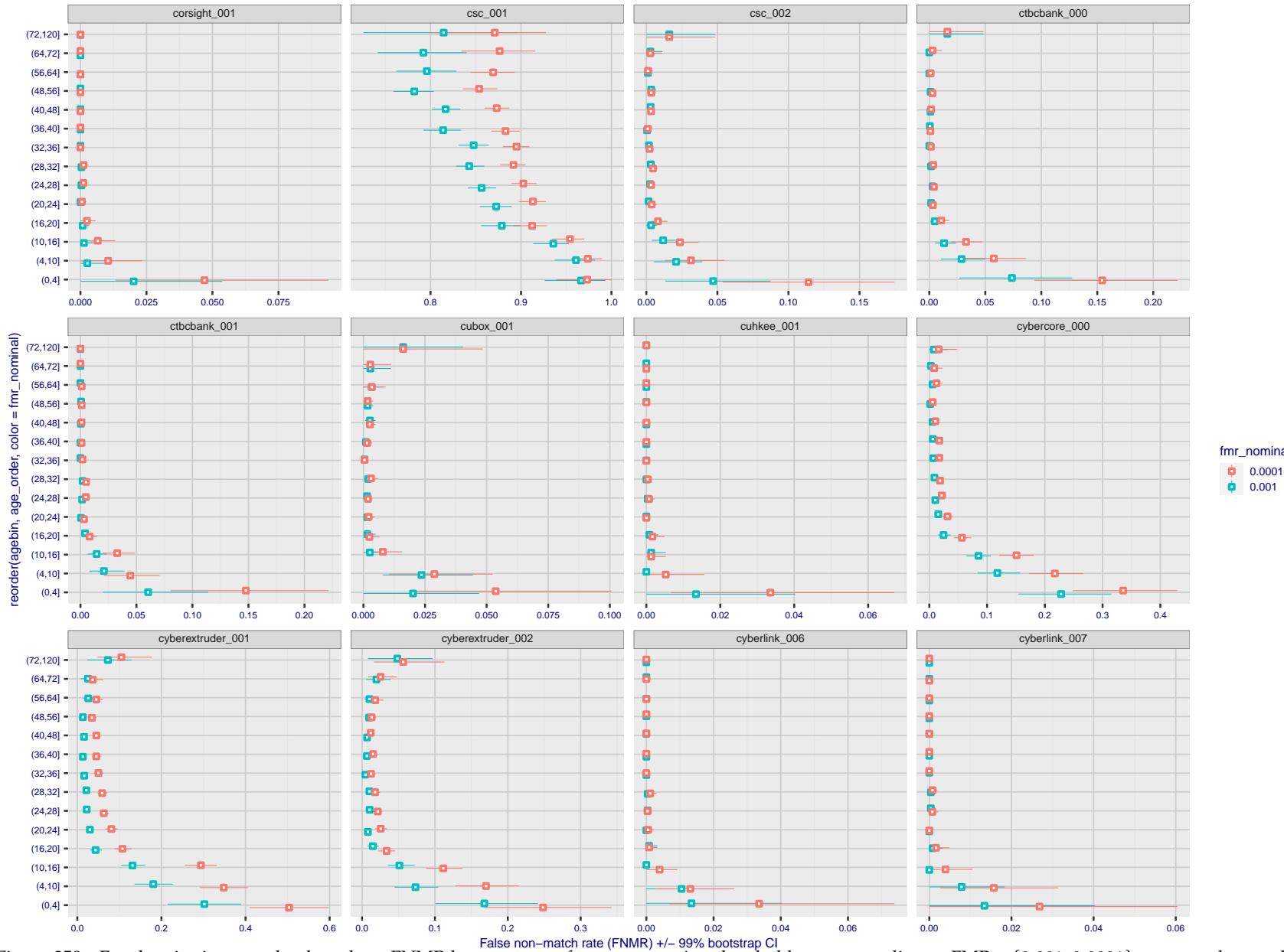


Figure 258: For the visa images, the dots show FNMR by age group for two operating thresholds corresponding to $FMR = \{0.001, 0.0001\}$ computed over all on the order of 10^{10} impostor scores. The FMR in each bin will vary also - see subsequent impostor heatmaps in sec. 3.6.2. Given a pair of face images taken at different times, we assign the comparison to the bin that is the arithmetic average of the subject's ages. This plot shows only the effect of age, not ageing. The number of comparisons in each bin is generally in the thousands, however the first and last bins are computed over 149 and 124 respectively. The error rates in some (adult) cases are zero, and in others the DET is flat so the error rates at the two thresholds are identical. The lines span 1% and 99% of bootstrap replicated FNMR estimates.



Figure 259: For the visa images, the dots show FNMR by age group for two operating thresholds corresponding to $FMR = \{0.001, 0.0001\}$ computed over all on the order of 10^{10} impostor scores. The FMR in each bin will vary also - see subsequent impostor heatmaps in sec. 3.6.2. Given a pair of face images taken at different times, we assign the comparison to the bin that is the arithmetic average of the subject's ages. This plot shows only the effect of age, not ageing. The number of comparisons in each bin is generally in the thousands, however the first and last bins are computed over 149 and 124 respectively. The error rates in some (adult) cases are zero, and in others the DET is flat so the error rates at the two thresholds are identical. The lines span 1% and 99% of bootstrap replicated FNMR estimates.

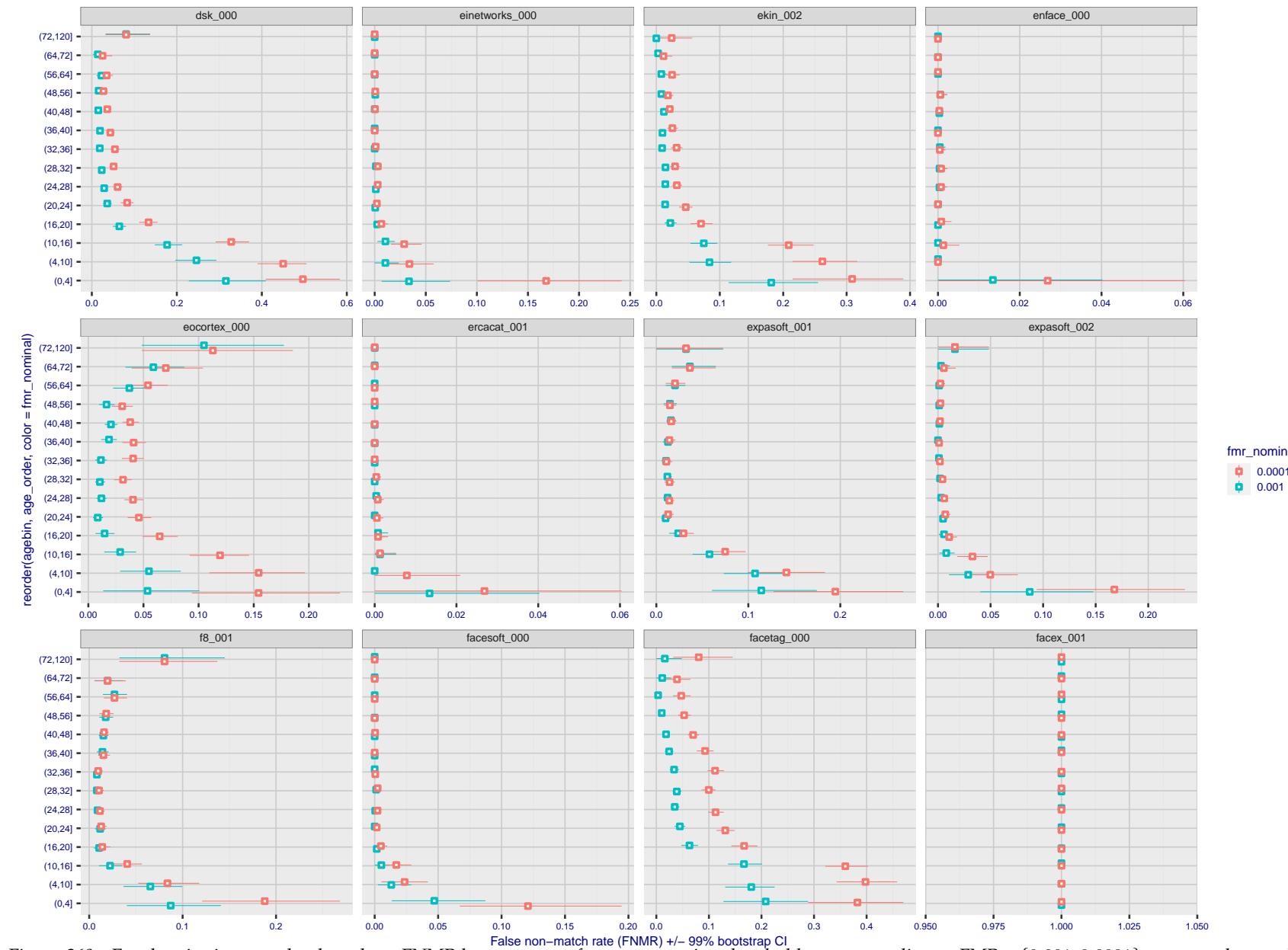


Figure 260: For the visa images, the dots show FNMR by age group for two operating thresholds corresponding to $FMR = \{0.001, 0.0001\}$ computed over all on the order of 10^{10} impostor scores. The FMR in each bin will vary also - see subsequent impostor heatmaps in sec. 3.6.2. Given a pair of face images taken at different times, we assign the comparison to the bin that is the arithmetic average of the subject's ages. This plot shows only the effect of age, not ageing. The number of comparisons in each bin is generally in the thousands, however the first and last bins are computed over 149 and 124 respectively. The error rates in some (adult) cases are zero, and in others the DET is flat so the error rates at the two thresholds are identical. The lines span 1% and 99% of bootstrap replicated FNMR estimates.



Figure 261: For the visa images, the dots show FNMR by age group for two operating thresholds corresponding to $FMR = \{0.001, 0.0001\}$ computed over all on the order of 10^{10} impostor scores. The FMR in each bin will vary also - see subsequent impostor heatmaps in sec. 3.6.2. Given a pair of face images taken at different times, we assign the comparison to the bin that is the arithmetic average of the subject's ages. This plot shows only the effect of age, not ageing. The number of comparisons in each bin is generally in the thousands, however the first and last bins are computed over 149 and 124 respectively. The error rates in some (adult) cases are zero, and in others the DET is flat so the error rates at the two thresholds are identical. The lines span 1% and 99% of bootstrap replicated FNMR estimates.

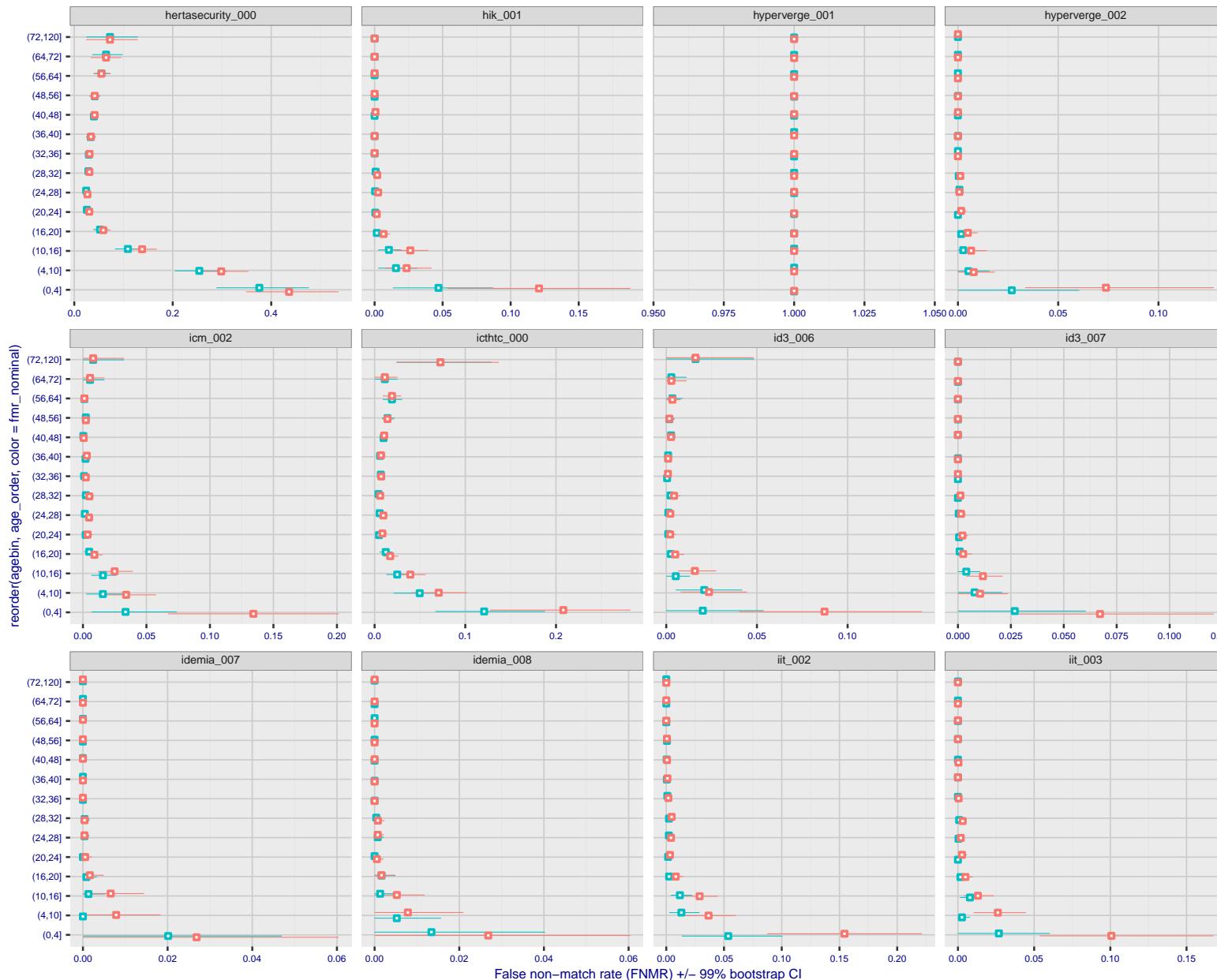


Figure 262: For the visa images, the dots show FNMR by age group for two operating thresholds corresponding to $FMR = \{0.001, 0.0001\}$ computed over all on the order of 10^{10} impostor scores. The FMR in each bin will vary also - see subsequent impostor heatmaps in sec. 3.6.2. Given a pair of face images taken at different times, we assign the comparison to the bin that is the arithmetic average of the subject's ages. This plot shows only the effect of age, not ageing. The number of comparisons in each bin is generally in the thousands, however the first and last bins are computed over 149 and 124 respectively. The error rates in some (adult) cases are zero, and in others the DET is flat so the error rates at the two thresholds are identical. The lines span 1% and 99% of bootstrap replicated FNMR estimates.

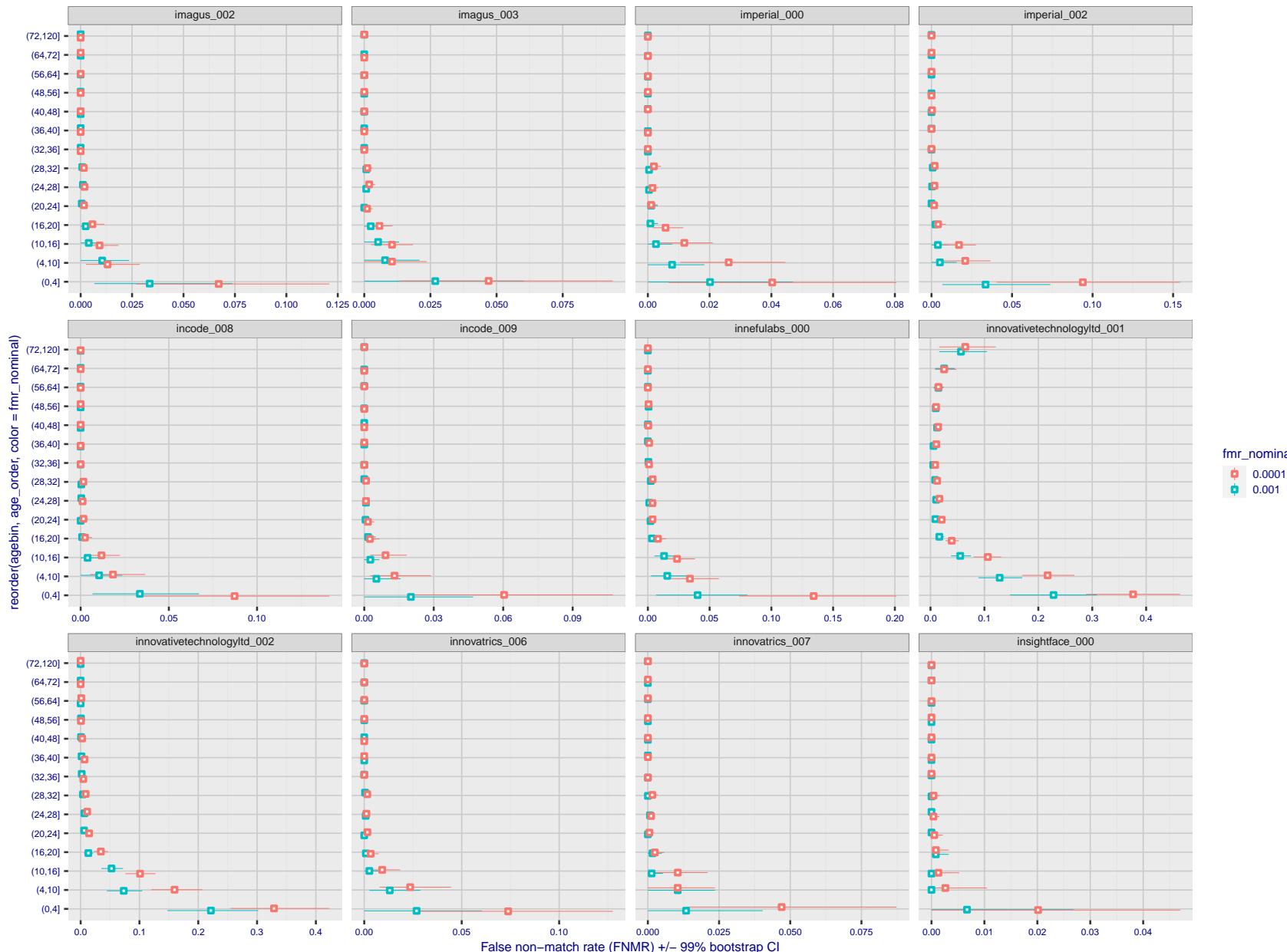


Figure 263: For the visa images, the dots show FNMR by age group for two operating thresholds corresponding to $FMR = \{0.001, 0.0001\}$ computed over all on the order of 10^{10} impostor scores. The FMR in each bin will vary also - see subsequent impostor heatmaps in sec. 3.6.2. Given a pair of face images taken at different times, we assign the comparison to the bin that is the arithmetic average of the subject's ages. This plot shows only the effect of age, not ageing. The number of comparisons in each bin is generally in the thousands, however the first and last bins are computed over 149 and 124 respectively. The error rates in some (adult) cases are zero, and in others the DET is flat so the error rates at the two thresholds are identical. The lines span 1% and 99% of bootstrap replicated FNMR estimates.

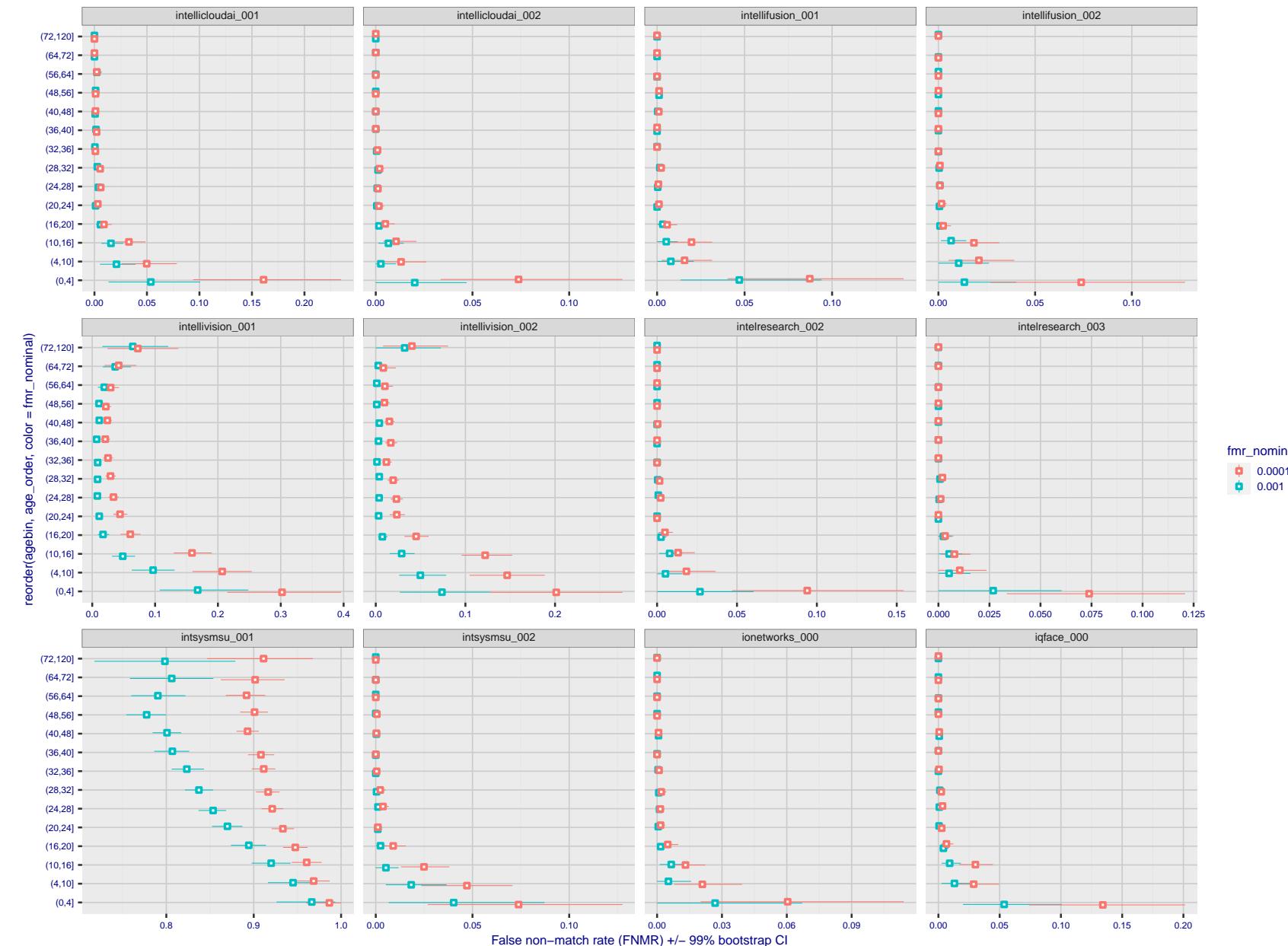


Figure 264: For the visa images, the dots show FNMR by age group for two operating thresholds corresponding to $FMR = \{0.001, 0.0001\}$ computed over all on the order of 10^{10} impostor scores. The FMR in each bin will vary also - see subsequent impostor heatmaps in sec. 3.6.2. Given a pair of face images taken at different times, we assign the comparison to the bin that is the arithmetic average of the subject's ages. This plot shows only the effect of age, not ageing. The number of comparisons in each bin is generally in the thousands, however the first and last bins are computed over 149 and 124 respectively. The error rates in some (adult) cases are zero, and in others the DET is flat so the error rates at the two thresholds are identical. The lines span 1% and 99% of bootstrap replicated FNMR estimates.

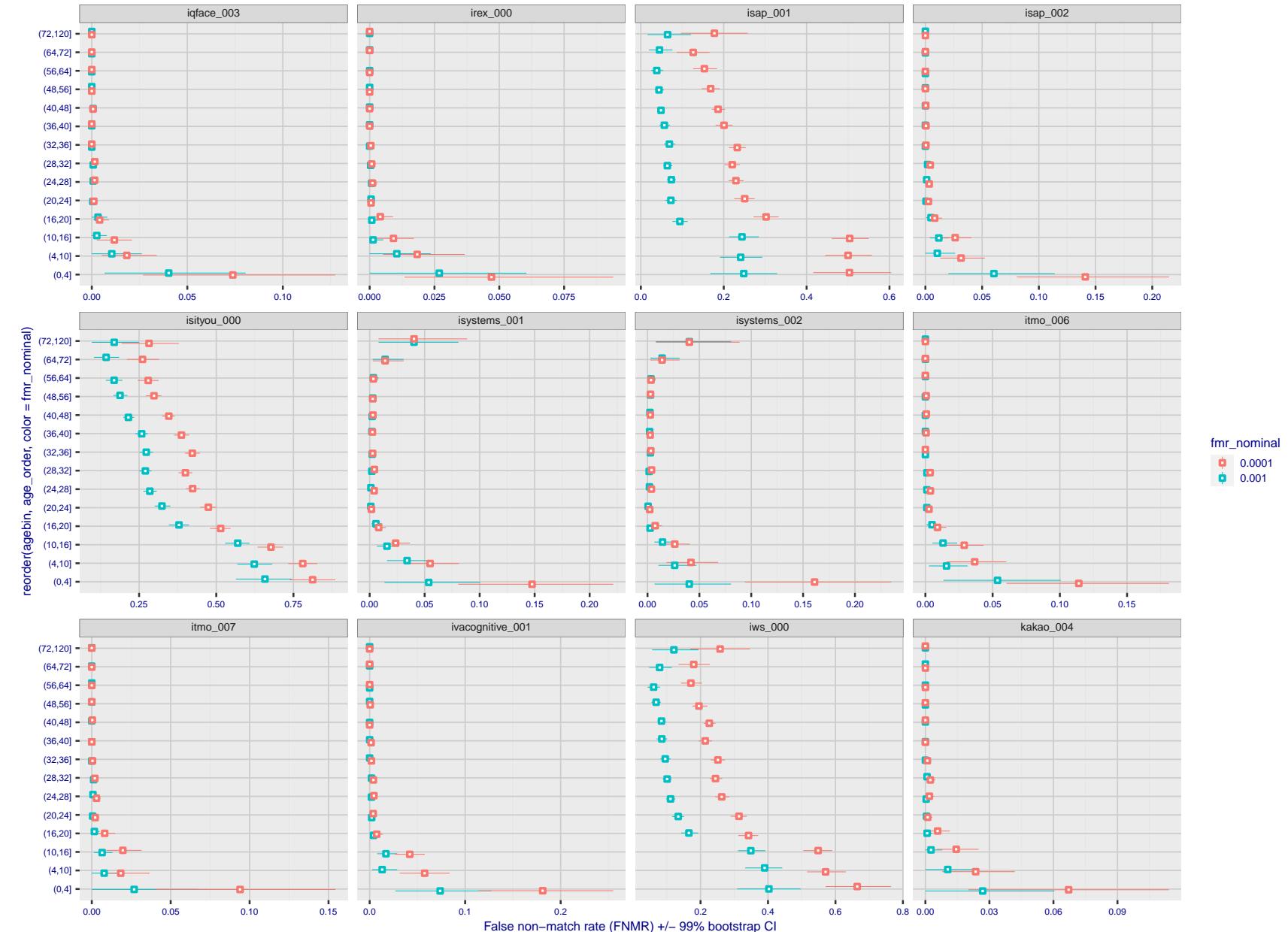


Figure 265: For the visa images, the dots show FNMR by age group for two operating thresholds corresponding to $FMR = \{0.001, 0.0001\}$ computed over all on the order of 10^{10} impostor scores. The FMR in each bin will vary also - see subsequent impostor heatmaps in sec. 3.6.2. Given a pair of face images taken at different times, we assign the comparison to the bin that is the arithmetic average of the subject's ages. This plot shows only the effect of age, not ageing. The number of comparisons in each bin is generally in the thousands, however the first and last bins are computed over 149 and 124 respectively. The error rates in some (adult) cases are zero, and in others the DET is flat so the error rates at the two thresholds are identical. The lines span 1% and 99% of bootstrap replicated FNMR estimates.

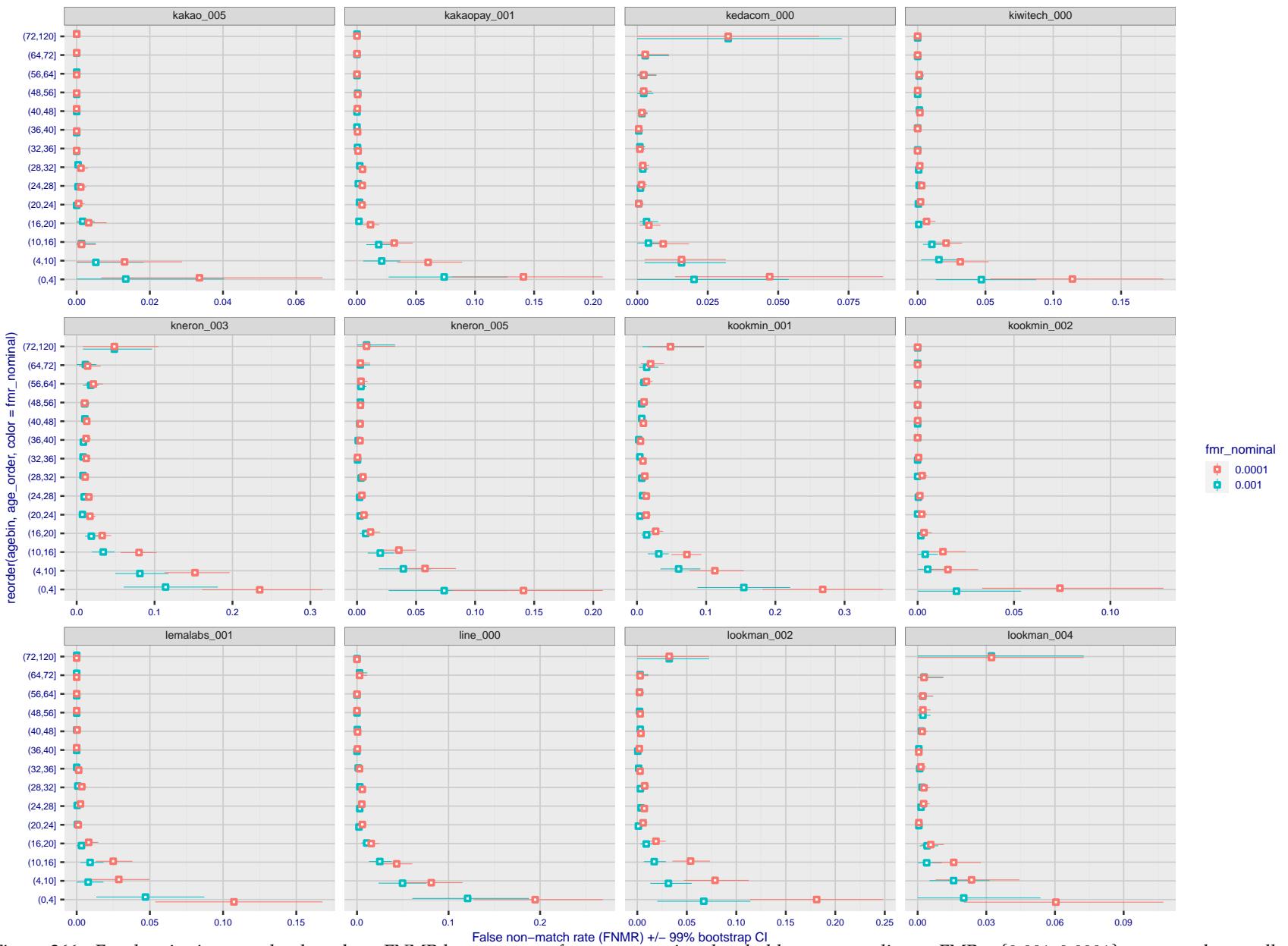


Figure 266: For the visa images, the dots show FNMR by age group for two operating thresholds corresponding to $FMR = \{0.001, 0.0001\}$ computed over all on the order of 10^{10} impostor scores. The FMR in each bin will vary also - see subsequent impostor heatmaps in sec. 3.6.2. Given a pair of face images taken at different times, we assign the comparison to the bin that is the arithmetic average of the subject's ages. This plot shows only the effect of age, not ageing. The number of comparisons in each bin is generally in the thousands, however the first and last bins are computed over 149 and 124 respectively. The error rates in some (adult) cases are zero, and in others the DET is flat so the error rates at the two thresholds are identical. The lines span 1% and 99% of bootstrap replicated FNMR estimates.

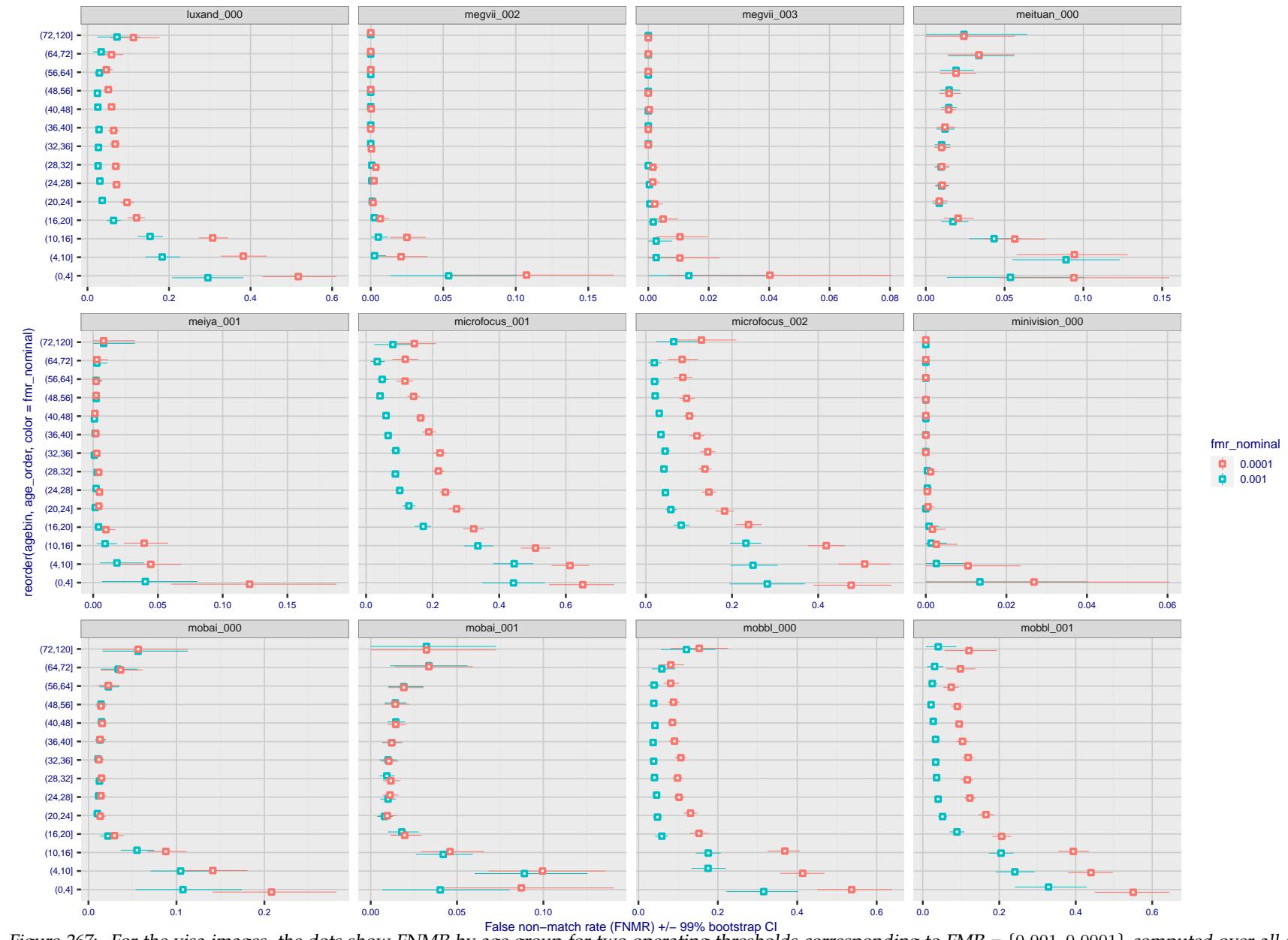


Figure 267: For the visa images, the dots show FNMR by age group for two operating thresholds corresponding to $FMR = \{0.001, 0.0001\}$ computed over all on the order of 10^{10} impostor scores. The FMR in each bin will vary also - see subsequent impostor heatmaps in sec. 3.6.2. Given a pair of face images taken at different times, we assign the comparison to the bin that is the arithmetic average of the subject's ages. This plot shows only the effect of age, not ageing. The number of comparisons in each bin is generally in the thousands, however the first and last bins are computed over 149 and 124 respectively. The error rates in some (adult) cases are zero, and in others the DET is flat so the error rates at the two thresholds are identical. The lines span 1% and 99% of bootstrap replicated FNMR estimates.



Figure 268: For the visa images, the dots show FNMR by age group for two operating thresholds corresponding to $FMR = \{0.001, 0.0001\}$ computed over all on the order of 10^{10} impostor scores. The FMR in each bin will vary also - see subsequent impostor heatmaps in sec. 3.6.2. Given a pair of face images taken at different times, we assign the comparison to the bin that is the arithmetic average of the subject's ages. This plot shows only the effect of age, not ageing. The number of comparisons in each bin is generally in the thousands, however the first and last bins are computed over 149 and 124 respectively. The error rates in some (adult) cases are zero, and in others the DET is flat so the error rates at the two thresholds are identical. The lines span 1% and 99% of bootstrap replicated FNMR estimates.

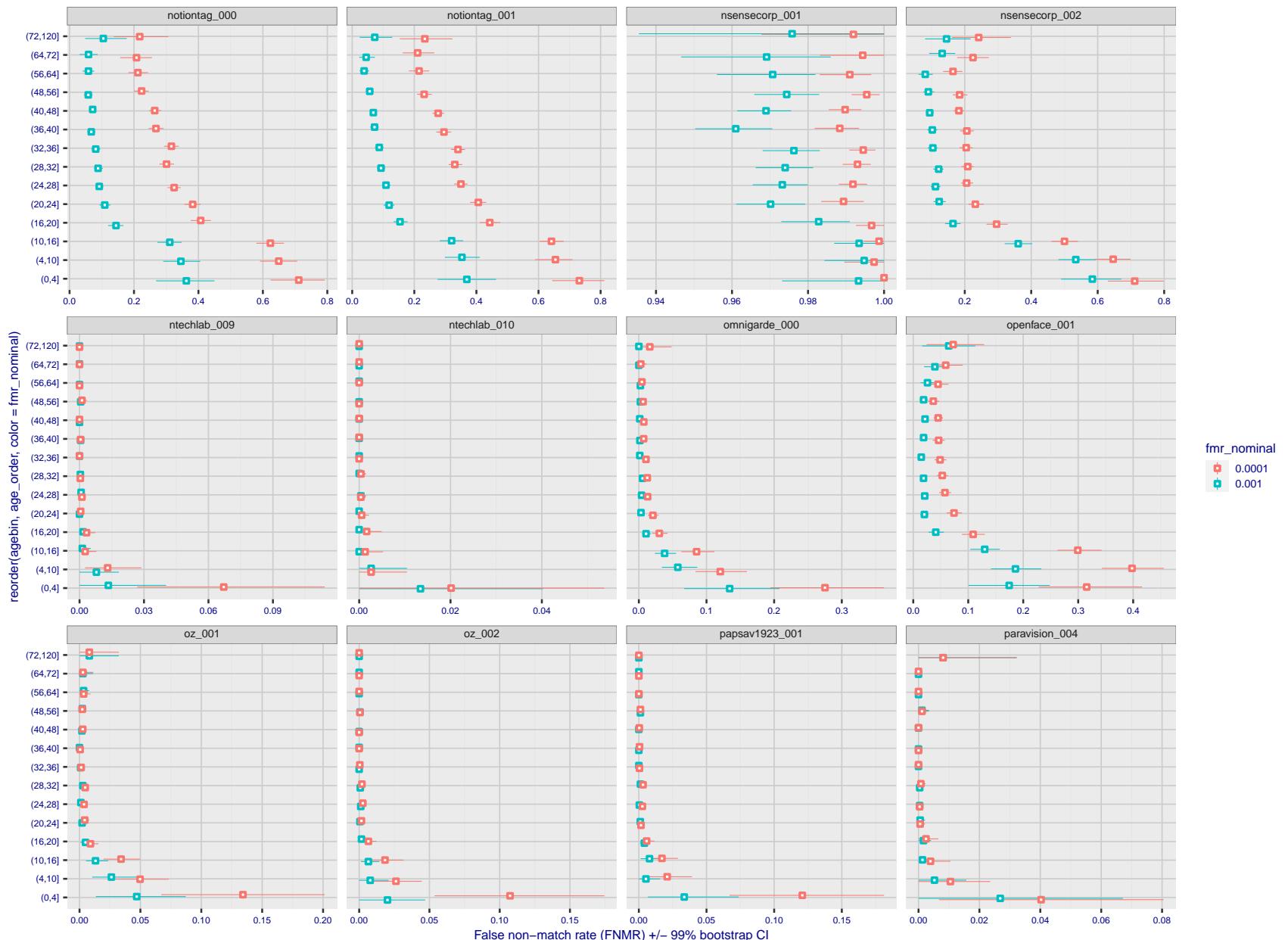


Figure 269: For the visa images, the dots show FNMR by age group for two operating thresholds corresponding to $FMR = \{0.001, 0.0001\}$ computed over all on the order of 10^{10} impostor scores. The FMR in each bin will vary also - see subsequent impostor heatmaps in sec. 3.6.2. Given a pair of face images taken at different times, we assign the comparison to the bin that is the arithmetic average of the subject's ages. This plot shows only the effect of age, not ageing. The number of comparisons in each bin is generally in the thousands, however the first and last bins are computed over 149 and 124 respectively. The error rates in some (adult) cases are zero, and in others the DET is flat so the error rates at the two thresholds are identical. The lines span 1% and 99% of bootstrap replicated FNMR estimates.



Figure 270: For the visa images, the dots show FNMR by age group for two operating thresholds corresponding to $FMR = \{0.001, 0.0001\}$ computed over all on the order of 10^{10} impostor scores. The FMR in each bin will vary also - see subsequent impostor heatmaps in sec. 3.6.2. Given a pair of face images taken at different times, we assign the comparison to the bin that is the arithmetic average of the subject's ages. This plot shows only the effect of age, not ageing. The number of comparisons in each bin is generally in the thousands, however the first and last bins are computed over 149 and 124 respectively. The error rates in some (adult) cases are zero, and in others the DET is flat so the error rates at the two thresholds are identical. The lines span 1% and 99% of bootstrap replicated FNMR estimates.



Figure 271: For the visa images, the dots show FNMR by age group for two operating thresholds corresponding to $FMR = \{0.001, 0.0001\}$ computed over all on the order of 10^{10} impostor scores. The FMR in each bin will vary also - see subsequent impostor heatmaps in sec. 3.6.2. Given a pair of face images taken at different times, we assign the comparison to the bin that is the arithmetic average of the subject's ages. This plot shows only the effect of age, not ageing. The number of comparisons in each bin is generally in the thousands, however the first and last bins are computed over 149 and 124 respectively. The error rates in some (adult) cases are zero, and in others the DET is flat so the error rates at the two thresholds are identical. The lines span 1% and 99% of bootstrap replicated FNMR estimates.

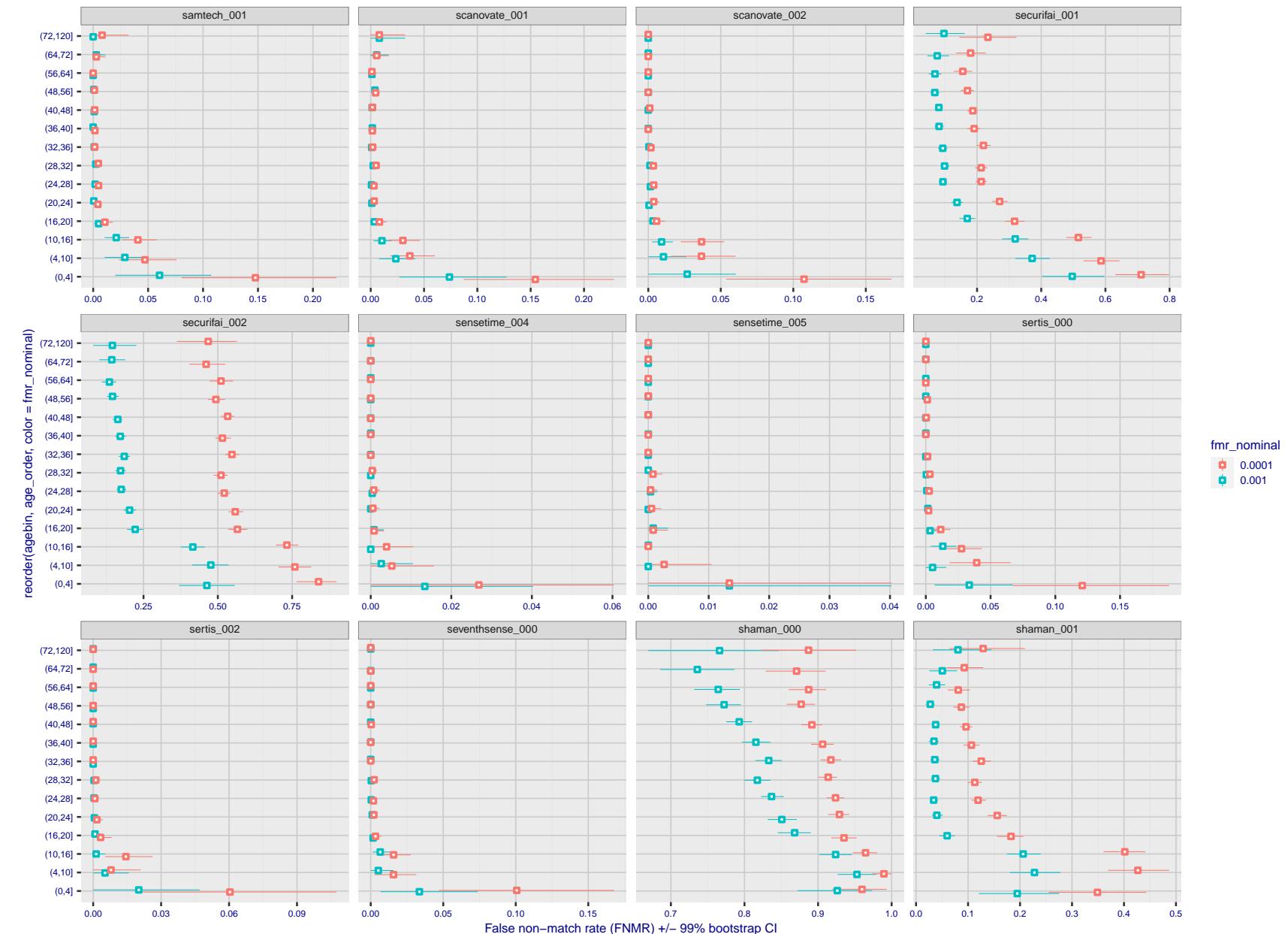


Figure 272: For the visa images, the dots show FNMR by age group for two operating thresholds corresponding to $FMR = \{0.001, 0.0001\}$ computed over all on the order of 10^{10} impostor scores. The FMR in each bin will vary also - see subsequent impostor heatmaps in sec. 3.6.2. Given a pair of face images taken at different times, we assign the comparison to the bin that is the arithmetic average of the subject's ages. This plot shows only the effect of age, not ageing. The number of comparisons in each bin is generally in the thousands, however the first and last bins are computed over 149 and 124 respectively. The error rates in some (adult) cases are zero, and in others the DET is flat so the error rates at the two thresholds are identical. The lines span 1% and 99% of bootstrap replicated FNMR estimates.



Figure 273: For the visa images, the dots show FNMR by age group for two operating thresholds corresponding to $FMR = \{0.001, 0.0001\}$ computed over all on the order of 10^{10} impostor scores. The FMR in each bin will vary also - see subsequent impostor heatmaps in sec. 3.6.2. Given a pair of face images taken at different times, we assign the comparison to the bin that is the arithmetic average of the subject's ages. This plot shows only the effect of age, not ageing. The number of comparisons in each bin is generally in the thousands, however the first and last bins are computed over 149 and 124 respectively. The error rates in some (adult) cases are zero, and in others the DET is flat so the error rates at the two thresholds are identical. The lines span 1% and 99% of bootstrap replicated FNMR estimates.



Figure 274: For the visa images, the dots show FNMR by age group for two operating thresholds corresponding to $FMR = \{0.001, 0.0001\}$ computed over all on the order of 10^{10} impostor scores. The FMR in each bin will vary also - see subsequent impostor heatmaps in sec. 3.6.2. Given a pair of face images taken at different times, we assign the comparison to the bin that is the arithmetic average of the subject's ages. This plot shows only the effect of age, not ageing. The number of comparisons in each bin is generally in the thousands, however the first and last bins are computed over 149 and 124 respectively. The error rates in some (adult) cases are zero, and in others the DET is flat so the error rates at the two thresholds are identical. The lines span 1% and 99% of bootstrap replicated FNMR estimates.

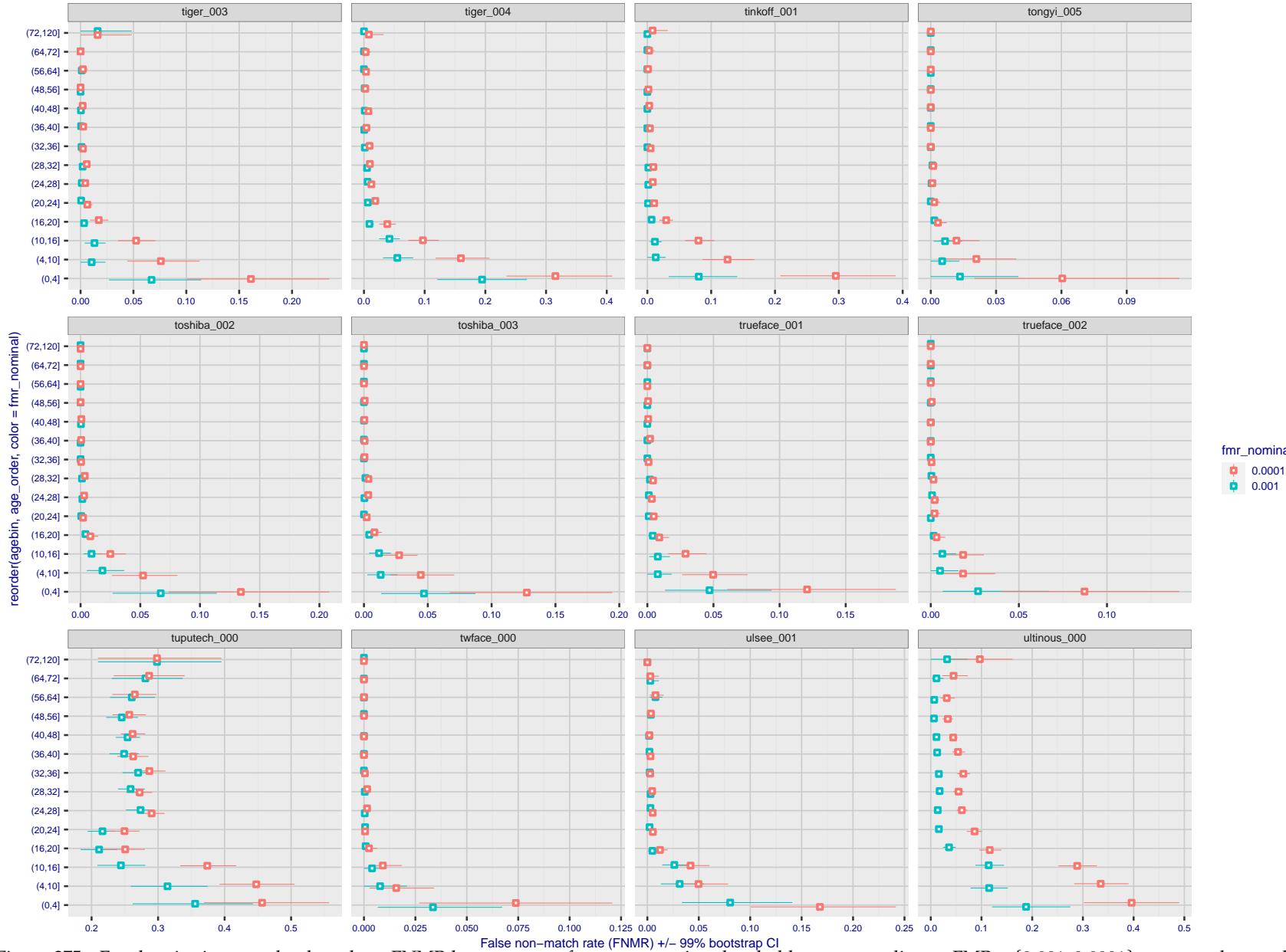


Figure 275: For the visa images, the dots show FNMR by age group for two operating thresholds corresponding to $FMR = \{0.001, 0.0001\}$ computed over all on the order of 10^{10} impostor scores. The FMR in each bin will vary also - see subsequent impostor heatmaps in sec. 3.6.2. Given a pair of face images taken at different times, we assign the comparison to the bin that is the arithmetic average of the subject's ages. This plot shows only the effect of age, not ageing. The number of comparisons in each bin is generally in the thousands, however the first and last bins are computed over 149 and 124 respectively. The error rates in some (adult) cases are zero, and in others the DET is flat so the error rates at the two thresholds are identical. The lines span 1% and 99% of bootstrap replicated FNMR estimates.

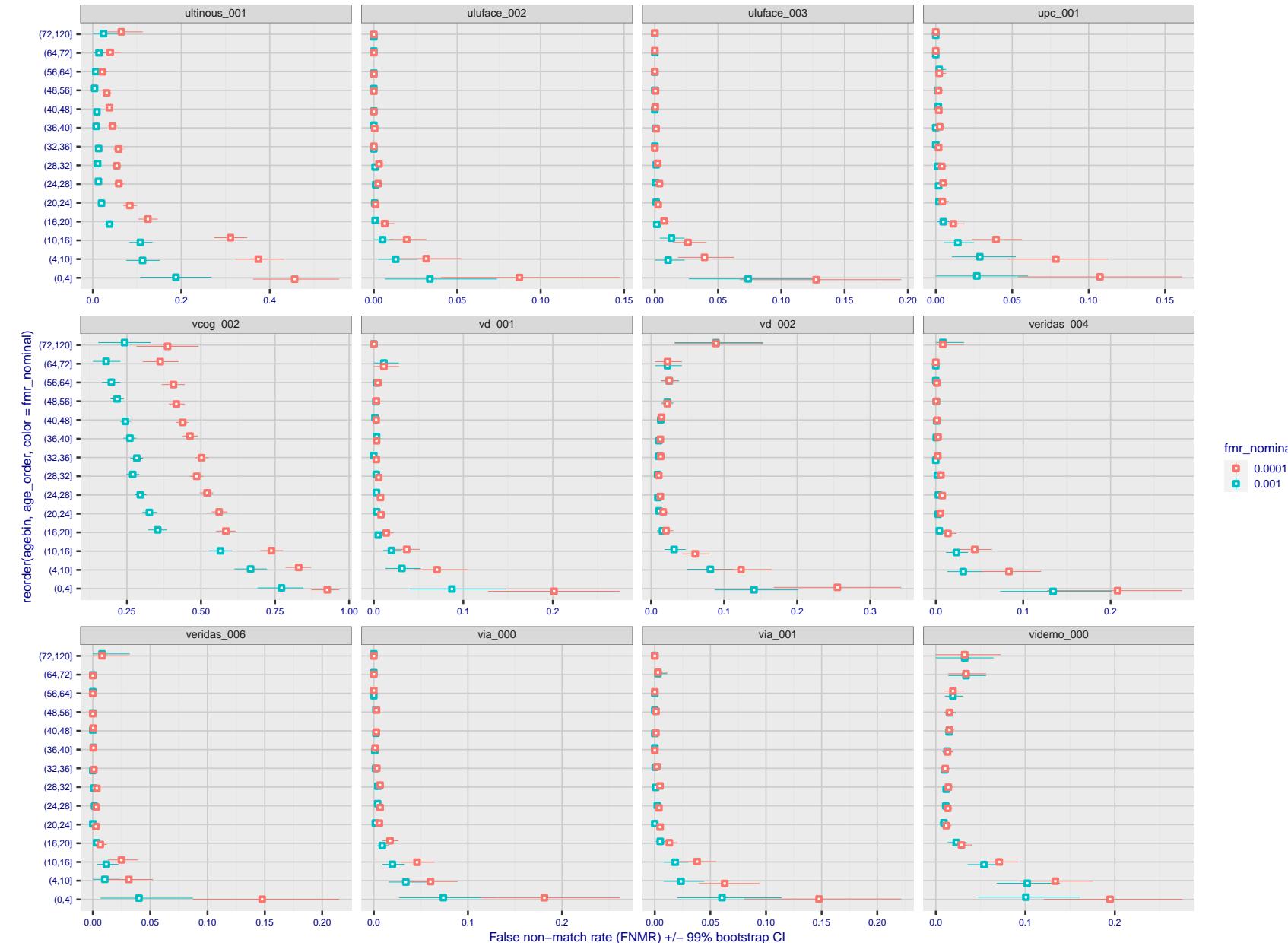


Figure 276: For the visa images, the dots show FNMR by age group for two operating thresholds corresponding to $FMR = \{0.001, 0.0001\}$ computed over all on the order of 10^{10} impostor scores. The FMR in each bin will vary also - see subsequent impostor heatmaps in sec. 3.6.2. Given a pair of face images taken at different times, we assign the comparison to the bin that is the arithmetic average of the subject's ages. This plot shows only the effect of age, not ageing. The number of comparisons in each bin is generally in the thousands, however the first and last bins are computed over 149 and 124 respectively. The error rates in some (adult) cases are zero, and in others the DET is flat so the error rates at the two thresholds are identical. The lines span 1% and 99% of bootstrap replicated FNMR estimates.

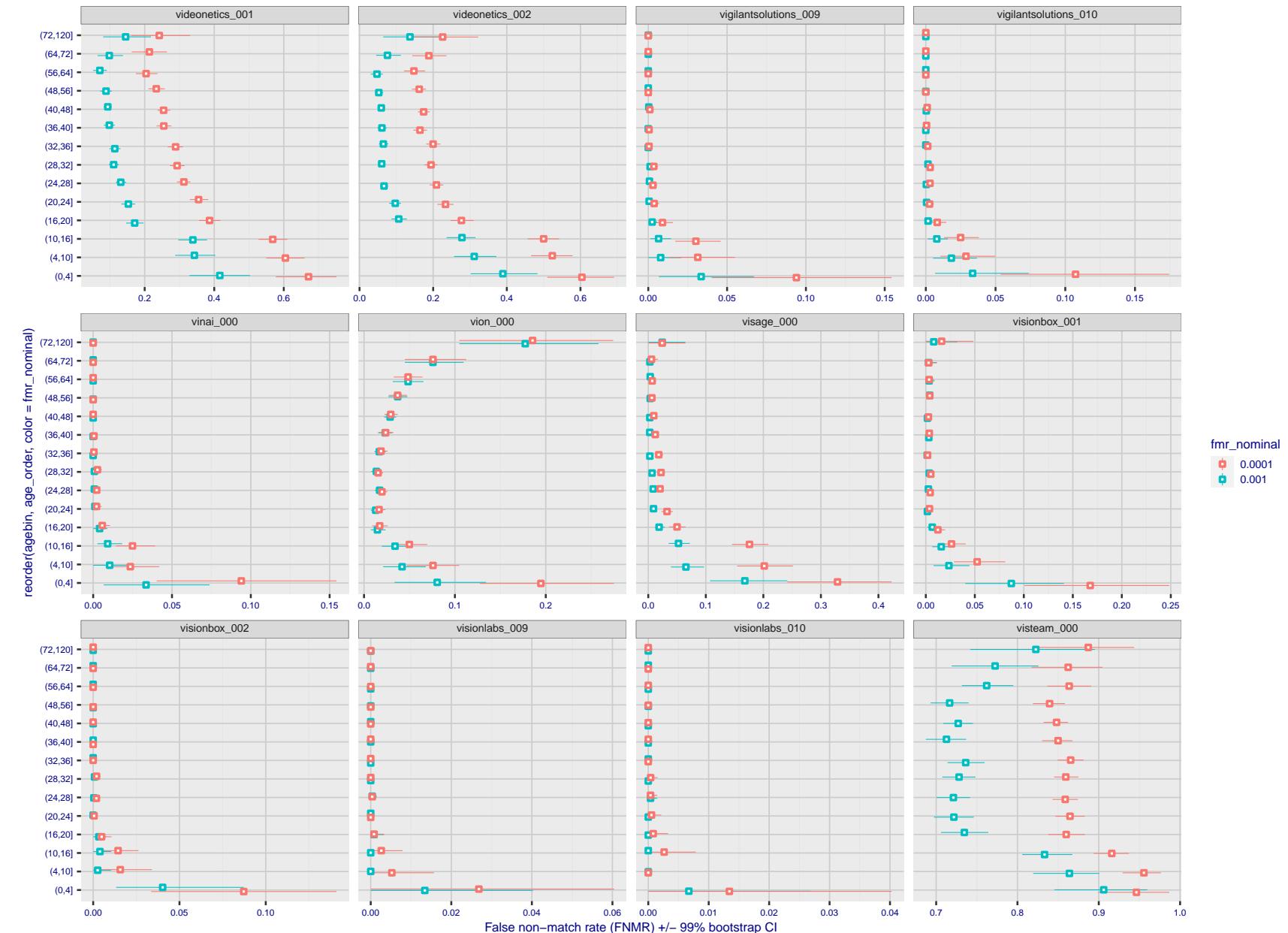


Figure 277: For the visa images, the dots show FNMR by age group for two operating thresholds corresponding to $FMR = \{0.001, 0.0001\}$ computed over all on the order of 10^{10} impostor scores. The FMR in each bin will vary also - see subsequent impostor heatmaps in sec. 3.6.2. Given a pair of face images taken at different times, we assign the comparison to the bin that is the arithmetic average of the subject's ages. This plot shows only the effect of age, not ageing. The number of comparisons in each bin is generally in the thousands, however the first and last bins are computed over 149 and 124 respectively. The error rates in some (adult) cases are zero, and in others the DET is flat so the error rates at the two thresholds are identical. The lines span 1% and 99% of bootstrap replicated FNMR estimates.

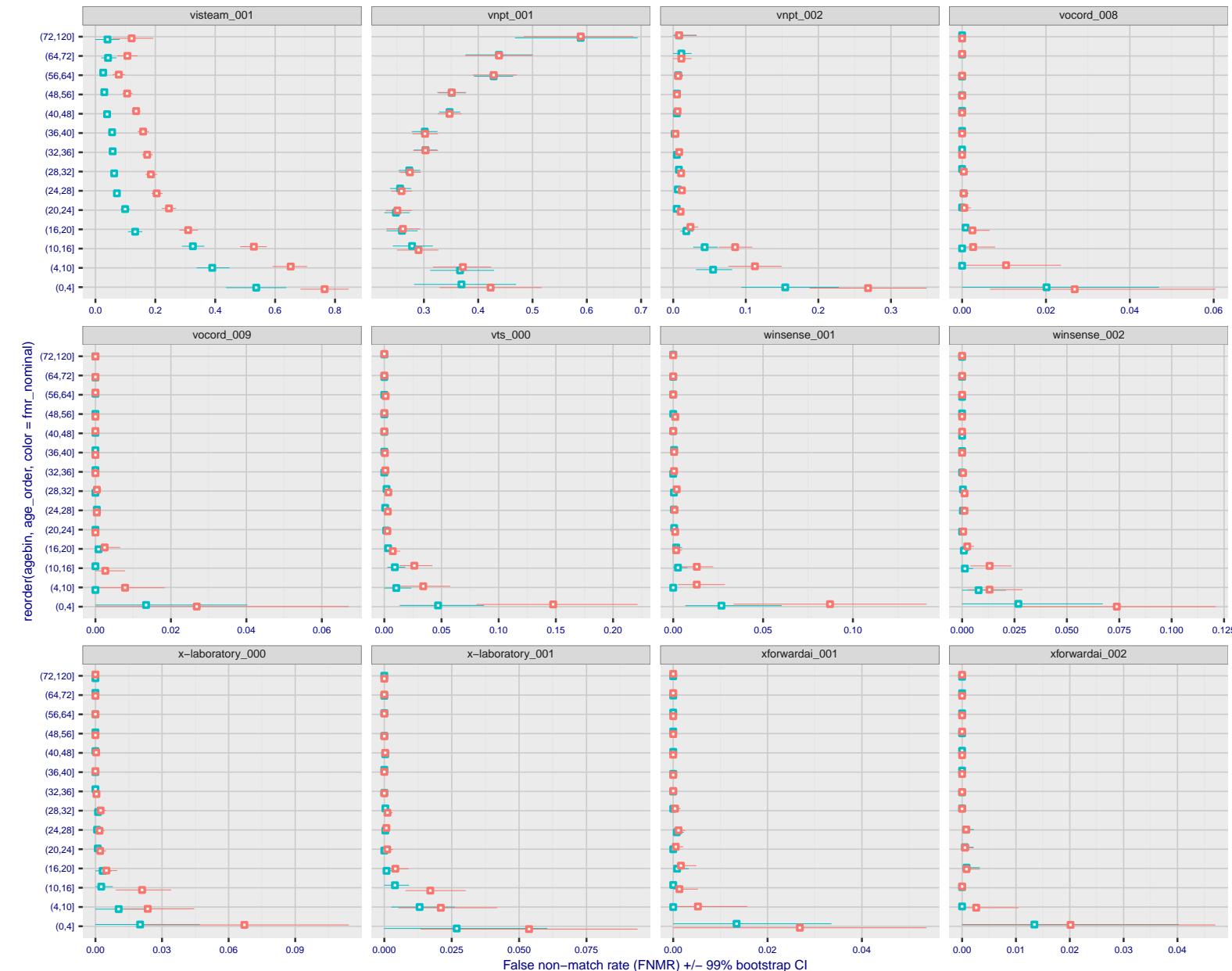


Figure 278: For the visa images, the dots show FNMR by age group for two operating thresholds corresponding to $FMR = \{0.001, 0.0001\}$ computed over all on the order of 10^{10} impostor scores. The FMR in each bin will vary also - see subsequent impostor heatmaps in sec. 3.6.2. Given a pair of face images taken at different times, we assign the comparison to the bin that is the arithmetic average of the subject's ages. This plot shows only the effect of age, not ageing. The number of comparisons in each bin is generally in the thousands, however the first and last bins are computed over 149 and 124 respectively. The error rates in some (adult) cases are zero, and in others the DET is flat so the error rates at the two thresholds are identical. The lines span 1% and 99% of bootstrap replicated FNMR estimates.



Figure 279: For the visa images, the dots show FNMR by age group for two operating thresholds corresponding to $FMR = \{0.001, 0.0001\}$ computed over all on the order of 10^{10} impostor scores. The FMR in each bin will vary also - see subsequent impostor heatmaps in sec. 3.6.2. Given a pair of face images taken at different times, we assign the comparison to the bin that is the arithmetic average of the subject's ages. This plot shows only the effect of age, not ageing. The number of comparisons in each bin is generally in the thousands, however the first and last bins are computed over 149 and 124 respectively. The error rates in some (adult) cases are zero, and in others the DET is flat so the error rates at the two thresholds are identical. The lines span 1% and 99% of bootstrap replicated FNMR estimates.

Caveats: None.

3.6 Impostor distribution stability

3.6.1 Effect of birth place on the impostor distribution

Background: Facial appearance varies geographically, both in terms of skin tone, cranio-facial structure and size. This section addresses whether false match rates vary intra- and inter-regionally.

Goals:

- ▷ To show the effect of birth region of the impostor and enrollee on false match rates.
- ▷ To determine whether some algorithms give better impostor distribution stability.

Methods:

- ▷ For the visa images, NIST defined 10 regions: Sub-Saharan Africa, South Asia, Polynesia, North Africa, Middle East, Europe, East Asia, Central and South America, Central Asia, and the Caribbean.
- ▷ For the visa images, NIST mapped each country of birth to a region. There is some arbitrariness to this. For example, Egypt could reasonably be assigned to the Middle East instead of North Africa. An alternative methodology could, for example, assign the Philippines to *both* Polynesia and East Asia.
- ▷ FMR is computed for cases where all face images of impostors born in region r_2 are compared with enrolled face images of persons born in region r_1 .

$$\text{FMR}(r_1, r_2, T) = \frac{\sum_{i=1}^{N_{r_1, r_2}} H(s_i - T)}{N_{r_1, r_2}} \quad (5)$$

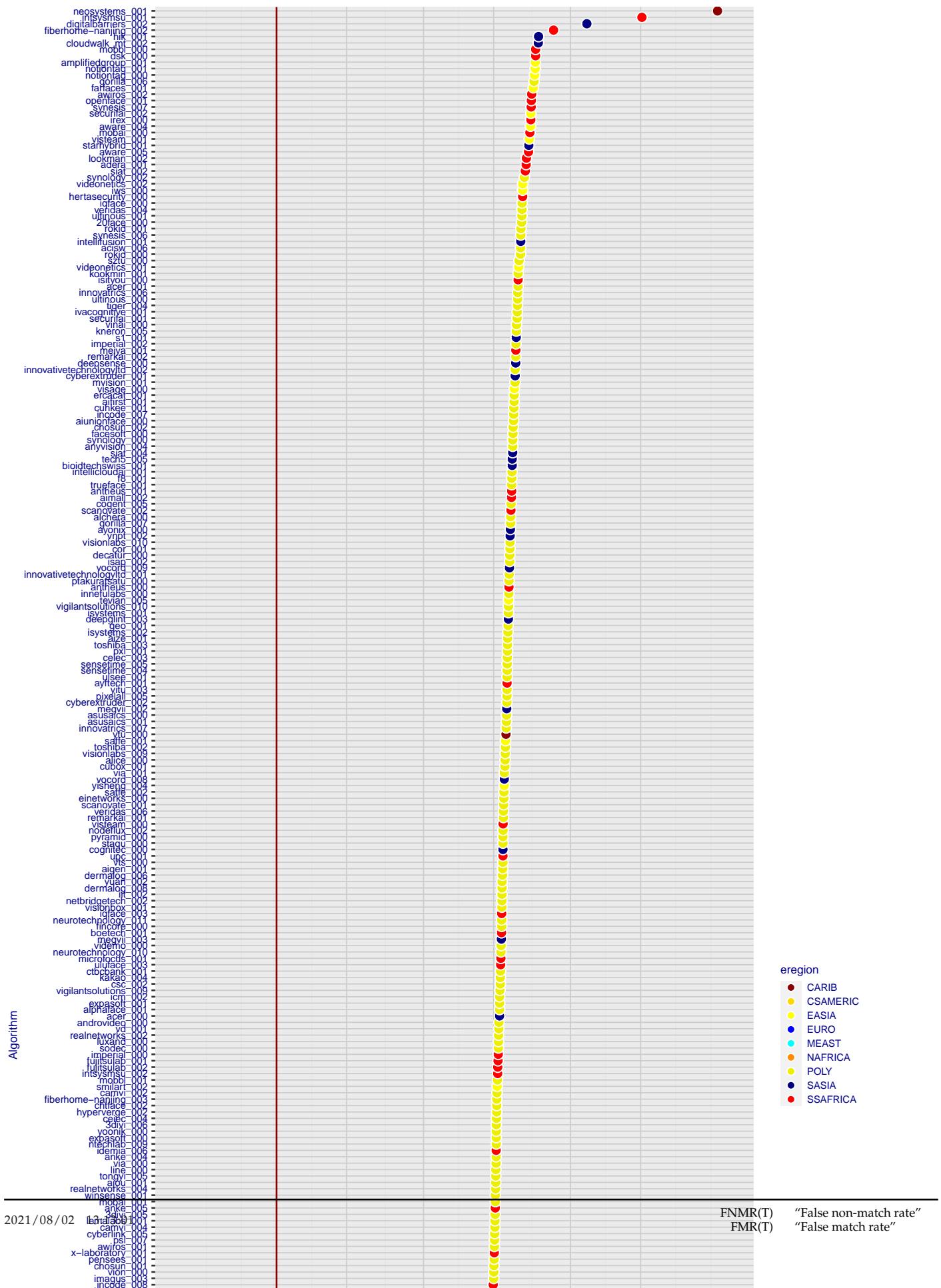
where the same threshold, T , is used in all cells, and H is the unit step function. The threshold is set to give $\text{FMR}(T) = 0.001$ over the entire set of visa image impostor comparisons.

- ▷ This analysis is then repeated by country-pair, but only for those country pairs where both have at least 1000 images available. The countries¹ appear in the axes of graphs that follow.
- ▷ The mean number of impostor scores in any cross-region bin is 33 million. The smallest number of impostor scores in any bin is 135000, for Central Asia - North Africa. While these counts are large enough to support reasonable significance, the number of individual faces is much smaller, on the order of $N^{0.5}$.
- ▷ The numbers of impostor scores in any cross-country bin is shown in Figure ??.

Results: Subsequent figures show heatmaps that use color to represent the base-10 logarithm of the false match rate. Red colors indicate high (bad) false match rates. Dark colors indicate benign false match rates. There are two series of graphs corresponding to aggregated geographical regions, and to countries. The notable observations are:

- ▷ The on-diagonal elements correspond to within-region impostors. FMR is generally above the nominal value of $\text{FMR} = 0.001$. Particularly there is usually higher FMR in, Sub-Saharan Africa, South Asia, and the Caribbean. Europe and Central Asia, on the other hand, usually give FMR closer to the nominal value.
- ▷ The off-diagonal elements correspond to across-region impostors. The highest FMR is produced between the Caribbean and Sub-Saharan Africa.
- ▷ Algorithms vary.

¹These are Argentina, Australia, Brazil, Chile, China, Costa Rica, Cuba, Czech Republic, Dominican Republic, Ecuador, Egypt, El Salvador, Germany, Ghana, Great Britain, Greece, Guatemala, Haiti, Hong Kong, Honduras, Indonesia, India, Israel, Jamaica, Japan, Kenya, Korea, Lebanon, Mexico, Malaysia, Nepal, Nigeria, Peru, Philippines, Pakistan, Poland, Romania, Russia, South Africa, Saudi Arabia, Thailand, Trinidad, Turkey, Taiwan, Ukraine, Venezuela, and Vietnam.



- ▷ We computed the same quantities for a global FMR = 0.0001. The effects are similar.

Caveats:

- ▷ The effects of variable impostor rates on one-to-many identification systems may well differ from what's implied by these one-to-one verification results. Two reasons for this are a) the enrollment galleries are usually imbalanced across countries of birth, age and sex; b) one-to-many identification algorithms often implement techniques aimed at stabilizing the impostor distribution. Further research is necessary.
- ▷ In principle, the effects seen in this subsection could be due to differences in the image capture process. We consider this unlikely since the effects are maintained across geography - e.g. Caribbean vs. Africa, or Japan vs. China.

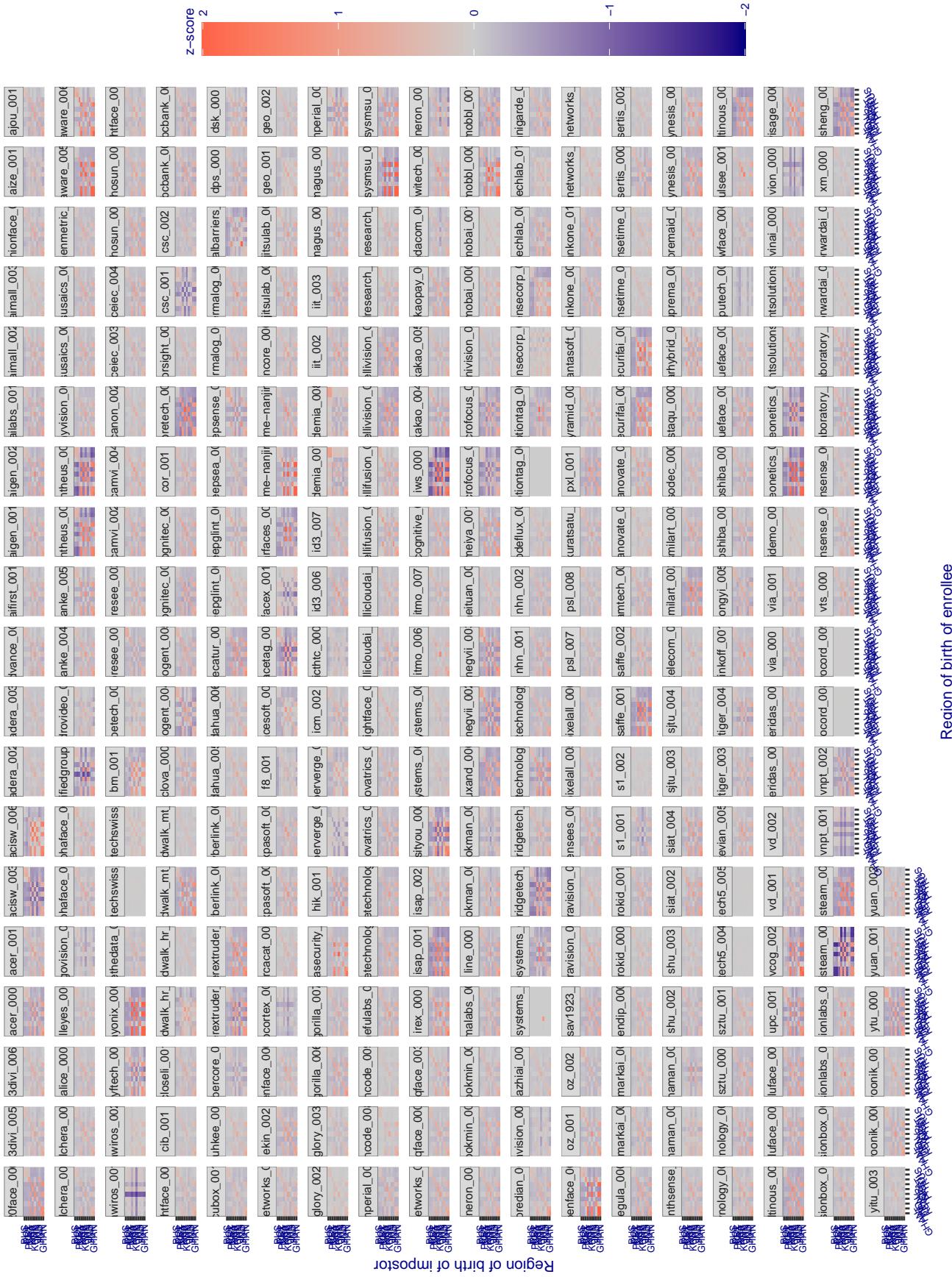


Figure 281: For visa images, the heatmap shows how the mean of the impostor distribution for the country pair (a,b) is shifted relative to the mean of the global impostor distribution, expressed as a number of standard deviations of the global impostor distribution. This statistic is designed to show shifts in the entire impostor distribution, not just tail effects that manifest as the anomalously high (or low) false match rates that appear in the subsequent figures. The countries are chosen to show that skin shifts in the Asian populations with the Yitu and Tong YiTrans algorithms, is accompanied by positive shifts in the European populations. This reversal relative to most other algorithms, may derive from use of nationally weighted training sets. The figure is computed from same-sex and same-age impostor pairs.

3.6.2 Effect of age on impostors

Background: This section shows the effect of age on the impostor distribution. The ideal behaviour is that the age of the enrollee and the impostor would not affect impostor scores. This would support FMR stability over sub-populations.

Goals:

- ▷ To show the effect of relative ages of the impostor and enrollee on false match rates.
- ▷ To determine whether some algorithms have better impostor distribution stability.

Methods:

- ▷ Define 14 age group bins, spanning 0 to over 100 years old.
- ▷ Compute FMR over all impostor comparisons for which the subjects in the enrollee and impostor images have ages in two bins.
- ▷ Compute FMR over all impostor comparisons for which the subjects are additionally of the same sex, and born in the same geographic region.

Results:

The notable aspects are:

- ▷ Diagonal dominance: Impostors are more likely to be matched against their same age group.
- ▷ Same sex and same region impostors are more successful. On the diagonal, an impostor is more likely to succeed by posing as someone of the same sex. If $\Delta \log_{10} \text{FMR} = 0.2$, then same-sex same-region FMR exceeds the all-pairs FMR by factor of $10^{0.2} = 1.6$.
- ▷ Young children impostors give elevated FMR against young children. Older adult impostor give elevated FMR against older adults. These effects are quite large, for example if $\Delta \log_{10} \text{FMR} = 1.0$ larger than a 32 year old, then these groups have higher FMR by a factor of $10^1 = 10$. This would imply an FMR above 0.01 for a nominal (global) FMR = 0.001.
- ▷ Algorithms vary.
- ▷ We computed the same quantities for a global FMR = 0.0001. The effects are similar.

Note the calculations in this section include impostors paired across all countries of birth.

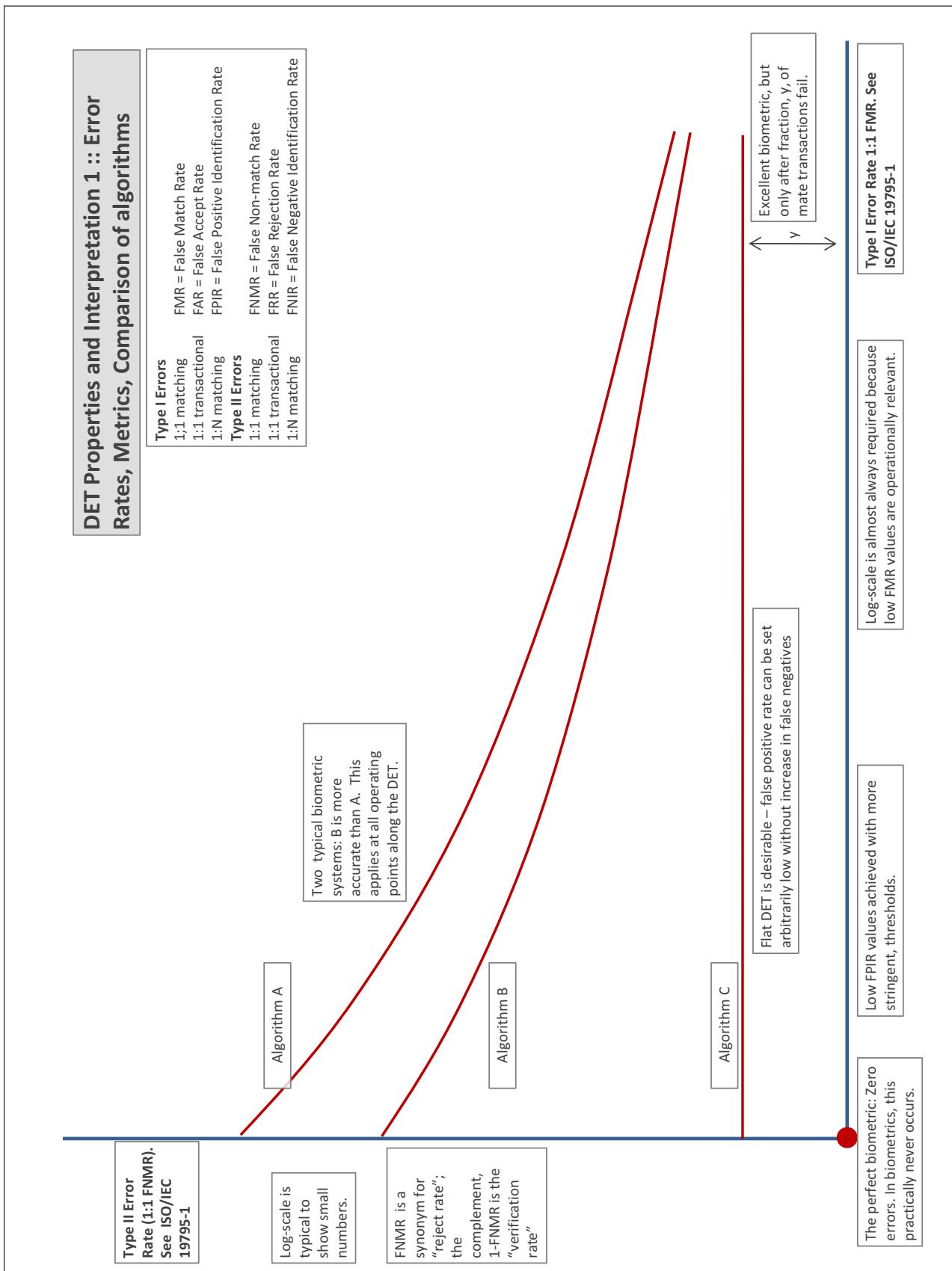
Accuracy Terms + Definitions

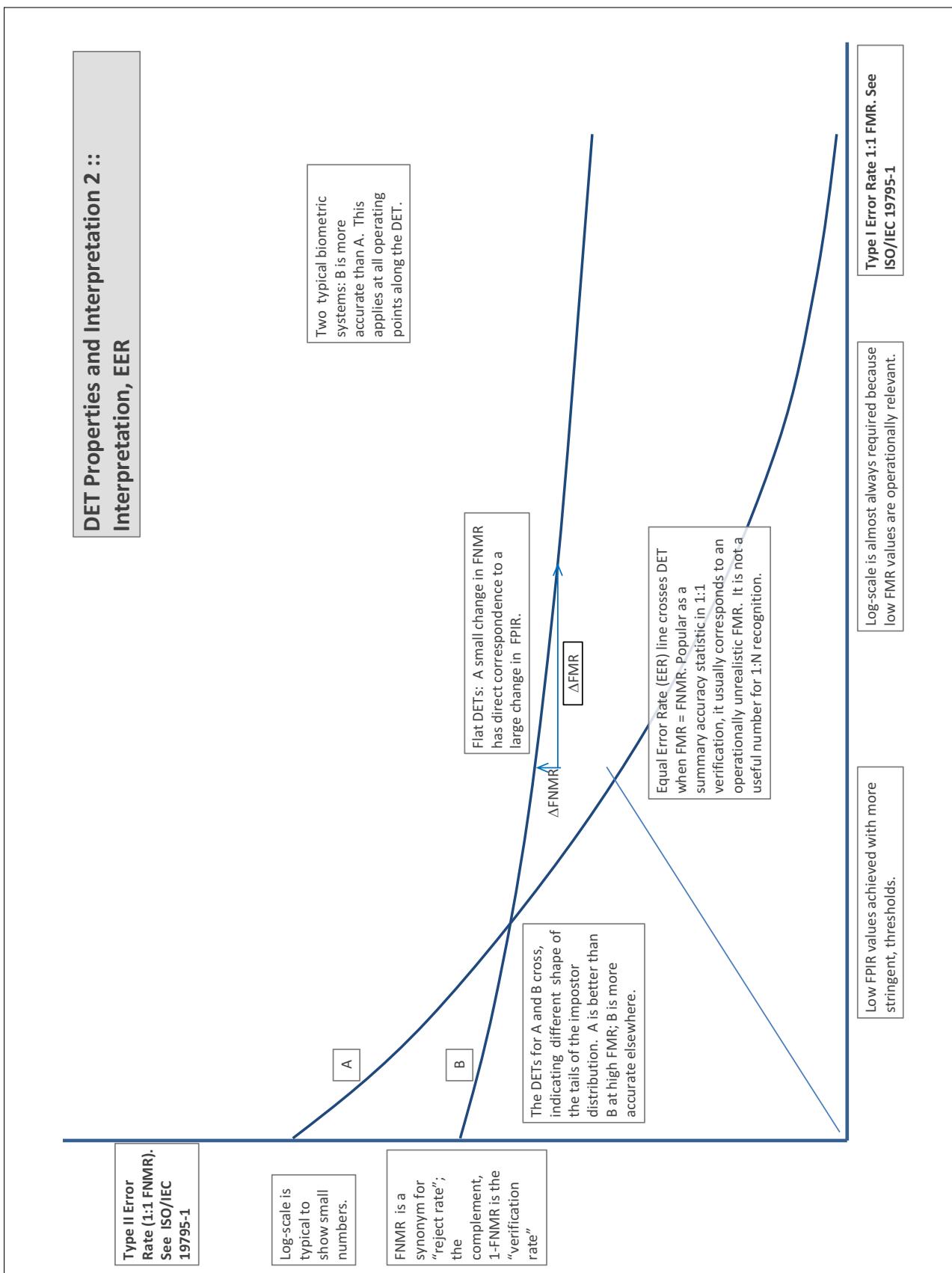
In biometrics, Type II errors occur when two samples of one person do not match – this is called a **false negative**. Correspondingly, Type I errors occur when samples from two persons do match – this is called a **false positive**. Matches are declared by a biometric system when the native comparison score from the recognition algorithm meets some **threshold**. Comparison scores can be either **similarity scores**, in which case higher values indicate that the samples are more likely to come from the same person, or **dissimilarity scores**, in which case higher values indicate different people. Similarity scores are traditionally computed by **fingerprint** and **face** recognition algorithms, while dissimilarities are used in **iris recognition**. In some cases, the dissimilarity score is a distance; this applies only when **metric** properties are obeyed. In any case, scores can be either **mate** scores, coming from a comparison of one person's samples, or **nonmate** scores, coming from comparison of different persons' samples. The words **genuine** or **authentic** are synonyms for mate, and the word **impostor** is used as a synonym for nonmatch. The words mate and nonmatch are traditionally used in identification applications (such as law enforcement search, or background checks) while genuine and impostor are used in verification applications (such as access control).

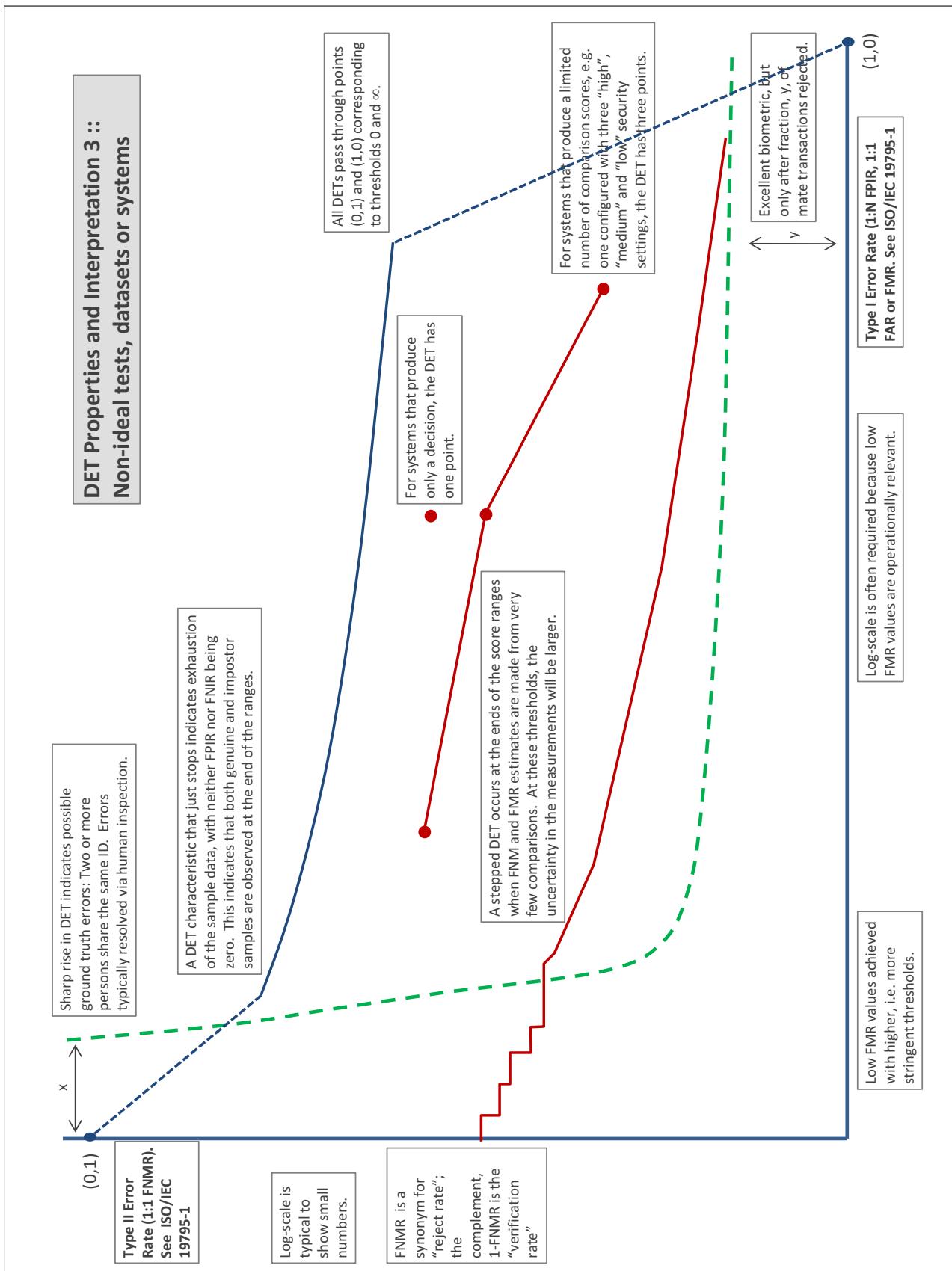
A **error tradeoff** characteristic represents the tradeoff between Type II and Type I classification errors. For verification this plots false non-match rate (FNMR) vs. false match rate (FMR) parametrically with T.

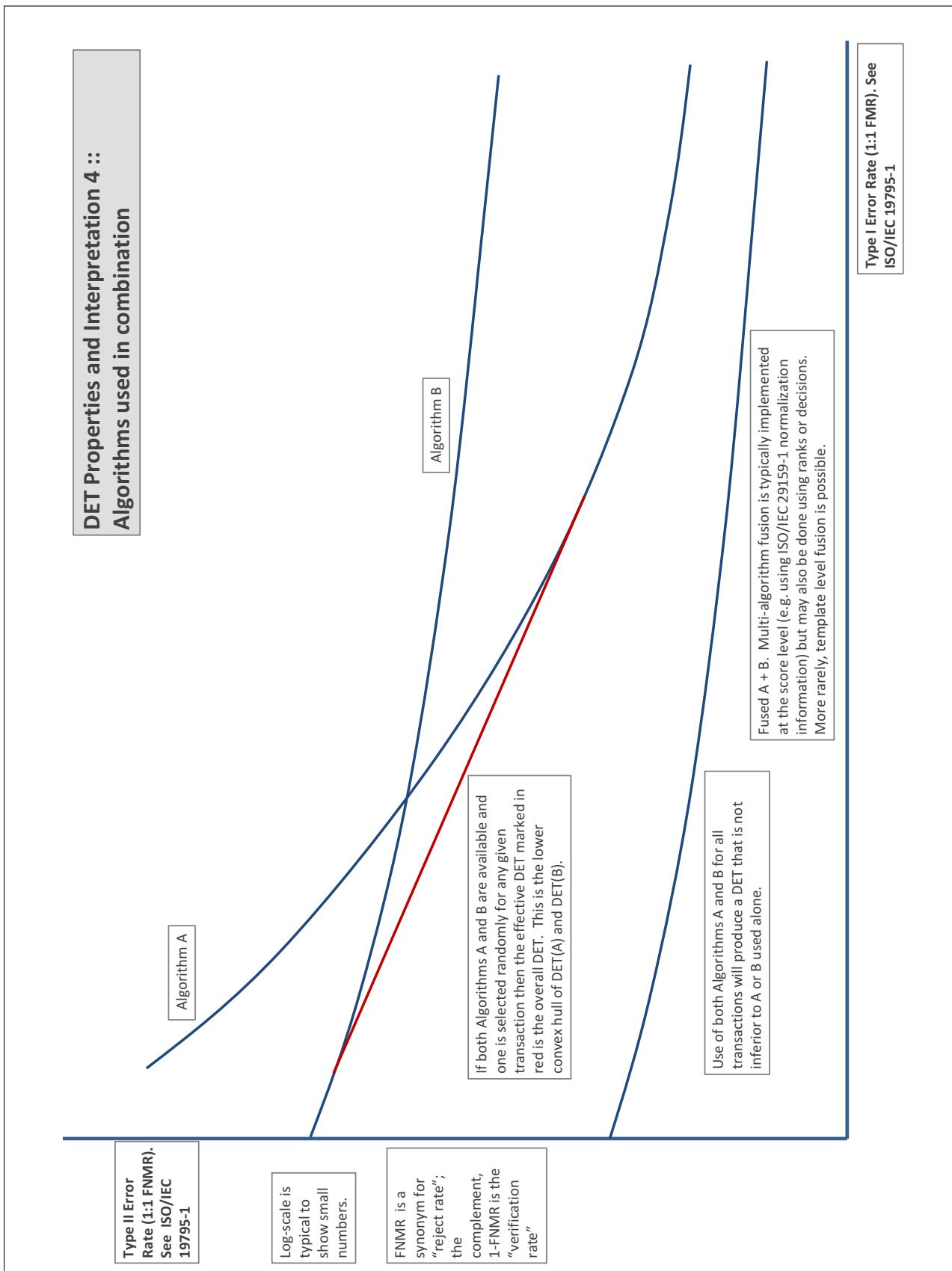
The error tradeoff plots are often called **detection error tradeoff (DET)** characteristics or **receiver operating characteristic (ROC)**. These serve the same function but differ, for example, in plotting the complement of an error rate (e.g., $TMR = 1 - FNMR$) and in transforming the axes most commonly using logarithms, to show multiple decades of FMR. More rarely, the function might be the inverse Gaussian function.

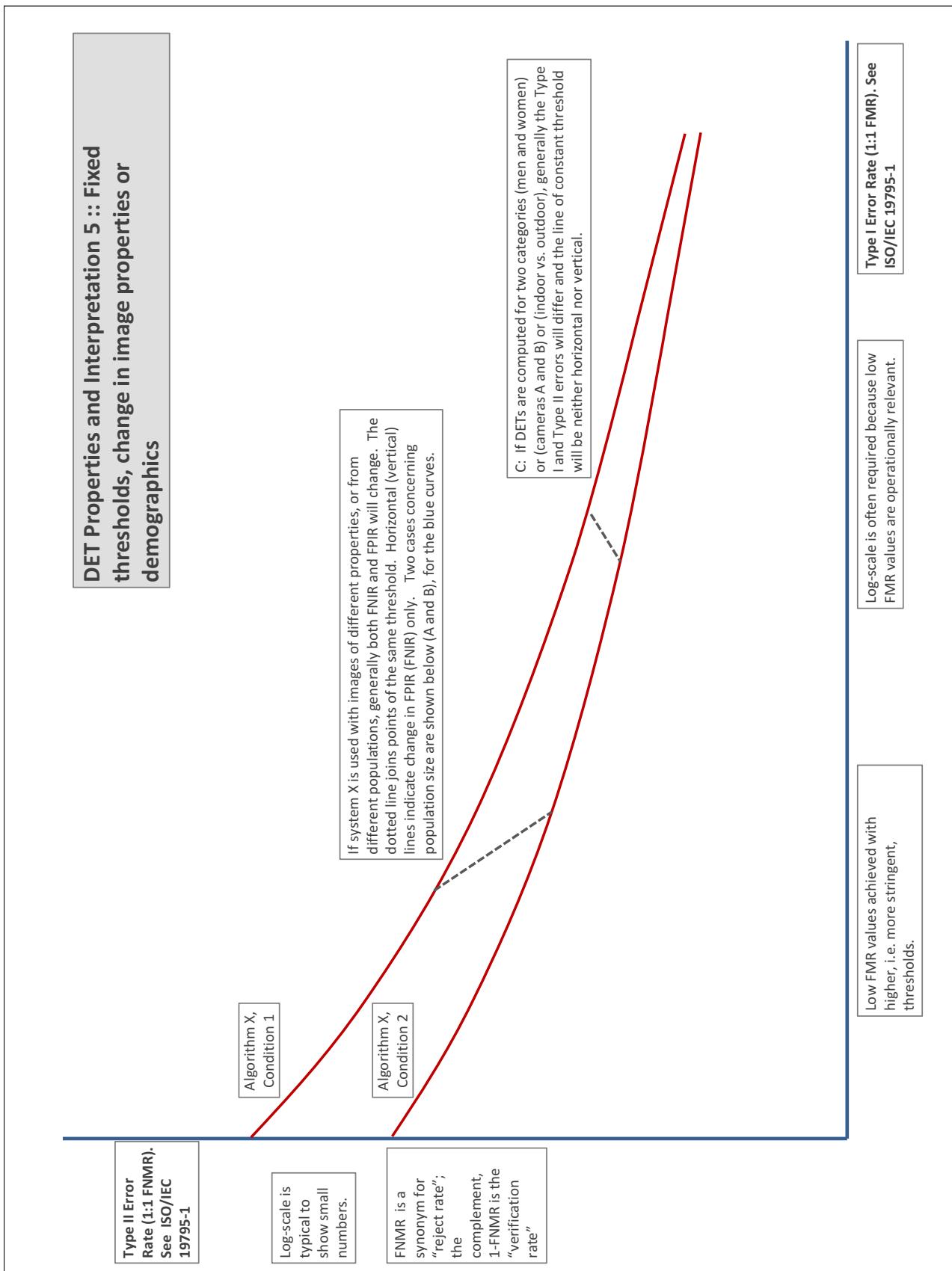
More detail and generality is provided in formal biometrics testing standards, see the various parts of [ISO/IEC 19795 Biometrics Testing and Reporting](#). More terms, including and beyond those to do with accuracy, see [ISO/IEC 2382-37 Information technology -- Vocabulary -- Part 37: Harmonized biometric vocabulary](#)











References

- [1] P. Jonathon Phillips, Amy N. Yates, Ying Hu, Carina A. Hahn, Eilidh Noyes, Kelsey Jackson, Jacqueline G. Cavazos, Géraldine Jeckeln, Rajeev Ranjan, Swami Sankaranarayanan, Jun-Cheng Chen, Carlos D. Castillo, Rama Chellappa, David White, and Alice J. O'Toole. Face recognition accuracy of forensic examiners, superrecognizers, and face recognition algorithms. *Proceedings of the National Academy of Sciences*, 115(24):6171–6176, 2018.